EFFECT OF ANCHORAGE SLIP AND INELASTIC SHEAR ON SEISMIC RESPONSE OF REINFORCED CONCRETE FRAMES

by

JABER ALSIWAT

A thesis submitted to
the Faculty of Graduate Studies and Research
in partial fulfilment of the requirements
for the degree of
DOCTORATE OF PHILOSOPHY
in Civil Engineering*

Department of Civil Engineering
University of Ottawa
Ottawa, Canada

January, 1993

* The Ph. D. of Civil Engineering Program
is a joint program with Carleton University
administered by the Ottawa-Carleton
Institute for Civil Engineering

ISBN 0-315-82591-X

UNIVERSITÉ D'OTTAWA
UNIVERSITY OF OTTAWA

Abstract

Reinforced Concrete structures located in regions of high seismic activity are expected to develop inelastic deformations in their critical regions. Therefore, inelastic dynamic analysis is required to obtain reliable predictions of structural behavior during an earthquake. Tests on reinforced concrete elements and subassemblages have shown that anchorage slip and inelastic shear deformations can be as significant as those due to inelastic flexure, in the critical regions. Hence, a proper seismic analysis should include inelastic deformations due to anchorage slip, shear and flexure. Flexural response has been researched extensively in the past. Research on the effects of anchorage slip and shear inelasticity is scarce in the literature.

The effect of anchorage slip and inelastic shear on seismic response of moment-resisting reinforced concrete frames is investigated in this study. A hysteretic model for anchorage slip is developed in the first phase of the project. The model consists of a primary curve and a set of hysteretic rules. The primary curve is developed based on assuming inelastic strain distribution along the embedded length of reinforcing bars. Considerations are given for conditions existing at interior joints, exterior joints, and column-foundation interface. Hysteretic rules are derived based on observations from available experimental data. The model is verified against a large volume of experimental data conducted on single straight and hooked bars, as well as interior and exterior joints. In the second phase of the project, the hysteretic anchorage-slip model is implemented into the nonlinear dynamic analysis program Drain 2D. A recently derived hysteretic model for shear is also implemented into the program. Two major subroutines, SLIPM and SHEARM, are added in order to trace out nonlinearity in the anchorage-slip and shear models. The program is enhanced with calculations of ductility demand and energy dissipation factors. Related input and output features of the program are also enhanced. In the final phase of the project, The enhanced computer program is used to determine the seismic response of three reinforced concrete frames that were designed for this purpose. Emphasis is placed on determining effects of individual deformation components on ductility demands and overall deformation characteristics of the frames. The effect of interaction of the fundamental period of vibration of the structure and the frequency content of ground motion are also investigated. The study shows that anchorage slip reduces flexural ductility demand by up to 42%. The amount of reduction is shown to depend on the level of inelasticity experienced by the structure. Overall behavior of the structures is not affected significantly by anchorage slip. Inelastic shear is shown to have very little effect on the behavior of the frames investigated.

Acknowledgment

I would like to express my deep gratitude to Dr. M. Saatcioglu, thesis supervisor, for his guidance and encouragement throughout the course of this study. Thanks are also due to my fellow graduate students for many fruitful discussions. The financial support provided by the Ministry of Higher Education of the Kingdom of Saudi Arabia, and by the Department of Civil Engineering, University of Ottawa, is highly appreciated.

Special thanks are extended to my mother for her continuous prayers and relentless support, and to my wife and children for their patience and sacrifice.

Table of Contents

List of Tables

List of Figures

Notations

Unless otherwise defined as they appear in the text, the following definition of symbols is adopted in this study:

A	Cross sectional area
A_b	Cross sectional area of the bar
A_o	Surface area of pull-out cone
b_c	Core dimension measured center to center of the perimeter hoop
c	Depth of the neutral axis measured from the extreme concrete compression fibre
[C]	Damping matrix
C_c	Concrete cover measured from extreme tension fibre to the center of the bar
C_s	Smaller of; side cover measured to steel centroid, and one half the center to center bar spacing in the layer
d	Section depth measured to the main tension reinforcement
d_b	Diameter of reinforcing bar
d_e	Edge distance measured to the outside of the bar surface
E	Elastic modulus
E_c	Elastic modulus of concrete
EDF	Energy dissipation factor
E_s	Elastic modulus for steel
f_c	Concrete stress
f'_c	Cylinder strength of concrete
f_{cc}	Confined concrete strength
f'_{co}	Unconfined concrete strength
f_{cs}	Steel stress at the pushed end of an interior bar

$\{F_D\}$	Damping force vector
$[f]_{el}$	Elastic flexibility matrix
f_i	Spring flexibility at end i
$\{F_I\}$	Inertia force vector
f_j	Spring flexibility at end j
f_l	Lateral confining pressure
f_s	Steel stress
F_s	Steel force
$\{F_s\}$	Elastic force vector
$[f]_{tot}$	Total flexibility matrix
f_u	Ultimate steel stress
f_y	Yield steel stress
$f1_{i,j}$	Flexibility of anchorage slip spring at ends i and j
$f2_{i,j}$	Flexibility of shear spring at ends i and j
$f3_{i,j}$	Flexibility of flexural spring at ends i and j
G	Shear Modulus
H_l	Height of lugs
I	Moment of inertia
k	Unloading slope in the shear model
K	Strength enhancement factor for confined concrete; Confinement and bar spacing factor for bond stress
[K]	Stiffness matrix
k_e	Elastic stiffness
$[K_G]$	geometric stiffness matrix
$[K_m]$	Member stiffness matrix
k_p	Plastic stiffness
K_{se}	Elastic stiffness of the spring
K_{sp}	Plastic stiffness of the spring
K_{tr}	Confinement factor for calculation of bond stress
k_u	Unloading stiffness

k_y	Controlling slope in the shear model
L	Length of member
l_d	Development length of the bar
L_e	Elastic length of an embedded bar
LL	Lead-in length of the hook
L_{pc}	Depth of pull-out cone measured to the outside of vertical reinforcement
L_{p1}	Length of the yield plateau region of an embedded bar
L_{p2}	Length of the strain hardening region of an embedded bar
L_t	Total embedded length of the bar
[M]	Mass matrix
M	Bending moment
M_{cr}	Bending moment value at cracking
M_L	Linear moment
M_m, M'_m	Characteristic moment in the shear model
M_o	Characteristic moment value of the anchorage slip model
M_p, M'_p	Characteristic moment values in the shear model
M_{ub}	Unbalanced moment
M_y	Bending moment value at yield
n	Number of reinforcing bars
P_1, P_2, P_3	Characteristic force values of the hook force-deformation model
p	Perimeter of the bar
P	Hook force
r	Hardening ratio of the cantilever
s	Lateral spacing of ties
S	Reinforcement slip
s_l	Center to center spacing of longitudinal reinforcement
S_l	Spacing of lugs
S_1, S_2	Ratio of the post cracking and post yielding stiffness to the elastic stiffness in the shear model

T	Period of vibration
t	Time
u	Bond stress
u_{ACI}	bond stress based on ACI committee 408 empirical relationships
u_{cr}	critical bond stress for formation of a cone
u_e	Elastic bond stress
u_f	frictional bond stress
u_1, u_3	Characteristic bond stress values for the local bond slip model
$\{U\}$	Displacement vector
$\{U^{\cdot}\}$	Velocity vector
$\{U^{\cdot\cdot}\}$	Acceleration vector
$\{U^{\cdot\cdot}_g\}$	Ground acceleration vector
u, $u^{\cdot}$, $u^{\cdot\cdot}$	displacement, velocity and acceleration, respectively
X, Y	Center to center spacing between a group of bars in the two orthogonal directions
Δ	Increment of
δ, δ_h	Hook deformation
δ_c	Deformation at the pushed end of an interior bar
δ_{ext}	Total extension of reinforcement
Δf_{sh}	Increment of steel stress between the stress value at yield and its value at the beginning of strain hardening
δ_r	Recovered deformation
δ_t	Total deformation
δ_u	Unrecovered deformation
δ_1, δ_2, δ_3	Characteristic deformation values of the hook force-deformation model
ξ	Damping ratio as a percentage of critical damping
ε_c	Concrete strain
ε_s	Steel strain
ε_{sh}	Steel strain at the beginning of strain hardening
ε_u	Ultimate steel strain

ε_y	Yield strain
ε_1	Concrete strain corresponding to confined strength of concrete
ε_{50}	Concrete strain on the descending branch of stress-strain curve of confined concrete corresponding to 50% reduction in confined strength
ε_{85}	Concrete strain on the descending branch of stress-strain curve of confined concrete corresponding to 15% reduction in confined strength
ε_{01}	Concrete strain corresponding to unconfined strength of concrete
ε_{085}	Concrete strain on the descending branch of stress-strain curve of unconfined concrete corresponding to 15% reduction in unconfined strength
γ	Shear distortion
γ_e	Elastic shear distortion
γ_t	Total shear distortion
γ_y, γ_p, γ_m, γ_{cr}	Characteristic shear distortion values in the shear model
λ	A factor that depends on concrete type (λ = 1.0 for normal weight concrete)
μ	Ductility demand
μ_{fl}	Flexural ductility demand
μ_{sh}	Shear ductility demand
μ_{sl}	Slip ductility demand
ϕ	Curvature
θ_e	Elastic rotation
θ_{max}	maximum chord rotation
θ_p	Plastic rotation
θ_r	Recovered anchorage slip rotation
θ_t	Total anchorage slip rotation
θ_u	Unrecovered anchorage slip rotation

Chapter 1

Introduction

1.1 The Problem

During severe earthquakes, reinforced concrete moment-resisting frames are expected to deform into the inelastic range. Inelastic structural performance during an earthquake is governed by the ability of the structure to experience large inelastic deformations in critical regions without a significant loss of strength. Following current design philosophy of strong columns and weak beams, inelastic deformations in a moment resisting frame are usually concentrated in the girders, at beam-column joints. Because it is difficult to avoid inelasticity in the first story columns, hinging also occurs in the ground level columns, at the column-foundation interface. The energy input by the ground motion at the base of a structure is dissipated by hysteretic behavior of structural elements in these regions. Hysteretic loops of reinforced concrete elements in their critical regions are characterized by stiffness degradation during unloading and reloading.

In order to gain insight into the behavior of critical regions of reinforced concrete structures, a number of experimental studies have been undertaken in the last two decades. Tests were performed on full and half-scale reinforced concrete elements , as well as interior and exterior joints. In addition, a large number of anchorage tests were performed on straight and hooked bars. These tests have demonstrated the degrading nature of hysteretic loops of reinforced concrete elements. The tests have also pointed out that the majority of deformations in these regions are attributed to three important modes of behavior. These are; inelastic flexure, inelastic shear, and reinforcement extension and/or slippage in the adjoining member. The latter is referred to in literature as "anchorage slip". In addition to the experimental work, the subject of inelastic dynamic analysis of reinforced concrete structures has been advanced rapidly in recent years. The widespread use of digital computers coupled with development of sophisticated mathematical modelling made it possible for researchers to analyze large scale structures with little cost. The current trend in the advancement of high speed personal computers will make it possible for structural engineers to perform accurate dynamic analyses that are more reliable than the approximate code equations. The accuracy of such analyses, however, is dependant on the degree of accuracy achieved in modelling structural elements.

Modelling of reinforced concrete elements for dynamic inelastic analysis has received wide interest from many researchers in recent years. Member modelling techniques with various degrees of complexity have been proposed. In addition, a number of hysteretic models have been developed to describe the behavior of critical regions of structural members for dynamic analysis. However, most of these hysteretic models were representatives of flexural dominant response and gave little or no attention to other modes of deformation. Effect of inelastic shear and anchorage slip were either ignored, or crudely lumped together with flexural deformations. Dynamic analysis of reinforced concrete structures incorporating individual deformation components due to flexure, shear, and anchorage slip has not been carried out to date due to lack of hysteretic models simulating inelastic effects of shear and anchorage slip.

1.2 Previous Research

The review of previous research is conducted in three parts. Those related to dynamic inelastic analysis of structures are presented first. Mechanical member modelling techniques are presented next, followed by a review of available hysteretic models for flexure, shear, and anchorage slip.

1.2.1 Inelastic Dynamic Analysis of Structures

The subject of inelastic dynamic analysis of structures received interest from researchers in the past two decades. The ability of a large number of structures to withstand earthquake forces that exceed the code specified design loads, tempted many researchers to gain insight into the inelastic behavior of such structures. Early studies focused on the analysis of simple structures that behave in elasto-plastic or bilinear manner. Penzien [1] studied seismic behavior of a single-degree-of-freedom system having an elasto-plastic force-deformation characteristic. The main parameters investigated were the lateral strength and natural period of the system, and percentage of critical damping in the system. The study showed that inelasticity in the system was a source of damping that resulted in reduction of dynamic response. Berg [2] studied the behavior of symmetrical single bay multistory frames subjected to ground motion. The beams and columns were assumed to have elasto-plastic moment-rotation relationships. The author concluded that viscous damping and formation of plastic hinges during response provided energy dissipation, thus reducing the amplitude of response. Clough and Benuska [3] investigated inelastic behavior of three multistory frames when subjected to ground motion. Frames of ten, twenty, and thirty stories high and three bays wide were analyzed. The study focused on determining ductility requirements for such structures under severe earthquakes. All frame members were assumed to have a bilinear moment-rotation relationship. The study showed that the ductility requirements of the girders of such frames was in the order of 4 to 6. Columns were shown to remain elastic throughout the response, except in the upper stories. Period and height of the frames were shown not to have a significant effect on the amount and distribution of inelastic deformations. Goel and Berg [4] studied the behavior of three multistory single-bay steel frames. Ten, twenty five, and forty story frames were considered in the analysis. Three different idealizations for girder behavior, namely; elastic, elasto-plastic, and Ramberg-Osgood function were used in the study. The frames were subjected to three distinctly different ground motions. All columns were assumed to remain elastic throughout response. The study showed that inelasticity in the girders reduced response by 50%. It was also pointed out that the period of structure and characteristics of ground motion were the most important factors affecting structural response. The study also showed that the elasto-plastic idealization overestimated response when compared with the Ramberg-Osgood idealization. Suko and Adams [5] analyzed a ten-story-single-bay frame subjected to Taft earthquake. The frame members were assumed to follow a moment-rotation relationship that included the effects of secondary moments due to axial loads, and joint distortions. In deriving the moment-rotation relationship, the initial axial load and location of point of contraflexure were determined based on gravity loads. While these studies gave insight into inelastic response of structures, their generalization to reinforced concrete structures cannot be made because of the nature of the hysteretic models used.

Experimental observations from quasi-static and simulated earthquake tests conducted on reinforced concrete elements showed that stiffness degradation occurred in such elements. This led researchers to conclude that elasto-plastic and bilinear models, used widely for their simplicity, were not appropriate for reinforced concrete structures. The first study to include the effect of stiffness degradation in the analysis of reinforced concrete structures was reported by Clough [6]. The author conducted a parametric study on a single-degree-of-freedom system, subjected to ground excitation using three different hysteretic models, namely; elasto-plastic, bilinear, and degrading stiffness models. A total of 192 cases were investigated. Variables included in the analysis were the period of vibration, damping ratio, yield strength, and intensity and characteristics of ground motion. The study showed that the displacement time history response for the degrading stiffness model was quite different from those of elasto-plastic and bilinear models. It also showed that the displacement ductility demand for structures with short periods of vibration were significantly larger for the degrading stiffness model than that for the elasto-plastic and bilinear models. Displacement ductility demand for structures with high period of vibration, however, was not affected by stiffness degradation. This is probably due to the fact that structures with short period of vibration will undergo a large number of cycles during the response as compared to structures with long period of vibration. Therefore, the dissipated energy in structures with short period of vibration, and hence the ductility demand, will be affected by the type of hysteretic model used. Ductility demand was found to be directly proportional to the intensity of earthquake and inversely proportional to yield strength and period of the structure.

Takeda et al. [7], studied response of statically determinate reinforced concrete specimens subjected to quasi-static and simulated earthquake loading. Five specimens were included in the study. The specimens were cantilever columns with a mass attached at their tips. Two specimens were subjected to quasi-static type loading, one to harmonic base excitation, and the other two were subjected to a simulated earthquake excitation. The aim of the study was to compare measured and predicted responses of the specimens. The analytical predictions of response were determined using the step-by-step integration method with linear variation of acceleration within each step. A proposed degrading stiffness hysteretic model was used to represent the force-displacement relationship. The response of the specimens based on the proposed hysteretic model was shown to compare favourably with the measured response.

The investigation of the effect of stiffness degradation on the inelastic response of structures was extended by Chopra and Christopher to multistory buildings [8]. Two eight-story shear type buildings, with different periods of vibration, were analyzed under twenty simulated ground motions. Both the bilinear and degrading hysteretic models were considered in modelling story shear-story drift relationships. The study showed that stiffness degradation resulted in an increase in ductility demand for stiff buildings but had little effect on the ductility demand for flexible buildings.

Otani and Sozen [9, 10], analyzed a small-scale one-bay, three-story reinforced concrete frame. The aim of the study was to correlate the predicted response with that obtained from laboratory testing. Each frame member was modelled by two imaginary line elements, one linearly elastic and the other inelastic. Two rotational springs were added at the ends of the flexible line element to simulate the behavior of reinforcement extension within the joint. Rigid links were used at the two ends of each member simulating the portion of the member within the joint. The resulting equation of motion of the system was integrated numerically using the linear acceleration method. The study showed that the analytical predictions of the response compared favourably with the measured value for large amplitude oscillations. However, for low and medium amplitude oscillations the predicted results gave higher frequencies than those observed experimentally.

Takayanagi and Schnobrich [11] analyzed two models of ten-story coupled shear walls. Each coupling beam was modelled as a line element with one rotational spring at each end. The flexibility of the rotational springs included the effects of inelastic flexural and shear deformations within the member, and rotations due to anchorage slip at the ends of the member. Inelastic flexural stiffness was derived by considering the force deformation relationship of a cantilever representing one half the length of the coupling beam. The effect of inelastic shear was introduced by a factor equal to the ratio of elastic shear deformation to total deformation. Flexibility due to anchorage slip was determined based on assuming a constant bond along the development length of the bar. Rigid links were used to represent the portion of the beam inside the wall. Modified Takeda's model that reflected pinching and strength decay was used to represent the hysteresis of the springs. The coupling walls were modelled by dividing them into small segments and representing each segment with a spring. Modified Takeda's model that reflected the effect of axial load moment interaction was used for these springs. The study showed that analytical predictions of the coupled walls based on the proposed procedure agreed with the measured response. It also showed that inelastic actions in the coupling beams played a major role in the overall response of the coupled wall systems since they controlled axial loads in the walls which control the wall yield moment.

Anderson and Townsend [12] investigated the effect of hysteretic modelling on inelastic behavior of a ten-story single-bay reinforced concrete frame subjected to earthquake loading. Four hysteretic models were used in the study; the bilinear model, degrading bilinear model, degrading trilinear model, and degrading trilinear connection model. Each element of the frame was represented by two parallel line elements, one for elastic and the other for elasto-plastic response. In the case of degrading trilinear connection model, two hinges, with lengths equal to the depth of the member, were inserted between the ends of the line elements and the rigid joint links. This was done to simulate the effects of anchorage slip and shear deformation in the joint core. The rest of the member was assumed to follow the degrading trilinear model. The study showed that stiffness degradation of reinforced concrete elements had a pronounced effect on their inelastic response. The study also showed that out of the four hysteretic models considered in the study, the degrading trilinear connection model was the most appealing one. It resulted in inelastic deformations that were concentrated near the ends of the member, a phenomenon that complied with experimental observations.

Soleimani et al. [13], examined the behavior of two interior beam-column joints under quasi-static loading. The aim of the study was to correlate the measured and predicted responses of subassemblages. In the analytical program, each beam was divided into elastic and inelastic zones. Two nonlinear springs were added at the ends of the beams to simulate the effects of reinforcement extension and/or slip within the joint. The initial stiffness of the spring was chosen such that when fixed end rotations due to anchorage slip was included, the overall stiffness of the member was reduced by 33%. Clough's model with 2% strain hardening was used to complete the hysteresis. The extent of the spread of inelasticity into the member was determined from moment distribution along the member. A constant reduced effective stiffness was used in this region. Clough's hysteretic model was used to trace out the flexural flexibility in inelastic regions throughout the history of loading. The study showed that concentrated rotations at the beam-column interface, caused by anchorage slip, contributed significantly to the overall deformations of the joints. Up to 35% of the total lateral displacements of the subassemblages were attributed to anchorage slip.

Emori and Schnobrich [14] analyzed a model of ten-story three-bay reinforced concrete frame-wall system. The structure had been tested on the earthquake simulator at the University of Illinois, Urbana. The input base motion used in both the analytical and experimental programs was a modified version of the N-S component of El Centro 1940 earthquake. Each frame member was modelled as a line element with plastic deformations concentrated at springs, one at each end of the member. An alternative approach was also considered to model the frame elements by dividing predetermined plastic lengths at member ends into layers. This is known as the layer model. A multiple spring model was used for modelling the shear wall. Takeda's hysteretic model was used to trace inelastic deformations of both the beam plastic regions and shear wall multiple springs. The computed response based on the adopted mechanical models gave a good agreement when compared with the measured response. The authors concluded that the predictions of inelastic response of reinforced concrete structures based on concentrated spring model for frame members and multiple spring model for shear walls led to satisfactory results. If variable axial loads in columns were expected to alter the behavior of the structure, the authors recommended using the layered model since it accounted for axial load-moment interaction. In another study [15], the authors analyzed a wall-frame system that had been tested under quasi-static type of loading using the same modelling techniques. Good correlation was found between the analytical and experimental results.

Humar [16] Investigated the effect of stiffness degradation on inelastic response and ductility requirements of reinforced concrete frames with flexible beams. Each frame member was modelled as a flexible elastic line element with one spring at each end to account for inelastic deformations within the member. To isolate the effect of stiffness degradation, both the bilinear and stiffness degrading models were used in the analysis. Takeda's model was used to express the hysteretic behavior for the stiffness degrading case. Elastic analysis was also performed in an attempt to correlate inelastic response to the elastic one. Both single and multistory frames with a single bay were subjected to a modified El Centro 1940 N-S accelerogram. The study showed that stiffness degradation resulted in a higher ductility demand for the girders of single-story frames. A similar conclusion was obtained for the girders of multistory frames, especially in the upper stories. In correlating the elastic response to inelastic response, the study showed that the elastic force reduction factor was generally lower than the ductility demand, but in the same order of magnitude.

Banon et al. [17] analyzed 32 large scale reinforced concrete members and subassemblages under quasi-static type of loading. The specimens had been tested previously by different researchers. The aim of the study was to test the ability of a number of damage indicators in predicting the amount of damage sustained by the elements during testing. In modelling the members for dynamic analysis, inelastic deformations were lumped at the ends of each member in two concentrated springs. Two additional springs were added to model deformations due to inelastic shear and reinforcement slippage. The elastic portion of the member was divided into two parts joined together at the contraflexure point. This was done to account for differences in member rigidity in the positive and negative directions. Degrees of freedom at the joints connecting the two elastic elements were condensed out at the element level. The study showed that results of inelastic analysis based on one component model correlated well with the measured values. The study also showed that flexural damage ratio, defined as the ratio between the initial elastic flexural stiffness and the secant stiffness at maximum displacement, and the normalized dissipated energy were good indicators of damage in a reinforced concrete element.

Saatcioglu et al. [18] investigated response of a twenty-story coupled shear wall system. The aim of the study was to examine the effect of interaction between axial load and moment on the response of the system. Effects of variations in post yield, unloading, and reloading slopes of the force-deformation hysteresis, as well as strength decay, shear yielding, and pinching of hysteretic model were investigated. Coupling beams were modelled using one component models with elastic line elements having two springs one at each end for inelastic deformations. A modified one component model was used in modelling the shear walls. Each wall was modelled as a line element with two nonlinear springs whose properties changed with changing axial load. A modified version of Takeda's model was used to represent the force-deformation hysteresis. Strength degradation was introduced in the coupling beams via a user specified strength decay guideline. A second pair of springs was used to model inelastic shear deformations. A modified Takeda's model with a reduced reloading slope to simulate pinching was used for the shear springs. The study showed that changes in stiffness and strength of the wall due to axial load-moment interactions significantly affected maximum moments and shear forces of the individual walls. In addition, rotational ductilities of coupling beams were found to increase with rapid strength decay. Variation of post yielding, unloading, and reloading stiffnesses of the force - deformation relationship did not show any apparent effect on response of the system. It was also shown that inelastic response was insensitive to shear yielding and pinching of hysteretic loops. A similar study was conducted by Keshavarzian and Schnobrich [19]. The authors analyzed a 6-story and a 10-story coupled shear wall buildings subjected to alternating static loads as well as simulated ground motions in an effort to determine the axial load moment interaction effects. Each coupling beam was modelled as an elastic line element with one nonlinear spring at each end. Walls were represented as line elements with an inner elastic region and two plastic regions, one at each end. The lengths of the plastic regions varied during response. The stiffness of the plastic region was assumed to be constant throughout the region and was determined from an appropriate moment-curvature hysteretic model. The effect of varying axial load on the stiffness of both the elastic and inelastic portions of the line element were included by using axial load-moment interaction curves. The study showed that while the inclusion of axial load moment interaction affected the maximum forces and moments of individual walls significantly, its effect on the overall response of the system was negligible. Comparisons of the wave form of top level displacement, base overturning moment, and base shear, with and without the inclusion of axial load effect showed similar responses for the analyzed systems.

Saiidi [20] studied the response of a simple cantilever system using four different hysteretic models, namely; elasto plastic, bilinear, clough's model, and a proposed Q-hyst model. The performance of the four hysteretic models was tested by comparing their results with those obtained using Takeda's model. The study showed that results obtained using the elasto plastic and bilinear models did not agree with those obtained by using Takeda's model. Clough's model was shown to produce reasonable agreement, whereas excellent agreement was obtained from the Q-hyst model.

Al-Haddad and Wight [21], investigated the effect of relocating plastic hinges away from the column faces on seismic response of reinforced concrete moment resisting frames. Each girder was modelled as an elastic member with a pair of springs at the ends; i.e the one component model. The location of the springs were taken at one beam depth away from the column face. Modified Clough's hysteretic rules with stiffness degradation during unloading were applied to the springs. Columns, however, were assumed to consist of two parallel line elements consisting of an elastic, and an elasto-plastic element. Moment-axial load interaction was considered in the analysis. A total of three frames subjected to two different ground motions, namely; El Centro 1940 NS and Taft 1952 S21W were used in the investigation. The study showed that relocating plastic hinges one beam depth away from the joint did not affect strength and stiffness of frames with normal span to depth ratios. For beams with a short span to depth ratio (less than 7), the study showed that a higher ductility demand was anticipated at the relocated plastic hinges.

Filippou and Issa [22] studied the inelastic behavior of two reinforced concrete interior beam column subassemblages subjected to quasi-static type of loading. The specimens had been tested previously under alternating cyclic loading. The aim of the study was to test a newly developed member modelling technique. The technique was based on decomposing each element of the structure into a number of subelements, each of which represented a different mechanism which affected the behavior. In modelling the subassemblages, each beam was divided into three subelements; an elastic subelement, a spread plasticity subelement, and a joint subelement. The spread plasticity subelement represented flexural inelastic deformations near the ends of the member whereas the joint subelement modelled the concentrated rotations at the member joint interface due to anchorage slip. Effects of inelastic shear were not included in the analysis. Columns were assumed to remain elastic. The study showed that results based on the proposed modelling approach correlated well with experimental findings.

Paultre and Mitchell [23, 24] analyzed a series of six-story reinforced concrete buildings under several different earthquake records. The aim of the study was to assess the seismic design requirements of the 1984 Canadian concrete code [25]. Three of the buildings were designed for western Canada while the other three were designed for the eastern part of Canada. The design and details corresponding to three levels of ductility in the 1990 National Building Code of Canada [26] were considered. One building in each region was designed and detailed using an R value of 4.0, while the other two buildings were designed and detailed using R values of 2.0 and 1.5, respectively. The dynamic analysis was performed using a modified version of the computer program Drain-2D. Each frame girder was modelled using the one component model with an elastic line element and a pair of springs at the ends. Inelastic deformations due to flexure, shear, and anchorage slip were lumped together and assigned to the nonlinear springs at the ends of the member. A hysteretic model that recognizes pinching and strength degradation was used to describe the hysteretic relationship at hinging regions. Columns, however, were modelled using the non-degrading bi-linear model. A semi-rigid connection element was used to model joint deformations. The study showed that buildings designed with R values equal to 1.5 and 2.0 exhibit large shear distortion in the joint region resulting in high values of interstory drift. Structures designed with R values of 4.0 were shown to satisfy the condition of ductile behavior and exhibit little joint shear deformation.

1.2.2 Modelling Reinforced Concrete Members for Inelastic Dynamic Analysis

Modelling reinforced concrete elements for inelastic dynamic analysis is a complex problem that has been investigated by many researchers during the past two decades. Two major challenges were faced by researchers who attempted to tackle this problem. One was the fact that reinforced concrete members exhibited severe stiffness degradation in their critical regions. The other challenge was that, under severe load reversal, these regions of degrading stiffness spread away from the critical zones into the rest of the member. This means that for an accurate modelling of the member, one has to trace the spread of nonlinearity throughout the time history, a process that will add to the complexity of nonlinear dynamic analysis. Hence simplified modelling techniques have been adopted in the past for reinforced concrete elements. These modelling techniques consist of two parts; a mechanical member model, and hysteretic models to represent inelastic force-deformation relationships. Such models are simple enough to be used in nonlinear dynamic analysis programs and yet represent the main features of reinforced concrete response.

1.2.2.1 Reinforced Concrete Mechanical Member Models

Several techniques have been proposed in the past for modelling elements of structures for dynamic analysis. Clough et al. [27] proposed the two component model in which each member was divided into two imaginary parallel elements, as shown in Figure 1.1a. One of these was elasto-plastic representing yielding, and the other was linear elastic representing strain hardening. The nature of the model made it applicable only to elements that behaved in a bilinear manner, and could not be extended to elements of degrading stiffness, such as reinforced concrete elements. Extension of the two component model to multi-component model to represent cracking and different levels of yielding has been reported by Otani [28].

Another technique, called one component model, was proposed by Giberson [29]. The model, shown in Figure 1.1b, consists of an elastic line element and two nonlinear springs, one at each end of the member. All inelastic deformations are assumed to be lumped at the springs. In determining the characteristics of each spring, the inflection point is assumed to be located at the center of the member. Hence, deformations in each spring are dependant on the moment at that end of the member only. Although reinforced concrete members are expected to develop inelastic deformations away from their ends, and their points of inflection are not expected to remain stationary at the center, this model has been used widely for reinforced concrete elements due to it's simplicity and versatility. Results obtained from dynamic analysis of reinforced concrete elements and frames using the one component model showed good agreement with the measured response under simulated earthquake loadings [17]. Other researchers have suggested using the one component model in which the location of the inflection point is based on the initial conditions [5].

A more refined but tedious model was proposed by Otani and Sozen [9, 10]. The model, referred to as the two cantilever model, divides each element into an elastic line element and inelastic line element. The flexibility of the inelastic line element is obtained by dividing the line into two cantilevers, as shown in Figure 1.1c. The moment rotation relationship at the ends of the inelastic line element were derived as a function of the location of the contraflexure point. The slopes of the end moment - tip deflection and end moment - tip rotation relationships are determined by using a cantilever of unit length.

The moment rotation relationship, thus obtained, changes by the change in end moments and shifts rapidly when moments change sign, making the method impractical for general purpose inelastic dynamic analysis [9, 28].

Takayanagi and Schnobrich [11] proposed a multi-spring approach, shown in Figure 1.1d, for modelling walls in frame-wall systems. Each spring represents a short segment of the wall and handles both elastic and inelastic deformations. By knowing the moment distribution along the wall, the flexural flexibility of each spring can be evaluated from a prescribed moment - curvature hysteretic model. The flexibility of the entire wall is determined by combining the contributions of individual springs.

A distributed flexibility model was developed by Takizawa [30]. It is based on assuming a parabolic distribution of flexibility along the member, as shown in Figure 1.1e. The reduced flexibility at the ends of the member is determined from a specified trilinear moment-curvature hysteretic relationship. Elastic flexibility is assumed at the center of the member. By knowing the distribution of the flexibility along the member, the element flexibility matrix is determined through integration.

Soleimani et al. [13] presented a member model for reinforced concrete girders in which the spread of inelasticity is considered. The model, shown in Figure 1.1f, divides each member into three segments; an inner elastic zone, and two inelastic zones at the ends. A reduced effective rigidity is used at the inelastic zones and is assumed to be related to the curvature distribution. The length of the inelastic zones is variable, and depends on moment distribution along the member. Clough's hysteretic model is used to trace the moment-curvature relationship. The same approach was adopted by Keshavarzian and Schnobrich [19], and Roufaiel and Meyer [31].

Emori and Schnobrich [15] proposed an alternative to the one component model, called the layer model. Instead of lumping plastic deformations in concentrated springs at the ends of the member, the layered model accounts for spread of inelasticity by specifying pre-determined plastic lengths at each end of the member, as shown in Figure 1.1g. The plastic lengths are divided into small segments each of which is further divided into layers across the cross section. The moment curvature relationship of each segment is derived from constitutive laws of materials. Inelastic deformations at each end of the member are determined from the curvature distribution in the plastic region. The layered model accounts for axial load-moment interaction. Its practicality, however, is limited due to the excessive computational effort involved.

A super girder element model, shown in Figure 1.1h, was proposed by Filippou and Issa [22]. It is based on dividing each girder of the frame into a number of subelements each of which models a specific mechanism. Three subelements were presented, namely: the elastic subelement, spread plasticity subelement, and the joint subelement. The spread plasticity subelement consists of two plastic regions at the ends of the member connected by a rigid link. Two springs, one at each end, connected by a rigid link were used for the joint subelement. The joint subelement is used to represent the fixed end rotations resulting from anchorage slip within the joint at the ends of the member. The authors pointed out some of the limitations of the one component model, namely, the inaccuracy in determining the post yield stiffness of moment-rotation relationship, as compared to the super girder model.

1.2.2.2 Hysteretic models for Reinforced Concrete Elements

A. Hysteretic Models for Flexure

Hysteretic behavior of reinforced concrete in flexure was first simulated by elasto-plastic and bilinear models. However, experimental observations from quasi-static and simulated earthquake tests of reinforced concrete elements [7, 32, 33, 34, 35], indicated significant stiffness degradation in these elements. This led researchers to conclude that elasto-plastic and bilinear models, shown in Figures 1.2a and 1.2b, are not applicable to reinforced concrete elements, although used widely for their simplicity.

The first degrading stiffness model for reinforced concrete elements was proposed by

Clough [6]. This model is similar to the bilinear model except that reloading after a load reversal is aimed at the previous maximum point, a phenomenon that was observed in tests. Unloading from any point on the primary curve is parallel to the elastic branch of the curve. Reloading after small amplitude cycles is always directed towards the previous maximum. Clough's model is shown in Figure 1.2c.

A more detailed model, shown in Figure 1.2d, was proposed by Takeda et al. in 1970 [7]. It is based on experimental results of five reinforced concrete cantilever columns tested under static and simulated earthquake loading. The model consists of a trilinear primary curve with break points at cracking and yielding. The stiffness of the unloading branch from the primary curve reduces as a function of the maximum displacement reached in that direction. Reloading after a load reversal is aimed at the second previous maximum in the direction of loading. From thereon loading is directed towards the previous maximum. The merits of Takeda's model include treatment of small amplitude cycles, as well as stiffness degradation during unloading from the primary curve. Neither of these features are addressed in Clough's model.

Imbeault and Nielsen [36] also proposed a degrading stiffness model. Their model, shown in Figure 1.2e, is similar to the bilinear model except that unloading from the primary curve is not parallel to the elastic stiffness, but reduces as a function of the maximum displacement reached in the loading direction. Unloading prior to reaching the previous maximum (small amplitude cycles) takes place with the same slope as the unloading slope from the previous maximum.

Other researchers used variations of Takeda's model for dynamic analysis of reinforced concrete structures. Otani and Sozen [9] used a bilinear primary curve instead of trilinear, as shown in Figure 1.2f. Unloading from the primary curve was taken to be parallel to the initial elastic branch. Small amplitude cycles were treated as in Takeda's model. Powell [37] implemented Takeda's model with a bilinear primary curve into the computer program Drain-2D. A larger reloading stiffness than Takeda's was empirically specified as shown in Figure 1.2g. Takayanagi and Schnobrich [11] incorporated the effect of axial load on the primary curve of Takeda's model. The primary curve was shifted up based on the values of cracking and yield moments at a given level of axial load, as shown in Figure 1.2h. The authors also introduced pinching and strength decay in Takeda's model. In another study, Takayanagi et al. [38] introduced pinching and strength decay options in Powell's version of Takeda's model. The model was then incorporated into the computer program Drain-2D. A similar approach to that of Takayanagi and Schnobrich was adopted by Saatcioglu et al. [18]. Axial load effects were introduced in Powell's version of Takeda's model, as shown in Figure 1.2i. The model was then implemented in the computer program Drain-2D.

Riddell and Newmark [39] derived a new hysteretic model that is closely related to Clough's and Takeda's Models. The model eliminates some of the unrealistic features when treating small amplitude cycles, especially as they apply to Clough's model. Their model, shown in Figure 1.2j, consists of a bilinear primary curve with the break point at the yield moment. Reloading is always directed to the immediate previous maximum, thus preventing net negative energy during small amplitude cycles. Only a small improvement in the accuracy (6% as compared to Clough's model) was reported by the authors.

A simple model, know as the Q-Hyst model, was proposed by Saiidi [20]. It is based on a bilinear primary curve with a break point at the yield moment. Stiffness degradation during unloading from the primary curve is considered by specifying the slope of the unloading branch as a function of the displacement reached in that direction. Reloading is directed towards the maximum yield excursion reached in either direction. Saiidi's Model is shown in Figure 1.2k.

A degrading trilinear hysteretic model developed in Japan was reported by Otani [28]. The model, shown in Figure 1.2l, has a trilinear primary curve with break points at cracking and yielding. Prior to yielding, unloading and reloading follow the same branches as those of the bilinear model. Once the yield point is exceeded, the unloading point on the primary curve is treated as the new yield point. The behavior between the new positive and negative yield points is the same as that of the bilinear behavior with degrading stiffness.

Roufaiel and Meyer [31] proposed a hysteretic moment-curvature relationship for determining effective elastic rigidity of reinforced concrete members. The model, shown in Figure 1.2m, consists of a bilinear primary curve and a set of empirically derived rules. Unloading from the primary curve takes place with a reduced slope which is a function of the previous maximum displacement. The crack closing phenomenon was incorporated in the model by specifying a pinched bilinear reloading branch. The degree of pinching was expressed empirically as a function of the shear span ratio. Strength degradation was also expressed in the model.

B. Hysteretic Models for Shear

Hysteresis loops for shear force - shear deformation relationship of reinforced concrete elements are distinctly different than those for flexure. While flexural response results in stable hysteresis loops before reaching the onset of strength decay, shear response is characterized by pinched hysteresis loops resulting in smaller energy dissipation per loop. Stiffness degradation during unloading is more pronounced in shear response than that for flexure.

Hysteretic modelling of shear deformations of reinforced concrete elements has been lagging behind due to the lack of sufficient experimental data. Many researchers have either ignored its effect or included it by simple modification of existing flexural models to account for pinching phenomenon. Banon et al. [17] proposed a combined hysteretic model for shear and reinforcement slip. The model is based on a bilinear primary curve with unloading parallel to the elastic branch. Pinching of hysteresis loops are introduced by specifying a bilinear reloading curve with a break point at the zero moment axis as shown in Figure 1.3a. The slope of the first segment of the reloading branch is taken as 50% of the post yield slope. Strength decay is empirically introduced to the model. Other researchers modified existing flexural models to account for features of shear hysteretic response. Takayanagi and Schnobrich [11] introduced pinching and strength decay in

Takeda's model as shown in Figure 1.3b. Takayanagi et al. [38] modified Powell version of Takeda's model for the same effect. Their model is shown in Figure 1.3c. Roufaiel and Meyer [31] incorporated pinching and strength decay in a hysteretic moment-curvature relationship having rules similar to that of Takeda's and used for damage assessment of reinforced concrete frames.

Recently, a hysteretic model for shear force - shear deformation relationship was proposed by Ozcebe and Saatcioglu [40]. The model, shown in Figure 1.3d, is based on experimental data obtained from testing reinforced concrete columns under inelastic moment and shear reversals. The model consists of a primary curve and a set of empirically derived rules. The primary curve is derived using the Compression Field Theory [41] and includes the effect of interaction between flexure, shear, and axial load. Stiffness degradation during unloading is considered by specifying a bilinear unloading branch with slopes expressed as a function of the maximum displacement attained in a given direction. Pinching of the loops is introduced by specifying bilinear reloading branch. Strength decay is also incorporated in the model. To date, this model has not been incorporated in a nonlinear dynamic analysis program.

C. Hysteretic Models for Slip

The problem of reinforcement anchorage slip takes place within the adjoining members of reinforced concrete structures. It arises when cracks are formed at the interface of two elements. The steel crossing the crack is stressed within the adjoining member giving rise to extension and/or slippage of reinforcement that produces a wider crack and rigid body rotation at the end of the member. This results in stiffness reduction that is not accounted for in flexural and shear calculations.

Anchorage slip and the associated reduction in member stiffness has been researched in the past two decades. Experimental research was performed on full and half-scale cantilever beams and columns [34, 35, 42-44], as well as interior and exterior joints [13, 23, 35, 45-50]. In addition, a large number of pull-out tests were performed on straight and hooked bars [51-61]. The behavior of anchored bars has also been investigated numerically [62-68]. These studies have shown that member deformation attributed to anchorage slip may account for up to 50% of total deformations of the member.

Alarmed by the significance of slip contribution to total deformation, some researchers attempted to model this phenomenon for dynamic analysis. Otani and Sozen [9] assumed a constant bond stress along the development length of the bar as shown in Figure 1.4a. The total extension of the bar at the member joint interface was determined from the area of the triangular strain diagram. The concentrated rotation at the member end due to slip was determined by assuming the center of rotation to be located at the level of compression steel. The primary moment-slip rotation curve was idealized by two linear segments with the break point at a moment level equals to half the yield moment. Simplified Takeda's rules were then employed to complete the hysteresis. A similar approach was adopted by Takayanagi and Schnobrich [11] and Emori and Schnobrich [14, 15] when modelling frame-wall structure systems..

Soleimani et al. [13] adopted a hysteretic model for fixed end rotations resulting from anchorage slip. The model was used for analytical predictions of reinforced concrete joint response under quasi-static loading. It consists of a bilinear primary curve with a break point at yield moment. The elastic stiffness of the primary curve is taken as 33% of the elastic flexural stiffness. Strain hardening ratio is taken as that for the moment curvature relationship. Clough's hysteretic rules are employed to complete the hysteresis.

Banon et al. [17] proposed a hysteretic model for combined slip and shear effect . This model has been described previously under shear hysteretic models.

Filippou et al. [66, 67] presented a numerical model to describe the behavior of reinforced concrete beam-column joints. The method, shown in figure 1.4b, is based on dividing top and bottom layers of reinforcement into finite segments and satisfying equilibrium and compatibility at the ends of each segment as well as at the faces of the joint. The resulting nonlinear equations are solved iteratively by specifying the unknown boundary conditions at two opposite faces of the joint and marching along each reinforcement layer to solve for the unknown boundary conditions at the other face. The process continues until equilibrium and compatibility are satisfied at both faces of the joint. Later [22], the authors proposed a Clough-type hysteretic model for moment-slip rotation relationship in which pinching was introduced. The primary curve was determined using the above described numerical model and was idealized by two linear segments with a break point at the yield point, as shown in Figure 1.4c. Reloading in the strong direction is aimed at a moment value equal to the yield moment in the weak direction. This results in pinching of hysteresis loops. From thereon loading is directed towards the previous maximum.

Morita and Kaku [69] presented a hysteretic model for moment-slip rotation relationship for reinforced concrete joints. The model, shown in figure 1.4d, consists of a primary curve and a set of hysteretic rules which are based on experimental observations. In constructing the primary curve, the total deformation at the face of the joint is taken as the elongation of the reinforcing bar in the anchorage region. The bar elongation is computed as the area under the strain diagram. Prior to yielding, the strain distribution is determined by assuming a constant bond stress whose value is expressed empirically on the basis of the strain at the loaded end. After yielding, yield penetration is introduced empirically. For straight bars, the yield penetration is limited to the column width and the sum of the yield penetration length and the elastic length is limited to the column width plus one half the beam width. For hooked bars, however, the yield penetration length is limited to the lead-in length of the bar, and the sum of the yield length and the elastic length is limited to the lead-in length plus the curved portion of the hook. Once the total deformation at the loaded end is determined, slip rotation is calculated by assuming the center of rotation to be located at the compression steel. The primary curve is idealized by two linear segments with a break point at the yield. The slope of the post yield segment is determined by joining the yield point with the post yield point corresponding to the yield penetration limit. A set of empirically derived rules are then introduced to complete the hysteresis.

1.3 Conclusions from Previous Research

The following conclusions can be made from the review of previous research:

-Reinforced concrete structures may develop inelastic deformations during earthquakes. Inelasticity may be relied upon for dissipation of seismic induced energy, and may not necessarily be an undesirable behavior.

-Dynamic inelastic analysis of structures proves to be an effective tool to gain insight into seismic behavior of reinforced concrete structures. However, the reliability of the results depends, to a great extent, on the reliability of models used in the analysis.

-Tests of reinforced concrete components and subassemblages under cyclic loading indicate that there are three components of deformations generated during loading. These components include deformations due to flexure, shear and anchorage slip. Depending on the structural element under consideration, either one, two, or all three components can be very significant. Therefore, proper analysis of reinforced concrete structures should include hysteretic models for all three components.

-The state-of-the-art indicates that a number of reliable hysteretic models are available for flexure. Particularly, that proposed by Takeda et al. [7], and various other simplified versions of this model may be suitable for dynamic analysis of reinforced concrete structures.

-There is lack of hysteretic models for shear and anchorage slip. With the exception of one recent model for shear, which has not been used for dynamic analysis yet, and another model for anchorage slip, which is not suitable for response history analysis of multistory structures, no generalized model is available.

- More research is needed to study the effects of individual deformation components on dynamic inelastic response of reinforced concrete structures.

1.4 Objective and Scope

The objective of this study is to establish the significance of inelastic deformation components on the seismic response of moment-resisting reinforced concrete framed structures. Emphasis is placed on isolating and modelling different components of inelastic deformations. Of particular interest is the effect of inelastic shear and anchorage slip on overall behavior of structures as well as behavior in the critical regions. To achieve this objective, the following scope of research is adopted.

1. Review of the state-of-the-art in terms of modelling reinforced concrete structures for inelastic dynamic analysis. This part of the project focuses on defining a mechanical member model to be used in the dynamic analysis, as well as hysteretic models for flexural, shear, and anchorage slip deformations. The findings of this part of the project are summarized in this chapter.

2. Development of a hysteretic model for anchorage slip deformations. The model should reflect the basic features of behavior observed in experimental data, and should be simple enough to be incorporated in a nonlinear dynamic analysis program. As a first step in the development of the model, the primary force - deformation relationship of single straight and hooked bars, anchored in exterior and interior joints, needs to be determined. The force - deformation relationship obtained can then be extended to determine the primary moment - anchorage slip relationship. The complete hysteretic relationship can be obtained by defining a set of rules based on experimental observations.

3. Incorporating the anchorage slip hysteretic model, developed in this study, together with a recently developed shear model, into the computer program Drain-2D. This requires modification of the one component model used by the program by adding two pairs of springs, one at each end, to account for shear and anchorage slip deformations. In addition, two subroutines, one to trace out nonlinearity in the shear model and the other to trace out nonlinearity in the anchorage slip model, need to be added to the

program. The program also needs to be enhanced with ductility demand calculation.

4. Design of three reinforced concrete moment resisting frames based on the requirements of the 1990 NBC of Canada and CSA A23.3 - M84. The frames should be representative of those built in practice.

5. Using the enhanced computer program to perform inelastic dynamic analysis of the selected frames aimed at determining the effects of inelastic shear and anchorage slip on their response. In addition, the effects of anchorage slip and inelastic shear need to be examined in light of variations in structural and ground motion parameters. The parameters considered are; period of vibration of the structure, characteristics of ground motion, degree of damage sustained by the structure, as well as shear strength of structural members.

Chapter 2

Proposed Moment-Anchorage Slip Hysteretic Model

2.1 Introduction

Hysteretic models used for dynamic analysis of reinforced concrete structures consist of a primary curve, and a set of rules usually based on experimental observations to define the complete hysteretic behavior. The basic advantage of such approach is that the model obtained is simple enough to be incorporated in a nonlinear dynamic analysis, and yet retains the basic observed features of the behavior. The alternative is to use constitutive material models under cyclic loading and compute member behavior starting at the sectional level. This approach is prone to accumulation of errors due to the uncertainty in the cyclic stress-strain curve of concrete, and has not been successful in the past. This makes the former approach an attractive choice.

This chapter presents the analytical procedure used in developing a new hysteretic model for moment-anchorage slip rotation relationship. The procedure for constructing the primary force-deformation relationship for straight and hooked bars in concrete is presented first. This requires sectional analysis at the end of the member. Constitutive material models needed for this analysis are discussed in Section 2.3. This is followed by the extension of the procedure to determine monotonic moment-anchorage slip rotation curve at the member joint interface. The rules for defining the complete hysteretic model for moment-slip rotation relationship are then presented. Finally analytical predictions based on the proposed model are compared with published results of tests conducted on single bars as well as interior and exterior joints.

2.2 Assumptions Made in the Analysis

The following assumptions were made in developing the hysteretic moment-anchorage slip rotation model:

1. Bond stress in the yield region of the bar is limited to the frictional bond stress, whereas in the elastic region an average value based on the equation proposed by ACI Committee 408 is assumed.
2. For straight bars, bond stress in the elastic region will adjust itself based on the remaining elastic portion of the bar until such time that the average bond exceeds the peak bond on the local bond-slip model.
3. Pull-out failure for a straight embedded bar is assumed to take place when the average bond stress in the elastic portion of the bar exceeds the peak bond on the local bond-slip model.
4. For a hooked bar, the average bond stress in the elastic portion of the lead-in length is limited to the value proposed by ACI committee 408. The hook contributes to the resistance of the applied load only if the lead-in length is not sufficient for developing the load.
5. The pull-out cone (see Figure 2.4b) is assumed to form when the bond stress near the loaded end of the bar exceeds a critical level of bond stress or when yielding takes place. The critical bond stress for reinforcing bars is assumed to be the same as that established for bolts and welded headed studs.
6. The length of the pull out cone is approximated by the depth of the cover concrete in the joint measured to the out side of the longitudinal steel.
7. Yield penetration in the compression zone of reinforcing bars of interior joints is negligible.
8. Plain sections before bending remain plain after bending.
9. Stress-strain relationship for confined concrete developed on the basis of concentrically loaded specimens is applicable to members under strain gradient.

2.3 Material Modelling

2.3.1 Constitutive Model for Steel

Steel stress-strain relationships used in the analysis are shown in Figure 2.1. Two idealized shapes were considered in the preliminary analysis. In the first case, Figure 2.1a, a trilinear curve with a linear strain hardening portion was considered. In the second case, a parabolic curve was used to represent the strain hardening portion. The preliminary analysis showed that the shape of the steel stress-strain curve in the post yield region had a pronounced effect on the force deformation relationship of the bar. Hence, the shape shown in Figure 2.1b, which is a more accurate representation of the actual behavior, is used throughout this study. The curve is defined by the following expressions:

$$f_s=\begin{cases} E_s\epsilon_s & \text{for} \quad \epsilon_s\le\epsilon_y \\ f_y & \text{for} \quad \epsilon_y<\epsilon_s\le\epsilon_{sh} \\ f_y+(f_u-f_y)\left[2\dfrac{\epsilon_s-\epsilon_{sh}}{\epsilon_u-\epsilon_{sh}}-\left(\dfrac{\epsilon_s-\epsilon_{sh}}{\epsilon_u-\epsilon_{sh}}\right)^2\right] & \text{for} \quad \epsilon_{sh}<\epsilon_s\le\epsilon_u \end{cases} \tag{2.1}$$

in which; f_y and f_u are stresses at yield and ultimate; and, ε_y, ε_{sh}, ε_u, are strain values at yield, strain hardening, and ultimate, respectively.

2.3.2 Constitutive Model for Concrete

A reliable stress-strain model for confined concrete is needed to determine compression resistance of concrete. Several models have been proposed for stress-strain curve of confined concrete [70, 71]. These models are empirical in nature, and lack the generality.

Recently, a stress-strain model for concrete was proposed by Saatcioglu and Razvi [72]. The model, shown in Figure 2.2, utilizes the concept of equivalent uniform confining pressure generated by lateral steel and is applicable to square, rectangular, and circular cross sections. Lateral reinforcement arrangement consisting of spirals, hoops, cross ties, welded wire fabric, or a combination of these can be handled by the model. The following relationships define the different branches of the model:

$$f_c = f_{cc}\left[2\left(\frac{\epsilon_c}{\epsilon_1}\right) - \left(\frac{\epsilon_c}{\epsilon_1}\right)\right]^{\left(\frac{1}{1+2K}\right)} \tag{2.2}$$

$$f_{cc} = (1+K)f'_{co} \tag{2.3}$$

$$K = \frac{k_1 k_2 f_l}{f'_{co}} \tag{2.4}$$

$$k_1 = 6.7(f_{le})^{-0.17} \tag{2.5}$$

$$f_{le} = k_2 f_l \tag{2.6}$$

$$k_2 = 0.26\sqrt{\left(\frac{b_c}{s}\right)\times\left(\frac{b_c}{s_l}\right)\times\left(\frac{1}{f_l}\right)} \tag{2.7}$$

$$\epsilon_1=\epsilon_{01}[1+5K] \tag{2.8}$$

$$\epsilon_{85}=260\frac{f_l}{f_y}\epsilon_1+\epsilon_{085} \tag{2.9}$$

Where; b_c is the core dimension measured center to center of the perimeter hoop, s is the spacing of ties, s_l is the center to center spacing of longitudinal reinforcement, and f_y is the yield strength of lateral steel. All the stress terms are expressed in MPa. Other variables are defined in Figure 2.2. In lieu of experimental data, ε_{01} and ε_{085} can be taken as $2\frac{f_c'}{E_c}$ and 0.0038 respectively, where f_c' is the cylinder strength of concrete.

2.4 Primary Force-displacement Curve for a Single Deformed Bar Embedded in Concrete

Examination of previous results of pull-out tests and finite element analyses [55, 66, 68] show that, at the post yield range of loading, the bar can be divided into four regions. These include; the elastic region, yield plateau region, strain hardening region, and pull out cone regions as shown in Figure 2.3. Calculation of the length of each of these regions enables the prediction of strain profile along the embedded length. The total deformation of the bar at the loaded end consists of the extension and the rigid body movement of the bar. The rigid body movement is discussed later in the chapter under "reinforcement slip".

2.4.1 Reinforcement Extension

The extension of reinforcement can be evaluated as the area under the strain diagram. This requires evaluation of the length of each of the four regions of the bar described earlier as follows:

2.4.1.1 Elastic Region

This is the portion of the bar that is stressed below the yield stress. In order to determine the length of this region, a small segment of an embedded bar is considered. Figure 2.4a, shows a bar segment within the elastic range. From equilibrium of forces;

$$\Delta F_s = u \times p \times \Delta x \tag{2.10}$$

where;

u = bond stress

p = perimeter of the bar

Integration over the entire length gives;

$$F_s = \int_0^{L_e} u(x) \times p \times dx \tag{2.11}$$

or

$$f_s \times A_b = \pi \times d_b \int_0^{L_e} u(x) dx \tag{2.12}$$

where f_s is the bar stress at the loaded end, A_b and d_b are the area and the diameter of the bar cross section, respectively. Substitution of the terms for A_b yields;

$$f_s = \frac{4}{d_b}\int_0^{L_e} u(x)dx \tag{2.13}$$

Several studies have been devoted to investigate the subject of bond between steel and concrete [54, 55, 73, 74, 75]. These studies showed that bond stress between a reinforcing bar and surrounding concrete is a complex phenomenon that depends on; bar size, concrete strength, bar surface geometry, concrete cover, lateral confinement, as well as location of the bar within the specimens. Furthermore, the studies showed that bond distribution changes with applied force, and hence, can not be described by a unique function. In addition, the studies showed that bond stress values scatter considerably. Under the same laboratory conditions bond stress was found to scatter by ±15% [56]. Therefore, it has been the practice to use an average constant bond stress along the development length of an embedded bar. ACI committee 408 [76] has proposed an empirical relationship for bond stress to be used for determining the development length for straight anchorage. It was based on reviewing a wide range of pull out tests with different bar spacing, concrete cover, and lateral confinement. Their formulae are adopted in this study as follows:

$$u_e = u_{ACI} = \frac{f_y \, d_b}{4 \, l_d} \quad Mpa \tag{2.14}$$

Where;

$$l_d = \frac{457 A_b}{K\sqrt{f_c^{\prime}}} \times \frac{f_y}{414} \geq 305 \ mm. \tag{2.15}$$

$$K = \text{smaller of } (C_c + K_{tr}),\ (C_s + \sum K_{tr}/n),\ 3d_b \tag{2.16}$$

$$K_{tr} = \frac{A_{tr}\, f_y}{10.34\ s} \leq d_b \tag{2.17}$$

s = spacing of transverse steel.

C_c = concrete cover measured from the extreme tension fibre to the center of the bar.

C_s = smaller of; the side cover measured to steel centroid, and one half the center-to-center bar spacing in the layer.

n = number of bars in the layer.

A_{tr} = area of transverse steel crossing the plane of splitting adjacent to a single anchored bar.

It should be noted that for girder reinforcement running through interior and exterior joints, the value of C_c is very large and for most practical applications the value of K can be approximated by 3 d_b. Once the bond stress over the elastic region is known, the length of this region is determined from Equation 2.13 as follows:

$$l_e = \frac{f_s . d_b}{4\ u_e} \tag{2.18}$$

2.4.1.2 Yield Plateau Region

This region covers the portion of the bar over which stress exceeds the yield stress but not high enough to put the material into strain hardening range. In force controlled tests, this region can never be sustained since steel strain will jump to strain hardening on the outset of yield. However, when deformation controlled tests are employed, the steel strain in the plateau region can be sustained. Since the material has yielded in this region, large local deformations take place, crushing the concrete around the steel lugs. Hence the local bond in this region can be approximated by frictional bond stress. Pochanart and Harmon [61] have investigated the frictional bond stress and obtained the following empirical relationship between the frictional bond stress and the surface geometry of the bar:

$$u_f = (5.5 - 0.07(\frac{S_l}{H_l})) \times \sqrt{\frac{f_c'}{27.6}} \tag{2.19}$$

Their equation is adopted in this study to determine the length of the yield plateau region, which is usually very small.

$$L_{p1} = \frac{\Delta f_{sh}\ d_b}{4\ u_f} \tag{2.20}$$

where, Δf_{sh} is the increment of steel stress between the stress value at yield and its value at the beginning of strain hardening.

2.4.1.3 Strain Hardening Region

This is the region of the bar over which the bar is stressed into the strain hardening range. Since the bar segment in this region experiences large local deformations due to yielding, the bond stress in the strain hardening region is assumed to be equal to the frictional bond stress given in Equation 2.19. The length of the strain hardening region, L_{p2}, can be determined from equilibrium of forces:

$$L_{p2} = \frac{\Delta f_s \, d_b}{4 \, u_f} \tag{2.21}$$

Where; Δf_s is the increment of bar stress beyond its value at the beginning of strain hardening, and u_f is the frictional bond stress.

2.4.1.4 Pull-out Cone Region

The pull out cone forms when concrete near the pulled end of the bar pulls out in form of a cone as shown in Figure 2.4b. This usually takes place when the bar yields in tension. However, when the embedment length is not sufficiently long the bond stress near the loaded end exceeds a critical value of bond associated with pulling-out of the cone. The critical bond stress was determined experimentally by Shaik and Yi [77] for anchored bolts and welded studs. Their recommendation, which was also adopted by the Prestressed Concrete Institute [78], can be used to determine the critical bond stress for a single bar as follows:

$$u_{cr} = \frac{2.8\lambda\sqrt{f_c'}A_0}{\pi d_b L_{pc}} \frac{d_e}{L_{pc}} \tag{2.22}$$

$$\frac{d_e}{L_{pc}} \leq 1.0 \tag{2.23}$$

$$A_0 = \sqrt{2}\pi L_{pc}(d_b + L_{pc}) \tag{2.24}$$

where; d_e is the edge distance measured to the outside of the bar surface and L_{pc} is the depth of the pull-out cone measured to the outside of the vertical reinforcement.

For a group of bars, with center-to-center spacing not exceeding (L_{pc}+d_b), the critical bond stress can be derived by assuming a truncated pyramid failure surface as follows :

$$u_{cr} = \frac{4\lambda\sqrt{f_c'}(X+2L_{pc})\ (Y+2L_{pc})}{n\ (\pi\ d_b\ L_{pc})} \leq \frac{2.8\lambda\sqrt{f_c'}A_0}{(\pi\ d_b\ L_{pc})} \tag{2.25}$$

Where X and Y are the center to center spacing between the bars in the two orthogonal directions. If one or more bar(s) is located near an edge, Equation 2.25 is modified by reducing the area of the truncated pyramid according to the edge distances [77]. The pull-out cone has been observed experimentally during pull-out tests [55, 57]. However, published experimental work on large scale beam column connections [46], and column footing connections [44], did not indicate pulling-out of the cone. This is probably due to the fact that concrete in the potential cone region in these elements is usually heavily confined by reinforcement cage, thus preventing the formation of the cone. Therefore, in this study the pull-out cone was assumed to form in pull-out tests and was ignored in joints.

Once the length of each region is determined, the strain profile is approximated by linear segments and the total extension of reinforcement, δ_{ext}, can be computed as the area under the strain diagram. Therefore;

$$\delta_{ext}=\epsilon_s L_{pc}+\frac{1}{2}(\epsilon_s+\epsilon_{sh})L_{p1}+\frac{1}{2}(\epsilon_{sh}+\epsilon_y)L_{p2}+\frac{1}{2}(\epsilon_y)L_e \tag{2.26}$$

2.4.2 Reinforcement Slip

When an embedded bar is stressed beyond yield, yielding penetrates into the bar reducing the available elastic length to develop the bar force. If the remaining elastic length of the bar is less than the required development length based on the average elastic bond stress, the bar will be stressed to the end. As the bar lugs at the end of the bar crush the supporting concrete keys, a permanent deformation in the form of a rigid body movement of the bar takes place. This is often referred to as reinforcement slip, and is shown in Figure 2.5d. Reinforcement slip is dependant on bond at the end of the bar. The amount of slip can be determined from an appropriate local-bond slip model. The local bond slip model used in this study was first initiated by Ciampi et al. [64] and Eligehausen et al. [56]. It was based on pull out tests performed on bars with a small embedment length, i.e. 5 d_b and covered a wide range of parameters. The monotonic envelope of the model consisted of three branches as shown in Figure 2.6. Other researchers complemented the model. Soroushian and Choi [60] studied the effect of bar size on peak and frictional bond stresses and obtained a relationship between the peak bond stress and the diameter of the bar. Pochanart and Harmon [61] examined the effect of bar surface geometry and developed relationships between peak and frictional bond stresses and the surface geometry of the bar. Only one bar diameter (25mm) was used in the experimental program. In this study, the relationships proposed by Soroushian and Choi, and Pochanart and Harmon are used to define the peak and frictional bond stresses, respectively. The following relationships define the three branches of the monotonic envelope:

$$u=u_1\left(\frac{S}{S_1}\right)^{\alpha} \qquad for\ S \le S_1 \tag{2.27}$$

$$u=u_1 \qquad for\ S_1 < S \le S_2 \tag{2.28}$$

$$u=u_1-(u_1-u_3)\times\frac{S-S_2}{S_3-S_2} \qquad for\ S_2 < S \le S_3 \tag{2.29}$$

where;

$$S_1=\sqrt{\frac{30}{f_c^{/}}}\ \ mm \tag{2.30}$$

$$S_2=3.0\ mm \tag{2.31}$$

$$S_3=clear\ distance\ between\ the\ lugs \tag{2.32}$$

$$u_1=(20-\frac{d_b}{4})\times\sqrt{\frac{f_c^{/}}{30}}\ \ Mpa \tag{2.33}$$

$$u_3=(5.5-0.07(\frac{S_l}{H_l}))\times\sqrt{\frac{f_c^{\prime}}{27.6}}\quad Mpa \tag{2.34}$$

$$\alpha=0.4 \tag{2.35}$$

In the above equations, $f_c^{\prime}$ is the concrete compressive strength, d_b is the bar diameter, and S_l and H_l are the spacing and height of lugs, respectively. As the bond stress at the end of the bar increases, bar slip increases following the local bond-slip model. Once the peak bond is reached the bar pulls out as a whole, marking the anchorage failure. Slip of the bar can be determined from the local bond-slip model described in Equation 2.27.

$$S=S_1(\frac{u}{u_1})^{2.5} \tag{2.36}$$

The total deformation at the loaded end of the bar, δ_t, can now be determined by superimposing the elongation of the bar to the slip of the bar as a whole. Therefore;

$$\delta_t=\epsilon_s L_{pc}+\frac{1}{2}(\epsilon_s+\epsilon_{sh})L_{p1}+\frac{1}{2}(\epsilon_{sh}+\epsilon_y)L_{p2}+\frac{1}{2}(\epsilon_y)L_e+S_1(\frac{u}{u_1})^{2.5} \tag{2.37}$$

where;

ε_s = strain at the loaded end of the bar.

ε_y, ε_{sh} = strain values at the beginning of yield and strain hardening regions, respectively.

L_{pc} = depth of the pull-out cone measured to the outside of the vertical reinforcement.

L_{p1}, L_{p2} =plastic lengths given by Equation 2.20 and 2.21, respectively.

$L_e = L_t - L_{pc} - L_{p1} - L_{p2} \leq L_d$

L_d = development length based on the bond stress given by Equation 2.14

S_1 = slip value at the peak bond stress in the local bond-slip model (Equations 2.30)
u_1 = peak bond stress in the local bond-slip model (Equations 2.33)
u = bond stress at the end of the bar.

Equation 2.37 is used to determine the primary force-displacement for a straight deformed bar embedded in concrete.

2.4.3 Hooked Bars

Deformation of hooked reinforcement in concrete is a complex phenomenon. As bar force increases, concrete supporting the hook may crush, causing rotation of the hook. In addition, loss of bond around the perimeter of the hook may cause slippage of the bar as a whole. Several studies have been initiated in the past to examine the behavior of hooked anchorage [52, 53, 79]. In a recent study, Soroushian et al. [59] developed an empirical model for force-deformation relationship of a hook embedded in confined concrete. The model, shown in Figure 2.7, is similar to that for local bond-slip, and is governed by the following equations:

$$P=\begin{cases} P_1\left(\dfrac{\delta}{\delta_1}\right)^{\alpha} & for\ \delta\le\delta_1 \\ P_1 & for\ \delta_1<\delta\le\delta_2 \\ P_1+(P_3-P_1)\times\dfrac{\delta-\delta_2}{\delta_3-\delta_2} & for\ \delta_2<\delta\le\delta_3 \end{cases} \tag{2.38}$$

where;
P_1 = 271 (0.05 d_b -0.25) kN, d_b in mm
P_3 = 147 (0.05 d_b - 0.25) kN, d_b in mm
δ_1 = 2.54 mm
δ_2 = 7.62 mm

$\delta_3 = 38$ mm

$\alpha = 0.2$

In the analytical procedure considered here the resistance of a hooked bar is assumed to consist of two parts; resistance of the lead-in length, and the hook resistance. The lead-in length is treated as in the case of a straight bar. If the lead-in length is not sufficiently long to resist the applied load, the excess force is taken by the hook. Referring to Figure 2.8, the total deformation at the loaded end of the hooked bar can be expressed as follows:

$$\delta_t = \epsilon_s L_{pc} + \frac{1}{2}(\epsilon_s + \epsilon_{sh}) L_{p2} + \frac{1}{2}(\epsilon_y + \epsilon_{sh}) L_{p1} + \frac{1}{2}(\epsilon_y + \epsilon_h) L_e + \delta_h \tag{2.39}$$

where:

ε_h = steel strain at the beginning of the hook.

$L_e = LL - L_{pc} - L_{p1} - L_{p2} \leq L_d$

LL = lead-in length of the hook.

All other variables are defined previously for Equation 2.37. Equation 2.39 is used to calculate the primary force-deformation curve for bars with hooked anchorage.

2.5 Bars Subjected to Pull From one Side and Push from the Other

In reinforced concrete moment resisting frames, the combination of lateral loads and gravity loads gives rise to moments of the same sense across interior joints. Therefore, the beam bars that are running through the joint are subjected to pull from one end and push from the other. When the lateral load is reversed, a complete reversal of moments takes place at both ends of joints. This results in closing the cracks and opening of new cracks in what used to be the compression zone. If the previous load stage produced yielding of tension reinforcement, the cracks are not fully closed upon load reversal. This results in cracks that are open throughout the entire depth of the member. In practical situations where the ratio of top to bottom reinforcement of the girder is not unity, cracks at interior joints stay open throughout the entire history of loading [66]. Therefore, in order to model anchorage slip at interior joints, the behavior of straight bars subjected to pull from one end and push from the other needs to be examined. This case is treated in much the same way as that of pull only, except that the elastic portion of the bar is required to develop the force at the pulled and pushed ends simultaneously. Yield penetration on the compression side was neglected since experimental studies have shown that bond stress at the pushed end increases significantly at the outset of yielding [55]. Slip of the bar as a whole is determined from the local bond slip model of confined concrete as before. In situations where the elastic length of the bar is higher than that required to develop both tensile and compressive forces, slippage of the bar does not take place. Figure 2.9 shows stress and strain distribution for a bar subjected to push from one end and pull from the other, while also undergoing slippage.

2.6 Unloading from Primary Force-deformation Curve

Unloading results in recovery of elastic deformations, while leaving residual deformation. The residual deformations consist of unrecovered plastic deformation and slippage of the bar as a whole. The unrecovered deformation, δ_u, can easily be determined by considering the shaded area of the strain distribution shown in Figure 2.10:

$$\delta_u = L_{pc}(\epsilon_s - \epsilon_y) + \frac{1}{2}L_{p1}(\epsilon_s + \epsilon_{sh} - 2\epsilon_y) + \frac{1}{2}L_{p2}(\epsilon_{sh} - \epsilon_y) + S \qquad (2.40)$$

All the terms in the above equation have been defined previously. The recovered deformation, δ_r, is the difference between the total and residual deformations and is given below:

$$\delta_r = \epsilon_y (L_t - \frac{L_e}{2}) \tag{2.41}$$

By defining the amount of unrecovered deformation, the slope of the unloading branch at any particular load can be determined. This is done by joining the unloading point with the unrecovered deformation point on the zero load axis.

2.7 Primary Moment-Slip Rotation Curve for a Reinforced Concrete Joint

In reinforced concrete frames, the beam reinforcement is usually continuous through interior joints and hooked in exterior joints. Regardless of the joint type, cracks are usually formed at beam-joint interface. The reinforcement at the interface extends under increasing flexural stresses, giving rise to a wider crack, and a rigid body rotation of the member. The amount of rotation is governed by the extent of the bar elongation which in turn, is governed by the level of tensile force applied on the bar. Therefore, determination of bar forces and associated bending moment, and the center of rotation of the member, is necessary to establish the primary moment-slip rotation relationship.

In this study, the primary moment-slip rotation curve is constructed by performing analysis of the critical section at member end, near the joint. The tension steel force for a given moment is determined from internal equilibrium of forces and is assumed to be equally divided between the bars of the same layer. Once the force in the bar is determined, the total deformation, δ_t, at the pulled end of the bar is calculated as outlined in the previous section. In interior joints, the bar deformation at one side of the joint is affected by the action on the other side. This is because at an interior joint the bars are subjected to pull from one end and push from the other. The magnitude of the compressive force at the pushed end of the bars is dependant on the equilibrium of forces at that end, and is assumed in this study to be equal to the pull force. Therefore, In constructing the primary moment-slip rotation curve for interior joints, the bar is assumed to be subjected to a compressive force that is equal in magnitude to the pulling force. The magnitude of the compressive force in both the top and the bottom reinforcement is limited to the yield force of the bottom bars. This is due to the fact that at late stages of response, cracks will stay open throughout the entire depth of the joint leaving the applied moment to be resisted by the coupling force in steel. Since the tensile yield force in the bottom layer of steel is usually less than that of the top layer, the compressive force in the top layer will never exceed the yield force of the bottom layer. For the bottom bars, yield penetration at the compression end is neglected since previous experimental work has shown it to be negligible [55, 66]. The slip rotation is then calculated by assuming the center of rotation to be at the neutral axis location:

$$\theta_t = \frac{\delta_t}{d-c} \tag{2.42}$$

in which;

d= section depth measured to the main tension reinforcement.

c= depth to the neutral axis from the extreme concrete compression fibre.

Unloading from the primary moment-rotation curve takes place in the same manner as for the force deformation curve. An expression similar to that given in Equation 2.40 can be obtained for the unrecovered rotation as shown below:

$$\theta_u = \theta_t - \theta_r = \frac{L_{pc}(\epsilon_s - \epsilon_y) + \frac{1}{2}L_{p1}(\epsilon_s + \epsilon_{sh} - 2\epsilon_y) + \frac{1}{2}L_{p2}(\epsilon_{sh} - \epsilon_y) + S}{d-c} \tag{2.43}$$

The unloading branch at a particular moment can be determined by joining the unloading point to the unrecovered slip rotation on the rotation axis.

2.8 Effect of Axial Load on the Primary Moment-slip Rotation Curve

Ductile reinforced concrete frames are usually designed on the basis of weak girders and strong columns in order to limit the formation of plastic hinges to the girder ends. This is done to avoid failure of columns which are responsible for overall strength and stability of the structure. Despite this design philosophy, however, plastic hinges are expected to form in the ground floor columns when subjected to severe ground motion. Therefore, the problem of bar slip and the associated fixed end rotation is expected to take place at the interface between the ground floor column and the foundation. In recent experimental studies [44], fixed end rotation at the interface between reinforced concrete columns and their foundation was found to be accountable for up to 50% of the total deformation at the tip of the column.

The effect of axial load on the primary moment-slip rotation curve presents itself in two ways, as shown in Figure 2.11. First, the axial load is included in sectional analysis, changing the magnitude of moment at a given level of deformation. For axial loads smaller than the balance load, the primary moment-slip rotation curve shifts up on the moment axis as the level of axial load increases. The second effect of axial load occurs during unloading from the primary curve. Since the force in tension reinforcement of a beam column member reaches zero before the moment is entirely released, the recovery of permanent slip rotation occurs prior to complete unloading of the moment. Hence, the unloading branch is taken as the line connecting the point at which unloading takes place to a point having a coordinate of (θ_u, M_0), where M_0 is the level of moment at which the strain in tension steel changes sign.

2.9 Hysteretic Model for Moment-Slip Rotation Relationship

The hysteretic model consists of the primary moment-slip rotation relationship and a set of rules defining the slopes of the various load stages during unloading and reloading. Calculation of the primary curve is discussed in the previous sections. It requires analysis of the critical section under increasing loads. Although this can be done relatively easily, it may become tedious and unnecessary to compute many points on the curve, especially if this is to be done for each and every member of a multistory structure. Therefore, it is more convenient to idealize the primary curve with two line segments, as shown in Figure 2.12. The first segment connects the zero point with a point on the primary curve that corresponds to the yield point. The yield point, defined as the point with a significant change in the rate of deformation, takes place when reinforcement in the outermost layer enters into the strain hardening range (i.e. strain of ε_{sh}). This is because the yield plateau region of the embedded bar is very small, and the effect of yielding on the bar extension is not significant until strain hardening is encountered. The second segment of the idealized primary curve connects the yield point to a point on the curve corresponding to a confined concrete strain of ε_{50}. If the actual primary curve is availabel, then idealization of the primary curve can best be obtained by equating the areas under the actual and idealized curves as will be shown later in Chapter 5.

In order to determine the slope of the unloading branch, the unrecovered slip rotation at the point of unloading must be estimated. To do this, one can make use of the idealized primary moment-slip rotation relationship of the section. By knowing the state of unrecovered slip at an intermediary point on the curve, say ε_{50}, linear interpolation or extrapolation can be used to determine its value at other points.

Once the primary curve is obtained and the slope of the unloading branch is known, the complete hysteretic model can be determined by defining the rules for reloading and unloading. These rules are based on experimental observations [44, 46] and the results of previous analytical studies [66, 22], and are summarized below.

2.9.1 Flexural Members with Symmetrical Cross-Sections:

Reinforced concrete girders with equal top and bottom reinforcement tend to have stable hysteretic loops [66]. Pinching of hysteretic loops is usually associated with slippage of the bar and asymmetry of the cross section. Since slippage of the bar prior to the initiation of pull-out constitutes only a small fraction of the total deformation at the loaded end, pinching of the hysteretic loops of symmetrical cross sections is negligible. The following rules are proposed for members with symmetrical cross sections (see Figure 2.13):

1. Condition: Member has not been loaded in either direction, yield moment has not been exceeded in the loading direction.
   Loading : Loading follows a line with slope k_e. (Ex: OA, OH).
   Unloading: Unloading follows the line of loading.
2. Condition: Member has not been loaded in the other direction, yield moment has been exceeded in the loading direction.
   Loading: Loading follows a line with slope k_p. (Ex: AB).
   Unloading: Unloading follows a line with slope k_u. The slope of this line is determined by interpolation/extrapolation between the initial elastic slope and the unloading slope at a point on the primary curve. (Ex: BC, DE).
3. Condition: Unloading from the primary curve after yielding.
   Loading: loading due to load reversal follows the unloading slope, k_u, until the unloading point on the primary curve is reached. From thereon, loading follows the primary curve. (Ex: BC, DE, IJ).
   Unloading: Subsequent unloading follows the previous loading slope.
4. Condition: Unloading is complete, member has not been loaded in the other direction.
   Loading: Loading follows a line connecting the point of zero moment to the yield point in the other direction. (Ex: EFH).

Unloading: Unloading follows a line of slope k_e in that direction. (Ex: FG).

5. Condition: Yield moment is exceeded in the opposite direction, member is loaded beyond yielding in the loading direction.

   Loading: Loading follows a line of slope k_p as in the case of condition 2. (Ex: HI).

   Unloading: Unload with a slope of k_u as in the case of condition 2. (Ex: IJ).

6. Condition: One or more inelastic loading cycle(s) have been completed.

   Loading: Loading is directed towards the previously reached maximum on the primary curve in that direction. From thereon, loading follows the primary curve. (Ex: JKDK', LMI)

   Unloading: Unloading takes place with slope k_u from the previously reached maximum point in the same direction. (Ex: KL, MN)

7. Condition: One or more loading cycle(s) have been completed. Previous unloading took place before reaching the previous maximum in that direction.

   Loading: Loading takes place towards the second previous maximum. From thereon, loading is along a line connecting the second previous maximum to the previous maximum on the primary curve in that direction. (Ex: NK, STDK', QRM).

   Unloading: Unloading takes place with slope k_u from the previously reached maximum point in that direction. (Ex: PQ, RS).

2.9.2 Flexural Members with Asymmetrical Cross-Sections:

In reinforced concrete frames, girders are usually designed with top reinforcement area in excess of that at the bottom reinforcement. This results in asymmetric member capacity in the two directions. Hysteretic loops of such members are characterized by pinching of the loops during loading to the strong direction. Such phenomenon has been shown experimentally by Viwathanatepa et al. [46], and numerically by Filippou et al. [66]. Pinching of the loops is believed to be largely due to crack closing. During loading in the strong direction, crack closing will take place at approximately the capacity in the weak direction bringing concrete surfaces into contact. This results in a sharp increase in the reloading slope after the crack closure. Figure 2.14 outlines the proposed rules for members with asymmetric cross section. These rules are summarized below:

Conditions 1 to 3 are identical to those of symmetrical cross sections.

4. Condition: Unloading is complete, member has not been loaded in the other direction, reloading is to the weak direction.

   Loading: Loading is directed towards the yield point in the weak direction.

   Unloading: Unload with slope k_e in that direction.

5. Condition: Unloading is complete, member has not been loaded in the other direction, loading is to the strong direction.

   Loading: Loading is directed towards a point on the primary curve in the strong direction having a moment coordinate equals to the yield moment in the weak direction. From thereon, loading follows the elastic loading line. (Ex:EFHI).

   Unloading: Unload with slope k_e in the strong direction. (Ex: FG)

6. Condition: One or more loading cycle(s) is complete, loading is to the weak direction.

   Loading: Loading is directed to the previously reached maximum point on the primary curve in that direction. From thereon, loading follows the primary curve (Ex: KLL').

   Unloading: Unloading before reaching the prėvious maximum takes place with a slope equals to the unloading slope at that point. (Ex: LM).

7. Condition: One or more loading cycle(s) is complete, loading is to the strong direction.

   Loading: Loading is directed towards a point on the unloading branch at the previous maximum point having a moment coordinate equals to the capacity in the weak direction (Ex: MNT). From thereon loading is along the unloading branch. (Ex: TJ)

   Unloading: Unload with a slope k_u equals to the unloading slope at the previous maximum point. (Ex: NP).

8. Condition: One ore more loading cycle(s) is complete, previous unloading took place prior to reaching the previous maximum.

   Loading: loading is directed towards the second previous maximum. From thereon, loading follows the line connecting the second previous maximum to the absolute maximum. (Ex: PQ, RS).

   Unloading: Unload parallel to the unloading at the previously reached maximum point in that direction. (Ex: QR).

2.9.3 Flexural Members Subjected to Axial Load:

Columns of reinforced concrete frames subjected to ground motion are expected to undergo severe moment reversal while subjected to axial loads. The effect of axial load on section behavior is reflected on the capacity of the section as well as the closure of the crack and associated behavior of reinforcement crossing the crack. In axially compressed members subjected to bending moment, tension reinforcement is expected to unload before complete unloading of the bending moment. Therefore, recovery of the permanent slip deformation will start prior to the zero moment level. This is reflected in the moment-slip rotation hysteretic model as a change in slope during unloading. The change in slope takes place at a moment level M_0, where the strain in the outmost layer of steel is zero. Referring to Figure 2.15, the following is a summary of proposed hysteretic rules for members subjected combined moment and axial force:

1. Condition: The yield moment has not been exceeded in the loading direction, the member has not been loaded in the other direction.
   Loading: loading follows slope k_e. (Ex: OA, OM).
   Unloading: Unloading follows the line of loading.
2. Condition: The yield moment has been exceeded in the loading direction, and the member has not been loaded in the other direction.
   Loading: Loading takes place with slope k_p. (Ex: AB, MN)
   Unloading: Unload with slope k_u as defined previously (Ex: BC, FG)
3. Condition: Unloading from the primary curve after yielding, moment is greater than M_0 (in absolute terms).
   Loading: Loading takes place with slope k_u. (Ex: BC, FG, NP)
   Loading: Unload with slope k_u.
4. Condition: Unloading from the primary curve, moment is smaller than M_0 (in absolute terms), and the member has not been loaded in the other direction.

Loading: Loading is directed to the previous maximum. (Ex: DB).

Unloading: Unloading is directed to the yield moment in the other direction (GHI).

5. Condition: Unloading is complete, the member has not been loaded in the other direction.

   Loading: Loading is towards the yield point in the other direction, from thereon loading follows the primary curve. (Ex: HIMN).

   Unloading: Unload with a slope equal to the elastic slope in the same direction. (Ex: IJ).

6. Condition: One or more inelastic loading cycle(s) have taken place.

   Loading : Loading is directed towards the previous maximum point on the primary curve, from thereon loading follows the primary curve (Ex: QRFZ).

   Unloading: Unload with the same slopes of the unloading branches from the previous maximum point (Ex: RS, ST).

7. Condition: One or more inelastic loading cycle(s) have taken place, previous unloading took place prior to reaching the previous maximum.

   Loading: Loading is directed towards the second previous maximum (Ex: WX)

   Unloading: Unload with the same slopes of the unloading branches from the previous maximum in that direction.

2.10 Comparison with Experimental Work

The procedure outlined in this chapter has been checked against a wide range of experimental data obtained by different researchers. The experimental work used for comparisons include tests that were conducted on single straight and hooked bars as well as half and full scale reinforced concrete joints.

2.10.1 Single Bars

Ueda et al. [57] tested twenty two specimens which simulated conditions that exist at exterior beam column joints. The test specimens consisted of straight and hooked bars embedded in confined concrete, representing a portion of a column. Both monotonic as well as cyclic loadings were considered. Fig 2.16 shows the comparison between the analytical and experimental force deformation relationships of selected specimens. Specimen number starting with the letter S denotes straight embedment, whereas the letter B indicates 90 degrees hook anchorage. Numbers used in the specimen labels refer to the size of the bar and the rank of the specimen in the group, respectively. Specimen; S61, S64, S101, S107, B81, and B103 were tested under monotonic type loading whereas specimens; S62, S103, S105, B85, and B104 were subjected to cyclic loading. The monotonic experimental envelopes for those specimens tested under cyclic loading were depicted from the peaks of the given cycles.

Similar test specimen with double embedded bars had been used earlier by Marques and Jirsa [53] to study the behavior of 90 and 180 degree hooked bars. Fig 2.17 shows comparison of experimental and analytical stress-displacement relationships for four specimens with 90 degree hooks. All of these specimens were tested under monotonic loading.

Viwathanatepa et al. [55], reported a comprehensive experimental program aimed at examining bond between reinforcing bars and concrete. The test specimens were reinforced concrete blocks having a height of 46" and thickness of 10". The width of the blocks varied according to the size of the bar. A total of seventeen specimens were tested under monotonic pull only, monotonic pull and push, and cyclic pull and push. Fig 2.18 shows the comparisons between analytical and experimental stress-displacement monotonic envelopes for four specimens. Specimen #3 was subjected to pull from one side while the other three specimens were subjected to simultaneous pull from one side and push from the other.

The proposed analytical model was also checked against previous analytical models. Included in the comparison are the models proposed by Otani and Sozen [9] and Morita and Kaku [69]. Both of these models fall in the same category as the proposed model since they are based on strain distribution along the bar. Analytical predictions based on numerical procedures reported by Ciampi et al. [65] and Ueda et al. [57] are also included in the comparisons. Figure 2.19 shows these comparisons for a selected number of specimens.

2.10.2 Large Scale Joints

Viwathanatepa et al. [46] reported the results of tests conducted on two half scale reinforced concrete interior beam-column joints. The cruciform shaped joint was pinned at the ends of the beams and at the top of the column. A 470 kip axial load was applied to the column via hydraulic jack. Gravity loads were simulated by lowering the two ends of the beams prior to testing. Lateral loading was applied at the lower end of the column. The two specimens were identical but were subjected to different loading histories. Specimen BC3 was subjected to a number of cycles with increasing magnitudes while specimen BC4 was subjected to one cycle of large amplitude. Figs 2.20 and 2.21 compare the measured hysteretic loops with those predicted using the proposed model for both specimens.

Saatcioglu and Ozcebe [44] tested seven full scale reinforced concrete columns under uniaxial and biaxial loading reversals. The columns were 1000 mm high and 350 mm by 350 mm in cross section. A constant axial load of 600 kN was maintained throughout the test. Lateral loading was applied at the tip of the cantilever via hydraulic jack. The experimental program included measurements of the slip rotation at the face of the footing for five of the specimens. Three of these specimens, namely; specimens U4, U6, and U7 were tested under unidirectional loading. Specimens B1 and B2 were tested under bidirectional loading. These were subjected to major inelastic deformations in the north-south direction while deformation in the east-west direction were limited to half of those in the north-south direction. Figure 2.22 shows the comparison between the experimental and the analytical primary moment-slip rotation curves. The complete analytical hysteretic curves for bidirectionally loaded specimens to be compared with those obtained experimentally are shown in Figure. 2.23. A cycle by cycle comparison for the three specimens tested under unidirectional loading is presented in Figure. 2.24.

The comparisons presented in Figures 2.16 to 2.19 for single bars indicate very good agreement between experimental results and predictions based on the proposed model. The analytical predictions based on Otani's model are shown to underestimate the inelastic deformation. While the analytical model proposed by Morita and Kaku shows good agreement with experimental data, it does not predict the pull-out capacity of the bar. The comparisons also show that predictions based on the proposed model are as good as the predictions of the numerical procedures with far less computational effort.

Predictions of the moment-slip rotation hysteresis based on the proposed model indicate good agreement with the measured values shown in Figures 2.20 to 2.24, with the exception of the east-west direction of the specimens subjected to bidirectional loading. This is due to the fact that those specimens were subjected to major inelastic deformations in the north-south direction which significantly affected the capacity in the east-west direction. Hence, when applied to bidirectional loading, the model is capable of predicting moment-slip rotation relationship in one direction provided that deformations in the orthogonal direction remain near elastic.

Chapter 3

Analytical Procedure

3.1 Introduction

The subject of dynamic analysis of structures is well documented in several textbooks [80, 81]. The state-of-the-art is capable of determining the response of any structural configuration to any type of loading provided that the structure can be modelled properly. Starting from the basic dynamic equilibrium, the equation of motion that governs the response of any particular system can be formulated with ease. Once the equation of motion is known, the response of the structure can be determined using any one of a number of solution methods available. In general, there are two main techniques for obtaining the response of a multi-degree-of-freedom system; namely, the method of mode superposition, and direct integration of the equations of motion. The former requires uncoupling the equation of motion by transforming them into a set of coordinates called the normal coordinates. Once the equations of motion are uncoupled, the solution of each equation is obtained either using approximate numerical integration techniques or in a closed form, depending on the complexity of the loading function. The solution of the system of equations is then expressed as the superposition of the solutions obtained for the individual normal coordinates. Since this method is based on the method of superposition, it can only be applied to linear systems in which the system parameters, namely; its mass, stiffness, and damping remain unchanged with time. In most practical dynamic systems, however, some of the system parameters, if not all, vary with time resulting in a nonlinear system of equations. The solutions of these equations can be obtained using the second technique, namely, the direct integration method. In this method, the equations of motion are solved directly using any of a number of approximate numerical integration techniques.

In reinforced concrete frame structures subjected to ground excitation, the basics for formulating the equation of motion of the system are no different than those for any system. Both the stiffness and mass matrices can be determined relative to a fixed reference coordinate system. Several simplifications, however, are needed in order for the solution to be practical. These simplifications are usually applied to the distribution of the mass of the structure and the modelling of individual members. The nonlinearity in the equation of motion for such structures is primarily due to the change in the structural stiffness while the mass of the structure stays constant.

This chapter reviews the analytical procedure used for obtaining inelastic response of framed reinforced concrete structures. The equation of motion of the system is presented first. This is followed by the description of the formulation of the structural mass, stiffness, and damping matrices. Particular emphasis is placed on the formulation of element flexibility matrix based on the one component model, which is modified to include inelastic shear and slip deformations. In addition, details of hysteretic models for flexure, shear, and anchorage slip, that are used in the study, are presented. Finally, the method of solution used for solving the system of nonlinear equation of motion is discussed.

3.2 Nonlinear Equation of Motion for a Multi-Degree-of-Freedom System

Consider a discrete multi-degrees-of-freedom system, shown in Figure 3.1, subjected to ground excitation. The equation of motion of this system at a given point in time is given by [80]:

$$[M]\{\ddot{U}\}+[C]\{\dot{U}\}+[K]\{U\} = -[M]\{\ddot{U}_g\} \tag{3.1}$$

in which; $\{U\}$, $\{\dot{U}\}$, $\{\ddot{U}\}$ are vectors for displacement, velocity, and acceleration along the structure degrees of freedom and relative to the ground. [M], [C], and [K], are the instantaneous mass, damping, and stiffness matrices, respectively. Once the values of the system parameters, namely; stiffness, mass, and damping matrices are defined, the equation of motion of the system is completely defined. In the following subsections, a systematic evaluation of the system parameters is outlined as applied to moment-resisting reinforced concrete frames.

3.2.1 Stiffness Matrix, [K]

The first step in evaluating the global stiffness matrix is the evaluation of stiffness matrix for individual elements of the structure. This can be accomplished by determining the element flexibility matrix in local coordinates and then inverting it to obtain the stiffness matrix. The member stiffness matrix thus obtained can then be transformed into element global coordinates using an appropriate transformation matrix. Once the element stiffness matrix is determined in global element coordinates, the stiffness matrix of the structure can be assembled from individual element stiffness matrices by matching the element degrees of freedom to the global degrees of freedom of the structure. The stiffness matrix of each element is added to the global stiffness matrix based on the correspondence between the element and global degrees of freedom. This method of constructing the structure stiffness matrix is usually referred to as the "direct stiffness method".

3.2.1.1 Element Flexibility Matrix

In order to determine the flexibility matrix of each element, a suitable mechanical element model is needed. Several techniques for modelling elements of framed structures for inelastic dynamic analysis have been proposed in the past. A review of these models can be found in Chapter 1. The one component model proposed by Giberson [29], is an attractive choice due to its simplicity and versatility and has been widely used for modelling reinforced concrete frame elements. Results obtained from dynamic analysis of reinforced concrete elements and frames using the one component model showed good agreement with the measured response under simulated earthquake loadings [12, 28]. A detailed presentation of the one component model in its original form is presented below. This is followed by the modification of the model to include inelastic shear and slip deformations.

A. <u>The One Component Model</u>

In its original form the one component model assumes that all inelastic deformations are concentrated at the ends of each member. Hence, each member is represented by an elastic line element, with two nonlinear springs, one at each end of the member. All inelastic deformations are assumed to be lumped at the springs. Referring to Figure 3.2, the total flexibility of the element corresponding to the outer rotational degrees of freedom can be expressed as the sum of the elastic and inelastic flexibilities as follows:

$$[f]_{tot} = \begin{bmatrix} f_{ii} & f_{ij} \\ f_{ji} & f_{jj} \end{bmatrix}_{el} + \begin{bmatrix} f_{ii} & f_{ij} \\ f_{ji} & f_{jj} \end{bmatrix}_{in} \tag{3.2}$$

Using the unit dummy load theorem and considering elastic shear deformations, the elastic flexibility matrix can be expressed as follows (see Figure 3.3)

$$[f]_{el} = \begin{bmatrix} \dfrac{L}{3EI} + \dfrac{1}{GAL} & -\dfrac{L}{6EI} + \dfrac{1}{GAL} \\ -\dfrac{L}{6EI} + \dfrac{1}{GAL} & \dfrac{L}{3EI} + \dfrac{1}{GAL} \end{bmatrix} \tag{3.3}$$

In the one component model, it is assumed that the inflection point of the member is located at the center for the purpose of determining inelastic flexibility matrix. Hence each member can be idealized as two cantilevers, as shown in Figure 3.4. This, however, implies that moment at one side of the member has no effect on the rotation of the spring at the other end, a drawback to otherwise an attractive model. Therefore, the off diagonal elements in the inelastic flexibility matrix in Equation 3.2 vanish, resulting in a diagonal matrix.

The flexibility of each spring can be determined by considering the force-deformation relationship of a cantilever with a length equal to half the member length. Initially the stiffness of the spring is set to a very large value. The post yield stiffness of the spring is determined by considering the elastic and inelastic components of the total post yield deflection of the tip of the cantilever. Details of determining the post yield stiffness of the springs are presented later in Chapter 4.

In order to determine the spring flexibility at any point of time during response, each spring is assigned a hysteretic moment-rotation relationship. The flexibility of the spring is determined based on the governing rules of the hysteretic model. By knowing the flexibility of the springs, total member flexibility at any time can be expressed as follows:

$$[f]_{tot} = \begin{bmatrix} \frac{L}{3EI}+\frac{1}{GAL}+f_i & -\frac{L}{6EI}+\frac{1}{GAL} \\ -\frac{L}{6EI}+\frac{1}{GAL} & \frac{L}{3EI}+\frac{1}{GAL}+f_j \end{bmatrix} \tag{3.4}$$

in which f_i and f_j are the current spring flexibility at end i and j, respectively.

B. Modification of The One Component Model to Include Inelastic Shear and Slip Deformations

In the original one component model inelastic deformations are lumped in two springs at the ends of the member. Since only one hysteretic moment-rotation relationship can be assigned to each spring, the model is capable of handling only one hysteretic model of deformation, usually flexure, or flexural deformation lumped with other deformations in one hysteretic model. Since this study focuses on modelling flexure, shear, and slip deformations separately, a modified version of the model is needed. This is accomplished by adding two pairs of springs, one pair at each end, as shown in Figure 3.5. One spring at each end is assigned the hysteretic relationship for shear, while the second spring is assigned the hysteretic relationship for anchorage slip. With the flexibility of each spring known at a given time step, the total flexibility of the member in the outer rotational degrees of freedom is given by:

$$[f]_{tot}=\begin{bmatrix} \dfrac{L}{3EI}+\dfrac{1}{GAL}+f1_i+f2_i+f3_i & -\dfrac{L}{6EI}+\dfrac{1}{GAL} \\ -\dfrac{L}{6EI}+\dfrac{1}{GAL} & \dfrac{L}{3EI}+\dfrac{1}{GAL}+f1_j+f2_j+f3_j \end{bmatrix} \tag{3.5}$$

In which; f1, f2, and f3 are the current flexibilities of anchorage slip, shear, and flexural springs; respectively, and are determined from the applicable hysteretic models.

The post and pre-yielding stiffness of each of the three springs needs to be determined prior to performing any analysis. This is done as part of the bookkeeping process of nonlinear analysis program, and will be discussed in detail in Chapter 4. The hysteretic rules for each model can then be used to determine the flexibility of each spring at a particular stage of response. These rules are described below.

C. Hysteretic Model for Flexure

Several hysteretic models for flexural response of reinforced concrete elements have been proposed in the last two decades. Chapter 1 contains a review of all available hysteretic flexural models. The model proposed by Takeda et al. [7] has been widely used by previous researchers, and is adopted in this research program as well. Only the general characteristics of this model are outlined here. Details of the hysteretic rules of the model can be found elsewhere [7, 9].

The original model consists of a trilinear primary curve with the break points at cracking and yielding points, as shown in Figure 3.6. The stiffness of the unloading branch from the primary curve is a function of the maximum displacement reached in either direction. Reloading after load reversal is aimed at the second previous maximum. From thereon loading is directed to the previous maximum. In this study, a bi-linear primary curve was adopted in the original Takeda's model. The stiffness of the unloading branch from the primary curve was expressed as a function of the elastic stiffness and the maximum displacement reached in either direction. The modified version of the model is shown in Figure 3.7.

D. Hysteretic Model for Shear

As outlined in Chapter 1, modelling hysteretic behavior of shear response has been lagging behind due to lack of experimental data. A hysteretic model for shear was proposed only recently by Ozcebe and Saatcioglu [40]. It is based on an experimental program carried out on full scale reinforced concrete columns tested under uniaxial and biaxial load reversals. The model consists of a primary curve and a set of rules that were derived from the experimental data. The primary curve can be determined by any acceptable procedure. The authors have used the Compression Field Theory [41] in their applications to establish the primary curves. Following are detailed hysteretic rules for the model as implemented in this study. Each condition number given below is also shown on the respective branch of the model in Figure 3.8.

1. Condition: Cracking load has not been exceeded in either direction, loading is in the positive direction

   Loading: Loading is along the line connecting the origin to the positive cracking point.

   Unloading: Unloading takes place along the loading path.

2. Condition: Cracking load has not been exceeded in either direction, loading is in the negative direction.

   Loading: Loading is along the line connecting the origin to the negative cracking point.

   Unloading: Unloading takes place along the loading path.

3. Condition: Loading is on the primary curve between the cracking and yielding points.

   Loading: loading takes place along the line connecting the cracking and the yield points.

   Unloading: unloading follows a line connecting the unloading point to the cracking point in the opposite direction.

4. Condition: Unloading after 3.

   loading: Loading follows a line joining the point of unloading to the cracking point in the opposite direction.

   Unloading: Unloading follows the loading path.

5. Condition: Loading on the primary curve after yielding.

   Loading: Loading follows the line connecting the yield point to the ultimate point.

   Unloading: Unload with a slope k given by :

$$k = k_y\left(1 - 0.05\frac{\gamma}{\gamma_y}\right) \tag{3.6}$$

where;

k_y = the slope of the line connecting the yield point in the quadrant where loading is reversed to the cracking point in the opposite direction.

γ = shear distortion at which unloading takes place.

γ_y = shear distortion at the yield point in the quadrant where loading is reversed.

6. Condition: Unloading after rule 5, moment is greater than the cracking moment.
   Loading: Loading takes place with a slope k given in rule 5.
   Unloading: Unload with a slope k given in rule 5.

7. Condition: Unloading after rule 5, moment is smaller than M_{cr}.
   Loading: Loading is directed to the previous peak.
   Unloading: Unload with a slope k given by:

$$k = 0.6\ k_y\left(1 - 0.07\frac{\gamma}{\gamma_y}\right) \tag{3.7}$$

in which γ and γ_y are as previously defined for Equation (3.6).

8. Condition: Reloading after rule 7.
   Loading: Loading takes place along the line connecting the point at which loading is reversed to the previous peak.
   Unloading: Unloading follows the loading path.

9. Condition: One or more loading cycle(s) have taken place, moment is zero.

Loading: If the cracking moment has not been exceeded in the direction of loading, then loading takes place along the line connecting zero load point to the cracking point. Otherwise loading is directed towards a point having the coordinates (M'_p, γ_p), where:

$$M'_p = M_p e^{\alpha(\frac{\gamma_p}{\gamma_y})} \tag{3.8}$$

in which:

M_p = moment at the previous peak.

$\alpha = 0.82(\frac{N}{N_0}) - 0.14 \qquad \leq 0.0$

γ_p = shear distortion at the previous peak.

γ_y = shear distortion at the yield point in the direction of loading.

N = applied axial load.

N_0 = nominal concentric axial load capacity.

$N_0 = 0.85\ f'_c\ (A_g - A_s) + A_s f_y$

Unloading : Unload with a slope k given in rule 7, but not less than the minimum unloading slope.

10. Condition: Unloading after rule 9.

Loading: Loading takes place with a slope k specified in rule 7.

Unloading: Unload on the same path of loading with a slope k.

11. Condition: One or more loading cycle(s) have occurred beyond yielding, reloading has exceeded the cracking moment.

Loading: loading follows a line connecting the point of intersection of the reloading branch below the cracking moment with a horizontal line drawn at the cracking moment, and a point having a coordinate (M'_m, γ_m) where;

$$M'_m = M_m e^{\beta n + \eta \frac{\gamma_m}{\gamma_y}} \tag{3.9}$$

in which;

$$\beta = -0.014\sqrt{\frac{\gamma_m}{\gamma_y}} \tag{3.10}$$

$$\eta = -0.01\sqrt{n} \tag{3.11}$$

M_m = moment on the primary curve corresponding to the maximum shear distortion reached in that direction.

γ_m = maximum shear distortion in the direction of loading.

n = successive number of cycles at the current maximum shear distortion in the direction of loading. The value of n increases by 1 every time the load is reversed within the range of $\gamma_m \pm \gamma_{cr}$.

γ_{cr} = shear distortion at the cracking moment.

Unloading: Unloading taHxs place with the slope k given in rule 5, but not less than the minimum unloading slope.

12. Condition: Unloading after rule 11. Load is greater than M_{cr}.
Loading: Loading takes place with a slope k as in rule 5.
Unloading: Unloading follows the loading path.

13. Condition: Unloading after rule 11, moment is below M_{cr}.
Loading: Loading is directed towards the previous peak.
Unloading: Unload with a slope k given in rule 7, but not less than the minimum

unloading slope.

14. Condition: Reloading after rule 13 before the zero moment is reached.
    Loading: Loading takes place along the line connecting the point at which loading is reversed to the previous peak.
    Unloading: Unloading follows the loading path.

E. Hysteretic Model for Slip

The slip hysteretic model used in this study has been presented in detail in Chapter 2. It consists of a primary curve and a set of hysteretic rules. The primary curve is determined by performing sectional analysis at the critical region of the member. This regions is located at the member-joint interface for beams and at the column-foundation interface for columns. Implicit in this procedure is the famous Bernoulli principle of plain section before bending remains plain after bending. Once the internal forces of the cross section are determined, the deformation of the tensile reinforcement is calculated by superimposing reinforcement extension and slip. The reinforcement extension is calculated by assuming a constant average bond over the elastic region and frictional bond over the plastic region. If the reinforcement is stressed to the end, then the slippage of the bar as a whole takes place. The amount of slip is calculated from a previously derived local bond - slip model and the bond at the end of the bar. The chord rotation due to reinforcement slip is determined by dividing the deformatHxn of tensile reinforcement by the distance between the reinforcement and the neutral axis. Once the primary curve is determined, the complete hysteresis is obtained by employing a set of rules which are based on previous experimental and numerical work. Hysteretic rules for anchorage slip model are described in details in Chapter 2 for conditions existing at interior joints, exterior joints and column-foundation interface. These rules have been combined to form a generalized hysteretic model for anchorage slip. Figure 3.9 depicts the various branches of the generalized hysteretic model that are used in the analysis. The number indicated on each branch refers to the number of the rule used to describe this branch in the computer program.

Once the flexibility matrix of each element is determined for the outer rotational degrees of freedom, the 2 by 2 element stiffness matrix along these degrees of freedom is obtained by inverting the flexibility matrix, thus;

$$[K_m]_{2\times2}=[\,f\,]^{-1}_{2\times2} \tag{3.12}$$

In addition to the rotational degrees of freedom, each element has an axial extension mode of deformation as shown in Figure 3.10. Assuming elastic axial deformations, the axial stiffness of the member remains constant as given by :

$$[K_a]=\frac{EA}{L} \tag{3.13}$$

The total 3 by 3 element stiffness matrix for local degrees of freedom can now be obtained by superimposing the stiffness of axial deformation and the element stiffness for the outer rotational degrees of freedom. The element stiffness matrix is then transformed to global element degrees of freedom by matching the local and global elements degrees of freedom as follows (Figure 3.10):

$$[K_m]_u=[A]^T\,[K_m]_\delta[A] \tag{3.14}$$

in which [A] is a 3 by 6 transformation matrix and is given by (Figure 3.10):

$$[A]=\begin{bmatrix} -\cos\theta & -\sin\theta & 0 & \cos\theta & \sin\theta & 0 \\ -\dfrac{\sin\theta}{L} & \dfrac{\cos\theta}{L} & 1 & \dfrac{\sin\theta}{L} & -\dfrac{\cos\theta}{L} & 0 \\ -\dfrac{\sin\theta}{L} & \dfrac{\cos\theta}{L} & 0 & \dfrac{\sin\theta}{L} & -\dfrac{\cos\theta}{L} & 1 \end{bmatrix} \tag{3.15}$$

The global stiffness matrix of the structure, [K], can then be assembled from the element matrices using the direct stiffness method.

3.2.1.2 Geometric Nonlinearity

In inelastic analysis of structures to dynamic loadings there exists two types of nonlinearity. The first type is attributed to the material behavior and is refereed to as material nonlinearity. In the second case, nonlinearity is attributed to the deformation of the structural elements and is termed geometric nonlinearity. Most of the geometric nonlinearity in framed structures can be accounted for by considering the P - Δ effect resulting from side sway of the columns. The P - Δ effect can be approximated by adding to the stiffness of the structure a geometric stiffness based on a constant column axial load caused by gravity loading [37]. Referring to Figure 3.11, the effect of P - Δ on the stiffness of each column can be determined as follows:

$$P\times\Delta + H\times L = 0 \tag{3.16}$$

Therefore;

$$\frac{H}{\Delta} = -\frac{P}{L} \tag{3.17}$$

and the geometric stiffness of the column in global degrees of freedom is given by:

$$K_G = \frac{P}{L}\begin{bmatrix} -1 & 0 & 0 & 1 & 0 & 0 \\ 0 & 0 & 0 & 0 & 0 & 0 \\ 0 & 0 & 0 & 0 & 0 & 0 \\ 1 & 0 & 0 & -1 & 0 & 0 \\ 0 & 0 & 0 & 0 & 0 & 0 \\ 0 & 0 & 0 & 0 & 0 & 0 \end{bmatrix} \tag{3.18}$$

In this study, the secondary effect of P -Δ is accounted for by adding to the stiffness of the structure the geometric stiffness given in Equation 3.18. The geometric stiffness is determined based on the state of the side sway of the structure and column axial loads based on gravity loads determined from static analysis prior to performing dynamic analysis.

3.2.2 Mass Matrix, [M]

The mass of any structure is usually distributed throughout the entire structure. To account accurately for this distribution, the structure must be assigned an infinite number of degrees of freedom making the analysis impractical. Hence, an idealized form of the mass matrix is needed.

For framed structures it is customary to lump the structural mass at the floor levels. Furthermore, since such structures are usually assigned degrees of freedom at the nodes, the mass of each floor is further divided between the joints according to the tributary area. This approach is used in this study. The resulting diagonal mass matrix is given by:

$$[M]=\begin{bmatrix} m_1 & & & \\ & m_2 & & \\ & & \cdot & \\ & & & m_n \end{bmatrix} \tag{3.19}$$

in which m_n is the lumped mass corresponding to degree of freedom n. For rotational degrees of freedom, the mass moment of inertia is zero and hence the corresponding entry in the mass matrix is set to zero.

3.2.3 Damping Matrix, [C]

Damping forces are forces that oppose the motion of the structure and are due largely to air resistance as well as external and internal frictions within the elements of the structure. These forces are complex in nature and very difficult to measure. Hence, it has been the practice to express damping forces as a function of velocity. This form of damping is usually referred to as viscous damping. Therefore, in the equation of motion of the structure, forces due to damping are usually related to the velocity vector by the damping matrix [C].

In this study a viscous type damping is used. The coefficients of the damping matrix are determined by expressing the damping matrix as a combination of stiffness and mass matrices. This is referred to as Raleigh damping and is given by:

$$[C]=\alpha[M]+\beta[K] \tag{3.20}$$

The coefficients α and β are proportionality constants and are derived using the orthogonality conditions for mass and stiffness matrices [80]. The resulting expression for these coefficients is given by :

$$\alpha = \frac{4\pi(T_j\xi_j - T_i\xi_i)}{(T_j^2 - T_i^2)} \tag{3.21}$$

$$\beta = \frac{T_i\ T_j\ (T_j\ \xi_i - T_i\ \xi_j)}{\pi\ (T_j^2 - T_i^2)} \tag{3.22}$$

in which;

T_i, T_j = periods of vibration for modes i and j; respectively.

ξ_i, ξ_j = damping ratios for modes i and j; respectively.

Once the mass, stiffness, and damping matrices are determined, the equation of motion of the system is completely defined. The right hand side of Equation 3.1 represents the loading due to the ground motion along the degrees of freedom, and will subsequently be referred to as P(t).

3.3 Solution of the Equations of Motion

The solution for the equations of motion of multi-degree-of-freedom systems can be obtained by one of two methods; the mode superposition method and the direct integration method. In the mode superposition method, the equations of motion are uncoupled by transforming them into normal coordinates. The response in each coordinate is determined using either closed form solutions or numerical integration techniques, depending on the complexity of the applied load. The response of the system is then determined by superimposing the response of individual normal coordinates. The accuracy of the response obtained from this method is a function of the accuracy of the employed integration technique and the number of modes included in the response. This method is based on the principle of superposition and is useful only for the solution of the equations of motion of linear systems. In the direct integration method, however, the equation of motion is integrated directly without transformation. This method is based on dividing the nonlinear response of the system in the time domain into a number of intervals during each of which the response is taken to be linear. This technique is referred to as the step-by-step integration technique and is used in this study.

3.3.1 Step-By-Step Integration

In order to perform the step-by-step integration, Equation 3.1 needs to be written in incremental form as follows:

$$[M]\{\Delta \ddot{U}\}+[C]\{\Delta \dot{U}\}+[K]\{\Delta U\} = \{\Delta P\} \tag{3.23}$$

Several techniques are available for the direct integration of Equation 3.23. These techniques are based on expressing the values of response quantities, namely; displacement, velocity, and acceleration at a given point of time as a function of their values at one or more previous intervals of time. In the constant acceleration method, for example, expressions for the response parameters at interval n+1 are determined as a function of those at interval n by assuming that the acceleration during the time step is constant and equals to its value at the beginning of the time step. On the other hand , the linear acceleration method assumes a linear variation of acceleration within the time step while the average acceleration method assumes a constant acceleration whose value is taken as the average between the values at the beginning and end of the time step. Usually only two of the response quantities are expressed as a function of their previous values. The third response quantity is obtained by forcing total equilibrium of the equations of motion at the point of time for which response quantities are desired. Other methods of integrating the equations of motion are available. Details on the accuracy of these methods and the conditions for their stability can be found elsewhere [80]. It is sufficient in this study to note that the average acceleration method is unconditionally stable and is suitable for the solutions of nonlinear systems with a large number of degrees of freedom.

In this study the average acceleration method is used due to its advantage of being unconditionally stable. Referring to Figure 3.12, the velocity and displacement at time n+1 are given by:

$$\dot{u}_{n+1}=\dot{u}_n+\frac{\Delta t}{2}(\ddot{u}_n+\ddot{u}_{n+1}) \tag{3.24}$$

$$u_{n+1}=u_n+\Delta t\dot{u}_n+\frac{\Delta t^2}{4}(\ddot{u}_n+\ddot{u}_{n+1}) \tag{3.25}$$

Rearranging Equations 3.24 and 3.25 in terms of Δu:

$$\Delta\dot{u}=-2\dot{u}_n+\frac{2}{\Delta t}\Delta u \tag{3.26}$$

$$\Delta\ddot{u}=-2\ddot{u}_n-\frac{4}{\Delta t}\dot{u}_n+\frac{4}{\Delta t^2}\Delta u \tag{3.27}$$

Substituting Equations 3.26 and 3.27 in the incremental equation of motion:

$$\left[\frac{4}{\Delta t^2}[M]+\frac{2}{\Delta t}[C]+[K]\right]\{\Delta U\} = \{\Delta P\}+[M]\left\{2\ddot{U}_n+\dot{U}_n\frac{4}{\Delta t}\right\}+[C]\{2\dot{U}_n\} \tag{3.28}$$

If the damping matrix is expressed as a combination of mass dependant and stiffness dependant damping, then

$$[C]=\alpha[M]+\beta[K_T] \tag{3.29}$$

Substituting Eq. 3.29 into Eq. 3.28,

$$\begin{aligned}\left[\left\{\frac{4}{\Delta t^2}+\frac{2\alpha}{\Delta t}\right\}[M]+\left\{\frac{2\beta}{\Delta t}+1\right\}[K_T]\right]\{\Delta U\} &= \\ \{\Delta P\}+[M]\left\{2\ddot{U}_n+\frac{4}{\Delta t}\dot{U}_n+2\alpha\dot{U}_n\right\}&+\beta[K_T]\{2\dot{U}_n\}\end{aligned} \tag{3.30}$$

Equation 3.30 can be written in the form:

$$[K_T^*]\{\Delta U\}=\{P^*\} \tag{3.31}$$

in which K_T^* and ΔP^* are the effective stiffness and loading at the beginning of the time step and are give by:

$$[K_T^*]=\left[\left\{\frac{4}{\Delta t^2}+\frac{2\alpha}{\Delta t}\right\}[M]+\left\{\frac{2\beta}{\Delta t}+1\right\}[K_T]\right] \tag{3.32}$$

$$\{\Delta P^*\}=\left\{\{\Delta P\}+[M]\left(2\ddot{U}_n+\frac{4}{\Delta t}\dot{U}_n+2\alpha\dot{U}_n\right)+\beta[K_T]\{2\dot{U}_n\}\right\} \tag{3.33}$$

At the beginning of each time step, the effective stiffness matrix is assembled based on mass matrix and the tangent static stiffness of the structure as well as damping coefficients. The load vector is assembled based on the velocity and acceleration at the beginning of the time step as well as the incremental ground acceleration. The solution for the displacement vector in Equation 3.31 can then be obtained using the well known Gauss elimination with back substitution. Once the displacements are known, the initial velocity and acceleration for the next time step are determined using Equations 3.24 - 3.27. The new tangent stiffness of the structure is determined by transforming the nodal displacements into element deformations and checking the yield status of each element.

The procedure described above is an approximate solution to the differential equation governing the response of the structure. It requires the equilibrium of the structure to be satisfied at discrete intervals of the time domain of response. The accuracy of the procedure is, therefore, dependant on the size of the selected time step as well as the accuracy of the numerical integration technique. If one or more elements of the structure yield within a given time step, another situation contributing to the inaccuracy of the procedure arises. This inaccuracy is caused by the equilibrium unbalance during overshooting of internal forces due to the assumption of constant stiffness within the time step. When stiffness dependant damping is used, the change in stiffness results in the disruption of damping force, upsetting the equilibrium as well. Such equilibrium unbalance could result in accumulation of errors unless its effect is minimized. Several procedures have been proposed to correct the equilibrium unbalance caused by yielding within a time step. One approach is to divide the time step that includes yielding of the element into a number of steps such that yielding of the element will coincide with the beginning of a new time step. This approach has been reported to be tedious and impractical for a general purpose computer program. The other approach, is based on applying a corrective load at the end of each time step to minimize the effect of equilibrium unbalance. This approach is widely used and was reported to give good accuracy as compared to subdividing the time step into a number of smaller intervals. Therefore the latter approach is used in this study. Details of the evaluation of the unbalanced loads will be given in Chapter 4.

Chapter 4

Computer Program

4.1 Introduction

Dynamic inelastic analysis has been performed using an enhanced version of the computer program Drain-2D developed by Kanaan and Powell at the university of California, Berkeley. Drain-2D is a general purpose computer program for static and dynamic analysis of planar structures. Only ground motion type of dynamic loading can be handled by the program. Both horizontal and vertical ground acceleration records can be specified at the base of the structure. Currently the program contains a library of six elements, namely; a truss element, a beam element, a beam-column element, an infill panel element, a connection element, and a degrading stiffness beam element. The latter is suitable for modelling reinforced concrete elements. The program structure is composed of a number of base subroutines common to all the elements, and a number of element subroutines. The base subroutines are designed to input structure and loading data, construct the global stiffness matrix from individual element matrices, construct mass and damping matrices from the input data, and solve for the nodal displacements. The base subroutines interact with various element subroutines that are designed to form the stiffness of each element from element information data and determine the response of each element based on the calculated nodal displacements. An output subroutine for each element type is designed to output individual element responses. Since this study focuses on reinforced concrete structures, all element subroutines that are not related to the degrading stiffness element were discarded. This was done in order to make the program manageable, especially after a major modification was implemented to the stiffness degrading element. In its original form, the program is limited to flexure type inelastic deformations. It has been modified in this study to include inelastic shear and slip deformations. This chapter describes the original program, and outlines the modifications introduced to include shear and slip deformations in the analysis. Verifications of the new additions to the program are also discussed.

4.2 Program Concept

In Drain-2D the structure is idealized as consisting of discrete elements with degrees of freedom at the nodes connecting the elements. Each node can have up to three degrees of freedom, two translational and one rotational, and provisions are made for either restraining a degree of freedom or combining a number of degrees of freedom. The mass of the structure is lumped at the joints resulting in a diagonal mass matrix. The global stiffness of the structure is assembled from individual element stiffnesses using the direct stiffness method. Damping can be specified as either mass dependant or stiffness dependant Raleigh damping. Ground motion is input as accelerations specified at time intervals and can differ for horizontal and vertical directions. The dynamic response is determined using the step-by-step integration technique, with the assumption of constant average acceleration during each time step. In assembling the stiffness matrix, the tangent stiffness at the beginning of each step is assumed to remain constant during the step. Hence, the nonlinear response is divided into a number of small intervals of linear responses. The stiffness of each element is updated at the beginning of each step, and if nonlinearity takes place during the step, errors due to overshooting of internal resistance are accounted for by applying a corrective load in the beginning of the next step.

Each reinforced concrete element of the structure is modelled as an elastic line element with one point spring at each end to account for inelastic flexural deformations. The moment hysteretic relationship of the spring is defined by a primary curve and a set of hysteretic rules as described in section 3.2. The elastic and post yield stiffnesses of the spring are determined such that the total chord rotation of a cantilever of half the length of the member is equal to that of the idealized model (see Figure 4.1). If the elastic stiffness of the spring is initially set to a very large value such that the yield rotation of the idealized cantilever is equal to that of the actual cantilever, then for post yield rotation to be modelled correctly, the hardening ratio forHxhe moment rotation curve of the idealized cantilever must be equal to that of the actual cantilever.

If the initial stiffness of the spring is denoted by K_{se}, and the hardening ratio of the moment rotation curve of the real cantilever is denoted by r, then the total rotation of the idealized cantilever is given by:

$$\theta_t = \frac{M_y L}{6EI} + \frac{M_y}{K_{se}} + \frac{(M-M_y)L}{r \times 6EI} + \frac{(M-M_y)}{r \times K_{se}} \tag{4.1}$$

Since the elastic rotation is given by

$$\theta_e = \frac{M_y L}{6EI} + \frac{(M-M_y)L}{6EI} + \frac{M_y}{K_{se}} \tag{4.2}$$

The plastic rotation of the idealized cantilever can now be determined as the difference between the total and the elastic rotations as follows:

$$\theta_p = \theta_t - \theta_e = \frac{L}{6EI}\left(\frac{1}{r}-1\right)(M-M_y) + \frac{M-M_y}{r \times K_{se}} \tag{4.3}$$

Rearranging Equation 4.3, we get:

$$\theta_p = \left[\frac{L}{6EI}\left(\frac{1}{r}-1\right) + \frac{1}{rK_{se}}\right](M-M_y) \tag{4.4}$$

from which

$$K_{sp}=\frac{M-M_y}{\theta_p}=\frac{1}{\frac{L}{6EI}\left(\frac{1-r}{r}\right)+\frac{1}{r\times K_{se}}} \tag{4.5}$$

The strain hardening ratio of the moment - rotation relationship of spring, p, can now be determined as the ratio between the post yield and the elastic stiffness as follows:

$$p=\frac{K_{sp}}{K_{se}}=\frac{r}{\frac{K_{se}(1-r)}{\frac{6EI}{L}}+1} \tag{4.6}$$

Equation 4.6 is the default option in Drain-2D for determining the post yield stiffness of the spring based on the value of the strain hardening ratio of M - θ (or P-δ), of a cantilever beam of length L/2, which needs to be specified by the user.

Once the flexibility of the springs is determined, the total member flexibility is constructed by superimposing elastic and inelastic flexibilities. The latter is inverted to get the member stiffness matrix. The total stiffness matrix of the structure is then assembled using the direct stiffness method.

4.2.1 Equilibrium Unbalance

In determining the response of a structure to ground excitation using the step-by-step integration technique, it is assumed that the structure behaves elastically during each step. If one or more element(s) of the structure develop inelastic deformations during a particular step, the assumption of elastic behavior is violated resulting in inaccuracy in the response. This inaccuracy is caused by the equilibrium unbalance during overshooting of internal forces due to the assumption of constant stiffness during the time step. When stiffness dependant damping is used, the change in stiffness results in the disruption of the damping force and hence upset of equilibrium as well. Such equilibrium unbalance could result in accumulation of errors unless its effect is minimized. Several procedures have been proposed to correct the equilibrium unbalance caused by yielding within a time step. One approach is to divide the time step that includes yielding of the element into a number of steps such that yielding of the element will coincide with the beginning of a new time step. This approach has been reported to be tedious and impractical for a general purpose computer program. The other approach, which is used in Drain-2D, is based on applying a corrective load at the end of each time step to minimize the effect of equilibrium unbalance. This approach was reported to give good accuracy as compared to subdividing the time step into a number of smaller intervals. To illustrate the procedure for correcting the equilibrium unbalance in Drain-2D, let us consider the equation of equilibrium for the structure shown in Figure 4.2 at the end of the i^{th} step, which is given by:

$$\{F_I\}+\{F_D\}+\{F_S\}=\{P\} \tag{4.7}$$

If we assume that the solution of the equilibrium equation for step i results in rotations at the ends of element n of $\Delta\theta_1$ and $\Delta\theta_2$ respectively, and if we further assume that the status at the two ends of element n at the beginning of step i is as shown in Figure 4.2c and d, respectively, then, the linear increments of moment at the two ends of the member are given by:

$$\begin{Bmatrix}\Delta ML_1^{(1)}\\ \Delta ML_2^{(1)}\end{Bmatrix}=\begin{bmatrix}\frac{L}{3EI}+\frac{L}{GAL}+f_{1e} & -\frac{L}{6EI}+\frac{1}{GAL}\\ -\frac{L}{6EI}+\frac{1}{GAL} & \frac{L}{3EI}+\frac{1}{GAL}+f_{2e}\end{bmatrix}^{-1}\begin{Bmatrix}\Delta\theta_1\\ \Delta\theta_2\end{Bmatrix} \tag{4.8}$$

However the moments calculated based on linear behavior within the time step are not correct due to the yielding at end 1 of the member. Assuming that the total rotations at the ends of the member remain the same as for the linear case, the actual moment at the ends of the member can be evaluated as a composition of two parts, $\Delta M^{(1)}$ and $\Delta M^{(2)}$. These terms can be expressed in terms of coefficient μ which is defined as the smallest ratio between the incremental linear moment and the increment of moment to the first yielding event. From Figure 4.2, the value of μ is given by:

$$\mu=\mu^{(1)}=\frac{My_1-Mi_1}{\Delta ML_1^{(1)}} \tag{4.9}$$

Therefore;

$$\Delta M_1^{(1)}=My_1-Mi_1=\mu\Delta ML_1^{(1)} \tag{4.10}$$

and

$$\Delta M_2^{(1)}=\mu\Delta ML_2^{(1)} \tag{4.11}$$

To determine the second increment of moment, a new cycle is started with a changed flexibility matrix of the element reflecting the change in the flexibility of the spring at end 1. The new linear increments of moment are given by:

$$\begin{Bmatrix}\Delta ML_1^{(2)}\\ \Delta ML_2^{(2)}\end{Bmatrix}=\begin{bmatrix}\frac{L}{3EI}+\frac{1}{GAL}+f_{1p} & -\frac{L}{6EI}+\frac{1}{GAL}\\ -\frac{L}{6EI}+\frac{1}{GAL} & \frac{L}{3EI}+\frac{1}{GAL}+f_{2e}\end{bmatrix}^{-1}\begin{Bmatrix}\Delta\theta_1\\ \Delta\theta_2\end{Bmatrix} \tag{4.12}$$

Since we have no yield events in the second cycle, the moment increments $\Delta M_1^{(2)}$, and $\Delta M_2^{(2)}$ are given by:

$$\begin{Bmatrix}\Delta M_1^{(2)}\\ \Delta M_2^{(2)}\end{Bmatrix}=(1-\mu^{(1)})\begin{Bmatrix}\Delta ML_1^{(2)}\\ \Delta ML_2^{(2)}\end{Bmatrix} \tag{4.13}$$

The total increment of moments at the two ends, ΔM_1 and ΔM_2 can now be determined by superimposing the values of $\Delta M^{(1)}$ and $\Delta M^{(2)}$. This leads to unbalance moments at the two ends, which are given by:

$$\begin{Bmatrix}M_{ub_1}\\ M_{ub_2}\end{Bmatrix}=\begin{Bmatrix}\Delta ML_1^{(1)}-\Delta M_1\\ \Delta ML_2^{(1)}-\Delta M_2\end{Bmatrix} \tag{4.14}$$

The above illustration of determining the unbalanced moments focused on a simple example, in which only one yield event at one end of a member took place during a given step. In reality, however, yielding may take place at both ends of a number of members, and there may be more than one yield event at each end of a member for a given step. The procedure for determining the unbalanced moments at the ends of each member in such cases is no different than the case discussed above, except the procedure is repeated for each member. The number of cycles required to determine the unbalance moments at the end of each member is dependant on the number of yield events that take place during the step. The convergence for determining the actual increment of moment at each end is reached when the $\Sigma\mu$ reaches 1.

Because of the change in stiffness of the structure, the elastic force vector, $\{F_S\}$, in Equation 4.7 changes to $\{F_S - \Delta F_S\}$, in which $\{\Delta F_S\}$ is the change in elastic force vector, and is equal to the vector of transformed unbalanced moments over the entire structure. Hence;

$$\{\Delta F_S\}=\{M_{ub}\} \tag{4.15}$$

In addition to equilibrium unbalance due to the change in elastic force vector, changes in stiffness will also result in damping force vector of $\{F_D + \Delta F_D\}$ for structures with stiffness dependant damping. The change in damping force vector, $\{\Delta F_D\}$, can be determined by summing the contributions of individual elements. The contribution of each element to $\{\Delta F_D\}$ is determined by multiplying the change in element stiffness, transformed into global coordinates, by the global velocity vector corresponding to the element degrees of freedom and the damping constant β. thus:

$$\{\Delta F_D\}=\beta[\Delta K]\{\dot{u}\} \tag{4.16}$$

The change of stiffness, ΔK, in Equation 4.16 may be positive or negative depending on the yield status of the element at the beginning and end of the step. The true equation of motion at the end of the i^{th} step can then be expressed as follows:

$$\{F_I\}+\{F_D+\Delta F_D\}+\{F_S-\Delta F_S\}=\{P\} \tag{4.17}$$

For equilibrium to be satisfied, a fictitious load vector must be added to the right hand side of Equation 4.17 to reflect the changes in elastic and damping forces as follows:

$$\{F_I\}+\{F_D+\Delta F_D\}+\{F_S-\Delta F_S\}=\{P+\Delta F_D-\Delta F_S\} \tag{4.18}$$

The fictitious load in Equation 4.18 is allowed to act for a very short period of time and is eliminated at the beginning of tne next time step by adding to the load vector a corrective load of $\{\Delta F_S - \Delta F_D\}$

4.3 Program Modification

The computer program Drain-2D in its original form contains a reinforced concrete element whose flexibility matrix includes inelastic deformations that are attributed to flexural deformations only. The major modifications introduced to the program in this study include the additions of inelastic shear and slip flexibilities to the flexibility of the element. This was accomplished by the addition of two pairs of springs to the one component model, one pair at each end, as shown in Figure 3.11. One of the springs was assigned the hysteretic moment-rotation relationship for shear while the other was assigned the slip moment-rotation relationship. With the flexibility of each spring known at the beginning of each step, the incremental rotation at each end can be expressed as follows :

$$\begin{Bmatrix} \Delta\theta_i \\ \Delta\theta_j \end{Bmatrix} = \begin{bmatrix} \frac{L}{3EI}+\frac{1}{GAL}+f1_i+f2_i+f3_i & -\frac{L}{6EI}+\frac{1}{GAL} \\ -\frac{L}{6EI}+\frac{1}{GAL} & \frac{L}{3EI}+\frac{1}{GAL}+f1_j+f2_j+f3_j \end{bmatrix} \begin{Bmatrix} \Delta M_i \\ \Delta M_j \end{Bmatrix} \qquad (4.19)$$

in which; f1, f2, and f3 are the current flexibilities of slip, shear, and flexural spring; respectively, and are determined from the applicable hysteretic models. Prior to performing any analysis, the post and pre-yield stiffnesses of the shear and slip springs need to be determine. The hysteretic rules for each model can then be used to determine the flexibility of each spring at a particular stage of response. In the following two subsections, the procedure for determining the elastic and post yield stiffnesses of the primary curves for shear and slip springs is outlined.

4.3.1 Slip Spring

Anchorage slip deformations take place in the critical regions which are usually located at the beam-column joints and the column-foundation interface. This is explained in details in Chapter 2. Hence, these deformations can be lumped in the form of concentrated rotations at the ends of each member. This can be accomplished by assigning the moment-anchorage slip rotation relationship directly to the slip spring. The pre-yield and post yield stiffnesses of the spring will, therefore, be the same as those of the primary moment-anchorage slip rotation relationship. The analytical procedure for determining the primary moment-slip rotation relationship has been covered in details in Chapter 2.

The post and pre-yield stiffnesses of the slip spring are input items for the computer program that must be specified by the user. In addition, the unloading slope at a control point on the primary curve, and the coordinates of that point must also be input. The unloading slope at any other point on the post yield primary curve is automatically determined by the program by interpolating/extrapolating the input slope at the control point.

4.3.2 Shear Spring

The shear spring stiffness prior to and after yielding are determined from the primary moment-shear distortion curve in a manner that is similar to that for flexural spring. Referring to Fig. 4.3, the post cracking spring stiffness can be determined by considering the total shear distortion of a cantilever of length L/2 having a support moment M having a value between the cracking and the yield moments as follows:

$$\gamma_t=\frac{2M_{cr}}{GAL}+\frac{M_{cr}}{K_{se}}+\frac{(M-M_{cr})}{\frac{GAL}{2}\times S_1}+\frac{(M-M_{cr})}{K_{se}\times S_1} \tag{4.20}$$

in which; K_{se} is the elastic stiffness of the spring and is taken by the program to be very large (10^8GA), and S_1 is the ratio between the post cracking and pre-cracking stiffness of the primary moment-shear distortion curve.

Since the elastic shear distortion is given by:

$$\gamma_e = \frac{2M_c}{GAL} + \frac{M_c}{K_{se}} + \frac{(M-M_c)}{\frac{GAL}{2}} \tag{4.21}$$

The plastic distortion contributed by the spring can be expressed as the difference between the total and the elastic distortions as given below:

$$\gamma_p = \gamma_t - \gamma_e = \frac{2}{GAL}\left(\frac{1}{S_1} - 1\right)(M-M_c) + \frac{(M-M_c)}{S_1 \times K_{se}} \tag{4.22}$$

or

$$\gamma_p = \left[\frac{2}{GAL}\left(\frac{1}{S_1} - 1\right) + \frac{1}{S_1 K_{se}}\right](M-M_c) \tag{4.23}$$

from which;

$$K_{spl} = \frac{M-M_c}{\theta_p} = \frac{1}{\frac{2}{GAL}\left(\frac{1-S_1}{S_1}\right) + \frac{1}{S_1 \times K_{se}}} \tag{4.24}$$

The ratio of the post-cracking to the elastic stiffness can now be expressed as:

$$p_1=\frac{K_{sp1}}{K_{se}}=\frac{S_1}{\frac{K_{se}(1-S_1)}{\frac{GAL}{2}}+1} \tag{4.25}$$

Equation 4.25 has been implemented in the program to determine the post-cracking stiffness of the shear spring based on the ratio between the post and the pre-cracking stiffnesses of the primary moment-shear distortion relationship. This ratio must be specified by the user as part of the input data to the program.

The same procedure is adopted to derive the post yield stiffness of the spring. From the total shear deformation, γ_T, and the elastic shear deformation, γ_e, the plastic deformation of the spring, γ_p, at a moment M greater than M_y is determined as follows:

$$\gamma_T=\frac{2M_c}{GAL}+\frac{M_c}{K_{se}}+\frac{\frac{GAL}{2}+K_{se}}{S_1\times K_{se}\times\frac{GAL}{2}}(M_y-M_c)+\frac{\frac{GAL}{2}+K_{se}}{S_2\times K_{se}\times\frac{GAL}{2}}(M-M_y) \tag{4.26}$$

$$\gamma_e=\frac{2M_c}{GAL}+\frac{M_c}{K_{se}}+\frac{M_y-M_c}{\frac{GAL}{2}}+\frac{M-M_y}{\frac{GAL}{2}} \tag{4.27}$$

$$\gamma_{P(M>M_y)}=\gamma_T-\gamma_e-\gamma_{P(M=M_y)} \tag{4.28}$$

$$\gamma_{P(M>M_y)}=\left(\frac{1}{S_2\times\frac{GAL}{2}}+\frac{1}{S_2\times K_{se}}-\frac{1}{\frac{GAL}{2}}\right)(M-M_y) \qquad (4.29)$$

the post yield stiffness is then given by;

$$K_{sp2}=\frac{M-M_y}{\gamma_P}=\frac{1}{\frac{2}{GAL}\left(\frac{1}{S_2}-1\right)+\frac{1}{S_2\times K_{se}}} \qquad (4.30)$$

$$p_2=\frac{K_{sp2}}{K_{se}}=\frac{S_2}{\frac{K_{se}(1-S_2)}{\frac{GAl}{2}}+1} \qquad (4.31)$$

Equation 4.31 has been impleHxnted in the program to determine the post yield stiffness of the shear spring.

Once the pre-yield and post-yield stiffnesses of each spring have been obtained, their stiffness at any time during the response can be determined from the applicable hysteretic rules. These rules have been discussed in details in Chapter 3.

In the present study, two major subroutines, SLIPM and SHEARM, have been written to describe the rules for shear and slip models. The Fortran coding of these subroutines is included in Appendix A. These subroutines were then introduced to Drain-2D via a calling sequence that traces out nonlinearity in each spring. It is possible that one or more spring(s) at either or both ends of any member will yield during a given time step. To illustrate the procedure of tracing out nonlinearity for the three springs, the following numerical example, involving a simple yielding system shown in Fig. 4.4, is presented.

Numerical Example

Initially, let $M_i = 0$, $\Delta\theta=18$, $k_1= 50$, $k_2 = 150$, $k_3 = 300$. Then;

$$k_{eff}=\frac{k_1 \times k_2 \times k_3}{k_1 \times k_2+k_1 \times k_3+k_2 \times k_3}=\frac{50\times150\times300}{50\times150+50\times300+150\times300}=33.33$$

$$\Delta ML^{(1)}=k_{eff}\times\Delta\theta=18\times33.33=600.$$

$$\mu_1^{(1)}=\frac{My_1-M_i}{\Delta ML_1}=\frac{100}{600}=0.1667 \quad (\textit{governs})$$

$$\mu_2^{(1)}=\frac{200}{600}=0.333$$

$$\mu_3^{(1)}=\frac{300}{600}=0.5$$

$$\therefore \quad \mu^{(1)}=0.1667$$

$$\Delta M_1^{(1)}=\Delta M_2^{(1)}=\Delta M_3^{(1)}=0.1667\times600=100.$$

$$M_t=M_i+\Delta M^{(1)}=0+100=100$$

$$\sum\mu=\mu_1=0.1667 \qquad \therefore factor=1-\sum\mu=0.8333$$

$$k_{eff}=\frac{20\times150\times300}{20\times150+20\times300+150\times300}=16.6667$$

$$\Delta ML^{(2)}=16.6667\times18=300$$

$$\mu_1^{(2)}=0.8333$$

$$\mu_2^{(2)}=\frac{200-100}{300}=0.333 \qquad \textit{(governs)}$$

$$\mu_3^{(2)}=\frac{300-100}{300}=0.6667$$

$$\therefore \mu^{(2)}=0.333$$

$$\Delta M^{(2)}=0.333\times300=100$$

$$M_t=M_t+\Delta M^{(2)}=100+100=200$$

$$\sum\mu=\mu^{(1)}+\mu^{(2)}=0.333+0.1667=0.5$$

$$factor=1-\sum\mu=1-0.5=0.5$$

$$k_{eff}=\frac{20\times30\times300}{20\times30+20\times300+30\times300}=11.53846$$

$$\Delta ML^{(3)}=11.53846\times18=207.69228$$

$$\mu_1^{(3)} = factor = 0.5$$

$$\mu_2^{(3)} = factor = 0.5$$

$$\mu_3^{(3)}=\frac{300-200}{207.6922}=0.48148 \qquad \textit{(governs)}$$

$$\therefore \mu^{(3)} = 0.48148$$

$$\Delta M^{(3)} = 0.48148 \times 207.69228 = 100.$$

$$M_t=M_t+\Delta M^{(3)}=200+100=300$$

$$\sum \mu = \sum \mu + \mu^{(3)} = 0.5 + 0.48148 = 0.98148$$

$$factor = 1 - \sum \mu = 1 - 0.98148 = 0.01852$$

$$k_{eff} = \frac{20\times30\times50}{20\times30+20\times50+30\times50} = 9.6774$$

$$\Delta ML^{(4)} = 9.6774 \times 18 = 174.1935$$

$$\mu_1^{(4)} = \mu_2^{(4)} = \mu_3^{(4)} = factor = 0.01852$$

$$\therefore \mu^{(4)} = 0.01852$$

$$\Delta M^{(4)} = 0.01852 \times 174.1935 = 3.226$$

$$M_t = M_t + \Delta M^{(4)} = 300 + 3.226 = 303.226$$

$$\sum \mu = \sum \mu + \mu^{(4)} = 0.98148 + 0.01852 = 1.0 \quad \therefore \textit{cycle is complete}$$

4.3.3 Ductility Demand

The amount of plastic deformations that can be sustained by elements of a structure without loss of strength is an indicator of the ability of the structure to withstand the ground motion and is usually known as "ductility". The most commonly used definition of ductility is rotational ductility and is given by [29] (see Fig. 4.5):

$$\mu_\theta = \frac{\theta_{max}}{\theta_y} \tag{4.32}$$

The rotations in Figure 4.5 and Equation 4.32 are the chord rotations of a cantilever beam with the moment M applied at the support. Therefore, in the one component model idealization, once the moment values are known at the ends, the chord rotation at each end is calculated based on the end moment and a cantilever length of L/2. In the present study, the calculations of the ductility demand factors have been added to the program. Ductility factors for each mode of deformation are determined individually and then compared with the combined factor based on total deformation.

Flexural Ductility Factor

Referring to Figure 4.6, the flexural ductility demand factor is given by:

$$\mu_{fl}=\frac{\theta max_{fl}}{\theta y_{fl}} \tag{4.33}$$

in which;

$$\theta y_{fl}=M_y\left(\frac{L}{6EI}+\frac{1}{ke_{fl}}\right) \tag{4.34}$$

$$\theta max_{fl}=\theta y_{fl}+(M-M_y)\left(\frac{L}{6EI}+\frac{1}{kp_{fl}}\right) \tag{4.35}$$

where; ke_{fl}, and kp_{fl} are the pre-yield and post yield stiffnesses of the flexural spring, respectively.

Shear Ductility Demand

The shear ductility demand factor is determined in a similar manner to flexure as follows:

$$\mu_{sh}=\frac{\theta max_{sh}}{\theta y_{sh}} \tag{4.36}$$

in which:

$$\theta y_{sh}=M_{cr}(\frac{2}{GAL}+\frac{1}{Ke_{sh}})+(M_y-M_{cr})(\frac{2}{GAL}+\frac{1}{kp1_{sh}}) \tag{4.37}$$

$$\theta max_{sh}=\theta y_{sh}+(M-M_y)(\frac{2}{GAL}+\frac{1}{kp2_{sh}}) \tag{4.38}$$

where; ke_{sh} is the elastic stiffness, $kp1_{sh}$ is the post-cracking stiffness, and $kp2_{sh}$ is the post-yield stiffness of the shear spring.

Slip Ductility Demand

Since slip deformations are concentrated at the member ends, there is no contribution from the elastic line element. Hence, the slip ductility demand factor is defined as follows:

$$\mu_{sl}=\frac{\theta max_{sl}}{\theta y_{sl}} \tag{4.39}$$

where;

$$\theta y_{sl}=\textit{yield rotation in the slip model}=\frac{M_y}{ke_{sl}} \tag{4.40}$$

$$\theta max_{sl}=\theta y_{sl}+\frac{(M-M_y)}{kp_{sl}} \tag{4.41}$$

ke_{sl}, and kp_{sl} are the elastic and post-yield stiffnesses in the slip model, respectively.

<u>Combined Ductility</u>

The combined ductility demand is determined by combining flexure, shear, and slip deformations as follows:

$$\mu=\frac{\theta_{max}}{\theta_y} \tag{4.42}$$

where;

θ_y = combined rotation at first yield. The first yield can be due to flexure, shear, or anchorage slip, whichever occurs first.

$\theta max=\theta max_{fl}+\theta max_{sh}+\theta max_{sl}$

All other variables are as defined before.

4.3.4 Energy Dissipation Factors

In response of structures to seismic loadings, the energy input by the ground motion at the base is expected to be dissipated through plastic hinge rotations in the critical regions. The ability of the structure to dissipate large amount of energy without a loss of strength is an indicator of its seismic resistance. The dissipated energy is usually measured as the ratio between plastic and elastic energies. This ratio is termed the "Energy Dissipation Factor (EDF)" and is given by (see Figure 4.7):

$$EDF=\frac{Plastic\ Energy}{Elastic\ Energy}=\frac{Dashed\ Area}{\frac{1}{2}\times M_y\times\theta_y} \tag{4.43}$$

In this study, the determination of energy dissipation factors has been implemented in Drain-2D. The program calculates and outputs both the individual and the combined energy factors at the ends of each element. Comparison of the individual factors with the total gives an indication of the degree of contribution of each spring to the dissipated energy. All energy dissipation factors are normalized to the elastic flexural energy in order to facilitate the comparison.

In addition to the above modification, the program input and output have been organized to reflect the new changes. The ratios of the post cracking and post yield stiffnesses to the elastic stiffness of the shear model have been added to the list of input data. Also added to the list of input data are the pre-yield and post-yield stiffnesses of the slip model. Two moment values, which are not required in the original program, have been included in the input list. These are; the cracking moment, which is required in the shear model, and the moment at which the force in the outermost tensile reinforcement crosses the zero value, which is needed in the slip model. The program output has been modified to include; envelope values for the rotation of shear and slip springs, combined and individual ductility demand factors, energy dissipation factors, and time history for the rotation of shear and slip springs.

4.4 Verification of the Computer Program

The changes implemented in Drain-2D have been verified at three stages. The first stage was at the end of completing the Fortran coding for the rules of the shear and slip models. The main objective of this check was to insure that the rules were coded correctly. This was accomplished by assuming a simple yield system and reading different cases of hypothetical displacement histories at the end of the spring. The output of moment-displacement history for each case was verified against manual calculations. Figure 4.8 and 4.9 show several checks for slip and shear models, respectively.

The second stage was at the end of introducing shear and slip models to Drain-2D. The primary objective of this stage was to insure that changes in the common blocks and the calling sequence of the subroutines, as well as the addition of the new subroutines, did not disturb the original program. This was accomplished by locking the shear and slip springs and comparing the result of analysis of a simple portal frame, shown in Figure 4.10, subjected to Taft 1952 S69E earthquake with the results of the same structure using the original program. Figure 4.11 shows the lateral displacement time history and the flexural hinge moment-rotation relationship of the left end of the girder for both cases.

The third and final check involved running the program for two simple systems. The first system, shown in Figure 4.12a, consisted of a cantilever of length 5m, supporting a mass of 15000 kg. It was subjected to a monotonic ground motion, as shown in Figure 4.12b. The program was run for four different cases:

i) Appropriate stiffnesses were specified for pre-yield and post yield stiffnesses of flexure, shear, and slip springs. The primary curve for the shear spring was taken to be bilinear.

ii) Shear and slip springs were locked, but a stiffness equal to the combined stiffness of the three springs was specified for the flexural spring.

iii) Shear and flexural springs were locked, but a stiffness equal to the combined stiffness of the three springs was specified for the slip spring.

iv) Flexure and slip springs were locked, but a stiffness equal to the combined stiffness of the three springs is specified for the shear spring.

Results obtained for the four cases were compared and found to be identical. Figure 4.13 shows time history of lateral displacement for the four cases. In addition; envelope values of forces, hinge rotations, as well as ductility demands and dissipated energy factors were found to be identical.

The second system used at this stage was the portal frame used earlier at the second stage, except that the shear and slip springs were then activated. The system was subjected to Taft 1952 S69E earthquake. The objective of this run was to check whether or not each spring followed its prescribed rules. Fig. 4.14, shows the moment-rotation hysteresis for the three springs in the left side of the beam. Each spring was found to follow closely the applicable hysteretic model.

Chapter 5

Selection of Structures and Earthquake Records for Dynamic Analysis

5.1 Introduction

The scope of this study includes dynamic inelastic analyses of reinforced concrete frame structures. It is important to conduct the analyses on realistic structures that are representative of those built in practice. Therefore, selection and design of structures form an important task of the current investigation. For seismic analysis of a frame structure, two sets of data need to be defined a priori. First, the structural properties of the frame, including the geometry, mass, stiffness, and strength, as well as damping characteristics must be defined. This can be accomplished by using the structure design. Second, the time history of the ground motion at the base of the frame needs to be specified. Selection of critical ground excitations can be made by considering the dynamic properties of the structure and the response spectra of available ground motions.

This chapter describes the method used in selecting the frames that are considered for dynamic analyses. Three frame structures were designed with periods covering most of the practical range. Once the sizes and reinforcement arrangements of the frame members are determined, their flexural, shear, and slip properties can be determined by examining the corresponding force - deformation characteristics for each member. From the latter, flexural and shear rigidity, as well as relevant parameters of flexural, shear and slip hysteretic models can be evaluated. In addition to selecting the frames, this chapter describes the procedure of selecting the ground motion to be used for each frame. The appropriate ground motion for each frame is determined by considering five available earthquake records. Once the selection is made, the earthquake intensity is scaled up or down to obtain the desired intensity of ground motion.

5.2 Design Procedure

Three frames, each forming part of a multistory reinforced concrete moment resisting building, were designed. Five, ten, and fifteen-story buildings were considered. Simplifying assumptions were made in order to avoid unwarranted complications in design. A square floor plan was selected for all buildings, as shown in Figure 5.1. Bay sizes were taken to be 6 m. All floors were assumed to have the same height of 4 m. A symmetrical building layout was selected to minimize the torsional effect. It was further assumed that the lateral design load was governed by the equivalent static earthquake loads specified in the 1990 NBC of Canada [26]. Thus the design of each frame was performed by considering the combination of factored dead loads, live loads, and earthquake loads. Following are the relevant design data used for buildings.

Dead Loads:

Roof = 3.50 kN/m^2

Floor = 5.00 kN/m^2

External Wall (all glazing) = 0.26 kN/m^2

Live Loads:

Roof (snow load) = 2.24 kN/m^2

Floor (office) = 2.40 kN/m^2

Earthquake Loads:

Velocity Zone, Z_v = 2

Acceleration Zone, Z_a = 2

Importance Factor, I = 1

Foundation Factor, F = 1

Ductility Level, R = 4.0

Material Strength:

Concrete Compressive Strength = 30 MPa

Reinforcement Yield Strength = 400 MPa

Once the equivalent static lateral loads on the building were determined, they were divided between the frames of the building such that the external frames carried half of the loads carried by the internal frames. The gravity loads were determined by considering the tributary area of each girder. The frames were analyzed statically using estimated section sizes to obtain design loads for each member. Once the design loads were determined, the design of each member was carried out according to the requirements of the CSA A23.3 - M84 [25]. The lateral drift effect was approximated by adding the P - Δ moment to the column design moment. The P - Δ moment was approximated by multiplying the design axial load by the interstory drift, magnified by a factor of 2.85 to account for inelasticity [82]. The frames were analyzed once more with the initial design sizes to obtain new design forces. The design was modified on the basis of the new design forces when necessary. Tables 5.1 to 5.3 show the final sectional sizes and reinforcement arrangements for all three frames. The geometry of the frames are shown in Figures 5.2 - 5.4.

5.3 Properties of Selected Frames

Prior to performing dynamic analysis of a frame, flexural and shear rigidities of members need to be determined. In addition, the elastic and post yield slopes of moment-flexural rotation, moment-shear distortion, and moment-anchorage slip rotation relationships, are required. Each of these quantities requires proper evaluation of force-deformation relationships of each member for the three modes of deformation, namely; flexure, shear, and anchorage slip.

5.3.1 Flexural Moment - Rotation Relationship

The hysteretic flexural behavior of members are modelled in this study by determining the moment - chord rotation relationship at each end, assuming the member consists of two cantilevers with equal lengths, connected at mid span. This can be achieved by first determining the sectional moment - curvature relationship. Once the moment curvature relationship is known, the chord rotation can be determined from the moment area theorem, for a given value of support moment.

The moment-curvature relationship of a reinforced concrete section prior to cracking can be determined from the beam theory as follows:

$$\phi = \frac{d\theta}{dx} = \frac{M}{EI} \tag{5.1}$$

where EI is determined by considering the transformed cross section. Once cracking of concrete takes place, the behavior of the material can no longer be taken to be linear and elastic. The curvature of the section at any moment greater than the cracking moment can only be determined by performing sectional analysis. Implicit in this approach is the assumption that plain sections before bending remain plain after bending. The procedure consists of assuming a strain value at the extreme compression side of the core concrete and iterating on the depth of the neutral axis, c, until equilibrium of internal forces is attained. The curvature is then determined as the ratio between the strain value and the distance to the neutral axis. Internal forces in the core concrete are determined by considering the stress -strain relationship for confined concrete which is described in details in Chapter 2. Concrete cover was assigned the stress strain relationship of unconfined concrete and was assumed to spall off at a strain of 0.004. The stress-strain curve for steel was taken to be bilinear in the elastic and yield platea regions with the behavior in the strain hardening region expressed by a parabolic function. The process was continued by incrementing the strain value until the ultimate capacity of the section was reached. The procedure described above is tedious to be carried out manually. A computer subroutine was written in this study to obtain the complete moment - curvature relationship of a given section. Figure 5.5 shows an example of the calculated moment - curvature relationships for a beam section. For columns, the axial load has a pronounced effect on the moment - curvature relationship. For axial loads up to the balance load, the yield moment increases with increasing axial load. This results in a shift in the moment - curvature relationship as shown in Figure 5.6. In this study, the moment - curvature relationship for columns are based on the axial load level determined from gravity loads, prior to dynamic analysis.

The moment - curvature relationship determined as described above is idealized as two line segments for the purpose of hysteretic modelling. Two criteria were considered in the idealization of the actual curves. First, the idealized curve should be as close as possible to the actual one. Secondly, the areas under the idealized and actual curves should be approximately equal. In beam sections, this can be achieved by passing a line between the ultimate point and a point on the curve having a moment coordinate equal to the average of the ultimate and first yield moment values. The intersection of this line with the line connecting the origin to the first yield point defines the yield point of the curve. This is shown in Figure 5.7. In columns, yielding of the cross section is a progressive phenomenon since there are usually more than one layer of reinforcement on the tension side of the section. This results in a moment - curvature curve relationship with a curved yield region. In addition, spalling of cover concrete is more pronounced in these sections resulting in a drop of capacity between the yield and ultimate points. This can be seen in Figure 5.8. In such cases the curve can be idealized by specifying an average yield curvature and determining the yield moment such that the area under the bilinear idealization and actual curve are equal. Figure 5.8 shows the actual and bilinearly idealized curves for a column section.

Once the moment - curvature relationship for each section is known, the flexural rigidity, EI, can be determined as the ratio between the yield moment and yield curvature. The elastic and post yield stiffnesses of the flexural hysteretic model are determined by calculating the moment - chord rotation relationship of the cantilevers making up the member. This is achieved by determining the curvature distribution along each cantilever at yield and ultimate, and using the moment area theorem to determine the corresponding cantilever tip deflections. The chord rotation is determined as the ratio between the tip deflection and the length of the cantilever. The resulting moment - rotation relationship is used to determine the flexural spring stiffness as outlined in Chapter 4.

5.3.2 Moment - Shear Distortion Relationship

The determination of shear response of reinforced concrete members is not a straight-forward problem. While the section may have ample capacity in shear, yielding of longitudinal reinforcement triggers yielding of the shear force - shear deformation relationship. This has been shown experimentally in a recent study [83]. Response of reinforced concrete members in shear has been determined by the Compression Field Theory [41] in the past. The theory is capable of determining the shear force - shear distortion relationship of a reinforced concrete section by utilizing the equilibrium and compatibility relationships of the section as well as the constitutive laws of steel and concrete. While the method provides a tool for determining the shear response, it underestimates the flexural yield moments [83].

Recently [84], an empirical relationship has been proposed for determining the shear force - shear deflection relationship of reinforced concrete cantilever members. The relationship is based on evaluation of large volume of experimental data. It relates the secant stiffness of the force - displacement relationship at a given displacement, to the initial stiffness and a reference displacement, as shown in Figure 5.9. The estimates of the initial tangent stiffness and the ultimate capacity of the section are needed to use this approach. The following expression describes the relationship:

$$\frac{K_s}{k_{so}} = \frac{1.0}{1.0+0.85\left(\frac{\Delta_s}{\Delta_{rs}}\right)} \tag{5.2}$$

in which; k_s is the secant stiffness between the origin and the point on the curve corresponding to displacement Δ_s, k_{so} is the initial tangent stiffness, and Δ_{rs} is the reference displacement corresponding to the intersection of the initial tangent stiffness and a horizontal line drawn at the capacity of the section.

The shear force- shear displacement relationship obtained using Eq. (5.2) is highly nonlinear in the ascending portion of the curve. This requires idealization of the curve to obtain a clear yield point. Idealization of the shear force - shear displacement curve is carried out in a manner similar to that used for the moment - curvature relationship. Three linear segments are used to represent the actual curve, as shown in Figure 5.10. The first segment connects the origin to the cracking point via the initial tangent stiffness. The force level at the yield point is determined based on the yield moment of the section determined from the plain section analysis. The deformation level at the yield point as well as the post yield slope of the curve, are determined such that the area under the actual and idealized curves are the same.

Once the idealized shear force - shear displacement relationship is known, the idealized moment-shear distortion strain primary curve can be obtained by relating the moments and shear forces via the cantilever length shear span. The resulting moment - shear distortion relationship is used to determine the stiffness of the shear spring as outlined in Chapter 4.

5.3.3 Moment - Anchorage Slip Rotation Relationship

The procedure for determining moment - anchorage slip rotation relationship at the joint of a reinforced concrete frame has been discussed in details in Chapter 2. The procedure is based on performing a sectional analysis at the end of the member near the joint and accounts for elongation as well as slippage of anchored reinforcement steel. The moment - anchorage slip rotation relationship obtained by the procedure described in Chapter 2 shows yielding at a moment corresponding to the onset of strain hardening at the outermost tension steel.

The moment - anchorage slip rotation relationship for a beam section can best be idealized as in the case of moment - curvature relationship, as shown in Figure 5.11. The post yield behavior is idealized by a line segment connecting the ultimate point to a point on the curve with a moment coordinate equals to the average between the ultimate and yield moments. The intersection of this line with the line connecting the origin to the initial yielding of the curve defines the yield point of the idealized curve. The idealized curve thus obtained is a good approximation of the actual curve both in terms of shape and the area under the curve.

The spalling of cover concrete in columns results in a valley shaped segment between the yield and the ultimate points. Hence, connecting the yield point to the ultimate point on the curve would clearly overestimate the post yield capacity of the section. A reasonable idealization of the curve for such sections can be obtained by fixing the yield rotation on the curve, and determining the yield moment such that the area under the actual and idealized curves are approximately the same. Once the yield point is determined, the curve can be idealized by two line segments connecting the origin, yield, and ultimate points as shown in Figure 5.12. The post and pre-yielding slopes of the idealized curve are used to define the elastic and post yield stiffnesses of the slip spring as described in Chapter 4.

Tables 5.4 to 5.6 show the properties of the five, ten and fifteen story frames, respectively.

5.4 Selection of Earthquake Records

In selecting the ground excitation to be used for each frame, it is necessary to consider the frequency characteristics of the ground motion as reflected by the response spectra. It is possible that two different earthquakes with the same intensity excite a given structure differently. The correlation between the response spectrum of a given earthquake record and the fundamental period of the structure is, therefore, very important in selecting earthquake records to be used in the analysis.

In this study, the earthquake records are selected by considering five different accelerograms. The response spectrum for each of these records is shown in Figure 5.13 [85]. The fundamental period of each frame is entered into the response spectra and the most critical earthquake is selected. During seismic, however, it is expected that yielding of some elements will take place, resulting in elongation of fundamental period of vibration. This may lead to another critical earthquake corresponding to the new period. Therefore, in the selection of earthquakes, consideration is given to the change in period of vibration during response by selecting more than one critical earthquakes corresponding to the expected range of the period.

By examining the response spectra shown in Figure 5.13, it can be seen that the spectrum for the

1940 El Centro E-W earthquake peaks over the long and intermediate range of periods. Since the fundamental period of the selected frames fall in this range, this earthquake has been selected for dynamic analysis of selected frames. In addition three other earthquake records, namely; the 1940 El Centro N-S earthquake, the 1952 Taft S69E earthquake, and the 1971 Pacoima Dam S16E earthquake, were used as part of a parametric study.

Chapter 6

Results of Dynamic Analysis

6.1 Introduction

In order to examine the effect of inelastic shear and anchorage slip on the seismic response of reinforced concrete frames, a series of dynamic analyses needs to be carried out. The complete seismic analysis of a given structure can be obtained by defining the physical properties of the structure and the characteristics of the ground motion. In the previous chapter, three reinforced concrete frames were designed, and a critical earthquake was selected based on response spectra analyses. While examining the response of these frames to a specified ground motion would give an indication of the importance of inelastic shear and anchorage slip on response, it is of interest to examine the interaction between the fundamental period of vibration of a structure and the frequency content of earthquake records. In addition, the shear design is expected to have significant effects on inelastic shear response. Therefore, additional analyses are required with different fundamental periods, earthquake records and shear design.

This chapter presents the results of dynamic analyses carried out in this study. First, the results of three frames selected in the previous chapter and subjected to the east-west component of the 1940 El Centro earthquake are presented. This is followed by examining the effects of selected parameters on response. The parameters considered are; period of the frame, characteristic of the ground motion, and the degree of inelasticity imposed by the earthquake. In addition, the effect of shear design is investigated. Three runs were carried out in each case. In the first run, only inelastic flexural deformations were permitted by locking the other springs. In the second and third runs, inelastic shear and anchorage slip deformations were included in the analysis by activating the shear and slip springs, respectively. The results for the three cases are compared by examining a series of response parameters such as; flexural ductility demand, time history of lateral displacement, and envelope values for lateral displacements. In addition, time histories of hinging region deformations as well as hysteretic relationships are presented for a selected number of cases.

6.2 Assumptions Made in the Analysis

The following assumptions were made in the analysis:

1. The mass of the structure consisted of dead load + 25% of live load and was lumped at the joints.
2. Raleigh damping, in which the damping matrix is a combination of mass and stiffness matrices, was assumed.
3. All frame girders were axially rigid. Axial deformations of columns were assumed to remain elastic.
4. The effect of interaction between column axial load and moment on the response of the frames was negligible
5. The column yield moment was approximated based on a constant axial load determined from specified dead load plus 25% of live load.
6. All beam-column joints were properly designed to prevent any joint shear deformations.
7. Inelastic deformations for each member were assumed to be lumped in plastic hinges at the ends of the clear span of the member. Rigid links were used to represent the portion of the member within the joint.
8. The properties of the inelastic flexure and shear springs were based on the behavior of a cantilever with half the length of the member.
9. The ground motion was applied in the plane of the frame. No vertical or torsional effect of ground motions were considered.
10. The frames were built on rigid foundations and were rigidly attached to the

foundation. Therefore, both the effect of soil-structure interaction and foundation uplift, if any, were ignored in this study.

6.3 Results for the Selected Frames

The five, ten, and fifteen story frames selected in Chapter 5 were subjected to the first 10 seconds of the E-W component of the 1940 El Centro earthquake. The peak ground acceleration of the earthquake record was normalized to 0.5g. Each frame was analyzed for three different cases. In the first case, only the flexure type inelastic deformations were permitted to take place. This was accomplished by assigning appropriate inelastic stiffnesses for the flexural springs while assigning very large values for stiffnesses of shear and slip springs throughout the response. In the second case, inelastic shear deformations were permitted in addition to inelastic flexural deformations by assigning appropriate post yield stiffnesses for shear springs while keeping the slip spring stiffnesses very large throughout the response. In the last case, inelastic flexure, shear, and anchorage slip deformations were included by assigning appropriate stiffness values for each spring.

The results are presented in Figures 6.1 to 6.6. Figure 6.1 shows the effect of inelastic shear and anchorage slip on time history of roof displacement for the three frames. As can be seen from this figure, the effect of inelastic shear is nonexistent while anchorage slip has a small effect on both the waveform, as well as the amplitude of displacement. In addition to the time history of roof displacement, the envelopes of lateral displacements were examined in order to show the effect on the overall behavior of the frames. The envelopes for floor displacements is shown for the three frames in Figure 6.2. While the envelope displacement values are slightly affected by anchorage slip, there is no apparent effect of inelastic shear on the response of all three frames.

The effect of inelastic shear and anchorage slip were also examined at the critical regions. This was accomplished by examining the effect on flexural ductility demands at the ends of the girders. Figure 6.3 shows the effect on ductility demand for the three frames. It can be seen from this figure that consideration of anchorage slip in the analysis results in a reduction in the maximum girder ductility demands, ranging from 10% for the five story frame to 21% for the fifteen story frame. Inelastic shear has no effect on flexural ductility demand. The reduction in flexural ductility demand, observed when slip deformations were included, can be attributed to the extra means of energy dissipation induced by hysteretic slip behavior, thus relieving some of the burden on flexural response. Very little energy is dissipated by shear and hence its effect is not apparent. Typical values for the contribution of flexure, shear, and anchorage slip to the dissipation of energy at the critical region of one of the girders of the ten story frame is shown in Figure 6.4. While anchorage slip contributes up to 30% of dissipated energy, the contribution of inelastic shear is very negligible. This is reflected in the area of hysteretic relationships for plastic deformations of flexure, shear and slip springs as shown in Figure 6.5. The corresponding chord rotations are shown in Figure 6.6b. It can be seen from Figure 6.6a and b that although flexural displacements are reduced by including anchorage slip deformations, total displacements remain roughly the same. This is due to the fact that the reduction in flexural displacement is compensated by displacement due to anchorage slip. Hence, the overall displacement is not affected significantly. The absence of shear effect on response can be attributed to high shear rigidity used in the selected structures. Structures with shorter spans and lower shear rigidities may develop higher effect of inelastic shear.

6.4 Parametric Study

A parametric study was conducted to gain more insight into the effects of inelastic shear and anchorage slip on response of reinforced concrete frames. The parameters considered were; period of vibration of the frame, characteristics of the earthquake, degree of damage sustained by the frame, and shear strengths of frame members. A total of 18 different cases, covering a wide range of parameters, were considered. The results of the parametric study are summarized in this section.

6.4.1 Effect of Period of Vibration

The period of vibration is one of the most important parameters controlling response of a structure to a given earthquake. Therefore, the effects of inelastic shear and anchorage slip on response of structures with varying periods of vibration need to be examined. To do so, two different hypothetical ten-story frames were derived from the original ten-story frame, designed in Chapter 5, by changing its mass and/or stiffness. One of the resulting frames had a period of 1.17 seconds, while the other had a period of 2.32 seconds. These frames, together with the original ten story frame (period of 3.2 seconds), were subjected to two earthquake records, namely; the E-W component of El Centro 1940 earthquake, and the S16E component of Pacoima Dam 1971 earthquake. The peak ground acceleration for both earthquakes was normalized to 0.5g.

The results of the analysis for El Centro earthquake are shown in Figures 6.7 to 6.9. It can be seen from these figures that the effect of anchorage slip on the overall behavior of the frames, as reflected in the time history of roof displacement and lateral displacement envelopes, is insignificant. While the waveform of roof displacement remained essentially the same, the amplitude of lateral displacements changed slightly by including anchorage slip. The change in displacement amplitudes is random. While the lateral displacement increased in the 1.17-second frame, it reduced in the 2.32-second frame, and remained roughly the same in the 3.2-second frame. On the other hand, the effect on ductility demand is substantial as shown in Figure 6.9. A reduction in ductility demand of 42% was obtained in the 2.32-second frame when the anchorage slip deformations were considered. It is clear from Figure 6.9 that the reduction in ductility demand increases with the level inelasticity (15.57% for the 3.2-second frame compared to 42% for the 2.32-second frame).

Similar observations can be made for the results of the Pacoima Dam earthquake shown in Figures 6.10 to 6.12. The only noticeable difference between the results of Pacoima Dam and El Centro earthquakes occurred in the waveform of roof displacement for the

1.17-second frame. This is shown in Figure 6.10a. While the amplitude of displacement did not change significantly, the waveform showed a pronounced change when deformations due to anchorage slip were included. The reduction in flexural ductility associated with deformations due to anchorage slip appears to be a function of the level of inelasticity as in previous cases. No effect of inelastic shear is observed on response of any of the three frames considered.

6.4.2 Effect of Ground Motion

It is evident from the results of the initial set of analyses that the interaction of period of vibration with the characteristics of ground motion constitutes a major parameter that controls response. To further examine this observation, the original ten-story frame, with a period of 3.2 second, was subjected to four different earthquakes. These were; the east - west component of El Centro 1940 earthquake, the north - south component of El Centro 1940 earthquake, the S69E component of the 1952 Taft earthquake, and the S16E component of the 1971 Pacoima Dam earthquake. All earthquake records were normalized to a peak ground acceleration of 0.5g. The effect of inelastic shear and anchorage slip on response was re-examined under different earthquake records. The results are given in Figures 6.13 to 6.15.

Examination of the roof displacement time history, shown in Figure 6.13, shows that although the amplitude and waveform of displacement changes from one earthquake record to another, the effect of anchorage slip on both of these quantities is negligible. A similar observation can be made from examining the lateral displacement envelopes in Figure 6.14. The effect of anchorage slip on the envelope values of lateral displacements is seen to be very little and inconsistent. Including anchorage slip in the analysis may increase or decrease the displacement amplitude depending on the earthquake record.

The variation of flexural ductility demand with height, for the four earthquakes considered is shown in Figure 6.15. The E-W component of El Centro earthquake is shown to produce more damage to the frame (as reflected in the maximum ductility demand) while the other earthquakes caused variable damage to a lesser degree. The reduction in ductility demand resulting from including anchorage slip deformations is shown to be dependent on the degree of inelasticity sustained by the frame. A reduction of 21% in the flexural ductility demand was obtained in the case of E-W component of El Centro earthquake. No appreciable effect of inelastic shear is shown in any response quantity for any of the earthquakes considered.

6.4.3 Effect of Intensity of Ground Motion

Examination of results of the previously investigated cases reveals that the effect of anchorage slip on response of frames becomes more apparent when the degree of inelasticity experienced by the structure is high. Hence, the response of the 3.2-second frame was examined for variable intensities of three selected earthquake records, namely; E-W component of El Centro 1940 earthquake, N-S component of El Centro 1940 earthquake, and S69E component of the 1952 Taft earthquake. Two values for the peak ground motion, namely; 0.5g and 0.65g, were used for the E-W component of El Centro earthqauke. Increasing the peak ground acceleration beyond 0.65g for this record resulted in unrealistically large ductility values at some joints signalling structural collapse. Hence this was not pursued. Three values of peak acceleration were used for the other two earthquakes. These were 0.5g, 0.75g, and 1.0g. It is not likely that an earthquake having a peak ground acceleration of 1.0g would ever take place. However, the emphasis here is on the degree of inelasticity sustained by the frame, regardless of the practicality of the earthquake record used.

The results of the analysis for the three earthquakes are shown in Figures 6.16 to 6.24. It can be seen from these figures that the effect of anchorage slip on lateral displacement is negligible. While the amplitudes of displacements increased with increasing the earthquake intensity, the effect of anchorage slip on the overall behavior of the frames did not increase significantly by increasing the intensity of ground motion. However, the effect on ductility demand increased by increasing the intensity of ground motion. Increasing the intensity of ground motion resulted in an increase in the amount of energy dissipated by anchorage slip in terms of fraction of the total dissipated energy. The percentage reduction in flexural ductility due to consideration of anchorage slip increased from 16% to 20% by increasing the peak ground acceleration from 0.5g to 0.65g in the case of E-W El Centro record. For the N-S component of El Centro and Taft records, the increase is more substantial. Increasing the peak acceleration from 0.5g to 1.0g increased the reduction in ductility from 6% to 15% and from 8% to 17% for El Centro N-S and Taft earthquakes, respectively. The effect of inelastic shear is not apparent in all cases.

6.4.4 Shear Rigidity and Shear Strength

In the previous analyses, the shear rigidity of frame members was based on an effective shear area of 0.833 of the gross sectional area. While the use of such effective shear area has been recommended by researchers [86], it is of interest to determine the effect of inelastic shear on the behavior of frames in light of variation in the shear rigidity. To do so, the basic ten-story frame (T = 3.2 seconds), was analyzed under the first 10 seconds of the E-W component of El Centro 1940 earthquake with the shear rigidity of members reduced to 30% of the gross shear rigidity. The frame was analyzed for three case. In the first case, elastic shear deformations were included together with inelastic flexural deformations. In the second and third cases, inelastic shear and inelastic shear with anchorage slip deformations were included, respectively. The results are compared with those of 83% shear rigidity as shown in Figures 6.25 to 6.27. These figures show that even with a reduced shear rigidity, equals to 30% of the gross, the behavior of the frame is controlled by flexure and anchorage slip, and the effect of inelastic shear is nonexistent.

In addition to the shear rigidity, the shear capacity of the section is a likely candidate for playing a role on the effect of inelastic shear on response. In most seismic design codes, the requirements for shear design are such to insure flexural yielding prior to shear yielding. Hence shear yielding in such cases is triggered by flexural yielding. However, in poor shear design cases, shear yielding may take place prior to flexural yielding. This case was investigated by analyzing the 3.2 second structure. In this case the shear yield capacity was reduced to 75% of that corresponding to flexural yielding. The results are compared in Figures 6.28 to 6.31 with those of the properly shear designed structure in which yielding of shear was triggered by flexural yielding although the shear capacity provided was in excess of that corresponding to flexural capacity.

Figure 6.28a and 6.28b show the hysteretic relationships for flexure and shear chord rotations for the cases of proper and poor shear design. It is clear from Figure 6.28b that shear behavior enters the inelastic range in the positive direction at a moment value of 133 kN. m., while yielding of flexure takes place at a moment of 178 kN. m. Therefore, the member behaves inelastically in shear while behaving elastically in flexure between these two moment values. This resulted in high shear ductility demand for the poorly shear designed structure. The maximum girder shear ductility demand increased from approximately 2.7 for the well shear designed case to approximately 8.5 for the poorly shear designed case. The hysteretic shear force - shear distortion relationship for the poorly designed structure also shows severe pinching of the loops during reloading in both directions. Despite the high ductility demand obtained for shear, the effect on flexural ductility demand and the overall behavior of the frame is still negligible as depicted in Figures 6.29 to 6.31.

6.4.5 Concluding Remarks

From all the cases investigated in this study it is clear that inelastic shear deformations have little or no effect on the behavior of frames selected for this investigation. While this observation can be generalized for structures with span lengths similar to or greater than those used in this study, it is likely that frames with shorter spans could show a more pronounced effect of inelastic shear deformations. Such cases have not been investigated in this study. On the other hand, the effect of anchorage slip deformations are apparent in all cases. The degree of effect on the response, however, depends on the interaction of period of vibration with the characteristics of ground motion. While some frames showed a significant effect of anchorage slip under a given earthquake, the effect was diminished under another earthquake. The most significant effect with implications on practice is that on flexural ductility demand. Including anchorage slip in the analysis results in a reduction of flexural ductility demand in the range of 6% to 42%. The overall displacement ductility was not significantly affected.

The effect of anchorage slip on response of frames is believed to be due to two major factors. One is the fact that allowing anchorage slip deformations change dynamic characteristics of the frame and hence its period of vibration. This results in a more flexible frame, behaving differently than otherwise. The second is that hysteretic behavior of anchorage slip deformations provides additional means of energy dissipation. This indicates that consideration of anchorage slip in the analysis relieves some of the burden from flexural action. The total energy dissipation which would have been provided by flexural hysteresis alone, is shared between anchorage slip and flexural hysteresis. In some cases up to 30% of total dissipated energy is provided by anchorage slip. This relief in energy dissipation demand results in a reduction in the amplitude of flexural chord rotations, and hence a reduction in the flexural ductility demand.

Chapter 7

Summary and Conclusions

7.1 Summary

The objective of this study was to determine the significance of inelastic shear and anchorage slip deformations on seismic response of moment-resisting reinforced concrete frames. The emphasis was placed on modelling flexural, shear, and anchorage slip deformations for inelastic dynamic analysis of frames. The study has been divided into four stages.

In the first stage, a comprehensive review of previous experimental and analytical work on inelastic behavior of reinforced concrete structures, as well as in the subject of modelling reinforced concrete members for dynamic analysis was carried out. The review revealed that inelasticity in reinforced concrete members is a potential source of energy dissipation and inelastic dynamic analysis is needed in order to gain more insight into the behavior of these structures. It also revealed that there are three main sources of inelastic deformations in the critical regions of reinforced concrete structures. These consist of, inelastic flexure, shear, and anchorage slip deformations. While the-state-of-the-art provides ample information for modelling reinforced concrete members for inelastic flexural analysis, there is lack of hysteretic models for inelastic shear and anchorage slip. A hysteretic model for shear was proposed only recently. The model has not been previously used for inelastic dynamic analysis. On the other hand, the efforts to model anchorage slip deformations ranged from a simple model, in which a constant bond stress is assumed throughout the development length of the anchoring steel, to a tedious but a more accurate model based on numerical techniques. No other reliable and reasonably simple hysteretic model had been proposed for anchorage slip.

A simplified hysteretic moment-slip rotation model was developed in the second stage. The model consists of a primary curve and a set of hysteretic rules based on experimental observations. The primary curve is determined by first examining the behavior of single bars embedded in concrete. From conventional sectional analysis at the critical section of the member, the internal tensile force in the extreme tension steel can be determined. Deformation of the tensile reinforcement is determined in two parts; extension, and slippage of the bar. For straight anchorage, the reinforcement extension part is determined by assuming constant average bond along the elastic portion and frictional bond along the plastic portion of the embedment length. If the bar is stressed to its end, slippage of the bar as a whole takes place. A previously derived local bond-slip model is applied at the end of the bar to determine the amount of slippage. For hooked bars, the applied load is resisted by the lead-in length and the hook. The lead-in length is treated as in the case of straight embedment. If the lead-in length is not sufficient to resist the applied load, the hooked portion of the bar contributes to the resistance. A previously derived force - deformation relationship for hooks is used to determine the hook deformation. Provisions have been made for bars of interior joints by considering the behavior of bars subjected to pull from one end and push from the other. Yield penetration in the compression side of interior joints was neglected. Since the yield force in the top steel of interior joints is usually higher than the yield force of bottom steel, and since cracks are expected to develop throughout the depth of the member after few inelastic cycles, the compression force in the top steel of interior joints can be limited to the tensile yield force of the bottom steel. Bar slip in interior joints is determined from the local bond-slip model as in the case of straight bars of exterior joints. The value of bond stress to be entered in the local bond - slip model is determined based on the tension and compression forces at the ends of the elastic portions of the bar. Once the total deformation of the outmost tension steel is known, rotation due to anchorage slip is determined by assuming the center of rigid body rotation to be located at the neutral axis. Unloading from the primary curve is determined by considering recovered and unrecovered deformations. All deformations resulting from plastic strains and slippage of the bar are considered unrecoverable. The primary curve of the model is idealized as two linear segments with a break point at the yield point. Sectional analysis at the yield point of the curve and at a point on the post yield branch is needed to determine the elastic and post yield slopes of the curve. Therefore, only little computational effort over and above that required for flexure, is needed to define the idealized monotonic moment-slip rotation curve. The model was generalized by applying empirically derived rules for reloading branches. It is applicable to both exterior and interior joints having hooked or straight anchorages. No strength degradation effect is considered in the model. Analytical predictions based on the proposed procedure showed good agreement when compared with results of tests conducted on single bars as well as large scale interior and exterior joints. The model showed limitations when applied to specimens subjected to bi-directional loading.

In the third stage, the proposed hysteretic model for anchorage slip was implemented in the computer program Drain-2D together with the recently developed shear hysteretic model. This was accomplished by modifying the one component model that was used in Drain-2D for member modelling. Two additional springs were added at each end of the one component model. One spring was assigned the hysteretic model for shear while the other was assigned the hysteretic model for anchorage slip. This required the addition of two major subroutines to the original program to trace out the nonlinearity in both the shear and slip springs. The program was also enhanced by adding calculations of individual flexure, shear, and slip ductility demands, as well as the overall displacement ductility demand. Calculations of individual and total dissipated energies were also added to the program. Other related input/output features of the program were also enhanced.

In the final stage of the study, the enhanced computer program was used to determine the effect of inelastic shear and anchorage slip on response of moment resisting reinforced concrete frames. Three frames were designed based on the requirements of the 1990 National Building Code of Canada [26] and Canadian Standard CAN3-A23.3-M84 for design of concrete structures [25]. A parametric study was also conducted to further investigate the effects of anchorage slip and shear inelasticity. The parameters considered were; period of vibration of frame, characteristics and intensity of ground motion, and shear rigidity and shear strength of frame members. Results of dynamic analysis indicated that anchorage slip had a pronounced effect on flexural ductility demands of girders. Reduction in flexural ductility demand of up to 42% was obtained in some cases. The amount of reduction in ductility was found to be influenced by the degree of inelasticity experienced by the structure. For a given period of vibration and a given earthquake motion, the percentage reduction in ductility demand generally increased with the increase of inelasticity in the critical regions. The reduction in flexural ductility demand was also found to vary with the ground motion. The interaction between the fundamental period of structure and the frequency characteristics of ground motion has led to varying degree of effects of anchorage slip on flexural ductility demand. The effect on the overall behavior of frames as reflected in the displacement time history and amplitude was less pronounced. Only one case out of the 18 different cases that were investigated, showed a notable variations in the displacement time history. On the other hand, the effect of inelastic shear on the behavior of frames was negligible in all cases. Even in the case of inadequate shear design, in which shear yielding took place prior to flexural yielding, the effect of inelastic shear on the behavior of critical regions as well as the overall behavior of the frame was negligible.

7.2 Conclusions

The following conclusions can be drawn from the present study:

1. The analytical approach for anchorage slip deformations developed in this research program, can be used to compute non-linear response of reinforced concrete structures both under monotonic and cyclic loadings. The proposed hysteretic model for anchorage slip provides a convenient tool for seismic analysis. The model is reasonably accurate and retains a degree of simplicity that is compatible with previous hysteretic models for flexure and shear.

2. The multiple-spring-one-component model, employed in this investigation, can be used effectively to conduct dynamic inelastic analysis of reinforced concrete structure, where inelasticity due to flexure, shear and anchorage slip is allowed for separately. The advantage of the multiple-spring-model is that the inelastic deformations components and associated ductility demands can be computed separately, permitting a more rational assessment of structural response.

3. The contribution of anchorage slip to total deformations is significant in the critical regions of reinforced concrete members. Up to 38% of total deformations in the critical regions are attributed to anchorage slip. This was also observed in previous quasi-static tests.

4. Including anchorage slip deformations in inelastic analysis of reinforced concrete frames may result in substantial reductions in flexural ductility demands. Up to 42% reduction in ductility have been obtained in some cases. The degree of reduction in flexural ductility demand increases with an increase in inelasticity. This implies that structural design and detailing may be largely in error if they are based on dynamic analysis where inelastic deformations due to anchorage slip are ignored.

5. The effect of anchorage slip on overall displacement amplitudes of reinforced concrete frames is not significant. However, The waveform of displacement time history may be affected significantly depending on the interaction between the frequency characteristics of the structure and the ground motion. While a given frame shows a considerable effect of anchorage slip when subjected to a particular earthquake, the effect could be less pronounced for another type of ground motion.

6. Allowing inelastic shear deformations in dynamic inelastic analysis of reinforced concrete frames does not produce a significant change in response. In eighteen cases considered in this investigation, neither the behavior of critical regions nor the overall response was affected by inelastic shear deformations.

7. Deformations due to anchorage slip contribute significantly to the dissipated energy at the critical regions. Up to 30% of total dissipated energy is provided by anchorage slip. The contribution of inelastic shear deformations to dissipated energy is negligible.

8. The effect of anchorage slip on flexural ductility demand increases by increasing the intensity of ground motion. Increasing the intensity of ground motion results in an increase in the amount of energy dissipated by anchorage slip in terms of total dissipated energy.

9. The effect of shear rigidity and shear strength on the inelastic response of the selected frames is negligible. Reducing shear rigidity to 30% of its gross value and shear capacity to 75% of flexural capacity results in no appreciable effect of inelastic shear on response.

7.3 Recommendation for Further Research

The following recommendations are made for future research:

1. The effect of anchorage slip and inelastic shear needs to be investigated under variable axial loads. Hence, the computer software needs to be enhanced to include the P - M interaction effect.

2. Other types of structures having shorter spans than the frames considered in this study need to be investigated. The effect of inelastic shear and anchorage slip on the behavior of coupled shear walls and shear wall - frame interactive systems is of interest.

3. The one component model used in this study is attractive due to its simplicity and versatility. The drawbacks of the model inherent in the assumption that plastic deformations are localized at member ends and that plastic deformations at one end depends on the action at that particular end only, needs to be investigated. It would be

interesting to compare the results obtained in this study using the one component model with those obtained using models that recognize the spread of inelasticity such as the super girder model.

4. A parametric study aimed at investigating the effects of modelling parameters on response of reinforced concrete structures is needed. Potential parameters for this study are; variations on post yield slopes of both shear and anchorage slip models, pinching of both shear and anchorage slip models, as well as having a linear instead of a bi-linear unloading branch in the anchorage slip model. Simplifications of both of these models is possible based on a such parametric study.

Bibliography

[1] Penzien, J., "Dynamic Response of Elasto-Plastic Frames," Journal of the Structural Division, American Society of Civil Engineers, Vol. 86, No. ST7, July 1960, pp. 81-94.

[2] Berg, G. V., "Response of Multi-Story Structures to Earthquake," Journal of the Structural Division, American Society of Civil Engineers, Vol. 87, No. EM2, April 1961, pp. 1-16.

[3] Clough, R. W., and Benuska, M., " Nonlinear Behavior of Tall Buildings," Journal of the Engineering Mechanics, American Society of Civil Engineers, Vol. 93, No. EM3, June 1967, pp. 129-146.

[4] Goel, S. C., and Berg, G. V., "Inelastic Earthquake Response of Tall Steel Frames," Journal of the Structural Division, American Society of Civil Engineers, Vol. 94, No. ST8, August, 1968, pp. 1907-1932.

[5] Suko, A. M., and Adams, P. F., "Dynamic Analysis of Multistory Frames," journal of the Structural Division, American Society of Civil Engineers, Vol. 97, No. ST10, October, 1971, pp. 2519-2533.

[6] Clough, R. W., " Effect of Stiffness Degradation on Earthquake Ductility Requirements," Report No 66-16, Structures and Material Research, Structural Engineering Laboratory, University of California, Berkeley. Oct. 1966, P. 67.

[7] Takeda, T., Sozen, M. A., and Nielsen, N. N., "Reinforced Concrete Response to Simulated Earthquakes," Journal of the Structural Division, American Society of Civil

Engineers, Vol.96, ST4, Dec. 1970, pp. 2557-2573.

[8] Chopra, A. K., and Christopher, K., "Effects of Stiffness Degradation on Ductility Requirements for Multistory Buildings," Journal of Earthquake engineering and Structural Dynamics, Vol. 2, 1973, pp. 35-45.

[9] Otani, S., and Sozen, M., " Behavior of Multistory Reinforced Concrete Frames During Earthquake," Structural Research Series No. 392, University of illinois, Urbana, Illinois, 1972, P. 551.

[10] Otani, S., "Analysis of Reinforced Concrete Frame Structures," Journal of the Structural Division, American Society of Civil Engineers, Vol. 100, No. ST7, July, 1974, pp. 1433-1449.

[11] Takayanagi, T., and Schnobrich, W. C., " Computed Behavior of Reinforced Concrete Shear Walls," Structural Research Series No. 434, University of Illinois, Urbana, Dec. 1976, P. 192.

[12] Anderson, J. C., and Townsend, W. H., "Models for Reinforced Concrete Frames with Degrading Stiffness," Journal of the Structural Division, American Society for Civil Engineers, Vol. 103, No. ST12, December, 1977, pp. 2361-2376.

[13] Soleimani, D., Popov, E. P., and Bertero, V. V., "Hysteretic Behavior of Reinforced Concrete Beam - Column Subassemblages," ACI Journal, Vol. 76, No. 11, Nov. 1979, 1179-1194.

[14] Emori, K., and Schnobrich, W. C., "Dynamic Analysis of Reinforced Concrete Frame-Wall Structures," Journal of Engineering Structures, Vol. 2, April, 1980, pp. 103-112.

[15] Emori, K., and Schnobrich, W. C., "Inelastic Behavior of Concrete Frame-Wall Structures," Journal of the Structural Division, American Society of Civil Engineers, Vol. 107, No. ST1, January, 1981, pp. 145-164.

[16] Humar, J., " Seismic Response of Reinforced Concrete Frames," Journal of the Structural Division, American Society of Civil Engineers, Vol. 107, No. ST7, July, 1981, pp. 1215-1232.

[17] Banon, H., Biggs, J. M., and Irvin, H. M., "Seismic Damage in Reinforced Concrete Frames," Journal of the Structural Division, American Society of Civil Engineers, Vol. 107, No. ST9, September, 1981, pp. 1713-1729.

[18] Saatcioglu, M., Derecho, A. T., and Corley, W. G., "Modelling Hysteretic Behavior of Coupled Walls for Dynamic Analysis, "Earthquake Engineering and Structural Dynamics, Vol. 11, 1983, pp. 711-726.

[19] Keshavarzian, M., and Schnobrich, W. C., "Inelastic Analysis of Reinforced Concrete Coupled Shear Walls," Journal of Earthquake Engineering and Structural Dynamics, Vol. 13, 1985, pp. 427-448.

[20] Saiidi, M., "Hysteresis Models for Reinforced Concrete," Journal of the Structural Division, American Society of Civil Engineering, Vol. 108, No. ST5, May, 1982.

[21] Al-Haddad, M., and Wight, J. K., "Relocating Beam Plastic Hinges Zones for Earthquake Resisitant Design of Reinforced Concrete Buildings," ACi structural Journal, March-April 1988.

[22] Filippou, F., and Issa, A., "Nonlinear Analysis of Reinforced Concrete Frames Under Cyclic Load Reversals," Earthquake Engineering Research Center, University of California, Berkeley, Report No. UCB/EERC - 88/12, September, 1988, P. 120.

[23] Paultre, P., and Mitchell, D., "Evaluation of Seismic Performance of of Concrete Frames Structures in Canada," Structural Engineering Series Report No. 87-4, McGill University, Montreal, 1987.

[24] Paultre, P., and Mitchell, D., "Assessment of Some Canadian Seismic Code Requirements for Concrete Frame Structures," Canadian Journal of Civil Engineering, Vol. 18, No. 3, 1991, pp. 343-357.

[25] CSA Standard CAN3-A23.3-M84, "Design of Concrete Structures for Buildings," Canadian Standard Association, Rexdale, Ontario, December 1984

[26] "National Building Code of Canada," National Research Council of Canada, Ottawa, 1990.

[27] Clough, R. W., Benuska, K. L., and Wilson, E. L., "Inelastic Earthquake Response of Tall Buildings," proceedings, Third World Conference on earthquake engineering, New Zealand, Vol. II, session II, 1965, pp. 68-89.

[28] Otani, S., "Nonlinear Dynamic Analysis of Reinforced Concrete Building Structures," Canadian Journal of Civil Engineering, Vol. 7, No. 2, 1980. pp. 333-344.

[29] Giberson, M., "Two Nonlinear Beams with Definition of Ductility," Journal of the Structural Division, American Siciety of Civil engineers, Vol. 95, No. ST2, February, 1969.

[30] Takizawa, H., "Notes on Some Basic Problems in Inelastic Analysis of Planar Reinforced Concrte Structures - Part I," Transaction of the Architectural Institute of Japan, No. 240, February, 1976, pp. 51-62.

[31] Roufaiel, M. S., and Meyer, C., "Analytical Modelling of Hysteretic Behavior of

Reinforced Concrete Frames," Journal of the structural Engineering, American Society of Civil Engineering, Vol. 113, No. 3, March, 1987, pp. 429-444.

[32] Bertero, V. V., Bresler, B., and Liao, H., "Stiffness Degradation of Reinforced Concrete Members Subjected to Cyclic Flexural Moments," Earthquake engineering Research Center, Report No. 69-12, University of California, Berkeley, December, 1969, P. 115.

[33] Popov, E. P., Bertero, V. V., and Krawinkler, H., "Cyclic Behavior of Three Reinforced Concrete Flexural Members with High Shear," Earthquake Engineering Research Center, Report No. EERC 72- 5, University of California, Berkeley, October, 1972, P. 78.

[34] Bertero, V. V., Popov, E. P., and Wang, T. Y., " Hysteretic Behavior of Reinforced Concrete Flexural Members with Special Web Reinforcement," Earthquake Engineering Research Center, Report No. EERC 74-9, University of California, Berkeley, August, 1974, P. 125.

[35] Bertero, V. V., and Popov, E. P., " Hysteretic Behavior of Ductile Moment Resisting Reinforced Concrete Frame Components," Earthquake Engineering Research Center, Report No. EERC 75-16, University of California, Berkeley, April 1975.

[36] Imbeault, F., and Nielsen, N., " Effect of Degrading Stiffness on the Response of Multistory Frames Subjected to Earthquakes," Proceedings of Fifth world Conference on Earthquake Engineering, Italy, 1973.

[37] Kanaan, A., E., and Powell, G. H., "Drain-2D User's Manual," Earthquake Engineering Research Center, Report No. EERC 73-22, University of California, Berkeley, 1973.

[38] Takayanagi, T., Derecho, A. T., and Corley, W. G., "Analysis of Inelastic Shear Deformation Effects in Reinforced Concrte Structural Wall Systems," Nonlinear Design of Concrete Structures, proceedings of the CSCE-ASCE-ACI-CEB International Symposium, University of Waterloo, Ontario, 1979, pp. 545-579.

[39] Riddell, R., and Newmark, N. M., "Force-Deformation Models for Nonlinear Analysis," Journal of the structural Division, American Society of Civil Engineering, Vol. 105, No. ST12, December, 1979, pp. 2773-2777.

[40] Ozcebe, G., and Saatcioglu, M., "Hysteretic Shear Model for Reinforced Concrete Members," Journal of the Structural Division, American Society of Civil Engineering, Vol. 15, No. 1, January, 1989, pp. 132-148.

[41] Collins, M., and Michell, D., "Shear and Torsion Design of Prestressed and Non-Prestressed Concrete Beams," PCI Journal, V.25, No.5, September-October, 1980, pp. 32-100.

[42] Brown, R. H., and Jirsa, J. O., "Reinforced Concrete Beams Under Load Reversals," ACI Journal, Proceedings, V. 68, No. 5,May, 1971, pp. 380-390.

[43] Ismail, H., and Jirsa, J. O., "Behavior of Anchored Bars under Cyclic Overloads Producing Inelastic Strains," ACI Journal,Vol. 69, No.7, pp. 443-438, July, 1972.

[44] Saatcioglu, M., and Ozcebe, G., "Effect of Bar Slip on Hysteretic Behavior of Concrete Columns," Proceedings, 5th Canadian Conference on Earthquake Engineering, Ottawa, Canada, July, 1987, pp. 833-839.

[45] Townsend, W. H., and Hanson, R. D., " Hysteretic loops for Concrete Beam - Column Connections," Fifth World Conference on Earthquake Engineering, Paper 137, Session 3D, Rome 1973.

[46] Viwathanatepa, S., Popov, E. P., and Bertero, V. V., "Seismic Behavior of Reinforced Concrete Interior Beam - Column Subassamblages," Earthquake Engineering Research Center, Report No. EERC 79-14, University of California, Berkeley, July, 1979.

[47] Seckin, M., "Hysteretic Behavior of Cast - In - Place Exterior Beam - Column Subassemblies," Ph. D. Thesis, Department of Civil Engineering, University of Toronto, 1981.

[48] Ehsani, M. R., and Wight, J. K., "Effect of Transverse Beams and Slab on the Behavior of Reinforced Concrete Beam-Column Connections," ACI Journal, Vol. 82, No. 2, March-April, 1985.

[49] Durrani, A. J., and Wight, K. L., "Behavior of Interior Beam - Column connections Under Earthquake Type Loadng," ACI Journal, Vol. 82, No. 3, May-June, 1985.

[50] Paulter, P., Castele, D., Rattray, S., and Mitchell, D., "Seismic Response of Reinforced Concrete Frame Subassemblages - A Canadian Code Perspective," Canadian Journal of Civil Engineering, Vol. 16, No. 5, 1989, pp. 627 - 649.

[51] Hassan, F. M. and Hawkins, N. M., " Effect of Post-Yield Loading Reversals on Bond Between Reinforcing Bars and Concrete," Report No. SM 73 - 2, Department of Civil Engineering, University of Washington, Seatle, Washington, March, 1973.

[52] Minor, J., and Jirsa, J. O., " Behavior of Bent Bar Anchorages," ACI Journal, Proceedings, Vol. 72, No. 4, April, 1975, pp. 141-149.

[53] Marques, J. L., and Jirsa, J. O., " A study of Hooked Bar Anchorages in Beam - Column Joints," ACI Journal, Vol. 72, No. 5, May, 1975, pp. 198-209.

[54] Bertero, V. V., Popov, E. P., and Viwathanatepa, S. " Bond of Reinforcing Steel:

Experimental and Mechanical Model," Paper Presented at the IASS Symposium on Nonlinear Behavior of Reinforced Concrete Spatial Structures, Vol. 2, pp. 3-17, Darmstadt, West Germany, July, 1978.

[55] Viwathanatepa, S., Popov, E. P., and Bertero, V. V., "Effects of Generalized Loadings on Bond of Reinforcing Bars Embedded in Confined Concrete Blocks," Earthquake Engineering Research Center, University of California, Berkeley, Report No. EERC 79-22, Aug. 1979

[56] Eligehausen, R., Popov, E. P., and Bertero, V. V., "local Bond Stress - slip Relationships of Deformed Bar under Generalized Excitations," Earthquake Engineering Research Center, University of California, Berkeley, Report No. 83/23, Oct. 1983.

[57] Ueda, T., Lin, I., and Hawkins, N. M., "Beam Bar Anchorages in Exterior Column - Beam Connections," ACI Journal, Vol. 83, No., 3, May - June, 1986.

[58] Hawkins, N. M., Lin, I., and Ueda, T., "Anchorages of Reinforcing Bars for Seismic Forces," ACI Structural Journal, September - October, 1987.

[59] Soroushian, P., Obaseki, K., Nagi, M., and Rojas, M., "Pull out Behavior of Hooked Bars in Exterior Beam - Column Connections," ACI Structural Journal, Vol. 82, No. 3, May - June, 1988.

[60] Soroushian, Parviz; and Choi, Ki-Bong, "Local Bond of Deformed Bars with Different Diameters in Confined Concrete," ACI Structural Journal, Vol. 86, No. 2, March-April 1989.

[61] Pochanart, S., and Harmon, T., "Bond Slip Model for Generalized Excitations Including Fatigue," ACI Material Journal, V. 86, No. 5, September - October, 1989

[62] Somayaji, S., and Shah, S. P., "Bond Stress Versus Slip Relationship and Cracking Response of Tension Members," ACI Journal, Vol. 78, No. 3, May - June, 1981.

[63] Tassios, T. P., and Yannopoulos, P. J., "Studies on Reinforced Concrete Members under Cyclic Loadings Based on Bond Stress - Slip Relationships," ACI Journal, Vol. 78,No. 3, May - June, 1981.

[64] Ciampi, V., Eligehausen, R., Bertero, V. V., and Popov, E. P., "Analytical Model for Deformed Bar Bond under Generalized Excitation," IABSE Colloquin. Advanced Mechanics of Reinforced Concrete, Final Report, Delft, June, 1981.

[65] Ciampi, V., Eligehausen, R., Bertero, V. V., and Popov, E. P., "Analytical Model for Concrete Anchorage of Reinforcing Bar Under Generalized Excitation," Earthquake Engineering Research Center, University of California, Berkeley, Report No. 82/23, Nov. 1982.

[66] Filippou, F. C., Popov, E. P., and Bertero, V. V., "Effect of Bond Deterioration on Hysteretic Behavior of Reinforce Concrete Joints," Earthquake Engineering Research Center, University of California, Berkeley, Report No. EERC 83/19, August, 1983.

[67] Filippou, F. C., Popov, E. P., and Bertero, V. V., "Modelling of Reinforced Concrete Joints Under Cyclic Excitations," ASCE, Vol. 109, No. 11, Nov. 1983.

[68] Filippou, F. C., "A Simple Model for Reinforcing Bar Anchorages under Cyclic Excitations," Earthquake Engineering Research Center, Report No. EERC 85/05, University of California, Berkeley, March, 1985.

[69] Morita, S., and Kaku, T., "Slippage of Reinforcement in Beam - Column Joint of Reinforced Concrete Frames," Proceedings, 8th World Conference on Earthquake Engineering, San Francisco, V. 6, 1984 pp. 477-484.

[70] Sheik, S. A., and Uzumeri, S. M., "Analytical Model for Concrete Confined in Tied Columns," Journal of the Structural Division, ASCE, Vol. 108, ST12, Dec. 1982, pp. 2703-2722.

[71] Park, R., Priestley, M. J. N., and Gill, W. P., "Ductility of Square Confined Concrete Columns," Journal of the structural Division, ASCE, Vol. 108, ST4, April 1982, pp. 929-950.

[72] Saatcioglu, M., and Razvi, S., "Strength and Ductility of Confined Concrete," Journal of the Structural Division, ASCE, Vol. 118, No. 6, 1992, pp. 1590-1607.

[73] Lutz, L., and Gergely, P., "Mechanics of Bond and Slip of Deformed Bars in Concrete," ACI Journal, Vol. 64, No. 11, November, 1967, pp. 711-721.

[74] Lutz, "Analysis of Stress in Concrete Near a Reinforced Bar Due To Bond and Transverse Cracking," ACI Journal, Vol. 67, No. 10, October, 1970

[75] Goto, Y., "Cracks Formed in Concrete Around Tension Bars," ACI Journal, Proceedings Vol. 68, No. 4, April 1971.

[76] ACI Committee 408, "Suggested Development, Splice, and Standard Hook Provision for Deformed Bars in Tension," ACI 408.1R.79, American Concrete Institute, Detroit, Michigan, 1979, 3pp.

[77] Shaik, A. F., and Yi, W. "In Place Strength of Welded Headed Studs," PCI Journal, V. 30, No. 21, March/April, 1985.

[78] Prestressed Concrete Institute," PCI Design Handbook - Precast and Prestressed Concrete," PCI, Chicago, pp. 6-6 to 6-8.

[79] Jirsa, J. O., and Marques, J. L. G., " A Study of Hooked Bar Anchorages in Beam-Column Joints," University of Texas at Austin,Report on Project 33, July, 1972, 86 pages.

[80] Humar, J. L., "Dynamics of Structures," Prentice-Hall Inc., Englewood cliffs, New Jersey, 1990.

[81] Clough, R. W., and Penzien, J., "Dynamics of Structures," Mc Graw-Hill, New York, 1975.

[82] "Concrete Design Handbook," Canadian Portland Cement Association, Ottawa, Ontario, 1985, pp. 11-1 to 11-20.

[83] Ozcebe, G., "Inelastic Response of Reinforced Concrete Columns under Unidirectional and Bidirectional Loading revesals," Ph. D. Thesis, University of Toronto, Toronto, Canada, 1987.

[84] Ozcebe, G., and Hakan, B., "Modelling of the Hysteretic Flexural and Shear Response of R/C Members Subjected to Simulated Seismic Loading," Proceedings, Ninth European Conference on Earthqauke Engineering, Moscow, 1990.

[85] Saatcioglu, M., Derecho, A. T., and Corley, W. G.," Coupled Walls in Earthquake-Resistant Buildings - Modelling Techniques and Dynamic Analysis," Construction Technology Laboratories, Portland Cement Association, Skokie, Illinois, June, 1980.

[86] Park, R., and Paulay, T.," Reinforced Concrete Structures," John Wiley & Sons, Inc., 1975.

Table 5.1 Sectional Sizes and Reinforcement Arrangement for the Five-Story Frame

Floor	Beam Section	Column Section	
		Interior Columns	Exterior Columns
1-4	300 by 600 with 6#15 top 4#15 bottom	500 by 500 with 12#20	400 by 400 with 12#20
5	300 by 600 with 5#15 top 3#15 bottom	500 by 500 with 12#20	400 by 400 with 12#20

Table 5.2 Sectional Sizes and Reinforcement Arrangement for the Ten-Story Frame

Floor	Beam Section	Column Section	
		Interior Columns	Exterior Columns
1-9	300 by 600 with 8#15 top 4#15 bottom	550 by 550 with 8#25	450 by 450 with 8#25
10	300 by 600 with 5#15 top 3#15 bottom	550 by 550 with 8#25	450 by 450 with 8#25

Note: All dimensions are in mm.

Table 5.3 Sectional Sizes and Reinforcement Arrangement for the Fifteen-Story Frame

Floor	Beam Section	Column Section	
		Interior Columns	Exterior Columns
1-5	300 by 600 with 10#15 top 5#15 bottom	550 by 550 with 12#25	450 by 450 with 8#25
6-14	300 by 600 with 10#15 top 5#15 bottom	550 by 550 with 8#25	450 by 450 with 8#25
15	300 by 600 with 6#15 top 4#15 bottom	550 by 550 with 8#25	450 by 450 with 8#25

Note: All dimensions are in mm.

Table 5.4 : Properties of the Five-Story Frame

Fundamental Period	1.96 s
Height	20 m
V/W	0.032
Beams Stiffness Parameters	
Floor Girders	
EI	36,329 kN.m^2
GA	1,463,313 kN
EA	4,676,537 kN
Roof Girders	
EI	30,312 kN.m^2
GA	1,463,313 kN
EA	4,676,537 kN
Columns Stiffness Parameters	
Exterior Columns	
EI	9,442 kN.m^2
GA	1,190,784 kN
EA	4,156,922 kN
Interior Columns	
EI	21,405 kN.m^2
GA	1,973,366 kN
EA	6,495,191 kN
Beams Yield Moments	
Floor Girders	
Positive Yield Moment	178.58 kN.m
Negative Yield Moment	263.67 kN.m
Roof Girders	
Positive Yield Moment	136.38 kN.m
Negative Yield Moment	220.16 kN.m
Columns Yield Moments[1]	
Exterior Columns	249.2 kN.m
Interior Columns	450.89 kN.m
Ground Motion	
Intensity	0.5g
Duration	10 seconds
Mass	
Floors	60.461 tons
Roof	44.469 tons

[1]Values given are for ground floor columns. Values for upper-story columns are determined base on the applicable axial load in each column.

Table 5.5 : Properties of the Ten-Story Frame

Fundamental Period	3.21 s
Height	40 m
V/W	0.023
Beams Stiffness Parameters	
Floor Girders	
EI	39,735 kN.m^2
GA	1,441,662 kN
EA	4,676,537 kN
Roof Girders	
EI	30,312 kN.m^2
GA	1,463,313 kN
EA	4,676,537 kN
Columns Stiffness Parameters	
Exterior Columns	
EI	22,690 kN.m^2
GA	1,552,756 kN
EA	5,261,104 kN
Interior Columns	
EI	42,214 kN.m^2
GA	2,388,000 kN
EA	7,859,181 kN
Beams Yield Moments	
Floor Girders	
Positive Yield Moment	178.37 kN.m
Negative Yield Moment	328.90 kN.m
Roof Girders	
Positive Yield Moment	136.38 kN.m
Negative Yield Moment	220.16 kN.m
Columns Yield Moments[1]	
Exterior Columns	386.57 kN.m
Interior Columns	675.54 kN.m
Ground Motion	
Intensity	Variable
Duration	10 seconds
Mass	
Floors	60.461 tons
Roof	44.469 tons

[1]Values given are for ground floor columns. Values for upper-story columns are determined based on the applicable axial load in each column.

Table 5.6 : Properties of the fifteen-Story Frame

Fundamental Period	4.47 s
Height	60 m
V/W	0.018
Beams Stiffness Parameters	
Floor Girders	
EI	47,593 kN.m^2
GA	1,441,662 kN
EA	4,676,537 kN
Roof Girders	
EI	36,329 kN.m^2
GA	1,463,313 kN
EA	4,676,537 kN
Columns Stiffness Parameters	
Exterior Columns	
EI	20,614 kN.m^2
GA	1,552,756 kN
EA	5,261,104 kN
Interior Columns	
EI[1]	71,670 kN.m^2
GA	2,388,000 kN
EA	7,859,181 kN
Beams Yield Moments	
Floor Girders	
Positive Yield Moment	320.10 kN.m
Negative Yield Moment	394.00 kN.m
Roof Girders	
Positive Yield Moment	178.58 kN.m
Negative Yield Moment	263.67 kN.m
Columns Yield Moments[2]	
Exterior Columns	424.243 kN.m
Interior Columns	859.11 kN.m
Ground Motion	
Intensity	0.5g
Duration	10 seconds
Mass	
Floors	60.461 tons
Roof	44.469 tons

[1]EI value is reduced at the 6th floor level to 42214 kN.m^2.

[2]Values given are for ground floor columns. Values for upper-story columns are determined based on the applicable axial load in each column.

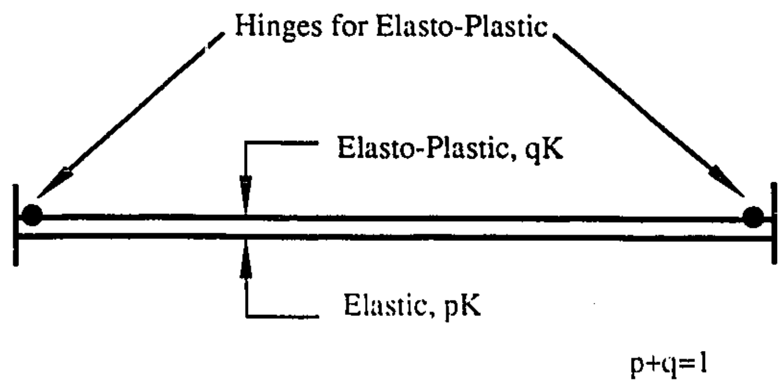

(a) Two Components Model by Clough et al. [27]

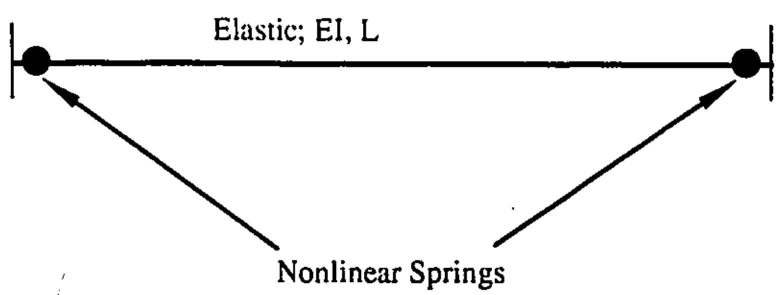

(b) One Component Model by Giberson [29]

Figure 1.1 Mechanical Member Models

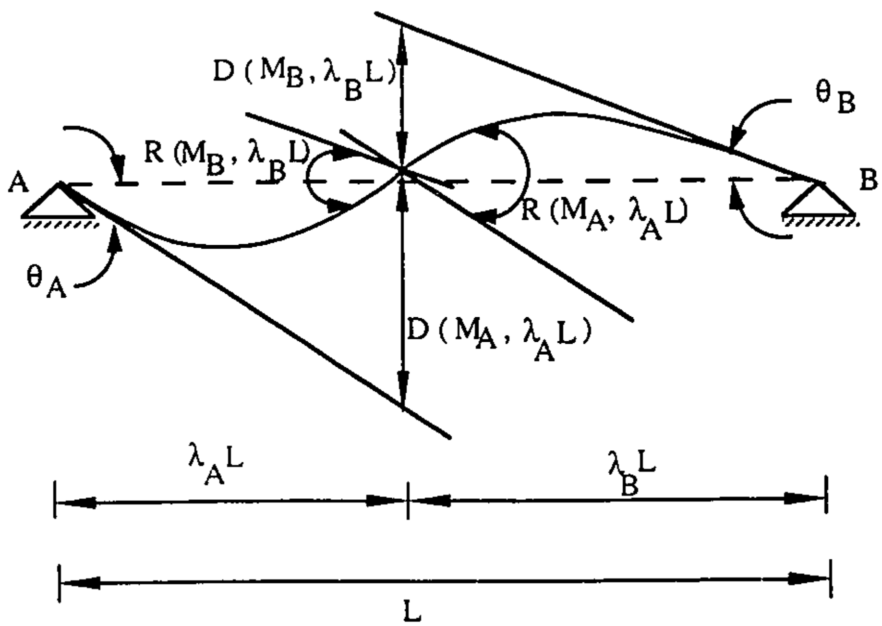

(c) Two Cantilever Model by Otani and Sozen [9]

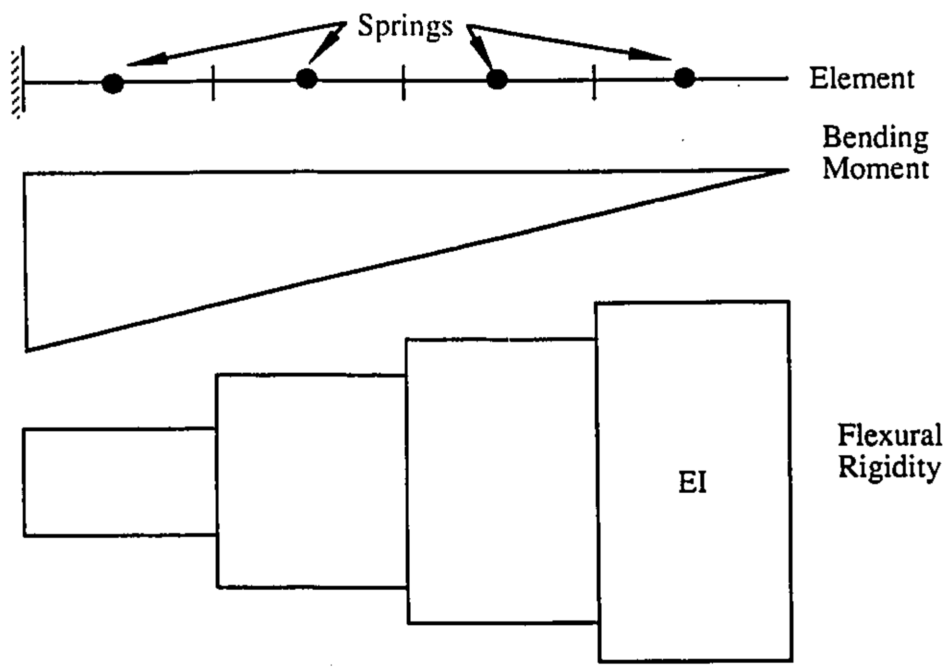

(d) Multi-spring Model by Emori and Schnobrich [11]

Figure 1.1 Continued

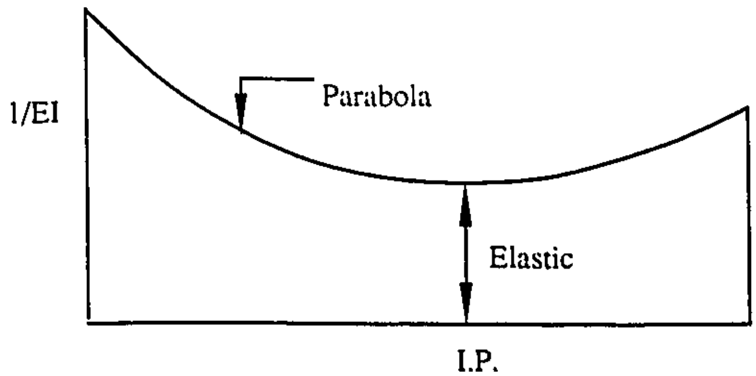

(e) Distributed Flexibility Model by Takizawa [30]

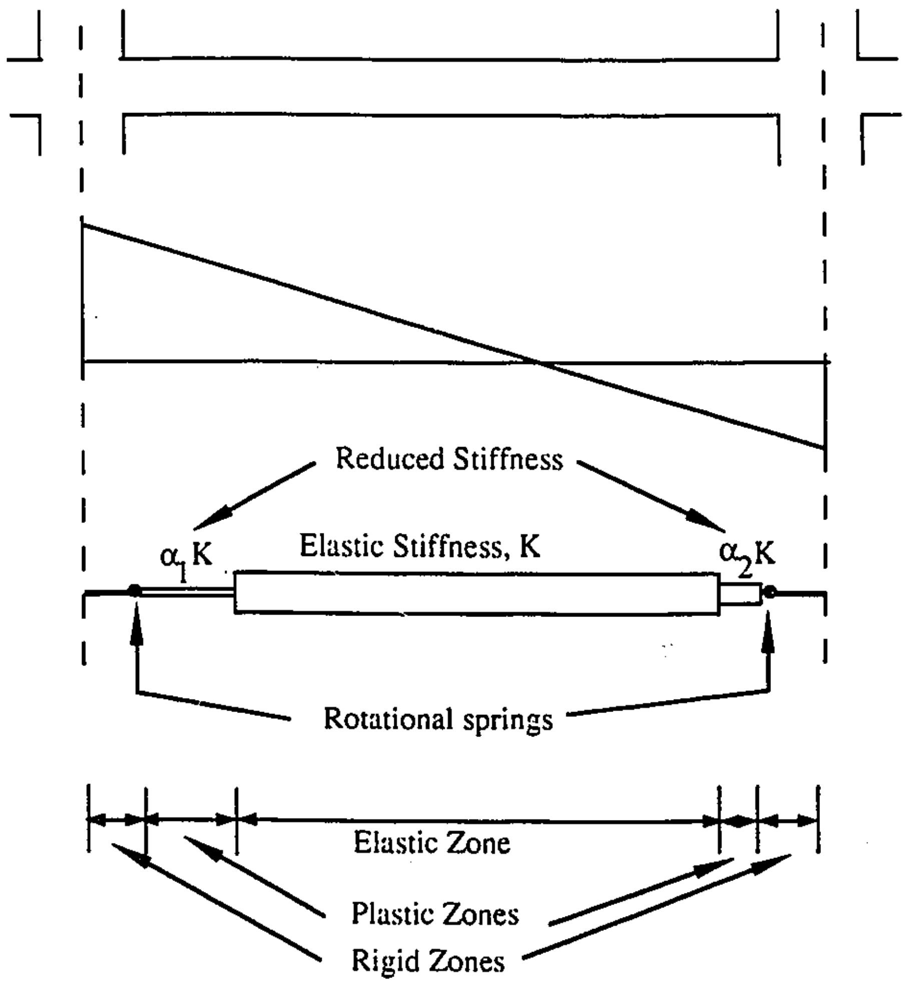

(f) Spread Plasticity Model by Soleimani et al. [13]

Figure 1.1 Continued

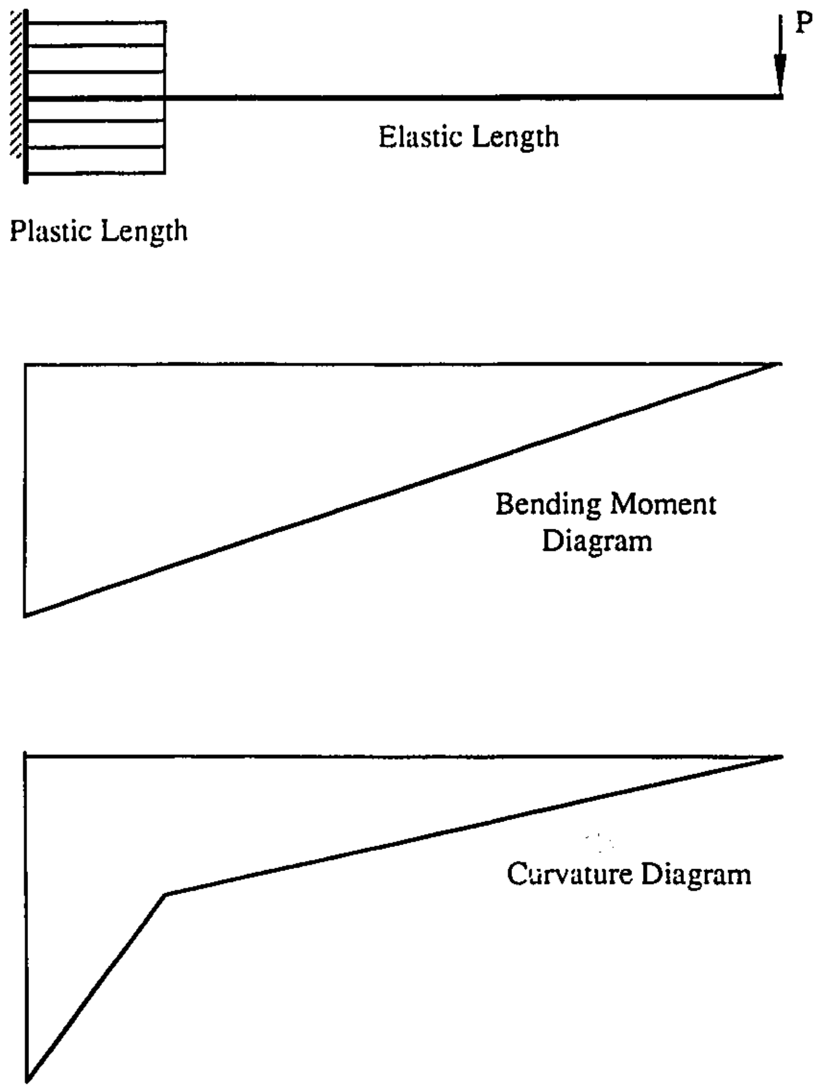

(g) Layer Model by Emori and Schnobrich [15]

Figure 1.1 Continued

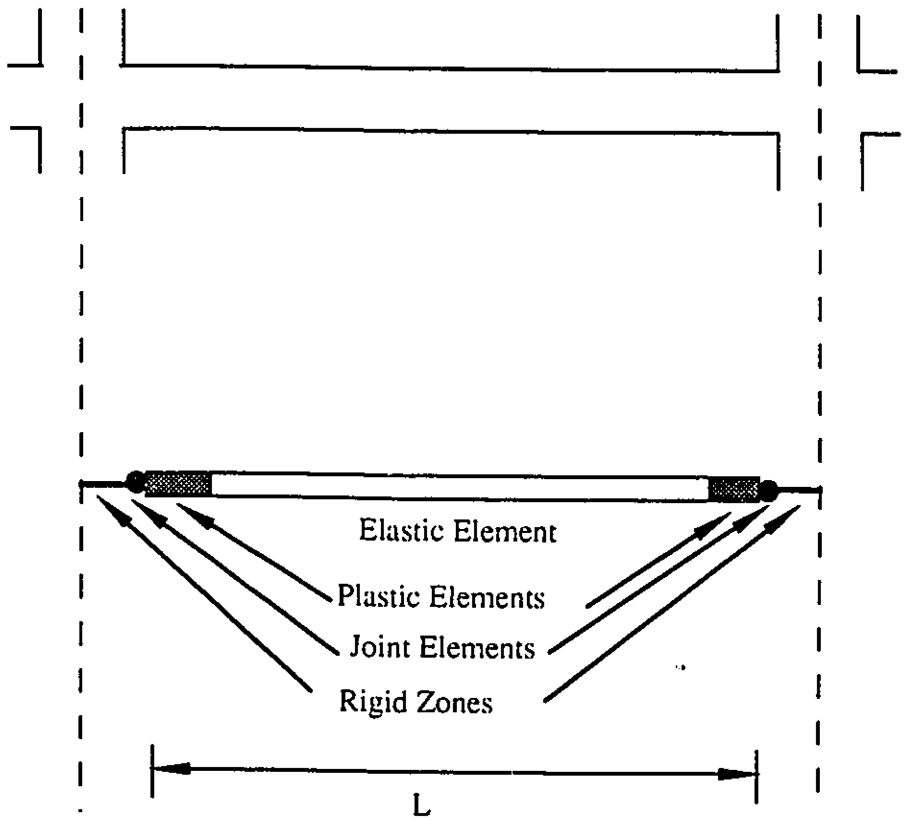

(h) Super Girder Model by Filippou and Issa [22]

Figure 1.1 Continued

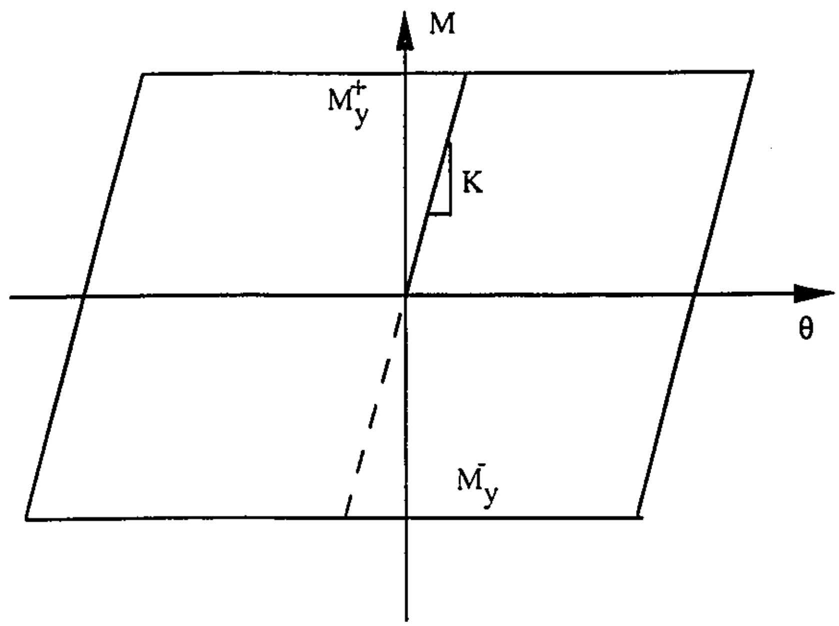

(a) Elasto - Plastic Hysteretic Model [1]

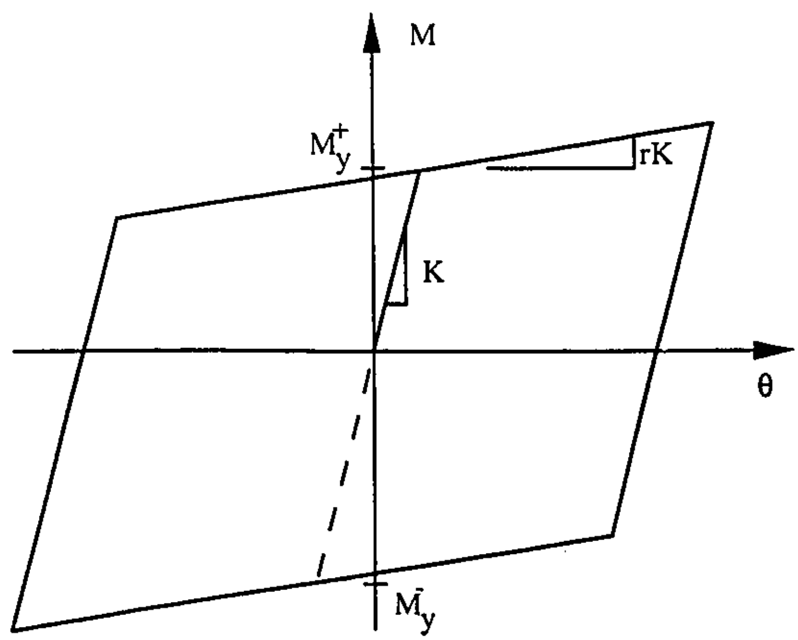

(b) Bilinear Hysteretic Model [3]

Figure 1.2 Hysteretic Models for Flexure

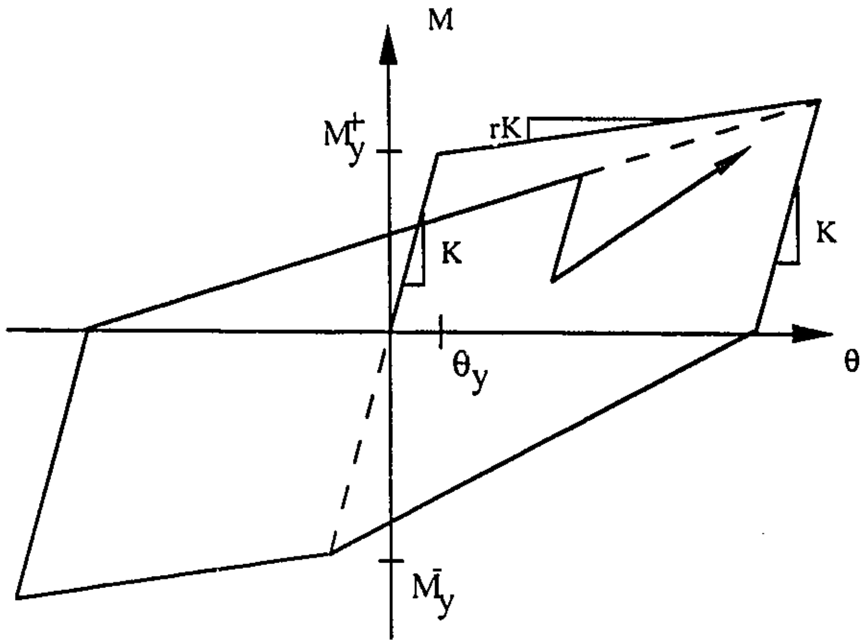

(c) Clough's Degrading Hysteretic Model [3]

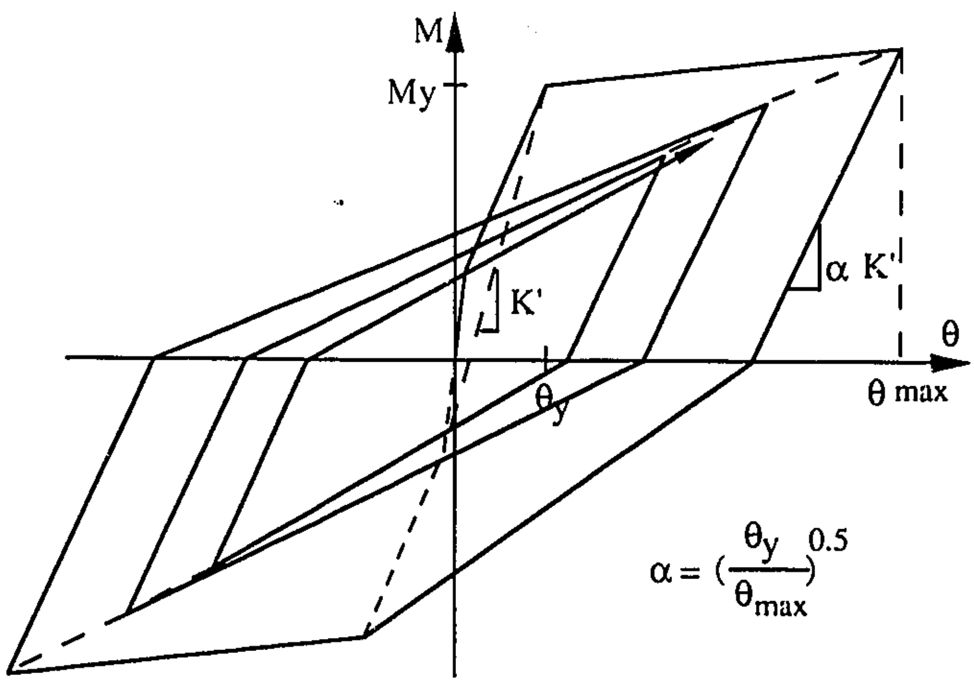

(d) Degrading Hysteretic Model by Takeda et al. [7]

Figure 1.2 Continued

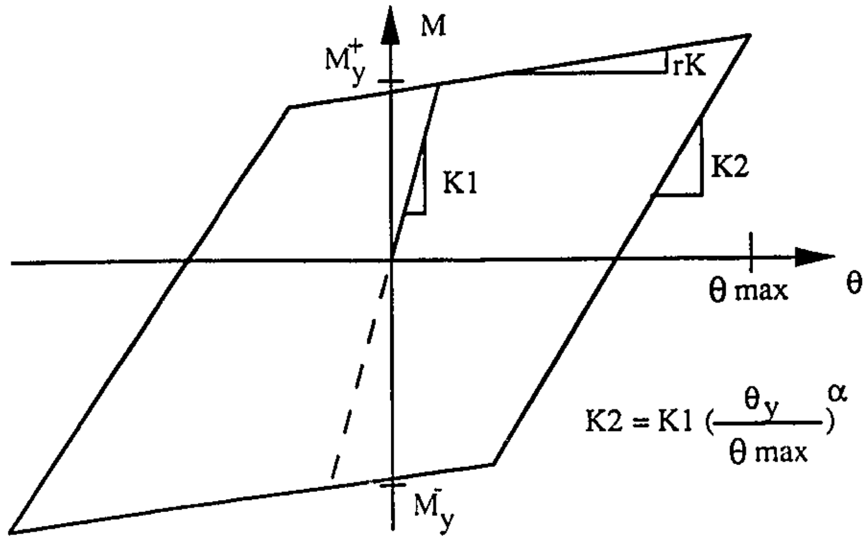

(e) Degrading Bilinear Model by Imbeault and Nielsen [36]

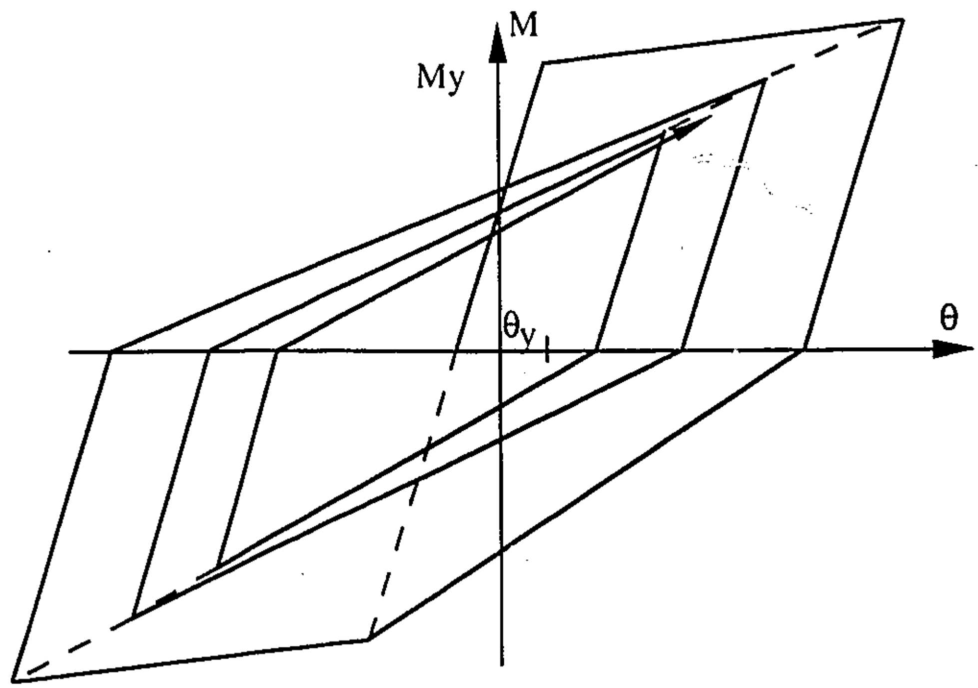

(f) Modified Takeda's Hysteretic Model by Otani and Sozen [9]

Figure 1.2 Continued

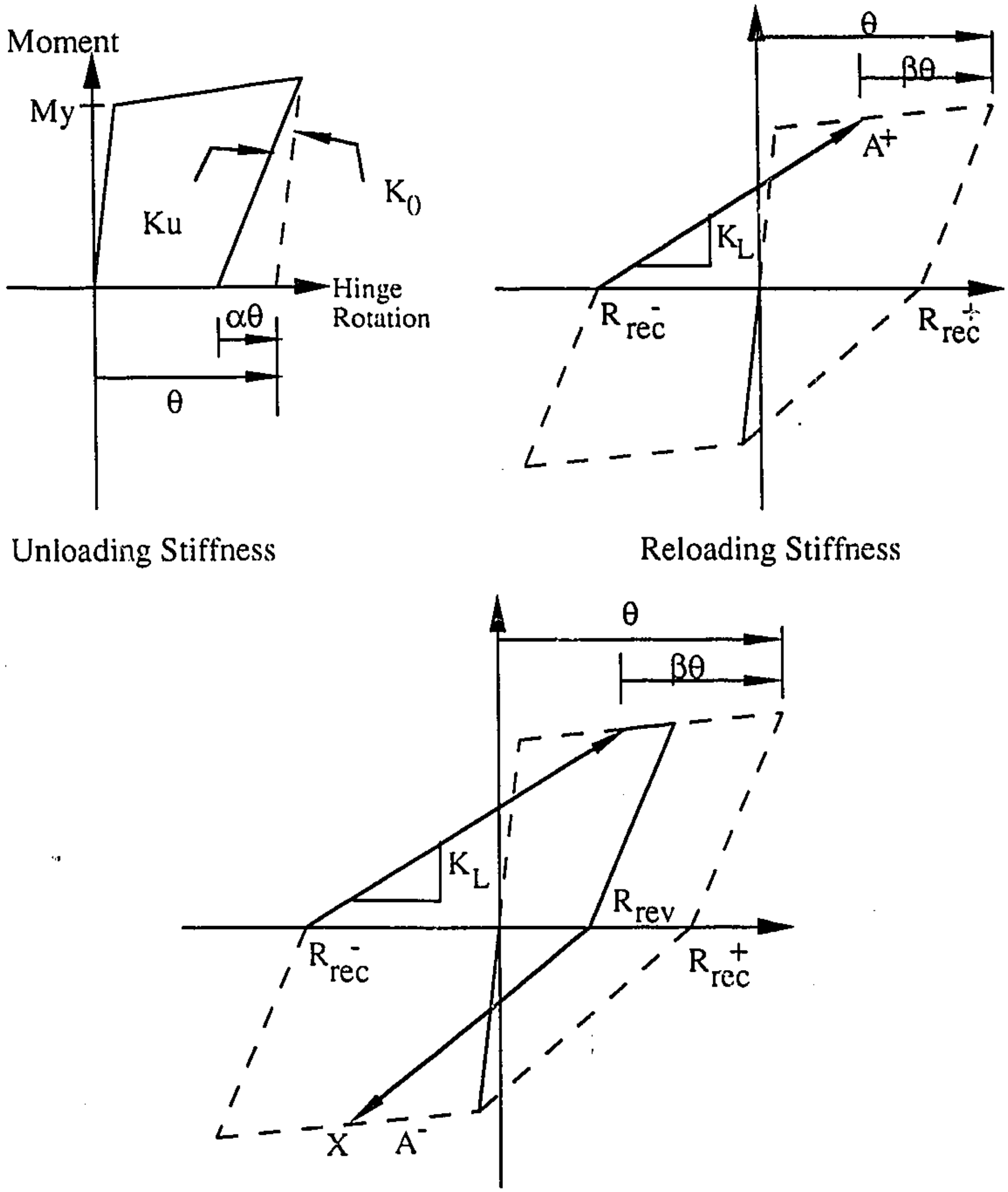

Unloading Stiffness

Reloading Stiffness

Reloading After Small Yield Excursion

(g) Modification of Takeda's Hysteretic Model by Powell [37]

Figure 1.2 Continued

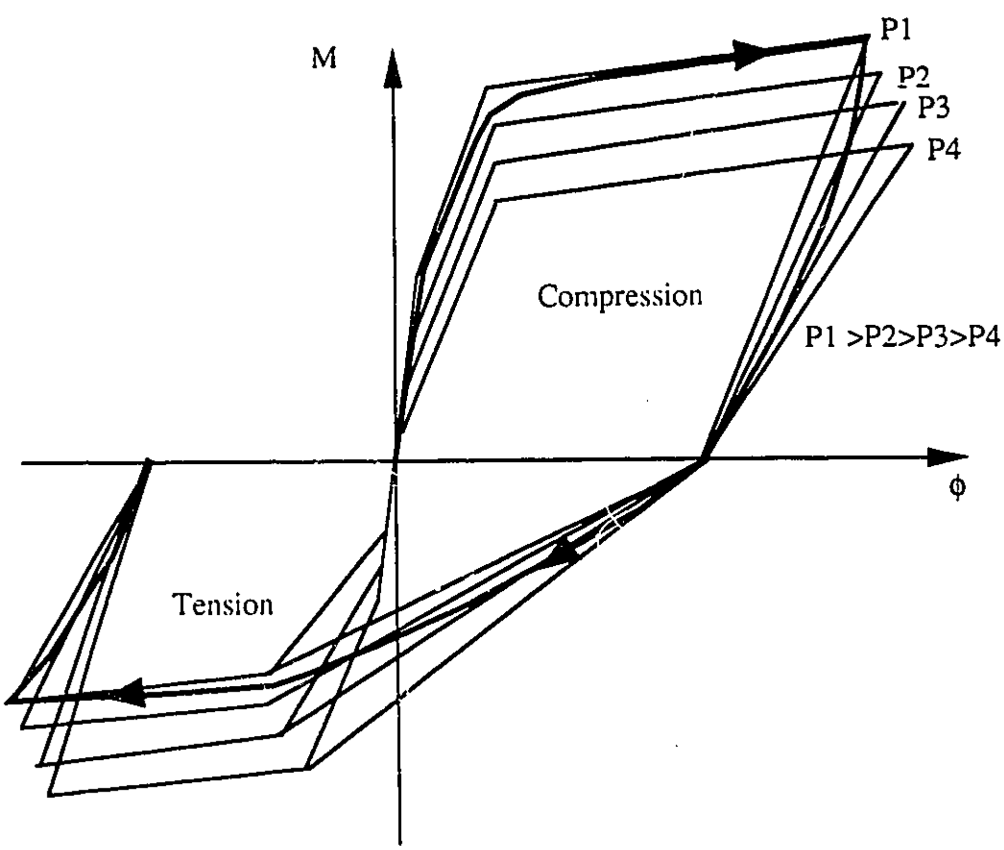

(h) Hysteretic Model Including the Effect of Changing Axial Load by Takayanagi and Schnobrich [11]

Figure 1.2 Continued

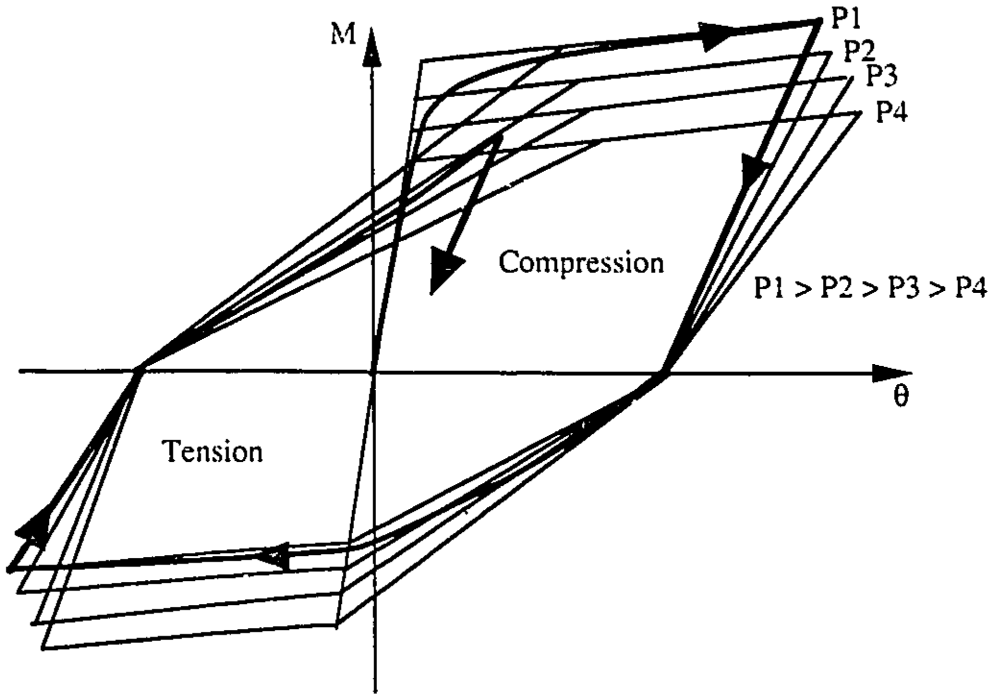

(i) Hysteretic Model Including the Effect of Changing Axial Load by Saatcioglu et al. [18]

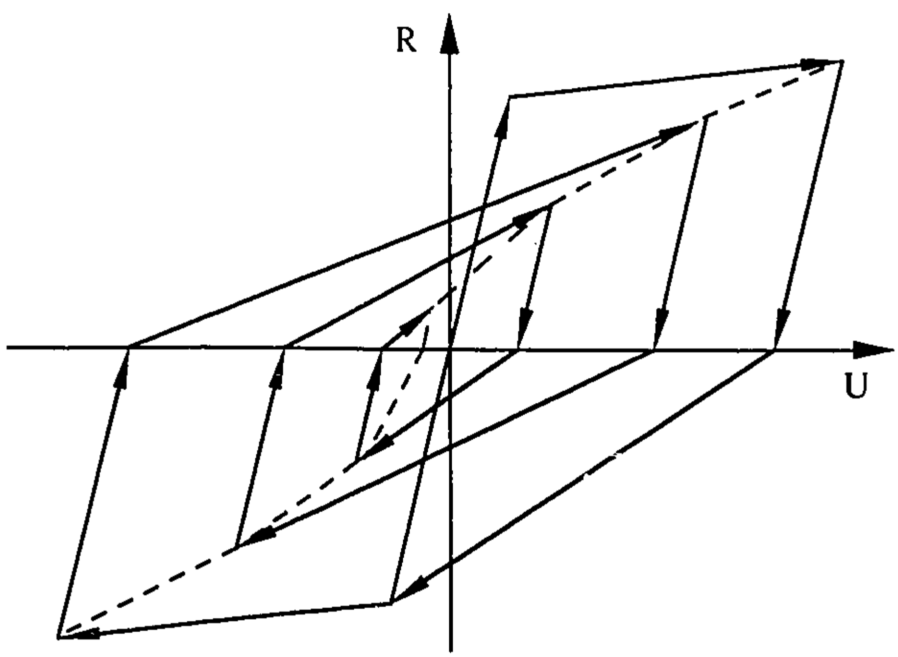

(j) Hysteretic Model by Riddle and Newmark [39]

Figure 1.2 Continued

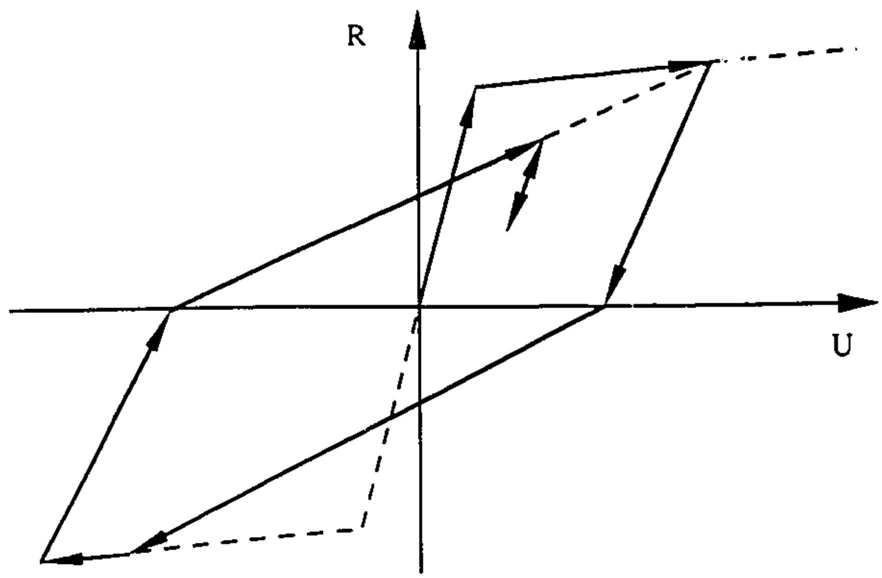

(k) Hysteretic Model by Saiidi [20]

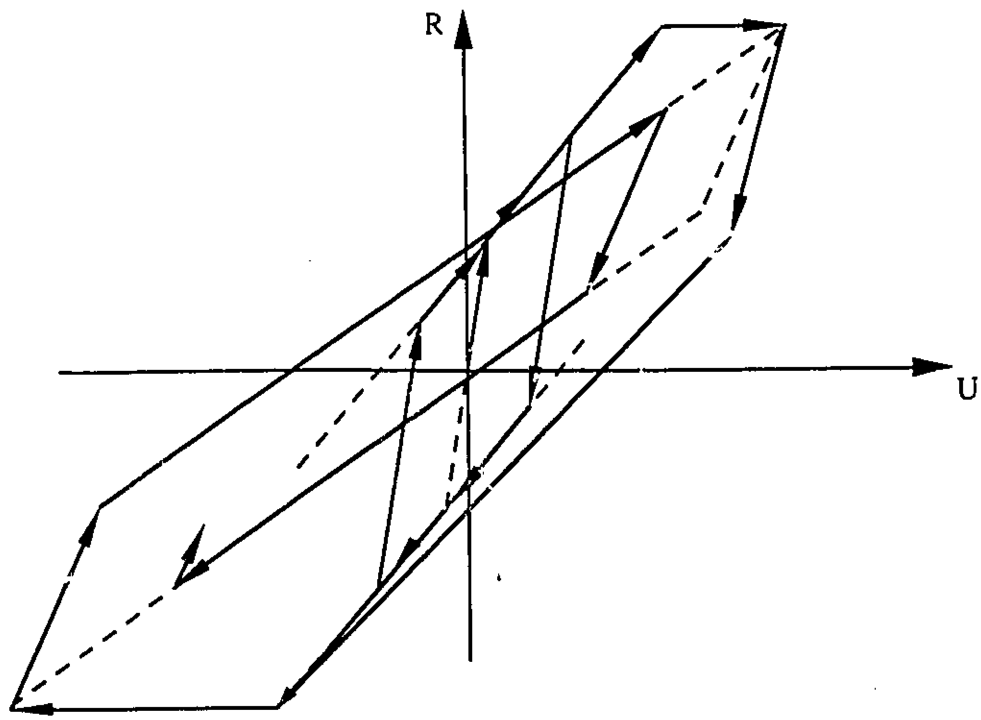

(l) Degrading Trilinear Hysteretic Model by Fukada [28]

Figure 1.2 Continued

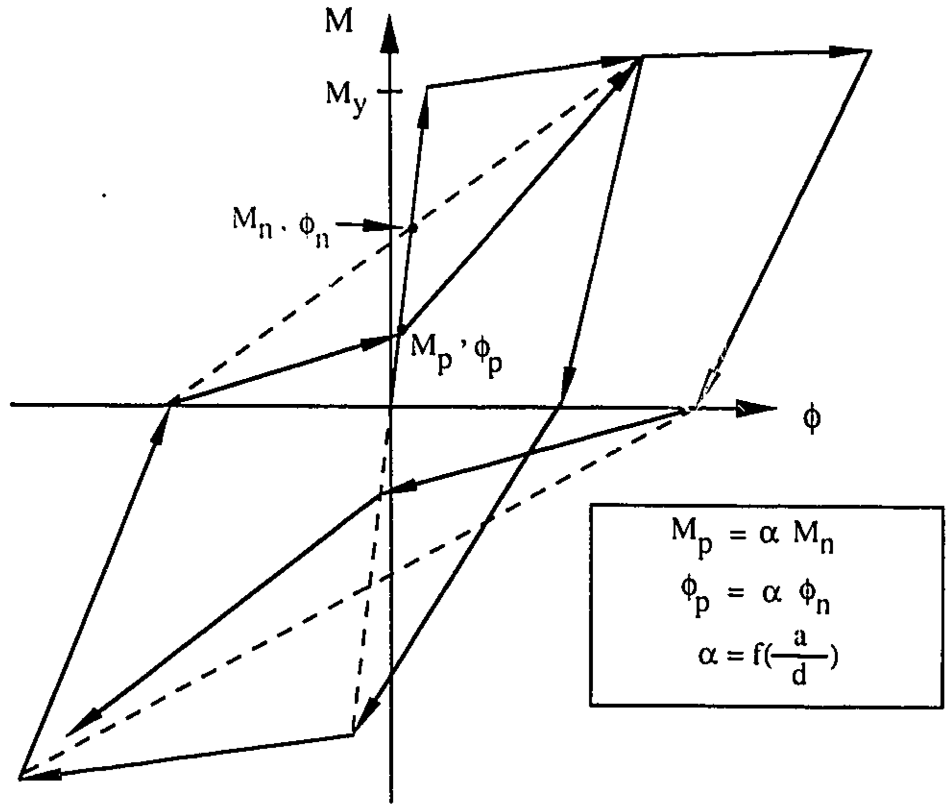

(m) Hysteretic Moment - Curvature Model by Roufaiel and Meyer [31]

Figure 1.2 Continued

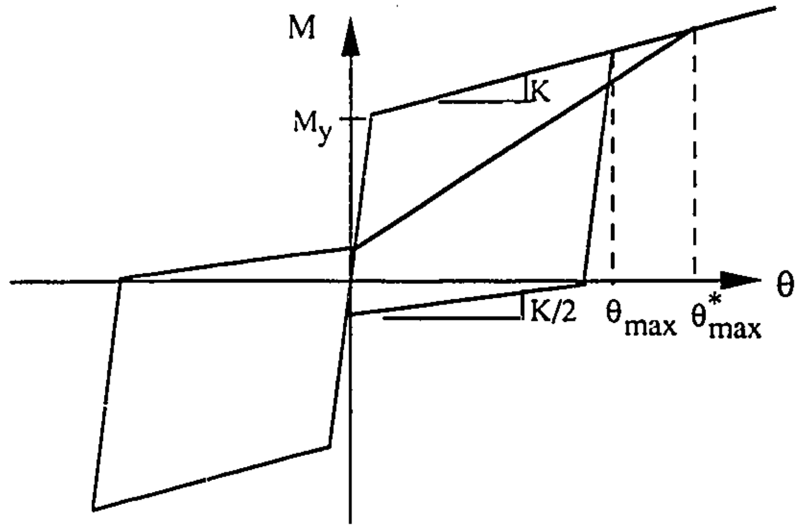

(a) Hysteretic Model by Banon et al. [17]

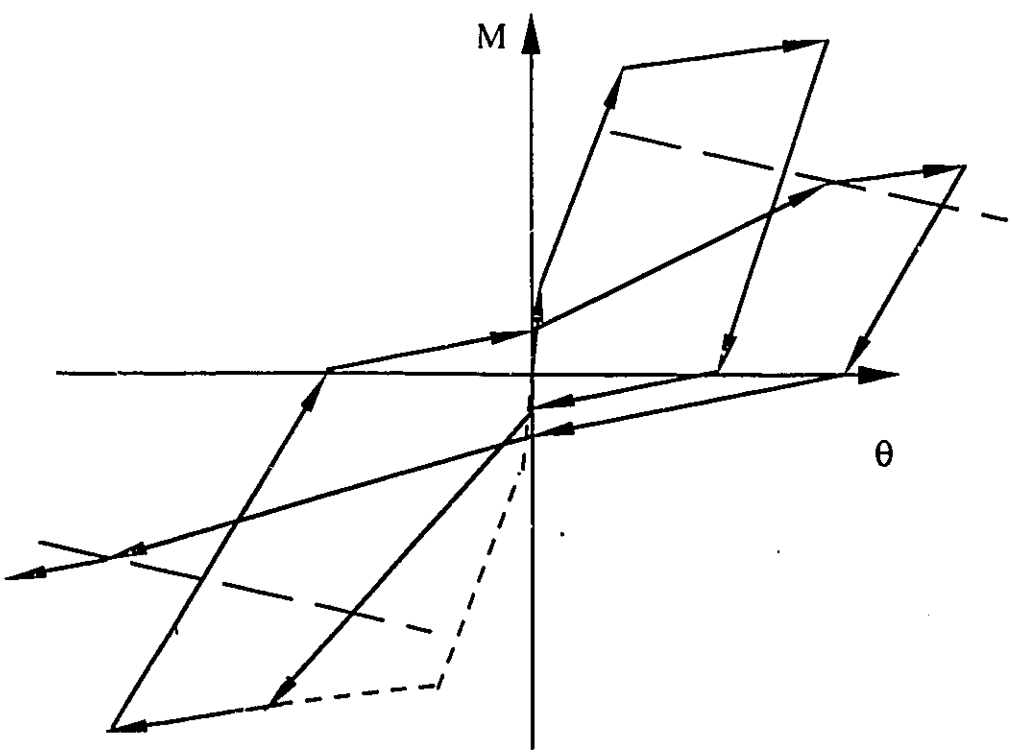

(b) Hysteretic Model Including Pinching by Takayanagi and Schnobrich [11]

Figure 1.3 Hysteretic Models for Shear

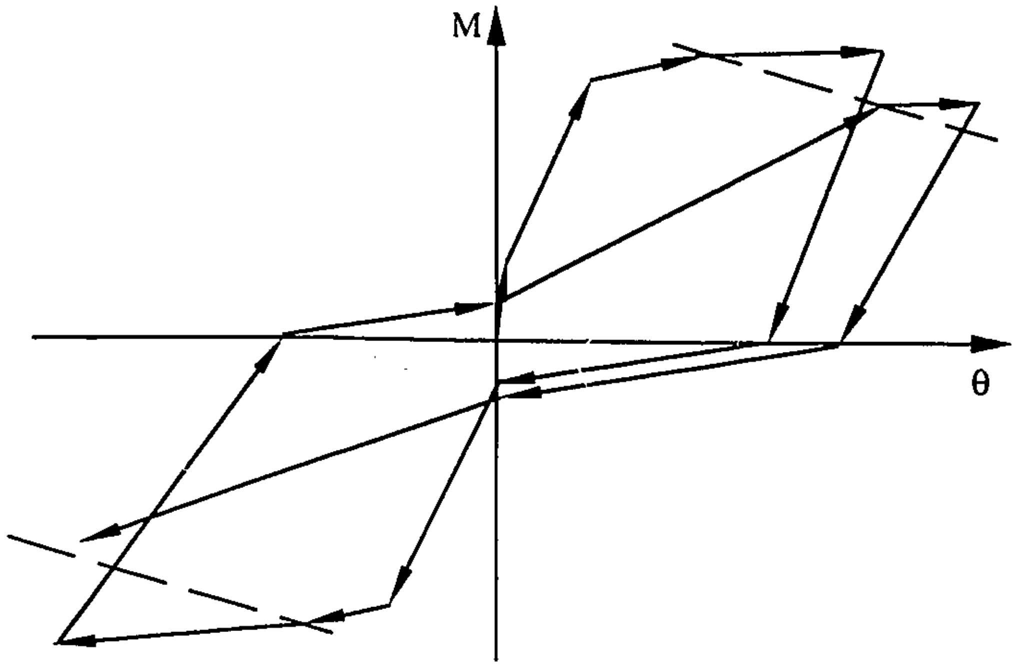

(c) Hysteretic Model Including Pinching and Strength Decay by Takayanagi et al. [38]

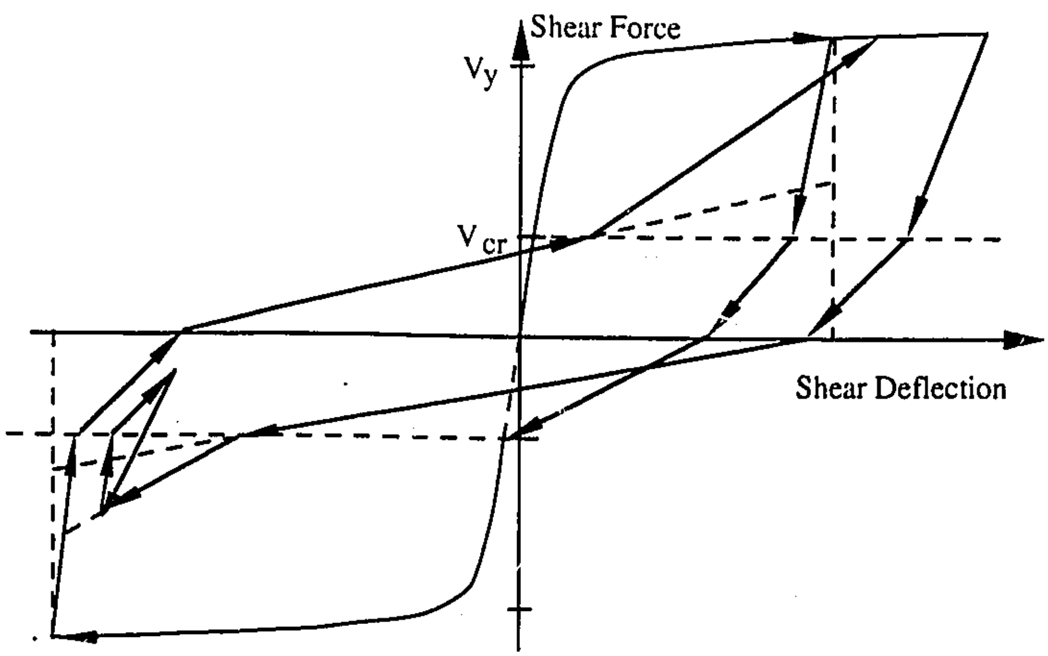

(d) Hysteretic Shear Model by Ozcebe and Saatcioglu [40]

Figure 1.3 Continued

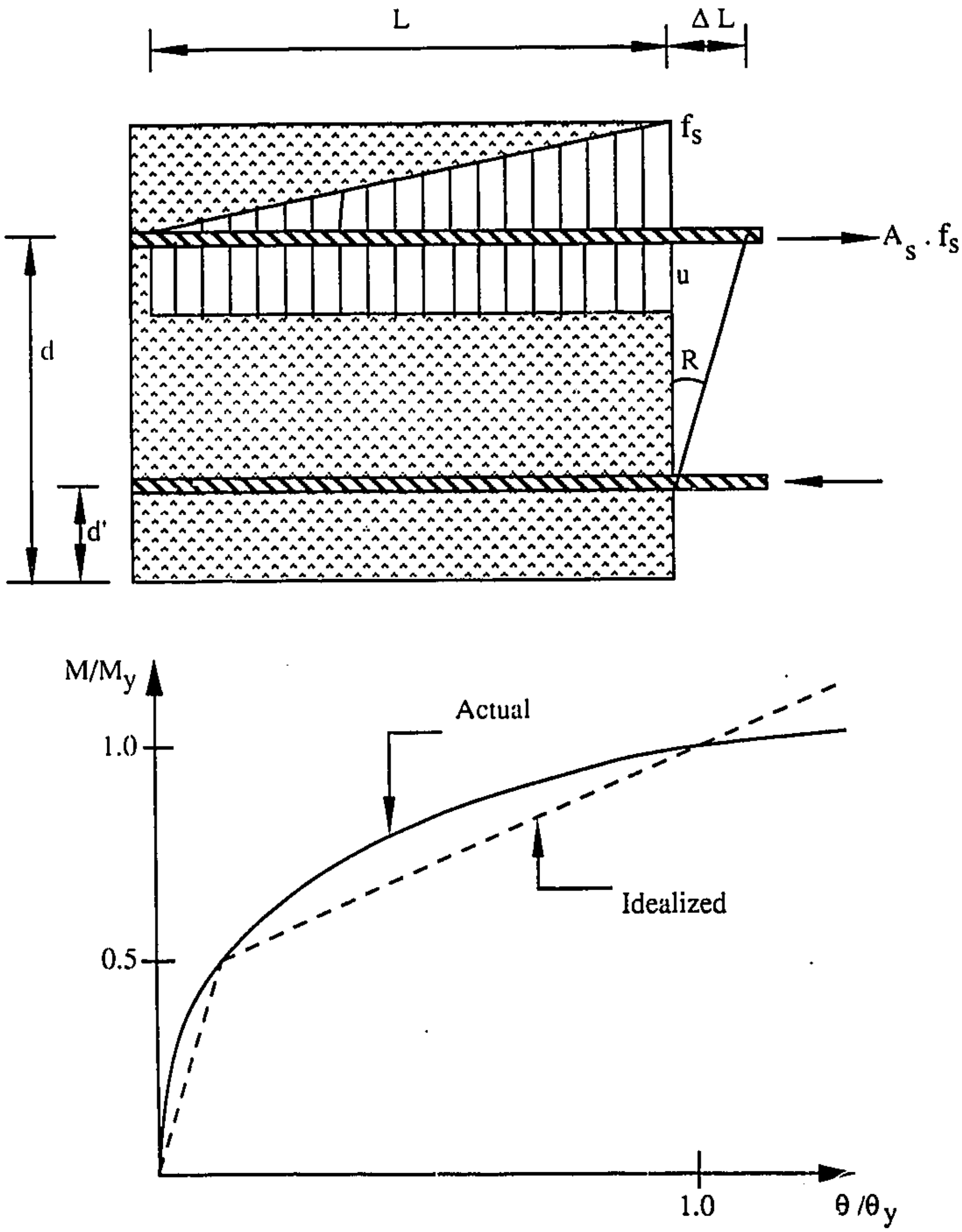

(a) Primary Moment -Anchorage Slip Model by Otani and Sozen [9]

Figure 1.4 Hysteretic Models for Anchorage-Slip

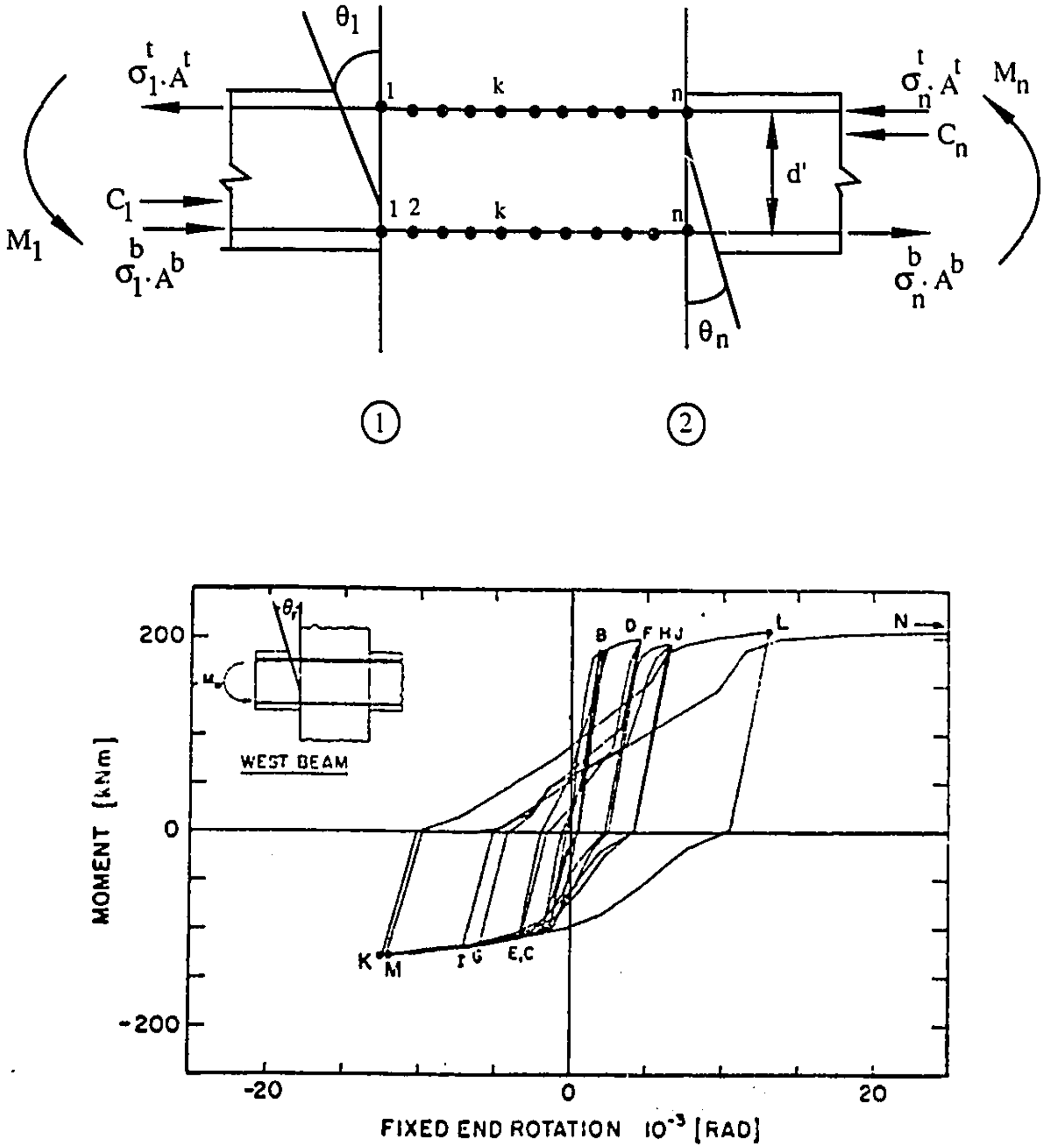

(b) Analytical Model by Filippou et al [66, 67]

Figure 1.4 Continued

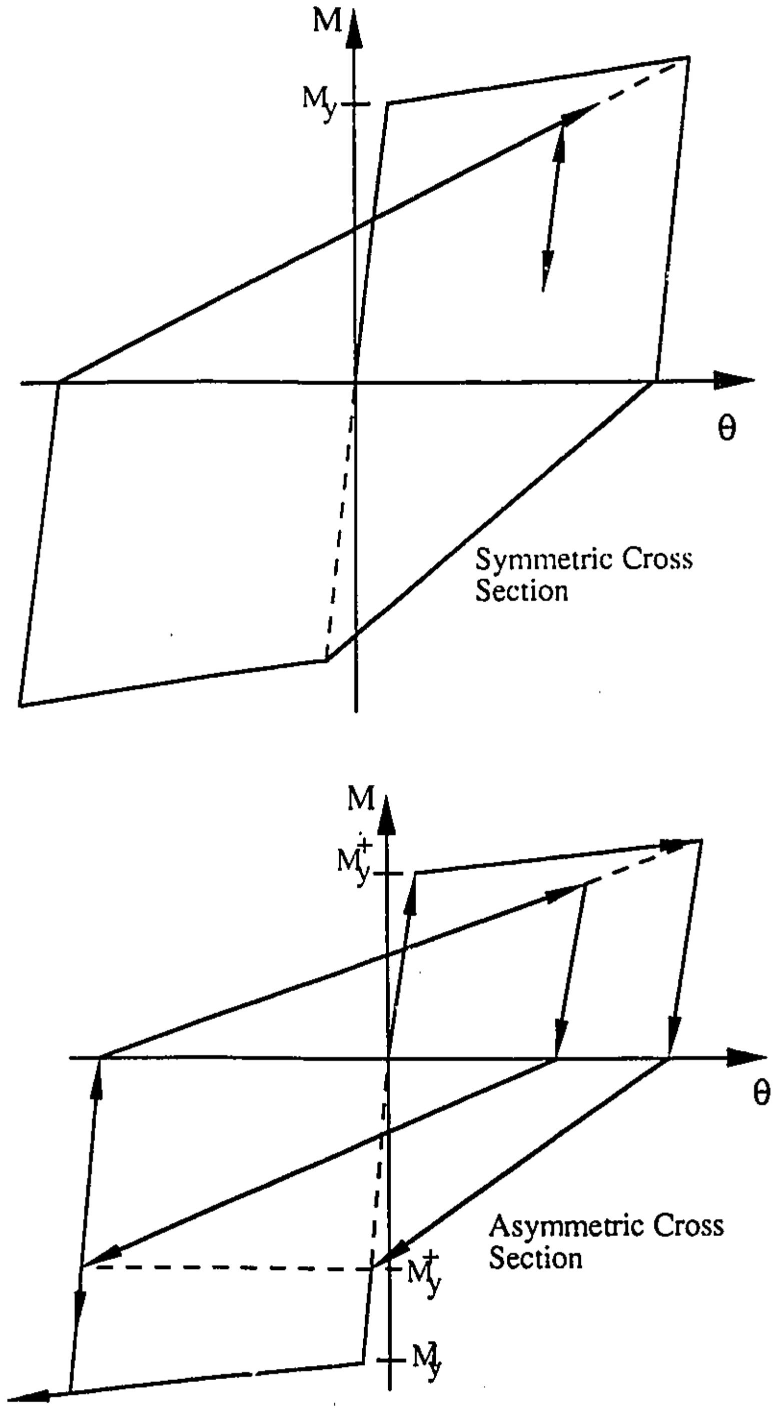

(c) Hysteretic Model by Filippou and Issa [22]

Figure 1.4 Continued

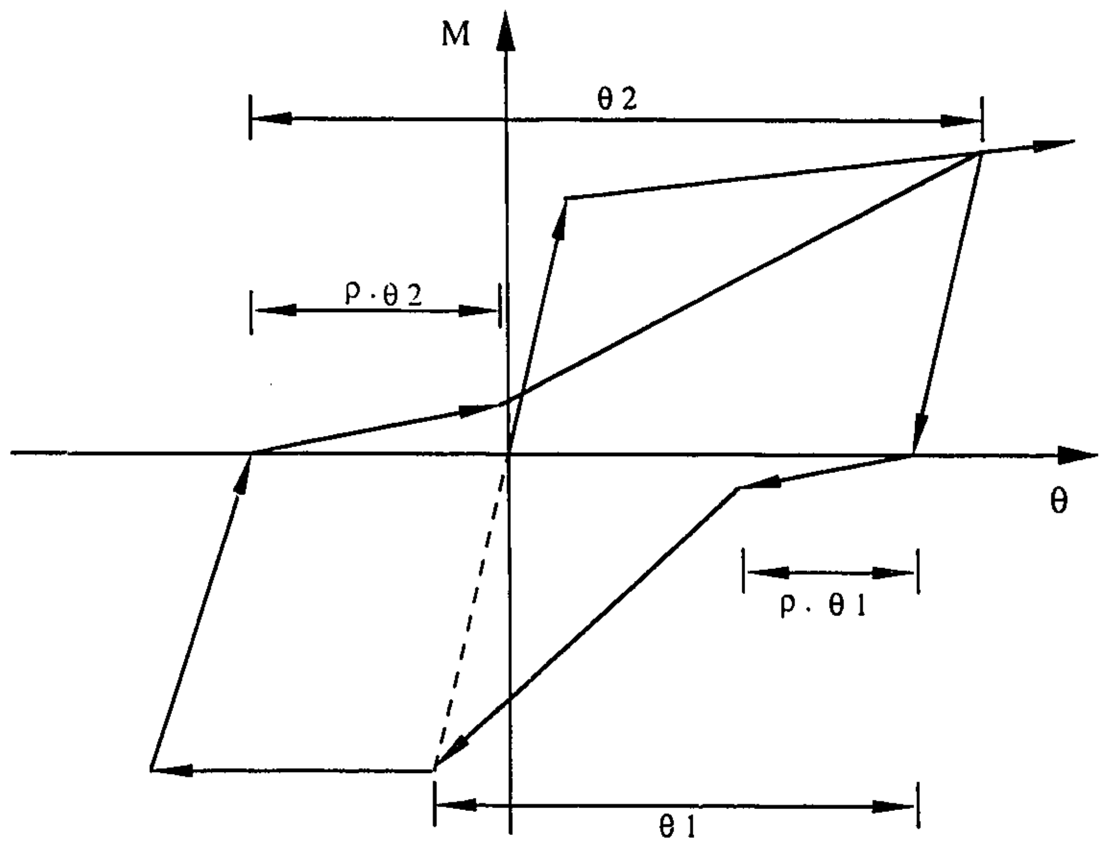

(d) Hysteretic Model by Morita and Kaku [69]

Figure 1.4 Continued

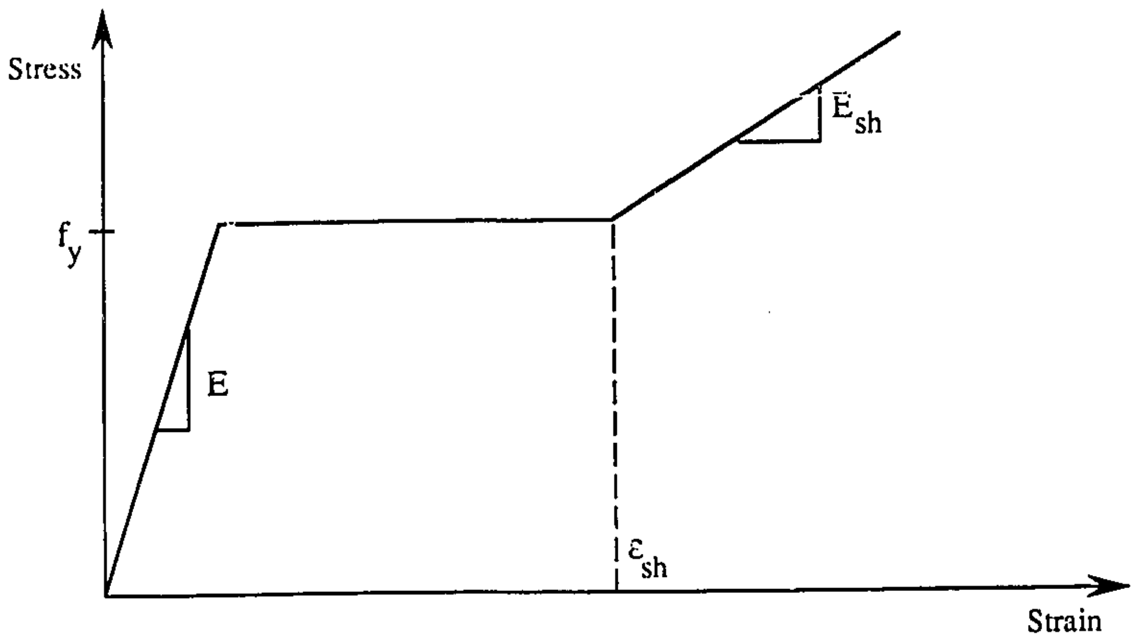

(a) Trilinear Idealization

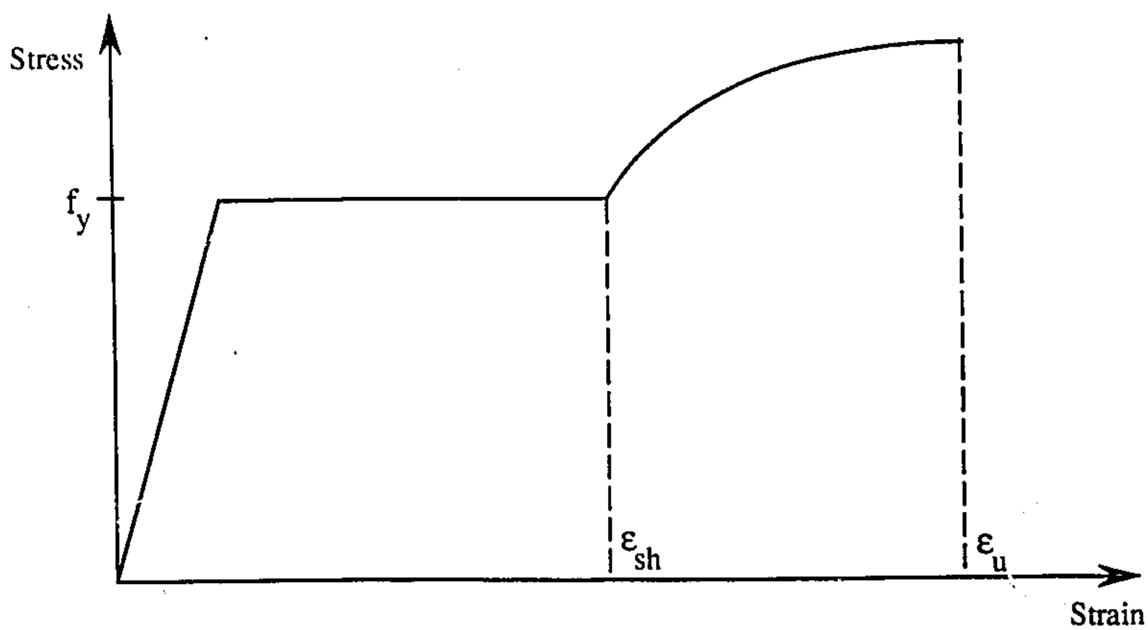

(b) Bilinear Idealization with Parabolic Strain Hardening

Fig. 2.1 Stress-Strain Relationships for Steel

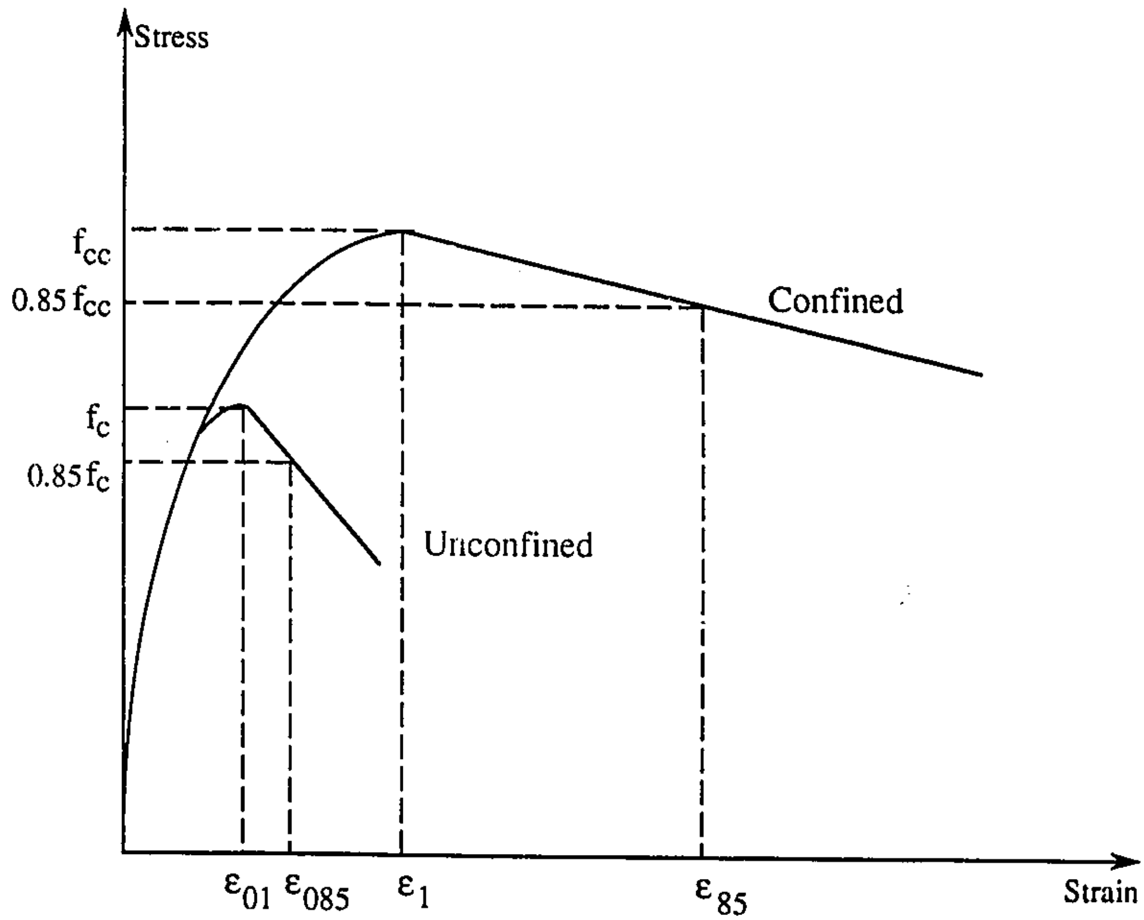

Figure 2.2 Concrete Stress-Strain Curve

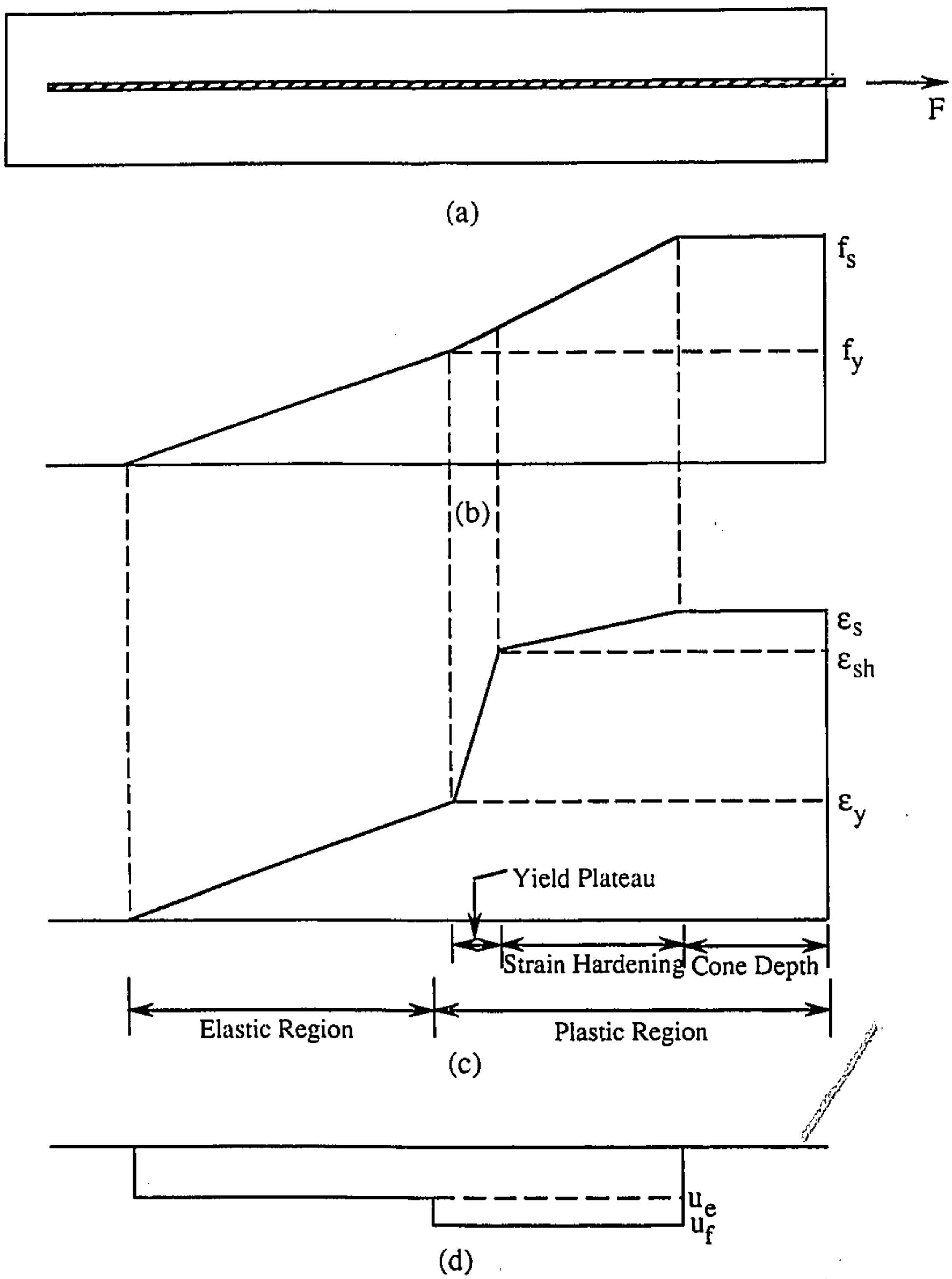

Figure 2.3 (a) Reinforcing Bar Embedded in Concrete; (b) Stress Distribution; (c) Strain Distributon; (d) Bond Stress Between Concrete and Steel

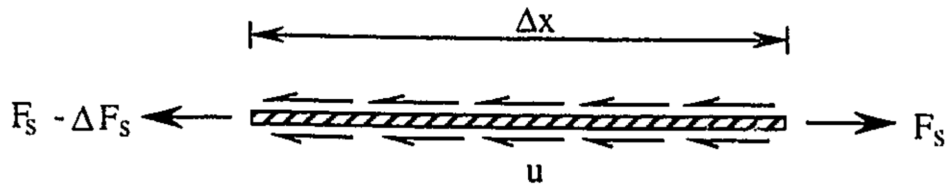

(a)

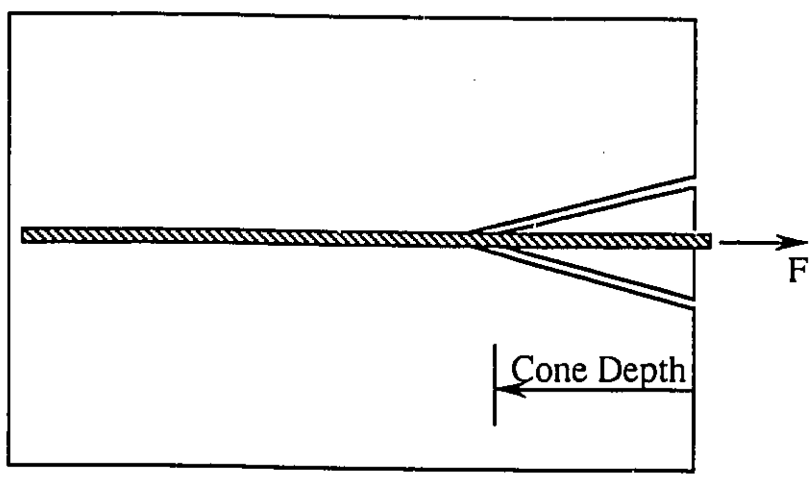

(b)

Fig. 2.4 (a) Forces Acting on a Bar Segment of the Elastic Region; (b) Pull-out Cone

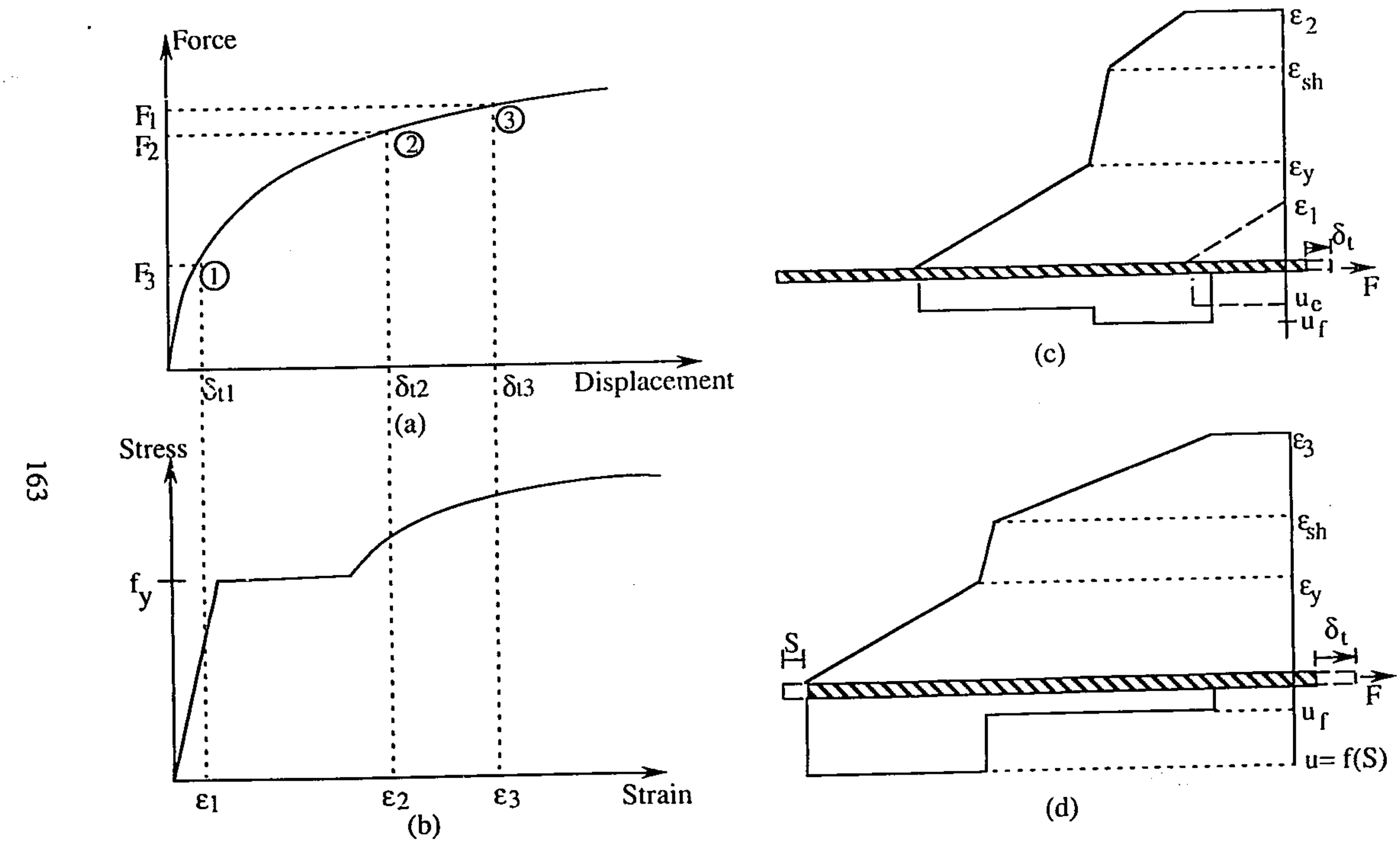

Figure 2.5 (a) Force Displacement Relationship of An Embedded Bar; (b) Stress-Strain Relationship (c) Strain Distribution and Bond Stress Along A Bar That Is Not Stressed To The End; (d) Strain Disribution and Bond Stress Along A Bar That Is Stressed To The End.

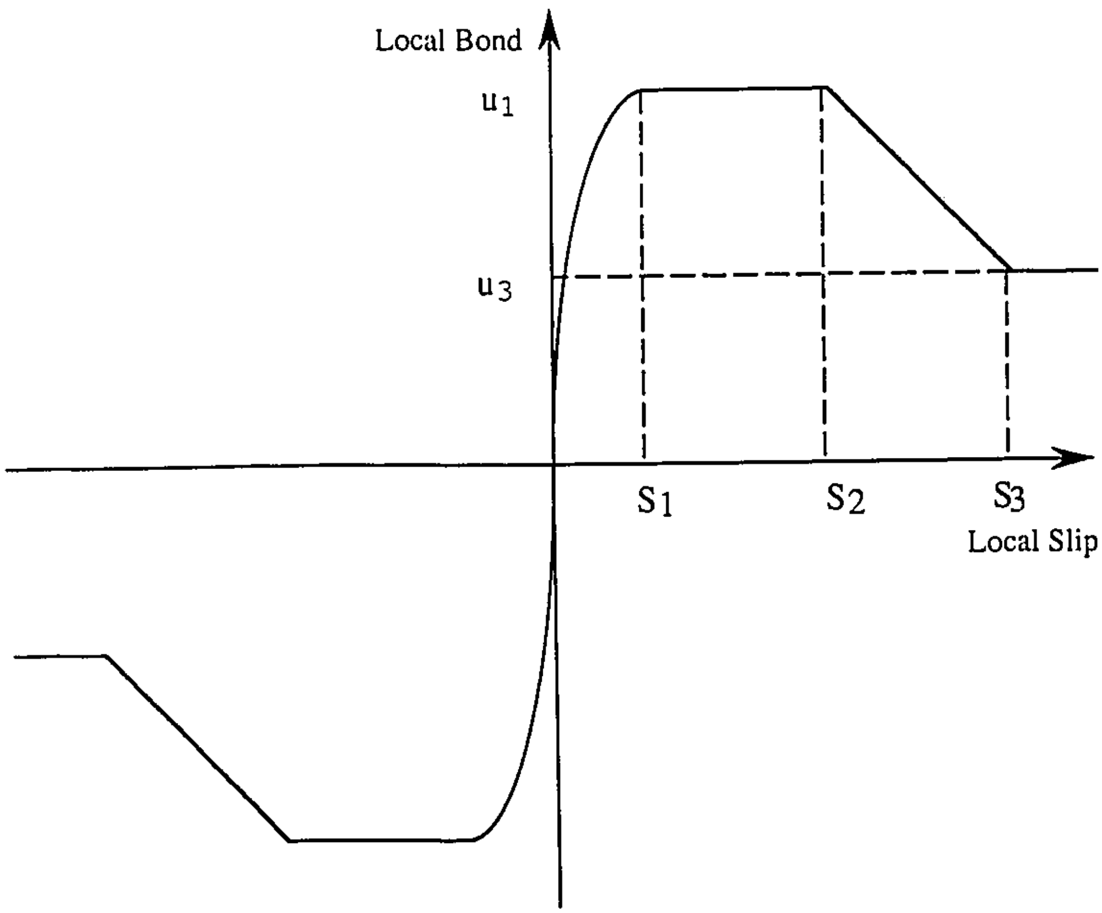

Figure 2.6 Local Bond-Slip Model

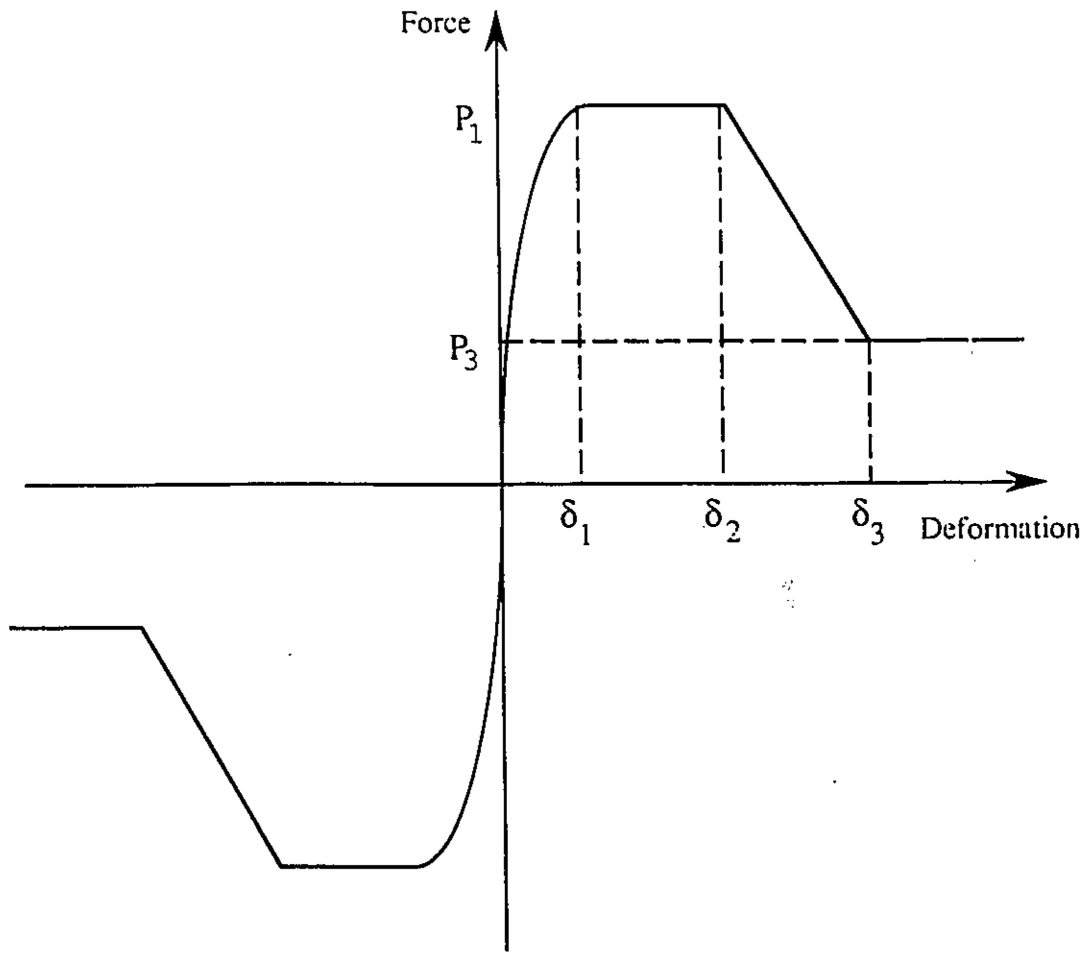

Figure 2.7 Force - Deformation Model for Hooks

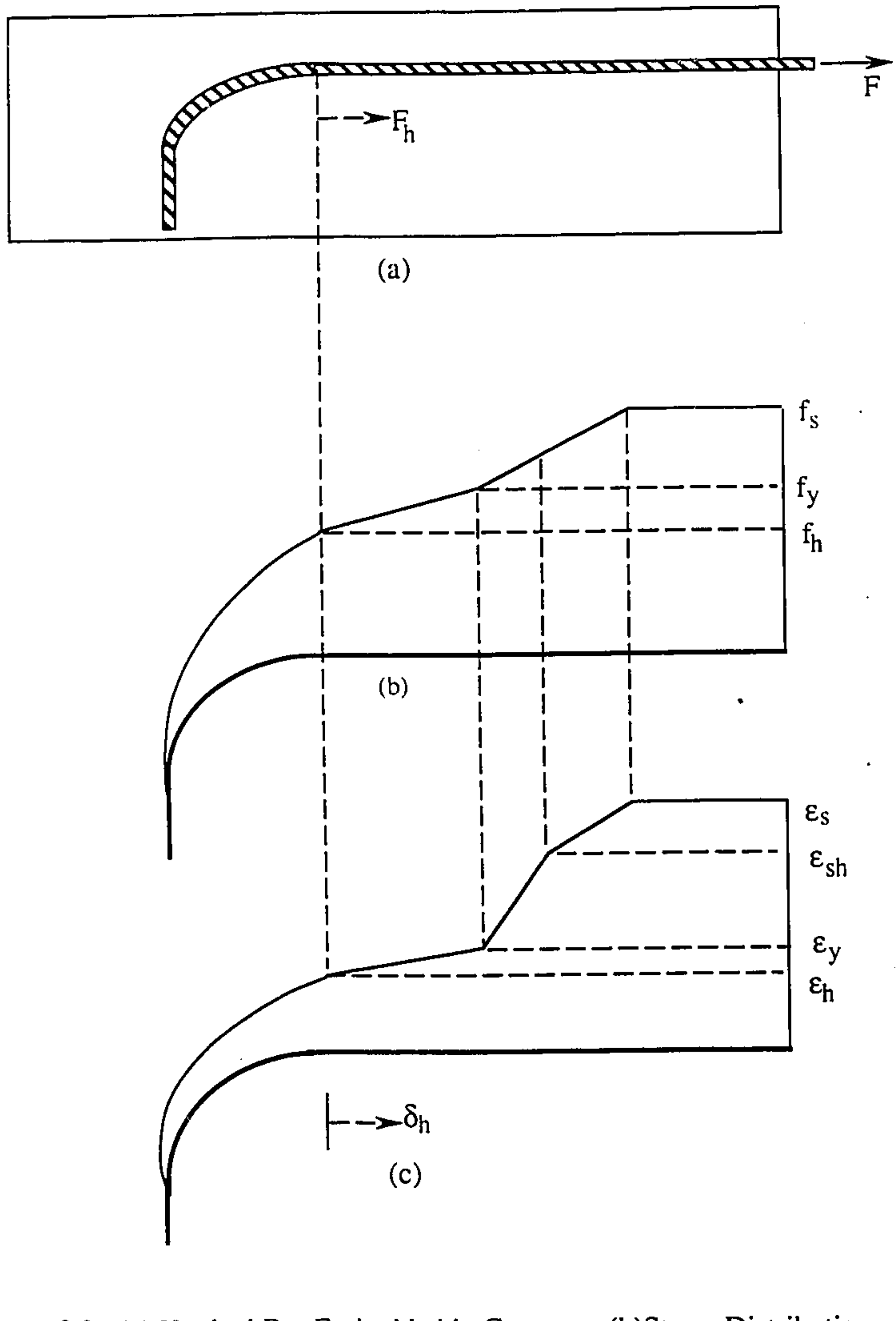

Figure 2.8 (a) Hooked Bar Embedded in Concrete; (b)Stress Distribution; (c) Strain Distribution

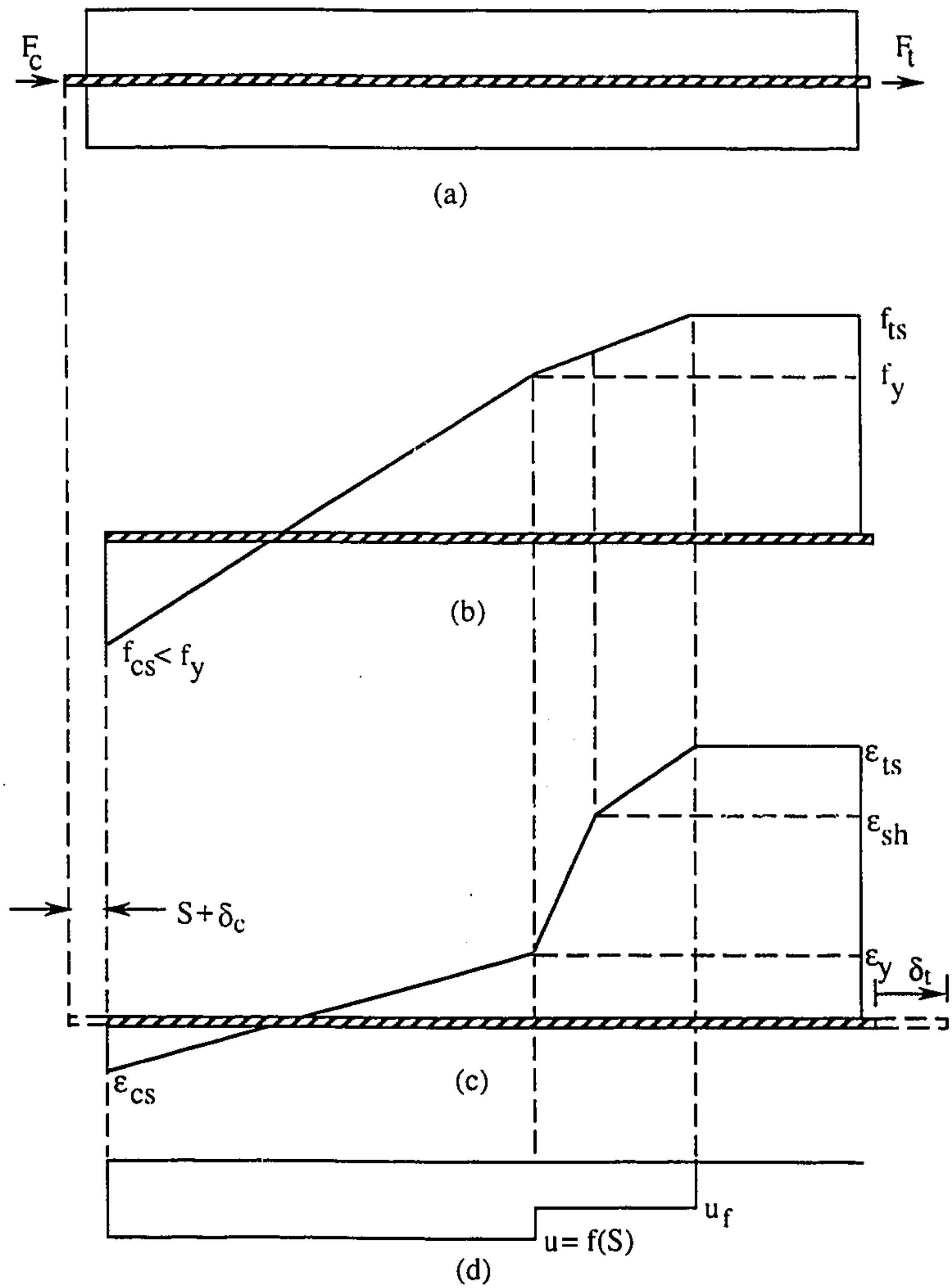

Figure 2.9 (a) Reinforcing Bar in Concrete Subjected to Pull and Push; (b) Stress Distribution; (c) Strain Distribution; (d) Bond Stress

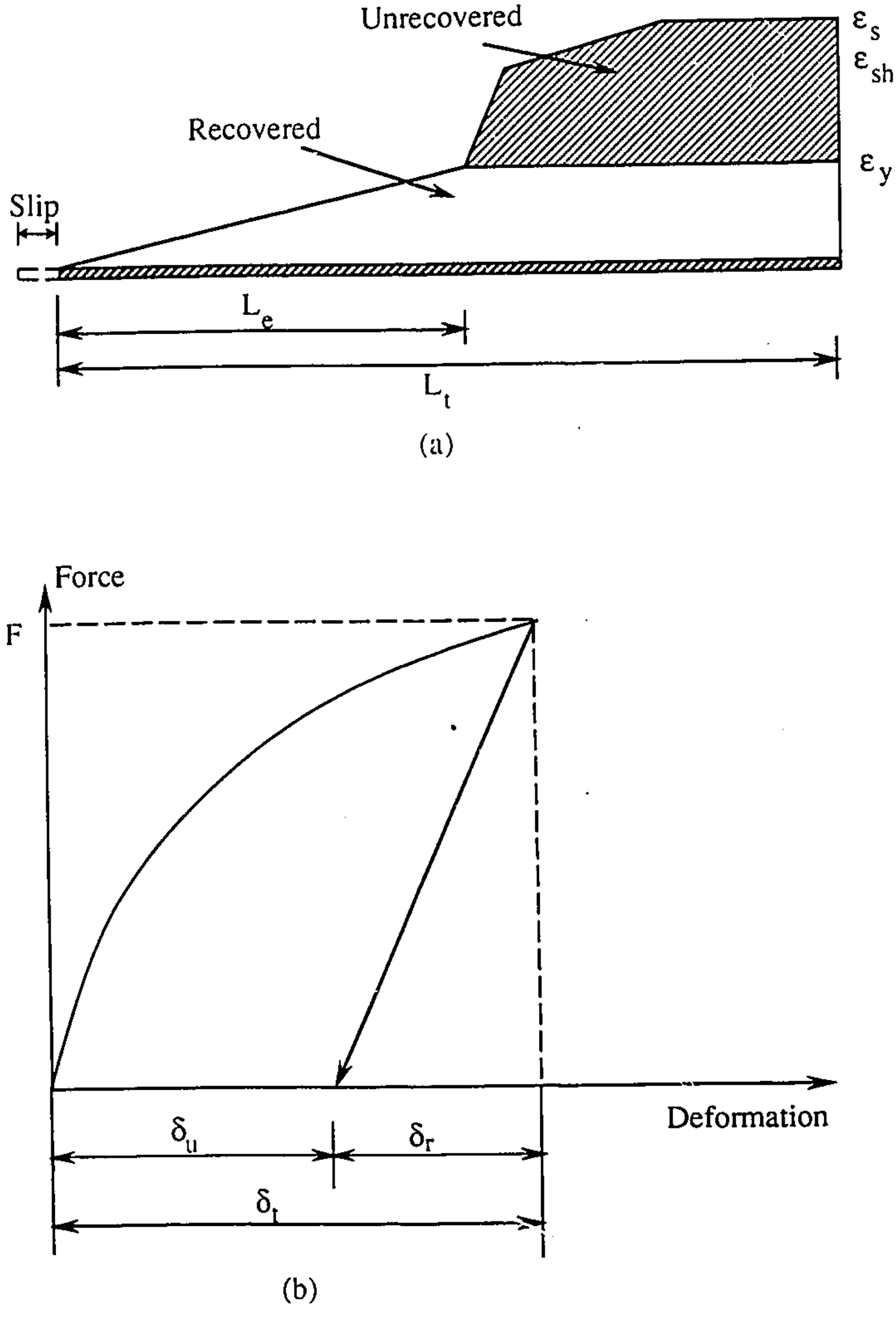

Figure 2.10 Recovered and Unrecovered Deformations

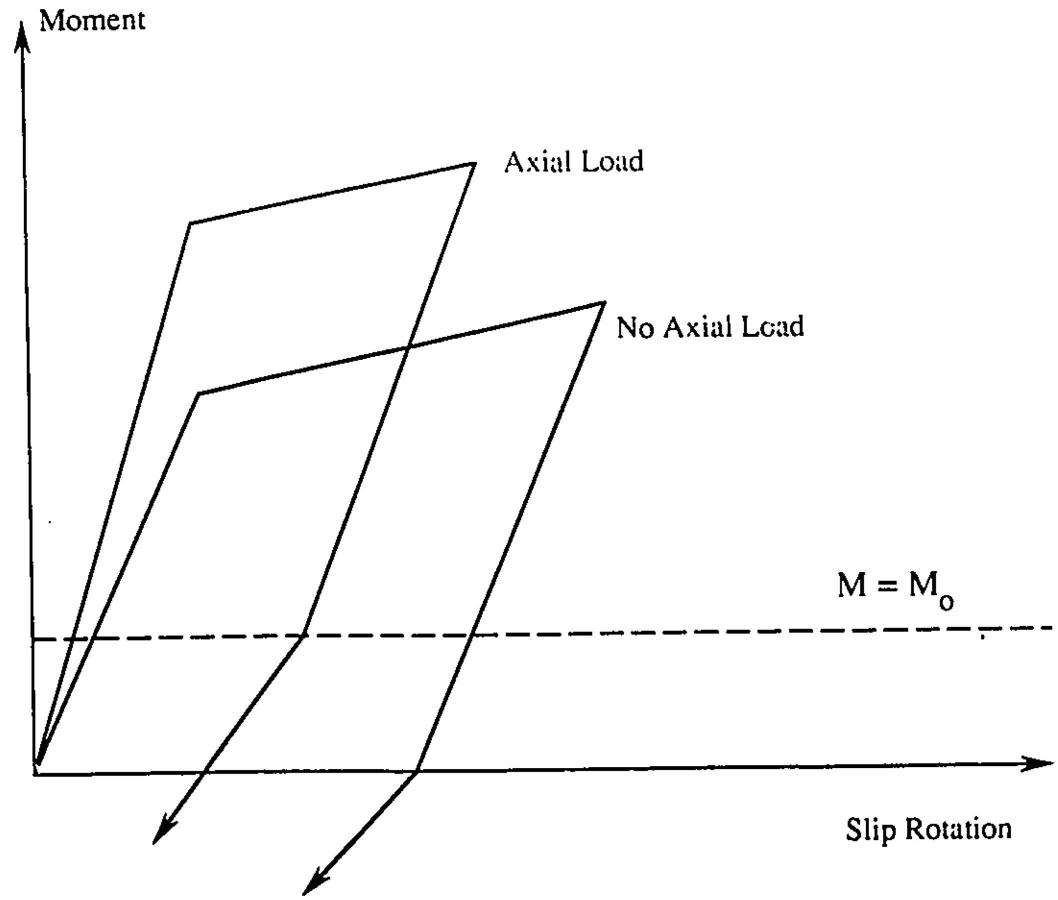

Figure 2.11 Effect of Axial Load on the Primary Moment-Slip Curve

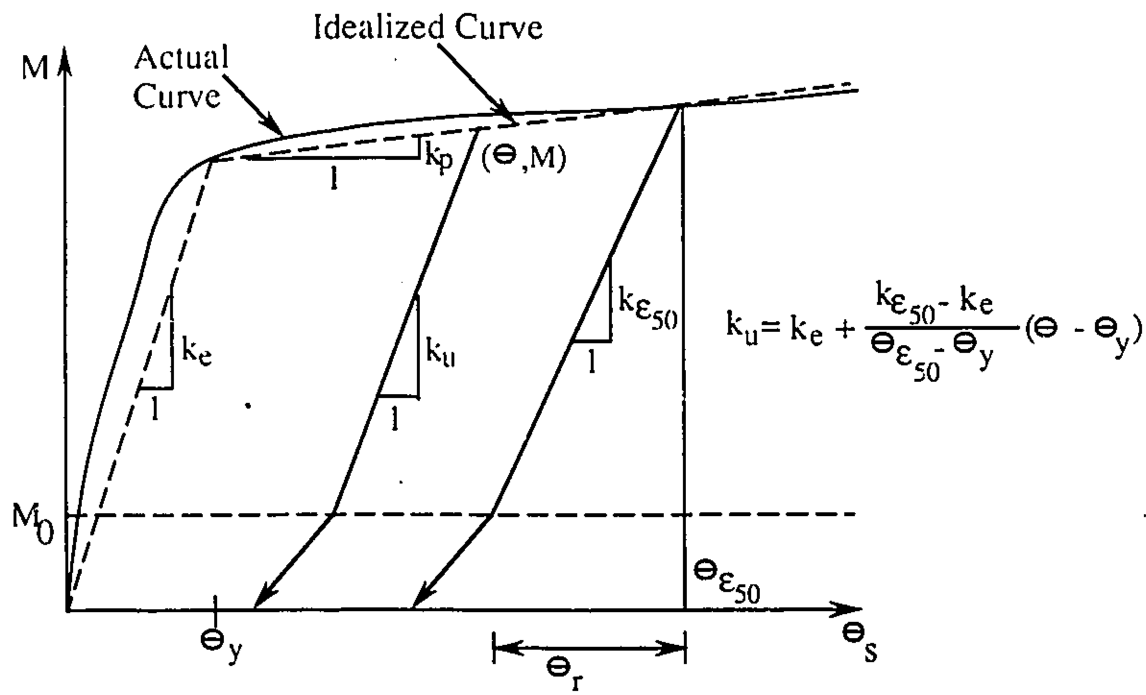

Figure 2.12 Idealized Primary Moment-Slip Relationship

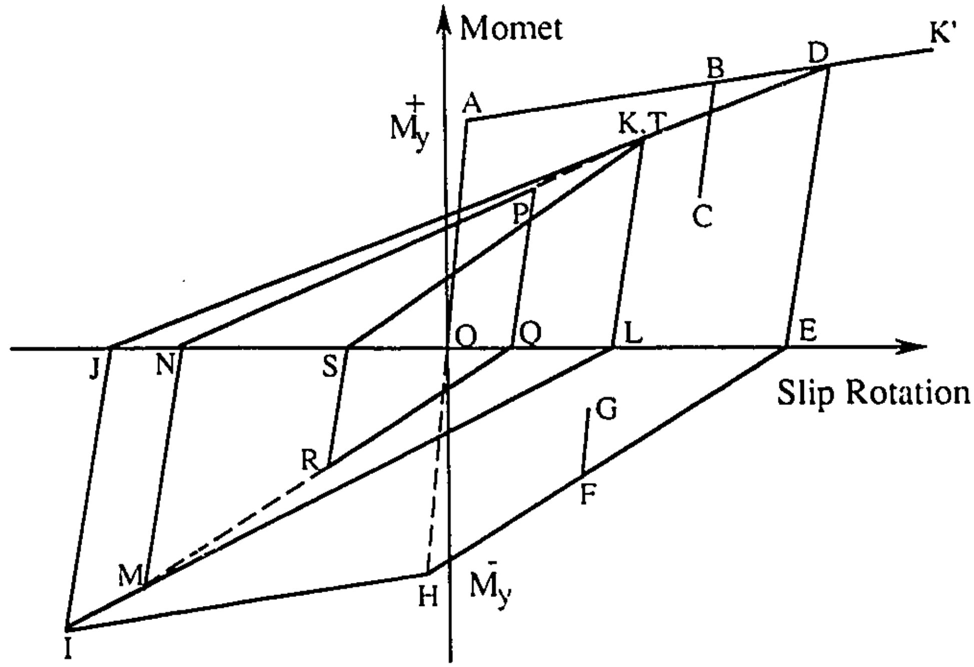

Figure 2.13 Hysteretic Model for Members with Symmetrical Cross Section

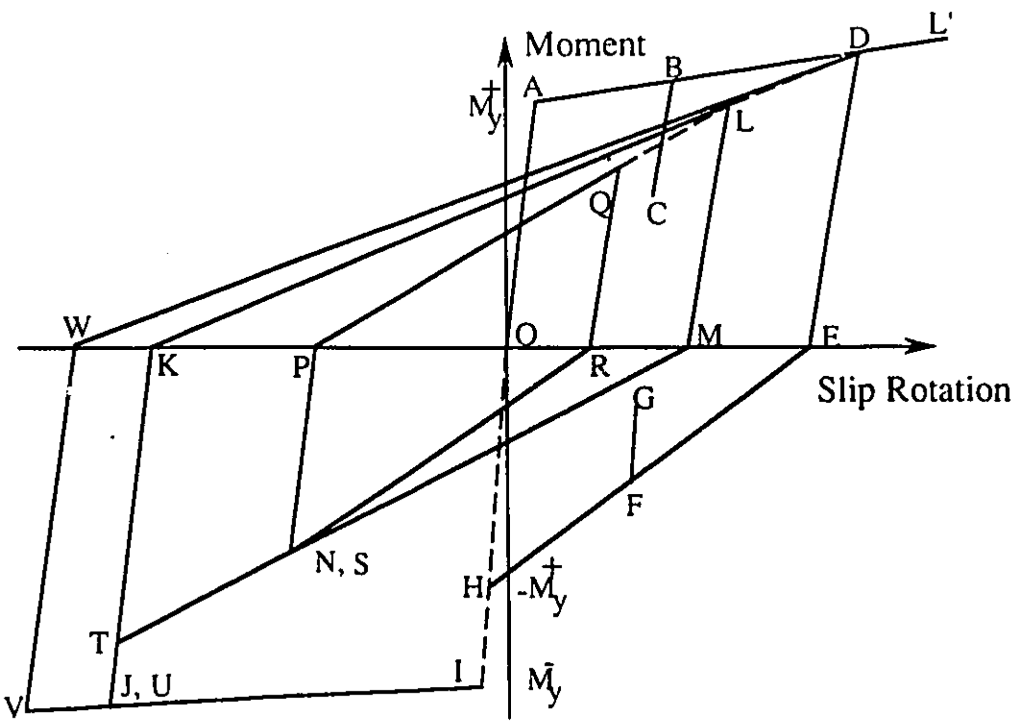

Figure 2.14 Hysteretic Model for Members with Asymmetrical Cross Section

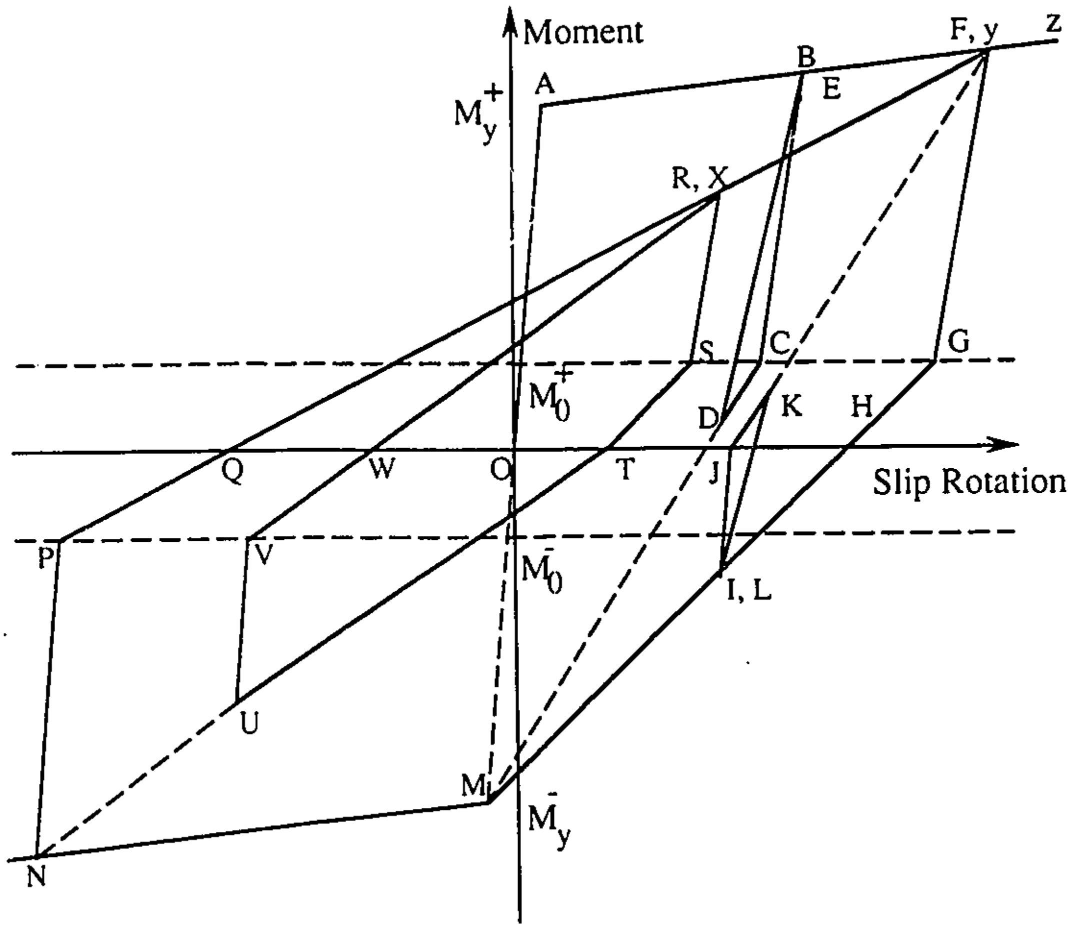

Figure 2.15 Hysteretic Model for Flexural Members Subjected to Axial Load

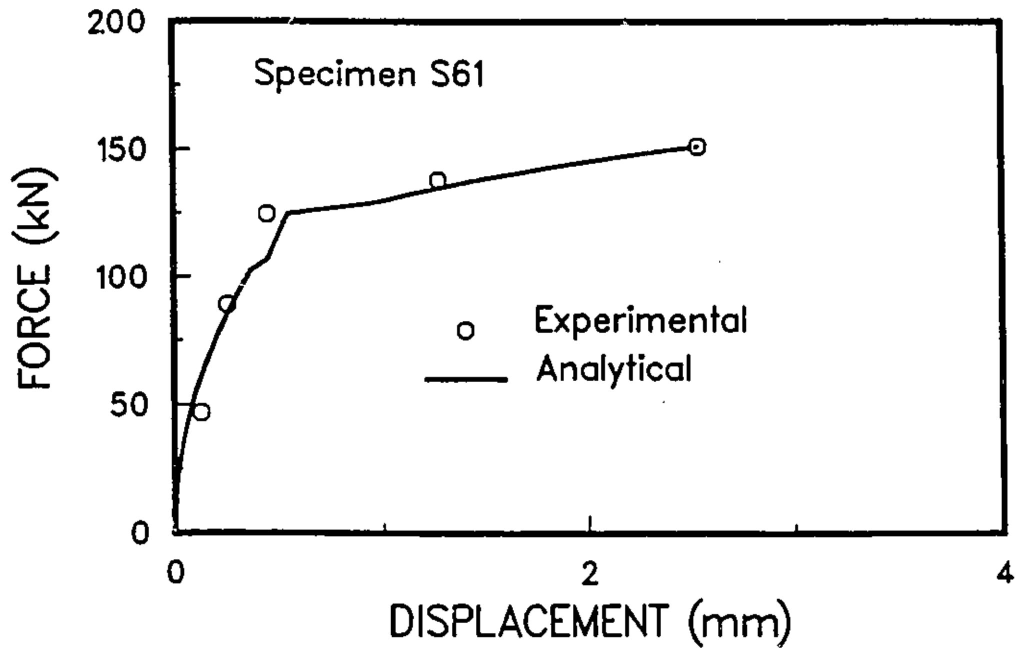

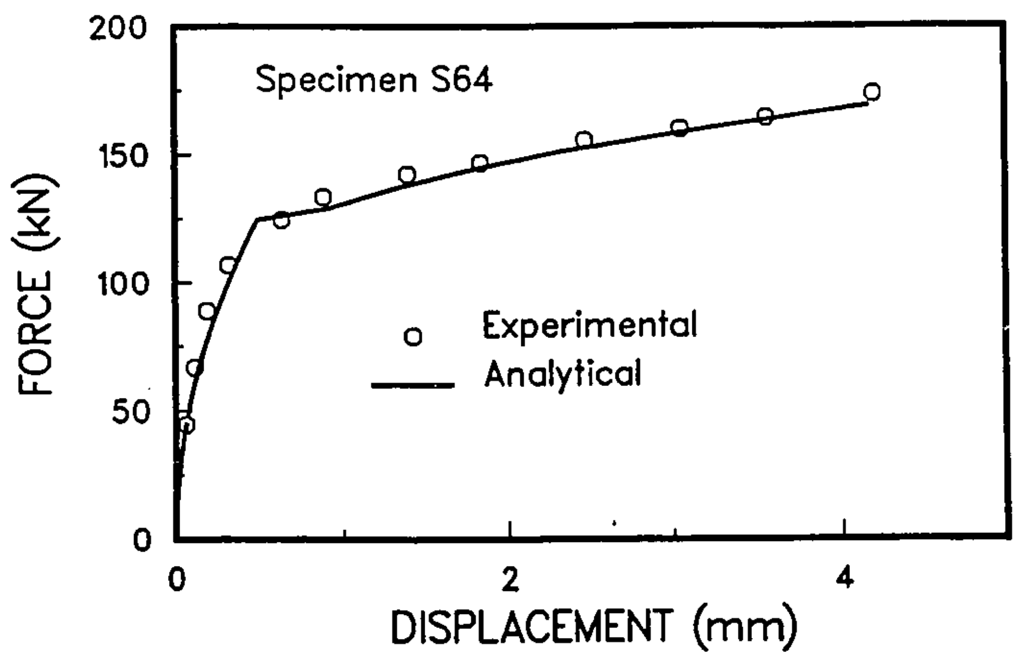

Figure 2.16 Analytical and Experimental Force-Deformation Relationships (Specimens Tested by Ueda et al. [57])

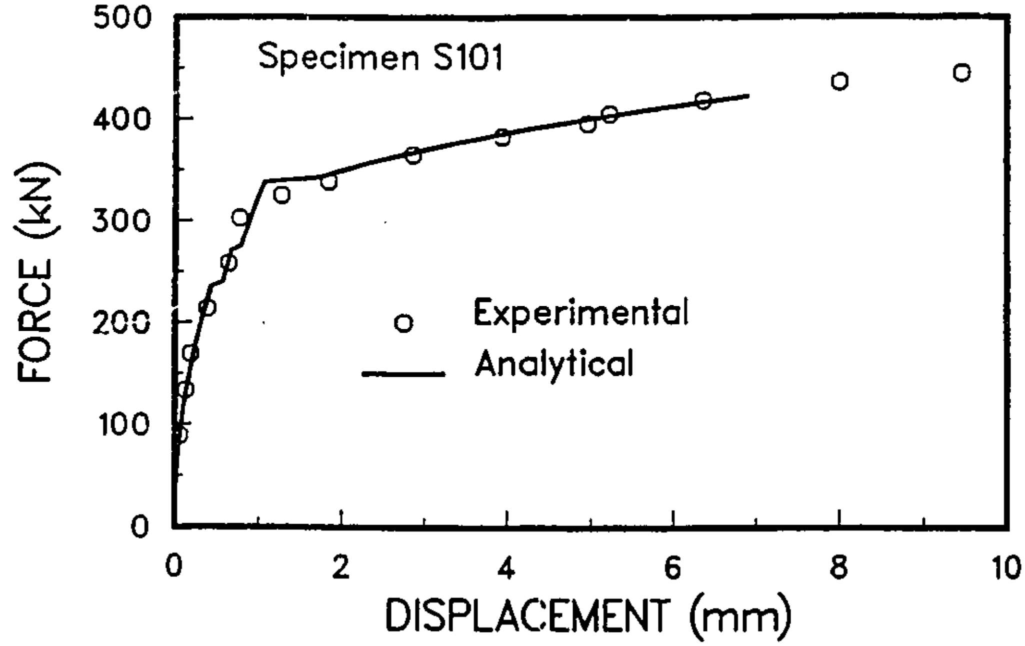

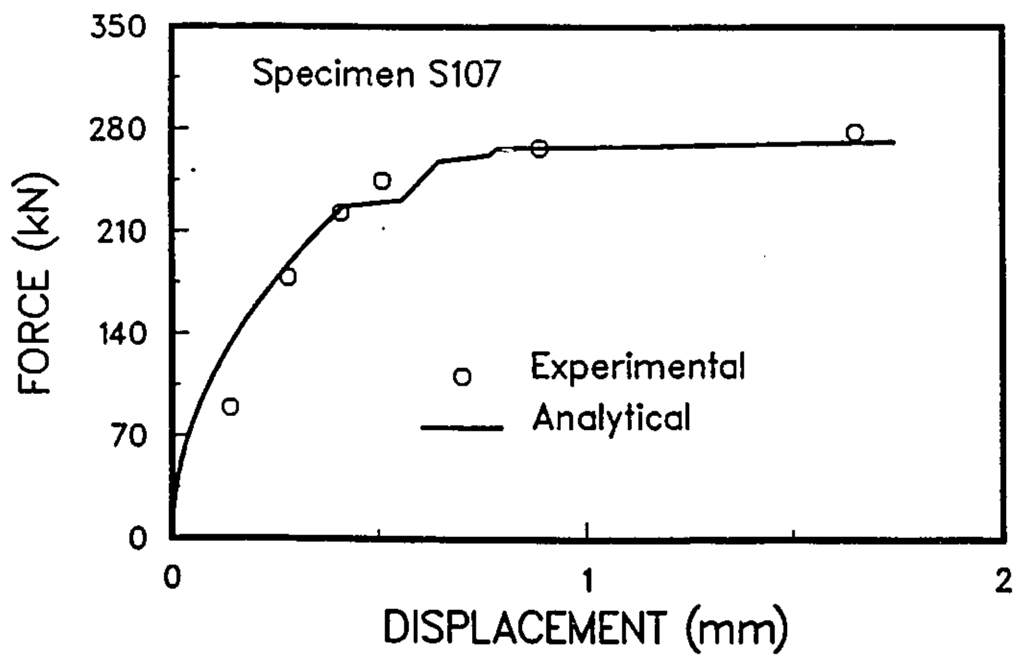

Figure 2.16 Continued

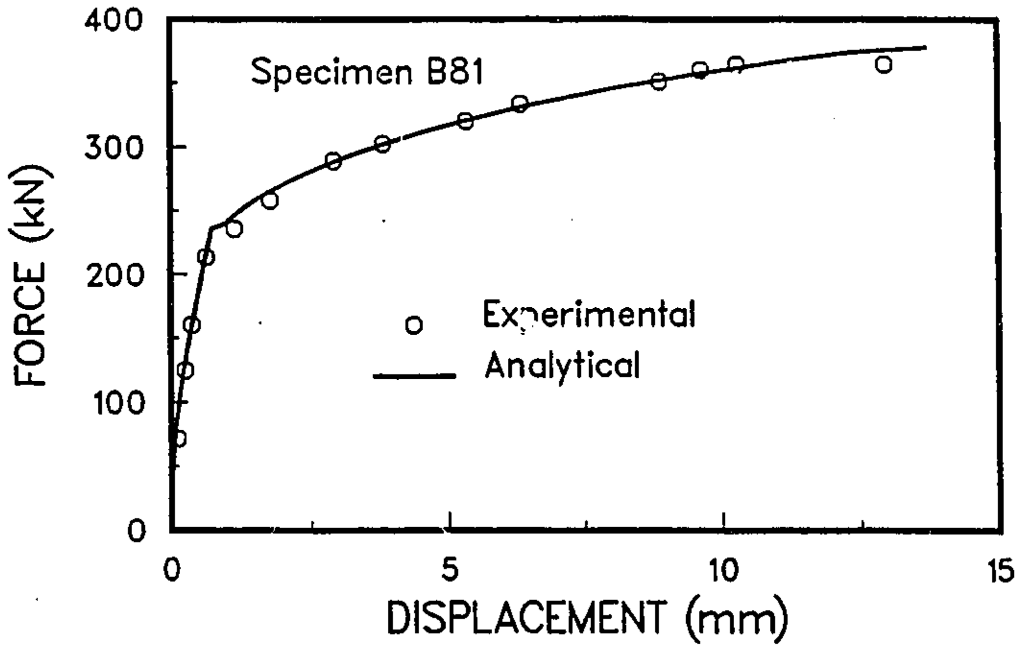

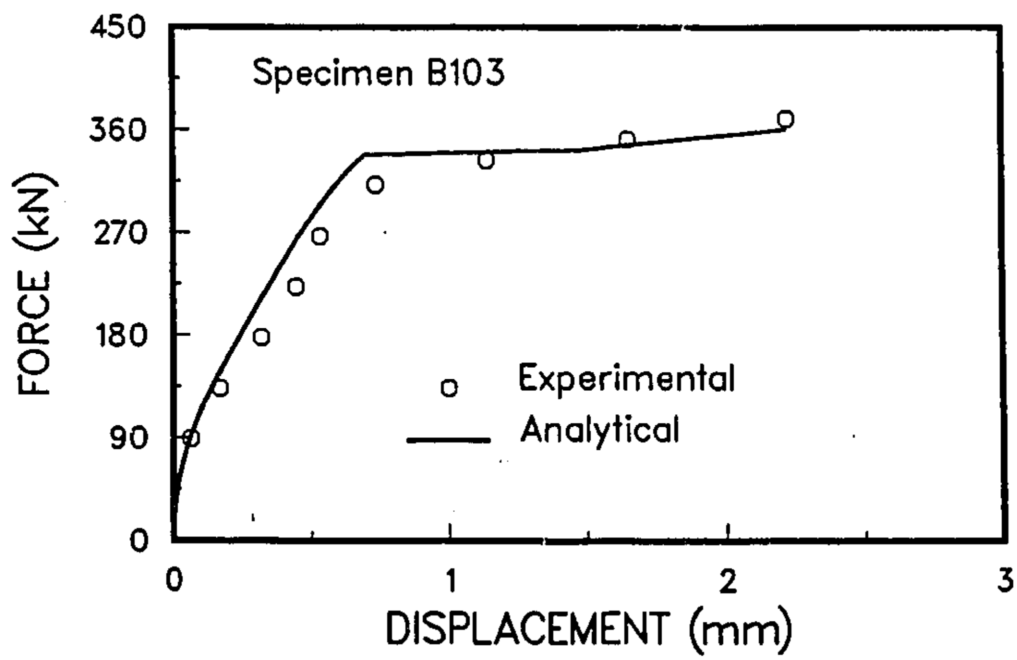

Figure 2.16 Continued

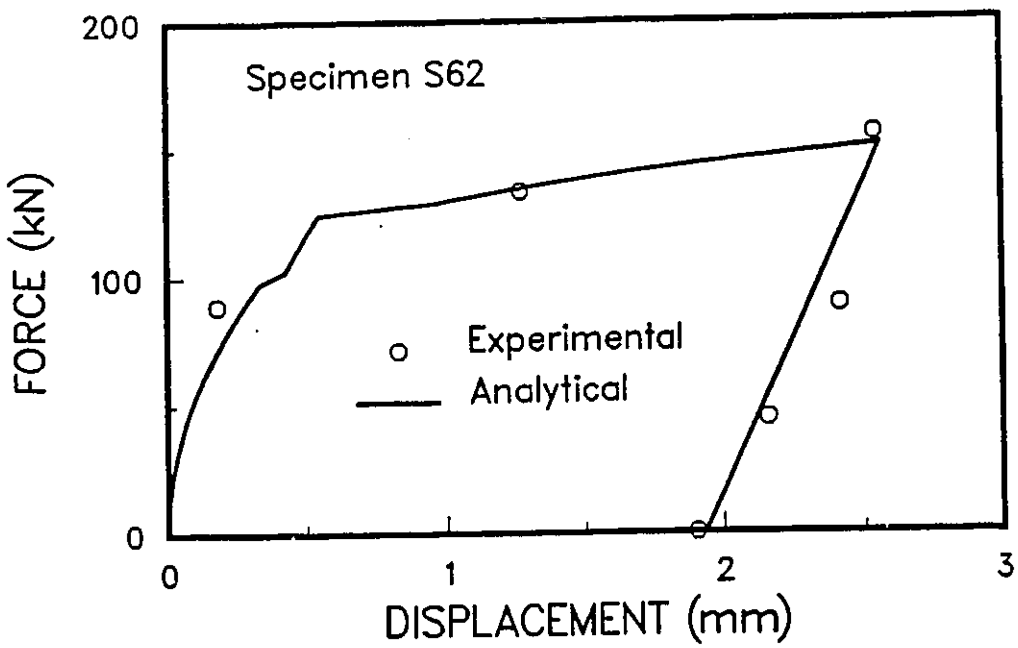

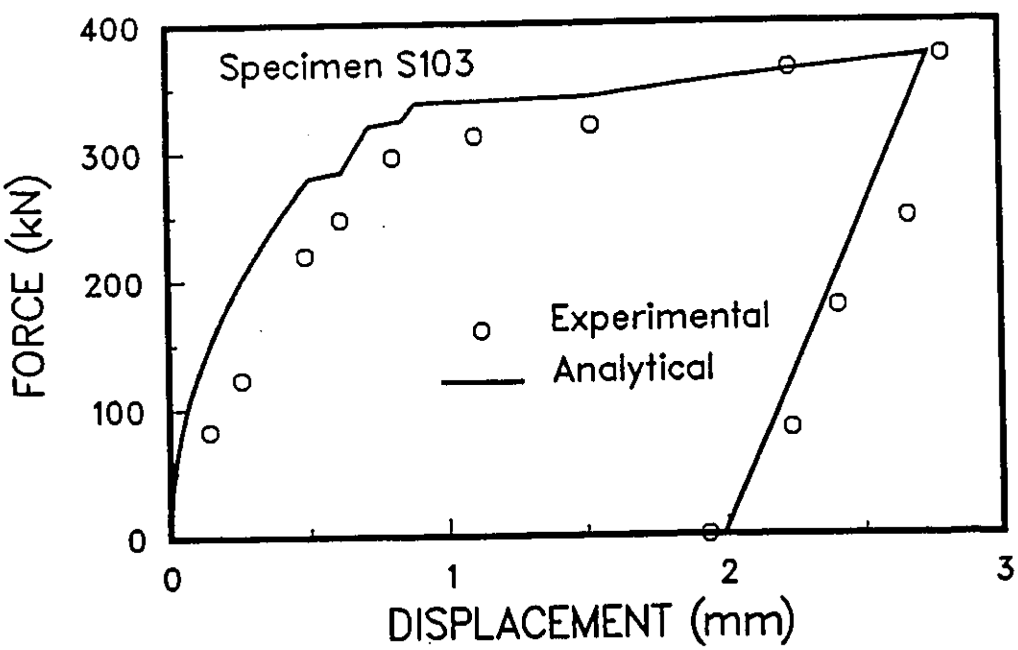

Figure 2.16 Continued

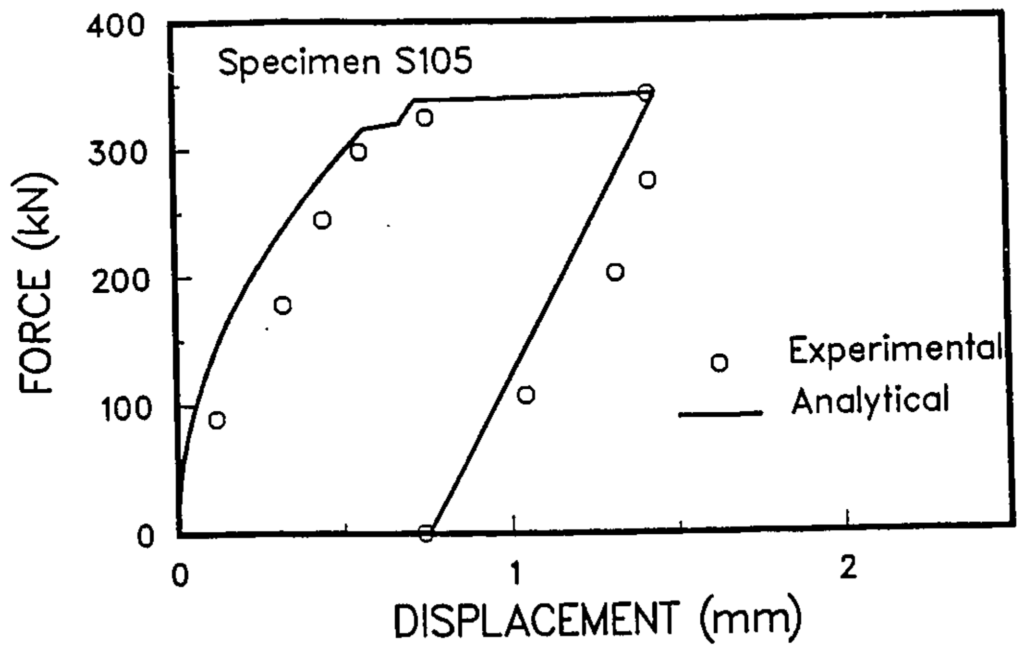

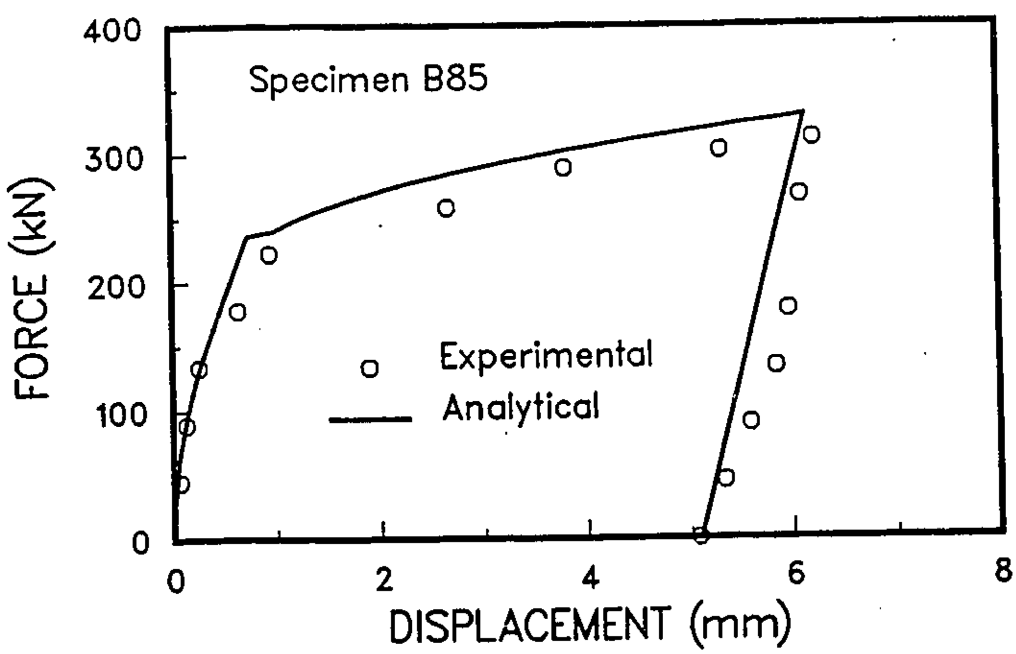

Figure 2.16 Continued

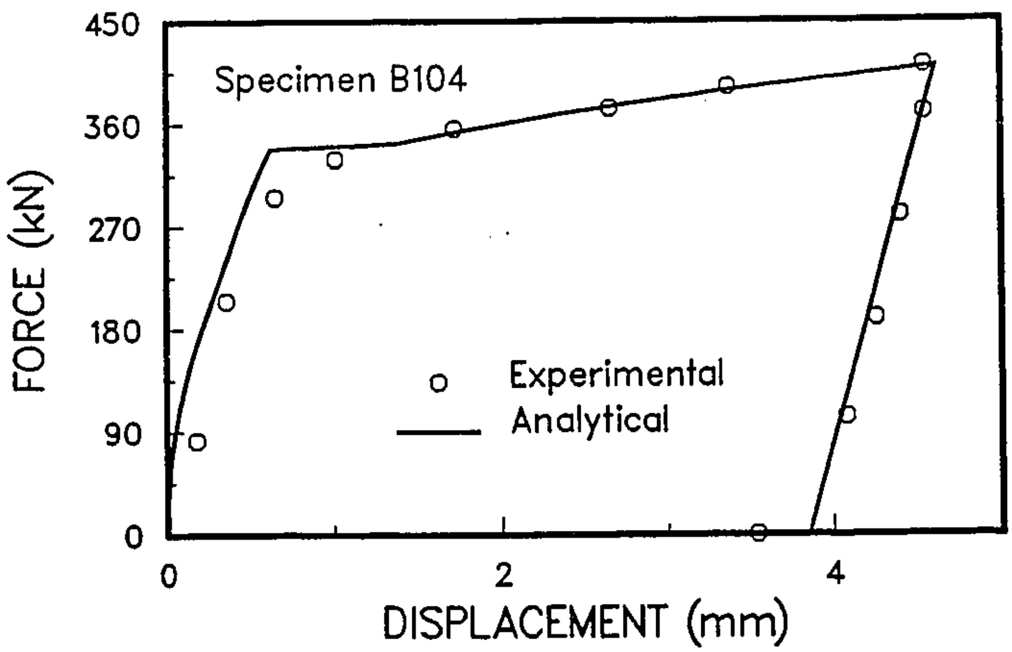

Figure 2.16 Continued

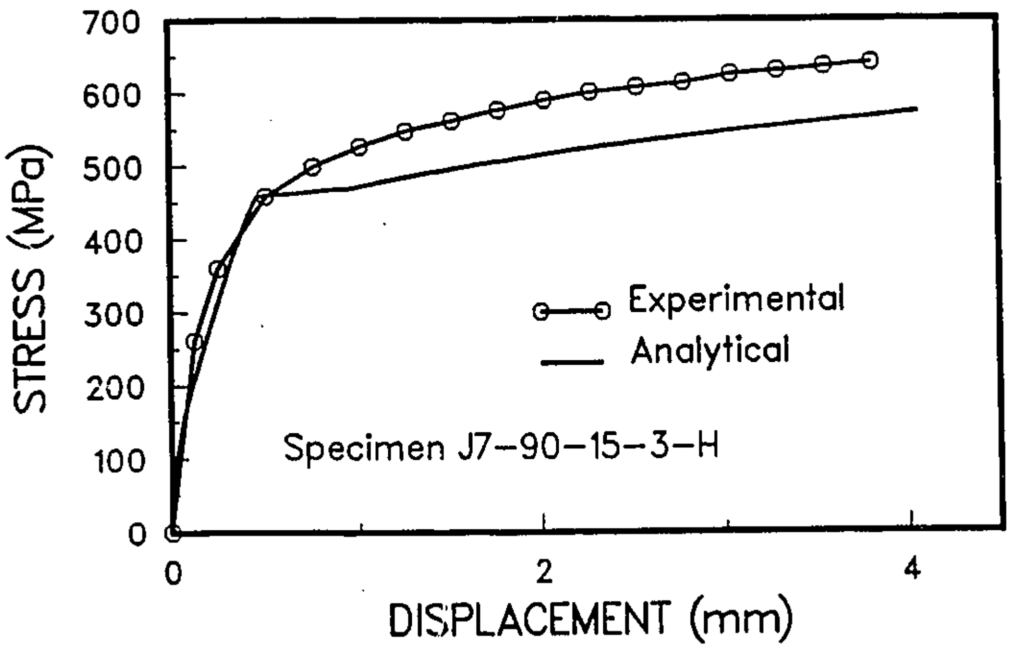

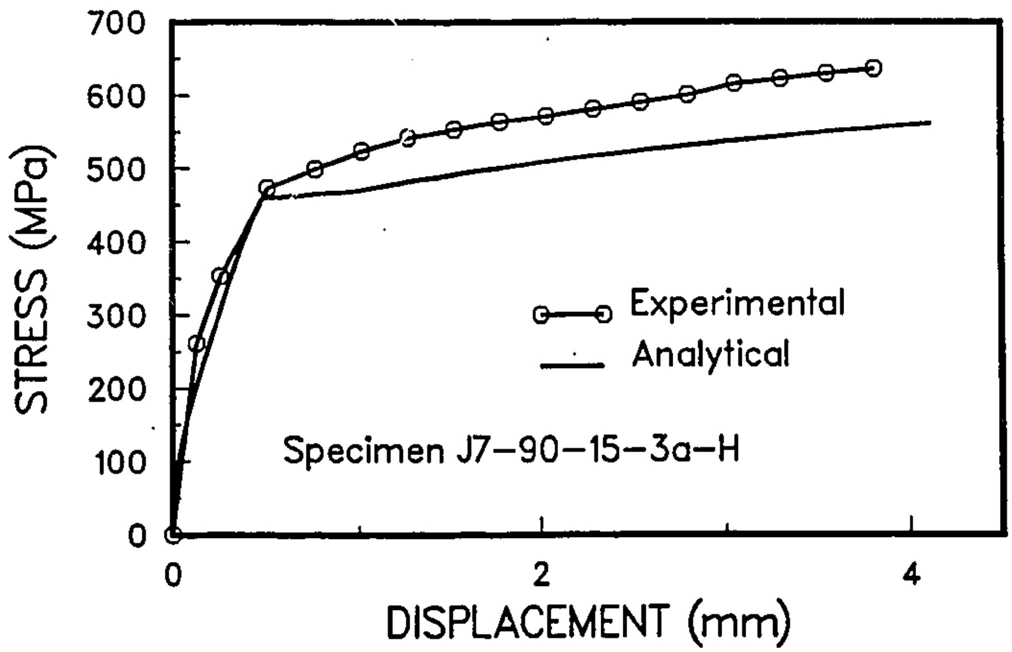

Figure 2.17 Analytical and Experimental Force-Deformation Relationships (Specimens Tested by Marques and Jirsa [53])

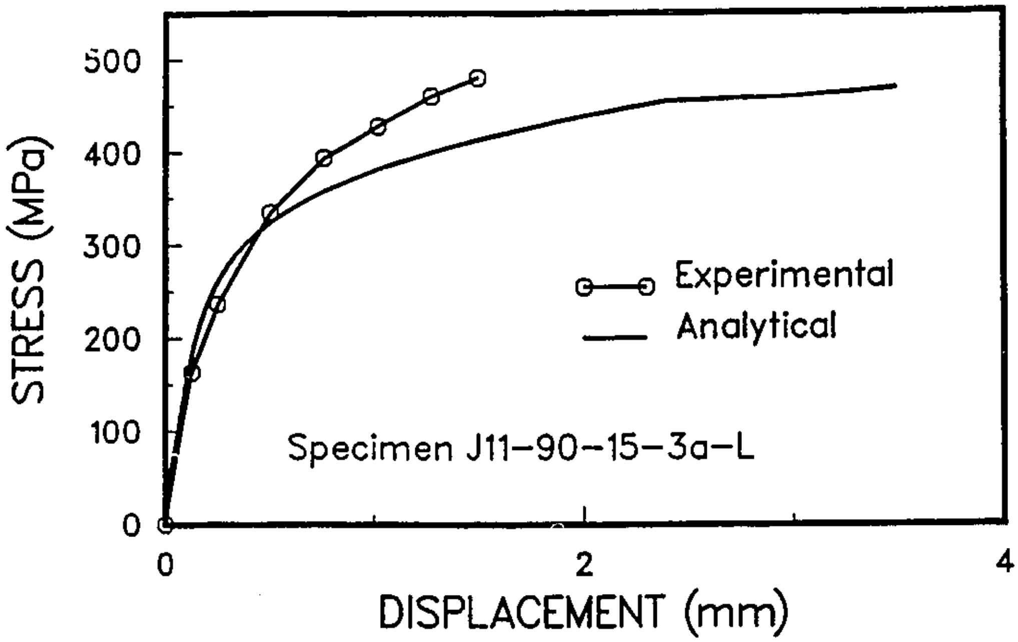

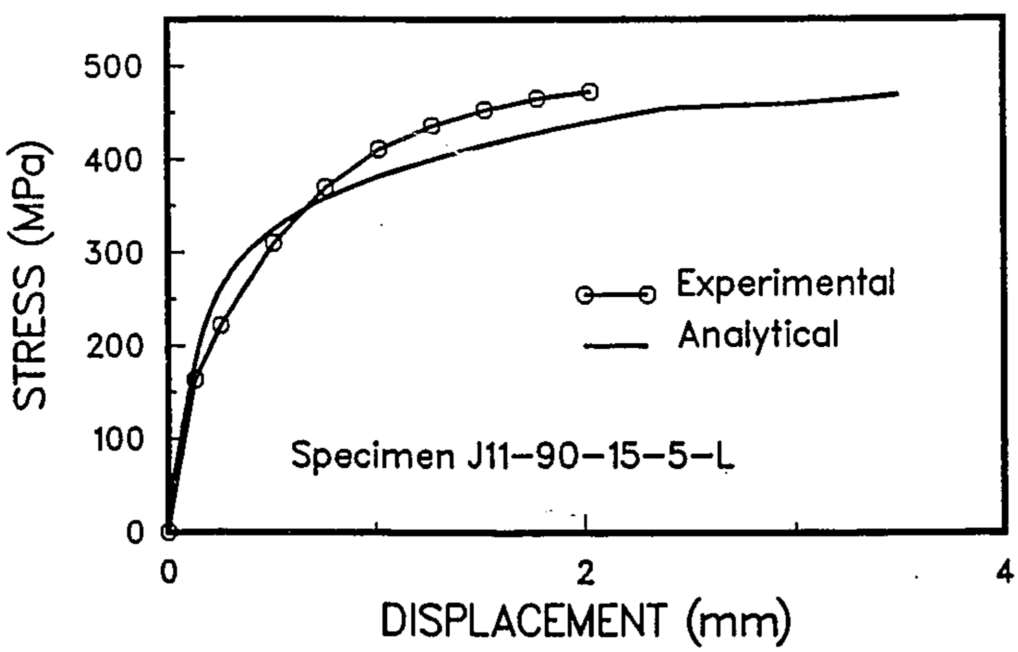

Figure 2.17 Continued

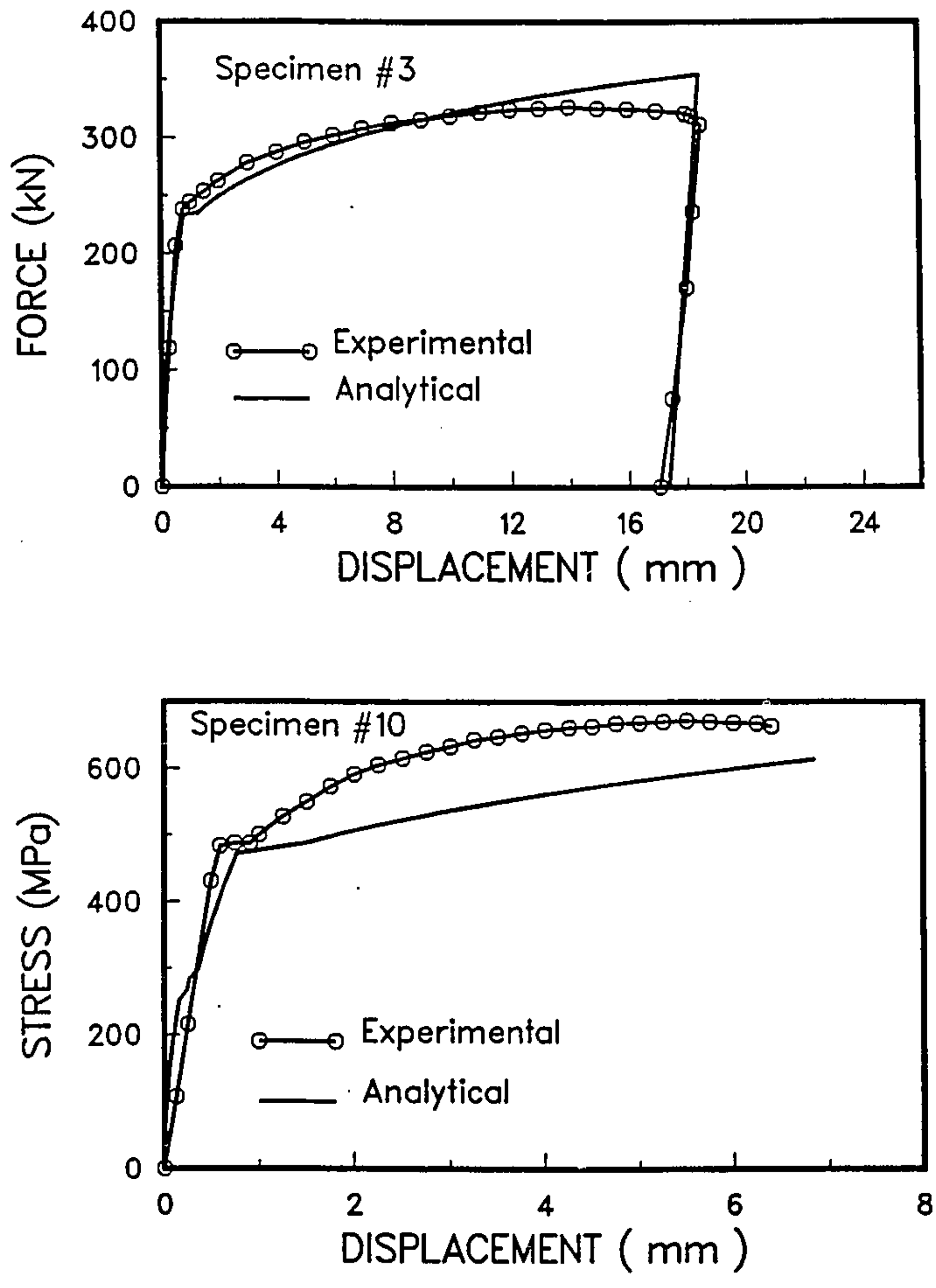

Figure 2.18 Analytical and Experimental Force-Deformation Relationships (Specimens Tested by Viwathanatepa et al. [55])

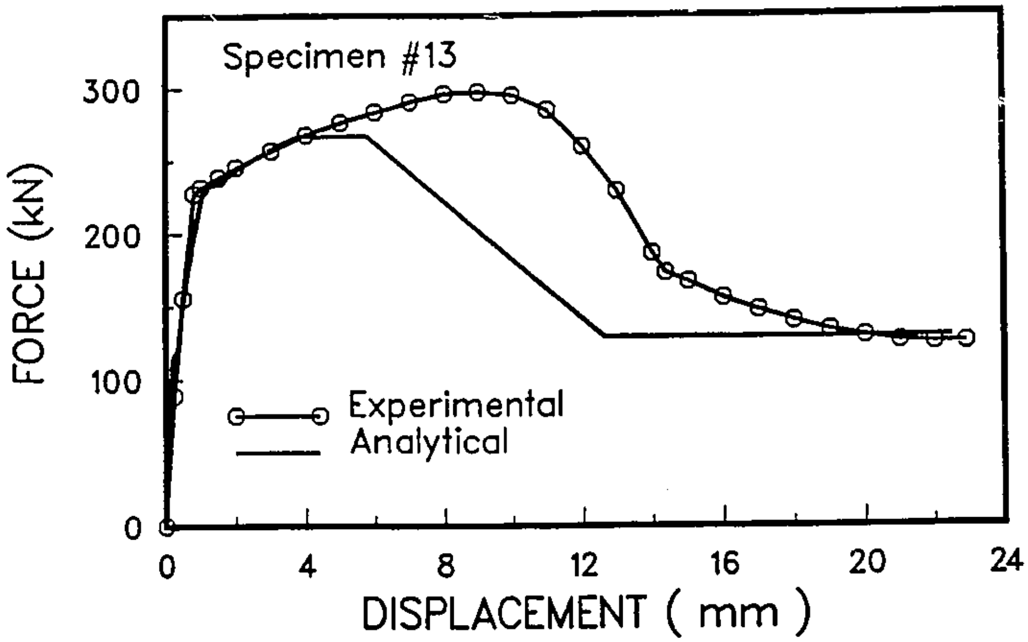

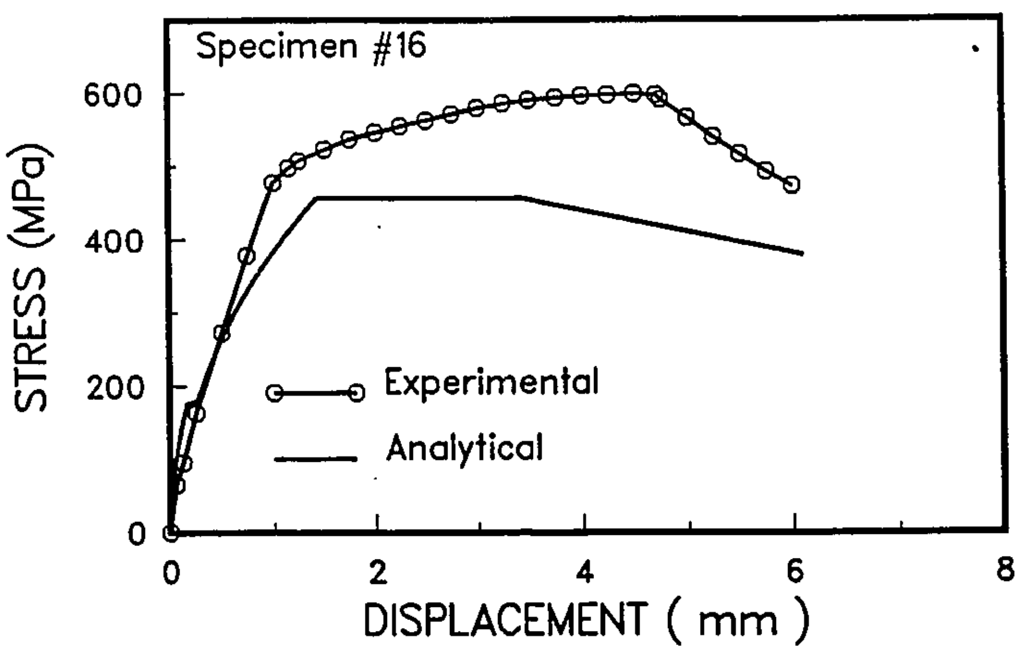

Figure 2.18 Continued

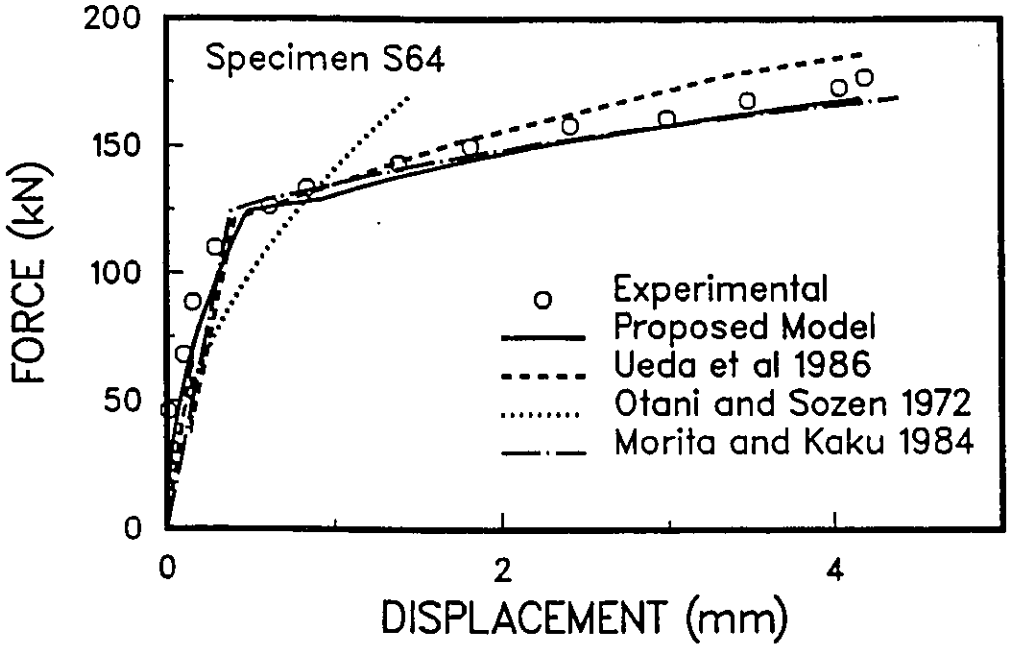

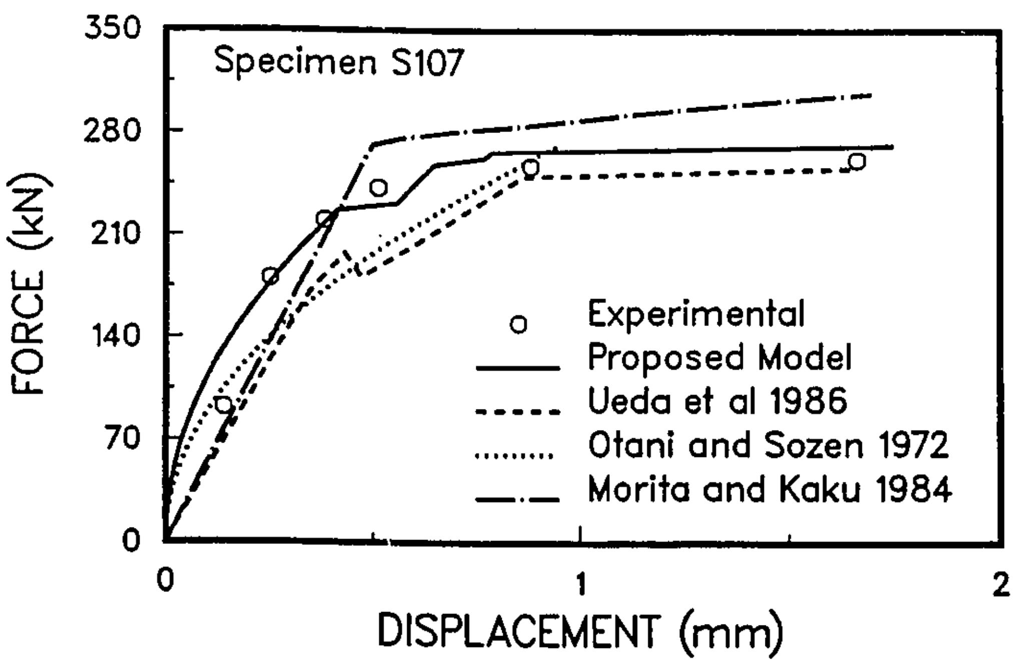

Figure 2.19 Comparisons with Previous Analytical Predictions

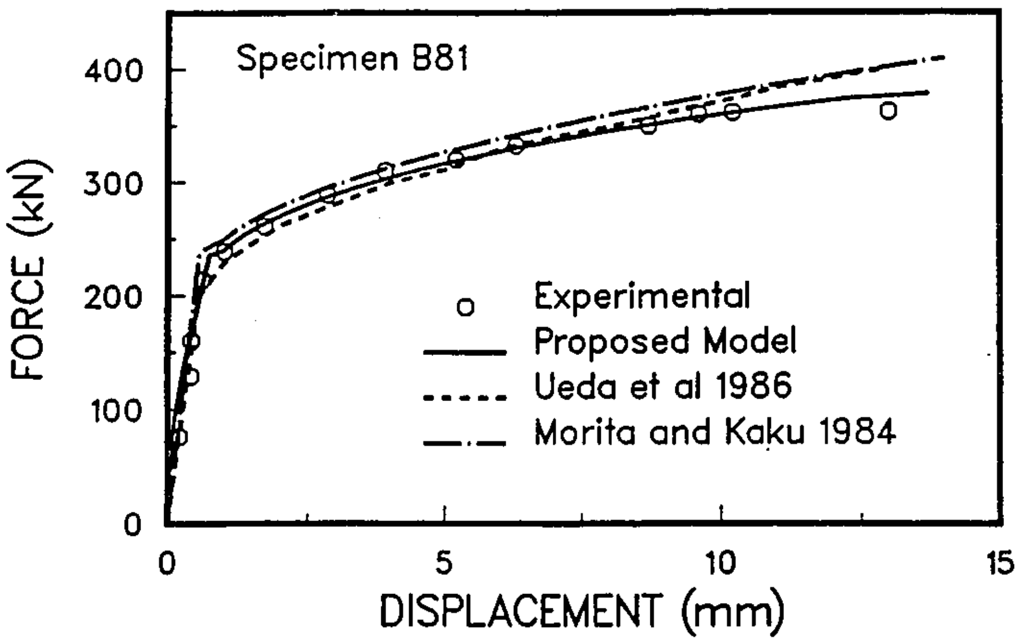

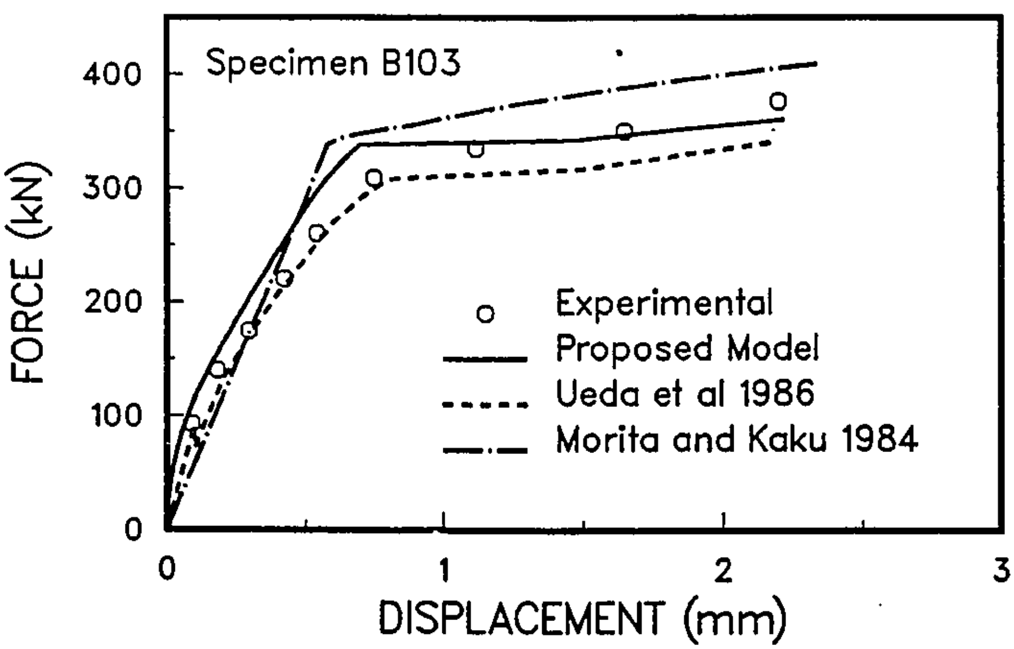

Figure 2.19 Continued

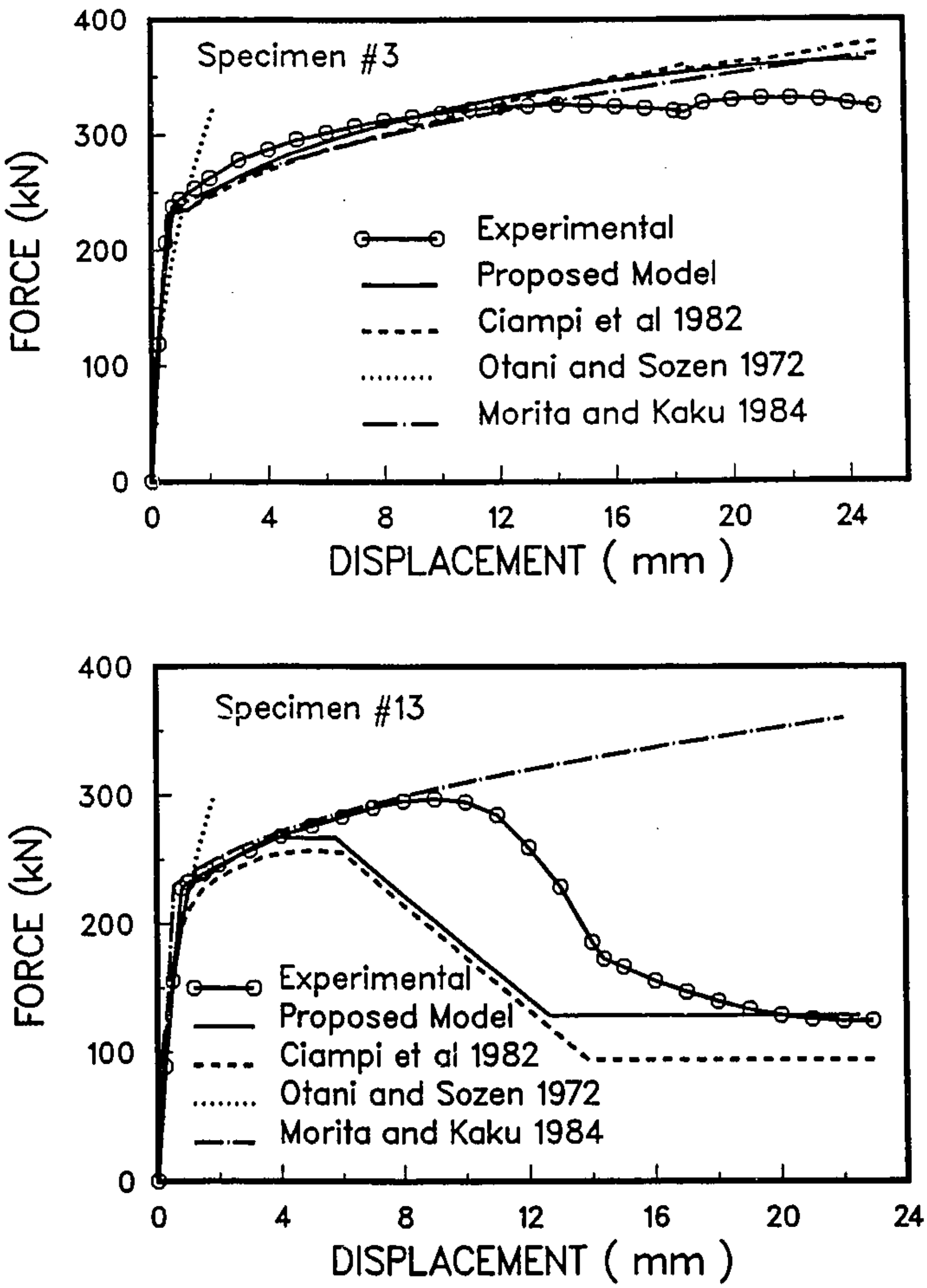

Figure 2.19 Continued

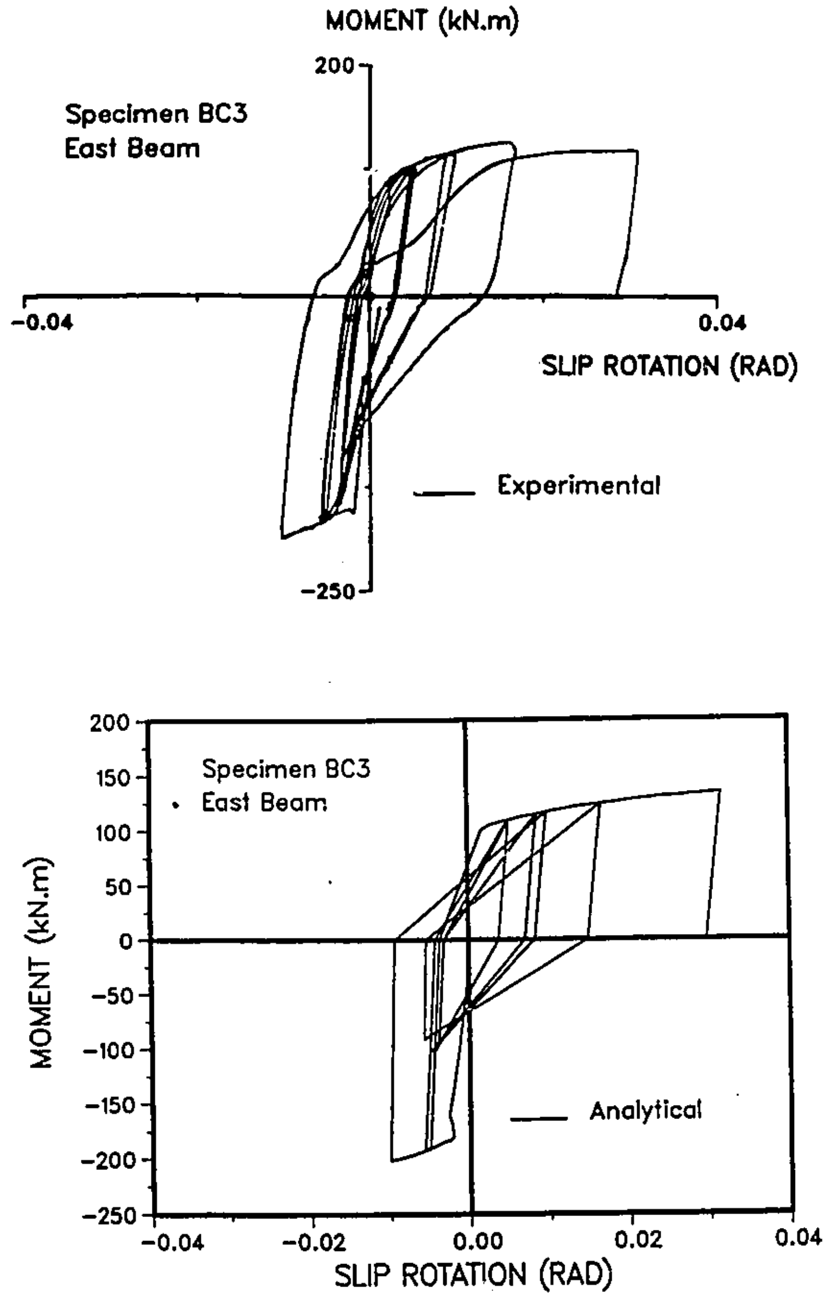

(a) East Beam

Figure 2.20 Analytical and Experimental Moment-Anchorage Slip Relationships (Specimens BC3 Tested by Viwathanatepa et al. [46])

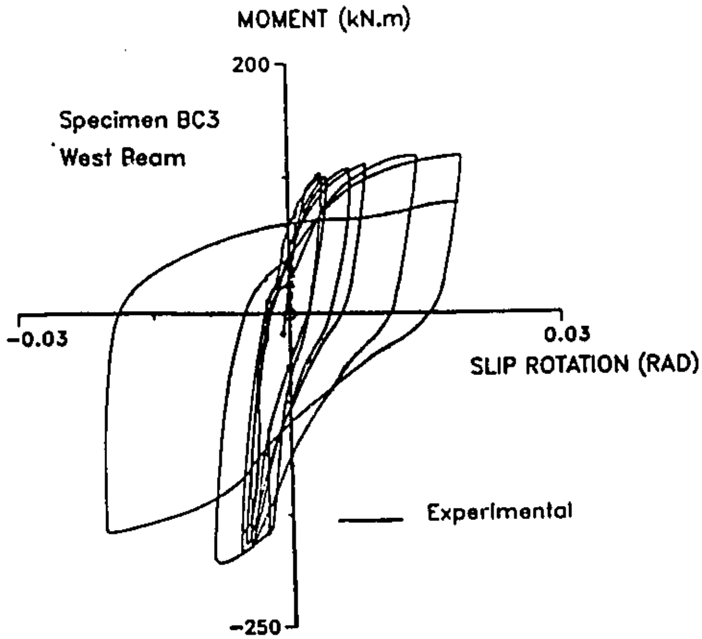

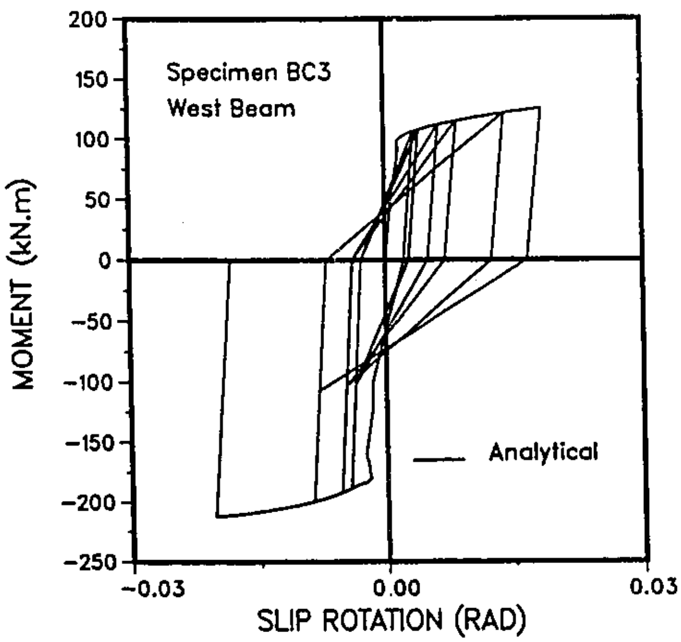

(b) West Beam

Figure 2.20 Continued

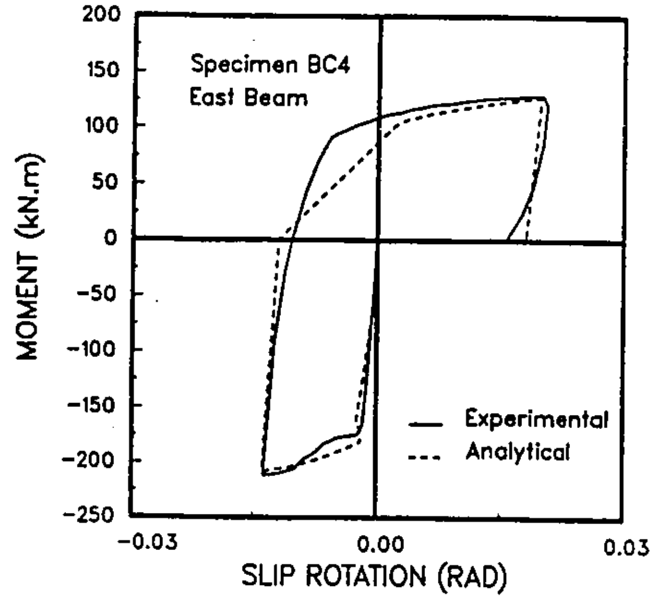

(a) East Beam

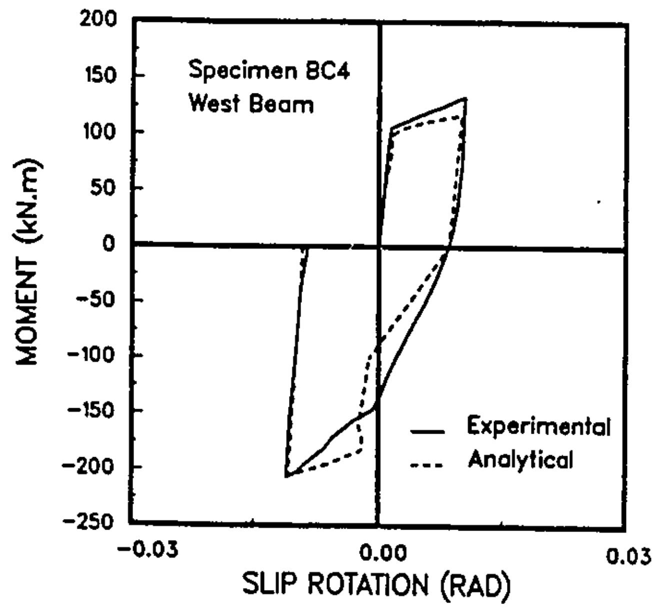

(b) West Beam

Figure 2.21 Analytical and Experimental Moment-Anchorage Slip Relationships (Specimens BC4 Tested by Viwathanatepa et al. [46])

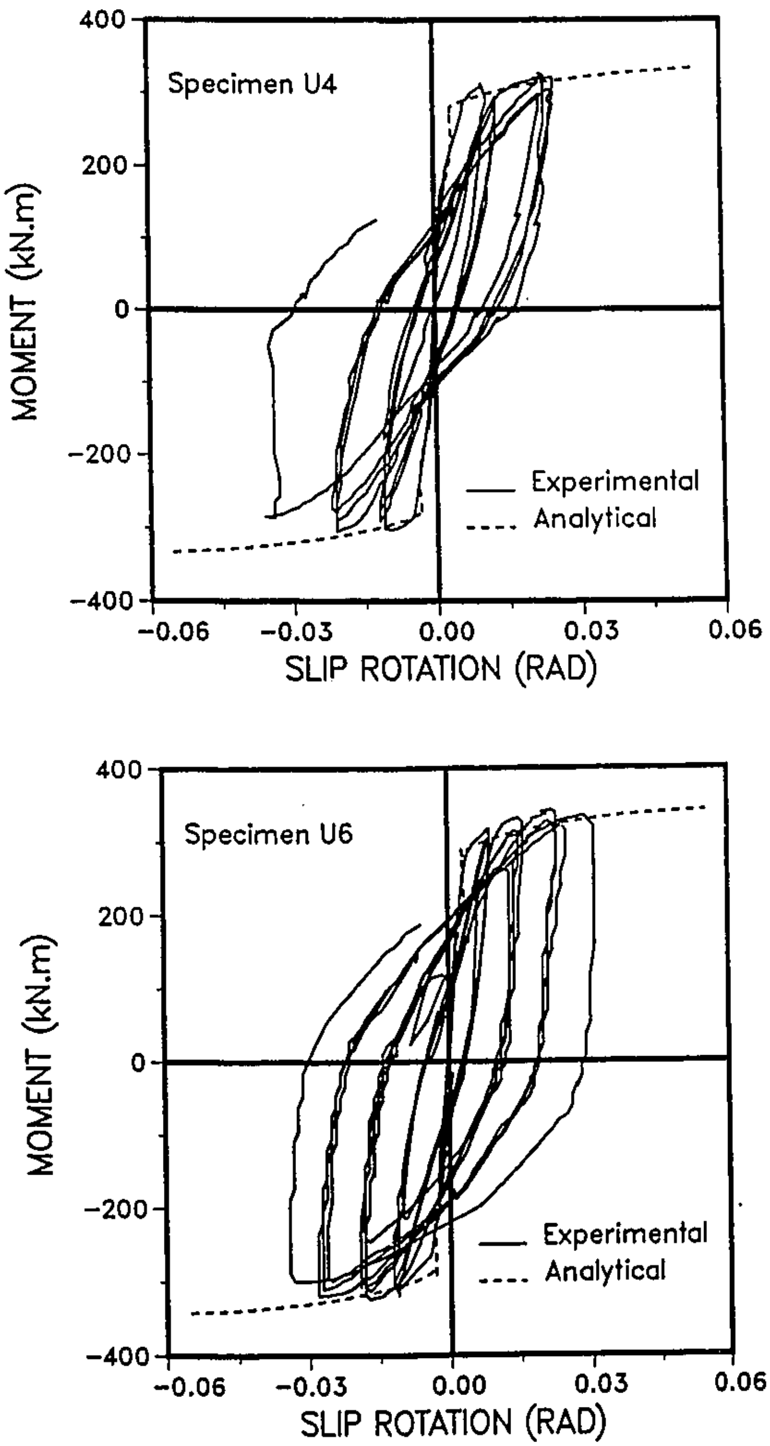

Figure 2.22 Analytical and Experimental Moment-Anchorage Slip Relationships (Specimens Tested by Saatcioglu and Ozcebe [44])

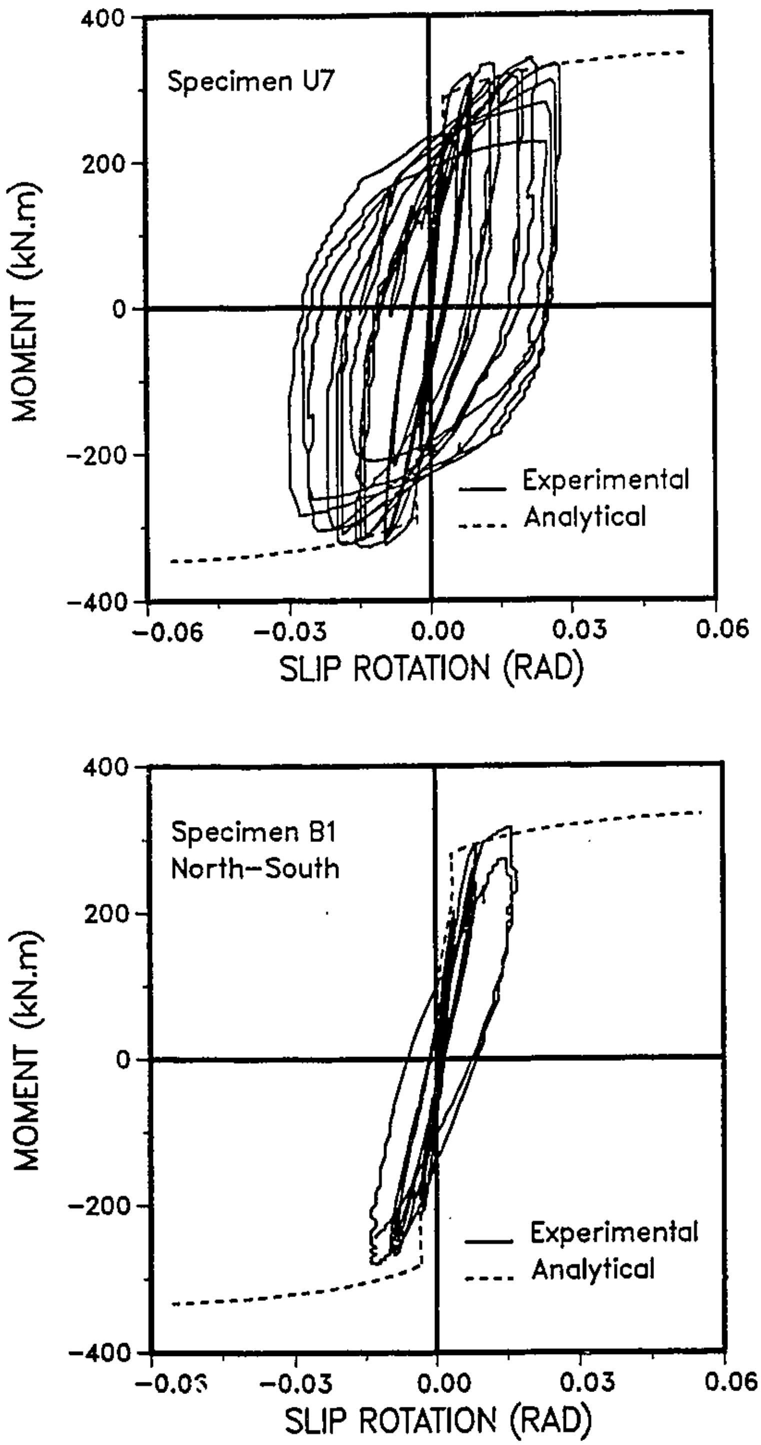

Figure 2.22 Continued

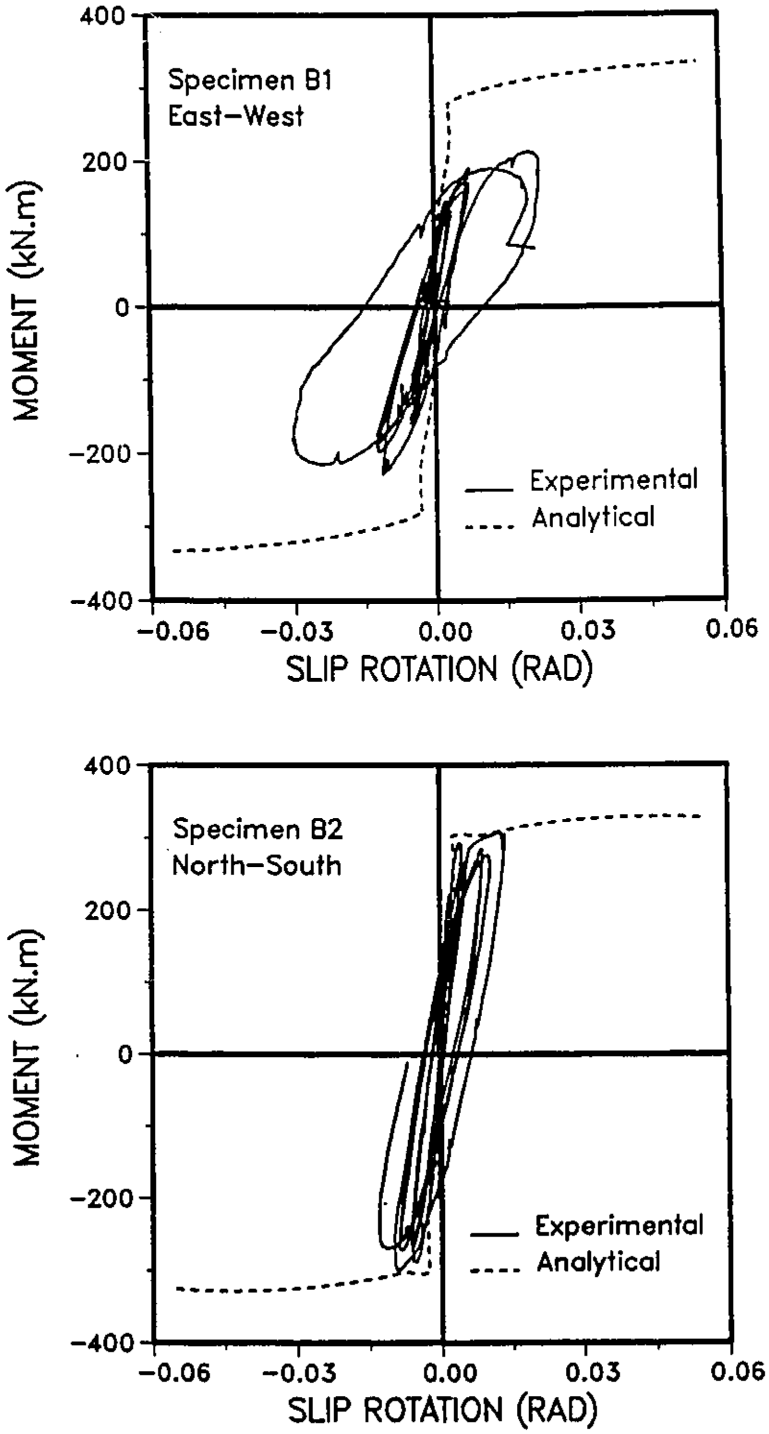

Figure 2.22 Continued

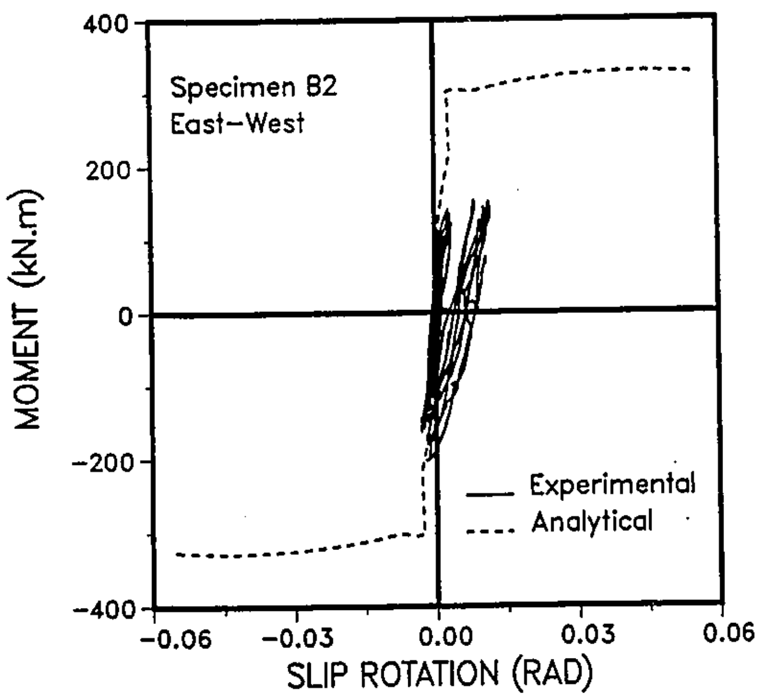

Figure 2.22 Continued

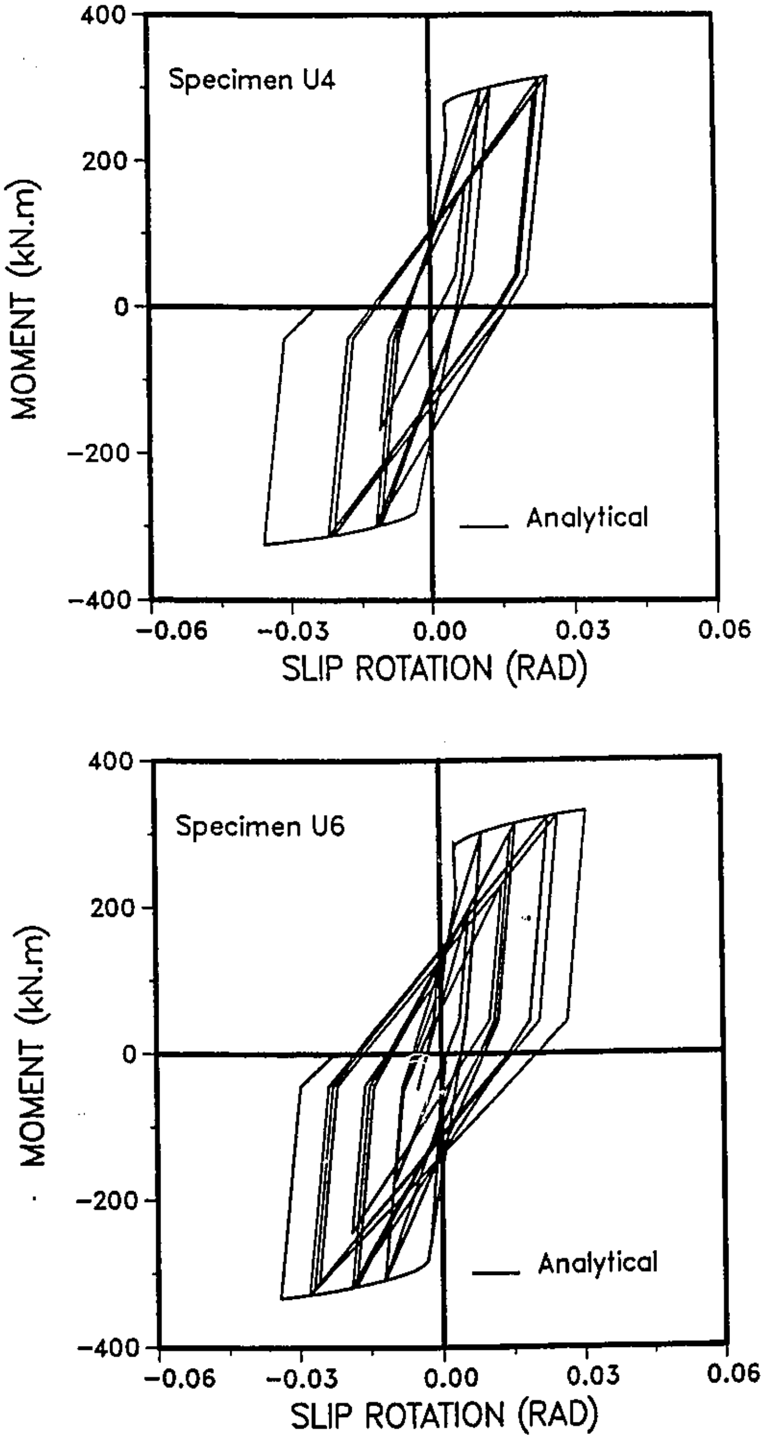

Figure 2.23 Analytical Hysteretic Relationships (Specimens Tested by Saatcioglu and Ozcebe [44])

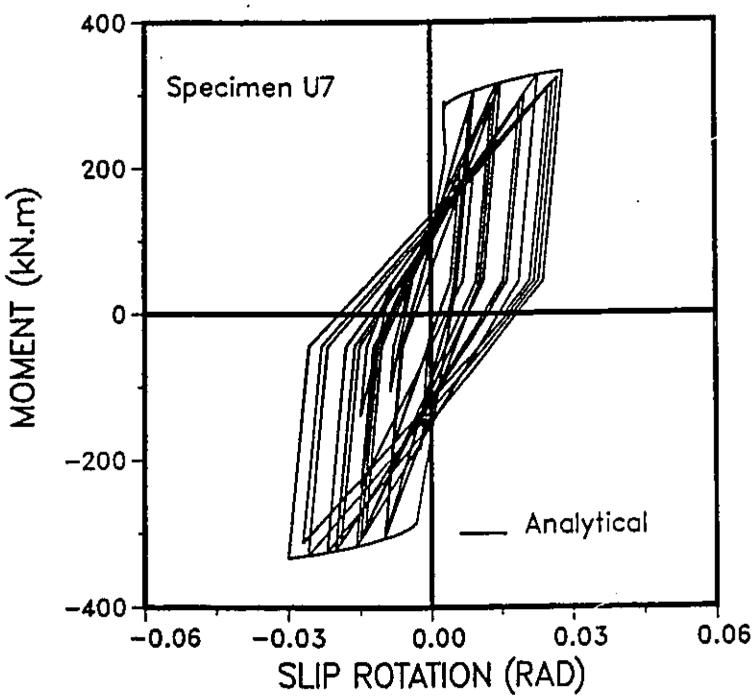

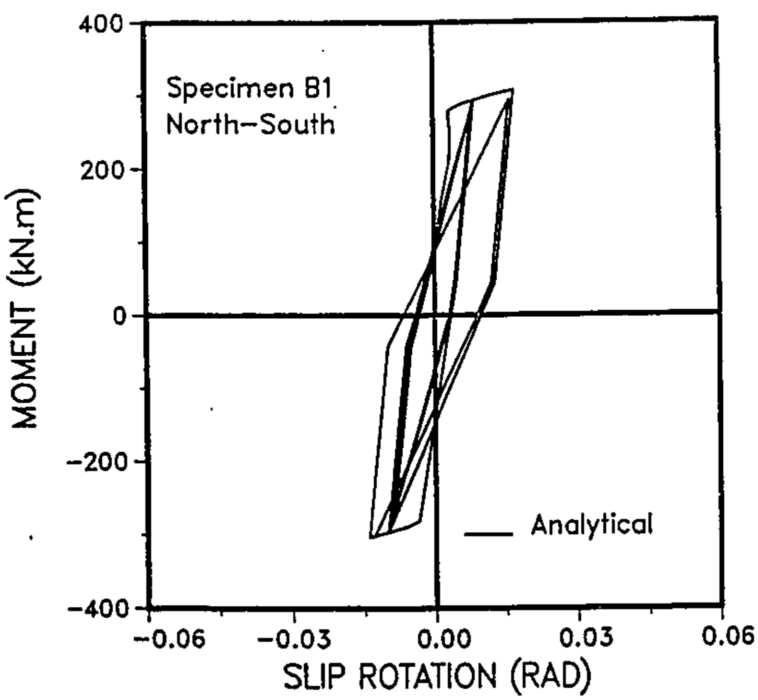

Figure 2.23 Continued

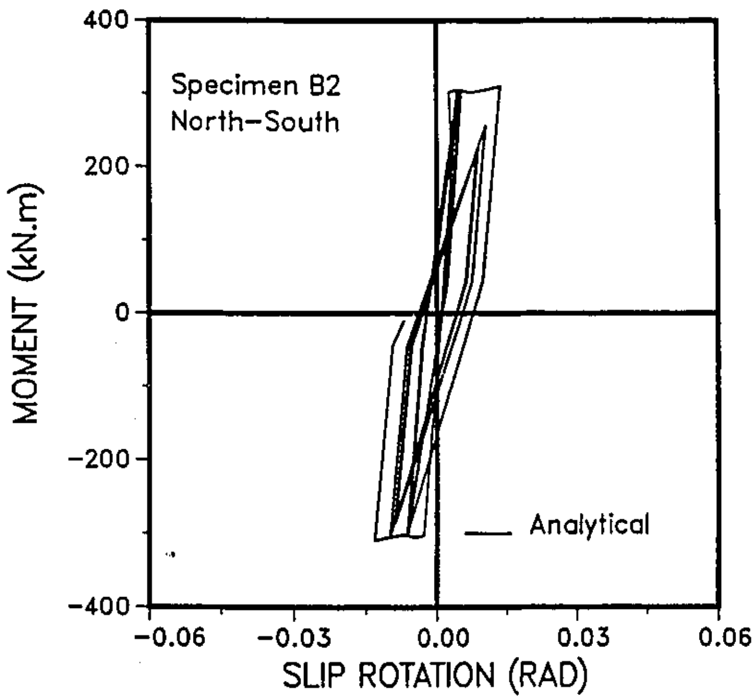

Figure 2.23 Continued

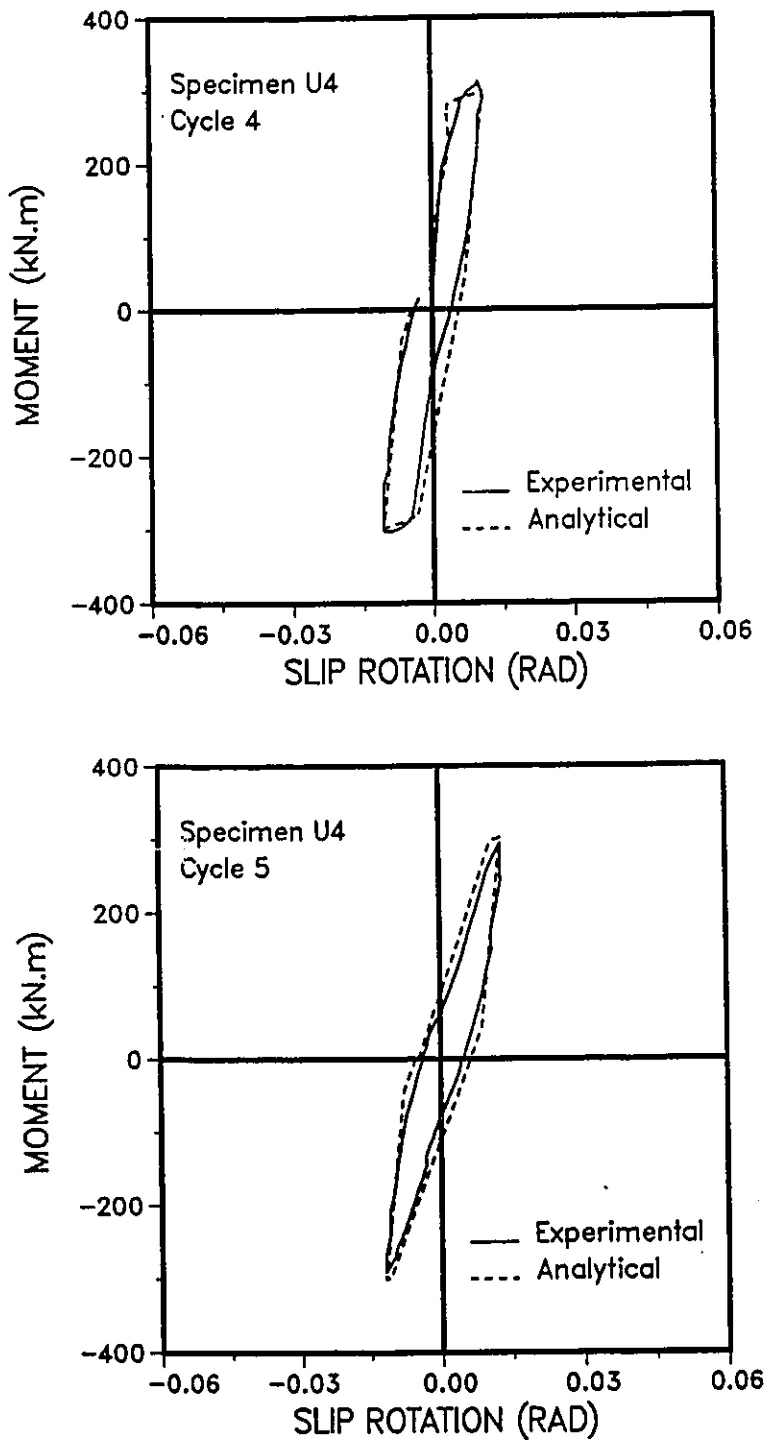

Figure 2.24 Comparisons Between Analytical and Experimental hysteretic Loops (Specimens Tested by Saatcioglu and Ozcebe [44])

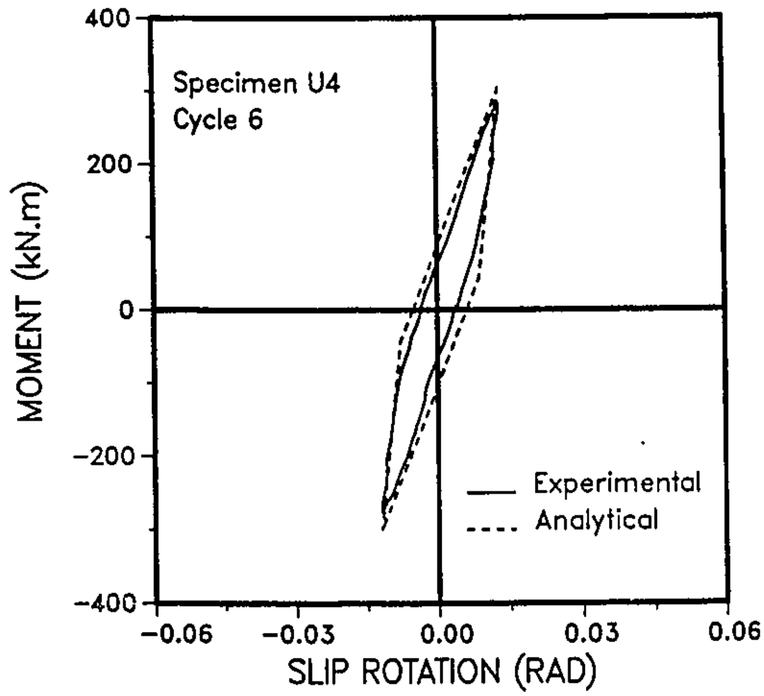

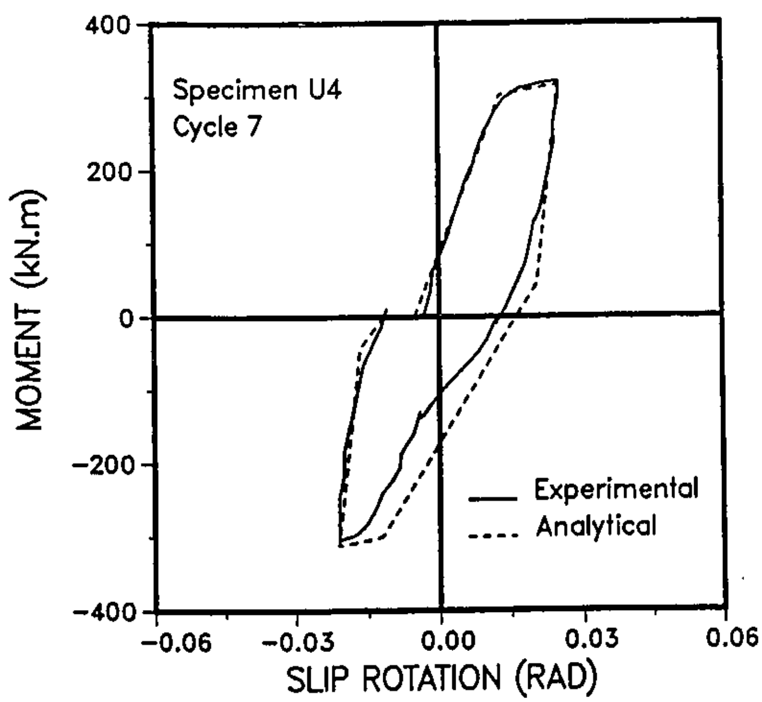

Figure 2.24 Continued

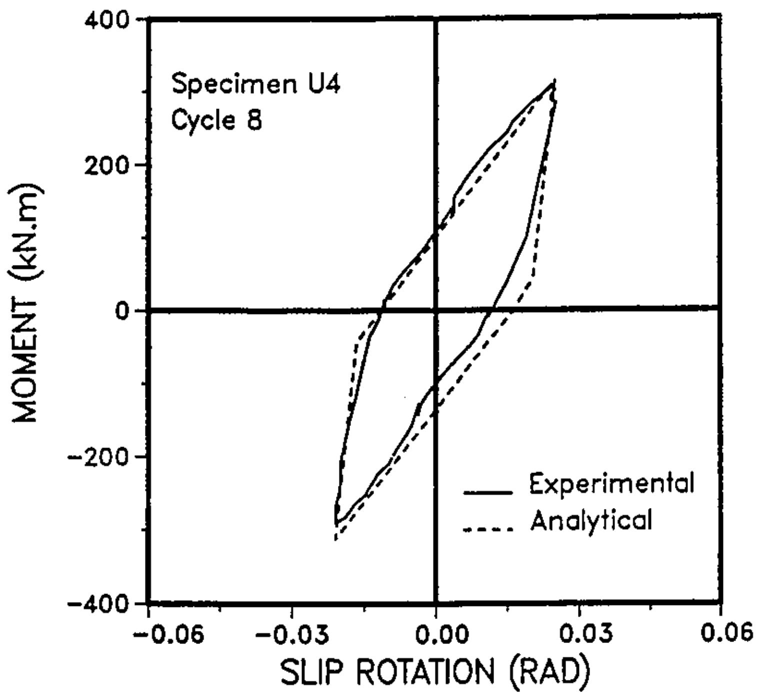

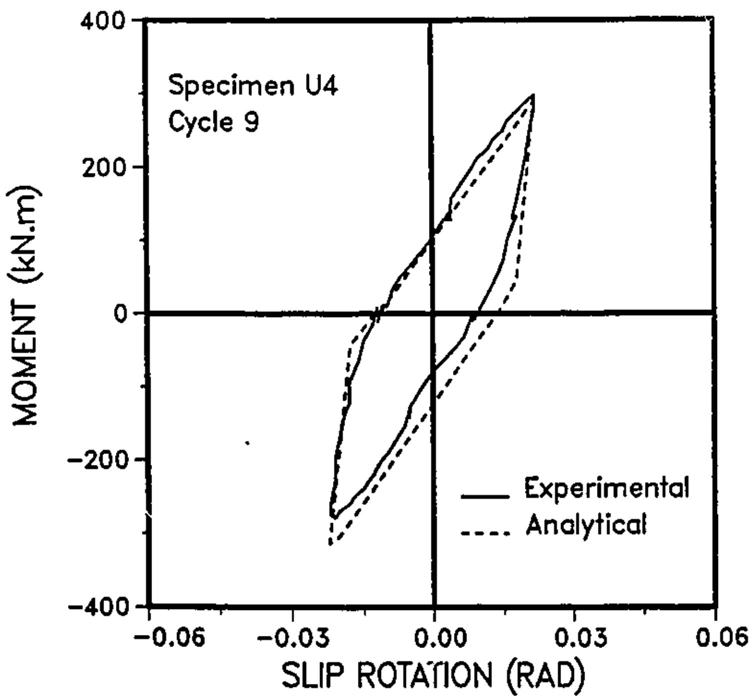

Figure 2.24 Continued

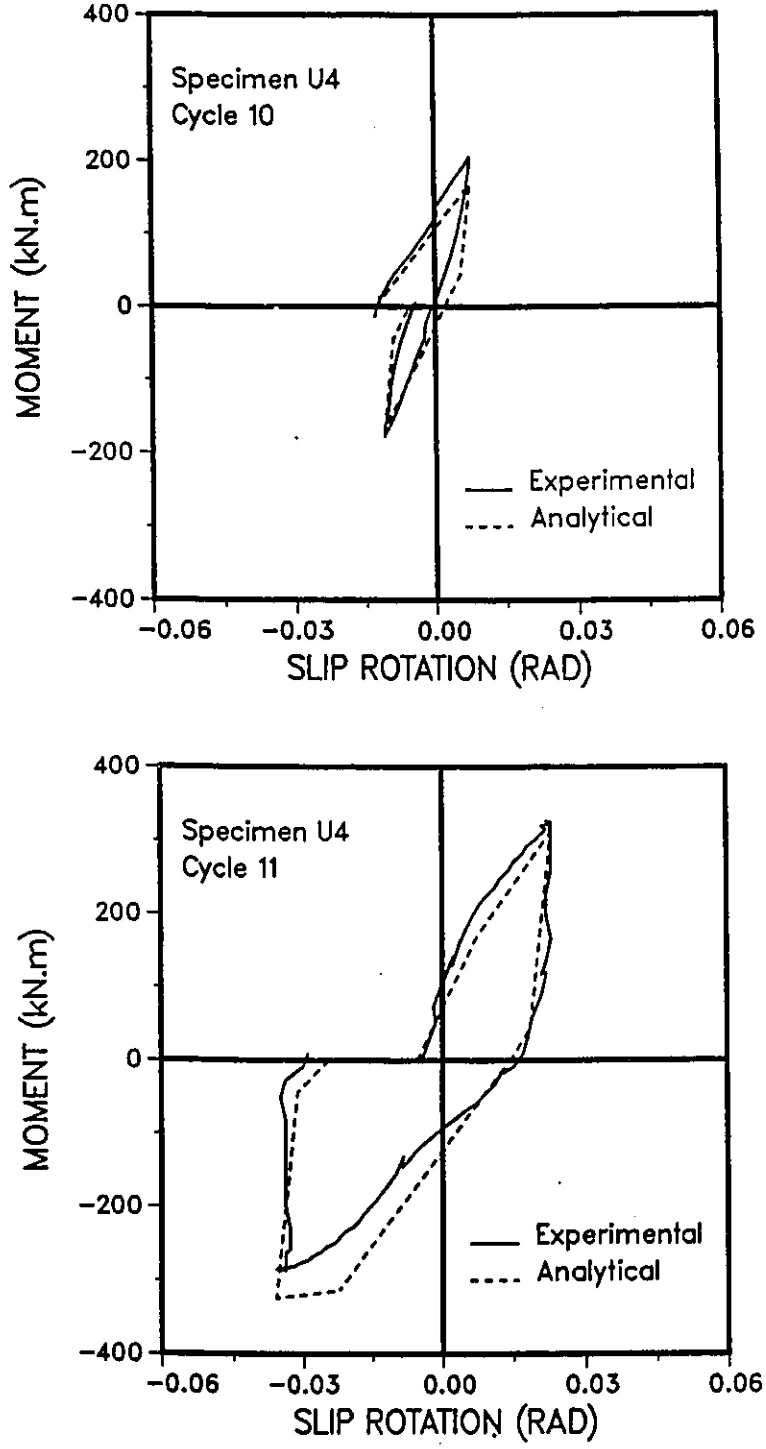

Figure 2.24 Continued

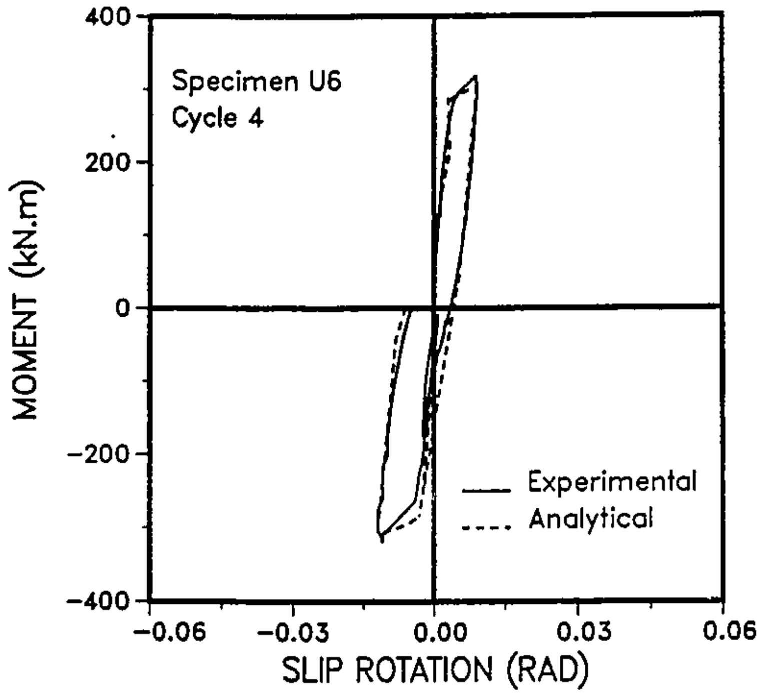

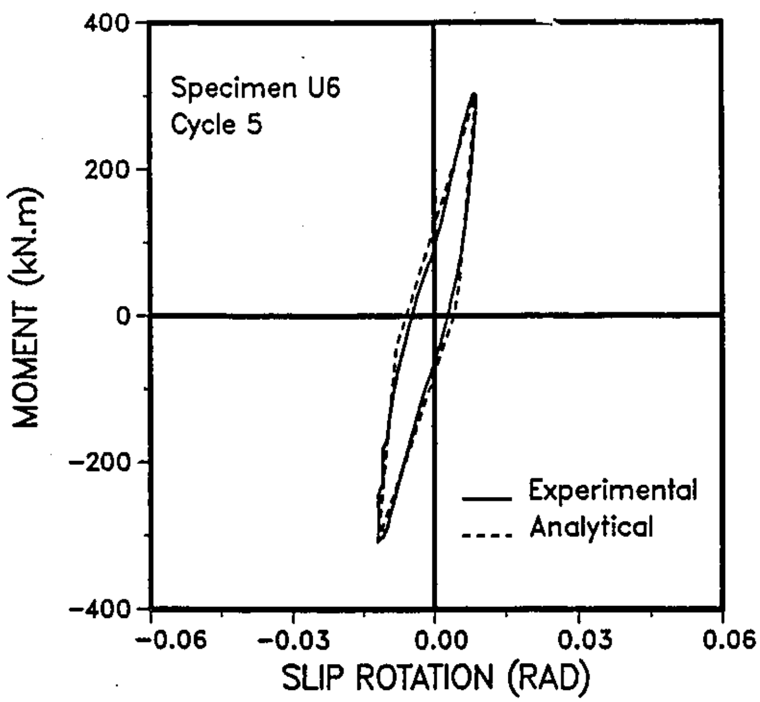

Figure 2.24 Continued

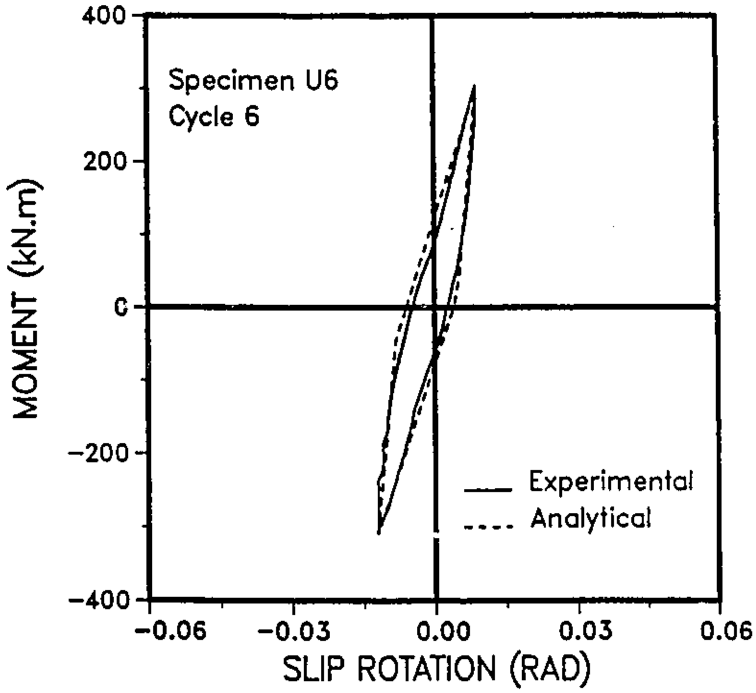

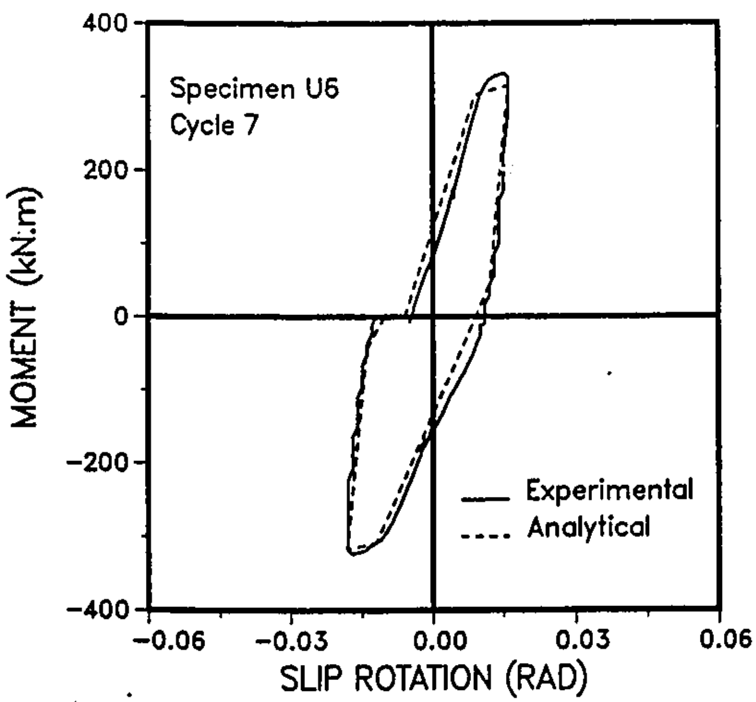

Figure 2.24 Continued

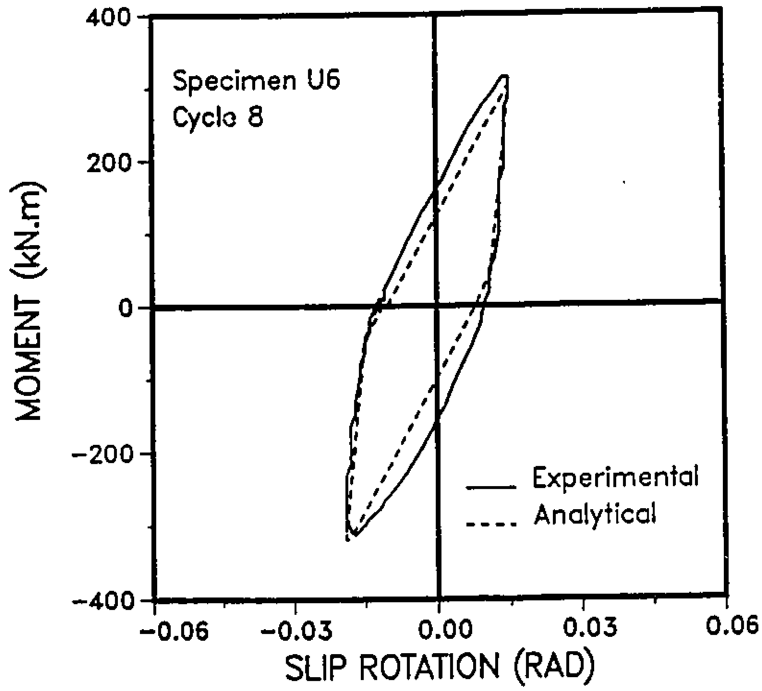

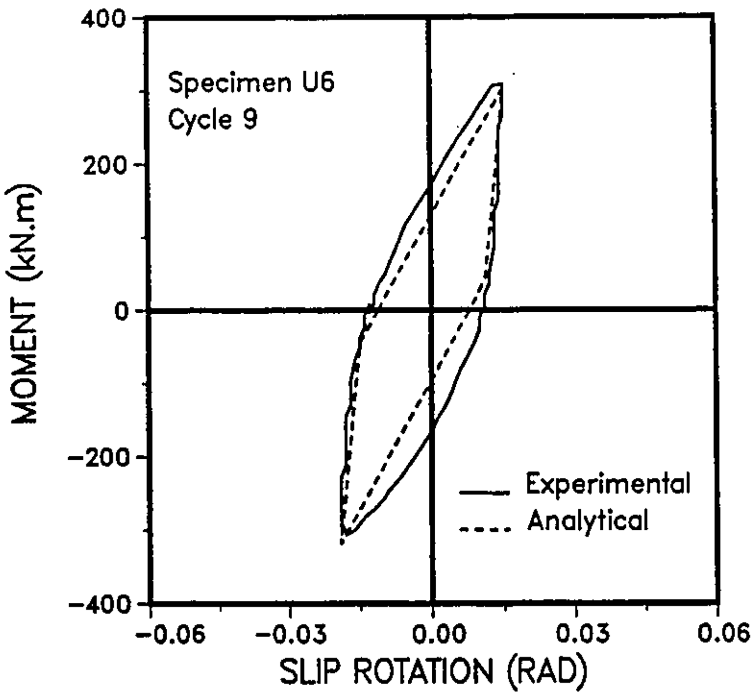

Figure 2.24 Continued

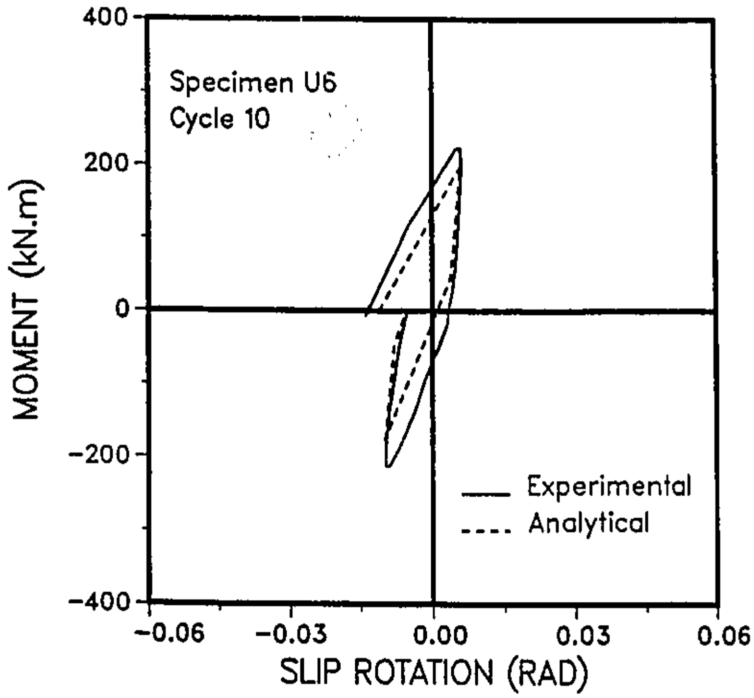

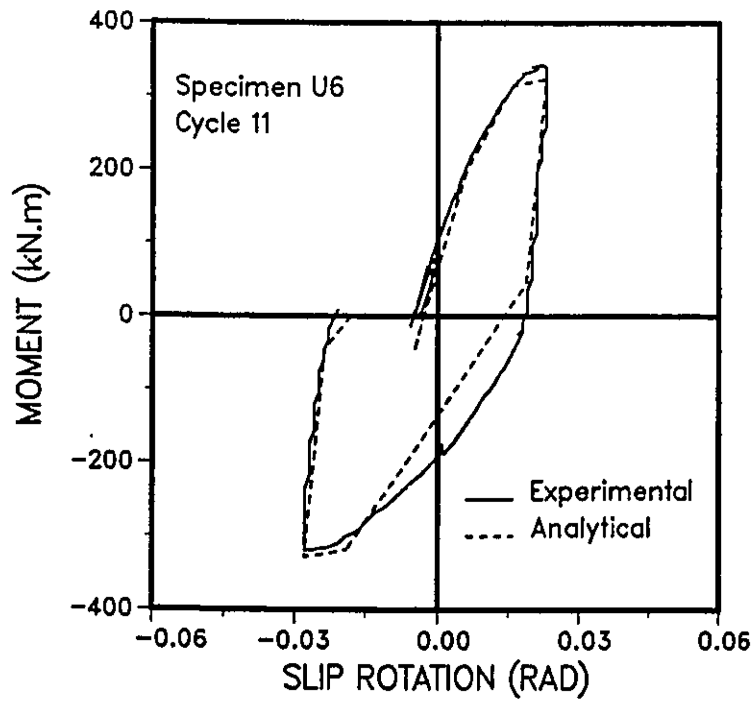

Figure 2.24 Continued

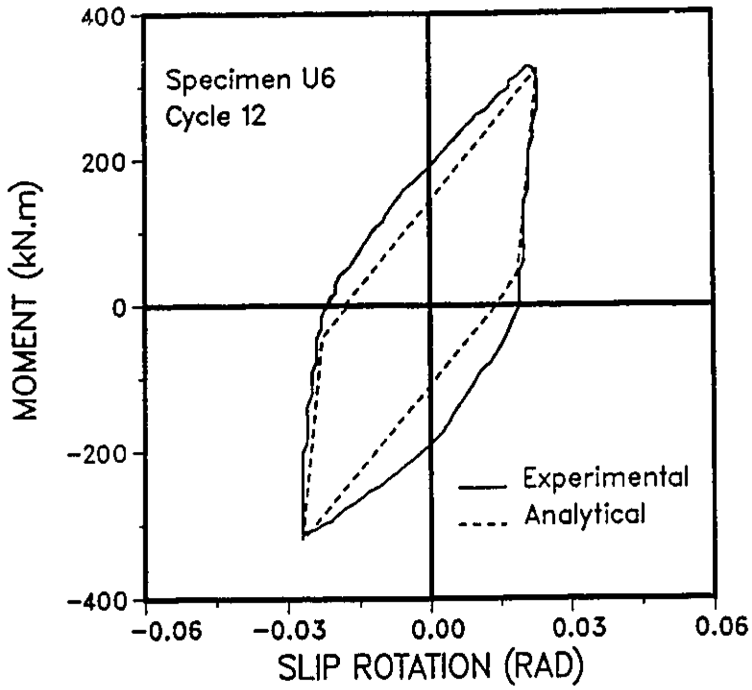

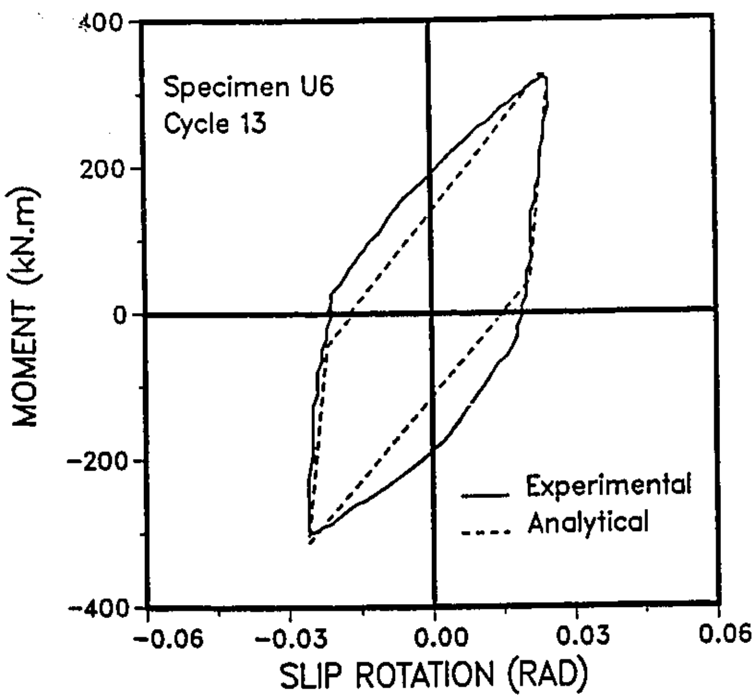

Figure 2.24 Continued

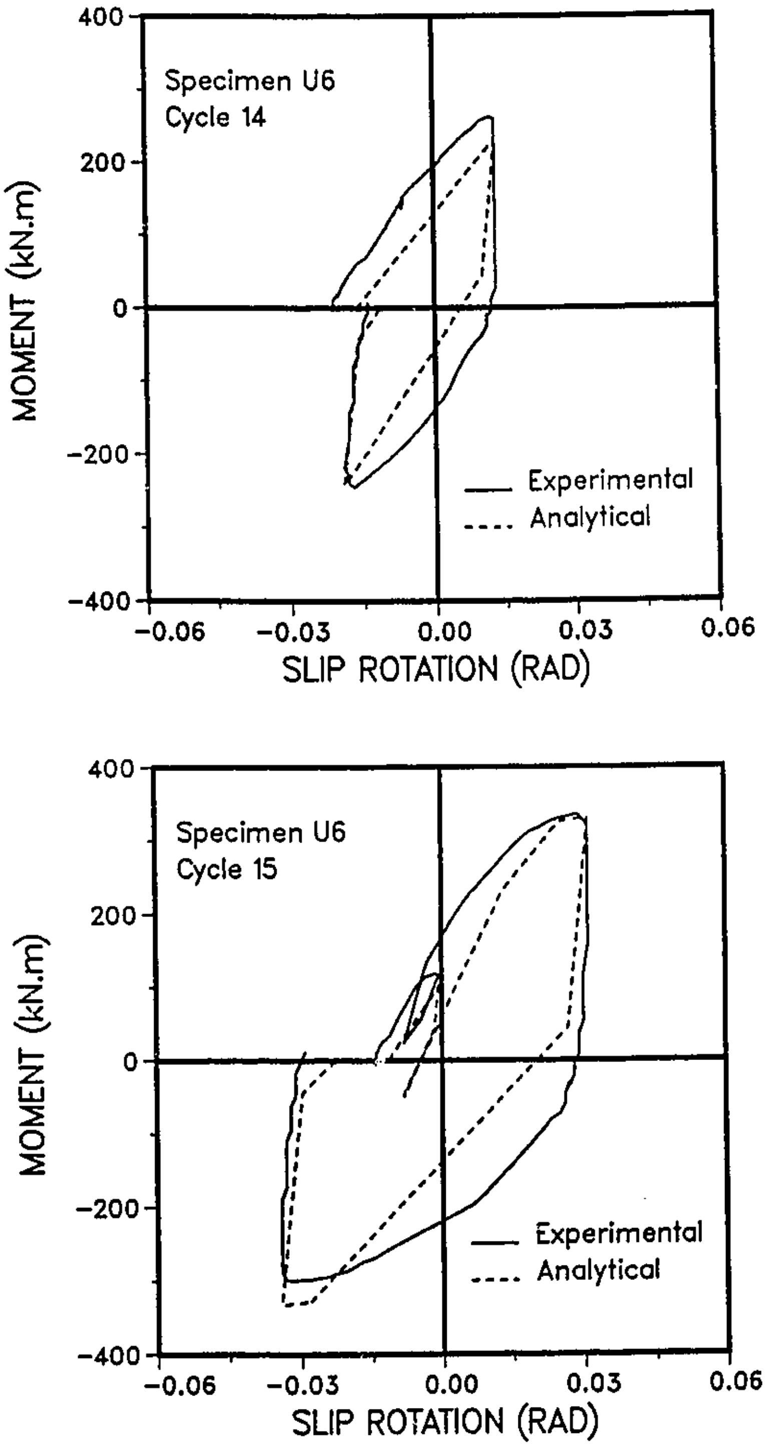

Figure 2.24 Continued

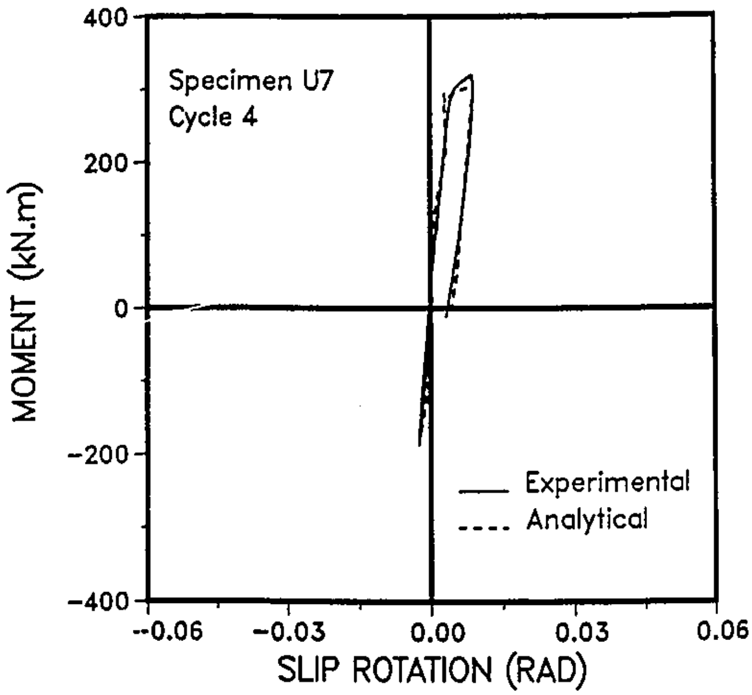

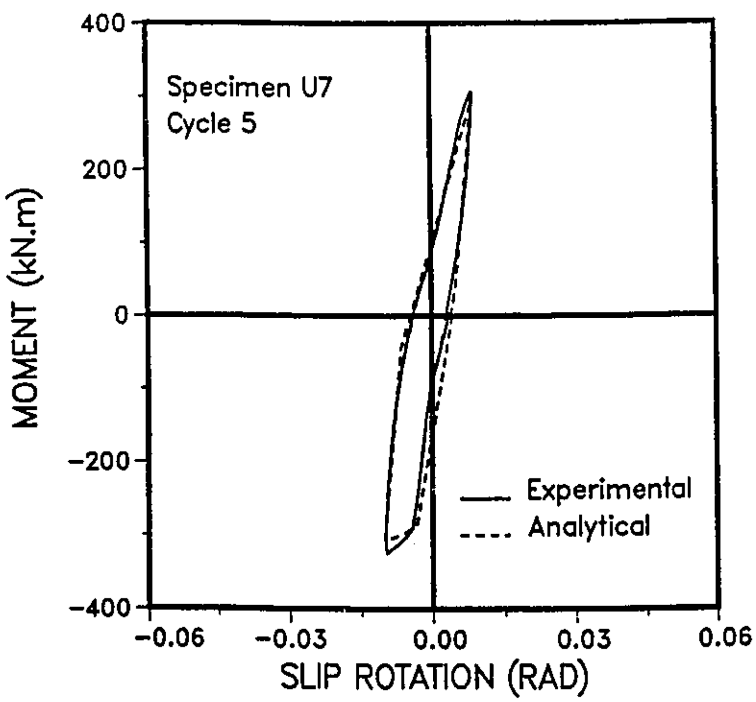

Figure 2.24 Continued

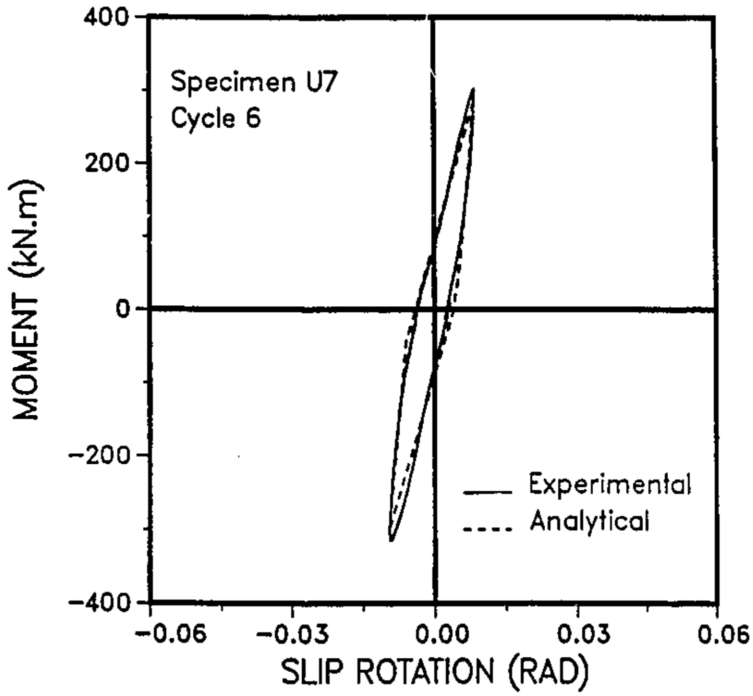

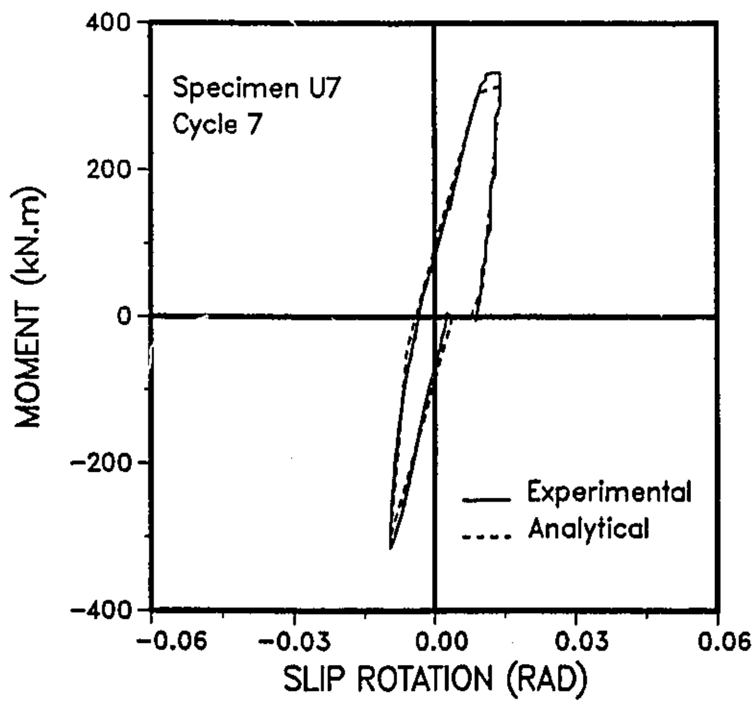

Figure 2.24 Continued

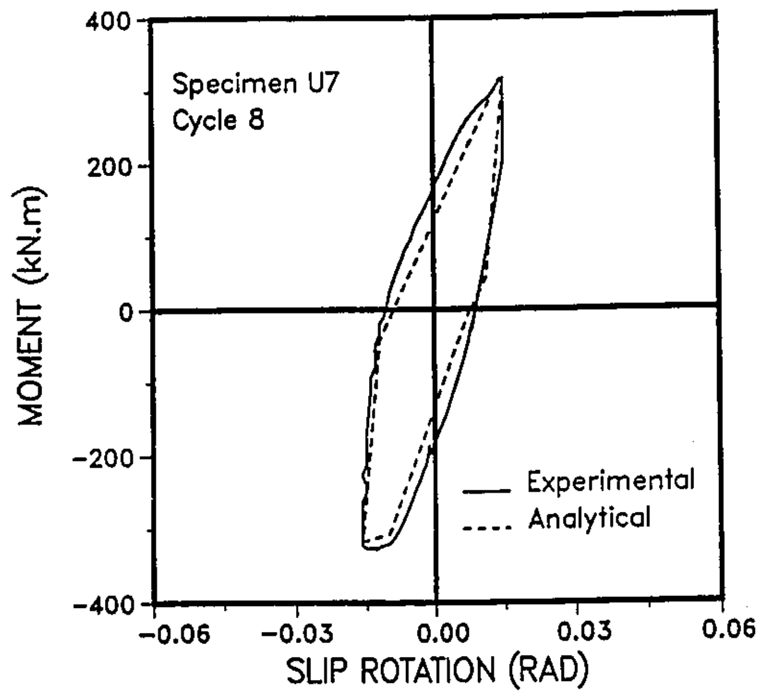

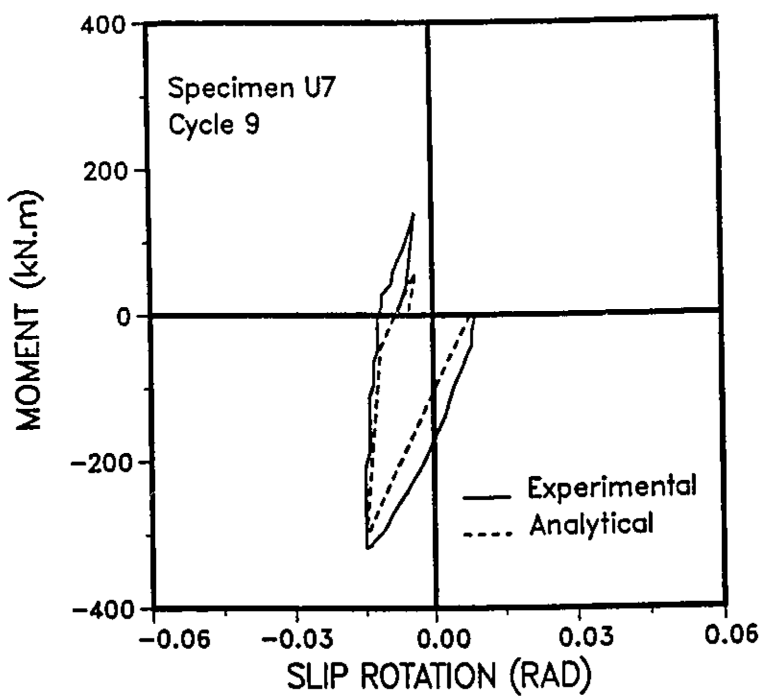

Figure 2.24 Continued

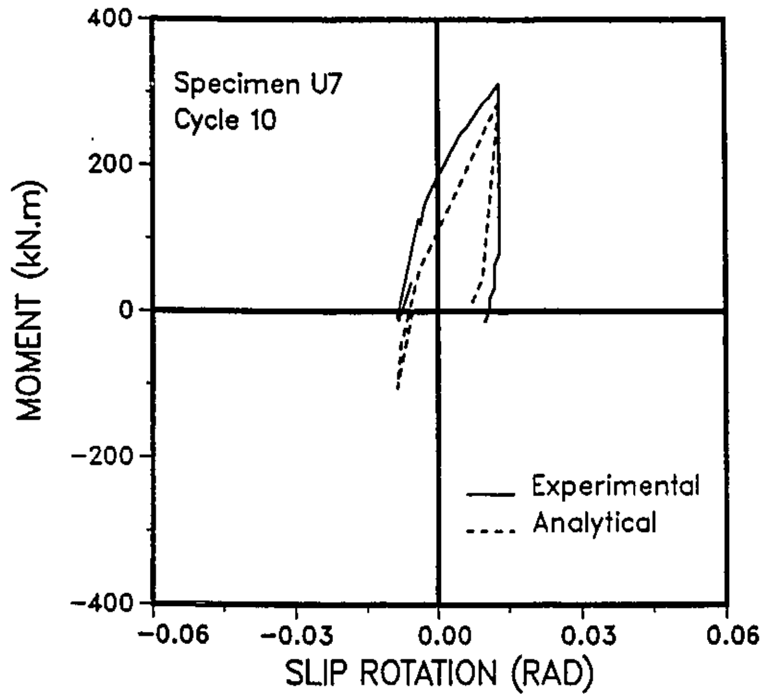

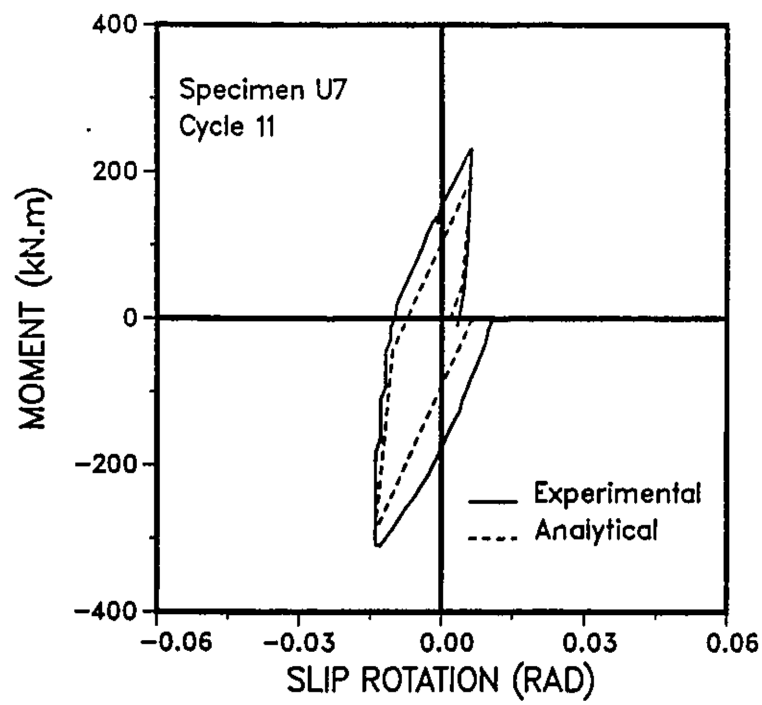

Figure 2.24 Continued

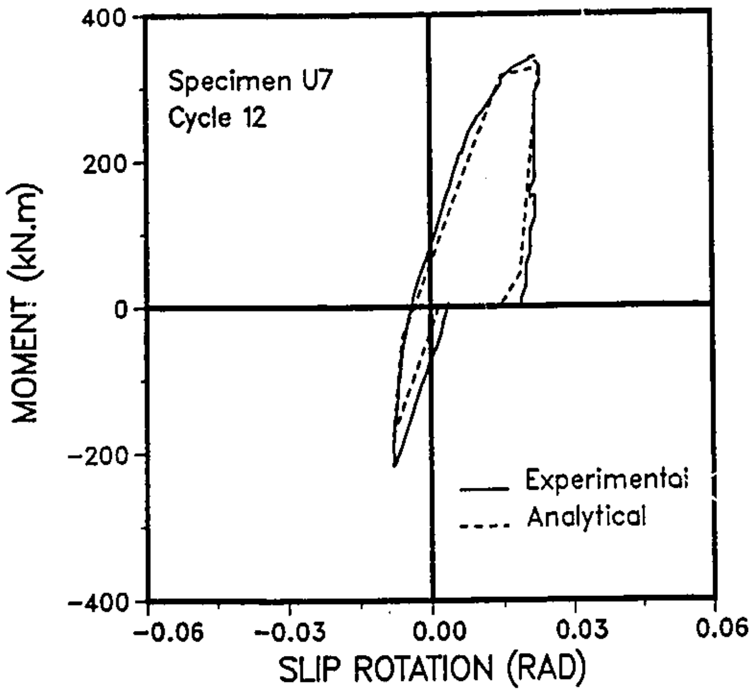

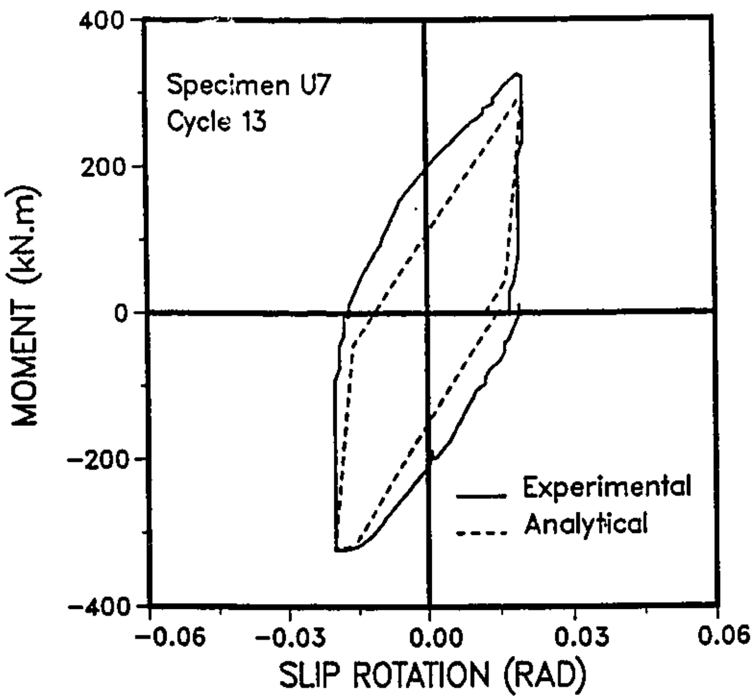

Figure 2.24 Continued

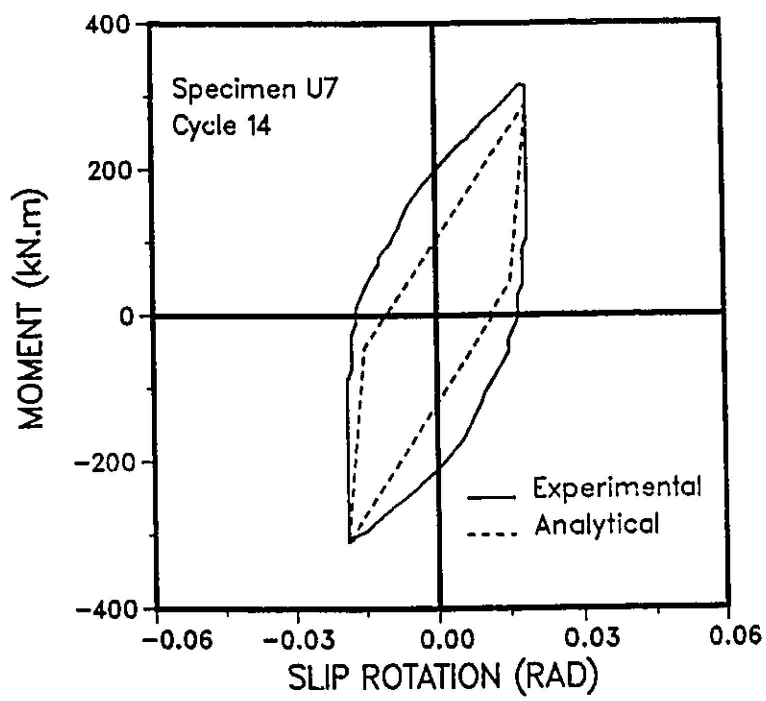

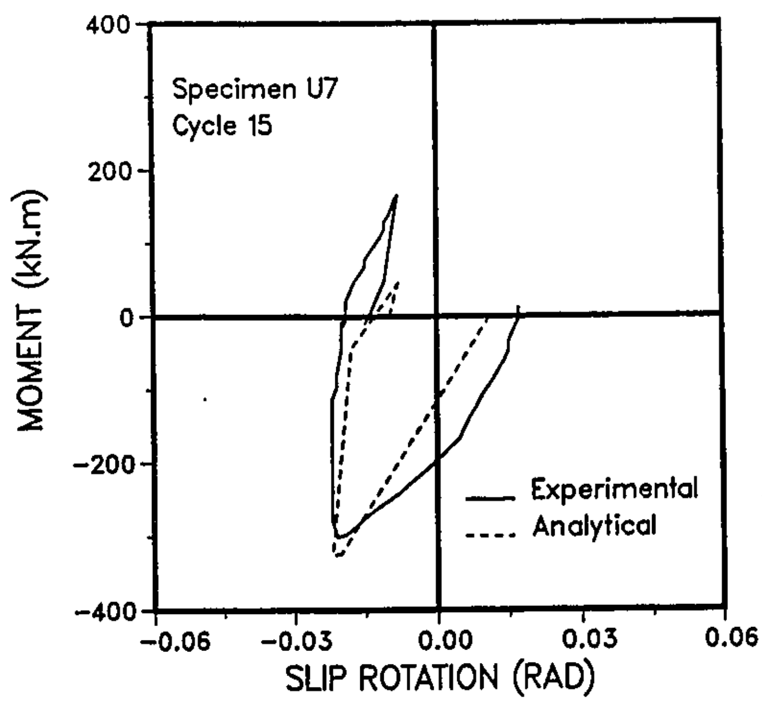

Figure 2.24 Continued

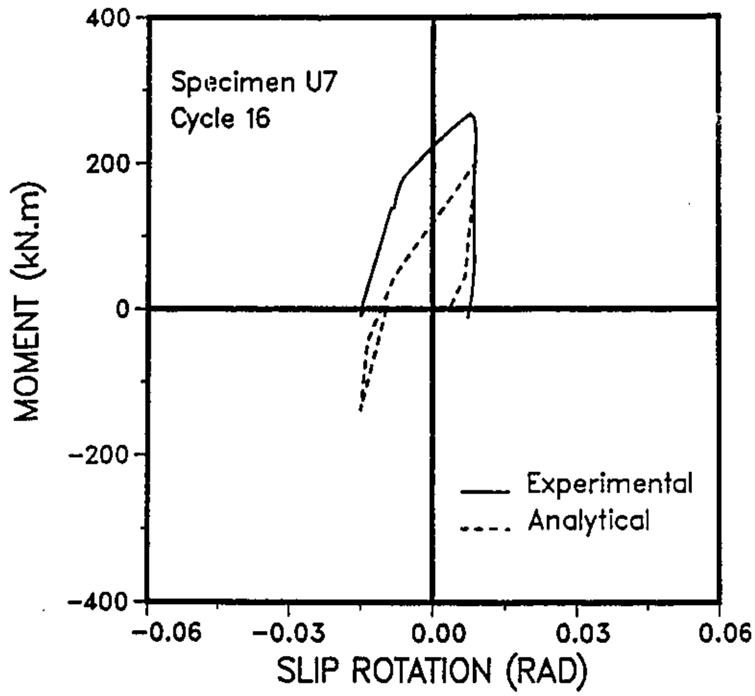

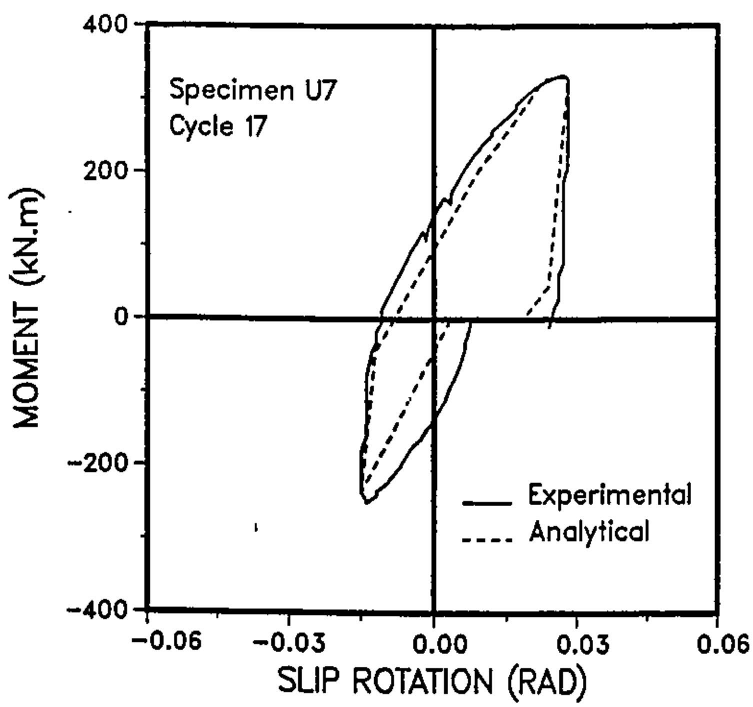

Figure 2.24 Continued

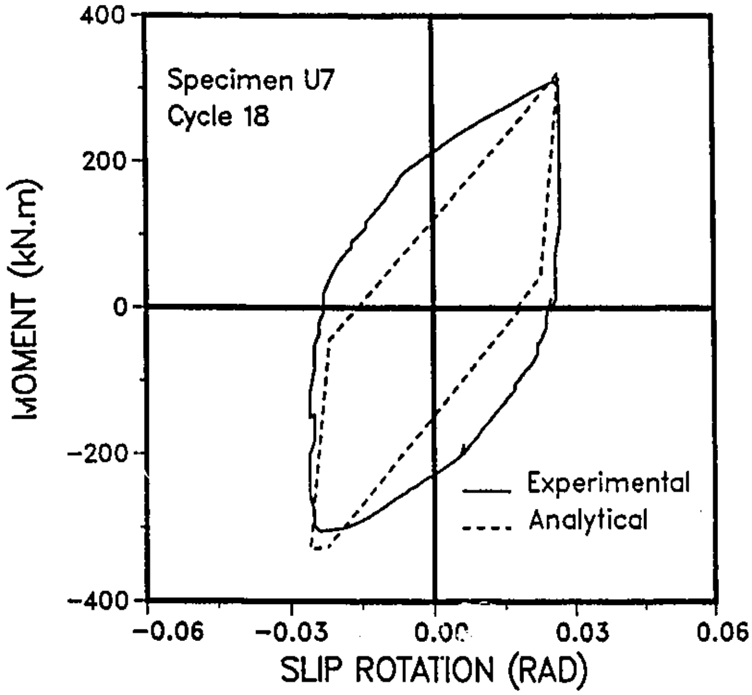

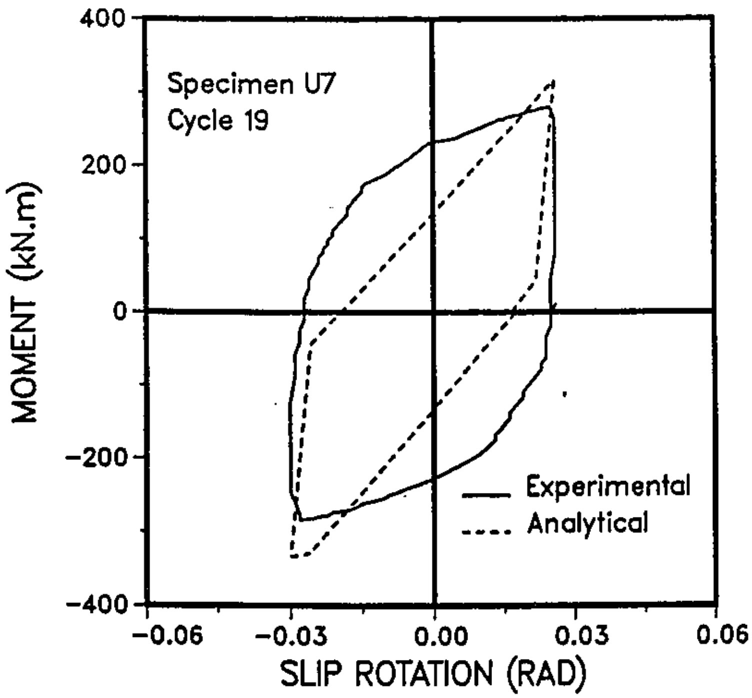

Figure 2.24 Continued

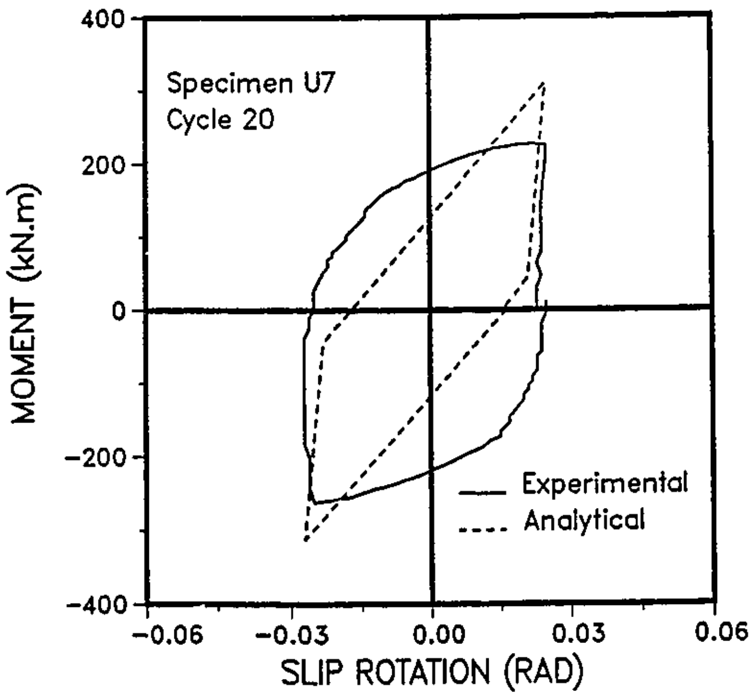

Figure 2.24 Continued

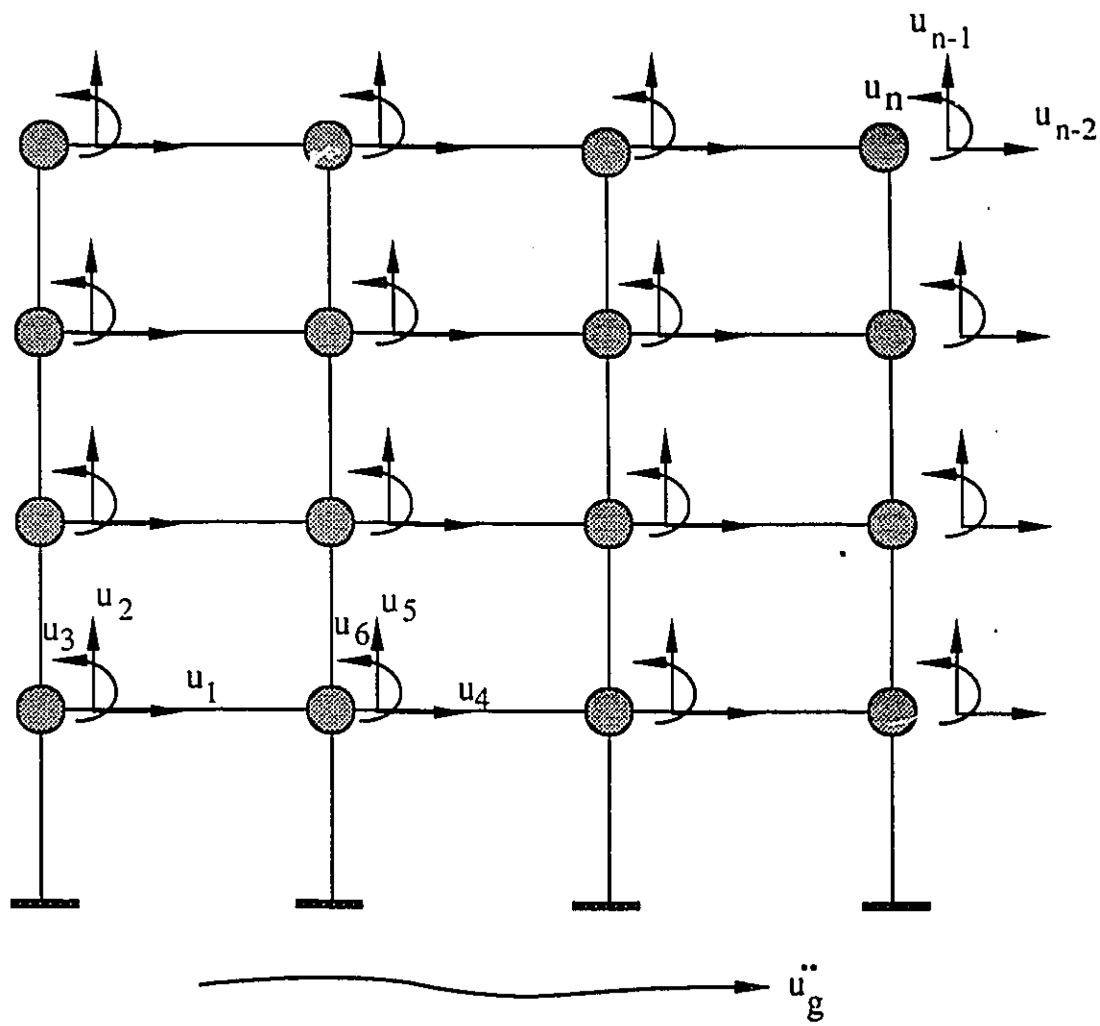

Figure 3.1 Discrete Parameters System

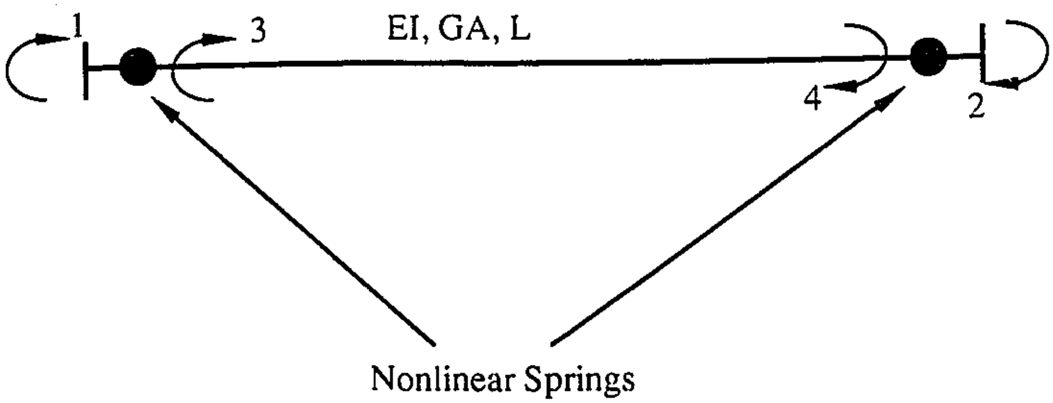

Figure 3.2 The One Component Model

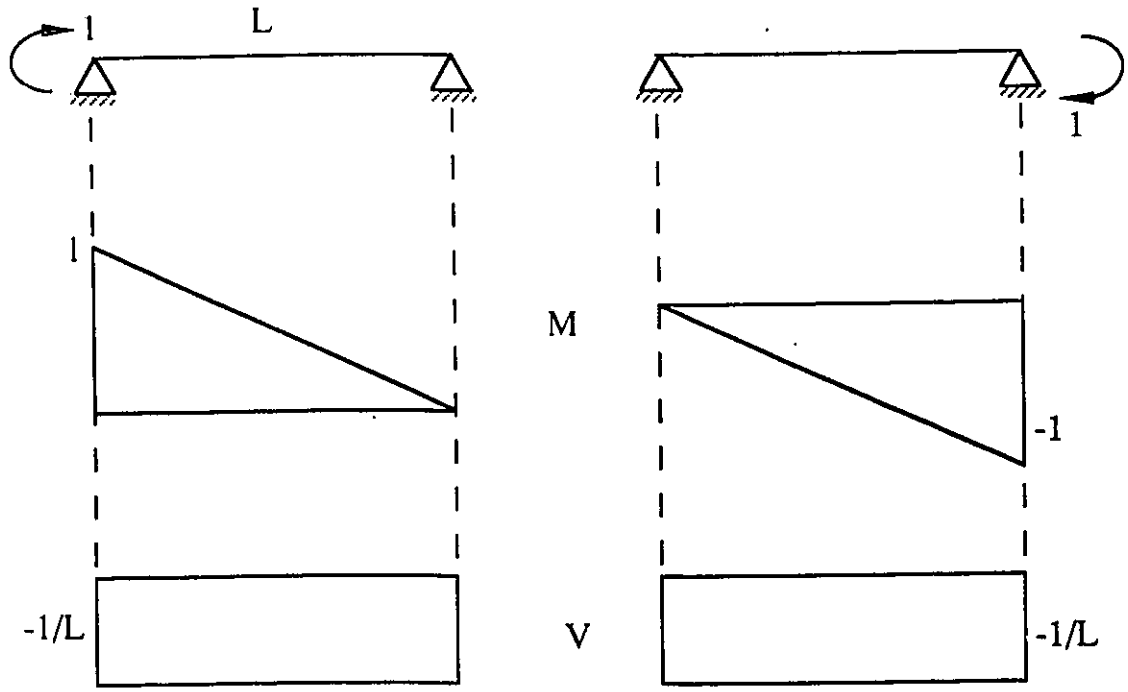

Figure 3.3 Derivation of Elastic Flexibility Coefficients

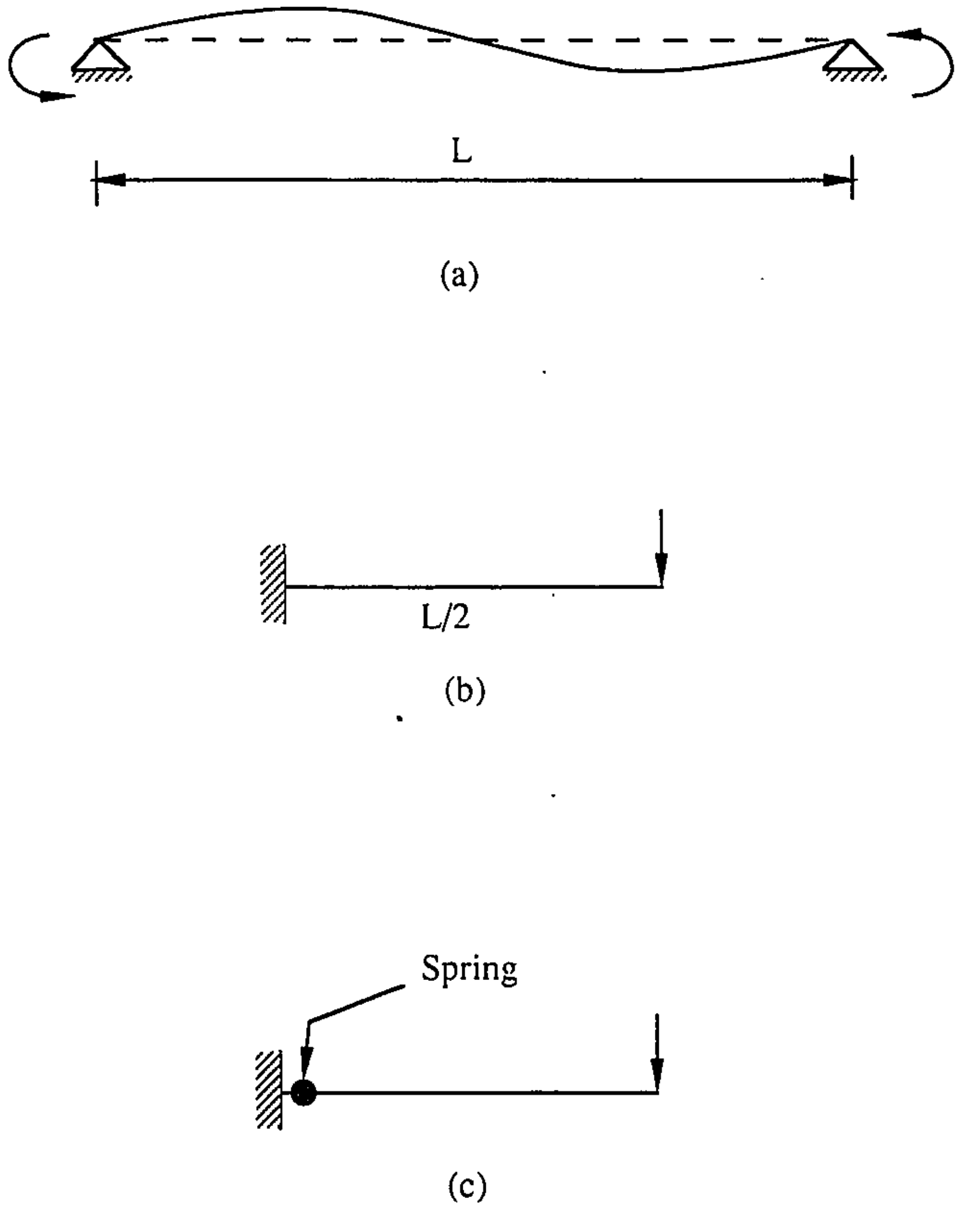

Figure 3.4 (a) Beam; (b) Actual Cantilever; (c) Idealized Cantilever

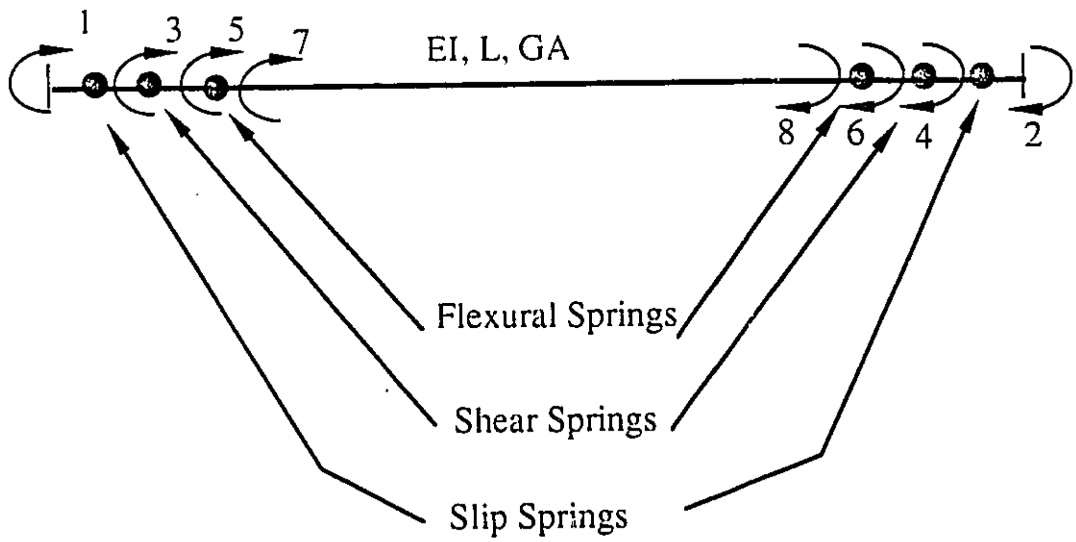

Figure 3.5 Modified One Component Model

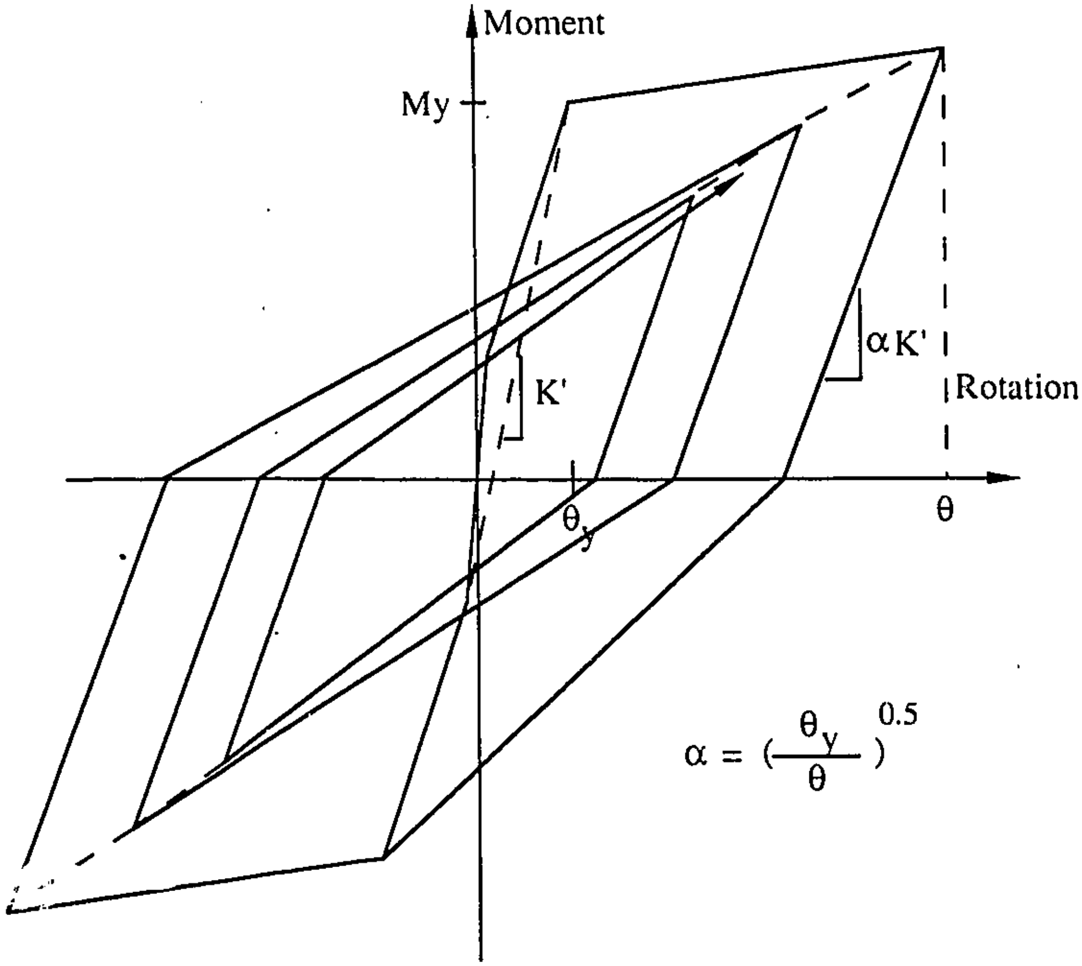

Figure 3.6 Takeda's Hysteretic Model

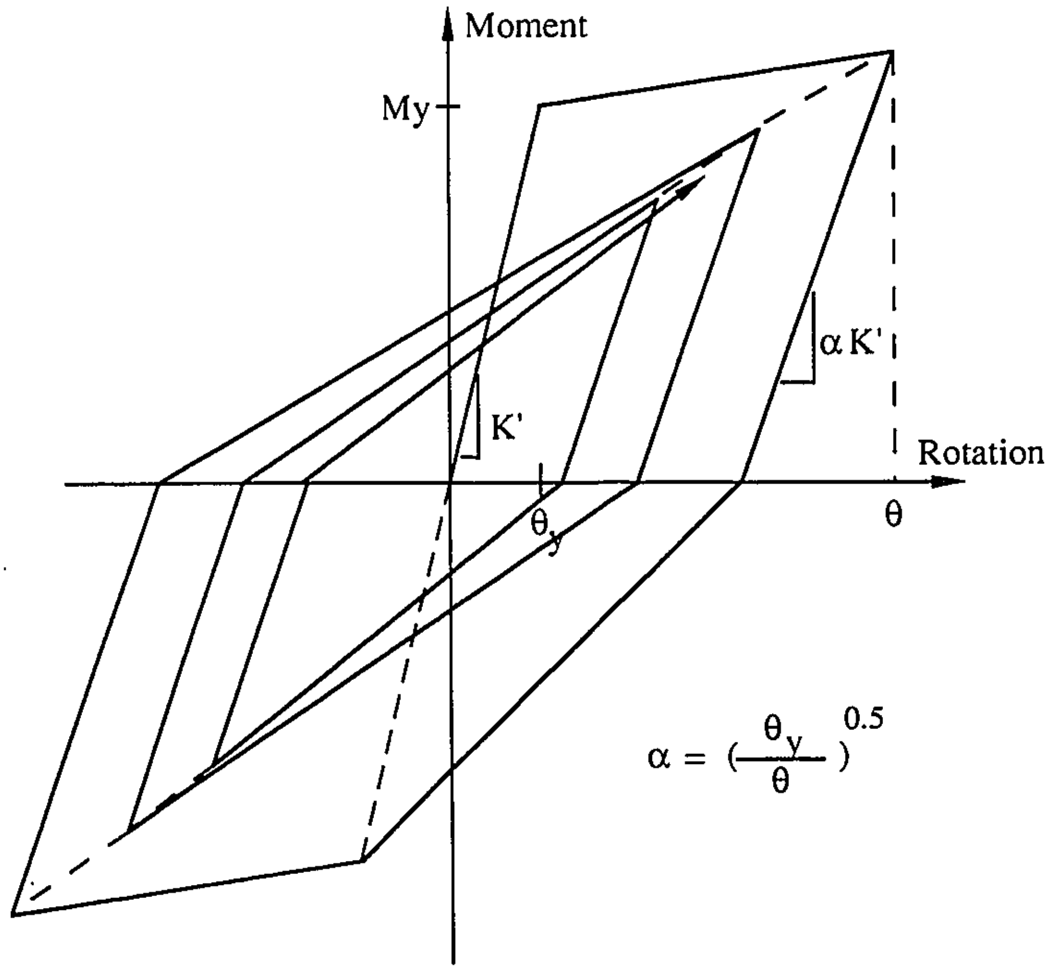

Figure 3.7 Modified Takeda's Hysteretic Model

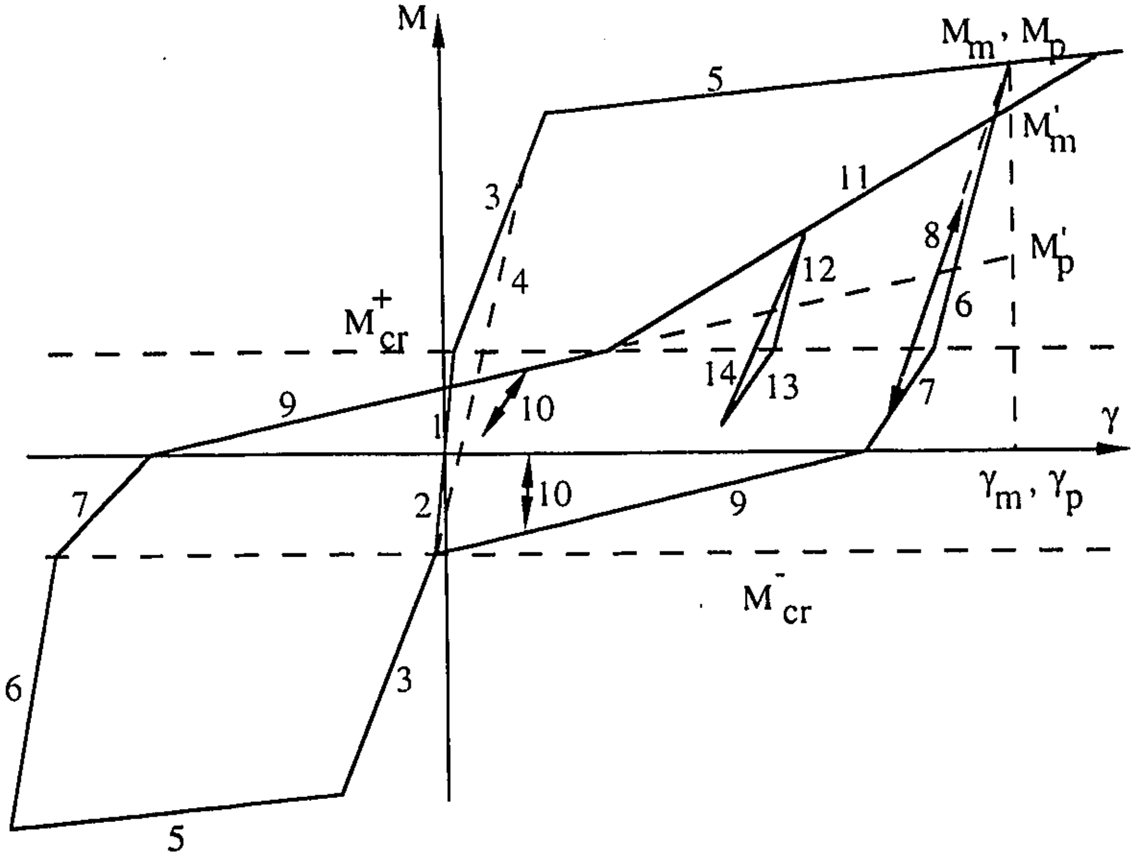

Figure 3.8 Hysteretic Model for Shear

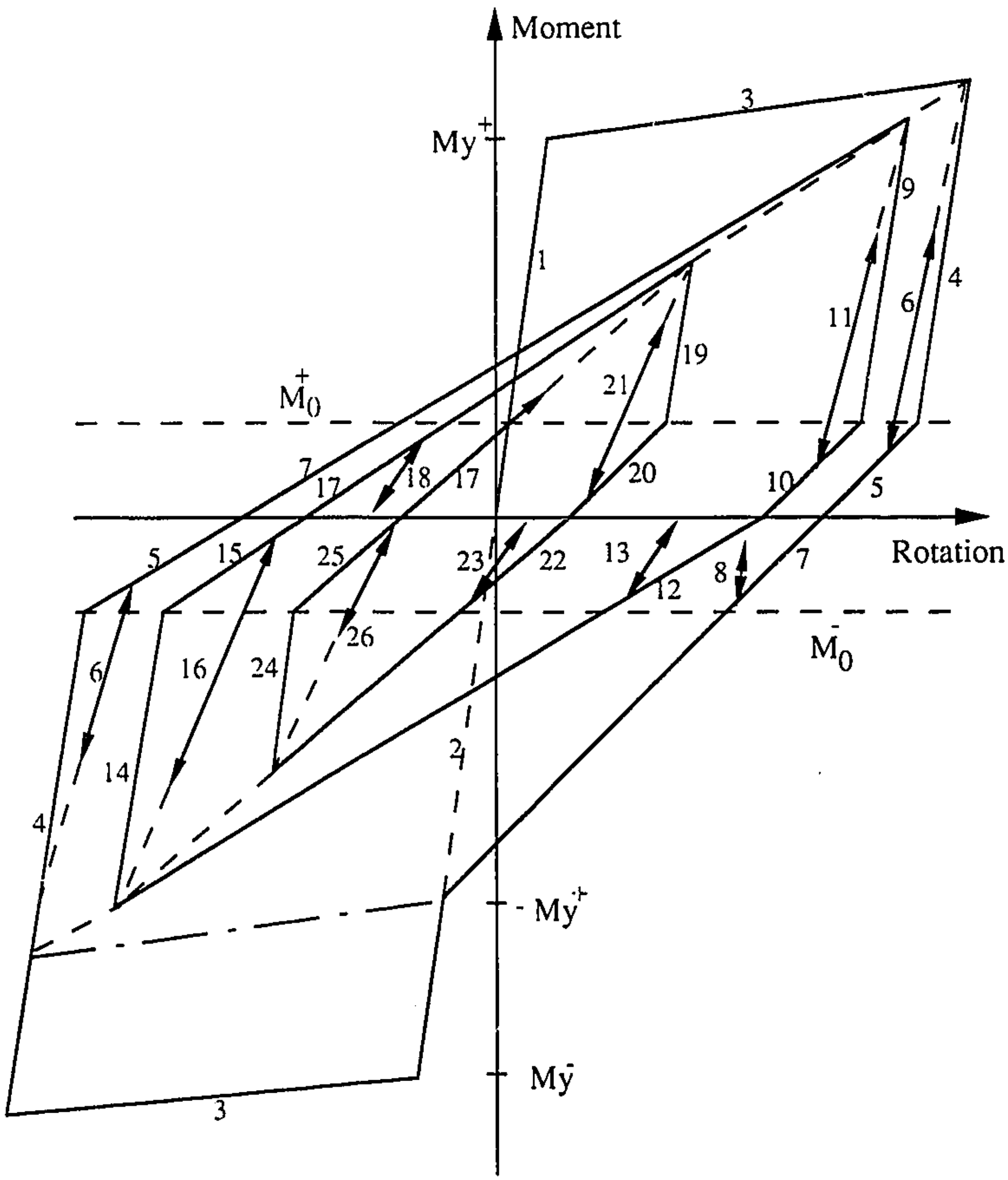

Figure 3.9 Generalized Slip Hysteretic Model

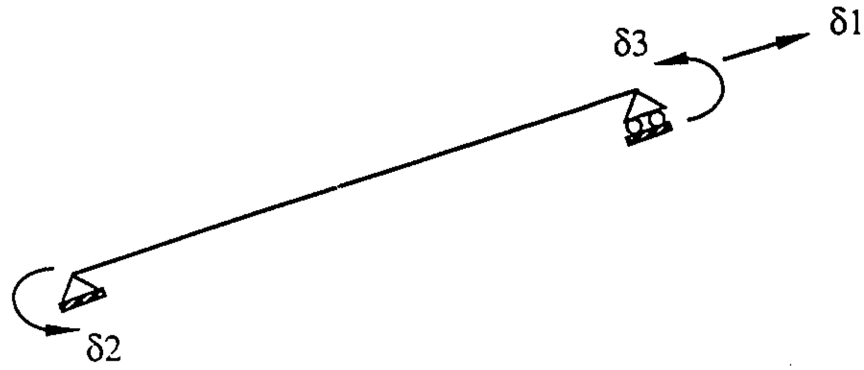

(a) Local Coordinates

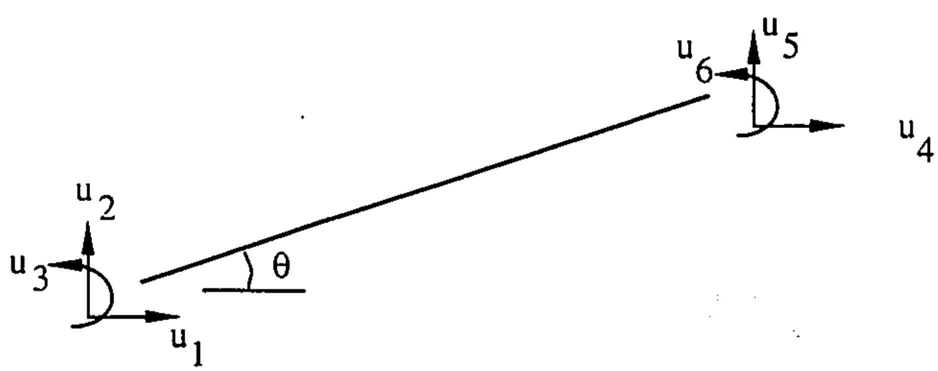

(b) Global Coordinates

Figure 3.10 Element Degrees of Freedom

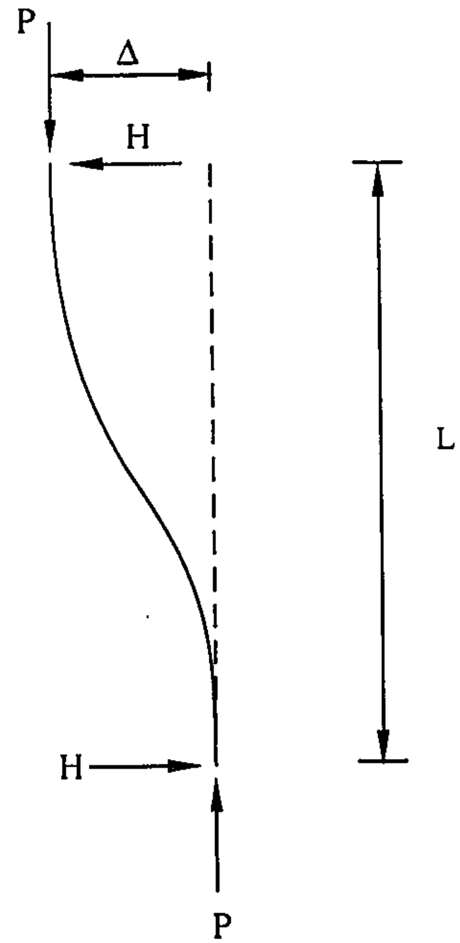

Figure 3.11 P - Δ Effect on Column Stiffness

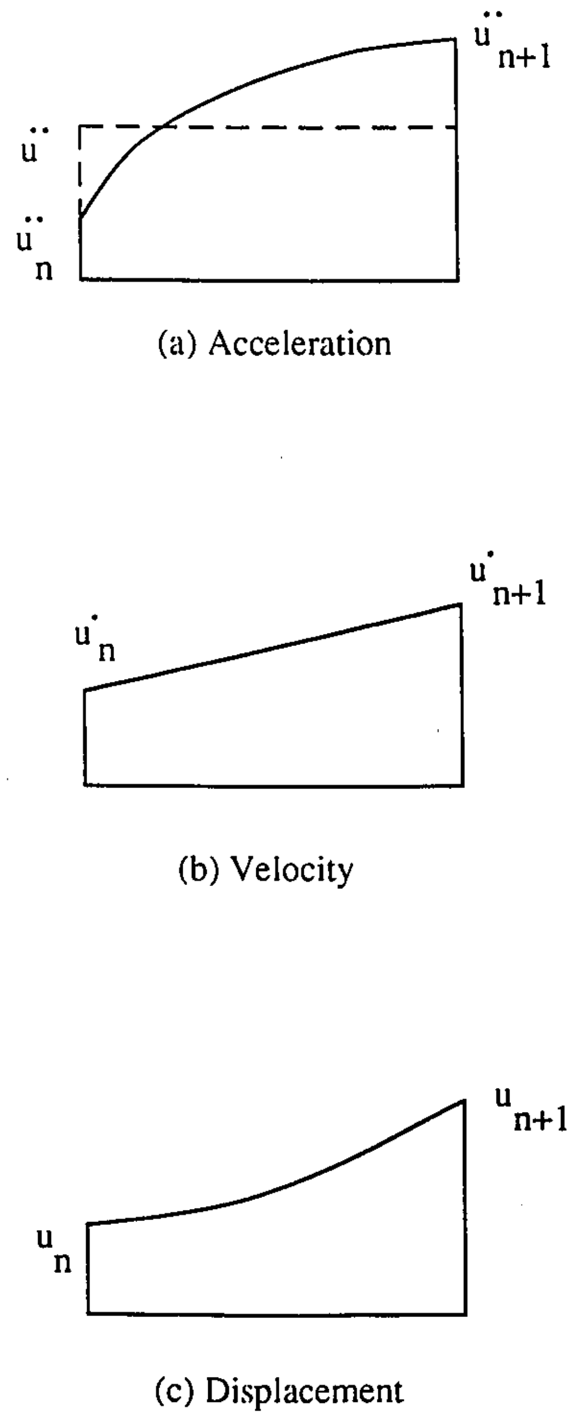

(a) Acceleration

(b) Velocity

(c) Displacement

Figure 3.12 Average Acceleration Method

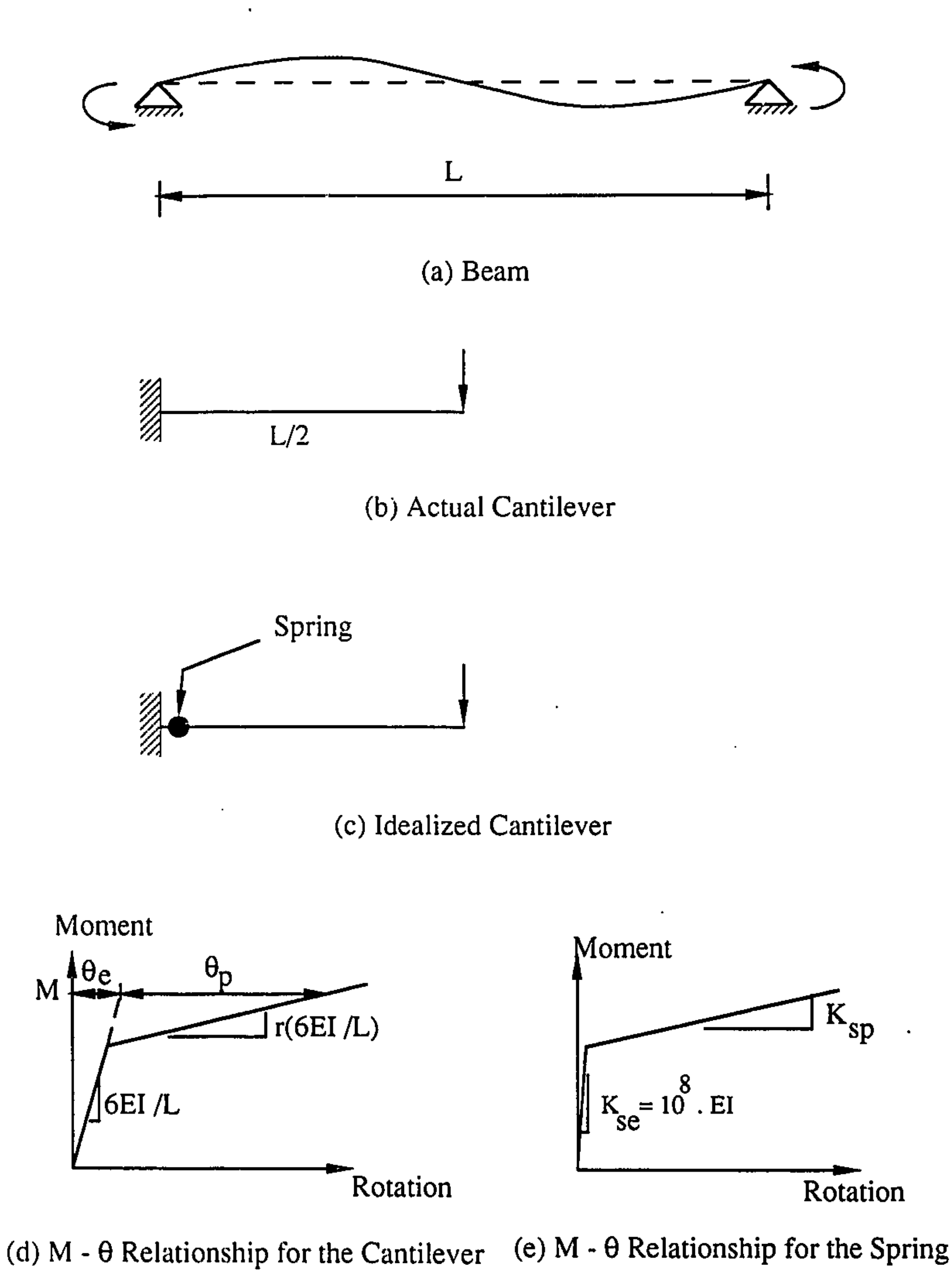

Figure 4.1 Derivation of Flexural Spring Stiffness

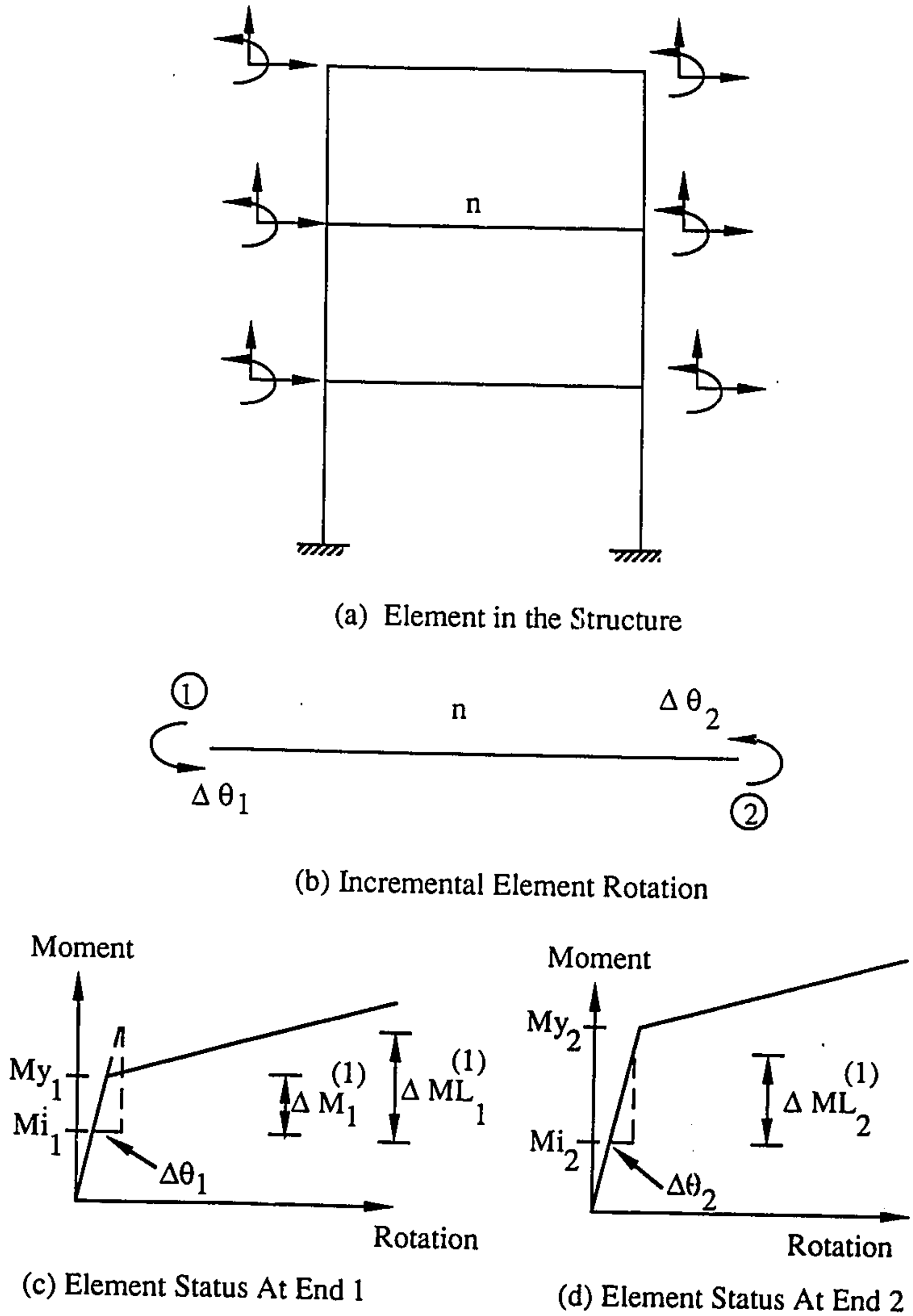

Figure 4.2 Determining Unbalanced Moment

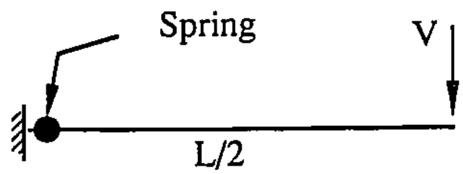

(a) Idealized Cantilever

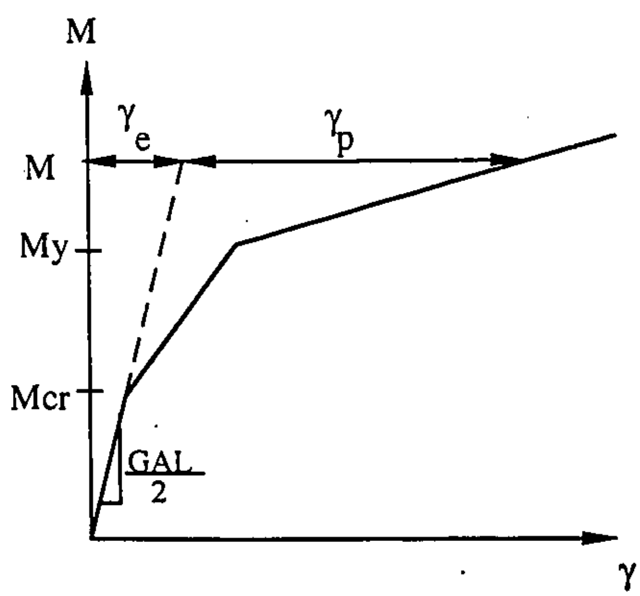

(b) M - γ Relationship

Figure 4.3 Derivation of Shear Spring Stiffness

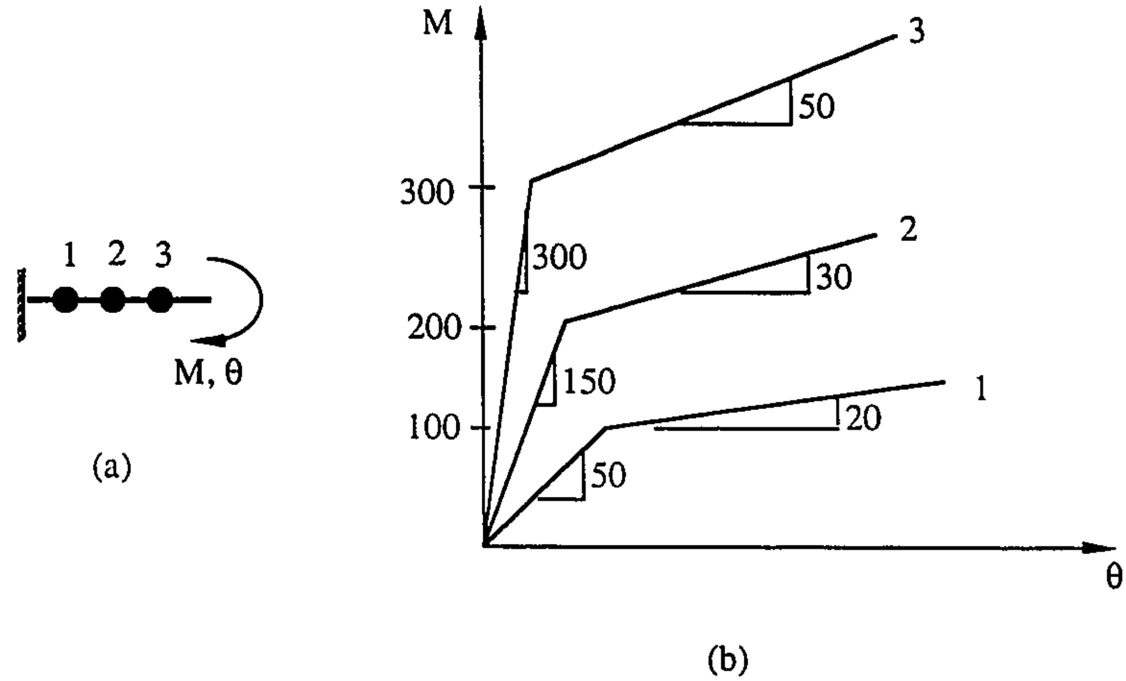

Figure 4.4 (a) Simple Yielding System; (b) M-θ Relationships

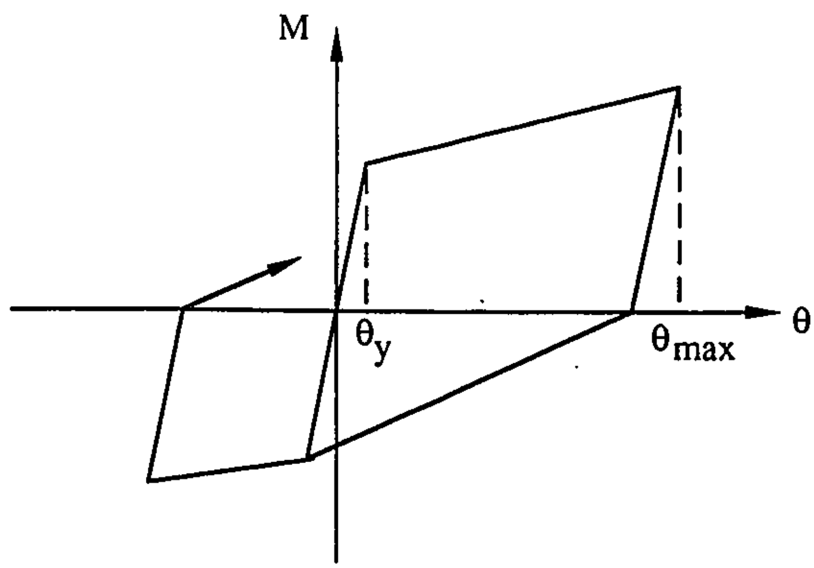

Figure 4.5 Definition of Ductility

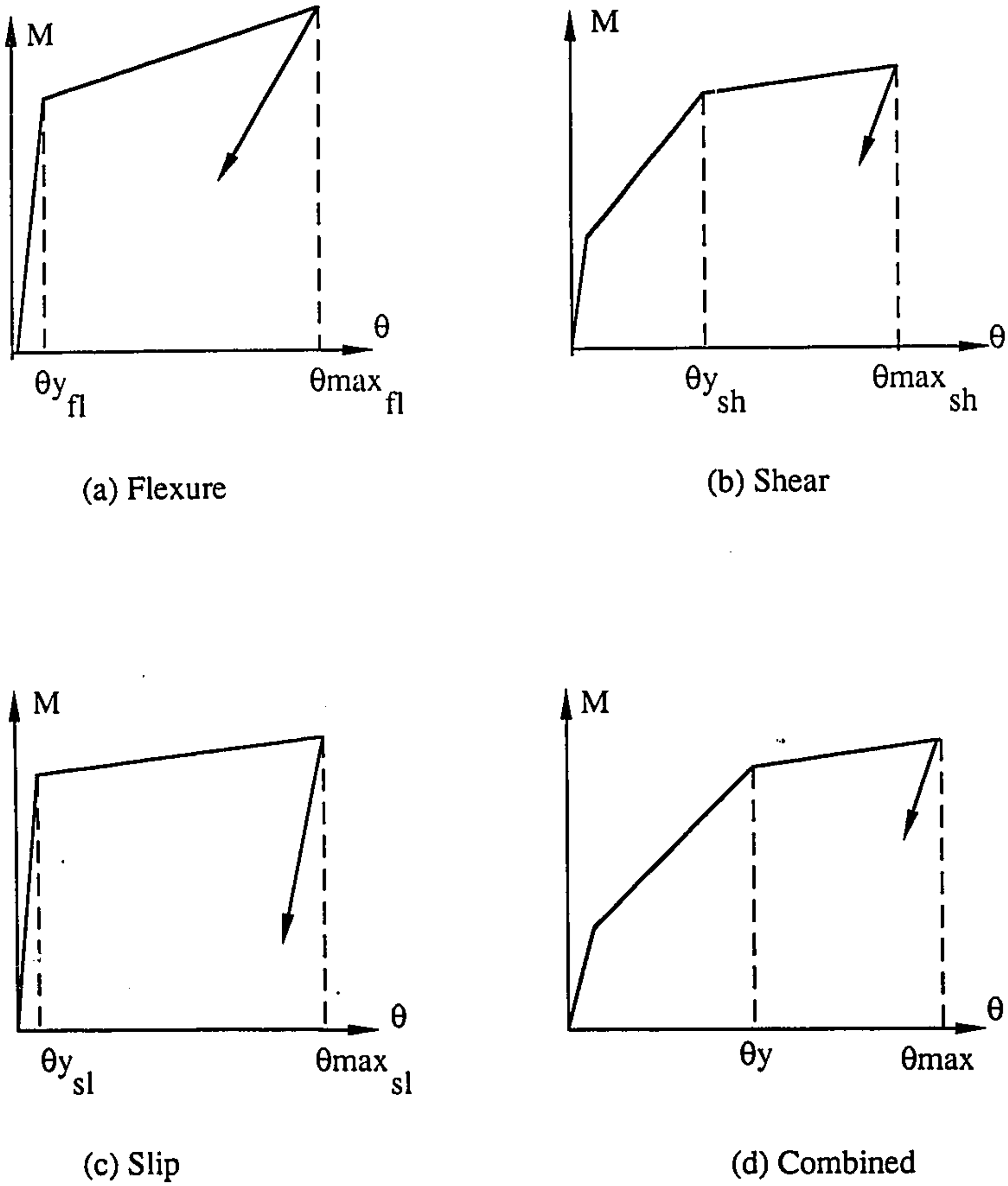

Figure 4.6 Individual and Combined Ductility

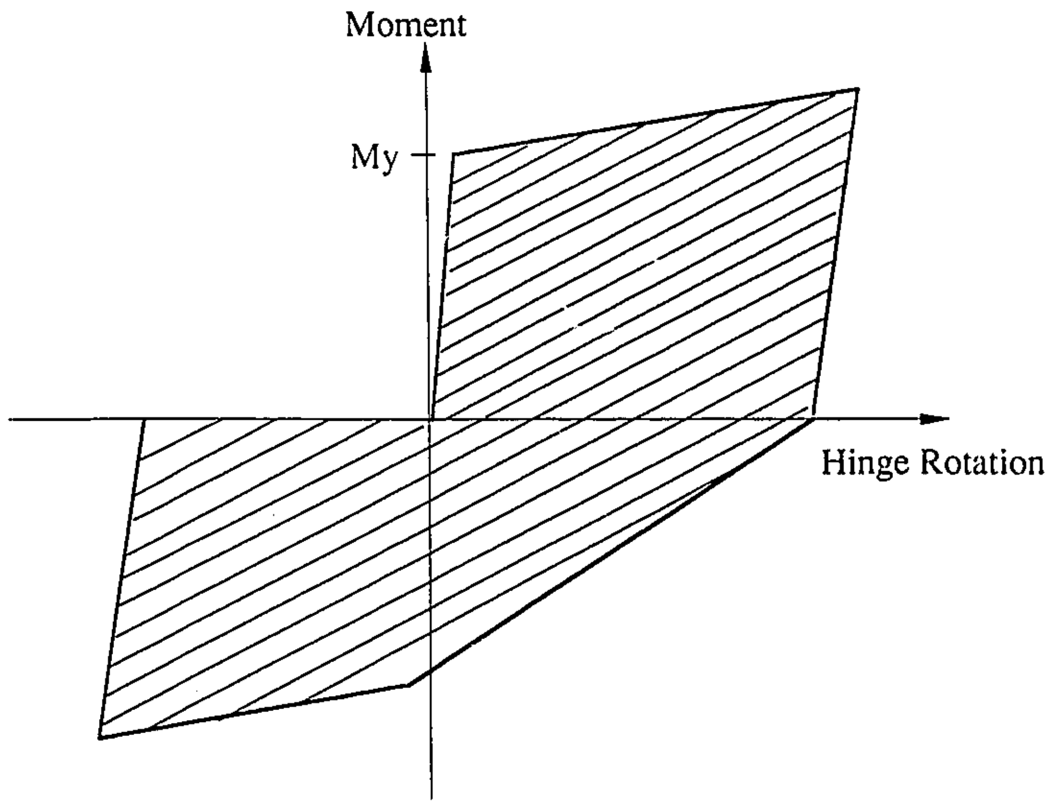

Figure 4.7 Definition of Energy Dissipation Factor

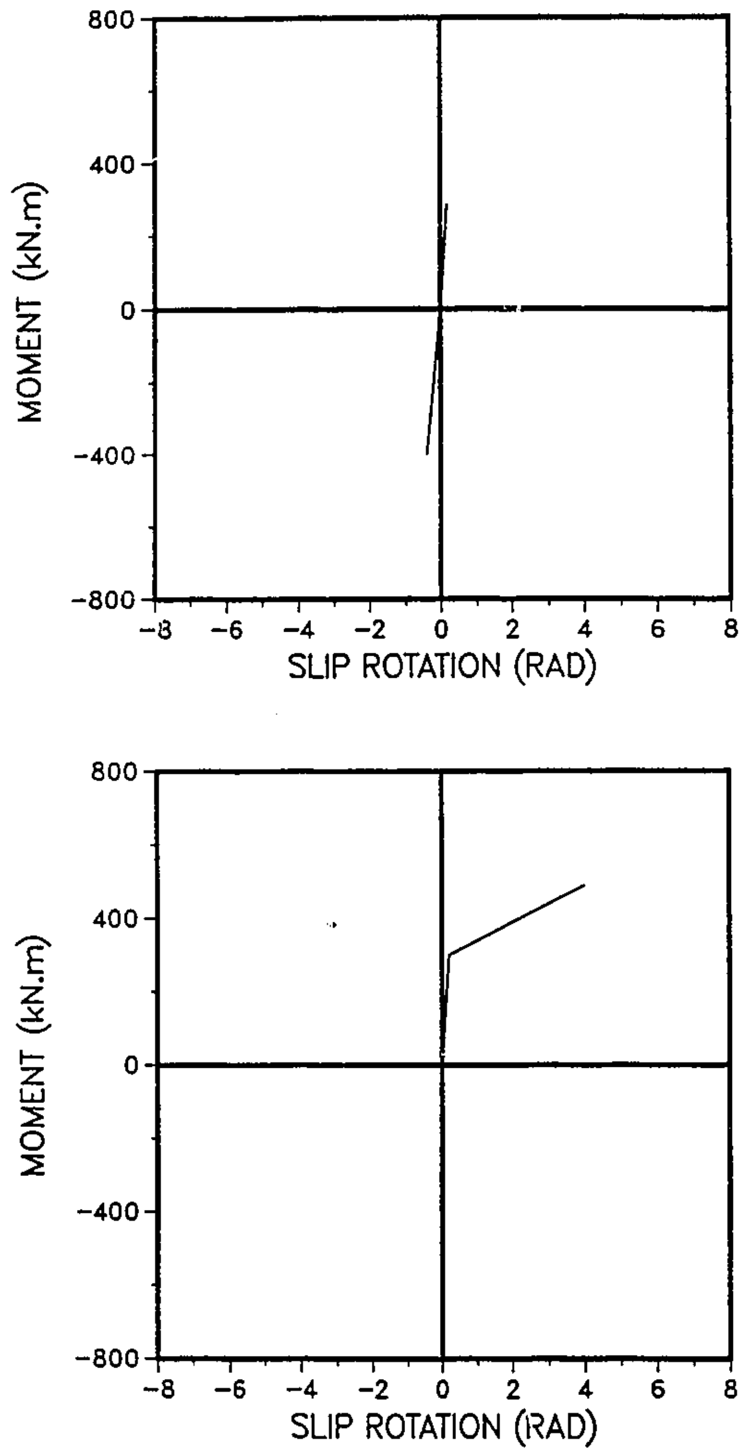

Figure 4.8 Verification of Slip Hysteretic Rules

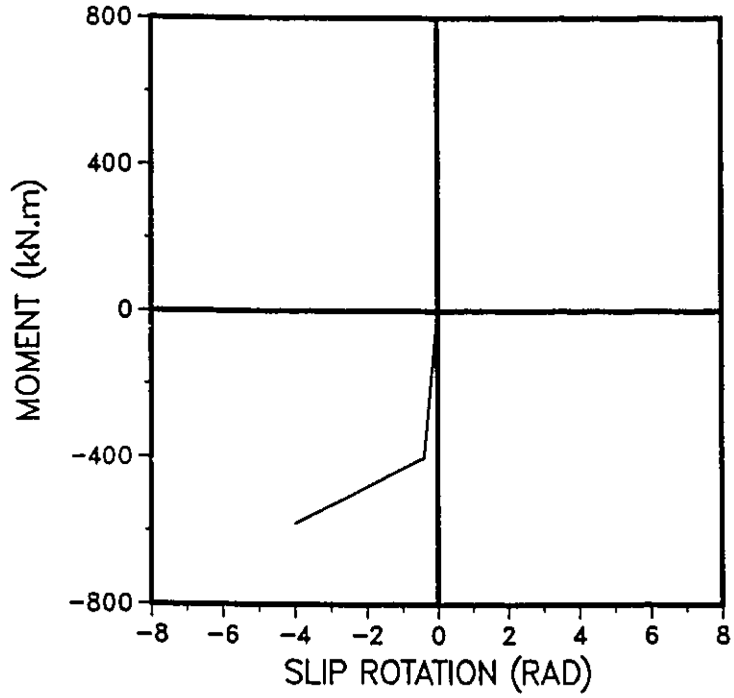

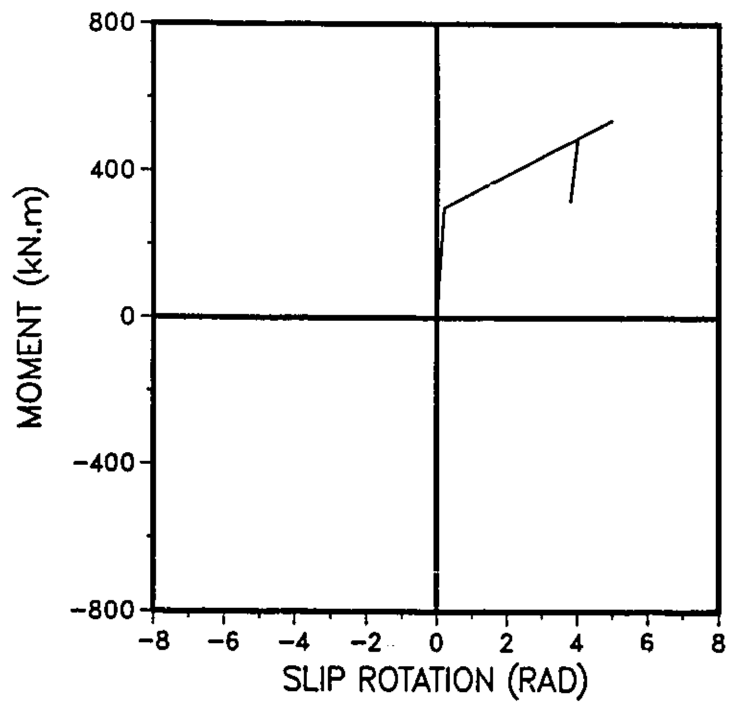

Figure 4.8 Continued

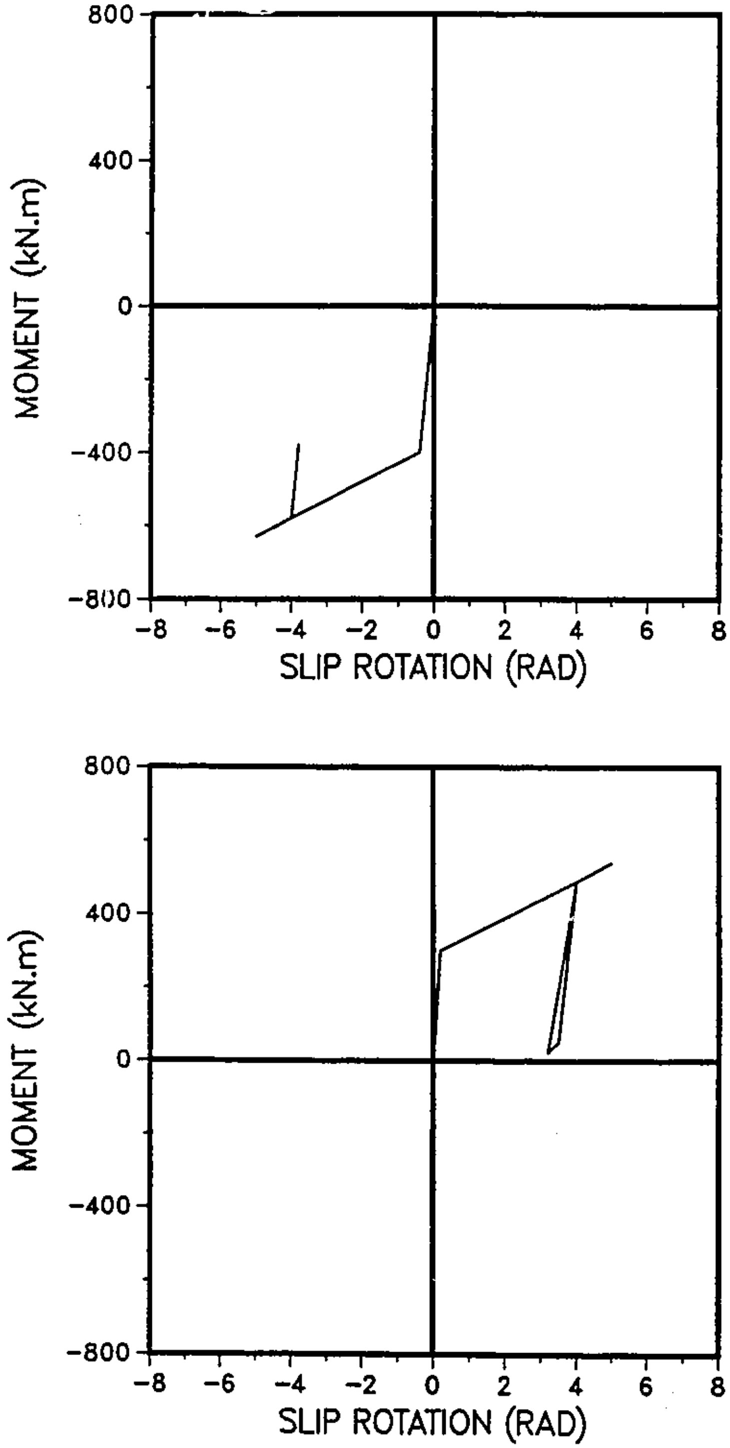

Figure 4.8 Continued

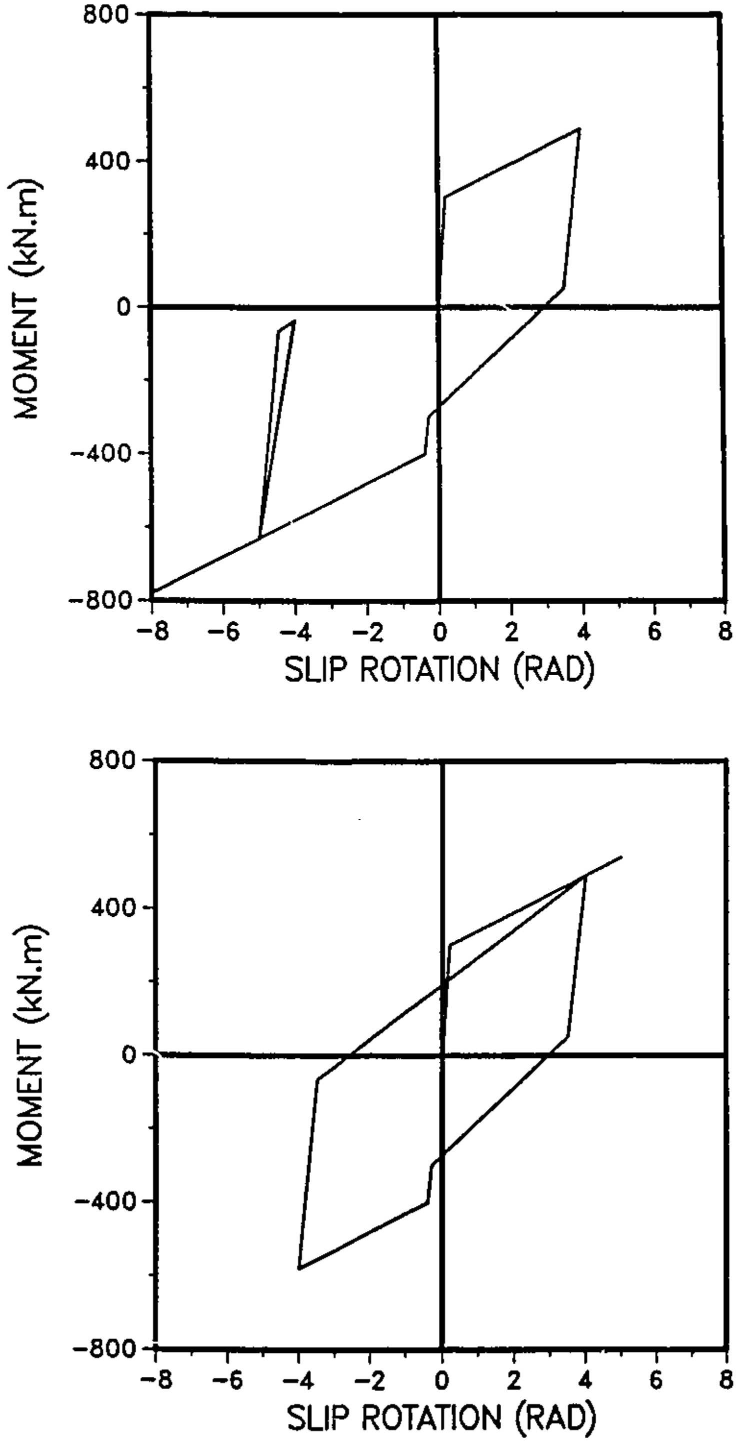

Figure 4.8 Continued

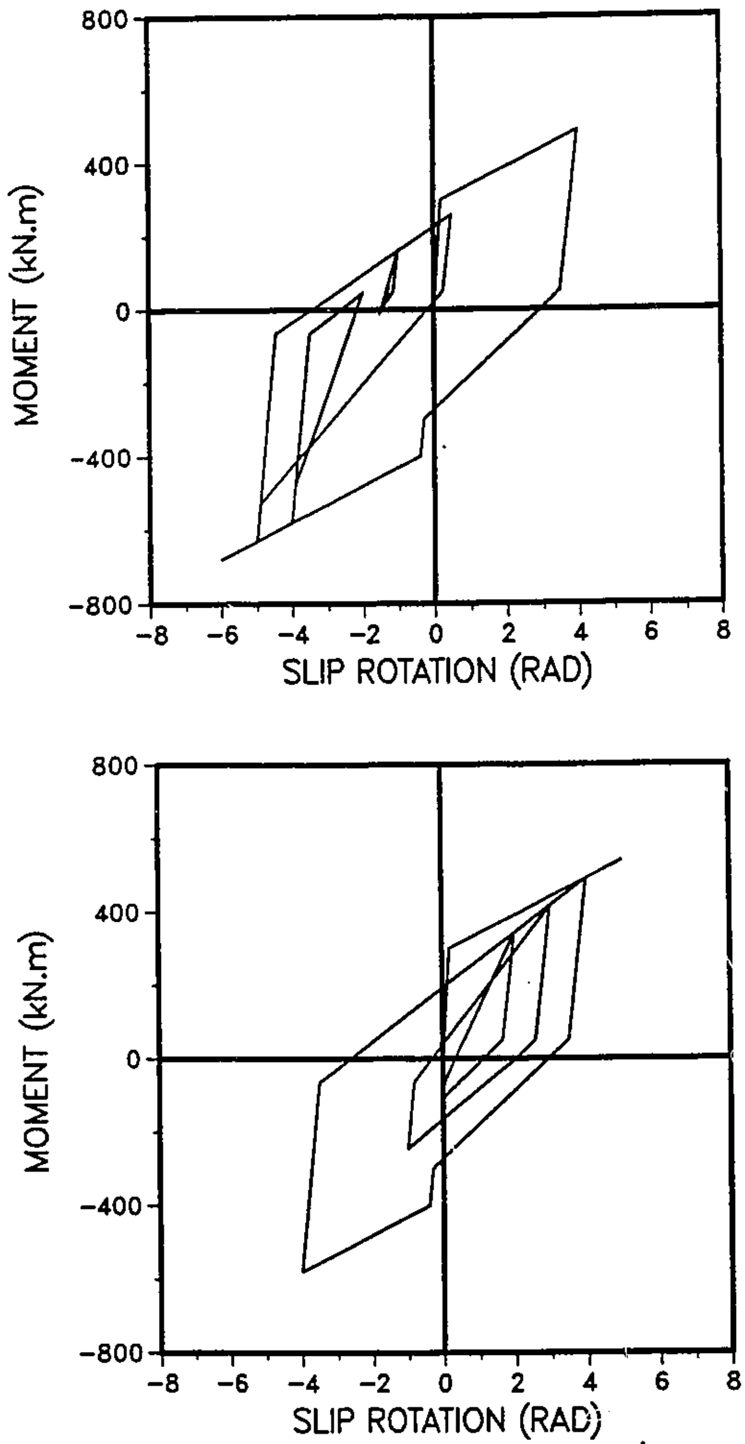

Figure 4.8 Continued

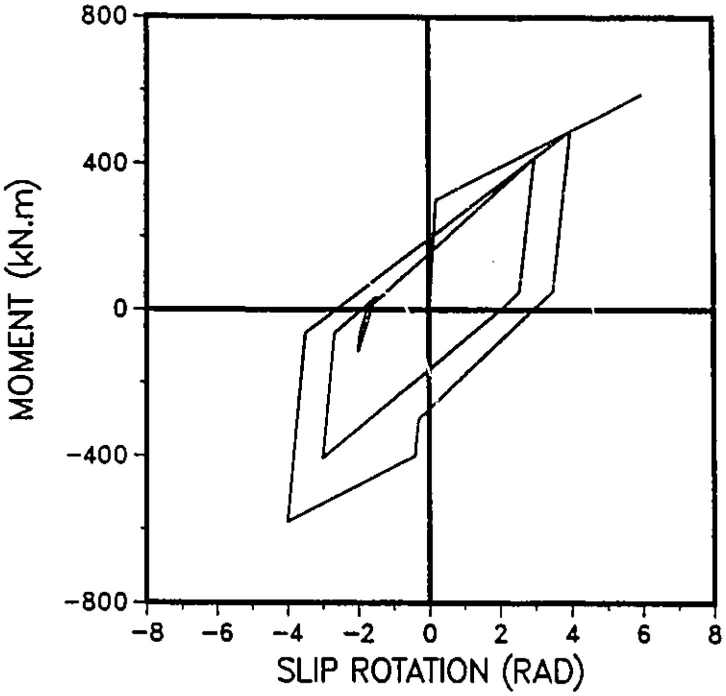

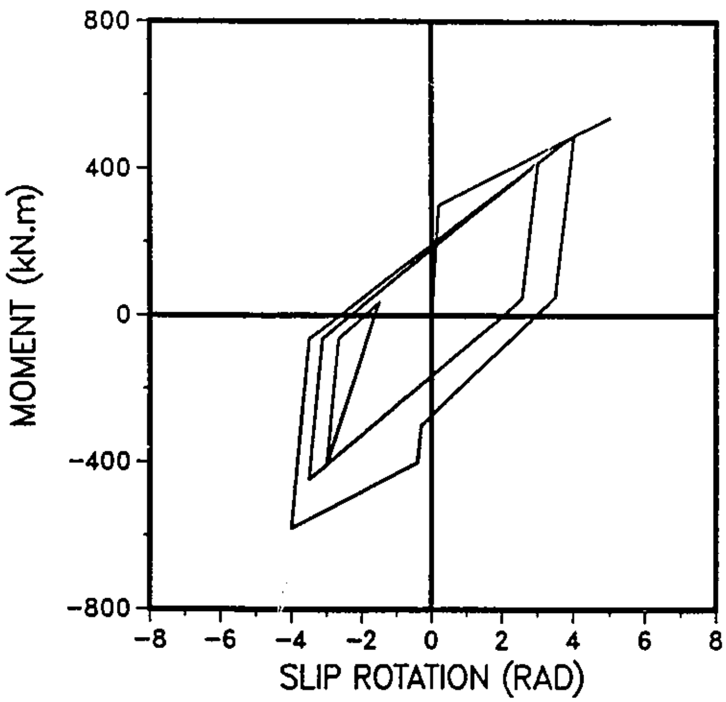

Figure 4.8 Continued

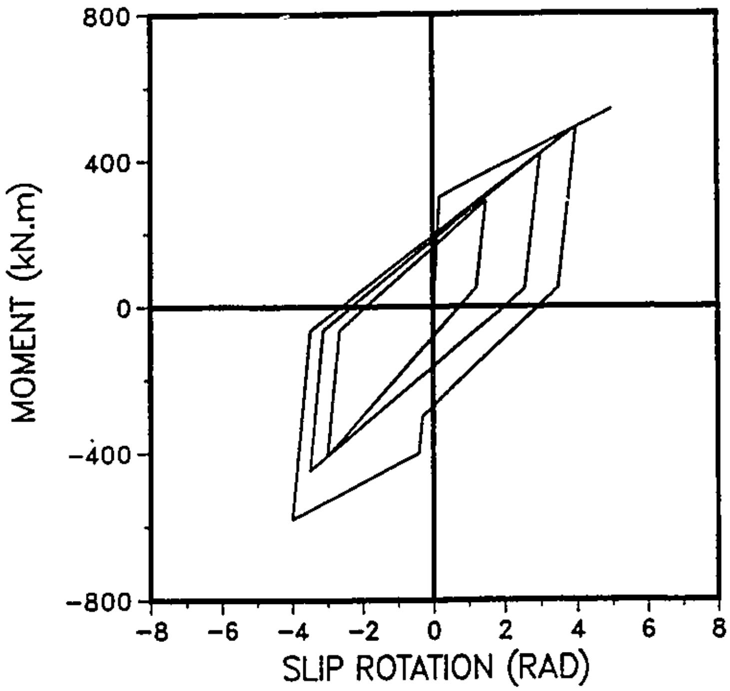

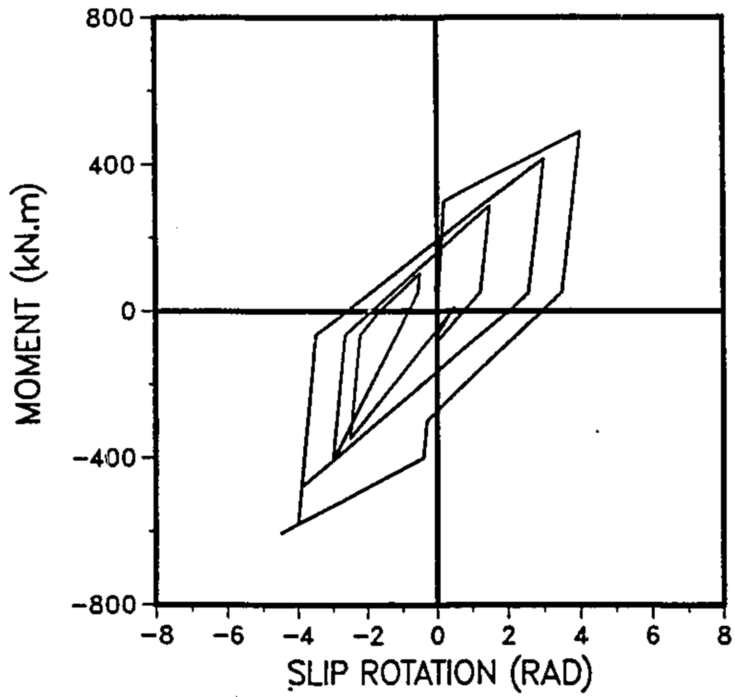

Figure 4.8 Continued

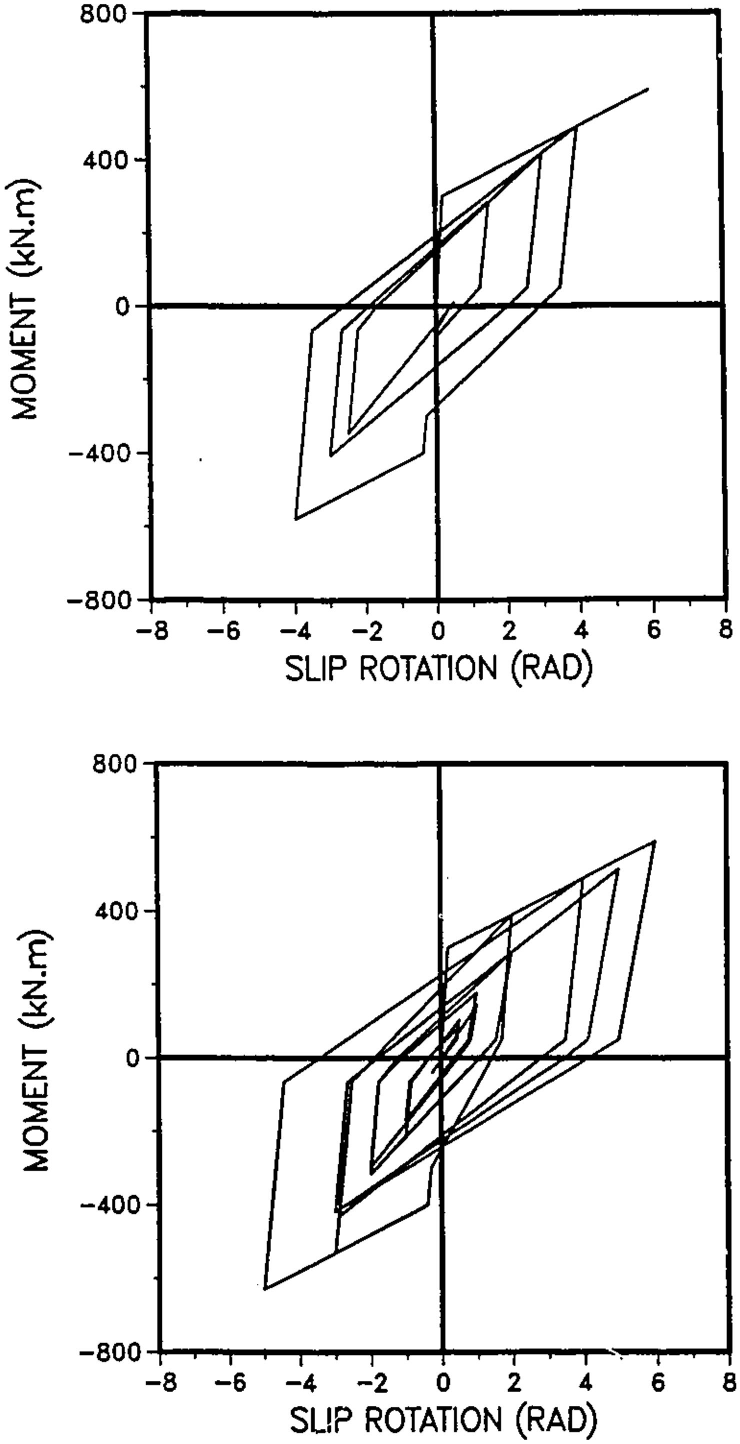

Figure 4.8 Continued

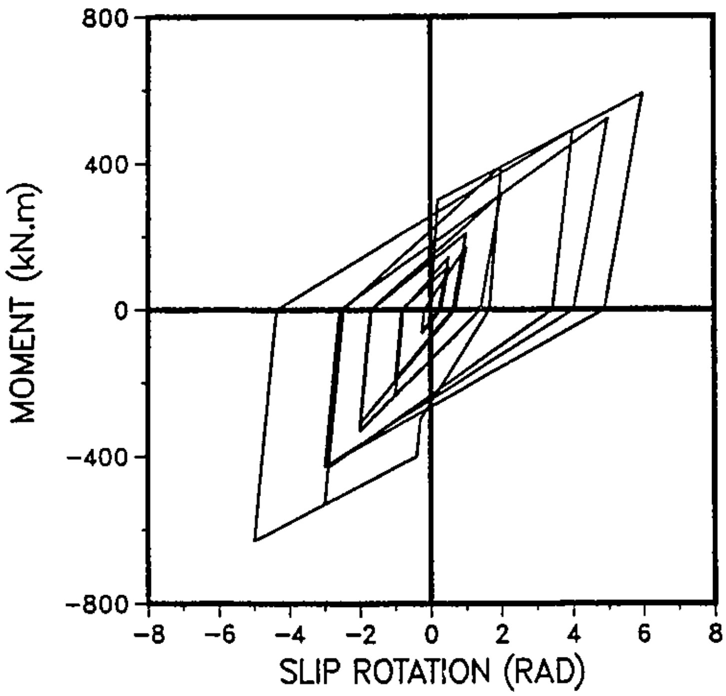

Figure 4.8 Continued

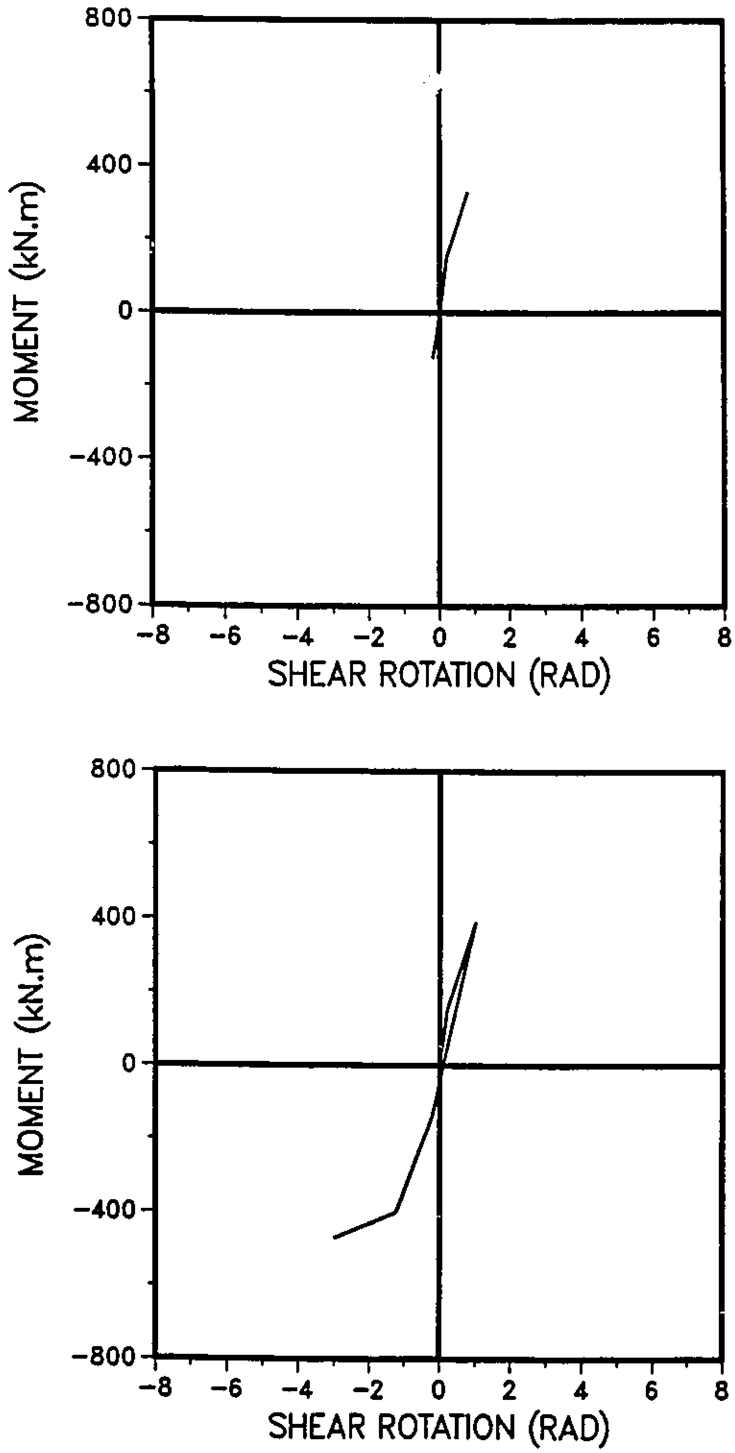

Figure 4.9 Verification of Shear Hysteretic Rules

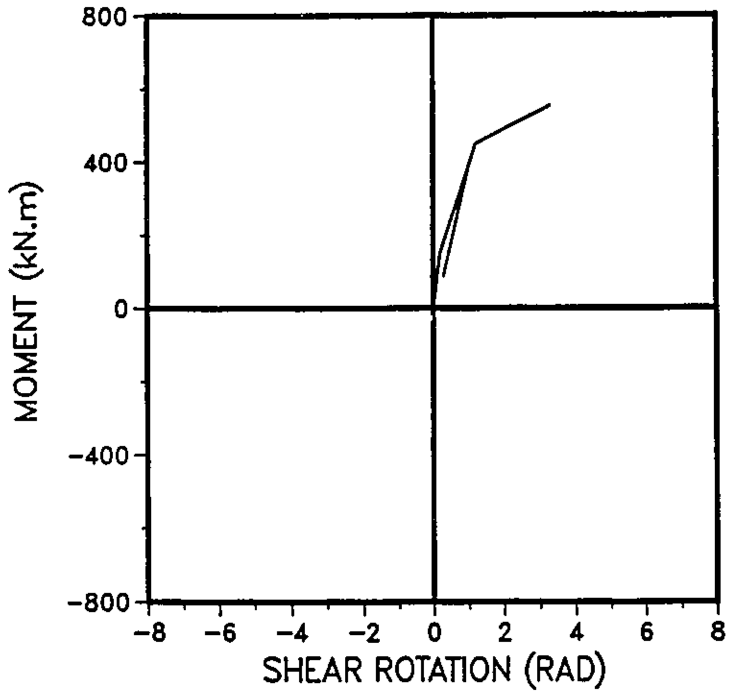

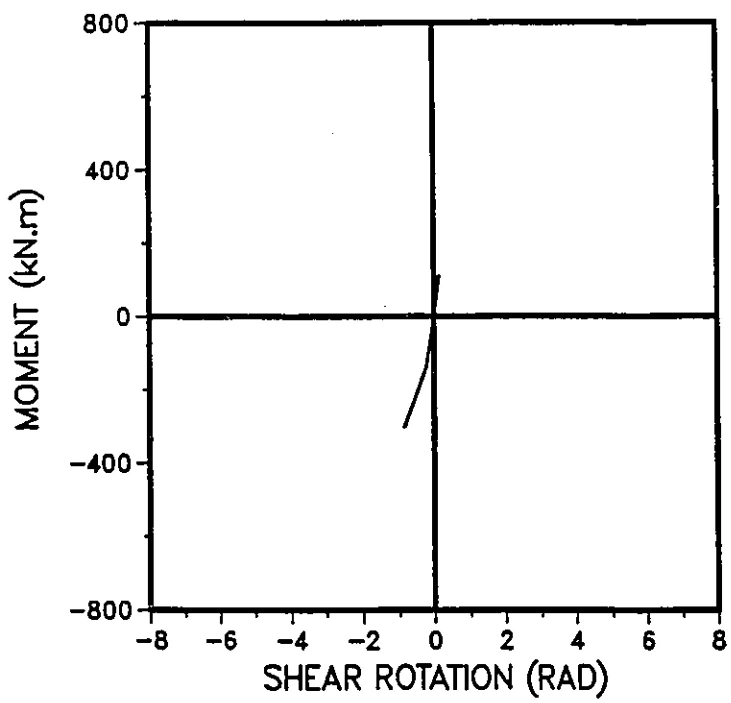

Figure 4.9 Continued

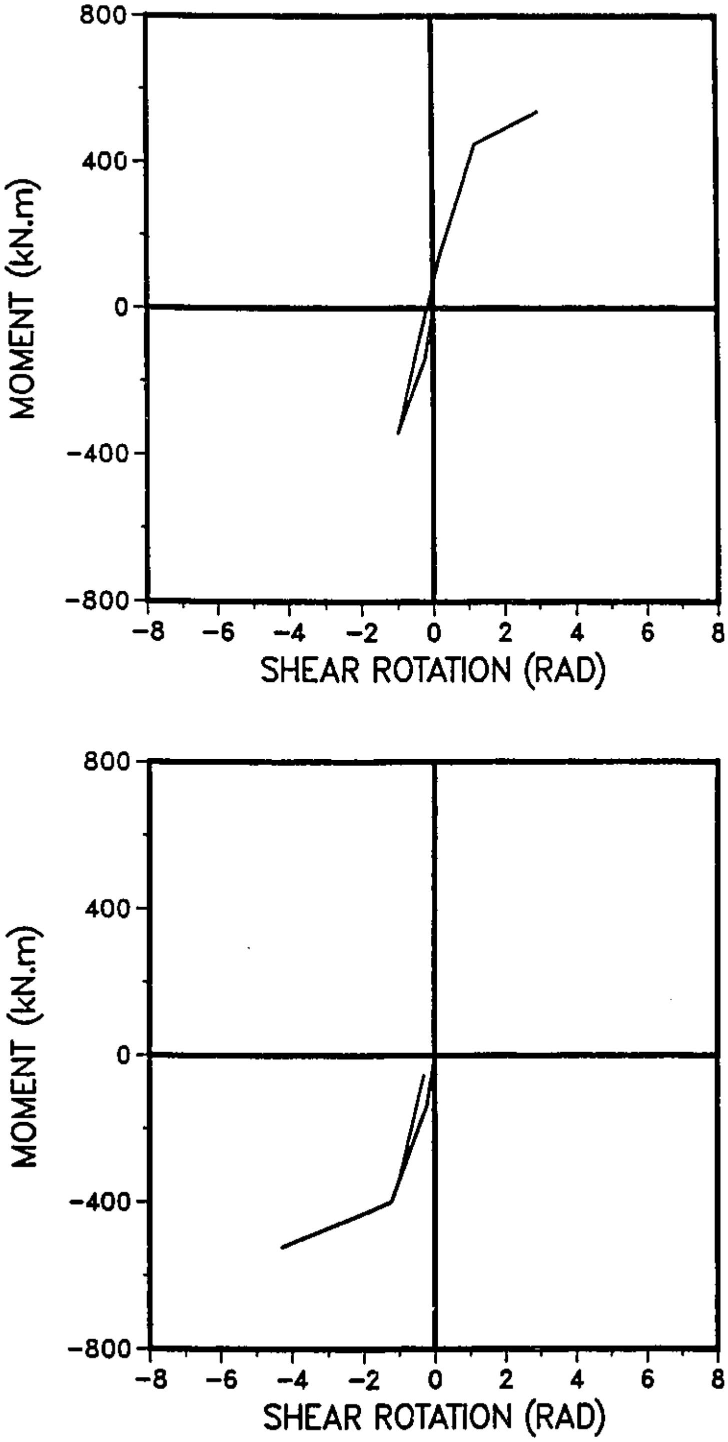

Figure 4.9 Continued

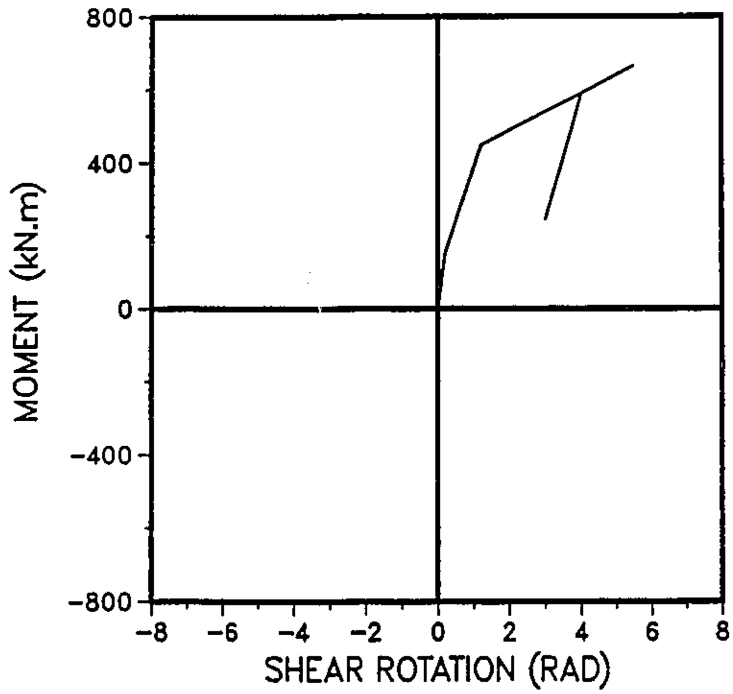

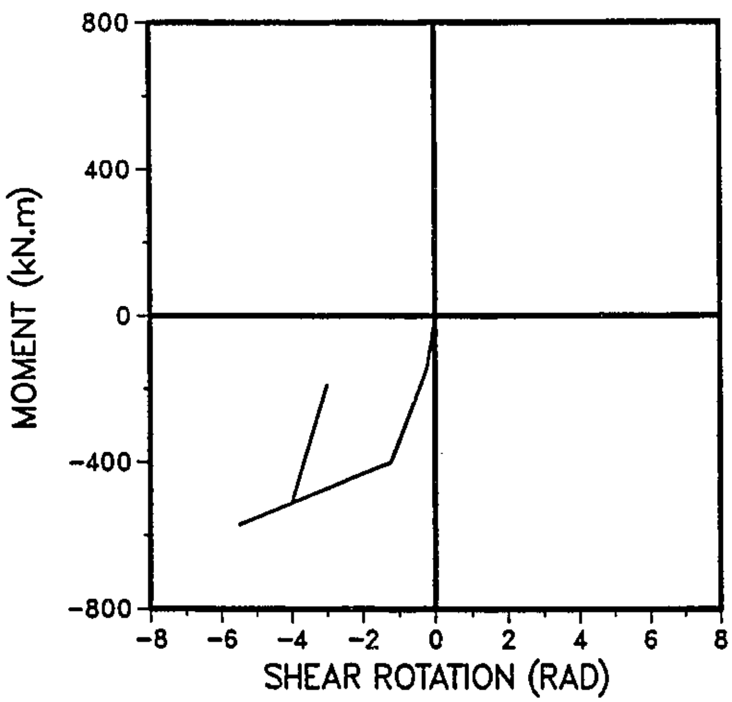

Figure 4.9 Continued

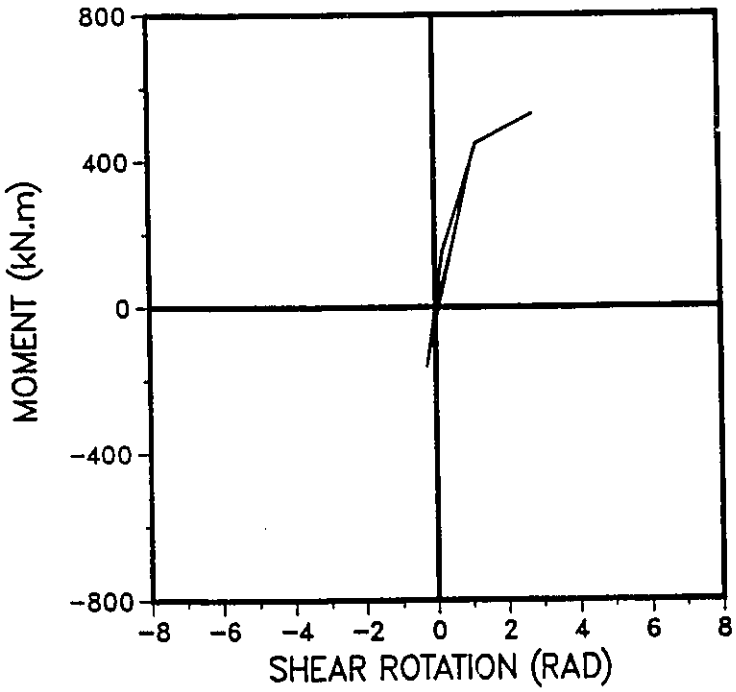

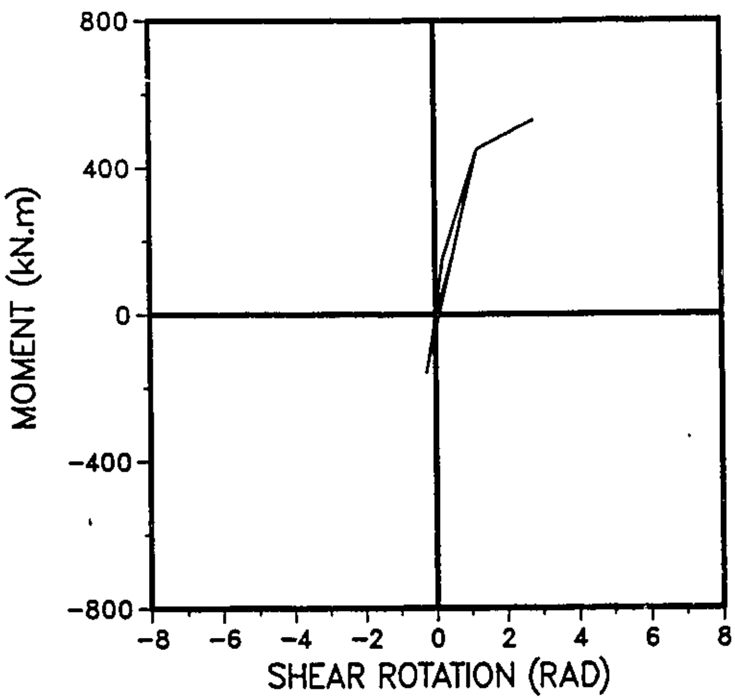

Figure 4.9 Continued

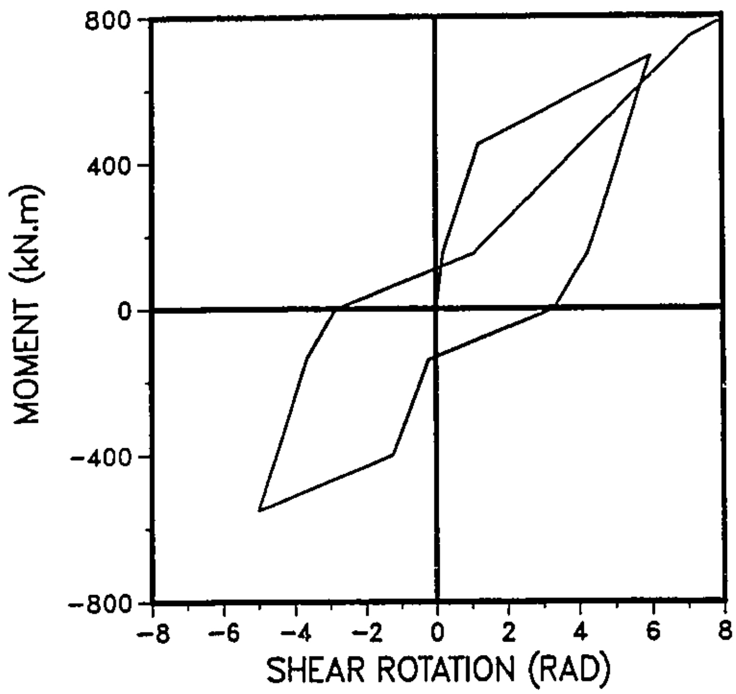

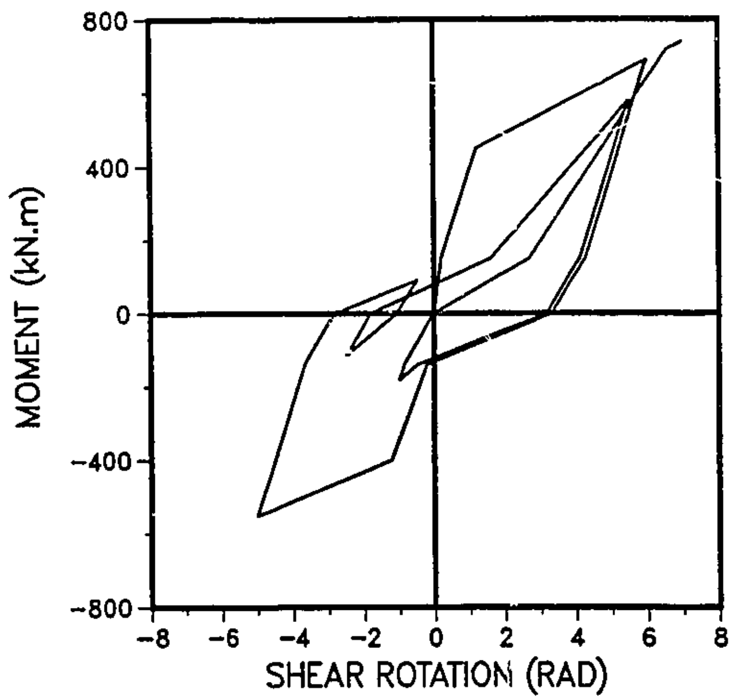

Figure 4.9 Continued

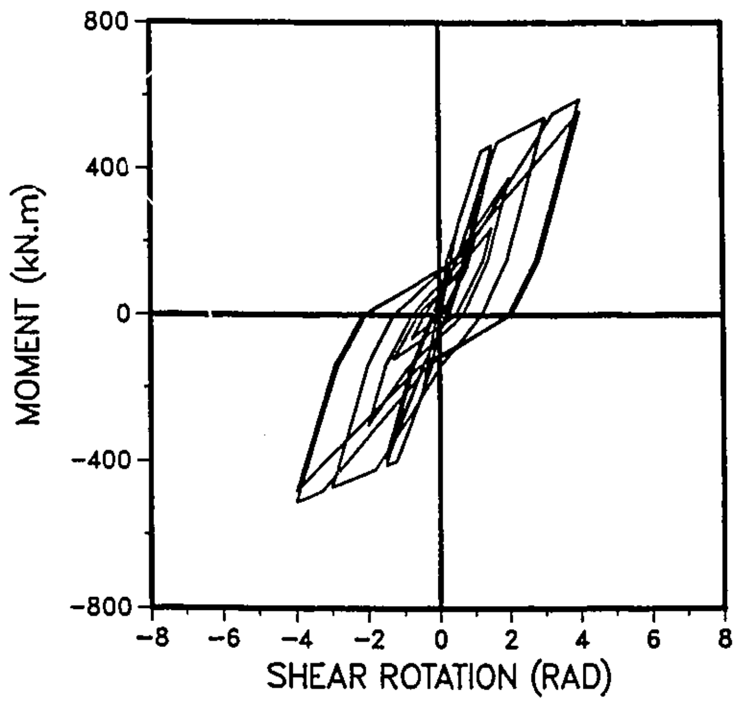

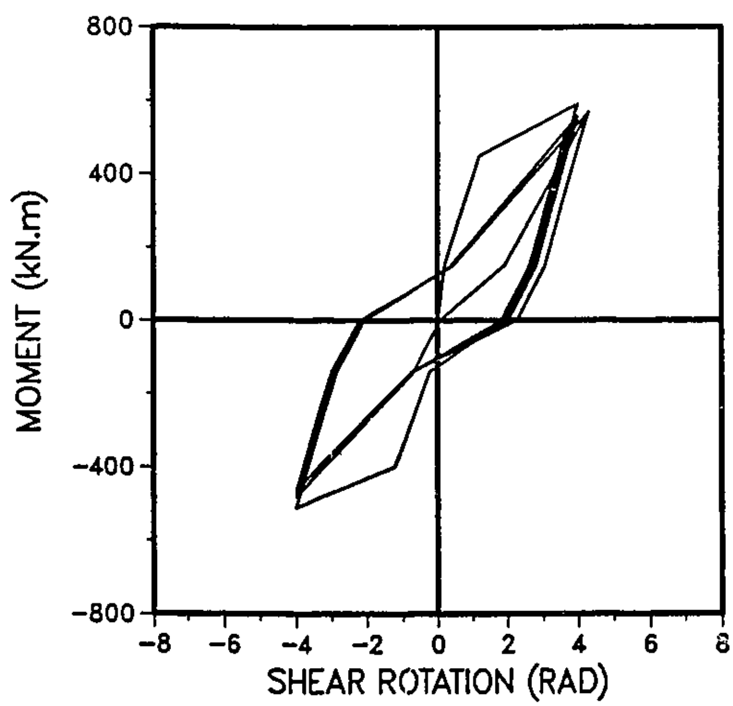

Figure 4.9 Continued

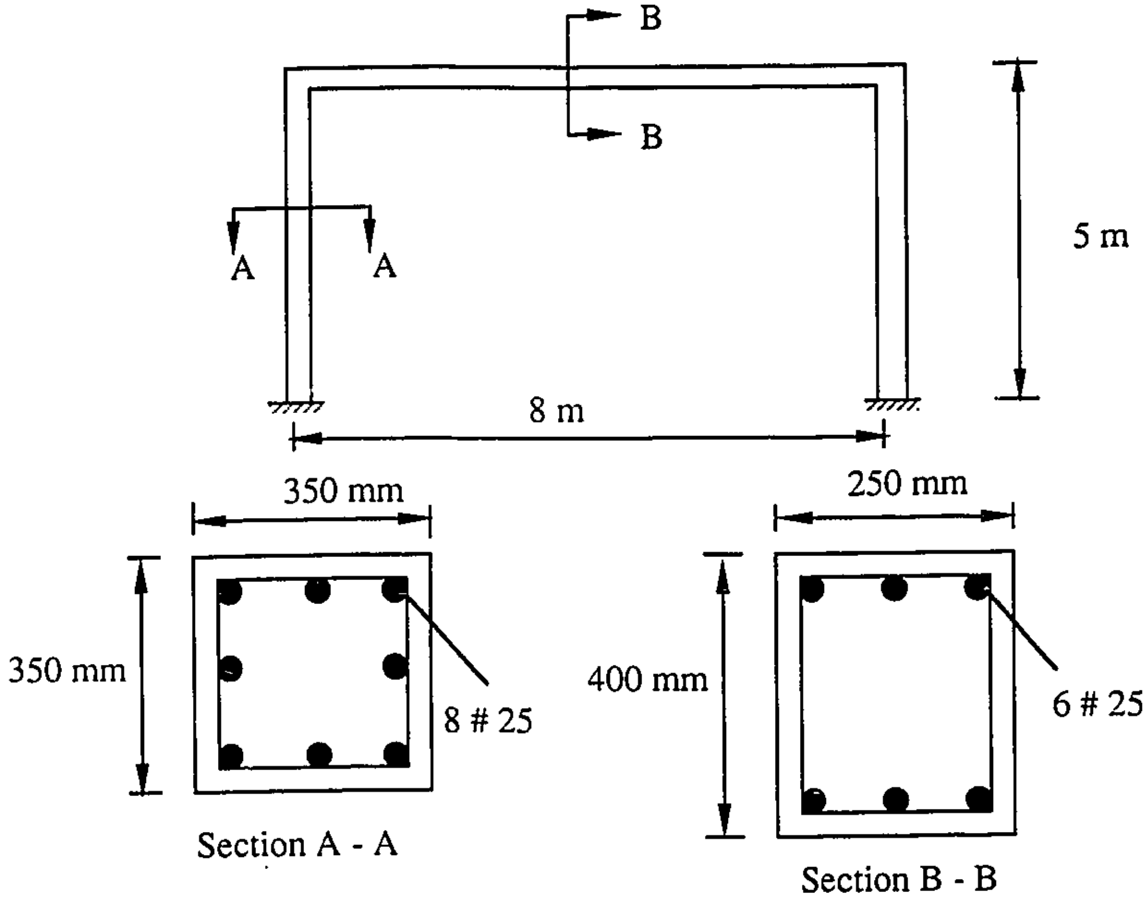

$M_y^{+} = M_y^{-} = 300$ kN.m
$M_{cr} = M0 = 50$ kN.m

$EI = 2 * 10^7$ N.m^2

$GA = 1.67 * 10^8$ N
$S1 = 0.55$
$S2 = 0.01$

$Ke_{slip} = 75*10^6$ N.m
$Kp_{slip} = 3.75*10^6$ N.m
$EA = 4151525520$ N

$M_y^{+} = M_y^{-} = 200$ kN.m
$M0 = 0.$
$EA = 4151525520$ N

$EI = 2.27 * 10^7$ N.m^2

$GA = 134225811$ N
$S1 = 0.55$
$S2 = 0.01$

$Ke_{slip} = 80*10^6$ N.m
$Kp_{slip} = 4*10^6$ N.m
$M_{cr} = 50$ kN.m

Figure 4.10 Portal Frame Used in the Second Stage

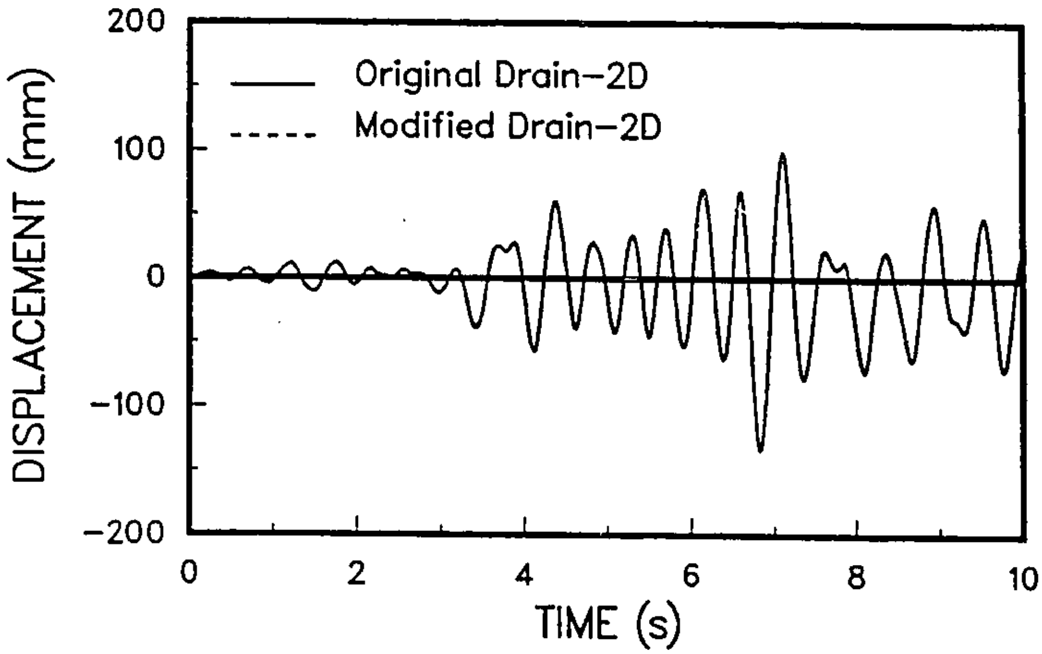

Figure 4.11 (a) Lateral Displacement Time History of Portal Frame

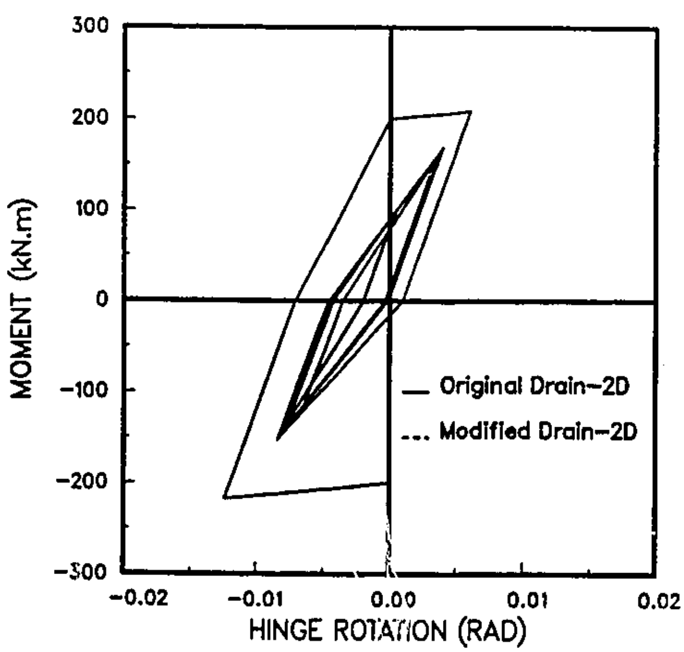

Figure 4.11 (b) Flexural Hinge Hysteretic Relationship at the Left End of the Portal Frame Girder.

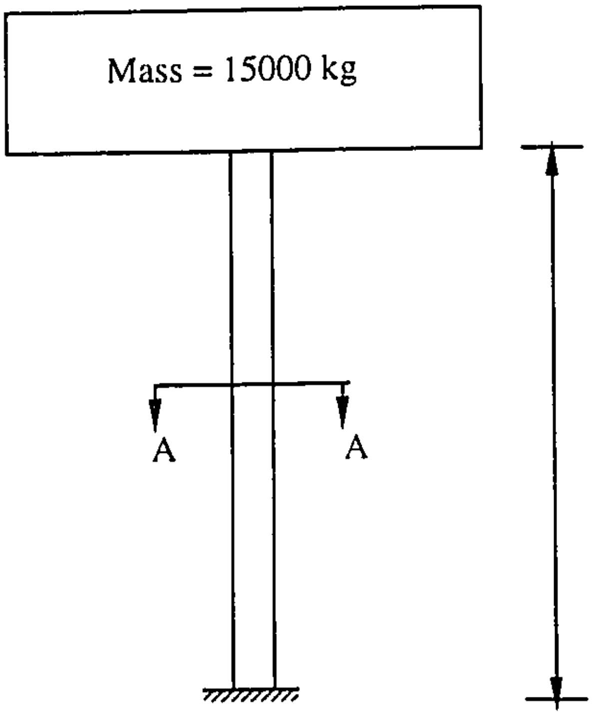

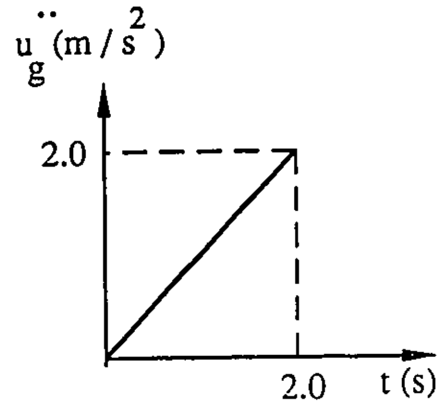

(b) Monotonic Ground Motion

(a) Cantilever System

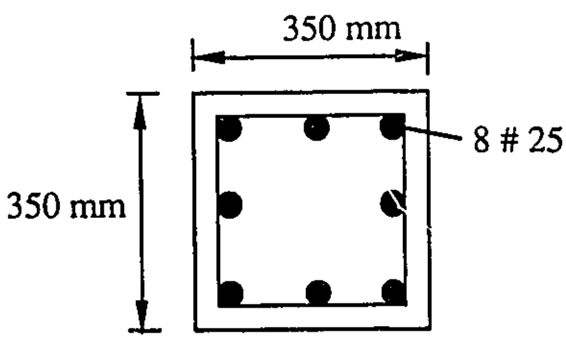

Section A - A

$M_y^+ = M_y^- = 300$ kN.m
$M_{cr} = M0 = 50$ kN.m

$EI = 2 * 10^7$ N.m^2

$GA = 1.67 * 10^8$ N
$S1 = 0.55$
$S2 = 0.01$

$Ke_{slip} = 75 * 10^6$ N.m
$Kp_{slip} = 3.75 * 10^6$ N.m
EA = 4151525520 N

Figure 4.12 Cantilever System Used in the Third Stage

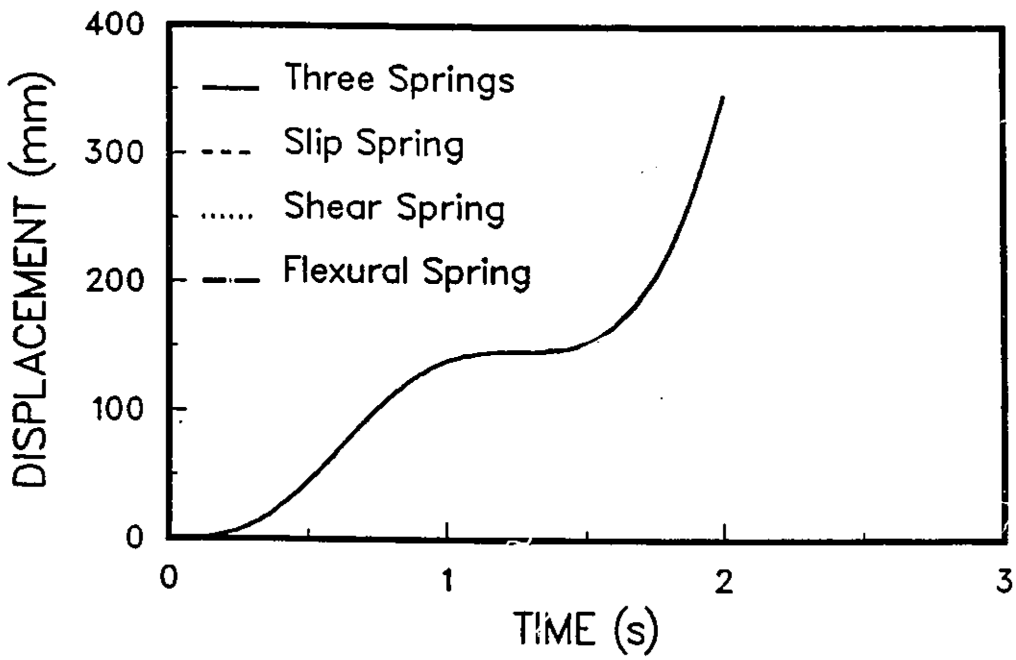

Figure 4.13 Lateral Displacement Time History of the Cantilever System

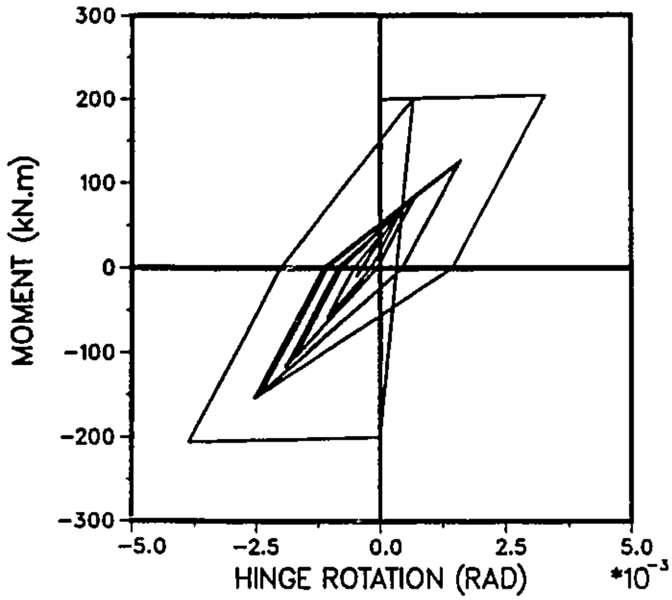

a) Flexure

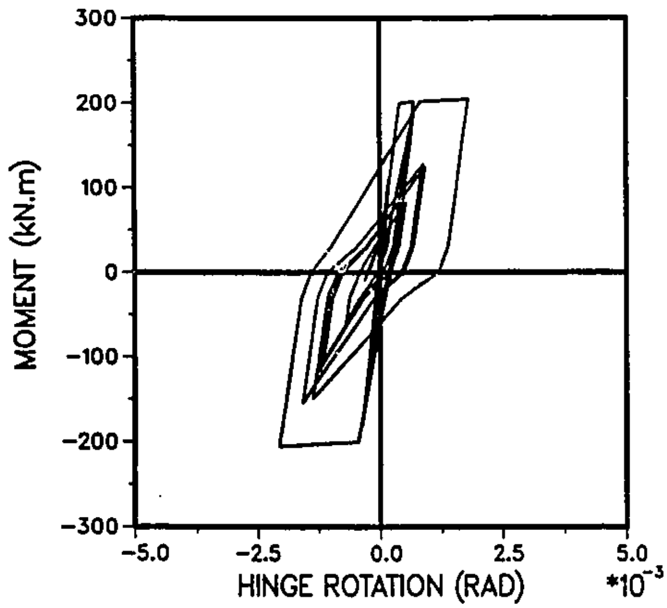

b) Shear

Figure 4.14 Moment-Hinge Rotation at the Left End of the Portal Frame Girder.

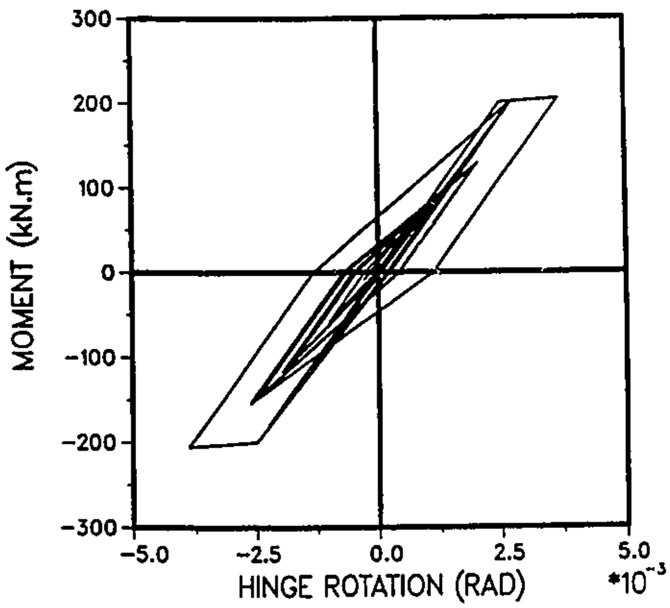

c) Anchorage Slip

Figure 4.14 Continued

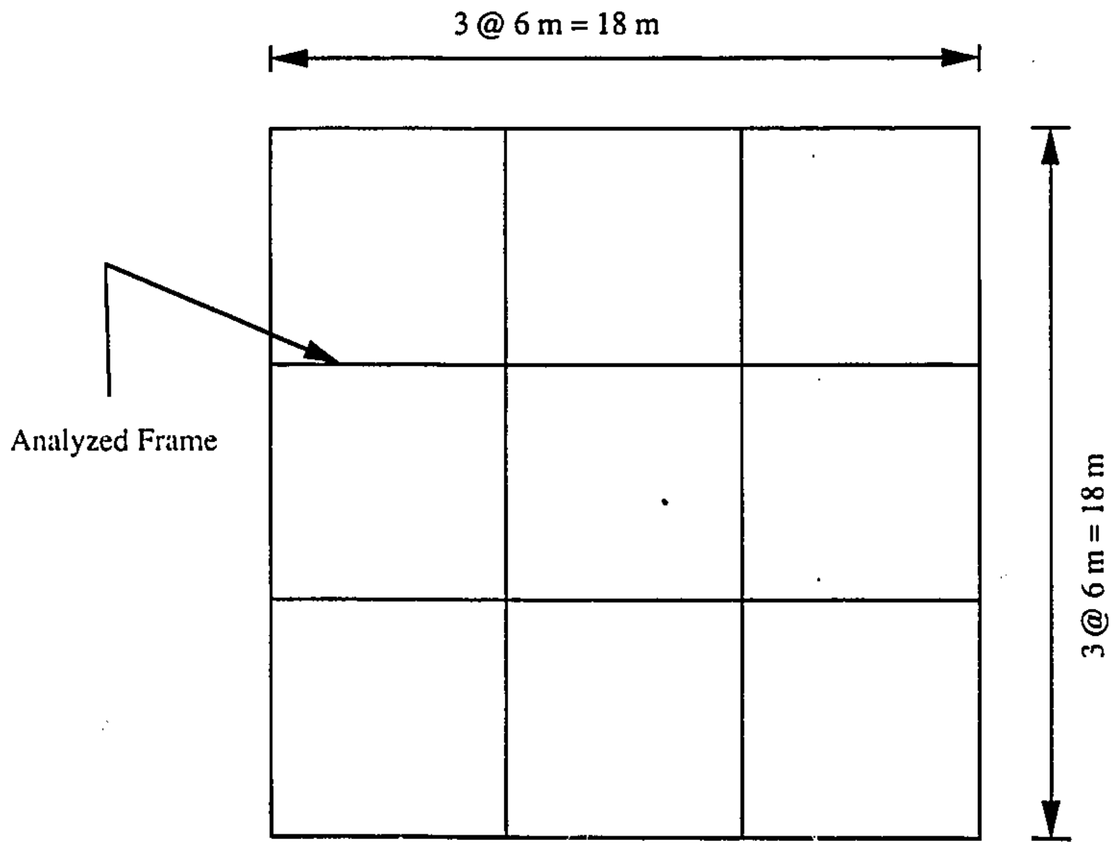

Figure 5.1 Plan View of the Building Considered

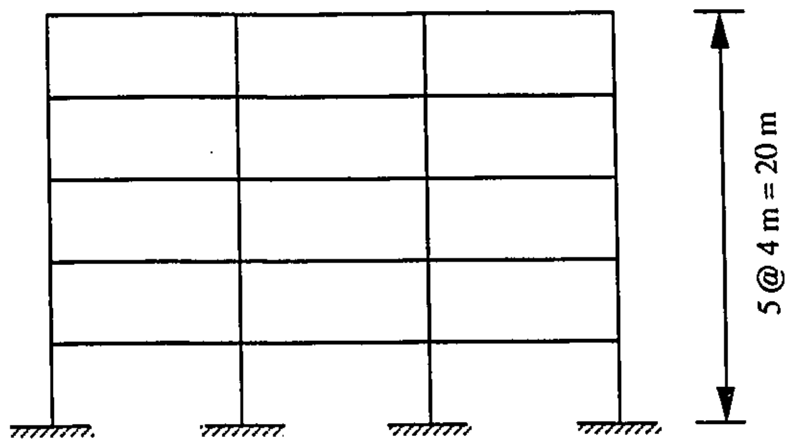

Figure 5.2 Five Story Frame

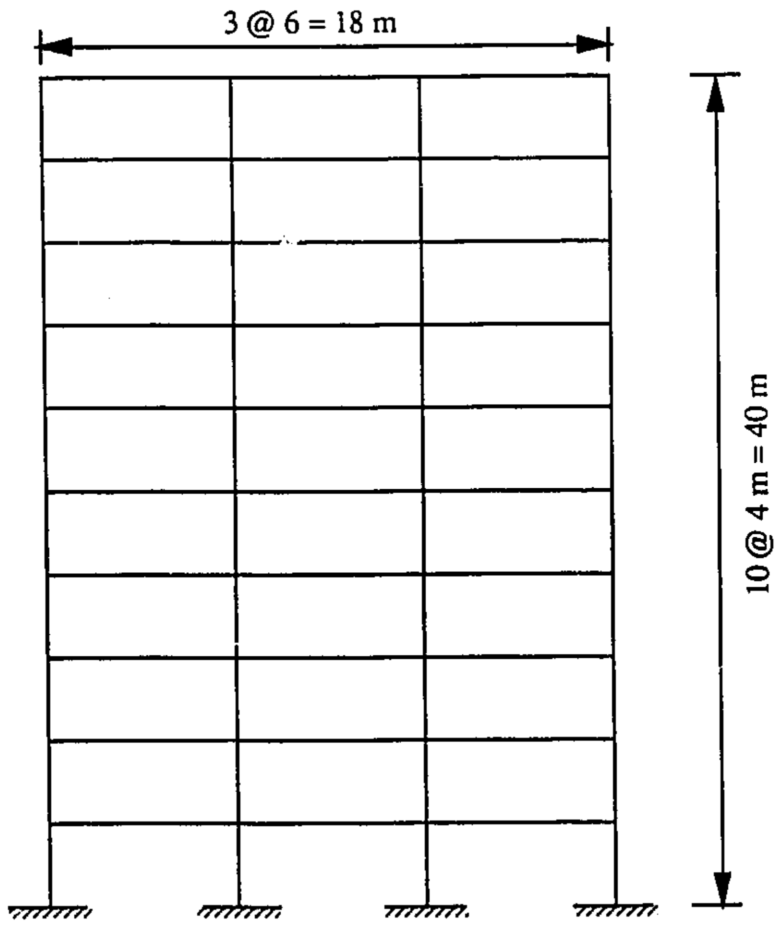

Figure 5.3 Ten Story Frame

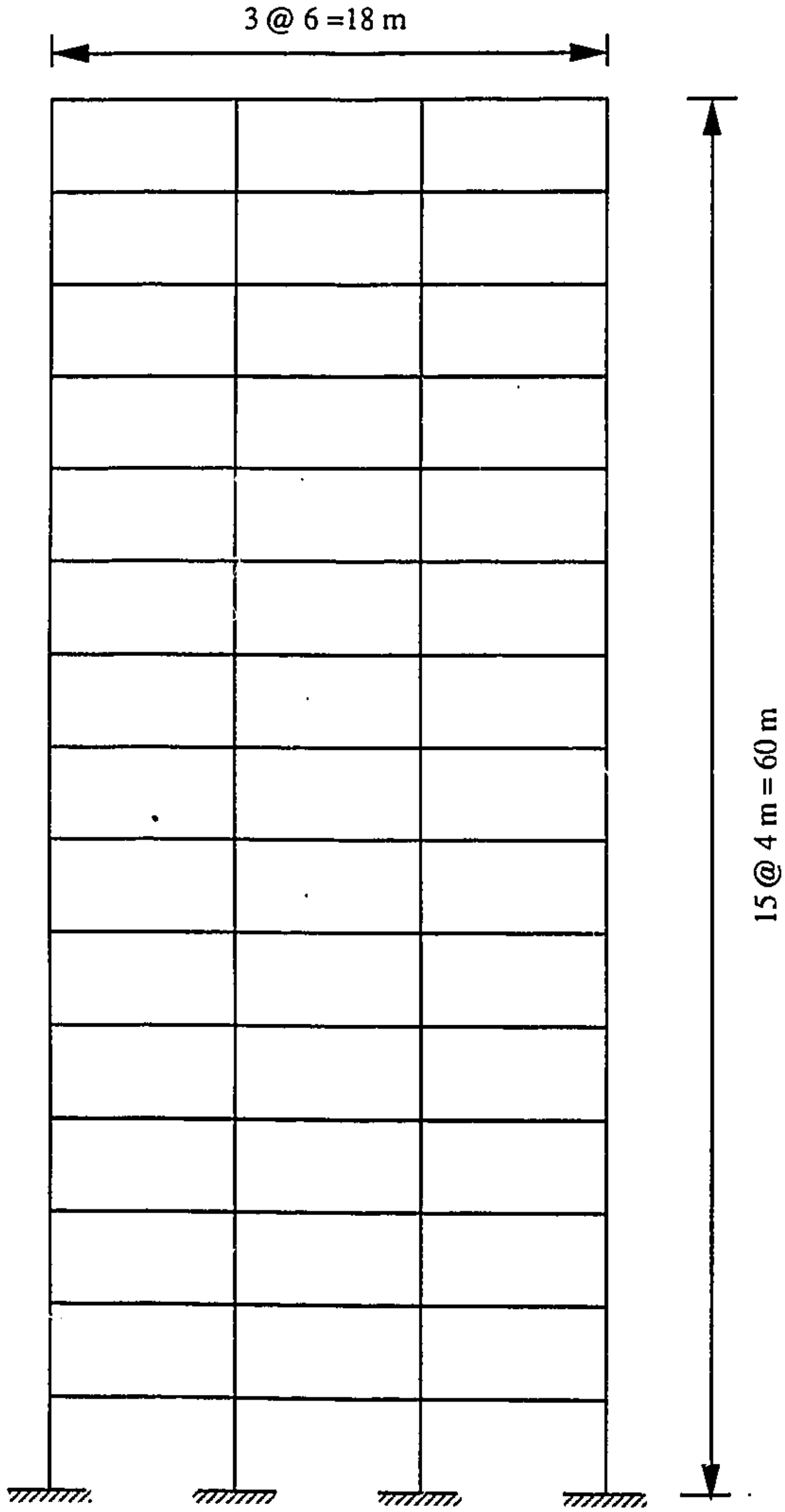

Figure 5.4 Fifteen Story Frame

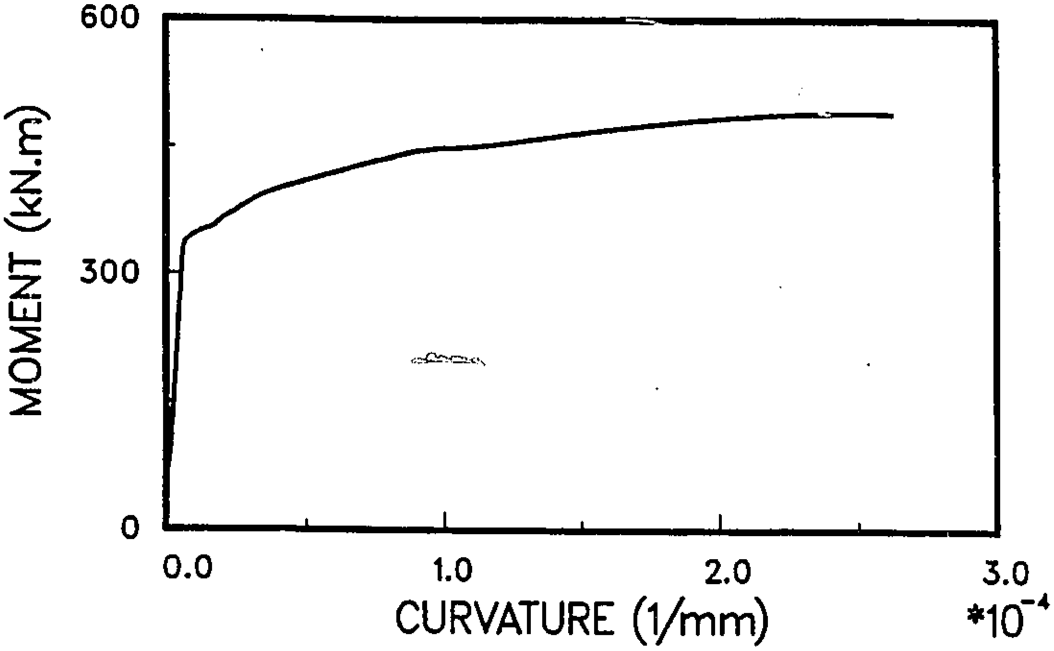

Figure 5.5 Typical Moment-Curvature Relationship for Girders

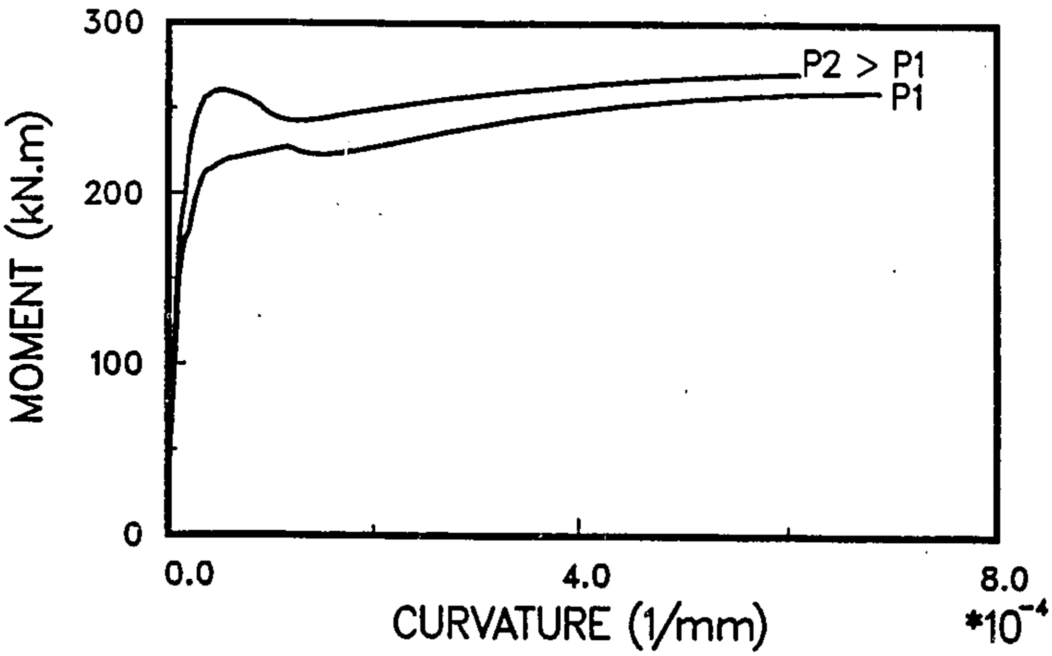

Figure 5.6 Effect of Axial Load on Moment-Curvature Relationship of Columns

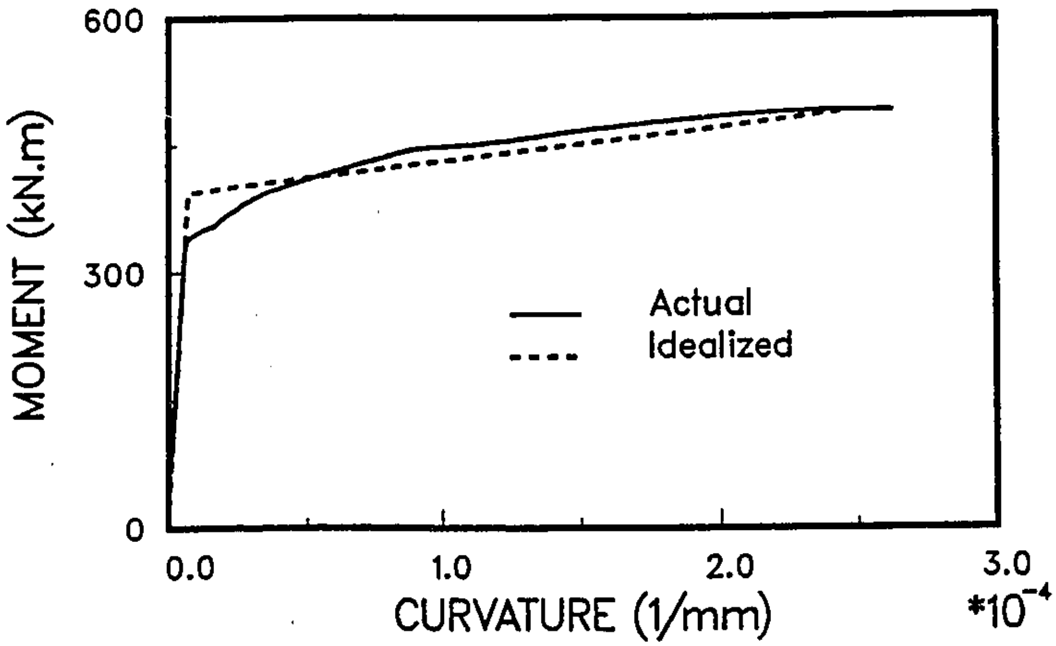

Figure 5.7 Idealization of Moment-Curvature Relationship of Girders

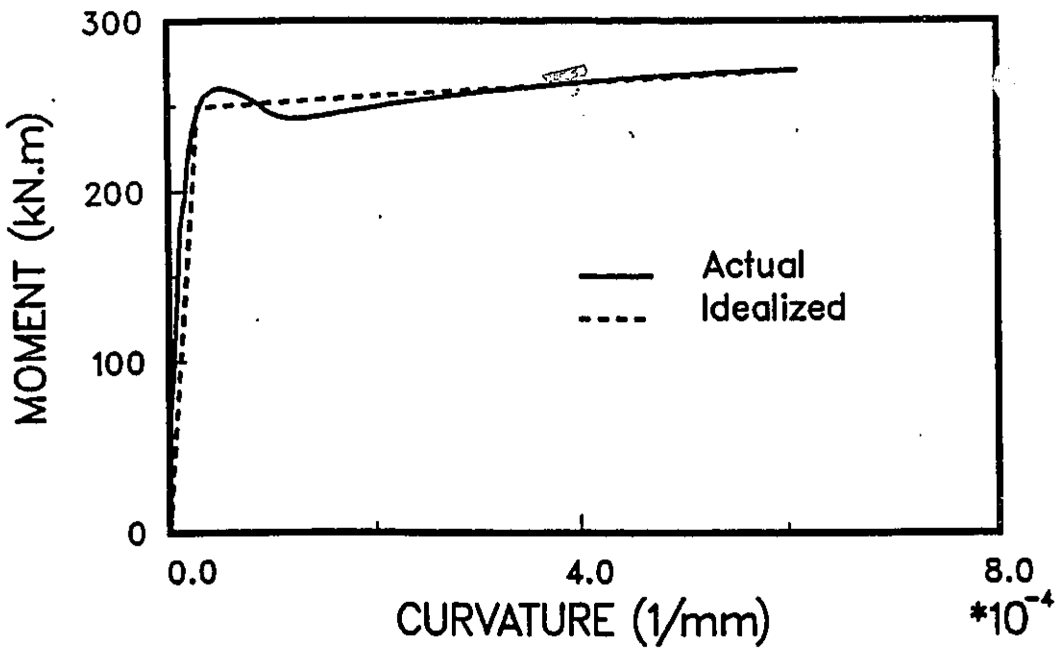

Figure 5.8 Idealization of Moment-Curvature Relationship of Columns

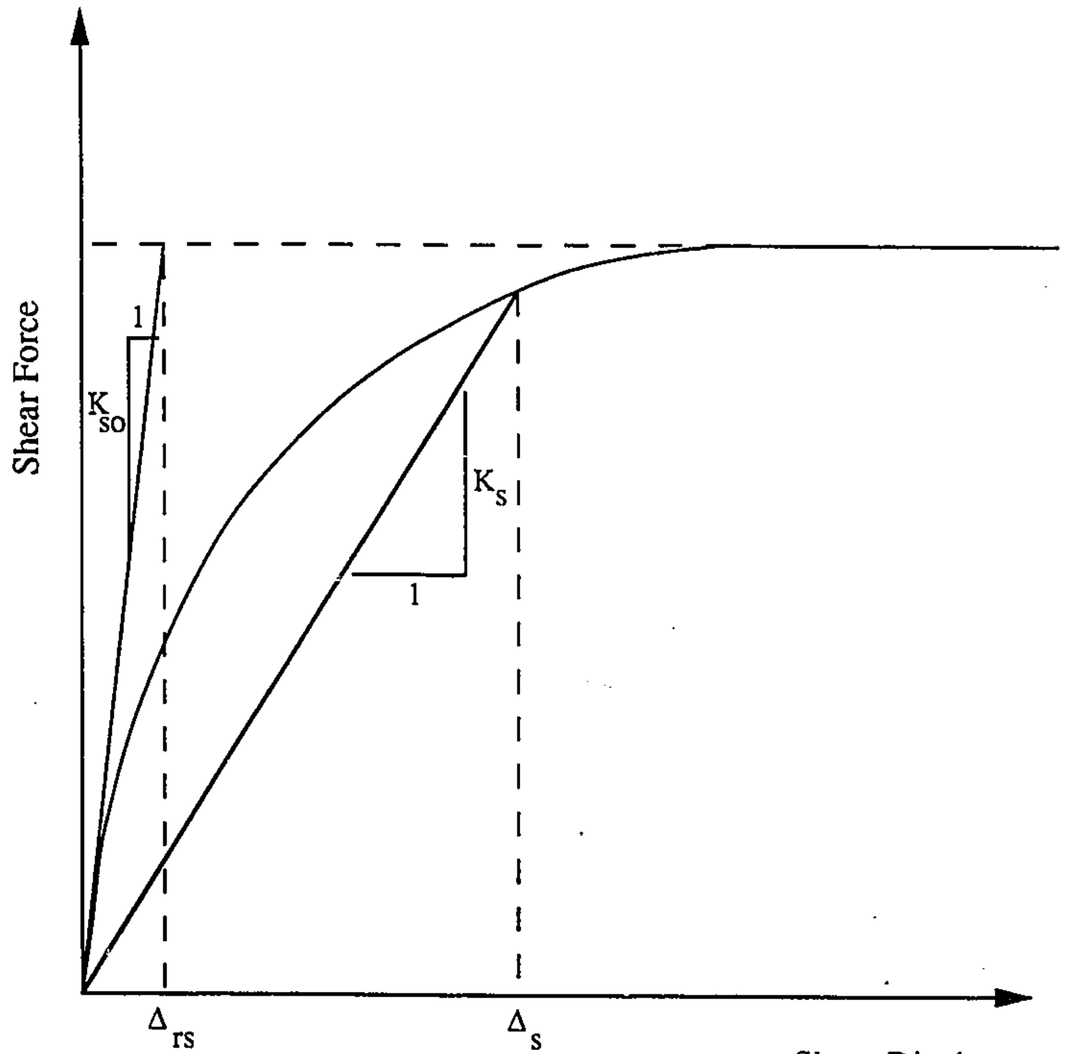

Figure 5.9 Shear Force - Shear Displacement Relationship

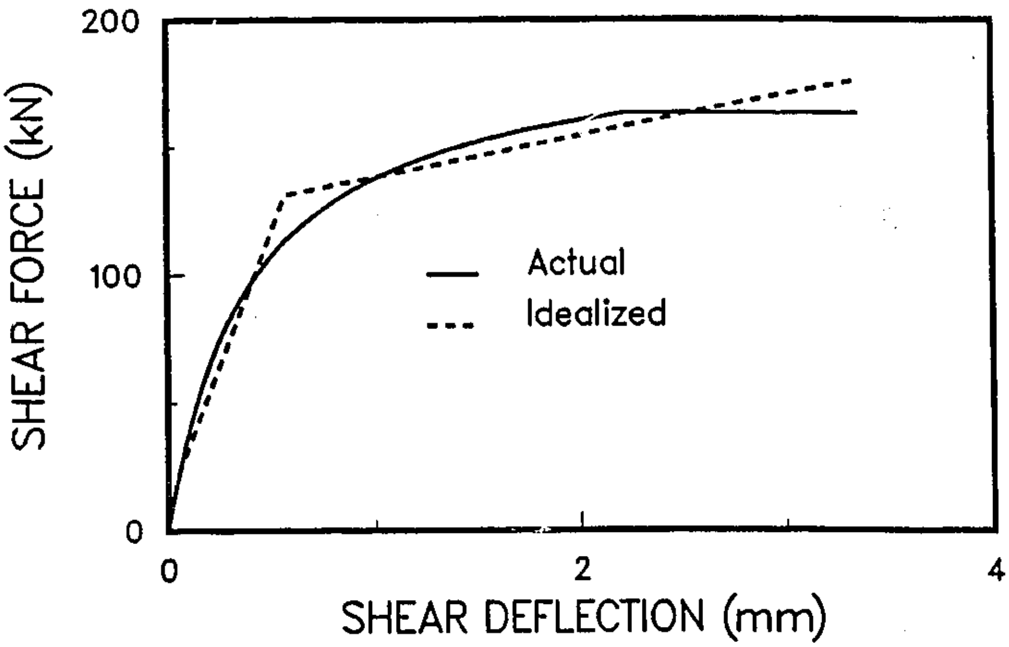

Figure 5.10 Idealization of Shear Force - Shear Deflection Relationship

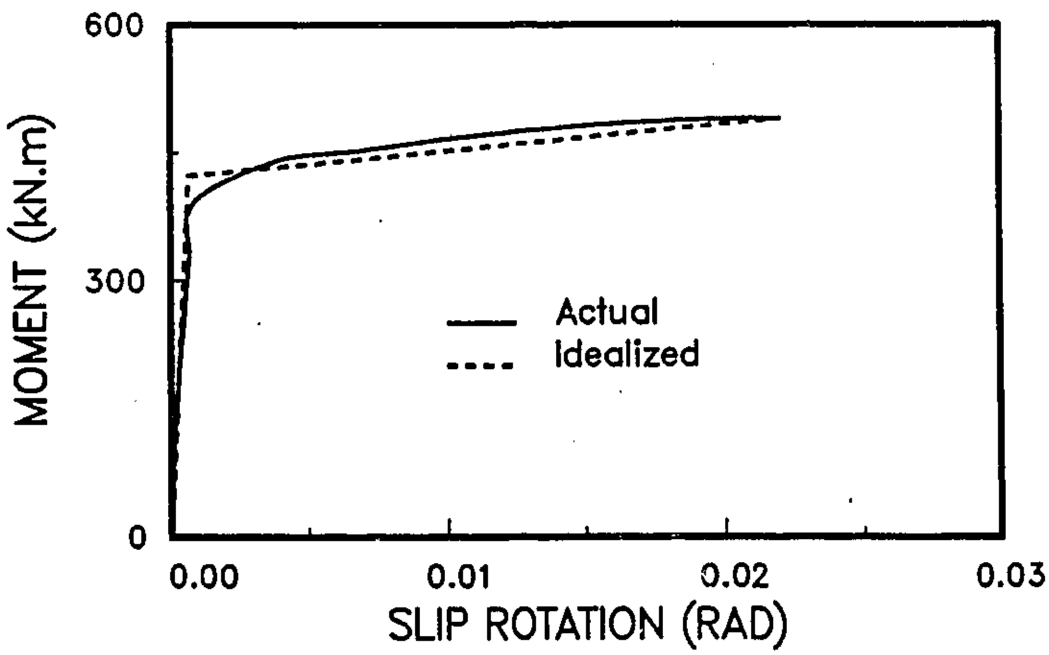

Figure 5.11 Idealization of Moment-Anchorage Slip Relationship of Girders

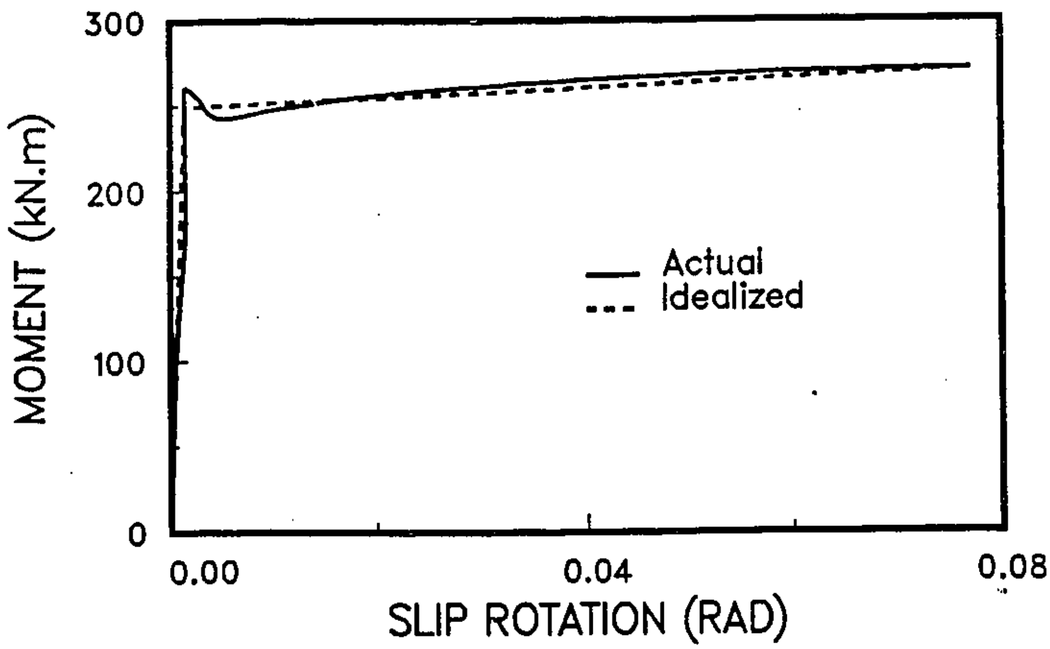

Figure 5.12 Idealization of Moment-Anchorage Slip Relationship of Columns

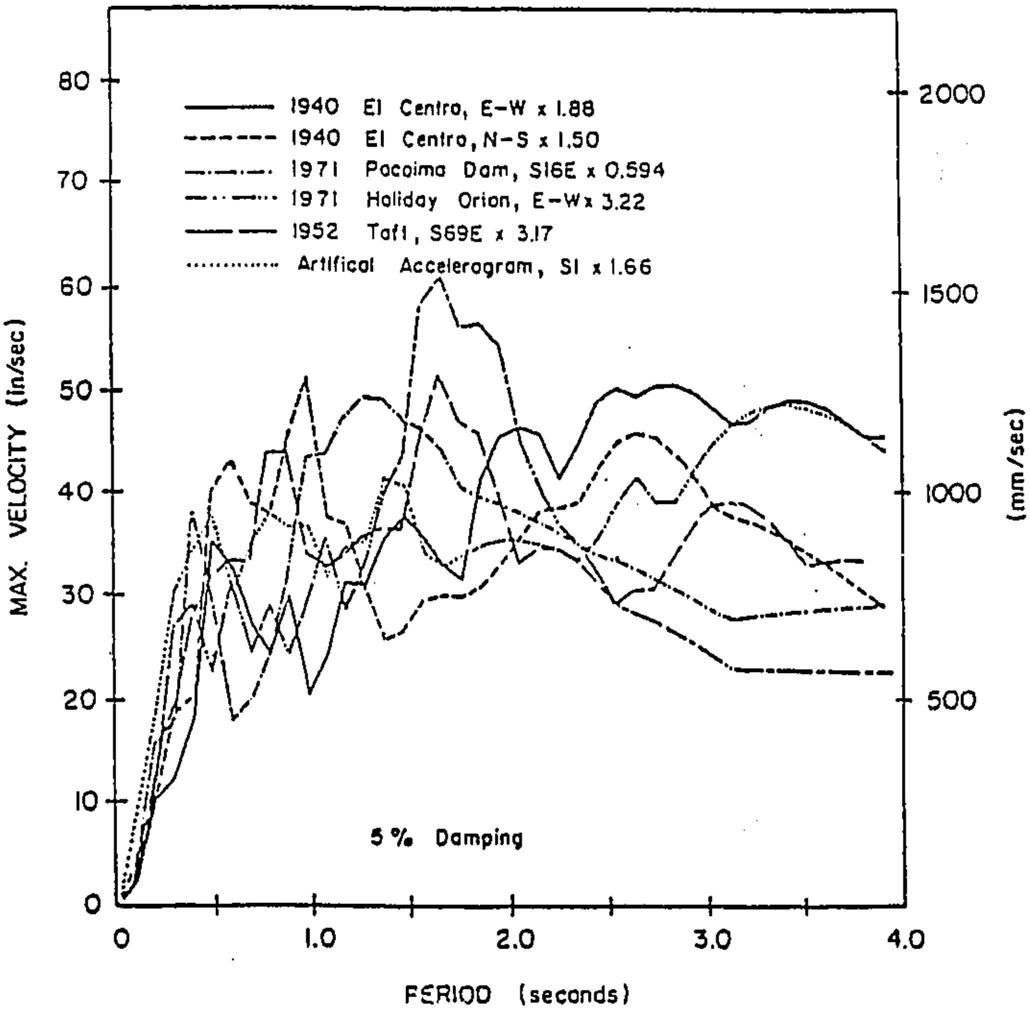

Figure 5.13 Response Spectra for Selected Earthquake records [85])

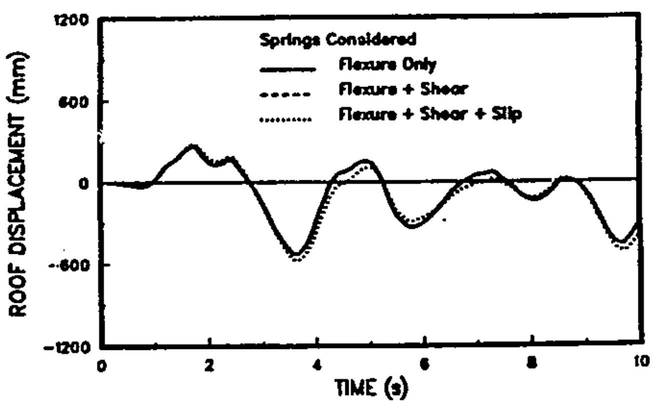

(a) Five-Story Frame

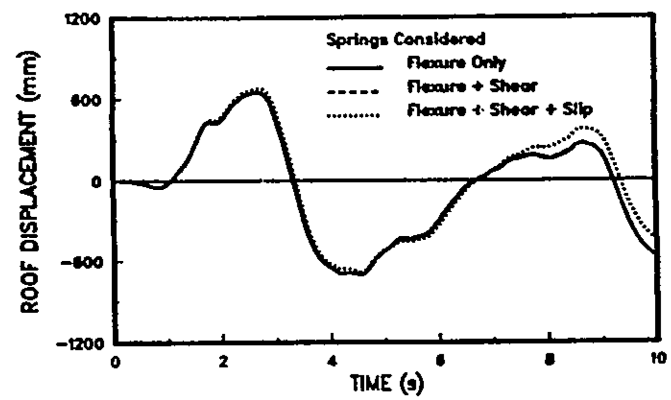

(b) Ten-Story Frame

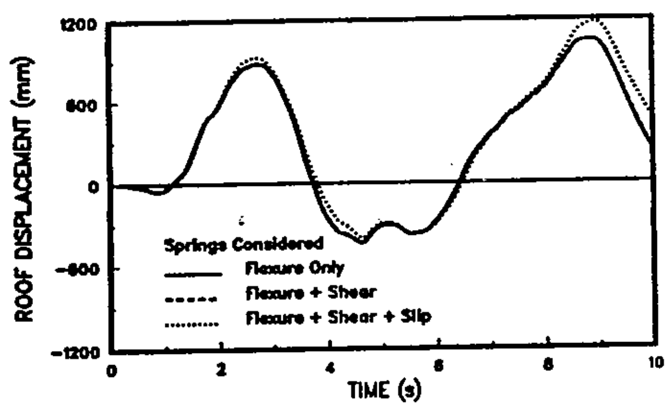

(c) Fifteen-Story Frame

Figure 6.1 Time History of Roof Displacement (El Centro 1940 E-W Earthquake)

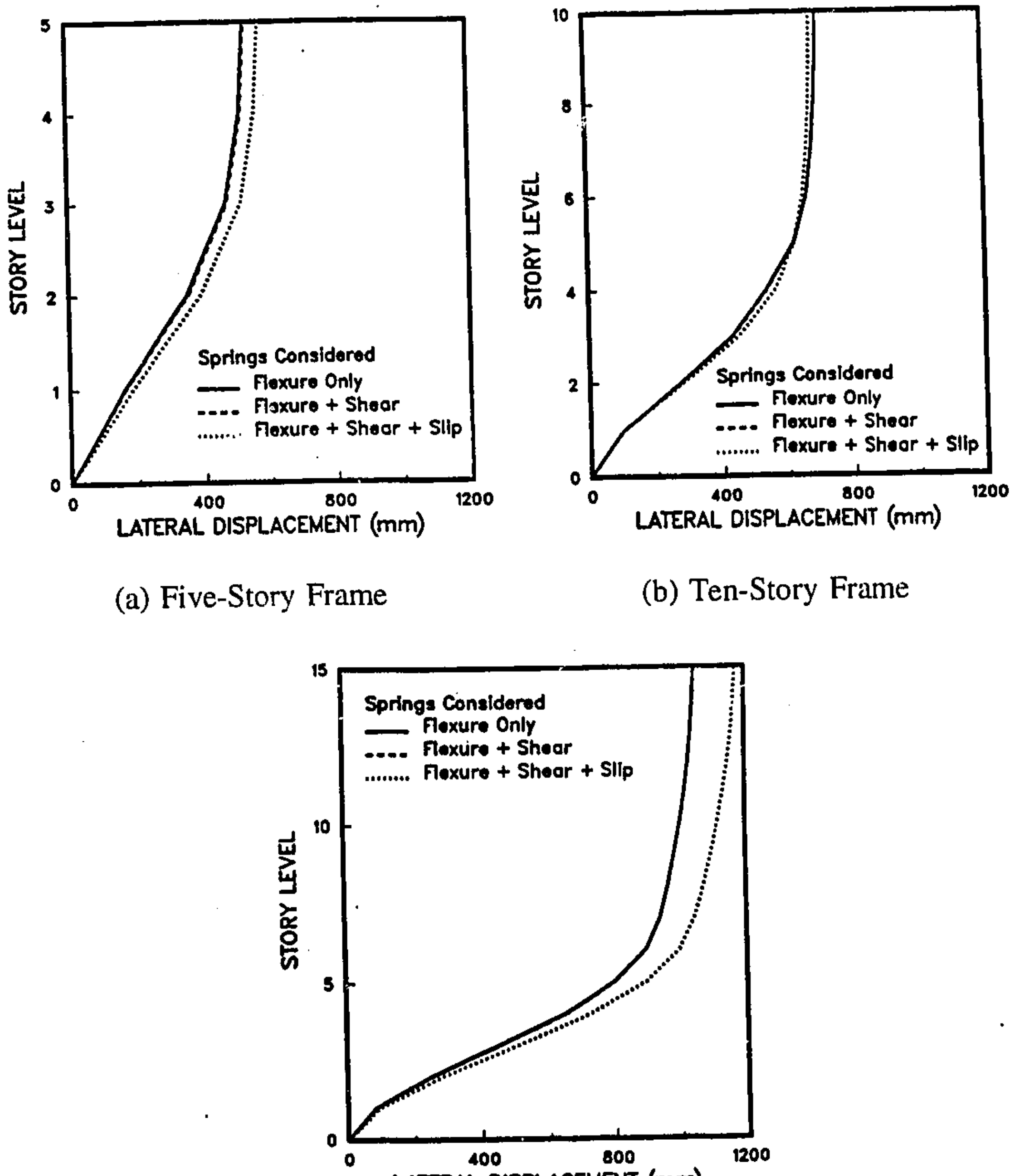

(a) Five-Story Frame

(b) Ten-Story Frame

(c) Fifteen-Story Frame

Figure 6.2 Lateral Displacement Envelopes (El Centro 1940 E-W Earthquake)

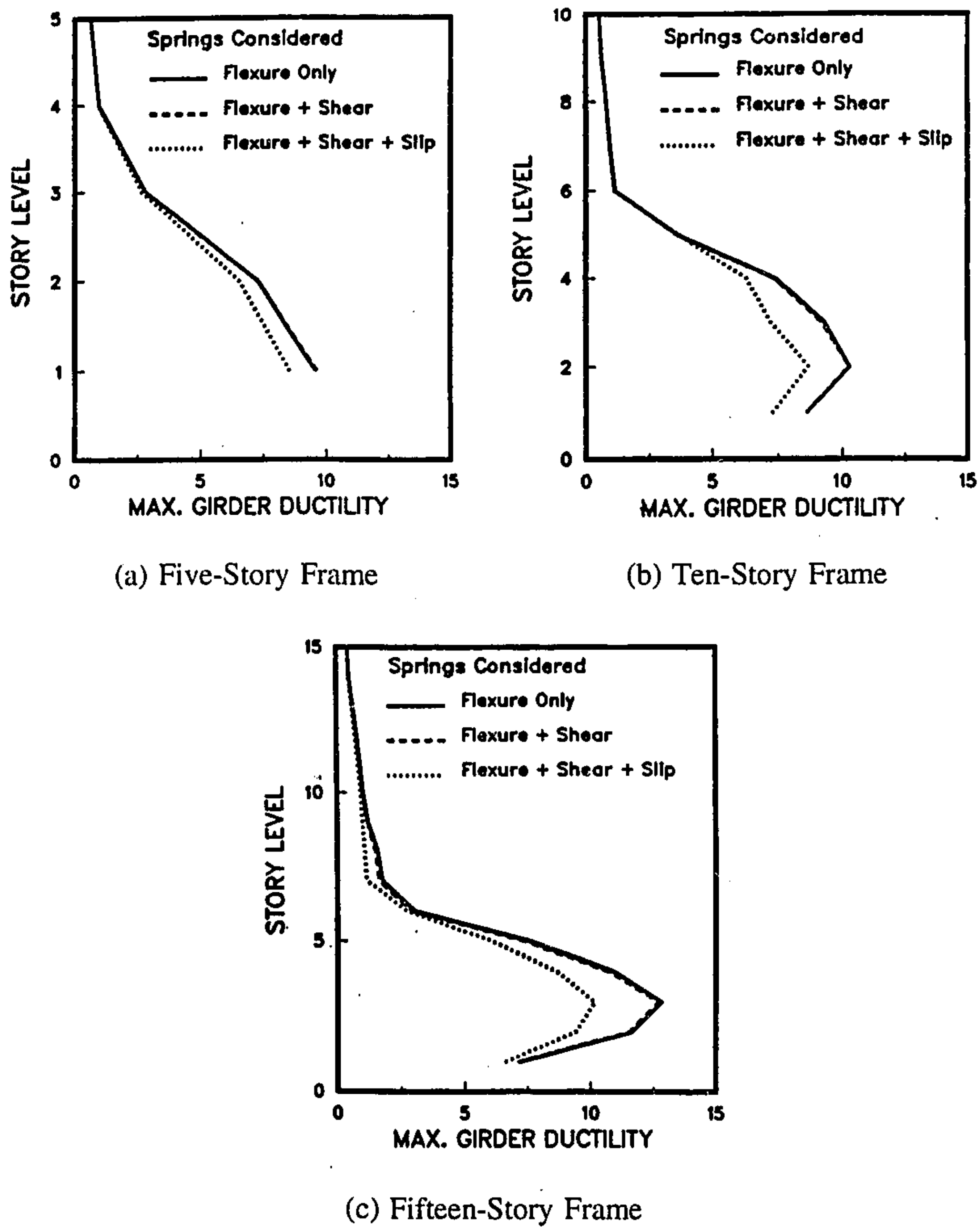

(a) Five-Story Frame

(b) Ten-Story Frame

(c) Fifteen-Story Frame

Figure 6.3 Maximum Girder Ductility Demand for Flexure (El Centro 1940 E-W Earthquake)

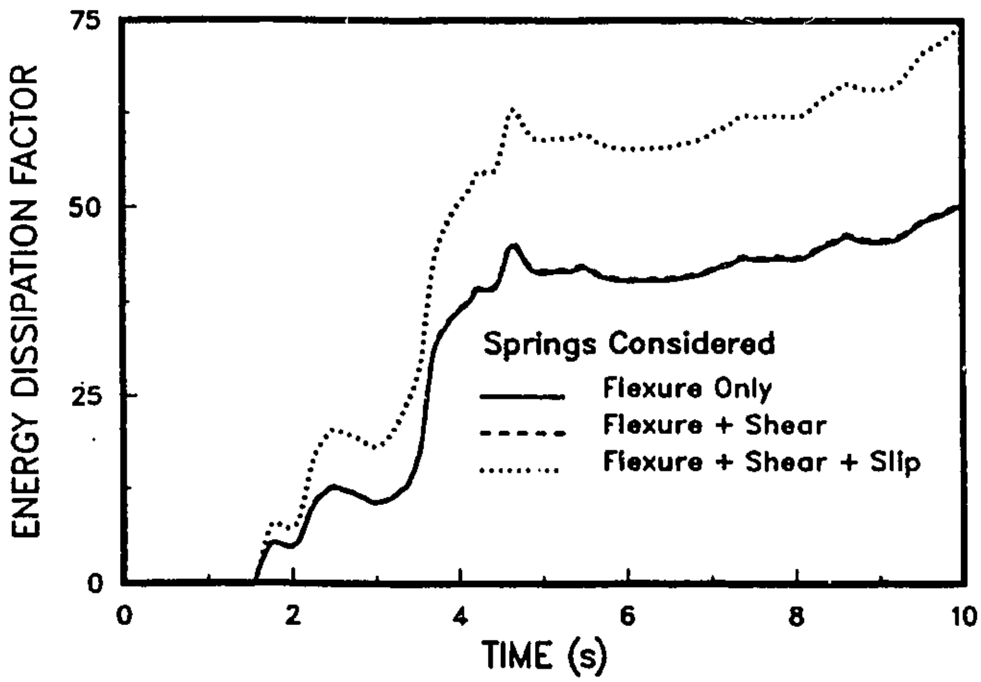

Figure 6.4 Typical Energy Dissipation Factors (Ten-Story, T=3.20 sec., El Centro 1940 E-W Earthquake)

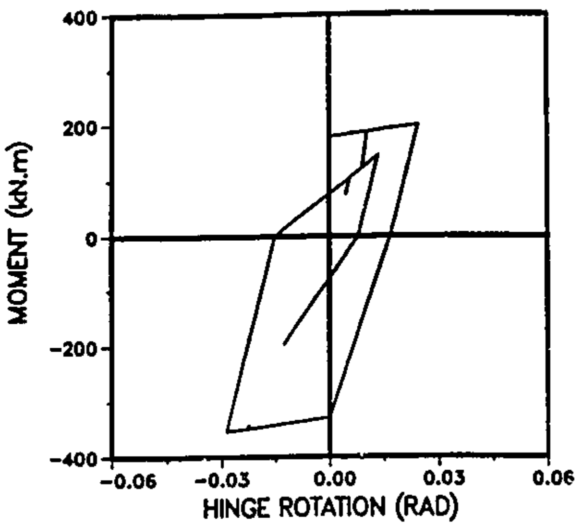

(a) Flexure

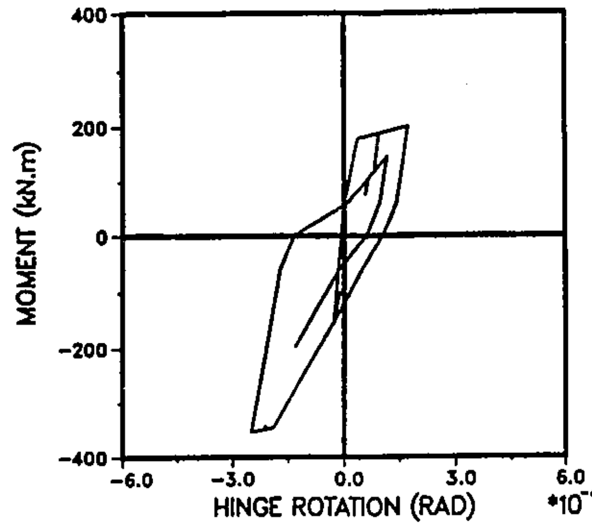

(b) Shear

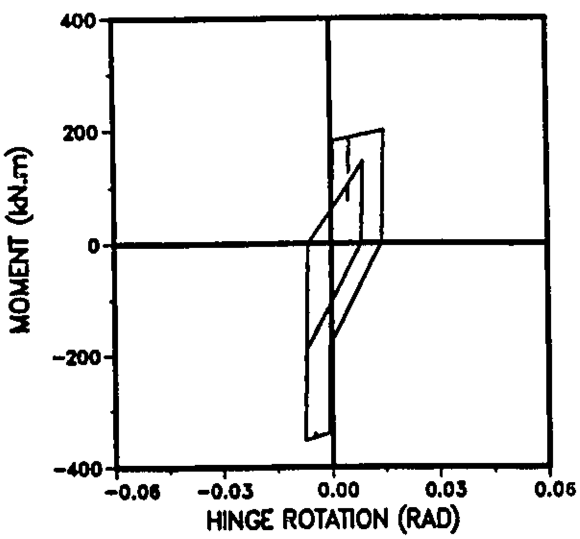

(c) Anchorage Slip

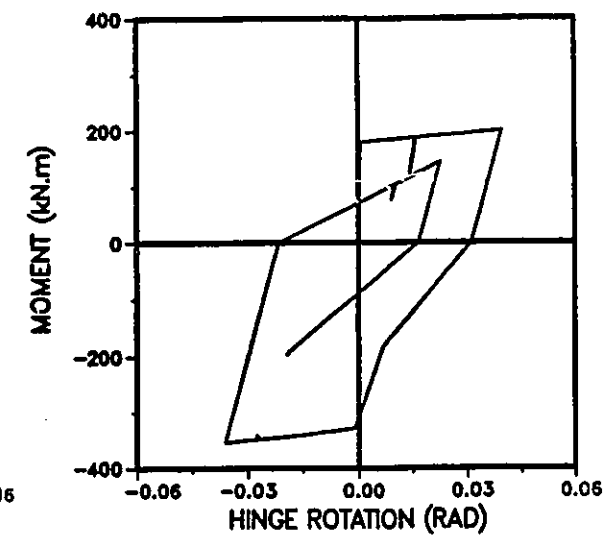

(d) Total

Figure 6.5 Plastic Hinge Hysteretic Relationships

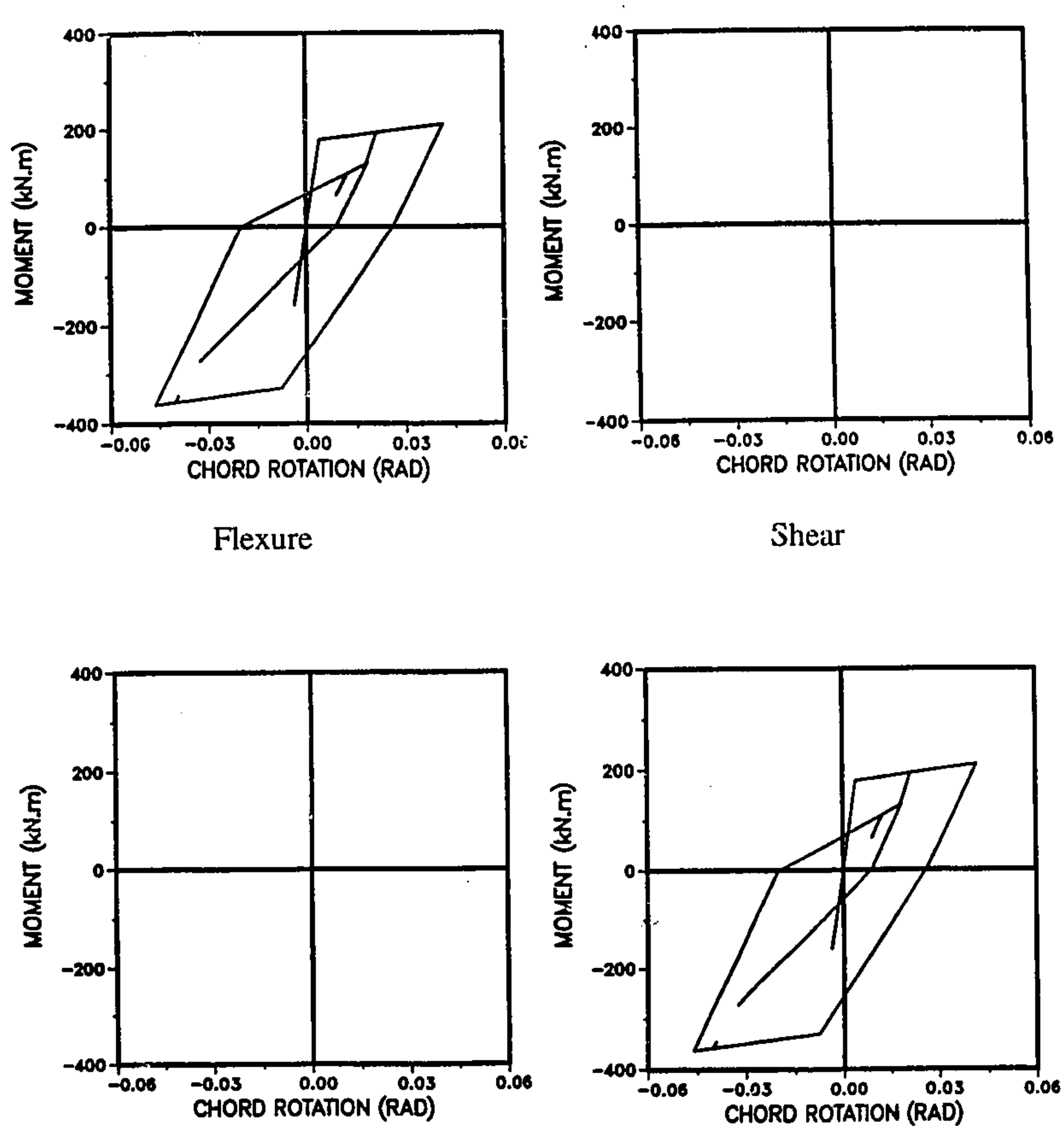

Figure 6.6(a) Total and Individual Chord Rotations Hysteretic Relationships
(Flexure Deformation Only)

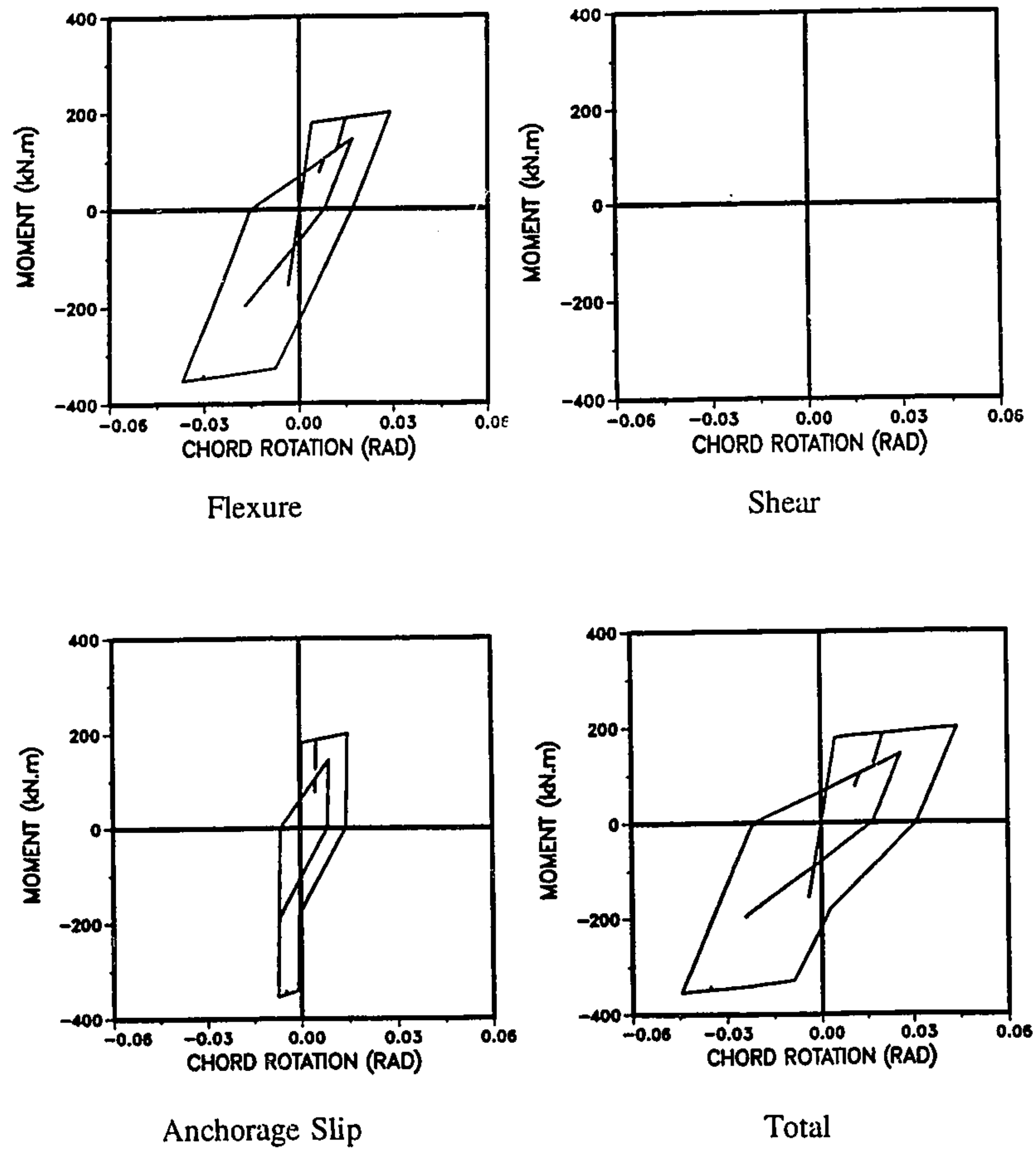

Figure 6.6(b) Total and Individual Chord Rotations Hysteretic Relationships (All Components of Deformation)

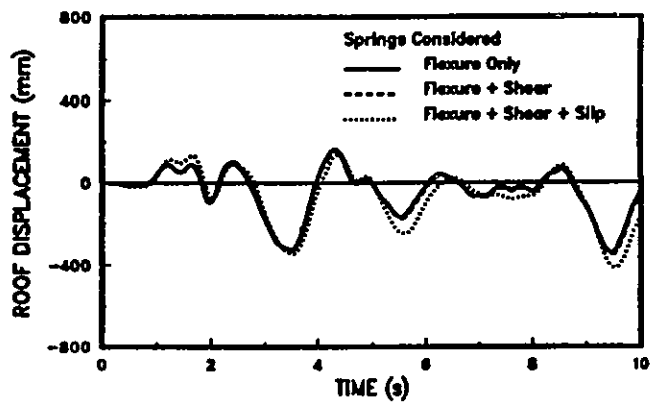

(a) T = 1.17 sec.

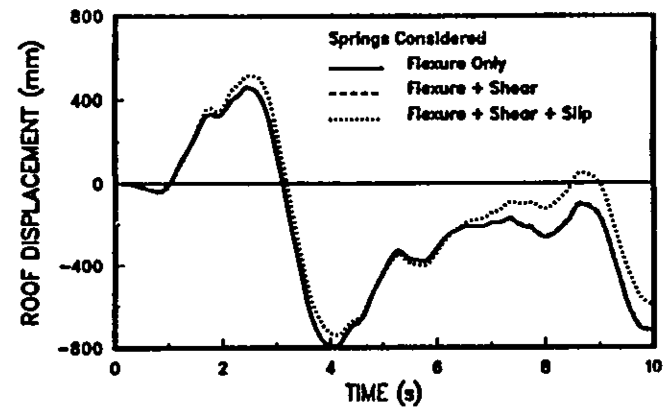

(b) T = 2.32 sec.

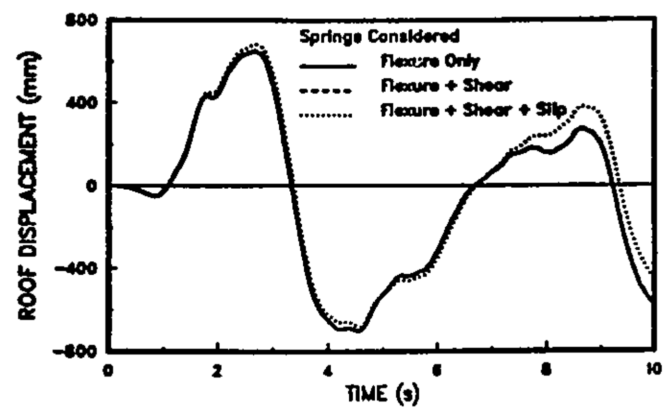

(c) T = 3.20 sec.

Figure 6.7 Time History of Roof Displacement (El Centro 1940 E-W Earthquake)

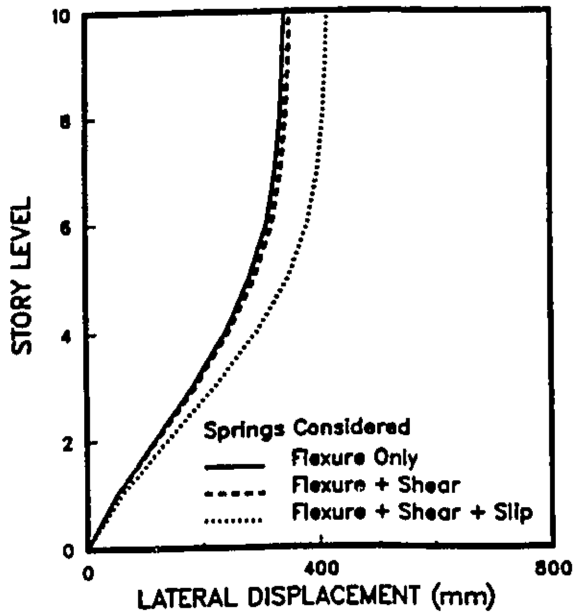

(a) T = 1.17 sec.

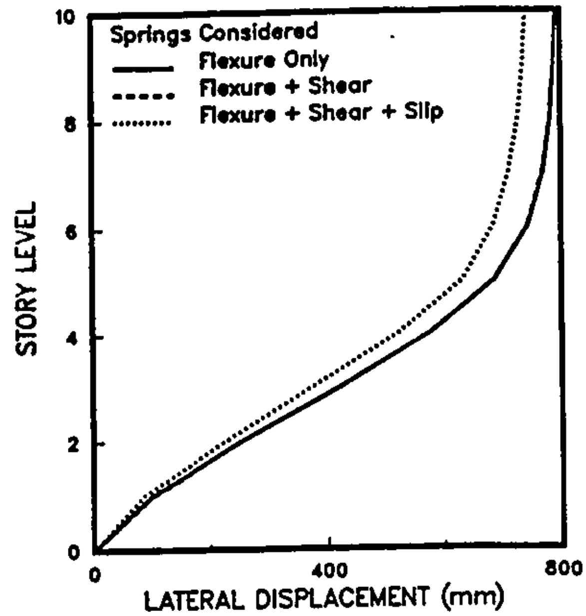

(b) T = 2.32 sec.

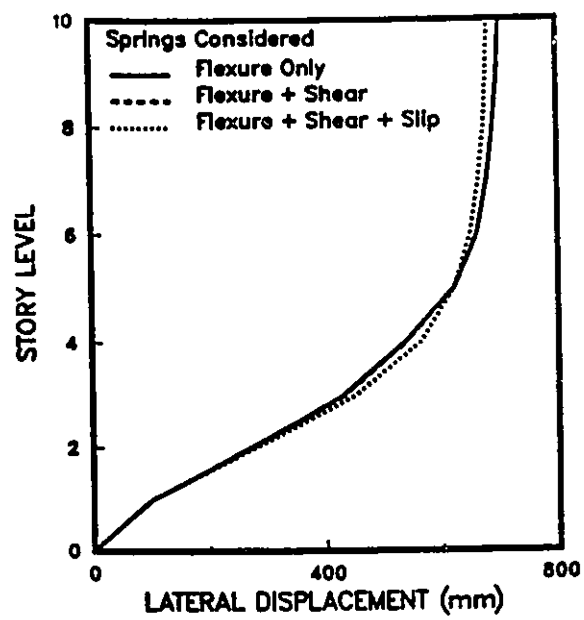

(c) T = 3.20 sec.

Figure 6.8 Lateral Displacement Envelopes (El Centro 1940 E-W Earthquake)

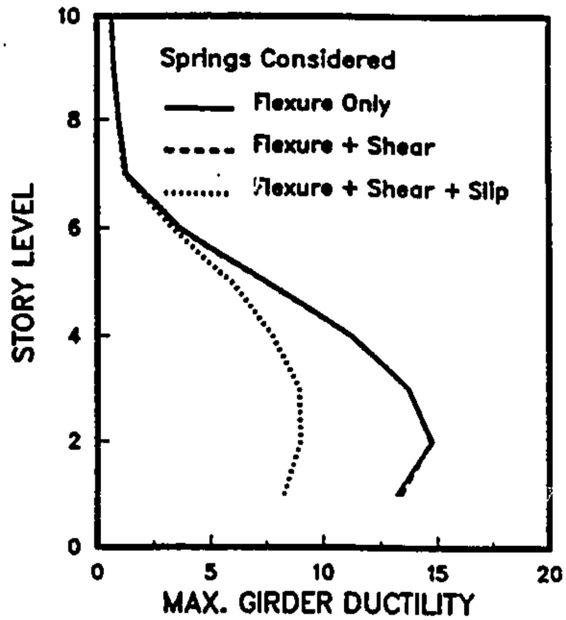

(a) T = 1.17 sec.

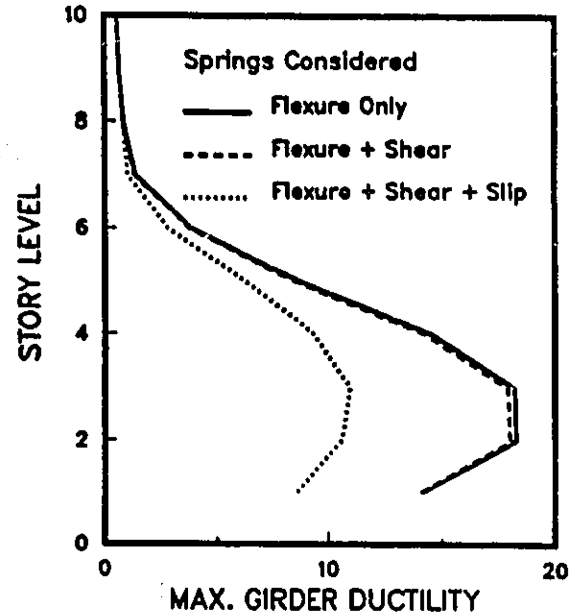

(b) T = 2.32 sec.

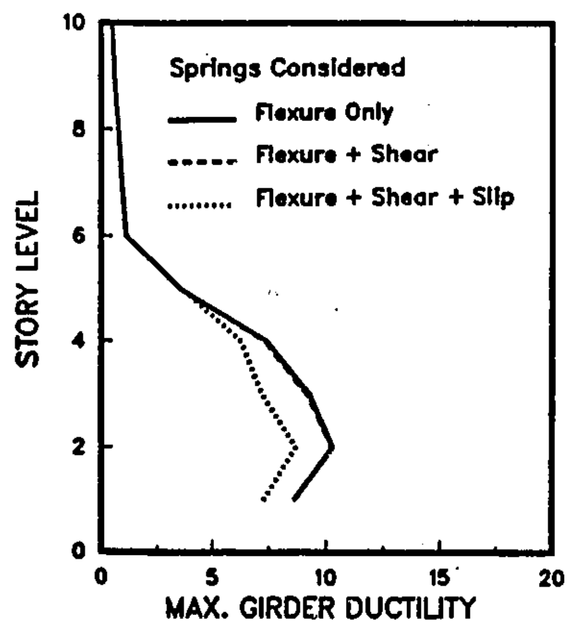

(c) T = 3.20 sec.

Figure 6.9 Maximum Girder Ductility Demand for Flexure (El Centro 1940 E-W Earthquake)

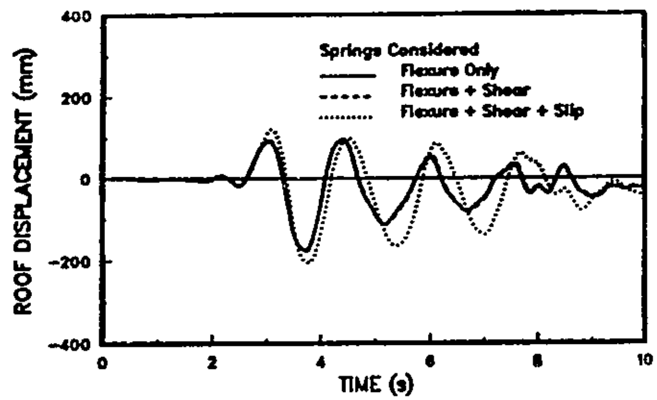

(a) T = 1.17 sec.

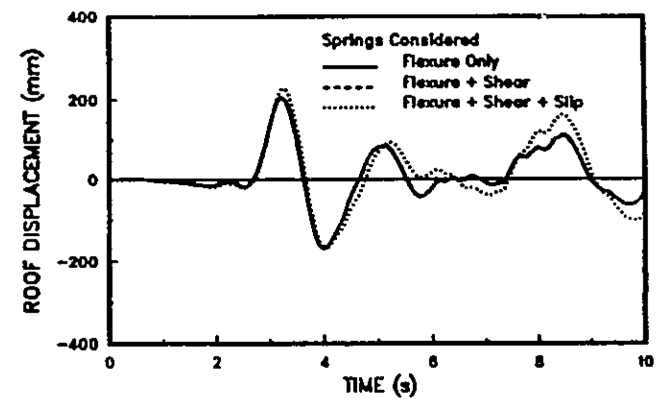

(b) T = 2.32 sec.

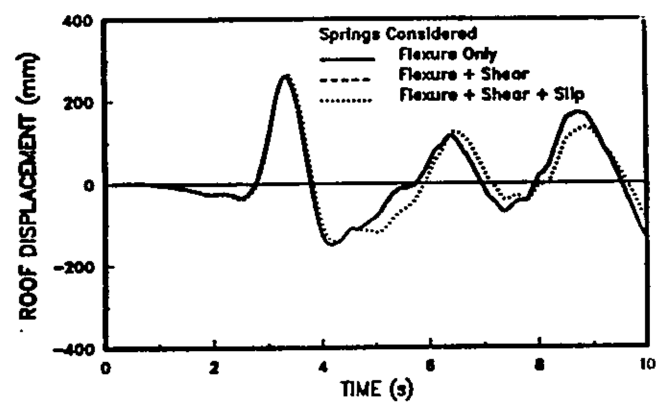

(c) T = 3.20 sec.

Figure 6.10 Time History of Roof Displacement (Pacoima Dam 1971 S16E Earthquake)

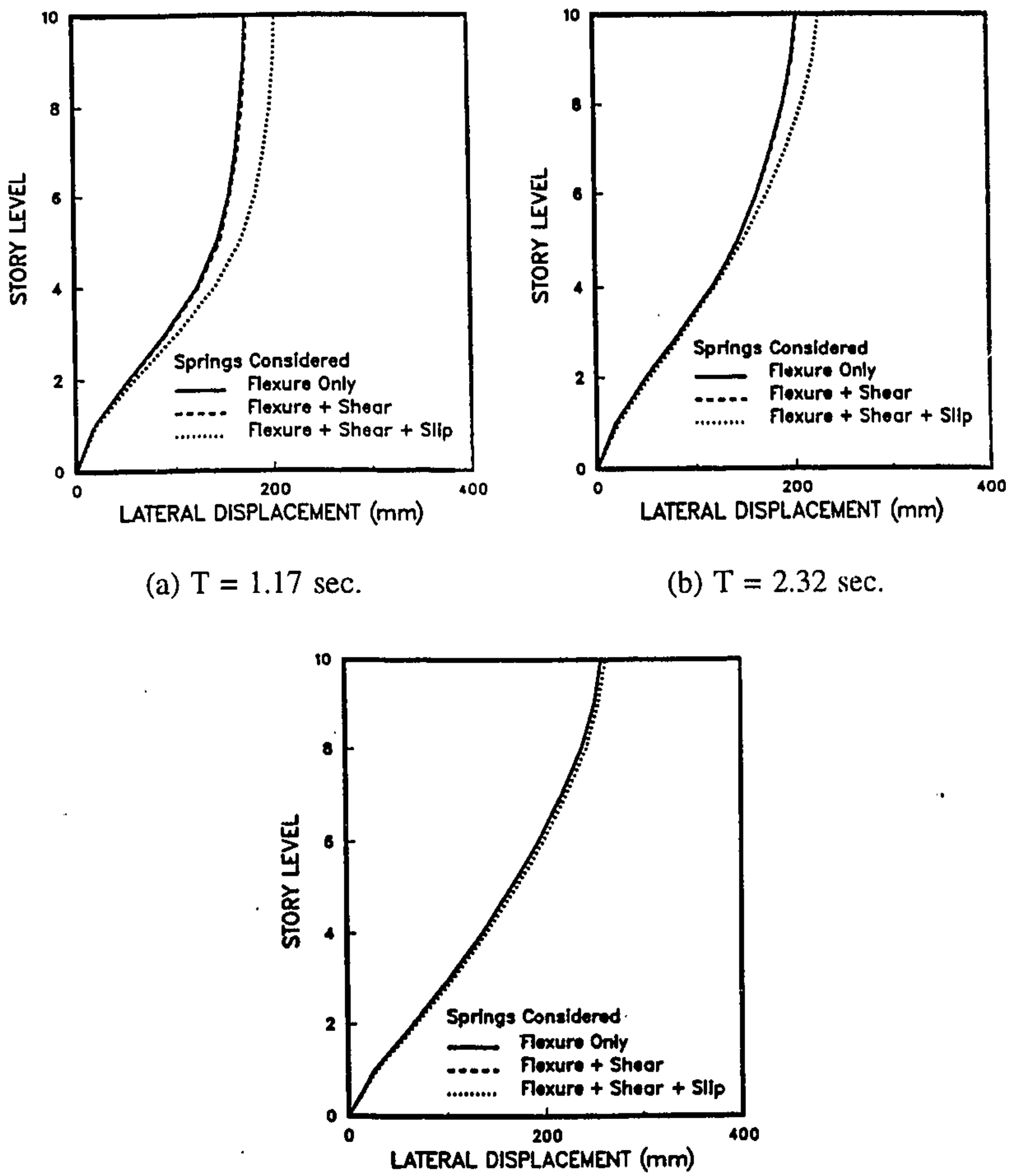

(a) T = 1.17 sec.

(b) T = 2.32 sec.

(c) T = 3.20 sec.

Figure 6.11 Lateral Displacement Envelopes (Pacoima Dam 1971 S16E Earthquake)

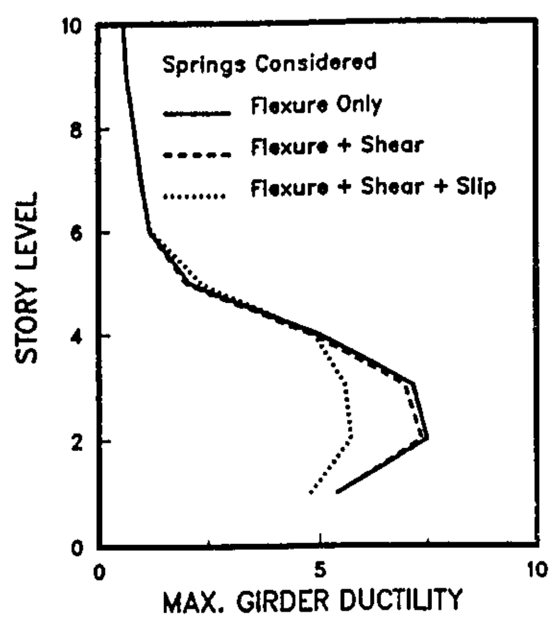

(a) T = 1.17 sec.

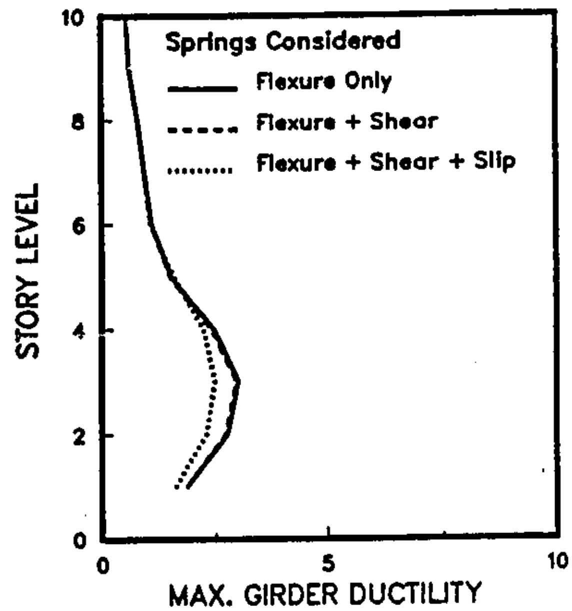

(b) T = 2.32 sec.

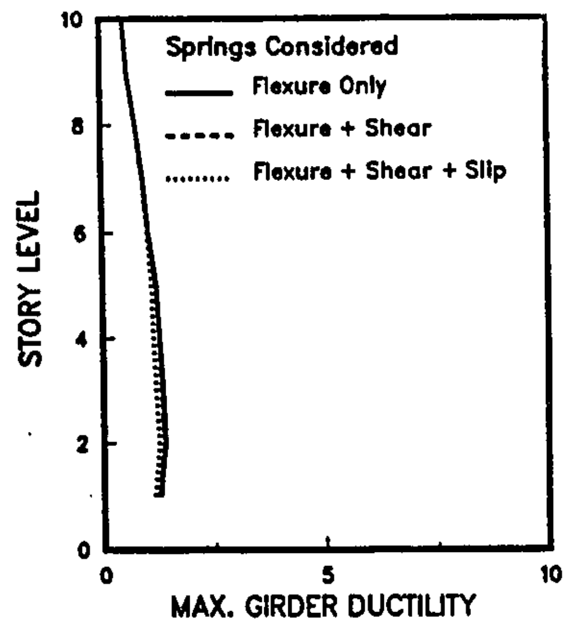

(c) T = 3.20 sec.

Figure 6.12 Maximum Girder Ductility Demand for Flexure (Pacoima Dam 1971 S16E Earthquake)

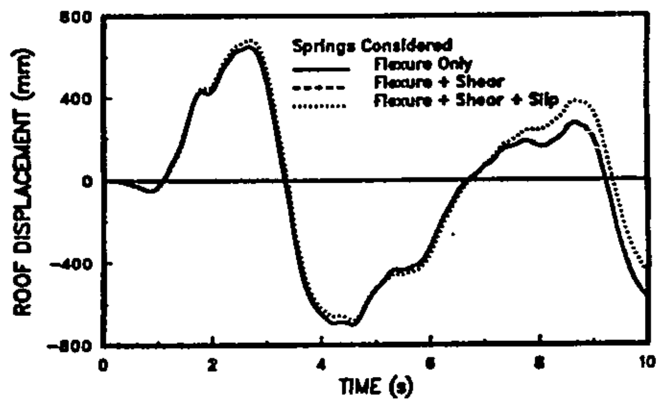

(a) El Centro E-W

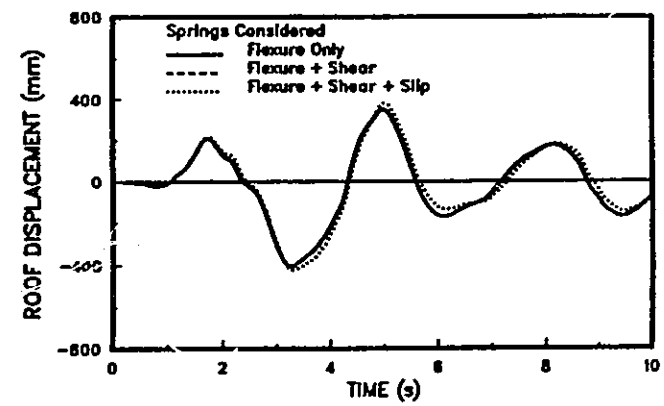

(b) El Centro N-S

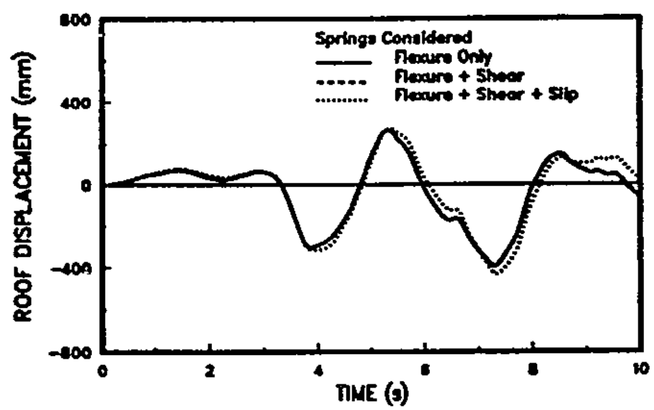

(c) Taft S69E

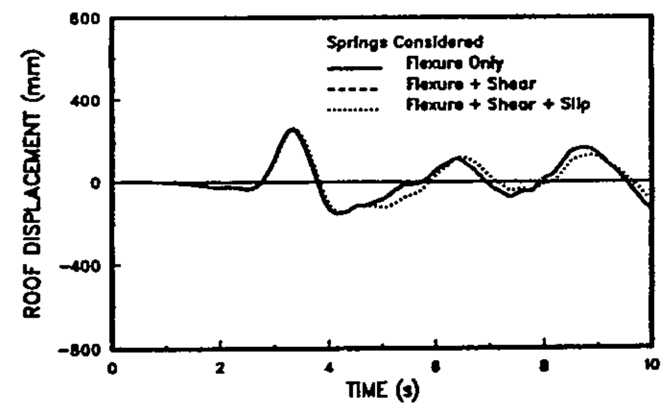

(d) Pacoima Dam S16E

Figure 6.13 Time History of Roof Displacement (Ten Story, T = 3.20 sec.)

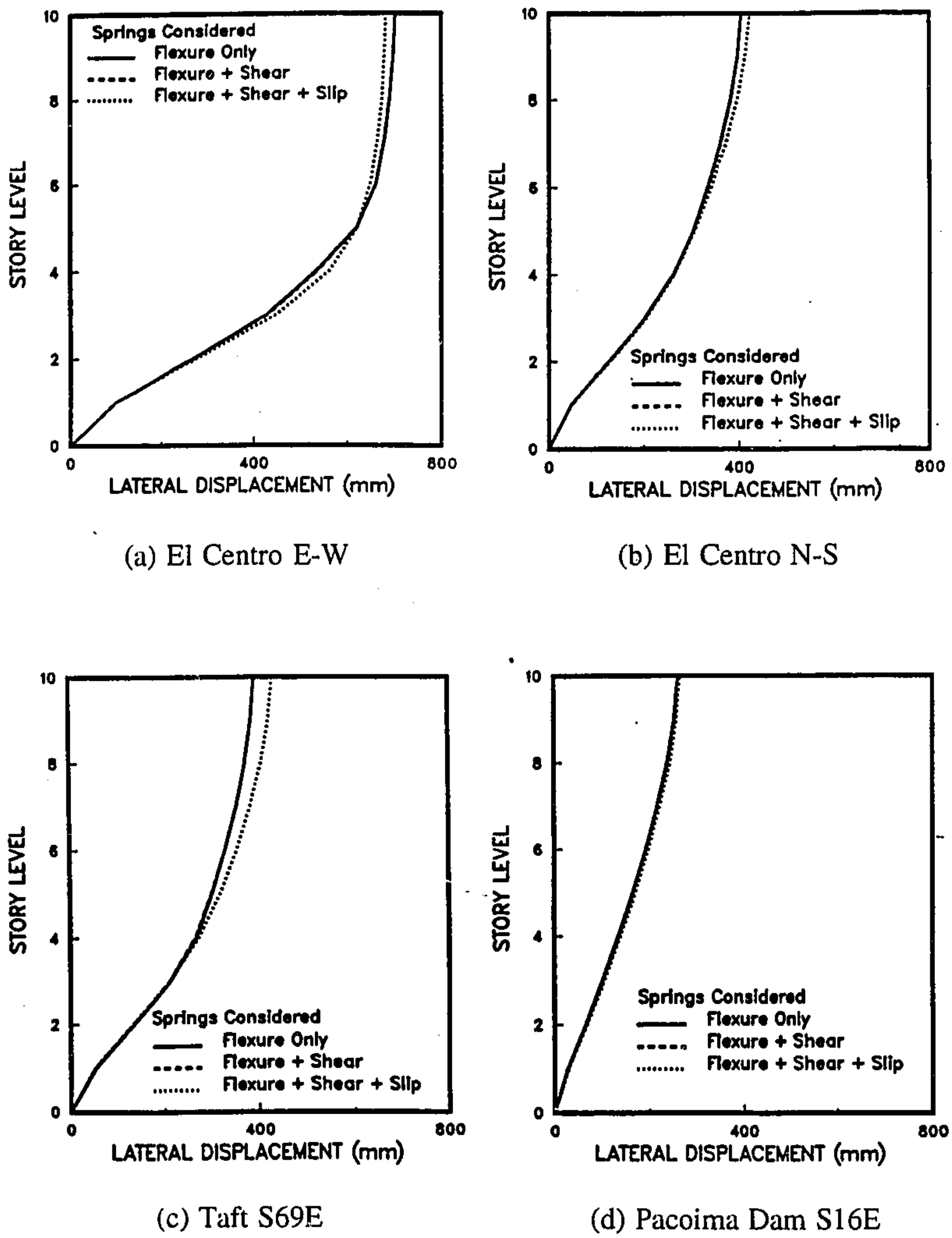

(a) El Centro E-W

(b) El Centro N-S

(c) Taft S69E

(d) Pacoima Dam S16E

Figure 6.14 Lateral Displacement Envelopes (Ten Story, T = 3.2 sec.)

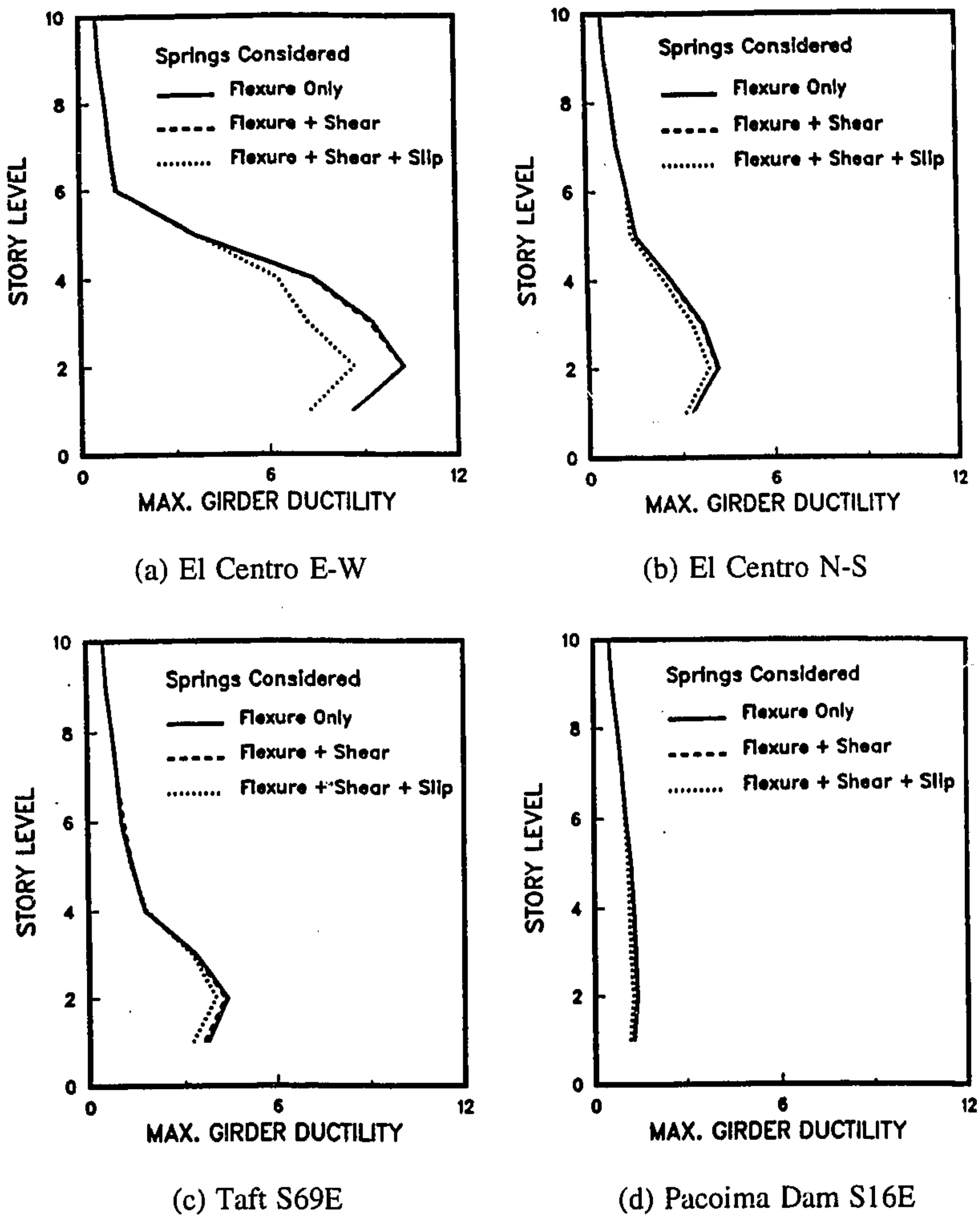

(a) El Centro E-W

(b) El Centro N-S

(c) Taft S69E

(d) Pacoima Dam S16E

Figure 6.15 Maximum Girder Ductility Demand for Flexure (Ten Story, T = 3.20 sec.)

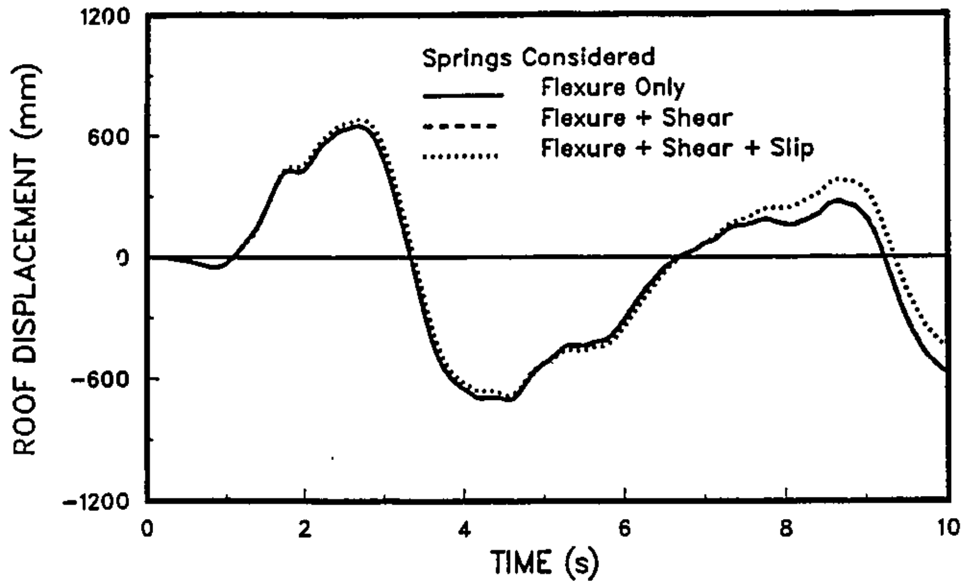

(a) Peak Ground Acceleration = 0.5g

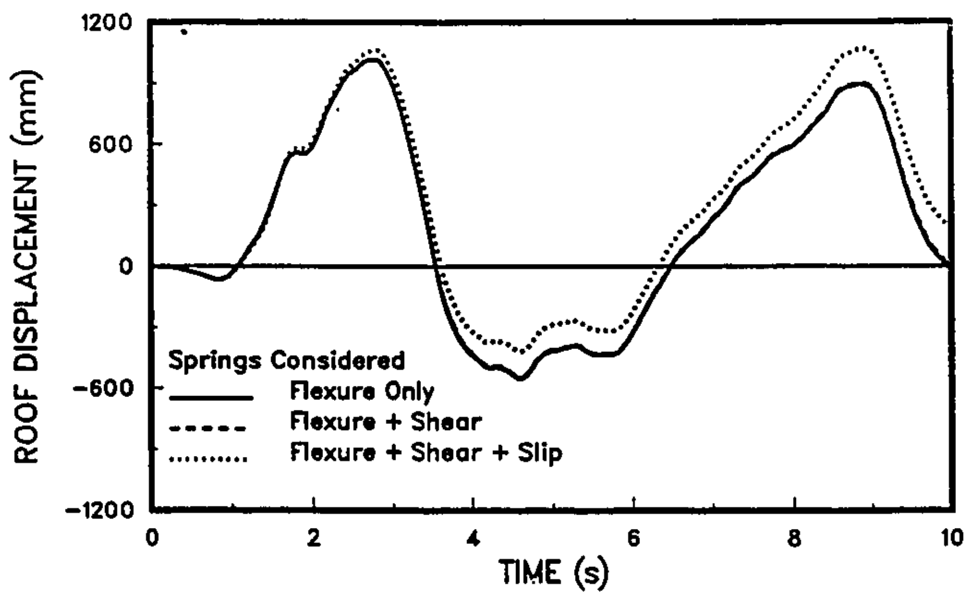

(b) Peak Ground acceleration = 0.65g

Figure 6.16 Time History of Roof Displacement (Ten Story, T = 3.20 sec., El Centro 1940 E-W Earthquake)

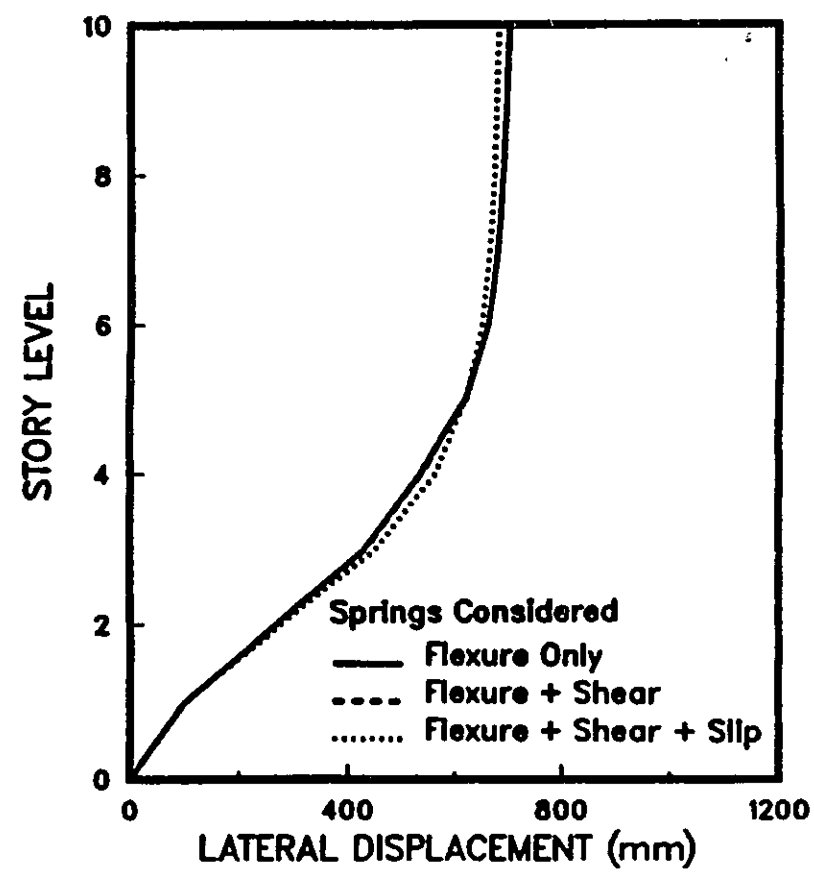

(a) Peak Ground acceleration = 0.5g

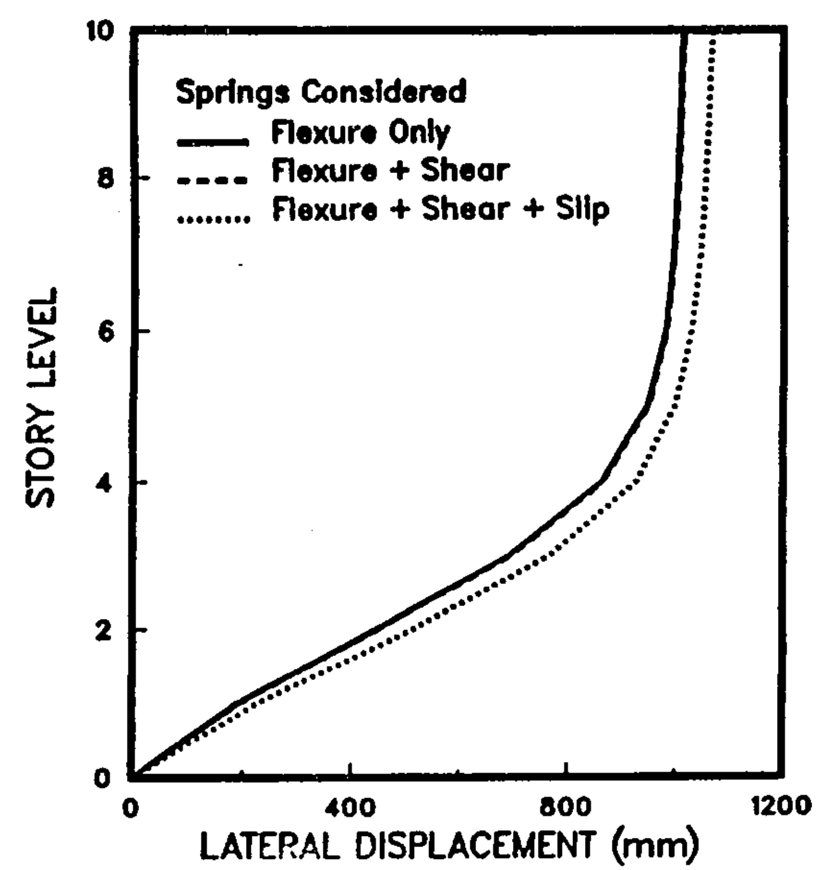

(b) Peak Ground acceleration = 0.65g

Figure 6.17 .Lateral Displacement Envelopes (Ten Story, T = 3.20 sec., El Centro 1940 E-W Earthquake)

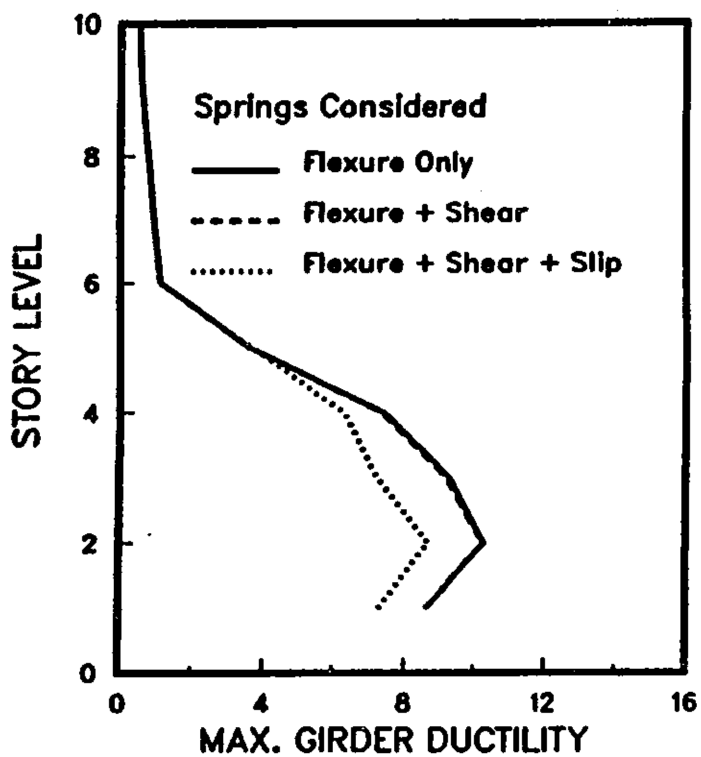

(a) Peak Ground acceleration = 0.5g

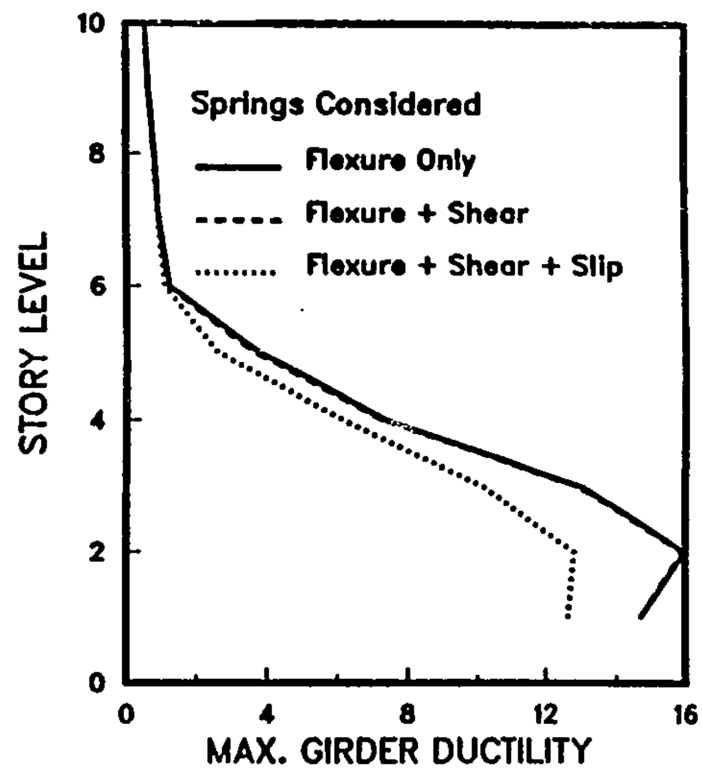

(b) Peak Ground acceleration = 0.65g

Figure 6.18 Maximum Girder Ductility Demand for Flexure (Ten Story, T=3.20 sec., El Centro 1940 E-W Earthquake)

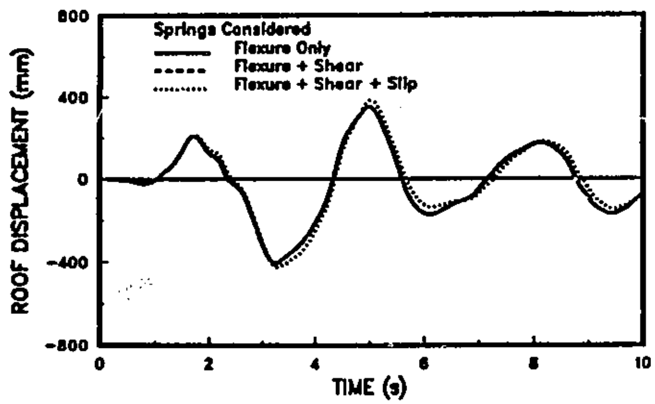

(a) Peak Ground Acceleration = 0.5g

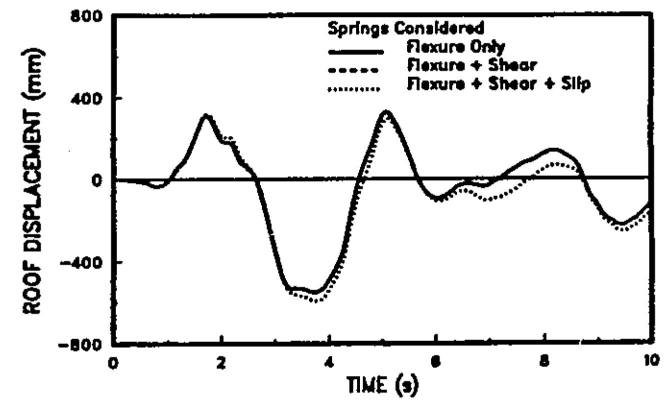

(b) Peak Ground acceleration = 0.75g

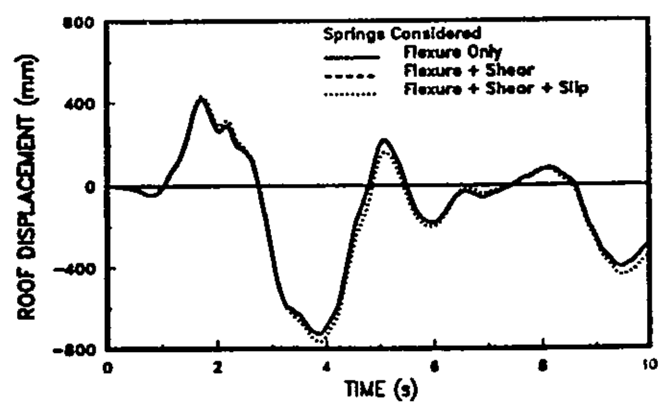

(c) Peak Ground acceleration = 1.0g

Figure 6.19 Time History of Roof Displacement (Ten Story, T = 3.20 sec., El Centro 1940 N-S Earthquake)

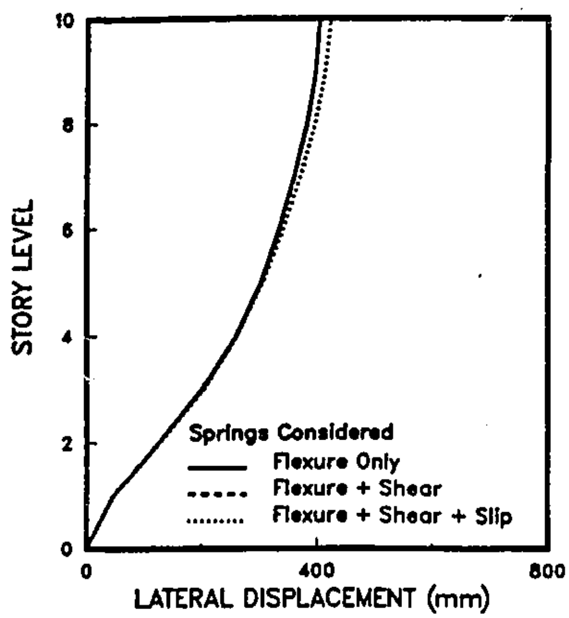

(a) Peak Ground Accel. = 0.5g

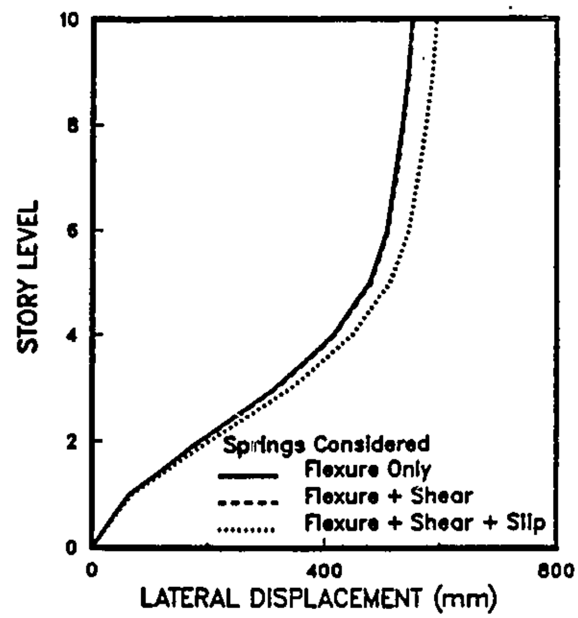

(b) Peak Ground Accel. = 0.75g

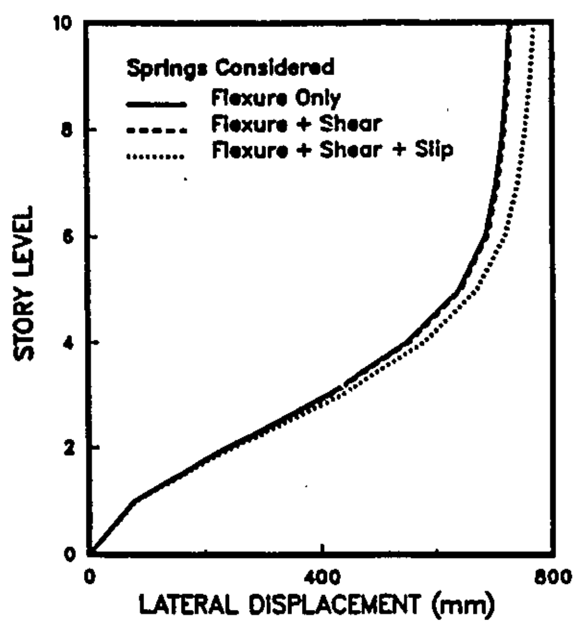

(c) Peak ground Accel. = 1.0g

Figure 6.20 Lateral Displacement Envelopes (Ten Story, T=3.20 sec., El Centro 1940 N-S Earthquake)

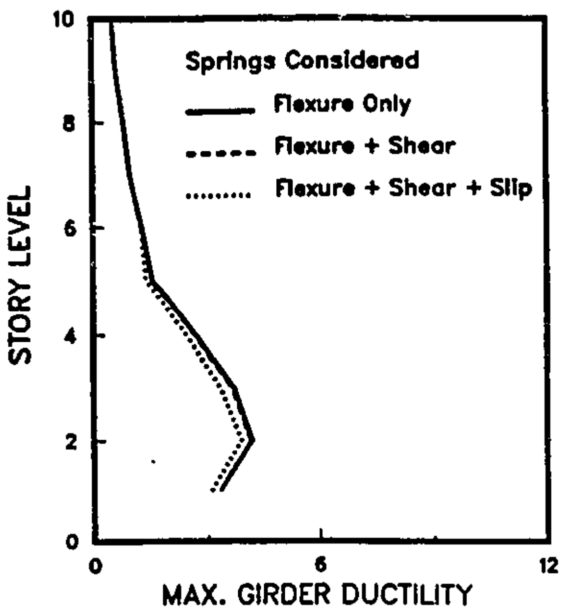

(a) Peak Ground Accel. = 0.5g

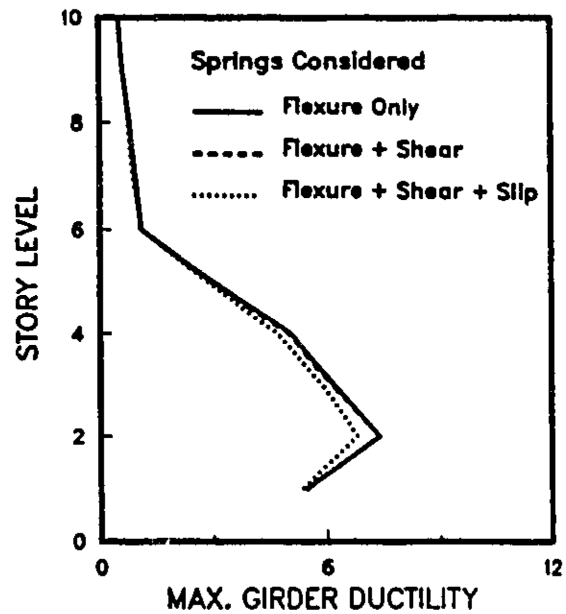

(b) Peak Ground Accel. = 0.75g

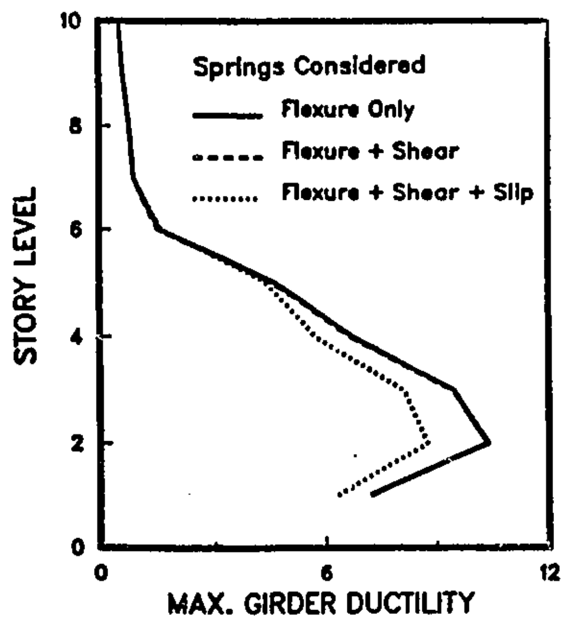

(c) Peak ground Accel. = 1.0g

Figure 6.21 Maximum Girder Ductility Demand for Flexure (Ten Story, T = 3.20 sec., El Centro 1940 N-S Earthquake)

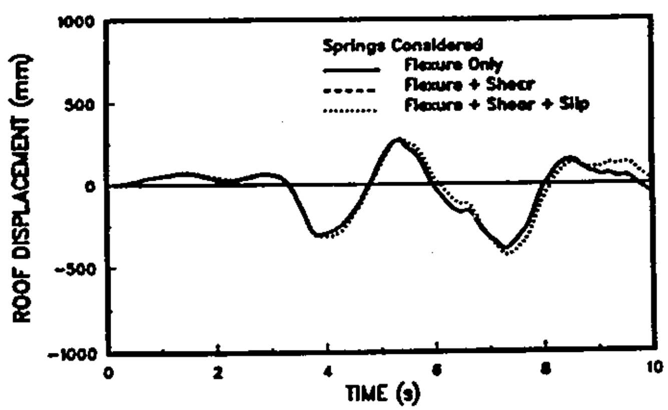

(a) Peak Ground Acceleration = 0.5g

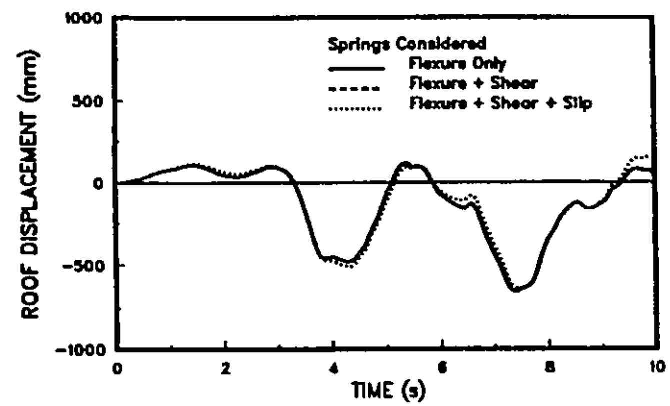

(b) Peak Ground acceleration = 0.75g

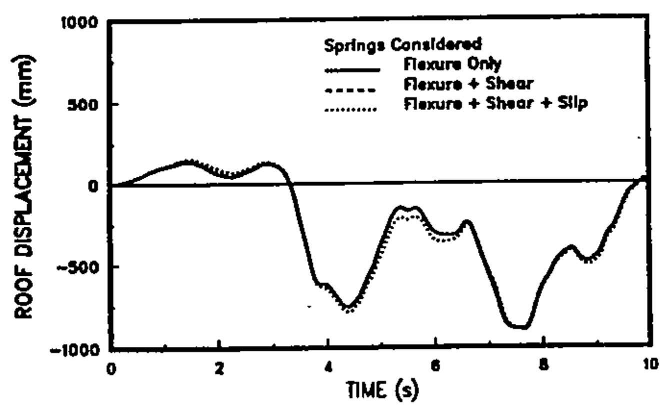

(c) Peak Ground acceleration = 1.0g

Figure 6.22 Time History of Roof Displacement (Ten Story, T = 3.20 sec., Taft 1952 S69E Earthquake)

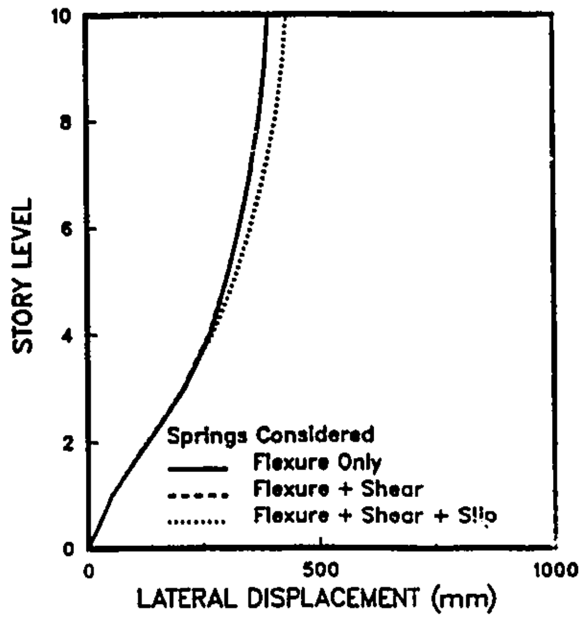

(a) Peak Ground Accel. = 0.5g

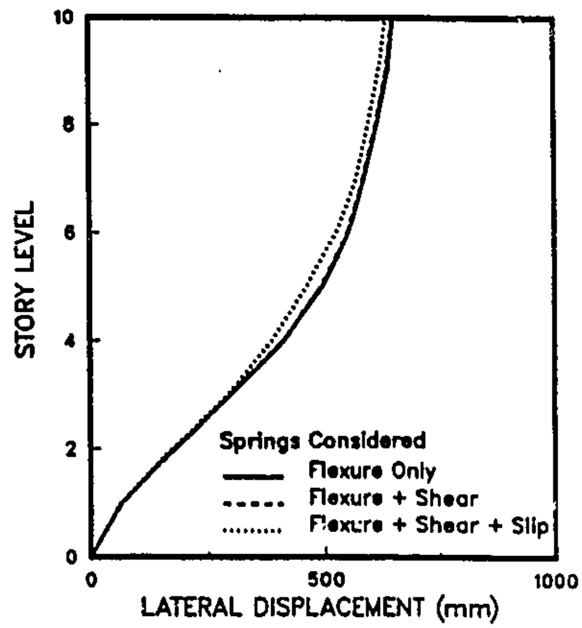

(b) Peak Ground Accel. = 0.75g

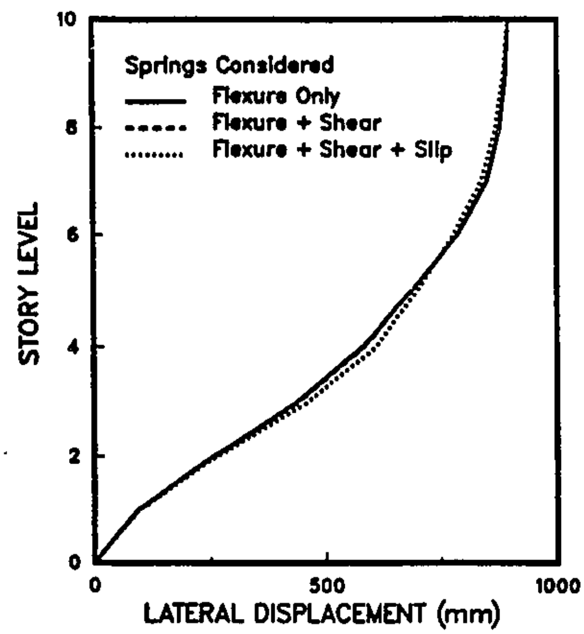

(c) Peak ground Accel. = 1.0g

Figure 6.23 Lateral Displacement Envelopes (Ten Story, T=3.20 sec., Taft 1952 S69E Earthquake)

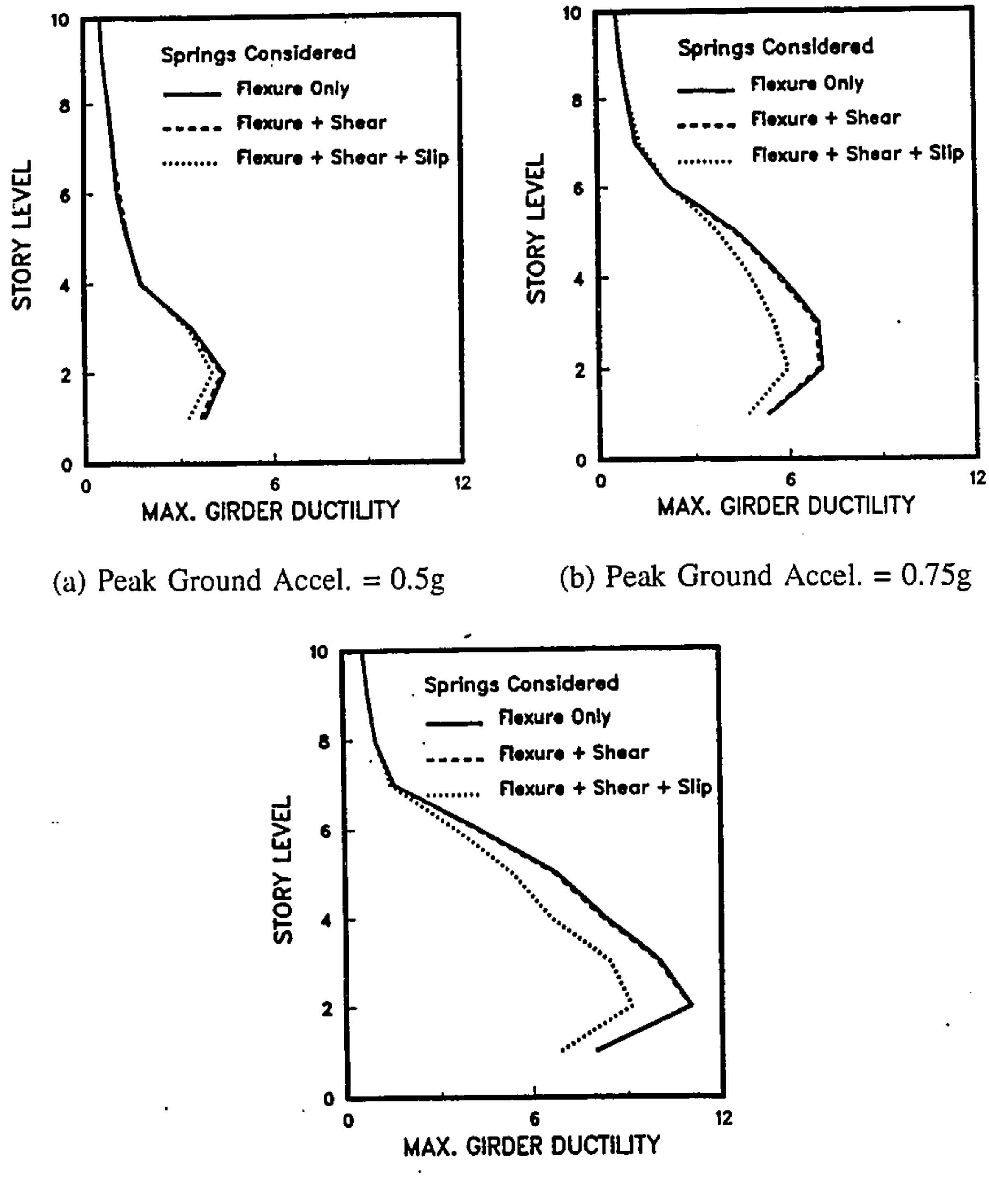

(a) Peak Ground Accel. = 0.5g

(b) Peak Ground Accel. = 0.75g

(c) Peak ground Accel. = 1.0g

Figure 6.24 Maximum Girder Ductility Demand for Flexure (Ten Story, T = 3.20 sec., Taft 1952 S69E Earthquake)

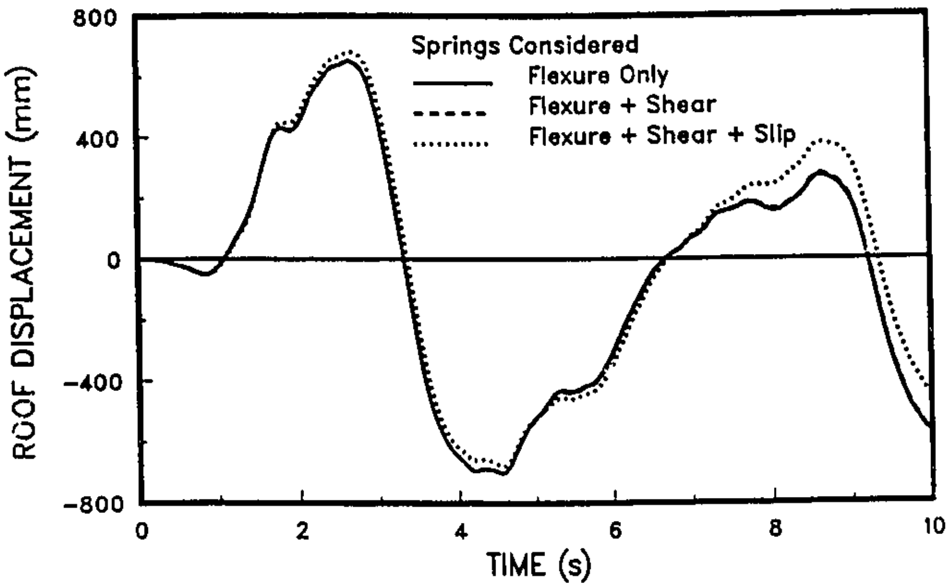

(a) GA = 83% of Gross GA

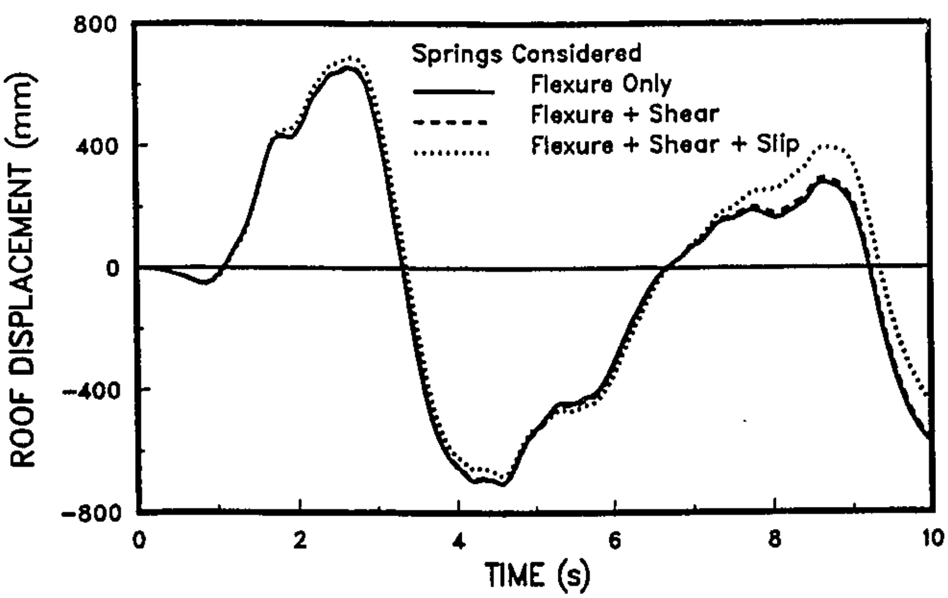

(b) GA = 30% of Gross GA

Figure 6.25 Time History of Roof Displacement (Ten Story, T = 3.20 sec., El Centro 1940 E-W Earthquake)

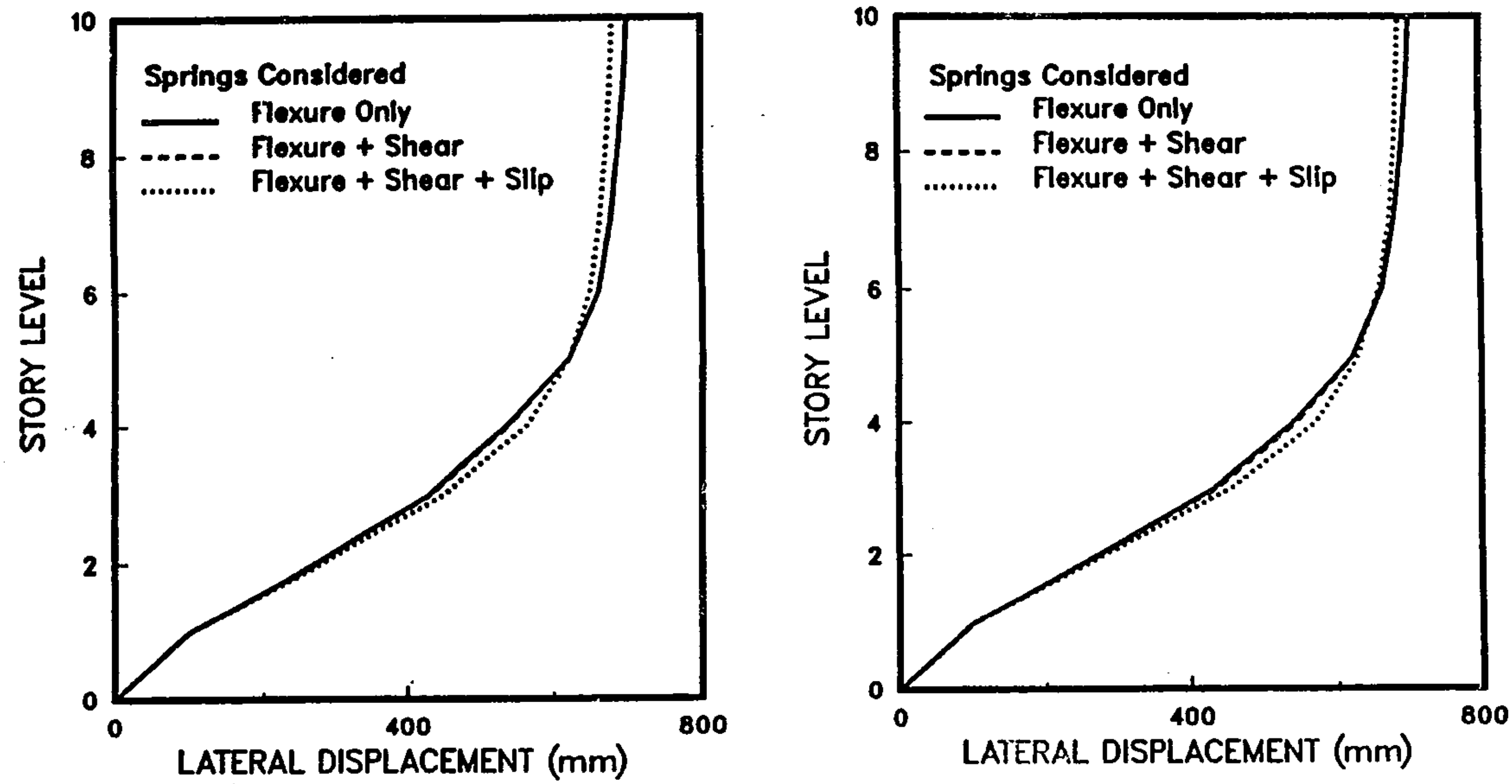

(a) GA = 83% of Gross GA

(b) GA = 30% of Gross GA

Figure 6.26 Lateral Displacement Envelopes (Ten Story, T = 3.20 sec., El Centro 1940 E-W Earthquake)

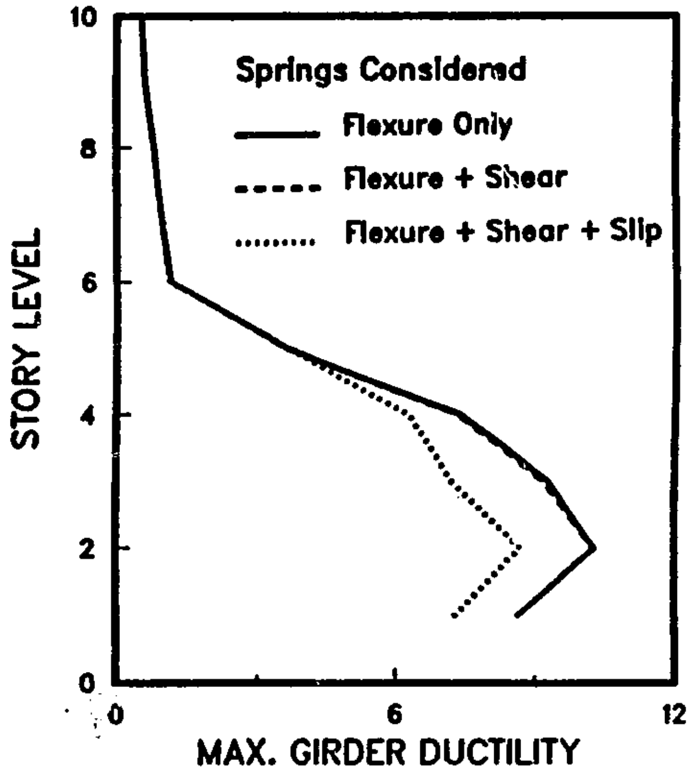

(a) GA = 83% of Gross GA

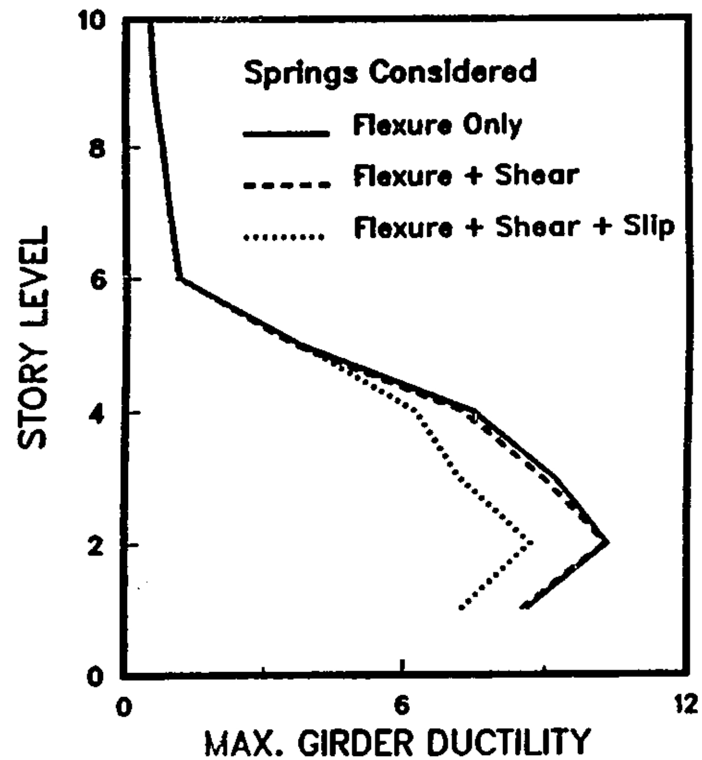

(b) GA = 30% of Gross GA

Figure 6.27 Maximum Girder Ductility Demand for Flexure (Ten Story, T = 3.20 sec., El Centro 1940 E-W Earthquake)

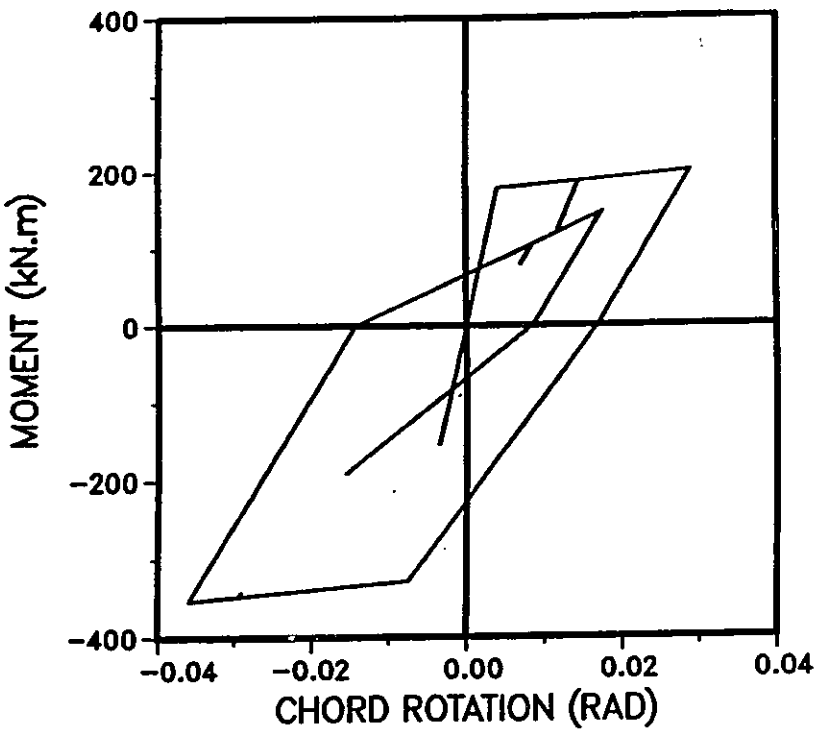

Flexure

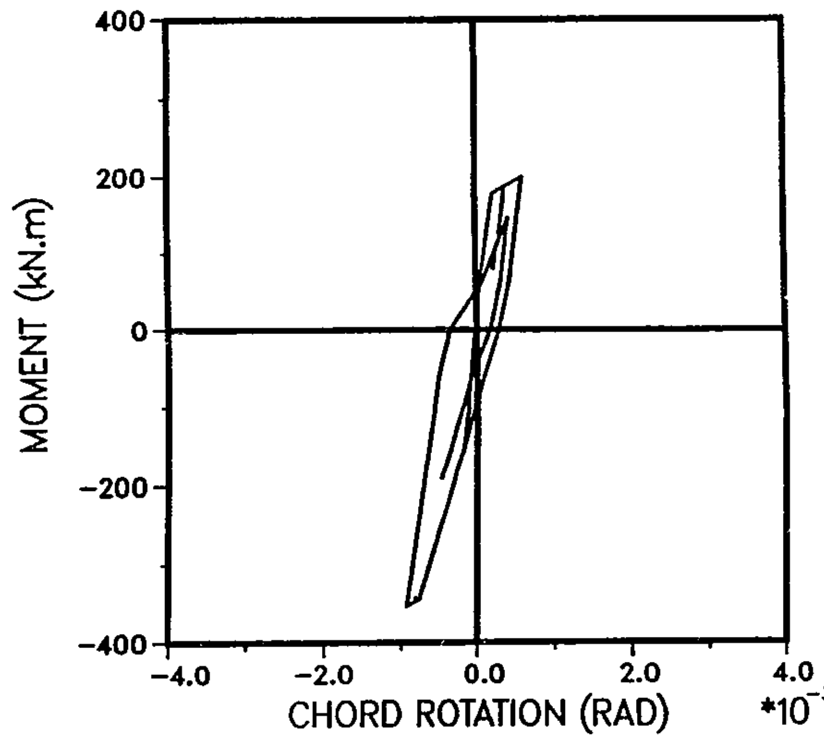

Shear

(a) Proper Shear Design

Figure 6.28 Hysteretic Relationships for Flexure and Shear Chord Rotations (Ten Story, T = 3.20 sec., El Centro 1940 E-W Earthquake)

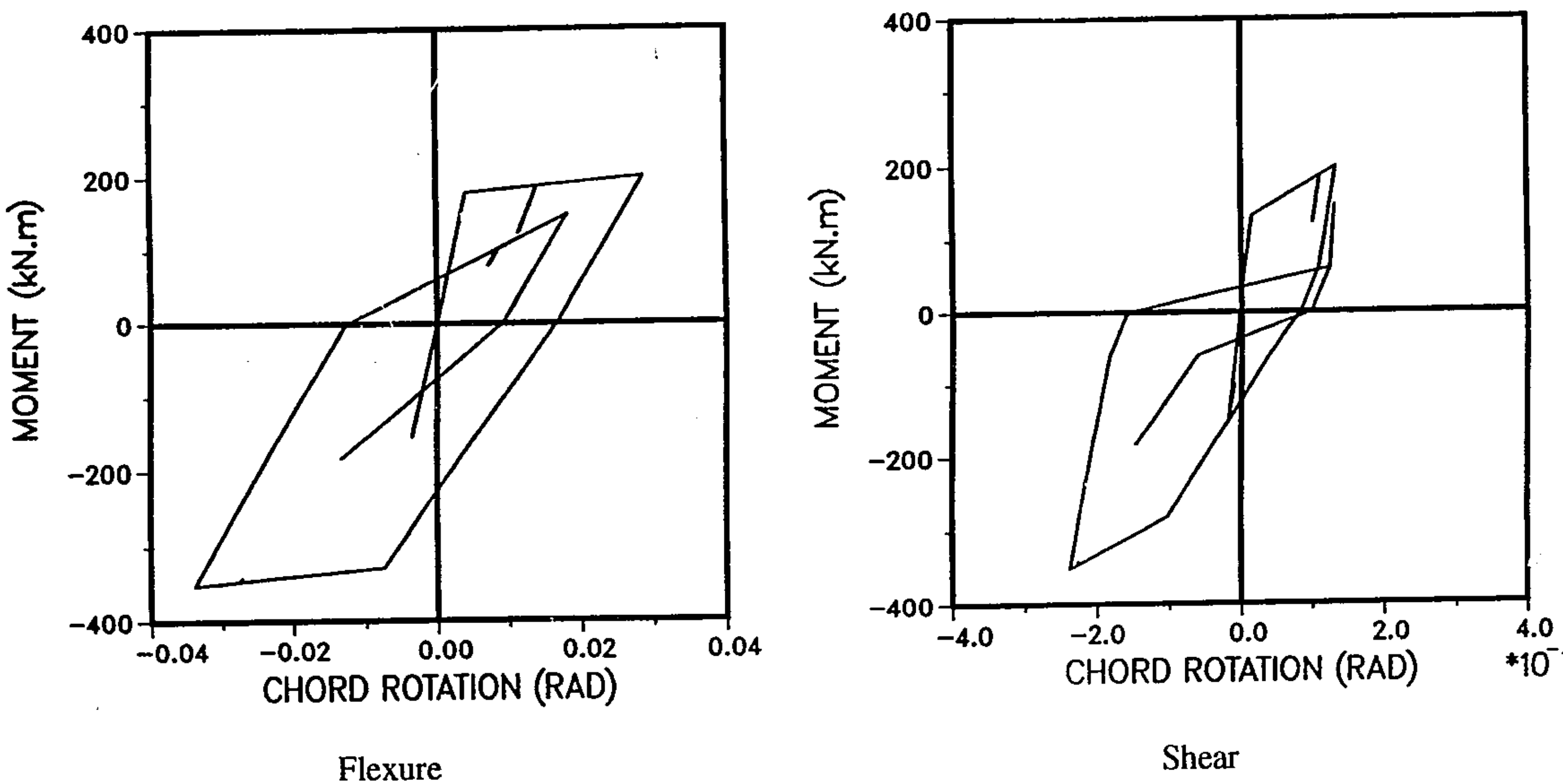

(b) Poor Shear Design

Figure 6.28 Continued

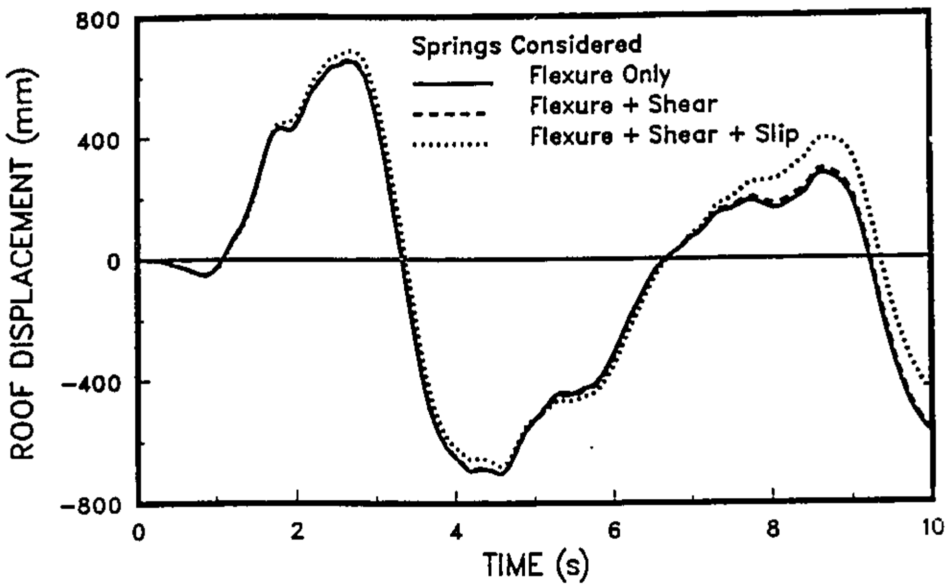

(a) Proper Shear Design

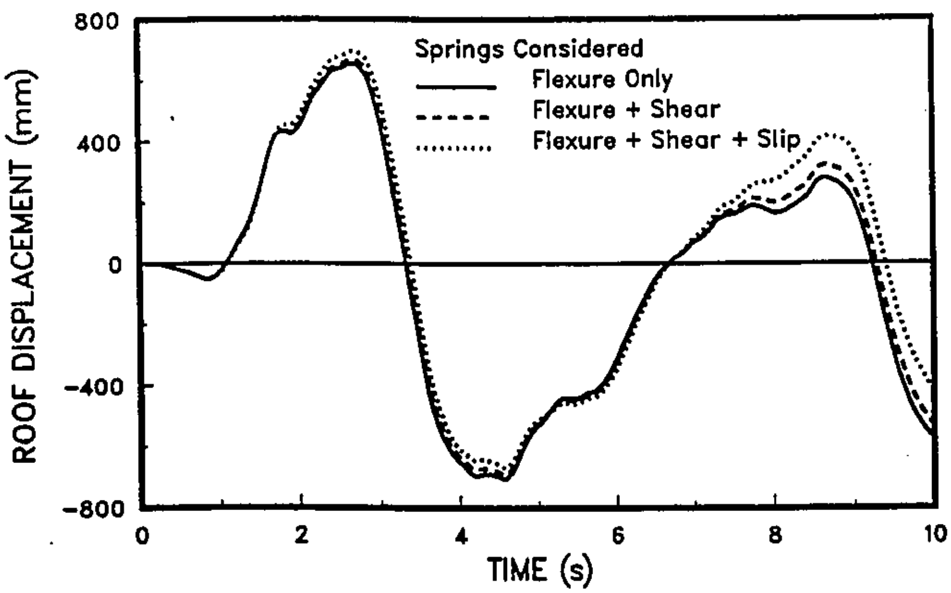

(b) Poor Shear Design

Figure 6.29 Time History of Roof Displacement (Ten Story, T = 3.20 sec., El Centro 1940 E-W Earthquake)

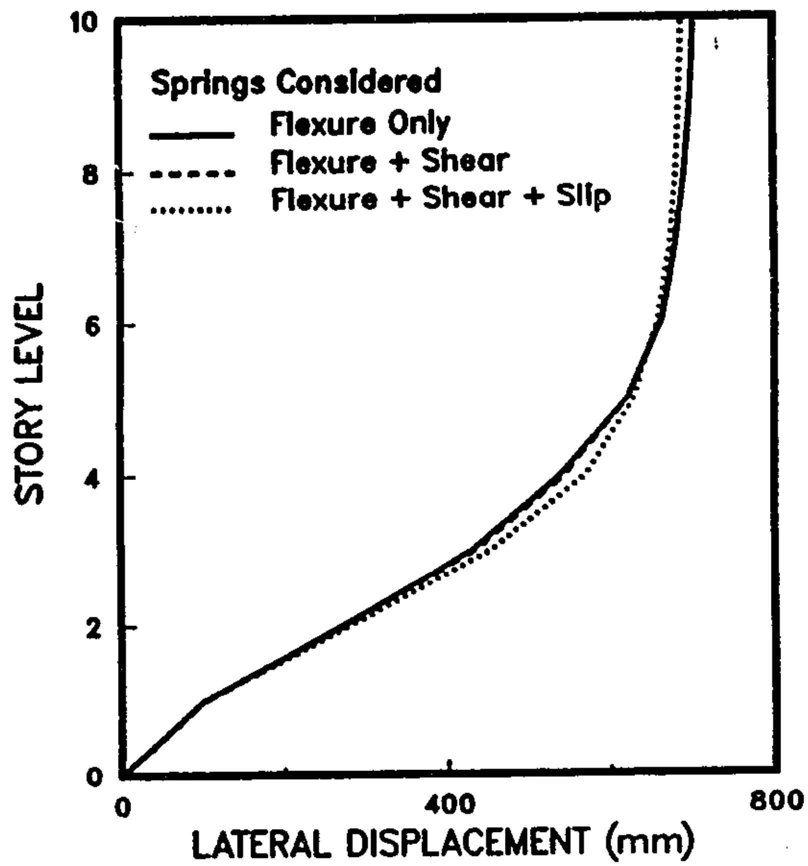

(a) Proper Shear Design

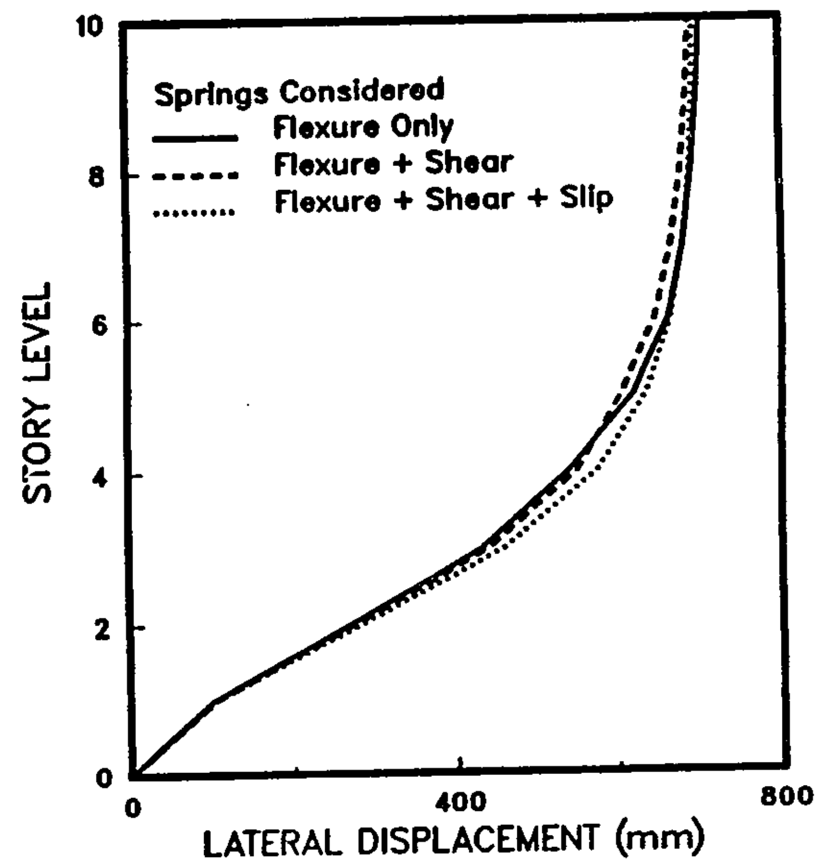

(b) Poor Shear Design

Figure 6.30 Lateral Displacement Envelopes (Ten Story, T = 3.20 sec., El Centro 1940 E-W Earthquake)

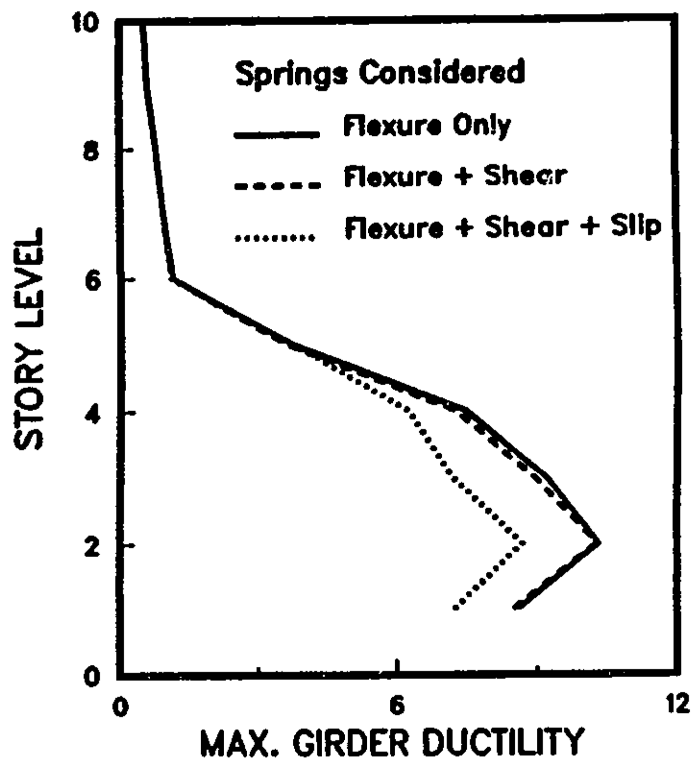

(a) Proper Shear Design

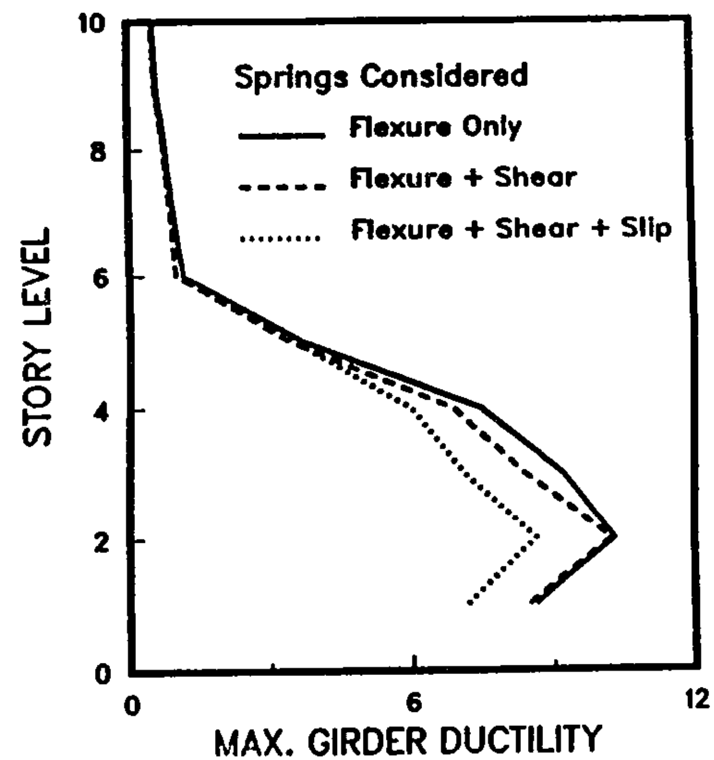

(b) Poor Shear Design

Figure 6.31 Maximum Girder Ductility Demand for Flexure (Ten Story, T = 3.20 sec., El Centro 1940 E-W Earthquake)

Appendix A

Fortran Listing for Subroutines SLIPM and SHEARM

```
C
C*******************************************************************
C*                                                                 *
C*                         SLIP MODEL                              *
C*                                                                 *
C*******************************************************************
C
      SUBROUTINE SLIPM(IEND,FACTOR,BM,ROTSL,KODESL,EKSL,IDK,KFAC,KSPRNG)
C
      IMPLICIT REAL*8(A-H,O-Z)
C
      COMMON/INFEL/ IMEM,IMEMD,KST,KSTD,LM(6),LMD(6),KGEOM,KGEOMD,
     *               FL,COSA,SINA,EC(4),A(2,6),
     1               BFII,BFJJ,BFIJ,EAL,EKHI3P,EKHJ3P,EKHFL(2),
     *               KODYX3(2),ND(4),
     2               KODYFL(2),BMYFL(2,6),RYFL(2,6),INDFL(2),INDUM(2),
     *               EKEPFL(2,6),REVPFL(2),
     3               BMTOT(2),SFTOT(2),FTOT(2),RTOTFL(2),RTPPFL(2),
     4               RTPNFL(2),RTSPFL(2),RTSNFL(2),SENP(8),SENN(8),
     5               TENP(8),TENN(8),SDACT(3),NODI,NODJ,KOUTDT,KDUM(3),
     6               EK1(2),RY1(2,2),RA(2,2),RB(2,2),BMA(2,2),BMB(2,2),
     7               RREC(2,2),ALPHA(2),BETA(2),EEXP
      COMMON/INFEL/  EKHI1P,EKHJ1P,EKHSL(2),KODYX1(2),KODYSL(2),
     +               BMYSL(2,17),RYSL(2,17),INDSL(2),EKEPSL(2,18),
     +               REVPSL(2,2),RTOTSL(2),RTPPSL(2),RTPNSL(2),
     +               RTSPSL(2),RTSNSL(2),SLRENP(2),SLRENN(2),
     +               TSLENP(2),TSLENN(2),
     +               MINDSL(2),EKUG(2,2),ROTUG(2,2),BMPIN(2,2),
     +               ROTPIN(2,2),RVPCSL(2,2),IPP(2,2),BMO(2,2),
     +               REVPMO(2,2),KDPSSL(2)
      COMMON/INFEL/  EKHI2P,EKHJ2P,EKHSH(2),KODYX2(2),KODYSH(2),
     +               BMYSH(2,16),RYSH(2,16),INDSH(2),EKEPSH(2,15),
     +               REVPSH(2,2),RTOTSH(2),RTPPSH(2),RTPNSH(2),
     +               RTSPSH(2),RTSNSH(2),SHRENP(2),SHRENN(2),
```

```
     +                TSHENP(2),TSHENN(2),
     +                RTOT(2),RTENP(2),RTENN(2),TRTENP(2),TRTENN(2),
     +                BMCR(2,2),RCR(2,2),MINDSH(2),RMAX(2,2),EKY(2,2),
     +                BMP(2,2),ROTP(2,2),BMPP(2,2),BMMP(2,2),ROTCRI(2,2),
     +                BMPN(2,2),ROTPN(2,2),BMPPN(2,2),RANGEL(2,2),
     +                RANGEU(2,2),RN(2,2),BETASH(2,2),GAMMA(2,2),
     +                BMMPN(2,2),KFLAG1(2),KFLAG2(2),REVPCR(2,2),
     +                KDPSSH(2)
      COMMON/INFEL/   EYRFL(2,2),ECRSH(2,2),EYRSH(2,2),EYR(2,2),ESRFL(2),
     +                ESRSH(2),ESRSL(2),ESRC(2),SENPFL(2),SENNFL(2),
     +                SENPSH(2),SENNSH(2),SENPSL(2),SENNSL(2),SENPC(2),
     +                SENNC(2),DFFL(2,2),DFSH(2,2),DFSL(2,2),DFC(2,2),
     +                EENGFL(2),ENGFL(2),EDFFL(2),EENGSH(2),ENGSH(2),
     +                EDFSH(2),EENGSL(2),ENGSL(2),EDFSL(2),TEENG(2),
     +                TENG(2),TDEF(2),
     +                PRBM(2),EIL,GAL2,P,PO,
     +                RYSHTL(2,16),RCRTL(2,2),RMAXTL(2,2),RMAXPL(2,2),
     +                ROTPTL(2,2),ROTPNT(2,2),REST(19)
      COMMON /WORK/   DVRI,DVRJ,BML(2),DBM(2),MINDFL(2),ST(2,2),W(4839)
C     SET REVERSAL MOMENT INDICATOR
C
      REMIND=1
      IF (INDSL(IEND).EQ.2) REMIND=-1
C
C     RULE 1. LOADING ELASTICALLY IN THE POSITIVE DIRECTION
C
      IF (KODYSL(IEND).NE.1) GO TO 30
      IF (REMIND*DBM(IEND).LT.0.) GO TO 20
      FAC=(BMYSL(IEND,1)-BMTOT(IEND))/DBM(IEND)
      IF (FAC.GE.FACTOR) GO TO 540
      FACTOR=FAC
      BM=BMYSL(IEND,1)
      ROTSL=RYSL(IEND,1)
      KFAC=IEND
```

```
      KSPRNG=1
      KODESL=3
      EKSL=EKEPSL(IEND,3)
      IDK=1
      GO TO 540
   20 FAC=-BMTOT(IEND)/DBM(IEND)
      IF (FAC.GE.FACTOR) GO TO 540
      FACTOR=FAC
      BM=0.
      ROTSL=0.
      KFAC=IEND
      KSPRNG=1
      KODESL=2
      EKSL=EKEPSL(IEND,2)
      IDK=2
      GO TO 540
   30 KODSL=KODYSL(IEND)
      GO TO(40,40,60,80,100,120,140,160,180,200,220,240,260,280,300,320,
     1340,360,380,400,420,440,460,480,500,520)KODSL
C
C     RULE 2. LOADING ELASTICALLY IN THE NEGATIVE DIRECTION
C
   40 IF (REMIND*DBM(IEND).LT.0.) GO TO 50
      FAC =(BMYSL(IEND,2)-BMTOT(IEND))/DBM(IEND)
      IF (FAC.GE.FACTOR) GO TO 540
      FACTOR=FAC
      BM=BMYSL(IEND,2)
      ROTSL=RYSL(IEND,2)
      KFAC=IEND
      KSPRNG=1
      KODESL=3
      EKSL=EKEPSL(IEND,4)
      IDK=2
      GO TO 540
```

```
   50 FAC=-BMTOT(IEND)/DBM(IEND)
      IF(FAC.GE.FACTOR)GO TO 540
      FACTOR=FAC
      BM=0.
      ROTSL=0.
      KFAC=IEND
      KSPRNG=1
      KODESL=1
      EKSL=EKEPSL(IEND,1)
      IDK=1
      GO TO 540
C
C     RULE 3. LOADING ON THE PRIMARY CURVE AFTER YIELDING.
C
   60 IDD=INDSL(IEND)
      IF (REMIND*DBM(IEND).LT.0.) GO TO 70
      MINDSL(IEND)=IDD+2
      GO TO 540
   70 KODYSL(IEND)=4
      IDB=3-IDD
      IKK=IDD+2
      IRR=IDB+2
      IUC=IDD+4
C
C     DETERMINE UNLOADING SLOPE
C
      EKU=EKEPSL(IEND,IDD)+(EKUG(IEND,IDD)-EKEPSL(IEND,IDD))/(ROTUG(IEND
     1,IDD)-RYSL(IEND,IDD))*(RTOTSL(IEND)-RYSL(IEND,IDD))
C
C     CHECK FOR MINIMUM SLOPE
C
      IF(DABS(BMYSL(IEND,IRR)).GT.DABS(BMYSL(IEND,IDB))) GO TO 75
      IF(DABS(BMYSL(IEND,IDD)).LT.DABS(BMYSL(IEND,IDB))) THEN
      BMPIN(IEND,IDB)=-(BMYSL(IEND,IDD))
```

```
      ROTPIN(IEND,IDB)=RYSL(IEND,IDB)-(BMYSL(IEND,IDB)-BMPIN(IEND,IDB)
     1)/EKEPSL(IEND,IDB)
      ELSE
      BMPIN(IEND,IDB)=BMYSL(IEND,IDB)
      ROTPIN(IEND,IDB)=RYSL(IEND,IDB)
      END IF
 75   EKUMIN=(BMYSL(IEND,IKK)-BMPIN(IEND,IDB))/(RYSL(IEND,IKK)-ROTPIN(IE
     1ND,IDB))
      IF(EKU.LE.EKUMIN) EKU=EKUMIN
      IF(EKU.GT.EKEPSL(IEND,IDD)) EKU=EKEPSL(IEND,IDD)
      EKEPSL(IEND,IUC)=EKU
      EKHSL(IEND)=EKEPSL(IEND,IUC)
      REVPMO(IEND,IDD)=RYSL(IEND,IKK)-(BMYSL(IEND,IKK)-BMO(IEND,IDD))/EK
     1U
      RVPCSL(IEND,IDD)=REVPMO(IEND,IDD)
C
C     CORDINATES OF THE POINT AT WHICH PINCHING OF THE CURVE TERMINATES.
C
      IF(DABS(BMYSL(IEND,IDD)).GT.DABS(BMYSL(IEND,IDB))) THEN
      RBM=-BMYSL(IEND,IDB)
      RR=RYSL(IEND,IDD)-(BMYSL(IEND,IDD)-RBM)/(EKEPSL(IEND,IDD))
      ROTPIN(IEND,IDD)=(RBM-RR*EKEPSL(IEND,IRR)-BMO(IEND,IDD)+REVPMO(IE
     1ND,IDD)*EKU)/(EKU-EKEPSL(IEND,IRR))
      BMPIN(IEND,IDD)=BMYSL(IEND,IKK)-(RYSL(IEND,IKK)-ROTPIN(IEND,IDD))*
     1EKU
        IF(DABS(BMPIN(IEND,IDD)).GE.DABS(BMYSL(IEND,IKK)))THEN
        BMPIN(IEND,IDD)=BMYSL(IEND,IKK)
        ROTPIN(IEND,IDD)=RYSL(IEND,IDD)
        ELSE
        END IF
      ELSE
      BMPIN(IEND,IDD)=BMYSL(IEND,IKK)
      ROTPIN(IEND,IDD)=RYSL(IEND,IKK)
      END IF
```

```
      FACTOR=0.
      KFAC=0
      KSPRNG=0
      GO TO 540
C
C     RULE. 4 UNLOADING FROM PRIMARY CURVE, MOMENT IS GREATER THAN MO
C
   80 IDD=INDSL(IEND)
      IF(REMIND*DBM(IEND).LT.0.)GO TO 90
      IPC=IDD+2
      FAC=(BMYSL(IEND,IPC)-BMTOT(IEND))/DBM(IEND)
      IF (FAC.GE.FACTOR)GO TO 540
      FACTOR=FAC
      BM=BMYSL(IEND,IPC)
      ROTSL=RYSL(IEND,IPC)
      KFAC=IEND
      KSPRNG=1
      KODESL=3
      EKSL=EKEPSL(IEND,IPC)
      IDK=IDD
      GO TO 540
   90 IUC=IDD+6
      FAC=(BMO(IEND,IDD)-BMTOT(IEND))/DBM(IEND)
      IF(FAC.GE.FACTOR) GO TO 540
      FACTOR=FAC
      BM=BMO(IEND,IDD)
      ROTSL=RVPCSL(IEND,IDD)
      KFAC=IEND
      KSPRNG=1
      KODESL=5
      IDB=3-IDD
C
C     DETERMINE UNLOADING SLOPE BELOW MO
C
```

```
      EKU=(BMPIN(IEND,IDB)-BMO(IEND,IDD))/(ROTPIN(IEND,IDB)-RVPCSL(IEND,
     1IDD))
      EKEPSL(IEND,IUC)=EKU
      EKSL=EKU
      REVPSL(IEND,IDD)=RVPCSL(IEND,IDD)-BMO(IEND,IDD)/EKU
      IDK=IDD
      GO TO  540
C
C     RULE 5. UNLOADING FROM PRIMARY CURVE, MOMENT IS LOWER THAN MO
C
  100 IDD=INDSL(IEND)
      IF(REMIND*DBM(IEND).LT.0.)GO TO 110
      KODYSL(IEND)=6
      IRR=IDD+2
      EKRL=(BMYSL(IEND,IRR)-BMYSL(IEND,5))/(RYSL(IEND,IRR)-RYSL(IEND,5))
      EKEPSL(IEND,9)=EKRL
      EKHSL(IEND)=EKRL
      KFAC=0
      KSPRNG=0
      FACTOR=0.
      GO TO 540
C
  110 MINDSL(IEND)=5
      KDPSSL(IEND)=KODYSL(IEND)
      FAC=-BMTOT(IEND)/DBM(IEND)
      IF(FAC.GE.FACTOR)GO TO 540
      FACTOR=FAC
      BM=0.
      ROTSL=REVPSL(IEND,IDD)
      KFAC=IEND
      KSPRNG=1
      KODESL=7
      IDK=3-IDD
      IDB=IDK
```

```
      EKLSL=BMPIN(IEND,IDB)/(ROTPIN(IEND,IDB)-REVPSL(IEND,IDD))
      EKEPSL(IEND,11)=EKLSL
      EKSL=EKEPSL(IEND,11)
      GO TO 540
C
C     RULE 6. RELOADING AFTER RULE 5.
C
  120 IDD=INDSL(IEND)
      IPC=IDD+2
      IF(REMIND*DBM(IEND).LT.0.)GO TO 130
      FAC=(BMYSL(IEND,IPC)-BMTOT(IEND))/DBM(IEND)
      IF(FAC.GE.FACTOR) GO TO 540
      FACTOR=FAC
      BM=BMYSL(IEND,IPC)
      ROTSL=RYSL(IEND,IPC)
      KFAC=IEND
      KSPRNG=1
      KODESL=3
      EKSL=EKEPSL(IEND,IPC)
      IDK=IDD
      GO TO 540
C
  130 IKK=IDD+6
      FAC=(BMYSL(IEND,5)-BMTOT(IEND))/DBM(IEND)
      IF(FAC.GE.FACTOR)GO TO 540
      FACTOR=FAC
      BM=BMYSL(IEND,5)
      ROTSL=RYSL(IEND,5)
      KFAC=IEND
      KSPRNG=1
      KODESL=5
      EKSL=EKEPSL(IEND,IKK)
      IDK=IDD
      GO TO 540
```

```
C
C     RULE 7. RELOADING TO THE PRIMARY CURVE AFTER RULE 5.
C
  140 IDD=INDSL(IEND)
      IF(REMIND*DBM(IEND).LT.0.) GO TO 150
      IUC=IDD+4
      FAC=(BMPIN(IEND,IDD)-BMTOT(IEND))/DBM(IEND)
      IF(FAC.GE.FACTOR)GO TO 540
      FACTOR=FAC
      BM=BMPIN(IEND,IDD)
      ROTSL=ROTPIN(IEND,IDD)
      KFAC=IEND
      KSPRNG=1
      KODESL=4
      EKSL=EKEPSL(IEND,IUC)
      IDK=IDD
      GO TO 540
C
  150 IF(DABS(BMTOT(IEND)).GT.DABS(BMO(IEND,IDD)))THEN
      KODYSL(IEND)=9
      IKK=7
      IUC=IDD+4
      EKHSL(IEND)=EKEPSL(IEND,IUC)
      BMD=BMYSL(IEND,7)-BMO(IEND,IDD)
      ELSE
      KODYSL(IEND)=8
      IKK=6
      IUC=IDD+6
      EKHSL(IEND)=EKEPSL(IEND,IUC)
      BMD=BMYSL(IEND,6)
      END IF
C
C     CHECK FOR MINIMUM SLOPE.
C
```

```
      IDB=3-IDD
      EKUMIN=(BMPIN(IEND,IDB)-BMYSL(IEND,IKK))/(ROTPIN(IEND,IDB)-RYSL(IE
     1ND,IKK))
      IF(DABS(EKHSL(IEND)).LT.DABS(EKUMIN)) EKHSL(IEND)=EKUMIN
      IF(DABS(EKHSL(IEND)).LT.DABS(EKEPSL(IEND,11))) EKHSL(IEND)=EKEPSL
     1(IEND,11)
      REVPSL(IEND,IDD)=RYSL(IEND,IKK)-BMD/EKHSL(IEND)
      IF(DABS(BMTOT(IEND)).GT.DABS(BMO(IEND,IDD))) REVPMO(IEND,IDD)=REVP
     1SL(IEND,IDD)
      FACTOR=0.
      KFAC=0
      KSPRNG=0
      GO TO 540
C
C     RULE 8. UNLOADING AFTER RULE 7, MOMENT IS BELOW MO
C
  160 IDD=INDSL(IEND)
      IF(REMIND*DBM(IEND).LT.0.) GO TO 170
      FAC=(BMYSL(IEND,6)-BMTOT(IEND))/DBM(IEND)
      IF(FAC.GE.FACTOR)GO TO 540
      FACTOR=FAC
      BM=BMYSL(IEND,6)
      ROTSL=RYSL(IEND,6)
      EKSL=EKEPSL(IEND,11)
      KODESL=7
      KFAC=IEND
      KSPRNG=1
      IDK=IDD
      GO TO 540
C
  170 FAC=-BMTOT(IEND)/DBM(IEND)
      IF(FAC.GE.FACTOR) GO TO 540
      FACTOR=FAC
      BM=0.
```

```
      ROTSL=REVPSL(IEND,IDD)
      IDK=3-IDD
      IDB=IDK
      KODESL=12
      KFAC=IEND
      KSPRNG=1
      EKLSL=BMPIN(IEND,IDB)/(ROTPIN(IEND,IDB)-REVPSL(IEND,IDD))
      EKEPSL(IEND,14)=EKLSL
      EKSL=EKLSL
      GO TO 540
C
C     RULE 9. UNLOADING AFTER RULE 7, MOMENT IS GREATER THAN MO
C
  180 IDD=INDSL(IEND)
      IF(REMIND*DBM(IEND).LT.0.)GO TO 190
      FAC=(BMYSL(IEND,7)-BMTOT(IEND))/DBM(IEND)
      IF(FAC.GE.FACTOR) GO TO 540
      FACTOR=FAC
      BM=BMYSL(IEND,7)
      ROTSL=RYSL(IEND,7)
      EKSL=EKEPSL(IEND,11)
      KODESL=7
      KFAC=IEND
      KSPRNG=1
      IDK=IDD
      GO TO 540
C
  190 IUC=IDD+6
      FAC=(BMO(IEND,IDD)-BMTOT(IEND))/DBM(IEND)
      IF(FAC.GE.FACTOR) GO TO 540
      FACTOR=FAC
      BM=BMO(IEND,IDD)
      ROTSL=REVPMO(IEND,IDD)
      KFAC=IEND
```

```
      KSPRNG=1
      KODESL=10
      EKSL=EKEPSL(IEND,IUC)
C     CHECK FOR MINIMUM SLOPE
      IDB=3-IDD
      EKUMIN=(BMO(IEND,IDD)-BMPIN(IEND,IDB))/(REVPMO(IEND,IDD)-ROTPIN(IE
     1ND,IDB))
      IF(DABS(EKSL).LT.DABS(EKUMIN)) EKSL=EKUMIN
      IF(DABS(EKSL).LT.DABS(EKEPSL(IEND,11))) EKSL=EKEPSL(IEND,11)
      REVPSL(IEND,IDD)=REVPMO(IEND,IDD)-BMO(IEND,IDD)/EKSL
      EKEPSL(IEND,13)=EKSL
      IDK=IDD
      GO TO 540
C
C     RULE 10. UNLOADING AFTER RULE 7, MOMENT IS BELOW MO
C
  200 IDD=INDSL(IEND)
      IF(REMIND*DBM(IEND).LT.0.) GO TO 210
      KODYSL(IEND)=11
      EKRL=(BMYSL(IEND,7)-BMYSL(IEND,8))/(RYSL(IEND,7)-RYSL(IEND,8))
      EKEPSL(IEND,9)=EKRL
      EKHSL(IEND)=EKRL
      KFAC=0
      KSPRNG=0
      FACTOR=0.
      GO TO 540
C
  210 MINDSL(IEND)=8
      KDPSSL(IEND)=KODYSL(IEND)
      FAC=-BMTOT(IEND)/DBM(IEND)
      IF(FAC.GE.FACTOR) GO TO 540
      FACTOR=FAC
      BM=0.
      ROTSL=REVPSL(IEND,IDD)
```

```
      KFAC=IEND
      KSPRNG=1
      KODESL=12
      IDK=3-IDD
      IDB=IDK
C     DETRMINE RELOADING SLOPE.
      EKLSL=BMPIN(IEND,IDB)/(ROTPIN(IEND,IDB)-REVPSL(IEND,IDD))
      EKSL=EKLSL
      EKEPSL(IEND,14)=EKSL
      GO TO 540
C
C     RULE 11. RELOADING FROM RULE 10.
C
  220 IDD=INDSL(IEND)
      IF(REMIND*DBM(IEND).LT.0.) GO TO 230
      FAC=(BMYSL(IEND,7)-BMTOT(IEND))/DBM(IEND)
      IF(FAC.GE.FACTOR) GO TO 540
      FACTOR=FAC
      BM=BMYSL(IEND,7)
      ROTSL=RYSL(IEND,7)
      KODESL=7
      KFAC=IEND
      KSPRNG=1
      EKSL=EKEPSL(IEND,11)
      IDK=IDD
      GO TO 540
C
  230 FAC=(BMYSL(IEND,8)-BMTOT(IEND))/DBM(IEND)
      IF(FAC.GE.FACTOR) GO TO 540
      FACTOR=FAC
      BM=BMYSL(IEND,8)
      ROTSL=RYSL(IEND,8)
      KODESL=10
      KFAC=IEND
```

```
      KSPRNG=1
      EKSL=EKEPSL(IEND,13)
      IDK=IDD
      GO TO 540
C
C     RULE 12. RELOADING AFTER RULE 10.
C
  240 IDD=INDSL(IEND)
      IUC=IDD+4
      IF(REMIND*DBM(IEND).LT.0.) GO TO 250
      FAC=(BMPIN(IEND,IDD)-BMTOT(IEND))/DBM(IEND)
      IF(FAC.GE.FACTOR) GO TO 540
      FACTOR=FAC
      BM=BMPIN(IEND,IDD)
      ROTSL=ROTPIN(IEND,IDD)
      KODESL=4
      KFAC=IEND
      KSPRNG=1
      EKSL=EKEPSL(IEND,IUC)
      IDK=IDD
      GO TO 540
C
  250 IF(DABS(BMTOT(IEND)).LE.DABS(BMO(IEND,IDD)))THEN
      KODYSL(IEND)=13
      IUC=IDD+6
      IKK=9
      BMD=BMYSL(IEND,9)
      ELSE
      KODYSL(IEND)=14
      IUC=IDD+4
      IKK=10
      BMD=BMYSL(IEND,10)-BMO(IEND,IDD)
      END IF
      EKHSL(IEND)=EKEPSL(IEND,IUC)
```

```
C
C     CHECK FOR MINIMUM SLOPE.
C
      IDB=3-IDD
      IRP=IPP(IEND,IDB)
      EKUMIN=(BMYSL(IEND,IRP)-BMYSL(IEND,IKK))/(RYSL(IEND,IRP)-RYSL(IEND
     1,IKK))
      IF(DABS(EKHSL(IEND)).LT.DABS(EKUMIN)) EKHSL(IEND)=EKUMIN
      IF(DABS(EKHSL(IEND)).LT.DABS(EKEPSL(IEND,14))) EKHSL(IEND)=EKEPSL(
     1IEND,14)
      REVPSL(IEND,IDD)=RYSL(IEND,IKK)-BMD/EKHSL(IEND)
      IF(DABS(BMTOT(IEND)).GT.DABS(BMO(IEND,IDD))) REVPMO(IEND,IDD)=REVP
     1SL(IEND,IDD)
      FACTOR=0.
      KFAC=0
      KSPRNG=1
      GO TO 540
C
C     RULE 13. UNLOADING AFTER RULE 12, MOMENT IS BELOW MO
C
 260  IDD=INDSL(IEND)
      IF(REMIND*DBM(IEND).LT.0.) GO TO 270
      FAC=(BMYSL(IEND,9)-BMTOT(IEND))/DBM(IEND)
      IF(FAC.GE.FACTOR) GO TO 540
      FACTOR=FAC
      BM=BMYSL(IEND,9)
      ROTSL=RYSL(IEND,9)
      KFAC=IEND
      KSPRNG=1
      KODESL=12
      EKSL=EKEPSL(IEND,14)
      IDK=IDD
      GO TO  540
C
```

```
 270  FAC=-BMTOT(IEND)/DBM(IEND)
      IF(FAC.GE.FACTOR) GO TO  540
      FACTOR=FAC
      BM=0.
      ROTSL=REVPSL(IEND,IDD)
      KFAC=IEND
      KSPRNG=1
      KODESL=17
      IDK=3-IDD
      IDB=IDK
C
C     DETRMINE RELOADING SLOPE.
C
      IRP=IPP(IEND,IDB)
      EKEPSL(IEND,17)=BMYSL(IEND,IRP)/(RYSL(IEND,IRP)-REVPSL(IEND,IDD))
      EKSL=EKEPSL(IEND,17)
      GO TO  540
C
C     RULE 14. UNLOADING AFTER RULE 12, MOMENT IS ABOVE MO
C
 280  IDD=INDSL(IEND)
      IF(REMIND*DBM(IEND).LT.0.)GO TO 290
      FAC=(BMYSL(IEND,10)-BMTOT(IEND))/DBM(IEND)
      IF(FAC.GE.FACTOR) GO TO 540
      FACTOR=FAC
      BM=BMYSL(IEND,10)
      ROTSL=RYSL(IEND,10)
      KODESL=12
      KFAC=IEND
      KSPRNG=1
      EKSL=EKEPSL(IEND,14)
      IDK=IDD
      GO TO 540
C
```

```
 290  IKK=IDD+6
      FAC=(BMO(IEND,IDD)-BMTOT(IEND))/DBM(IEND)
      IF(FAC.GE.FACTOR)GO TO  540
      FACTOR=FAC
      BM=BMO(IEND,IDD)
      ROTSL=REVPMO(IEND,IDD)
      KODESL=15
      KFAC=IEND
      KSPRNG=1
C
C     DETERMINE UNLOADING SLOPE BELOW MO
C
      EKEPSL(IEND,16)=EKEPSL(IEND,IKK)
      IDB=3-IDD
      IRP=IPP(IEND,IDB)
C
C     MINIMUM UNLOADING SLOPE.
C
      EKUMIN=(BMYSL(IEND,IRP)-BMO(IEND,IDD))/(RYSL(IEND,IRP)-REVPMO(IEND
     1,IDD))
      IF(DABS(EKEPSL(IEND,16)).LT.DABS(EKUMIN))  EKEPSL(IEND,16)=EKUMIN
      IF(DABS(EKEPSL(IEND,16)).LT.DABS(EKEPSL(IEND,14))) EKEPSL(IEND,16)
     1=EKEPSL(IEND,14)
      REVPSL(IEND,IDD)=REVPMO(IEND,IDD)-BMO(IEND,IDD)/EKEPSL(IEND,16)
      EKSL=EKEPSL(IEND,16)
      IDK=IDD
      GO TO 540
C
C     RULE 15. UNLOADING AFTER RULE 14.
C
 300  IDD=INDSL(IEND)
      IF(REMIND*DBM(IEND).LT.0.) GO TO 310
      KODYSL(IEND)=16
      EKRL=(BMYSL(IEND,10)-BMYSL(IEND,11))/(RYSL(IEND,10)-RYSL(IEND,11))
```

```
      EKEPSL(IEND,10)=EKRL
      EKHSL(IEND)=EKRL
      KFAC=0
      KSPRNG=0
      FACTOR=0.
      GO TO 540
C
 310  MINDSL(IEND)=11
      KDPSSL(IEND)=KODYSL(IEND)
      FAC=-BMTOT(IEND)/DBM(IEND)
      IF(FAC.GE.FACTOR) GO TO 540
      FACTOR=FAC
      BM=0.
      ROTSL=REVPSL(IEND,IDD)
      KFAC=IEND
      KSPRNG=1
      KODESL=17
C
C     DETRMINE RELOADING SLOPE.
C
      IDK=3-IDD
      IDB=IDK
      IRP=IPP(IEND,IDB)
      EKEPSL(IEND,17)=BMYSL(IEND,IRP)/(RYSL(IEND,IRP)-REVPSL(IEND,IDD))
      EKSL=EKEPSL(IEND,17)
      GO TO 540
C
C     RULE 16. RELOADING FROM RULE 15.
C
 320  IDD=INDSL(IEND)
      IF(REMIND*DBM(IEND).LT.0.)GO TO 330
      FAC=(BMYSL(IEND,10)-BMTOT(IEND))/DBM(IEND)
      IF(FAC.GE.FACTOR)GO TO 540
      FACTOR=FAC
```

```
      BM=BMYSL(IEND,10)
      ROTSL=RYSL(IEND,10)
      KODESL=12
      KFAC=IEND
      KSPRNG=1
      EKSL=EKEPSL(IEND,14)
      IDK=IDD
      GO TO 540
C
 330  FAC=(BMYSL(IEND,11)-BMTOT(IEND))/DBM(IEND)
      IF(FAC.GE.FACTOR) GO TO 540
      FACTOR=FAC
      BM=BMYSL(IEND,11)
      ROTSL=RYSL(IEND,11)
      KODESL=15
      KFAC=IEND
      KSPRNG=1
      EKSL=EKEPSL(IEND,16)
      IDK=IDD
      GO TO 510
C
C     RULE 17. RELOADING AFTER RULE 15.
C
 340  IDD=INDSL(IEND)
      IF(REMIND*DBM(IEND).LT.0.)GO TO 350
      IRP=IPP(IEND,IDD)
      FAC=(BMYSL(IEND,IRP)-BMTOT(IEND))/DBM(IEND)
      IF(FAC.GE.FACTOR) GO TO 540
      FACTOR=FAC
      BM=BMYSL(IEND,IRP)
      ROTSL=RYSL(IEND,IRP)
      KODESL=7
      KFAC=IEND
      KSPRNG=1
```

```
      EKSL=EKEPSL(IEND,11)
      IDK=IDD
      GO TO 540
C
  350 IF(DABS(BMTOT(IEND)).GT.DABS(BMO(IEND,IDD))) THEN
      KODYSL(IEND)=19
      IKK=13
      IUC=IDD+4
      EKHSL(IEND)=EKEPSL(IEND,IUC)
      BMD=BMYSL(IEND,13)-BMO(IEND,IDD)
      ELSE
      KODYSL(IEND)=18
      IKK=12
      IUC=IDD+6
      EKHSL(IEND)=EKEPSL(IEND,IUC)
      BMD=BMYSL(IEND,12)
      END IF
C
C     CHECK FOR MINIMUM SLOPE.
C
      IDB=3-IDD
      IRP=IPP(IEND,IDB)
      EKUMIN=(BMYSL(IEND,IRP)-BMYSL(IEND,IKK))/(RYSL(IEND,IRP)-RYSL(IEND
     1,IKK))
      IF(DABS(EKHSL(IEND)).LT.DABS(EKUMIN)) EKHSL(IEND)=EKUMIN
      IF(DABS(EKHSL(IEND)).LT.DABS(EKEPSL(IEND,17))) EKHSL(IEND)=EKEPSL(
     1IEND,17)
      REVPSL(IEND,IDD)=RYSL(IEND,IKK)-BMD/EKHSL(IEND)
      IF(DABS(BMTOT(IEND)).GT.DABS(BMO(IEND,IDD))) REVPMO(IEND,IDD)=REVP
     1SL(IEND,IDD)
      KFAC=0
      KSPRNG=0
      FACTOR=0.
      GO TO 540
```

```
C
C     RULE 18. UNLOADING FROM RULE 17, LOAD IS BELOW MO
C
 360  IDD=INDSL(IEND)
      IF(REMIND*DBM(IEND).LT.0.) GO TO 370
      FAC=(BMYSL(IEND,12)-BMTOT(IEND))/DBM(IEND)
      IF(FAC.GE.FACTOR) GO TO 540
      FACTOR=FAC
      BM=BMYSL(IEND,12)
      ROTSL=RYSL(IEND,12)
      KODESL=17
      KFAC=IEND
      KSPRNG=1
      EKSL=EKEPSL(IEND,17)
      IDK=IDD
      GO TO 540
 370  FAC=-BMTOT(IEND)/DBM(IEND)
      IF(FAC.GE.FACTOR) GO TO 540
      FACTOR=FAC
      BM=0.
      ROTSL=REVPSL(IEND,IDD)
      KODESL=22
      KFAC=IEND
      KSPRNG=1
      IDK=3-IDD
      IDB=IDK
C
C     DETERMINE RELOADING SLOPE.
C
      IRP=IPP(IEND,IDB)
      EKEPSL(IEND,18)=BMYSL(IEND,IRP)/(RYSL(IEND,IRP)-REVPSL(IEND,IDD))
      EKSL=EKEPSL(IEND,18)
      GO TO 540
C
```

```
C     RULE 19. UNLOADING FROM RULE 17, MOMENT IS HIGHER THAN MO
C
 380  IDD=INDSL(IEND)
      IF(REMIND*DBM(IEND).LT.0.)GO TO 390
      FAC=(BMYSL(IEND,13)-BMTOT(IEND))/DBM(IEND)
      IF(FAC.GE.FACTOR) GO TO 540
      FACTOR=FAC
      BM=BMYSL(IEND,13)
      ROTSL=RYSL(IEND,13)
      KODESL=17
      KFAC=IEND
      KSPRNG=1
      EKSL=EKEPSL(IEND,17)
      IDK=IDD
      GO TO 540
 390  IUC=IDD+6
      FAC=(BMO(IEND,IDD)-BMTOT(IEND))/DBM(IEND)
      IF(FAC.GE.FACTOR) GO TO 540
      FACTOR=FAC
      BM=BMO(IEND,IDD)
      ROTSL=REVPMO(IEND,IDD)
      KODESL=20
      KFAC=IEND
      KSPRNG=1
      EKEPSL(IEND,13)=EKEPSL(IEND,IUC)
      IDB=3-IDD
C
C     CHECK MINIMUM SLOPE
C
      IRP=IPP(IEND,IDB)
      EKUMIN=(BMYSL(IEND,IRP)-BMO(IEND,IDD))/(RYSL(IEND,IRP)-REVPMO(IEND
     1,IDD))
      IF(DABS(EKEPSL(IEND,13)).LE.DABS(EKUMIN))  EKEPSL(IEND,13)=EKUMIN
      IF(DABS(EKEPSL(IEND,13)).LE.DABS(EKEPSL(IEND,17))) EKEPSL(IEND,13)
```

```
     1=EKEPSL(IEND,17)
      EKSL=EKEPSL(IEND,13)
      REVPSL(IEND,IDD)=REVPMO(IEND,IDD)-BMO(IEND,IDD)/EKSL
      IDK=IDD
      GO TO 540
C
C     RULE 20. UNLOADING AFTER RULE 19.
C
  400 IDD=INDSL(IEND)
      IF(REMIND*DBM(IEND).LT.0.) GO TO 410
      KODYSL(IEND)=21
      EKRL=(BMYSL(IEND,13)-BMYSL(IEND,14))/(RYSL(IEND,13)-RYSL(IEND,14))
      EKEPSL(IEND,9)=EKRL
      EKHSL(IEND)=EKRL
      KFAC=0
      KSPRNG=0
      FACTOR=0.
      GO TO 540
  410 MINDSL(IEND)=14
      KDPSSL(IEND)=KODYSL(IEND)
      FAC=-BMTOT(IEND)/DBM(IEND)
      IF(FAC.GE.FACTOR)GO TO 540
      FACTOR=FAC
      BM=0.
      ROTSL=REVPSL(IEND,IDD)
      KFAC=IEND
      KSPRNG=1
      KODESL=22
      IDK=3-IDD
      IDB=IDK
C
C     DETERMINE RELOADING SLOPE.
C
      IRP=IPP(IEND,IDB)
```

```
      EKSL=BMYSL(IEND,IRP)/(RYSL(IEND,IRP)-REVPSL(IEND,IDD))
      EKEPSL(IEND,18)=EKSL
      GO TO 540
C
C     RULE 21. RELOADING FROM RULE 20.
C
  420 IDD=INDSL(IEND)
      IF(REMIND*DBM(IEND).LT.0.) GO TO 430
      FAC=(BMYSL(IEND,13)-BMTOT(IEND))/DBM(IEND)
      IF(FAC.GE.FACTOR) GO TO 540
      FACTOR=FAC
      BM=BMYSL(IEND,13)
      ROTSL=RYSL(IEND,13)
      KODESL=17
      KFAC=IEND
      KSPRNG=1
      EKSL=EKEPSL(IEND,17)
      IDK=IDD
      GO TO 540
  430 FAC=(BMYSL(IEND,14)-BMTOT(IEND))/DBM(IEND)
      IF(FAC.GE.FACTOR) GO TO 540
      FACTOR=FAC
      BM=BMYSL(IEND,14)
      ROTSL=RYSL(IEND,14)
      KODESL=20
      KFAC=IEND
      KSPRNG=1
      EKSL=EKEPSL(IEND,13)
      IDK=IDD
      GO TO  540
C
C     RULE 22. RELOADING TOWARDS U9/U10.
C
  440 IDD=INDSL(IEND)
```

```
      IF(REMIND*DBM(IEND).LT.0.) GO TO 450
      IRP=IPP(IEND,IDD)
      FAC=(BMYSL(IEND,IRP)-BMTOT(IEND))/DBM(IEND)
      IF(FAC.GE.FACTOR) GO TO  540
      FACTOR=FAC
      BM=BMYSL(IEND,IRP)
      ROTSL=RYSL(IEND,IRP)
      KODESL=12
      KFAC=IEND
      KSPRNG=1
      EKSL=EKEPSL(IEND,14)
      IDK=IDD
      GO TO 540
  450 IF(DABS(BMTOT(IEND)).LE.DABS(BMO(IEND,IDD))) THEN
      KODYSL(IEND)=23
      IUC=IDD+6
      IKK=15
      BMD=BMYSL(IEND,15)
      ELSE
      KODYSL(IEND)=24
      IUC=IDD+4
      IKK=16
      BMD=BMYSL(IEND,16)-BMO(IEND,IDD)
      END IF
      EKHSL(IEND)= EKEPSL(IEND,IUC)
C
C     CHECK FOR MINIMUM SLOPE.
C
      IDB=3-IDD
      IRP=IPP(IEND,IDB)
      EKUMIN=(BMYSL(IEND,IRP)-BMYSL(IEND,IKK))/(RYSL(IEND,IRP)-RYSL(IEND
     1,IKK))
      IF(DABS(EKHSL(IEND)).LT.DABS(EKUMIN))  EKHSL(IEND)=EKUMIN
      IF(DABS(EKHSL(IEND)).LT.DABS(EKEPSL(IEND,18)))  EKHSL(IEND)=EKEPSL
```

```
     1(IEND,18)
      REVPSL(IEND,IDD)=RYSL(IEND,IKK)-BMD/EKHSL(IEND)
      IF(DABS(BMTOT(IEND)).GT.DABS(BMO(IEND,IDD))) REVPMO(IEND,IDD)=REVP
     1SL(IEND,IDD)
      FACTOR=0.
      KFAC=0
      KSPRNG=1
      GO TO 540
C
C     RULE 23. UNLOADING FROM 22, MOMENT IS BELOW MO
C
  460 IDD=INDSL(IEND)
      IF(REMIND*DBM(IEND).LT.0.) GO TO 470
      FAC=(BMYSL(IEND,15)-BMTOT(IEND))/DBM(IEND)
      IF(FAC.GE.FACTOR) GO TO 540
      FACTOR=FAC
      BM=BMYSL(IEND,15)
      ROTSL=RYSL(IEND,15)
      KODESL=22
      KFAC=IEND
      KSPRNG=1
      EKSL=EKEPSL(IEND,18)
      IDK=IDD
      GO TO 540
  470 FAC=-BMTOT(IEND)/DBM(IEND)
      IF(FAC.GE.FACTOR) GO TO 540
      FACTOR=FAC
      BM=0.
      ROTSL=REVPSL(IEND,IDD)
      KFAC=IEND
      KSPRNG=1
      KODESL=17
      IDK=3-IDD
      IDB=IDK
```

```
C
C     DETERMINE RELOADING SLOPE.
C
      IRP=IPP(IEND,IDB)
      EKEPSL(IEND,17)=BMYSL(IEND,IRP)/(RYSL(IEND,IRP)-REVPSL(IEND,IDD))
      EKSL=EKEPSL(IEND,17)
      GO TO 540
C
C     RULE 24. UNLOADING AFTER RULE 22, MOMENT IS HIGHER THAN MO.
C
  480 IDD=INDSL(IEND)
      IF(REMIND*DBM(IEND).LT.0.) GO TO 490
      FAC=(BMYSL(IEND,16)-BMTOT(IEND))/DBM(IEND)
      IF(FAC.GE.FACTOR) GO TO 540
      FACTOR=FAC
      BM=BMYSL(IEND,15)
      ROTSL=RYSL(IEND,15)
      KODESL=22
      KFAC=IEND
      KSPRNG=1
      EKSL=EKEPSL(IEND,18)
      IDK=IDD
      GO TO 540
  490 FAC=(BMO(IEND,IDD)-BMTOT(IEND))/DBM(IEND)
      IF(FAC.GE.FACTOR) GO TO 540
      FACTOR=FAC
      BM=BMO(IEND,IDD)
      ROTSL=REVPMO(IEND,IDD)
      KODESL=25
      KFAC=IEND
      KSPRNG=1
C
C     DETERMINE UNLOADING SLOPE BELOW MO.
C
```

```
      IKK=IDD+6
      EKEPSL(IEND,16)=EKEPSL(IEND,IKK)
C
C     MIMINUM UNLOADING SLOPE.
C
      IDB=3-IDD
      IRP=IPP(IEND,IDB)
      EKUMIN=(BMYSL(IEND,IRP)-BMO(IEND,IDD))/(RYSL(IEND,IRP)-REVPMO(IEND
     1,IDD))
      IF(DABS(EKEPSL(IEND,16)).LT.DABS(EKUMIN)) EKEPSL(IEND,16)=EKUMIN
      IF(DABS(EKEPSL(IEND,16)).LT.DABS(EKEPSL(IEND,18))) EKEPSL(IEND,16)
     1=EKEPSL(IEND,18)
      EKSL=EKEPSL(IEND,16)
      REVPSL(IEND,IDD)=REVPMO(IEND,IDD)-BMO(IEND,IDD)/EKEPSL(IEND,16)
      IDK=IDD
      GO TO 540
C
C     RULE 25. UNLOADING AFTER RULE 24.
C
  500 IDD=INDSL(IEND)
      IF(REMIND*DBM(IEND).LT.0.)GO TO 510
      KODYSL(IEND)=26
      EKRL=(BMYSL(IEND,16)-BMYSL(IEND,17))/(RYSL(IEND,16)-RYSL(IEND,17))
      EKEPSL(IEND,10)=EKRL
      EKHSL(IEND)=EKRL
      KFAC=0
      KSPRNG=0
      FACTOR=0.
      GO TO 540
  510 MINDSL(IEND)=17
      KDPSSL(IEND)=KODYSL(IEND)
      FAC=-BMTOT(IEND)/DBM(IEND)
      IF(FAC.GE.FACTOR) GO TO 540
      FACTOR=FAC
```

```
      BM=0.
      ROTSL=REVPSL(IEND,IDD)
      KFAC=IEND
      KSPRNG=1
      KODESL=17
C
C     DETERMINE RELOADING SLOPE.
C
      IDK=3-IDD
      IDB=IDK
      IRP=IPP(IEND,IDB)
      EKEPSL(IEND,17)=BMYSL(IEND,IRP)/(RYSL(IEND,IRP)-REVPSL(IEND,IDD))
      EKSL=EKEPSL(IEND,17)
      GO TO 540
C
C     RULE 26. RELOADING FROM 25.
C
  520 IDD=INDSL(IEND)
      IF(REMIND*DBM(IEND).LT.0.) GO TO 530
      FAC=(BMYSL(IEND,16)-BMTOT(IEND))/DBM(IEND)
      IF(FAC.GE.FACTOR) GO TO 540
      FACTOR=FAC
      BM=BMYSL(IEND,16)
      ROTSL=RYSL(IEND,16)
      KODESL=22
      KFAC=IEND
      KSPRNG=1
      EKSL=EKEPSL(IEND,18)
      IDK=IDD
      GO TO 540
  530 FAC=(BMYSL(IEND,17)-BMTOT(IEND))/DBM(IEND)
      IF(FAC.GE.FACTOR) GO TO 540
      FACTOR=FAC
      BM=BMYSL(IEND,17)
```

```
      ROTSL=RYSL(IEND,17)
      KODESL=25
      KFAC=IEND
      KSPRNG=1
      EKSL=EKEPSL(IEND,16)
      IDK=IDD
  540 RETURN
      END
```

```
C*********************************************************************
C*                                                                   *
C*                           SHEAR MODEL                             *
C*                                                                   *
C*********************************************************************
      SUBROUTINE SHEARM(IEND,FACTOR,BM,ROTSH,KODESH,EKSH,IDK,KFAC,KSPRNG
     1)
      IMPLICIT REAL*8(A-H,O-Z)
C
      COMMON/INFEL/ IMEM,IMEMD,KST,KSTD,LM(6),LMD(6),KGEOM,KGEOMD,
     *                FL,COSA,SINA,EC(4),A(2,6),
     1                BFII,BFJJ,BFIJ,EAL,EKHI3P,EKHJ3P,EKHFL(2),
     *                KODYX3(2),ND(4),
     2                KODYFL(2),BMYFL(2,6),RYFL(2,6),INDFL(2),INDUM(2),
     *                EKEPFL(2,6),REVPFL(2),
     3                BMTOT(2),SFTOT(2),FTOT(2),RTOTFL(2),RTPPFL(2),
     4                RTPNFL(2),RTSPFL(2),RTSNFL(2),SENP(8),SENN(8),
     5                TENP(8),TENN(8),SDACT(3),NODI,NODJ,KOUTDT,KDUM(3),
     6                EK1(2),RY1(2,2),RA(2,2),RB(2,2),BMA(2,2),BMB(2,2),
     7                RREC(2,2),ALPHA(2),BETA(2),EEXP
      COMMON/INFEL/   EKHI1P,EKHJ1P,EKHSL(2),KODYX1(2),KODYSL(2),
     +                BMYSL(2,17),RYSL(2,17),INDSL(2),EKEPSL(2,18),
     +                REVPSL(2,2),RTOTSL(2),RTPPSL(2),RTPNSL(2),
     +                RTSPSL(2),RTSNSL(2),SLRENP(2),SLRENN(2),
     +                TSLENP(2),TSLENN(2),
     +                MINDSL(2),EKUG(2,2),ROTUG(2,2),BMPIN(2,2),
     +                ROTPIN(2,2),RVPCSL(2,2),IPP(2,2),BMO(2,2),
     +                REVPMO(2,2),KDPSSL(2)
      COMMON/INFEL/   EKHI2P,EKHJ2P,EKHSH(2),KODYX2(2),KODYSH(2),
     +                BMYSH(2,16),RYSH(2,16),INDSH(2),EKEPSH(2,15),
     +                REVPSH(2,2),RTOTSH(2),RTPPSH(2),RTPNSH(2),
     +                RTSPSH(2),RTSNSH(2),SHRENP(2),SHRENN(2),
     +                TSHENP(2),TSHENN(2),
     +                RTOT(2),RTENP(2),RTENN(2),TRTENP(2),TRTENN(2),
```

```
+                 BMCR(2,2),RCR(2,2),MINDSH(2),RMAX(2,2),EKY(2,2),
+                 BMP(2,2),ROTP(2,2),BMPP(2,2),BMMP(2,2),ROTCRI(2,2),
+                 BMPN(2,2),ROTPN(2,2),BMPPN(2,2),RANGEL(2,2),
+                 RANGEU(2,2),RN(2,2),BETASH(2,2),GAMMA(2,2),
+                 BMMPN(2,2),KFLAG1(2),KFLAG2(2),REVPCR(2,2),
+                 KDPSSH(2)
      COMMON/INFEL/  EYRFL(2,2),ECRSH(2,2),EYRSH(2,2),EYR(2,2),ESRFL(2),
+                 ESRSH(2),ESRSL(2),ESRC(2),SENPFL(2),SENNFL(2),
+                 SENPSH(2),SENNSH(2),SENPSL(2),SENNSL(2),SENPC(2),
+                 SENNC(2),DFFL(2,2),DFSH(2,2),DFSL(2,2),DFC(2,2),
+                 EENGFL(2),ENGFL(2),EDFFL(2),EENGSH(2),ENGSH(2),
+                 EDFSH(2),EENGSL(2),ENGSL(2),EDFSL(2),TEENG(2),
+                 TENG(2),TDEF(2),
+                 PRBM(2),EIL,GAL2,P,P0,
+                 RYSHTL(2,16),RCRTL(2,2),RMAXTL(2,2),RMAXPL(2,2),
+                 ROTPTL(2,2),ROTPNT(2,2),REST(19)
      COMMON /WORK/  DVRI,DVRJ,BML(2),DBM(2),MINDFL(2),ST(2,2),W(4839)
C
      IF(P0.EQ.0.)THEN
      ALPHSH=-0.14
      ELSE
      ALPHSH=0.82*(P/P0)-0.14
      END IF
      IF(ALPHSH.GT.0.) ALPHSH=0.
C
C
C     SET REVERSAL SHEAR INDICATOR.
      REMIND=1
      IF(INDSH(IEND).EQ.2) REMIND=-1
C
C     RULE 1. LOADING ELASTICALLY IN THE POSITIVE DIRECTION.
C
      IF(KODYSH(IEND).NE.1)GO TO 30
      IF(REMIND*DBM(IEND).LT.0.)GO TO 20
```

```
      FAC=(BMCR(IEND,1)-BMTOT(IEND))/DBM(IEND)
      IF(FAC.GE.FACTOR)GO TO 300
      FACTOR=FAC
      BM=BMCR(IEND,1)
      ROTSH=RCR(IEND,1)
      KFAC=IEND
      KSPRNG=2
      KODESH=3
      EKSH=EKEPSH(IEND,3)
      IDK=1
      GO TO 300
   20 FAC=-BMTOT(IEND)/DBM(IEND)
      IF(FAC.GE.FACTOR)GO TO 300
      FACTOR=FAC
      BM=0.
      ROTSH=0.
      KFAC=IEND
      KSPRNG=2
      KODESH=2
      EKSH=EKEPSH(IEND,2)
      IDK=2
      GO TO 300
   30 KODSH=KODYSH(IEND)
      GO TO (40,40,60,80,100,120,140,160,180,200,220,240,260,280)KODSH
C
C     RULE2. LOADING ELASTICALLY IN THE NEGATIVE DIRECTION.
C
   40 IF(REMIND*DBM(IEND).LT.0.)GO TO 50
      FAC=(BMCR(IEND,2)-BMTOT(IEND))/DBM(IEND)
      IF(FAC.GE.FACTOR)GO TO 300
      FACTOR=FAC
      BM=BMCR(IEND,2)
      ROTSH=RCR(IEND,2)
      KFAC=IEND
```

```
      KSPRNG=2
      KODESH=3
      EKSH=EKEPSH(IEND,4)
      IDK=2
      GO TO 300
   50 FAC=-BMTOT(IEND)/DBM(IEND)
      IF(FAC.GE.FACTOR)GO TO 300
      FACTOR=FAC
      BM=0.
      ROTSH=0.
      KFAC=IEND
      KSPRNG=2
      KODESH=1
      EKSH=EKEPSH(IEND,1)
      IDK=1
      GO TO 300
C
C     RULE. 3 LOADING ON THE PRIMARY CURVE BETWEEN CRACKING AND YIELD
C             POINTS

   60 IDD=INDSH(IEND)
      IF(REMIND*DBM(IEND).LT.0.)GO TO 70
      MINDSH(IEND)=IDD+2
      KDPSSH(IEND)=KODSH
      IKK=IDD+4
      FAC=(BMYSH(IEND,IDD)-BMTOT(IEND))/DBM(IEND)
      IF(FAC.GE.FACTOR)GO TO 300
      FACTOR=FAC
      BM=BMYSH(IEND,IDD)
      ROTSH=RYSH(IEND,IDD)
      KFAC=IEND
      KSPRNG=2
      KODESH=5
      EKSH=EKEPSH(IEND,IKK)
```

```
      IDK=IDD
      GO TO 300
   70 KODYSH(IEND)=4
      IDB=3-IDD
      IKK=IDD+2
      IRR=IDD+7
      IUC=IDD+9
      EKU=(BMYSH(IEND,IKK)-BMCR(IEND,IDB))/(RYSH(IEND,IKK)-RCR(IEND,IDB)
     1)
      RMAX(IEND,IDD)=RYSH(IEND,IKK)
      RN(IEND,IDD)=1.
      EKEPSH(IEND,7)=EKU
      EKEPSH(IEND,IRR)=EKEPSH(IEND,7)
      EKEPSH(IEND,IUC)=EKEPSH(IEND,7)
      EKHSH(IEND)=EKEPSH(IEND,7)
      REVPSH(IEND,IDD)=RYSH(IEND,IKK)-BMYSH(IEND,IKK)/EKU
C     IF(IMEM.EQ.3.AND.IEND.EQ.1)WRITE(6,*)REVPSH(IEND,IDD),EKHSH(IEND)
C
C     DETERMINE THE COORDINATES OF BMMP AND BMPP
C
      RYSHTL(IEND,IKK)=RYSH(IEND,IKK)+BMYSH(IEND,IKK)/GAL2
      BETASH(IEND,IDD)=-0.014*DSQRT(RYSHTL(IEND,IKK)/RYSHTL(IEND,IDD))
      GAMMA(IEND,IDD)=-0.01*DSQRT(RN(IEND,IDD))
      BMP(IEND,IDD)=BMYSH(IEND,IKK)
      ROTPTL(IEND,IDD)=RYSHTL(IEND,IKK)
      BMPP(IEND,IDD)=BMP(IEND,IDD)*DEXP(ALPHSH*ROTPTL(IEND,IDD)/RYSHTL(I
     1END,IDD))
      BMMP(IEND,IDD)=BMYSH(IEND,IKK)*DEXP(BETASH(IEND,IDD)*RN(IEND,IDD)+
     1GAMMA(IEND,IDD)*(RYSHTL(IEND,IKK)/RYSHTL(IEND,IDD)))
      IF(DABS(BMPP(IEND,IDD)).LE.DABS(BMCR(IEND,IDD)))THEN
      BMPP(IEND,IDD)=1.01*BMCR(IEND,IDD)
        IF(DABS(BMPP(IEND,IDD)).GT.DABS(BMP(IEND,IDD))) THEN
        BMPP(IEND,IDD)=BMP(IEND,IDD)
        ELSE
```

```
          END IF
         ELSE
         END IF
         IF(DABS(BMMP(IEND,IDD)).LT.DABS(BMPP(IEND,IDD)))THEN
         BMMP(IEND,IDD)=BMPP(IEND,IDD)
         ELSE
         END IF
         RMAXTL(IEND,IDD)=RYSHTL(IEND,IKK)
         RMAXPL(IEND,IDD)=RMAXTL(IEND,IDD)-BMMP(IEND,IDD)/GAL2
         ROTP(IEND,IDD)=ROTPTL(IEND,IDD)-BMPP(IEND,IDD)/GAL2
         KFAC=0
         KSPRNG=0
         FACTOR=0.
         GO TO 300
C
C        RULE. 4 UNLOADING FROM PRIMARY CURVE AFTER RULE 3.
C
   80    IDD=INDSH(IEND)
         IKK=IDD+2
         IF(REMIND*DBM(IEND).LT.0.)GO TO 90
         FAC=(BMYSH(IEND,IKK)-BMTOT(IEND))/DBM(IEND)
         IF(FAC.GE.FACTOR)GO TO 300
         FACTOR=FAC
         BM=BMYSH(IEND,IKK)
         ROTSH=RYSH(IEND,IKK)
         KFAC=IEND
         KSPRNG=2
         KODESH=3
         EKSH=EKEPSH(IEND,IKK)
         IDK=IDD
         GO TO 300
   90    FAC=-BMTOT(IEND)/DBM(IEND)
         IF(FAC.GE.FACTOR)GO TO 300
         FACTOR=FAC
```

```
      BM=0.
      ROTSH=REVPSH(IEND,IDD)
      KFAC=IEND
      KSPRNG=2
      KODESH=9
      IDK=3-IDD
      IDB=IDK
      IRR=IDB+2
      IKK=IDB+4
C
C     CALCULATE RELOADING SLOPE.
C
      IF(DABS(RMAX(IEND,IDB)).EQ.DABS(RCR(IEND,IDB)))THEN
      EKLSH=EKEPSH(IEND,7)
      ELSE
      EKLSH=BMPP(IEND,IDB)/(ROTP(IEND,IDB)-REVPSH(IEND,IDD))
      END IF
      EKEPSH(IEND,13)=EKLSH
      EKSH=EKEPSH(IEND,13)
C
C     DETERMINE THE BREAKING POINTS AT CRACKING LOAD AND AT THE PRIMARY
C     CURVE.
C
      RREMIN=-1.*REMIND
      IPC=IDB+14
      IF(DABS(RMAX(IEND,IDB)).EQ.DABS(RCR(IEND,IDB))) THEN
      ROTCRI(IEND,IDB)=RCR(IEND,IDB)
      KFLAG1(IEND)=3
      ELSE IF(DABS(RMAX(IEND,IDB)).LT.DABS(RYSH(IEND,IDB)))THEN
      ROTCRI(IEND,IDB)=REVPSH(IEND,IDD)+BMCR(IEND,IDB)/EKEPSH(IEND,13)
      IF(RREMIN*ROTCRI(IEND,IDB).GE.DABS(RMAXPL(IEND,IDB)))THEN
      ROTCRI(IEND,IDB)=0.99*RMAXPL(IEND,IDB)
        IF(RREMIN*ROTCRI(IEND,IDB).LE.RREMIN*REVPSH(IEND,IDD))THEN
           IF(BMCR(IEND,IDB)*ROTCRI(IEND,IDB).LT.0.)THEN
```

```
         REVPSH(IEND,IDD)=1.01*ROTCRI(IEND,IDB)
         ELSE
         REVPSH(IEND,IDD)=0.99*ROTCRI(IEND,IDB)
         END IF
       ROTSH=REVPSH(IEND,IDD)
       ELSE
       END IF
     EKEPSH(IEND,13)=BMCR(IEND,IDB)/(ROTCRI(IEND,IDB)-REVPSH(IEND,IDD))
     EKSH=EKEPSH(IEND,13)
     ELSE
     END IF
     EKEPSH(IEND,14)=(BMMP(IEND,IDB)-BMCR(IEND,IDB))/(RMAXPL(IEND,IDB)-
    1ROTCRI(IEND,IDB))
     IF(RREMIN*ROTCRI(IEND,IDB).LE.DABS(RCR(IEND,IDB)).AND.DABS(EKEPSH(
    1IEND,14)).GE.DABS(EKEPSH(IEND,IRR))) THEN
     RYSH(IEND,IPC)=RYSH(IEND,IRR)
     BMYSH(IEND,IPC)=BMYSH(IEND,IRR)
     EKEPSH(IEND,14)=(BMYSH(IEND,IPC)-BMCR(IEND,IDB))/(RYSH(IEND,IPC)-R
    1OTCRI(IEND,IDB))
     KFLAG1(IEND)=11
     KFLAG2(IEND)=3
     ELSE
     IF(DABS(EKEPSH(IEND,14)).LE.DABS(EKEPSH(IEND,IRR))) GO TO 95
     RYSH(IEND,IPC)=(RCR(IEND,IDB)*EKEPSH(IEND,IRR)-ROTCRI(IEND,IDB)*EK
    1EPSH(IEND,14))/(EKEPSH(IEND,IRR)-EKEPSH(IEND,14))
     IF(DABS(RYSH(IEND,IPC)).GE.DABS(RYSH(IEND,IDB)))THEN
95   IF(DABS(EKEPSH(IEND,14)).LE.DABS(EKEPSH(IEND,IKK))) THEN
     BMYSH(IEND,IPC)=BMYSH(IEND,IDB)
     RYSH(IEND,IPC)=RYSH(IEND,IDB)
      IF(RREMIN*ROTCRI(IEND,IDB).GE.DABS(RYSH(IEND,IDD))) THEN
      ROTCRI(IEND,IDB)=0.99*RYSH(IEND,IDB)
       IF(RREMIN*ROTCRI(IEND,IDB).LE.RREMIN*REVPSH(IEND,IDD))THEN
          IF(BMCR(IEND,IDB)*ROTCRI(IEND,IDB).LT.0.)THEN
          REVPSH(IEND,IDD)=1.01*ROTCRI(IEND,IDB)
```

```
      ELSE
      REVPSH(IEND,IDD)=0.99*ROTCRI(IEND,IDB)
      END IF
    ROTSH=REVPSH(IEND,IDD)
    ELSE
    END IF
   EKEPSH(IEND,13)=BMCR(IEND,IDB)/(ROTCRI(IEND,IDB)-REVPSH(IEND,IDD)
 1 )
   EKSH=EKEPSH(IEND,13)
   ELSE
   END IF
  EKEPSH(IEND,14)=(BMYSH(IEND,IDB)-BMCR(IEND,IDB))/(RYSH(IEND,IDB)-
 1ROTCRI(IEND,IDB))
  ELSE
  RYSH(IEND,IPC)=(BMYSH(IEND,IDB)-BMCR(IEND,IDB)+EKEPSH(IEND,14)*ROT
 1CRI(IEND,IDB)-EKEPSH(IEND,IKK)*RYSH(IEND,IDB))/(EKEPSH(IEND,14)-EK
 2EPSH(IEND,IKK))
  BMYSH(IEND,IPC)=BMYSH(IEND,IDB)+EKEPSH(IEND,IKK)*(RYSH(IEND,IPC)-R
 1YSH(IEND,IDB))
  END IF
  KFLAG1(IEND)=11
  KFLAG2(IEND)=5
  ELSE
  BMYSH(IEND,IPC)=BMCR(IEND,IDB)+EKEPSH(IEND,IRR)*(RYSH(IEND,IPC)-RC
 1R(IEND,IDB))
  KFLAG1(IEND)=11
  KFLAG2(IEND)=3
  END IF
  END IF
  ELSE
  ROTCRI(IEND,IDB)=REVPSH(IEND,IDD)+BMCR(IEND,IDB)/EKEPSH(IEND,13)
  IF(RREMIN*ROTCRI(IEND,IDB).GE.DABS(RMAXPL(IEND,IDB)))THEN
  ROTCRI(IEND,IDB)=0.99*RMAXPL(IEND,IDB)
    IF(RREMIN*ROTCRI(IEND,IDB).LE.RREMIN*REVPSH(IEND,IDD))THEN
```

```
        IF(BMCR(IEND,IDB)*ROTCRI(IEND,IDB).LT.0.)THEN
        REVPSH(IEND,IDD)=1.01*ROTCRI(IEND,IDB)
        ELSE
        REVPSH(IEND,IDD)=0.99*ROTCRI(IEND,IDB)
        END IF
     ROTSH=REVPSH(IEND,IDD)
     ELSE
     END IF
   EKEPSH(IEND,13)=BMCR(IEND,IDB)/(ROTCRI(IEND,IDB)-REVPSH(IEND,IDD))
   EKSH=EKEPSH(IEND,13)
   ELSE
   END IF
   EKEPSH(IEND,14)=(BMMP(IEND,IDB)-BMCR(IEND,IDB))/(RMAXPL(IEND,IDB)-
  1ROTCRI(IEND,IDB))
   IF(RREMIN*ROTCRI(IEND,IDB).LE.DABS(RCR(IEND,IDB)).AND.DABS(EKEPSH(
  1IEND,14)).GE.DABS(EKEPSH(IEND,IRR))) THEN
   RYSH(IEND,IPC)=RYSH(IEND,IKK)
   BMYSH(IEND,IPC)=BMYSH(IEND,IKK)
   EKEPSH(IEND,14)=(BMYSH(IEND,IPC)-BMCR(IEND,IDB))/(RYSH(IEND,IPC)-R
  1OTCRI(IEND,IDB))
   KFLAG1(IEND)=11
   KFLAG2(IEND)=5
   ELSE
C
C     BREAKING POINT ON THE PRIMARY CURVE.
C
   IF(DABS(EKEPSH(IEND,14)).LE.DABS(EKEPSH(IEND,IKK))) THEN
   BMYSH(IEND,IPC)=BMYSH(IEND,IKK)
   RYSH(IEND,IPC)=RYSH(IEND,IKK)
    IF(RREMIN*ROTCRI(IEND,IDB).GE.DABS(RYSH(IEND,IKK))) THEN
    ROTCRI(IEND,IDB)=0.99*RYSH(IEND,IKK)
     IF(RREMIN*ROTCRI(IEND,IDB).LE.RREMIN*REVPSH(IEND,IDD))THEN
        IF(BMCR(IEND,IDB)*ROTCRI(IEND,IDB).LT.0.)THEN
        REVPSH(IEND,IDD)=1.01*ROTCRI(IEND,IDB)
```

```
              ELSE
              REVPSH(IEND,IDD)=0.99*ROTCRI(IEND,IDB)
              END IF
            ROTSH=REVPSH(IEND,IDD)
            ELSE
            END IF
           EKEPSH(IEND,13)=BMCR(IEND,IDB)/(ROTCRI(IEND,IDB)-REVPSH(IEND,IDD)
     1 )
           EKSH=EKEPSH(IEND,13)
           ELSE
           END IF
          EKEPSH(IEND,14)=(BMYSH(IEND,IKK)-BMCR(IEND,IDB))/(RYSH(IEND,IKK)-
     1ROTCRI(IEND,IDB))
          ELSE
          RYSH(IEND,IPC)=(BMYSH(IEND,IDB)-BMCR(IEND,IDB)+EKEPSH(IEND,14)*ROT
     1CRI(IEND,IDB)-EKEPSH(IEND,IKK)*RYSH(IEND,IDB))/(EKEPSH(IEND,14)-EK
     2EPSH(IEND,IKK))
          BMYSH(IEND,IPC)=BMYSH(IEND,IDB)+EKEPSH(IEND,IKK)*(RYSH(IEND,IPC)-R
     1YSH(IEND,IDB))
          END IF
          KFLAG1(IEND)=11
          KFLAG2(IEND)=5
          END IF
          END IF
          GO TO 300
C
C         RULE. 5 LOADING ON THE PRIMARY CURVE AFTER YIELDING.
C
  100     IDD=INDSH(IEND)
          IDB=3-IDD
          IKK=IDD+4
          IF(REMIND*DBM(IEND).LT.0.) GO TO 110
          MINDSH(IEND)=IKK
          GO TO 300
```

```
 110  KODYSH(IEND)=6
      IUC=IDD+7
      RMAX(IEND,IDD)=RYSH(IEND,IKK)
C
C     DETERMINE UNLOADING SLOPE ABOVE MCR.
C
C     EKU=EKY(IEND,IDD)*(1.-0.05*RYSH(IEND,IKK)/RYSH(IEND,IDD))
      RYSHTL(IEND,IKK)=RYSH(IEND,IKK)+BMYSH(IEND,IKK)/GAL2
      SLR= 1-0.05*RYSHTL(IEND,IKK)/RYSHTL(IEND,IDD)
      EKU=SLR*EKY(IEND,IDD)/((1-SLR)*EKY(IEND,IDD)/GAL2+1.)
C
C     CHECK AGAINST MINIMUM SLOPE.
C
      IF(DABS(RMAX(IEND,IDB)).EQ.DABS(RCR(IEND,IDB)))THEN
      EKUMIN=(BMCR(IEND,IDB)-BMYSH(IEND,IKK))/(RCR(IEND,IDB)-RYSH(IEND,I
     1KK))
      ELSE
      EKUMIN=(BMPP(IEND,IDB)-BMYSH(IEND,IKK))/(ROTP(IEND,IDB)-RYSH(IEND,
     1IKK))
      END IF
      IF(EKU.LT.EKUMIN) EKU=EKUMIN
      IF(EKU.LT.EKEPSH(IEND,IKK)) EKU=EKEPSH(IEND,IKK)
      EKEPSH(IEND,IUC)=EKU
      EKHSH(IEND)=EKEPSH(IEND,IUC)
C
C     DETERMINE THE COORDINATES OF BMMP AND BMPP
C
      BETASH(IEND,IDD)=-0.014*DSQRT(RYSHTL(IEND,IKK)/RYSHTL(IEND,IDD))
      RN(IEND,IDD)=1.0
      GAMMA(IEND,IDD)=-0.01*DSQRT(RN(IEND,IDD))
      BMP(IEND,IDD)=BMYSH(IEND,IKK)
      ROTPTL(IEND,IDD)=RYSHTL(IEND,IKK)
      BMPP(IEND,IDD)=BMP(IEND,IDD)*DEXP(ALPHSH*ROTPTL(IEND,IDD)/RYSHTL(I
     1END,IDD))
```

```
      BMMP(IEND,IDD)=BMYSH(IEND,IKK)*DEXP(BETASH(IEND,IDD)*RN(IEND,IDD)+
     1GAMMA(IEND,IDD)*(RYSHTL(IEND,IKK)/RYSHTL(IEND,IDD)))
      IF(DABS(BMPP(IEND,IDD)).LE.DABS(BMCR(IEND,IDD)))THEN
      BMPP(IEND,IDD)=1.01*BMCR(IEND,IDD)
       IF(DABS(BMPP(IEND,IDD)).GT.DABS(BMP(IEND,IDD))) THEN
       BMPP(IEND,IDD)=BMP(IEND,IDD)
       ELSE
       END IF
      ELSE
      END IF
      IF(DABS(BMMP(IEND,IDD)).LT.DABS(BMPP(IEND,IDD)))THEN
      BMMP(IEND,IDD)=BMPP(IEND,IDD)
      ELSE
      END IF
      RMAXTL(IEND,IDD)=RYSHTL(IEND,IKK)
      RMAXPL(IEND,IDD)=RMAXTL(IEND,IDD)-BMMP(IEND,IDD)/GAL2
      ROTP(IEND,IDD)=ROTPTL(IEND,IDD)-BMPP(IEND,IDD)/GAL2
      REVPCR(IEND,IDD)=RYSH(IEND,IKK)-(BMYSH(IEND,IKK)-BMCR(IEND,IDD))/E
     1KU
      KFAC=0
      KSPRNG=0
      FACTOR=0.
      GO TO 300
C
C   RULE 6. UNLOADING FROM PRIMARY CURVE, MOMENT IS GREATER THAN
C           CRACKING MOMENT.
C
 120  IDD=INDSH(IEND)
      IKK=IDD+4
      IUC=IDD+7
      IF(REMIND*DBM(IEND).LT.0.)GO TO 130
      FAC=(BMYSH(IEND,IKK)-BMTOT(IEND))/DBM(IEND)
      IF(FAC.GE.FACTOR)GO TO 300
      FACTOR=FAC
```

```
      BM=BMYSH(IEND,IKK)
      ROTSH=RYSH(IEND,IKK)
      KFAC=IEND
      KSPRNG=2
      KODESH=5
      EKSH=EKEPSH(IEND,IKK)
      IDK=IDD
      GO TO 300
 130  FAC=(BMCR(IEND,IDD)-BMTOT(IEND))/DBM(IEND)
      IF(FAC.GE.FACTOR)GO TO 300
      FACTOR=FAC
      BM=BMCR(IEND,IDD)
      ROTSH=REVPCR(IEND,IDD)
      KFAC=IEND
      KSPRNG=2
      KODESH=7
      IDB=3-IDD
C
C     DETERMINE UNLOADING SLOPE BELOW MCR.
C
      SLR=0.6*(1-0.07*RYSHTL(IEND,IKK)/RYSHTL(IEND,IDD))
      EKU=SLR*EKY(IEND,IDD)/((1-SLR)*EKY(IEND,IDD)/GAL2+1.)
C
C     CHECK AGAINST MINIMUM UNLOADING SLOPE.
C
      IF(DABS(RMAX(IEND,IDB)).EQ.DABS(RCR(IEND,IDB)))THEN
      EKUMIN=(BMCR(IEND,IDB)-BMCR(IEND,IDD))/(RCR(IEND,IDB)-REVPCR(IEND,
     1IDD))
      ELSE
      EKUMIN=(BMPP(IEND,IDB)-BMCR(IEND,IDD))/(ROTP(IEND,IDB)-REVPCR(IEND
     1,IDD))
      END IF
      IF(EKU.LT.EKUMIN) EKU=EKUMIN
      IUC=IDD+9
```

```
      EKEPSH(IEND,IUC)=EKU
      EKSH=EKEPSH(IEND,IUC)
      REVPSH(IEND,IDD)=REVPCR(IEND,IDD)-BMCR(IEND,IDD)/EKEPSH(IEND,IUC)
      IDK=IDD
      GO TO 300
C
C     RULE 7. UNLOADING FROM PRIMARY CURVE, MOMENT IS BELOW MCR.
C
 140  IDD=INDSH(IEND)
      IF(REMIND*DBM(IEND).LT.0.)GO TO 150
      KODYSH(IEND)=8
      IKK=IDD+4
      IRR=IDD+6
      EKRL=(BMYSH(IEND,IKK)-BMYSH(IEND,IRR))/(RYSH(IEND,IKK)-RYSH(IEND,I
     1RR))
      EKEPSH(IEND,12)=EKRL
      EKHSH(IEND)=EKRL
      KFAC=0
      KSPRNG=2
      FACTOR=0.0
      GO TO 300
 150  IDB=3-IDD
      IKK=IDB+4
      IRR=IDB+2
      MINDSH(IEND)=IDD+6
      KDPSSH(IEND)=KODSH
      FAC=-BMTOT(IEND)/DBM(IEND)
      IF(FAC.GE.FACTOR)GO TO 300
      FACTOR=FAC
      BM=0.
      ROTSH=REVPSH(IEND,IDD)
      KFAC=IEND
      KSPRNG=2
      KODESH=9
```

```
      IDK=3-IDD
C
C     DETERMINE INITIAL RELOADING SLOPE.
C
      IF(DABS(RMAX(IEND,IDB)).EQ.DABS(RCR(IEND,IDB)))THEN
      EKLSH=BMCR(IEND,IDB)/(RCR(IEND,IDB)-REVPSH(IEND,IDD))
      ELSE
      EKLSH=BMPP(IEND,IDB)/(ROTP(IEND,IDB)-REVPSH(IEND,IDD))
      END IF
      EKEPSH(IEND,13)=EKLSH
      EKSH=EKLSH
C
C     DETERMINE THE BREAKING POINTS AT CRACKING LOAD AND AT THE PRIMARY
C     CURVE.
C
      RREMIN=-1.*REMIND
      IPC=IDB+14
      IF(DABS(RMAX(IEND,IDB)).EQ.DABS(RCR(IEND,IDB))) THEN
      ROTCRI(IEND,IDB)=RCR(IEND,IDB)
      KFLAG1(IEND)=3
      ELSE IF(DABS(RMAX(IEND,IDB)).LT.DABS(RYSH(IEND,IDB)))THEN
      ROTCRI(IEND,IDB)=REVPSH(IEND,IDD)+BMCR(IEND,IDB)/EKEPSH(IEND,13)
      IF(RREMIN*ROTCRI(IEND,IDB).GE.DABS(RMAXPL(IEND,IDB)))THEN
      ROTCRI(IEND,IDB)=0.99*RMAXPL(IEND,IDB)
        IF(RREMIN*ROTCRI(IEND,IDB).LE.RREMIN*REVPSH(IEND,IDD))THEN
           IF(BMCR(IEND,IDB)*ROTCRI(IEND,IDB).LT.0.)THEN
           REVPSH(IEND,IDD)=1.01*ROTCRI(IEND,IDB)
           ELSE
           REVPSH(IEND,IDD)=0.99*ROTCRI(IEND,IDB)
           END IF
        ROTSH=REVPSH(IEND,IDD)
        ELSE
        END IF
      EKEPSH(IEND,13)=BMCR(IEND,IDB)/(ROTCRI(IEND,IDB)-REVPSH(IEND,IDD))
```

```
      EKSH=EKEPSH(IEND,13)
      ELSE
      END IF
      EKEPSH(IEND,14)=(BMMP(IEND,IDB)-BMCR(IEND,IDB))/(RMAXPL(IEND,IDB)-
     1ROTCRI(IEND,IDB))
      IF(RREMIN*ROTCRI(IEND,IDB).LE.DABS(RCR(IEND,IDB)).AND.DABS(EKEPSH(
     1IEND,14)).GE.DABS(EKEPSH(IEND,IRR))) THEN
      RYSH(IEND,IPC)=RYSH(IEND,IRR)
      BMYSH(IEND,IPC)=BMYSH(IEND,IRR)
      EKEPSH(IEND,14)=(BMYSH(IEND,IPC)-BMCR(IEND,IDB))/(RYSH(IEND,IPC)-R
     1OTCRI(IEND,IDB))
      KFLAG1(IEND)=11
      KFLAG2(IEND)=3
      ELSE
      IF(DABS(EKEPSH(IEND,14)).LE.DABS(EKEPSH(IEND,IRR))) GO TO 155
      RYSH(IEND,IPC)=(RCR(IEND,IDB)*EKEPSH(IEND,IRR)-ROTCRI(IEND,IDB)*EK
     1EPSH(IEND,14))/(EKEPSH(IEND,IRR)-EKEPSH(IEND,14))
      IF(DABS(RYSH(IEND,IPC)).GE.DABS(RYSH(IEND,IDB)))THEN
 155  IF(DABS(EKEPSH(IEND,14)).LE.DABS(EKEPSH(IEND,IKK))) THEN
      BMYSH(IEND,IPC)=BMYSH(IEND,IDB)
      RYSH(IEND,IPC)=RYSH(IEND,IDB)
       IF(RREMIN*ROTCRI(IEND,IDB).GE.DABS(RYSH(IEND,IDB))) THEN
       ROTCRI(IEND,IDB)=0.99*RYSH(IEND,IDB)
        IF(RREMIN*ROTCRI(IEND,IDB).LE.RREMIN*REVPSH(IEND,IDD))THEN
           IF(BMCR(IEND,IDB)*ROTCRI(IEND,IDB).LT.0.)THEN
           REVPSH(IEND,IDD)=1.01*ROTCRI(IEND,IDB)
           ELSE
           REVPSH(IEND,IDD)=0.99*ROTCRI(IEND,IDB)
           END IF
        ROTSH=REVPSH(IEND,IDD)
        ELSE
        END IF
       EKEPSH(IEND,13)=BMCR(IEND,IDB)/(ROTCRI(IEND,IDB)-REVPSH(IEND,IDD)
     1 )
```

```
 EKSH=EKEPSH(IEND,13)
 ELSE
 END IF
 EKEPSH(IEND,14)=(BMYSH(IEND,IDB)-BMCR(IEND,IDB))/(RYSH(IEND,IDB)-
1ROTCRI(IEND,IDB))
 ELSE
 RYSH(IEND,IPC)=(BMYSH(IEND,IDB)-BMCR(IEND,IDB)+EKEPSH(IEND,14)*ROT
1CRI(IEND,IDB)-EKEPSH(IEND,IKK)*RYSH(IEND,IDB))/(EKEPSH(IEND,14)-EK
2EPSH(IEND,IKK))
 BMYSH(IEND,IPC)=BMYSH(IEND,IDB)+EKEPSH(IEND,IKK)*(RYSH(IEND,IPC)-R
1YSH(IEND,IDB))
 END IF
 KFLAG1(IEND)=11
 KFLAG2(IEND)=5
 ELSE
 BMYSH(IEND,IPC)=BMCR(IEND,IDB)+EKEPSH(IEND,IRR)*(RYSH(IEND,IPC)-RC
1R(IEND,IDB))
 KFLAG1(IEND)=11
 KFLAG2(IEND)=3
 END IF
 END IF
 ELSE
 ROTCRI(IEND,IDB)=REVPSH(IEND,IDD)+BMCR(IEND,IDB)/EKEPSH(IEND,13)
 IF(RREMIN*ROTCRI(IEND,IDB).GE.DABS(RMAXPL(IEND,IDB)))THEN
 ROTCRI(IEND,IDB)=0.99*RMAXPL(IEND,IDB)
   IF(RREMIN*ROTCRI(IEND,IDB).LE.RREMIN*REVPSH(IEND,IDD))THEN
      IF(BMCR(IEND,IDB)*ROTCRI(IEND,IDB).LT.0.)THEN
      REVPSH(IEND,IDD)=1.01*ROTCRI(IEND,IDB)
      ELSE
      REVPSH(IEND,IDD)=0.99*ROTCRI(IEND,IDB)
      END IF
   ROTSH=REVPSH(IEND,IDD)
   ELSE
   END IF
```

```
      EKEPSH(IEND,13)=BMCR(IEND,IDB)/(ROTCRI(IEND,IDB)-REVPSH(IEND,IDD))
      EKSH=EKEPSH(IEND,13)
      ELSE
      END IF
      EKEPSH(IEND,14)=(BMMP(IEND,IDB)-BMCR(IEND,IDB))/(RMAXPL(IEND,IDB)-
     1ROTCRI(IEND,IDB))
      IF(RREMIN*ROTCRI(IEND,IDB).LE.DABS(RCR(IEND,IDB)).AND.DABS(EKEPSH(
     1IEND,14)).GE.DABS(EKEPSH(IEND,IRR))) THEN
      RYSH(IEND,IPC)=RYSH(IEND,IKK)
      BMYSH(IEND,IPC)=BMYSH(IEND,IKK)
      EKEPSH(IEND,14)=(BMYSH(IEND,IPC)-BMCR(IEND,IDB))/(RYSH(IEND,IPC)-R
     1OTCRI(IEND,IDB))
      KFLAG1(IEND)=11
      KFLAG2(IEND)=5
      ELSE
C
C     BREAKING POINT ON THE PRIMARY CURVE.
C
      IF(DABS(EKEPSH(IEND,14)).LE.DABS(EKEPSH(IEND,IKK))) THEN
      BMYSH(IEND,IPC)=BMYSH(IEND,IKK)
      RYSH(IEND,IPC)=RYSH(IEND,IKK)
       IF(RREMIN*ROTCRI(IEND,IDB).GE.DABS(RYSH(IEND,IKK))) THEN
       ROTCRI(IEND,IDB)=0.99*RYSH(IEND,IKK)
        IF(RREMIN*ROTCRI(IEND,IDB).LE.RREMIN*REVPSH(IEND,IDD))THEN
           IF(BMCR(IEND,IDB)*ROTCRI(IEND,IDB).LT.0.)THEN
           REVPSH(IEND,IDD)=1.01*ROTCRI(IEND,IDB)
           ELSE
           REVPSH(IEND,IDD)=0.99*ROTCRI(IEND,IDB)
           END IF
        ROTSH=REVPSH(IEND,IDD)
        ELSE
        END IF

       EKEPSH(IEND,13)=BMCR(IEND,IDB)/(ROTCRI(IEND,IDB)-REVPSH(IEND,IDD)
```

```
     1 )
       EKSH=EKEPSH(IEND,13)
       ELSE
       END IF
      EKEPSH(IEND,14)=(BMYSH(IEND,IKK)-BMCR(IEND,IDB))/(RYSH(IEND,IKK)-
     1ROTCRI(IEND,IDB))
      ELSE
      RYSH(IEND,IPC)=(BMYSH(IEND,IDB)-BMCR(IEND,IDB)+EKEPSH(IEND,14)*ROT
     1CRI(IEND,IDB)-EKEPSH(IEND,IKK)*RYSH(IEND,IDB))/(EKEPSH(IEND,14)-EK
     2EPSH(IEND,IKK))
      BMYSH(IEND,IPC)=BMYSH(IEND,IDB)+EKEPSH(IEND,IKK)*(RYSH(IEND,IPC)-R
     1YSH(IEND,IDB))
      END IF
      KFLAG1(IEND)=11
      KFLAG2(IEND)=5
      END IF
      END IF
      GO TO 300
C
C     RULE 8. RELOADING AFTER RULE 7.
C
 160  IDD=INDSH(IEND)
      IKK=IDD+4
      IF(REMIND*DBM(IEND).LT.0.0)GO TO 170
      FAC=(BMYSH(IEND,IKK)-BMTOT(IEND))/DBM(IEND)
      IF(FAC.GE.FACTOR)GO TO 300
      FACTOR=FAC
      BM=BMYSH(IEND,IKK)
      ROTSH=RYSH(IEND,IKK)
      KFAC=IEND
      KSPRNG=2
      KODESH=5
      EKSH=EKEPSH(IEND,IKK)
      IDK=IDD
```

```
      GO TO 300
  170 IKK=IDD+9
      IRR=IDD+6
      FAC=(BMYSH(IEND,IRR)-BMTOT(IEND))/DBM(IEND)
      IF(FAC.GE.FACTOR)GO TO 300
      FACTOR=FAC
      BM=BMYSH(IEND,IRR)
      ROTSH=RYSH(IEND,IRR)
      KFAC=IEND
      KSPRNG=2
      KODESH=7
      EKSH=EKEPSH(IEND,IKK)
      IDK=IDD
      GO TO 300
C
C     RULE 9. RELOADING TO THE PRIMARY CURVE AFTER RULE 7, LOAD IS BELOW
C             CRACKING.
C
  180 IDD=INDSH(IEND)
      IRR=IDD+2
      MINDSH(IEND)=IDD+8
      IF(REMIND*DBM(IEND).LT.0.)GO TO 190
      FAC=(BMCR(IEND,IDD)-BMTOT(IEND))/DBM(IEND)
      IF(FAC.GE.FACTOR)GO TO 300
      FACTOR=FAC
      BM=BMCR(IEND,IDD)
      ROTSH=ROTCRI(IEND,IDD)
      KFAC=IEND
      KSPRNG=2
      IF(KFLAG1(IEND).EQ.3)THEN
      KODESH=3
      EKSH=EKEPSH(IEND,IRR)
      ELSE
      KODESH=11
```

```
      EKSH=EKEPSH(IEND,14)
      END IF
      IDK=IDD
      GO TO 300
 190  KODYSH(IEND)=10
      IDB=3-IDD
      IKK=IDD+9
      IRR=IDD+8
      IF(DABS(RMAX(IEND,IDD)).EQ.DABS(RCR(IEND,IDD)))THEN
      EKHSH(IEND)=EKEPSH(IEND,IDD)
      ELSE
      EKHSH(IEND)=EKEPSH(IEND,IKK)
      END IF
C
C     CHECK FOR MINIMUM SLOPE.
C
      IF(DABS(RMAX(IEND,IDB)).EQ.DABS(RCR(IEND,IDB))) THEN
      EKUMIN=(BMCR(IEND,IDB)-BMYSH(IEND,IRR))/(RCR(IEND,IDB)-RYSH(IEND,I
     1RR))
      ELSE
      EKUMIN=(BMPP(IEND,IDB)-BMYSH(IEND,IRR))/(ROTP(IEND,IDB)-RYSH(IEND,
     1IRR))
      END IF
      IF(DABS(EKHSH(IEND)).LT.DABS(EKUMIN))  EKHSH(IEND)=EKUMIN
      IF(DABS(EKHSH(IEND)).LT.DABS(EKEPSH(IEND,13)))  EKHSH(IEND)=EKEPSH
     1(IEND,13)
      REVPSH(IEND,IDD)=RYSH(IEND,IRR)-BMYSH(IEND,IRR)/EKHSH(IEND)
      KFAC=0
      KSPRNG=2
      FACTOR=0.
      GO TO 300
C
C     RULE 10. UNLOADING AFTER RULE 9.
C
```

```
200   IDD=INDSH(IEND)
      IKK=IDD+8
      IF(REMIND*DBM(IEND).LT.0.)GO TO 210
      FAC=(BMYSH(IEND,IKK)-BMTOT(IEND))/DBM(IEND)
      IF(FAC.GE.FACTOR)GO TO 300
      FACTOR=FAC
      BM=BMYSH(IEND,IKK)
      ROTSH=RYSH(IEND,IKK)
      KFAC=IEND
      KSPRNG=2
      KODESH=9
      EKSH=EKEPSH(IEND,13)
      IDK=IDD
      GO TO 300
210   FAC=-BMTOT(IEND)/DBM(IEND)
      IF(FAC.GE.FACTOR)GO TO 300
      FACTOR=FAC
      BM=0.
      ROTSH=REVPSH(IEND,IDD)
      KFAC=IEND
      KSPRNG=2
      KODESH=9
      IDK=3-IDD
      IDB=IDK
C
C     DETERMINE INITIAL RELOADING SLOPE.
C
      IF(DABS(RMAX(IEND,IDB)).EQ.DABS(RCR(IEND,IDB)))THEN
      EKLSH=BMCR(IEND,IDB)/(RCR(IEND,IDB)-REVPSH(IEND,IDD))
      ELSE
      EKLSH=BMPP(IEND,IDB)/(ROTP(IEND,IDB)-REVPSH(IEND,IDD))
      END IF
      EKEPSH(IEND,13)=EKLSH
      EKSH=EKLSH
```

```
C
C     DETERMINE THE BREAKING POINTS AT CRACKING LOAD AND AT THE PRIMARY
C     CURVE.
C
      RREMIN=-1.*REMIND
      IRR=IDB+2
      IKK=IDB+4
      IPC=IDB+14
      IF(DABS(RMAX(IEND,IDB)).EQ.DABS(RCR(IEND,IDB))) THEN
      ROTCRI(IEND,IDB)=RCR(IEND,IDB)
      KFLAG1(IEND)=3
      ELSE IF(DABS(RMAX(IEND,IDB)).LT.DABS(RYSH(IEND,IDB)))THEN
      ROTCRI(IEND,IDB)=REVPSH(IEND,IDD)+BMCR(IEND,IDB)/EKEPSH(IEND,13)
      IF(RREMIN*ROTCRI(IEND,IDB).GE.DABS(RMAXPL(IEND,IDB)))THEN
      ROTCRI(IEND,IDB)=0.99*RMAXPL(IEND,IDB)
        IF(RREMIN*ROTCRI(IEND,IDB).LE.RREMIN*REVPSH(IEND,IDD))THEN
           IF(BMCR(IEND,IDB)*ROTCRI(IEND,IDB).LT.0.)THEN
           REVPSH(IEND,IDD)=1.01*ROTCRI(IEND,IDB)
           ELSE
           REVPSH(IEND,IDD)=0.99*ROTCRI(IEND,IDB)
           END IF
        ROTSH=REVPSH(IEND,IDD)
        ELSE
        END IF
      EKEPSH(IEND,13)=BMCR(IEND,IDB)/(ROTCRI(IEND,IDB)-REVPSH(IEND,IDD))
      EKSH=EKEPSH(IEND,13)
      ELSE
      END IF
      EKEPSH(IEND,14)=(BMMP(IEND,IDB)-BMCR(IEND,IDB))/(RMAXPL(IEND,IDB)-
     1ROTCRI(IEND,IDB))
      IF(RREMIN*ROTCRI(IEND,IDB).LE.DABS(RCR(IEND,IDB)).AND.DABS(EKEPSH(
     1IEND,14)).GE.DABS(EKEPSH(IEND,IRR))) THEN
      RYSH(IEND,IPC)=RYSH(IEND,IRR)
      BMYSH(IEND,IPC)=BMYSH(IEND,IRR)
```

```
      EKEPSH(IEND,14)=(BMYSH(IEND,IPC)-BMCR(IEND,IDB))/(RYSH(IEND,IPC)-R
     1OTCRI(IEND,IDB))
      KFLAG1(IEND)=11
      KFLAG2(IEND)=3
      ELSE
      IF(DABS(EKEPSH(IEND,14)).LE.DABS(EKEPSH(IEND,IRR))) GO TO 215
      RYSH(IEND,IPC)=(RCR(IEND,IDB)*EKEPSH(IEND,IRR)-ROTCRI(IEND,IDB)*EK
     1EPSH(IEND,14))/(EKEPSH(IEND,IRR)-EKEPSH(IEND,14))
      IF(DABS(RYSH(IEND,IPC)).GE.DABS(RYSH(IEND,IDB)))THEN
215   IF(DABS(EKEPSH(IEND,14)).LE.DABS(EKEPSH(IEND,IKK))) THEN
      BMYSH(IEND,IPC)=BMYSH(IEND,IDB)
      RYSH(IEND,IPC)=RYSH(IEND,IDB)
       IF(RREMIN*ROTCRI(IEND,IDB).GE.DABS(RYSH(IEND,IDB))) THEN
       ROTCRI(IEND,IDB)=0.99*RYSH(IEND,IDB)
        IF(RREMIN*ROTCRI(IEND,IDB).LE.RREMIN*REVPSH(IEND,IDD))THEN
           IF(BMCR(IEND,IDB)*ROTCRI(IEND,IDB).LT.0.)THEN
           REVPSH(IEND,IDD)=1.01*ROTCRI(IEND,IDB)
           ELSE
           REVPSH(IEND,IDD)=0.99*ROTCRI(IEND,IDB)
           END IF
        ROTSH=REVPSH(IEND,IDD)
        ELSE
        END IF
       EKEPSH(IEND,13)=BMCR(IEND,IDB)/(ROTCRI(IEND,IDB)-REVPSH(IEND,IDD)
     1 )
       EKSH=EKEPSH(IEND,13)
       ELSE
       END IF
      EKEPSH(IEND,14)=(BMYSH(IEND,IDB)-BMCR(IEND,IDB))/(RYSH(IEND,IDB)-
     1ROTCRI(IEND,IDB))
      ELSE
      RYSH(IEND,IPC)=(BMYSH(IEND,IDB)-BMCR(IEND,IDB)+EKEPSH(IEND,14)*ROT
     1CRI(IEND,IDB)-EKEPSH(IEND,IKK)*RYSH(IEND,IDB))/(EKEPSH(IEND,14)-EK
     2EPSH(IEND,IKK))
```

```
 BMYSH(IEND,IPC)=BMYSH(IEND,IDB)+EKEPSH(IEND,IKK)*(RYSH(IEND,IPC)-R
1YSH(IEND,IDB))
 END IF
 KFLAG1(IEND)=11
 KFLAG2(IEND)=5
 ELSE
 BMYSH(IEND,IPC)=BMCR(IEND,IDB)+EKEPSH(IEND,IRR)*(RYSH(IEND,IPC)-RC
1R(IEND,IDB))
 KFLAG1(IEND)=11
 KFLAG2(IEND)=3
 END IF
 END IF
 ELSE
 ROTCRI(IEND,IDB)=REVPSH(IEND,IDD)+BMCR(IEND,IDB)/EKEPSH(IEND,13)
 IF(RREMIN*ROTCRI(IEND,IDB).GE.DABS(RMAXPL(IEND,IDB)))THEN
 ROTCRI(IEND,IDB)=0.99*RMAXPL(IEND,IDB)
   IF(RREMIN*ROTCRI(IEND,IDB).LE.RREMIN*REVPSH(IEND,IDD))THEN
      IF(BMCR(IEND,IDB)*ROTCRI(IEND,IDB).LT.0.)THEN
      REVPSH(IEND,IDD)=1.01*ROTCRI(IEND,IDB)
      ELSE
      REVPSH(IEND,IDD)=0.99*ROTCRI(IEND,IDB)
      END IF
   ROTSH=REVPSH(IEND,IDD)
   ELSE
   END IF
 EKEPSH(IEND,13)=BMCR(IEND,IDB)/(ROTCRI(IEND,IDB)-REVPSH(IEND,IDD))
 EKSH=EKEPSH(IEND,13)
 ELSE
 END IF
 EKEPSH(IEND,14)=(BMMP(IEND,IDB)-BMCR(IEND,IDB))/(RMAXPL(IEND,IDB)-
1ROTCRI(IEND,IDB))
 IF(RREMIN*ROTCRI(IEND,IDB).LE.DABS(RCR(IEND,IDB)).AND.DABS(EKEPSH(
1IEND,14)).GE.DABS(EKEPSH(IEND,IRR))) THEN
 RYSH(IEND,IPC)=RYSH(IEND,IKK)
```

```
      BMYSH(IEND,IPC)=BMYSH(IEND,IKK)
      EKEPSH(IEND,14)=(BMYSH(IEND,IPC)-BMCR(IEND,IDB))/(RYSH(IEND,IPC)-R
     1OTCRI(IEND,IDB))
      KFLAG1(IEND)=11
      KFLAG2(IEND)=5
      ELSE
C
C     BREAKING POINT ON THE PRIMARY CURVE.
C
      IF(DABS(EKEPSH(IEND,14)).LE.DABS(EKEPSH(IEND,IKK))) THEN
      BMYSH(IEND,IPC)=BMYSH(IEND,IKK)
      RYSH(IEND,IPC)=RYSH(IEND,IKK)
       IF(RREMIN*ROTCRI(IEND,IDB).GE.DABS(RYSH(IEND,IKK))) THEN
       ROTCRI(IEND,IDB)=0.99*RYSH(IEND,IKK)
        IF(RREMIN*ROTCRI(IEND,IDB).LE.RREMIN*REVPSH(IEND,IDD))THEN
           IF(BMCR(IEND,IDB)*ROTCRI(IEND,IDB).LT.0.)THEN
           REVPSH(IEND,IDD)=1.01*ROTCRI(IEND,IDB)
           ELSE
           REVPSH(IEND,IDD)=0.99*ROTCRI(IEND,IDB)
           END IF
        ROTSH=REVPSH(IEND,IDD)
        ELSE
        END IF
       EKEPSH(IEND,13)=BMCR(IEND,IDB)/(ROTCRI(IEND,IDB)-REVPSH(IEND,IDD)
     1 )
       EKSH=EKEPSH(IEND,13)
       ELSE
       END IF
      EKEPSH(IEND,14)=(BMYSH(IEND,IKK)-BMCR(IEND,IDB))/(RYSH(IEND,IKK)-
     1ROTCRI(IEND,IDB))
      ELSE
      RYSH(IEND,IPC)=(BMYSH(IEND,IDB)-BMCR(IEND,IDB)+EKEPSH(IEND,14)*ROT
     1CRI(IEND,IDB)-EKEPSH(IEND,IKK)*RYSH(IEND,IDB))/(EKEPSH(IEND,14)-EK
     2EPSH(IEND,IKK))
```

```
      BMYSH(IEND,IPC)=BMYSH(IEND,IDB)+EKEPSH(IEND,IKK)*(RYSH(IEND,IPC)-R
     1YSH(IEND,IDB))
      END IF
      KFLAG1(IEND)=11
      KFLAG2(IEND)=5
      END IF
      END IF
      GO TO 300
C
C     RULE 11. RELOADING TO THE PRIMARY CURVE, LOAD IS ABOVE MCR.
C
  220 IDD=INDSH(IEND)
      IKK=IDD+4
      IPC=IDD+14
      IRR=IDD+2
      IF(REMIND*DBM(IEND).LT.0.)GO TO 230
      MINDSH(IEND)=IDD+10
      FAC=(BMYSH(IEND,IPC)-BMTOT(IEND))/DBM(IEND)
      IF(FAC.GE.FACTOR)GO TO 300
      FACTOR=FAC
      BM=BMYSH(IEND,IPC)
      ROTSH=RYSH(IEND,IPC)
      KFAC=IEND
      KSPRNG=2
      IF(KFLAG2(IEND).EQ.3) THEN
      KODESH=3
      EKSH=EKEPSH(IEND,IRR)
      ELSE
      KODESH=5
      EKSH=EKEPSH(IEND,IKK)
      END IF
      IDK=IDD
      GO TO 300
  230 KODYSH(IEND)=12
```

```
      IDB=3-IDD
      IPC=IDD+2
      NPC=IDD+4
      IKK=IDD+7
      IUC=IDD+9
      IRR=IDD+10
      RANGEU(IEND,IDD)=RMAXTL(IEND,IDD)+RCRTL(IEND,IDD)
      RYSHTL(IEND,IRR)=RYSH(IEND,IRR)+BMYSH(IEND,IRR)/GAL2
      IF(REMIND*(RYSHTL(IEND,IRR)).GT.DABS(RANGEU(IEND,IDD)))THEN
      IF(DABS(RYSHTL(IEND,IRR)).LE.DABS(RYSHTL(IEND,IDD)))THEN
      BMYSH(IEND,IPC)=BMCR(IEND,IDD)+(RYSHTL(IEND,IRR)-RCRTL(IEND,IDD))*
     11./(1./EKEPSH(IEND,IPC)+1./GAL2)
      RYSH(IEND,IPC)=RYSHTL(IEND,IRR)-BMYSH(IEND,IPC)/GAL2
      EKEPSH(IEND,7)=(BMYSH(IEND,IPC)-BMCR(IEND,IDB))/(RYSH(IEND,IPC)-RC
     1R(IEND,IDB))
      EKEPSH(IEND,IKK)=EKEPSH(IEND,7)
      EKEPSH(IEND,IUC)=EKEPSH(IEND,7)
      ELSE
      SLR1=1-0.05*RYSHTL(IEND,IRR)/RYSHTL(IEND,IDD)
      SLR2=0.6*(1-0.07*RYSHTL(IEND,IRR)/RYSHTL(IEND,IDD))
      EKEPSH(IEND,IKK)=SLR1*EKY(IEND,IDD)/((1-SLR1)*EKY(IEND,IDD)/GAL2+
     11)
      EKEPSH(IEND,IUC)=SLR2*EKY(IEND,IDD)/((1-SLR2)*EKY(IEND,IDD)/GAL2+
     11)
      END IF
      ELSE
      END IF
      EKHSH(IEND)=EKEPSH(IEND,IKK)
C
C     CHECK AGAINST MINIMUM SLOPE.
C
      IF(DABS(RMAX(IEND,IDB)).EQ.DABS(RCR(IEND,IDB))) THEN
      EKUMIN=(BMCR(IEND,IDB)-BMYSH(IEND,IRR))/(RCR(IEND,IDB)-RYSH(IEND,I
     1RR))
```

```
      ELSE
      EKUMIN=(BMPP(IEND,IDB)-BMYSH(IEND,IRR))/(ROTP(IEND,IDB)-RYSH(IEND,
     1IRR))
      END IF
      IF(DABS(EKHSH(IEND)).LT.DABS(EKUMIN))  EKHSH(IEND)=EKUMIN
      IF(DABS(EKHSH(IEND)).LT.DABS(EKEPSH(IEND,14)))  EKHSH(IEND)=EKEPSH
     1(IEND,14)
      REVPCR(IEND,IDD)=RYSH(IEND,IRR)-(BMYSH(IEND,IRR)-BMCR(IEND,IDD))/E
     1KHSH(IEND)
C
C     DETERMINE THE COORDINATES OF THE NEW BMPP AND BMMP
C
      BMPN(IEND,IDD)=BMYSH(IEND,IRR)
      ROTPNT(IEND,IDD)=RYSHTL(IEND,IRR)
      BMPPN(IEND,IDD)=BMPN(IEND,IDD)*DEXP(ALPHSH*ROTPNT(IEND,IDD)/RYSHTL
     1(IEND,IDD))
      IF(DABS(BMPPN(IEND,IDD)).LT.DABS(BMPN(IEND,IDD)))THEN
      BMPP(IEND,IDD)=BMPPN(IEND,IDD)
      ROTPTL(IEND,IDD)=ROTPNT(IEND,IDD)
      ROTP(IEND,IDD)=ROTPTL(IEND,IDD)-BMPP(IEND,IDD)/GAL2
      ELSE
      END IF
      RANGEL(IEND,IDD)=RMAXTL(IEND,IDD)-RCRTL(IEND,IDD)
      IF(REMIND*RYSHTL(IEND,IRR).GT.DABS(RYSHTL(IEND,IDD))) THEN
      IF(REMIND*(ROTPTL(IEND,IDD)).GT.DABS(RANGEU(IEND,IDD)))THEN
      RN(IEND,IDD)=1.
      RMAXTL(IEND,IDD)=RYSHTL(IEND,IRR)
      RYSHTL(IEND,NPC)=RMAXTL(IEND,IDD)
      BMYSH(IEND,NPC)=BMYSH(IEND,IDD)+(RYSHTL(IEND,NPC)-RYSHTL(IEND,IDD)
     1)*1./(1./EKEPSH(IEND,NPC)+1./GAL2)
      BETASH(IEND,IDD)=-0.014*DSQRT(RYSHTL(IEND,NPC)/RYSHTL(IEND,IDD))
      GAMMA(IEND,IDD)=-0.01*DSQRT(RN(IEND,IDD))
      BMMPN(IEND,IDD)=BMYSH(IEND,NPC)*DEXP(BETASH(IEND,IDD)*RN(IEND,IDD)
     1+GAMMA(IEND,IDD)*(RYSHTL(IEND,NPC)/RYSHTL(IEND,IDD)))
```

```
IF(DABS(BMMPN(IEND,IDD)).LT.DABS(BMCR(IEND,IDD))) THEN
BMMP(IEND,IDD)=1.01*BMCR(IEND,IDD)
 IF(DABS(BMMP(IEND,IDD)).GT.DABS(BMYSH(IEND,NPC))) THEN
 BMMP(IEND,IDD)=BMYSH(IEND,NPC)
 ELSE
 END IF
ELSE
BMMP(IEND,IDD)=BMMPN(IEND,IDD)
END IF
IF (DABS(BMMP(IEND,IDD)).LT.DABS(BMPP(IEND,IDD)))THEN
BMMP(IEND,IDD)=BMPP(IEND,IDD)
ELSE
END IF
RMAX(IEND,IDD)=RMAXTL(IEND,IDD)-BMYSH(IEND,NPC)/GAL2
RYSH(IEND,NPC)=RMAX(IEND,IDD)
RMAXPL(IEND,IDD)=RMAXTL(IEND,IDD)-BMMP(IEND,IDD)/GAL2
ELSE IF(REMIND*(ROTPTL(IEND,IDD)).GE.DABS(RANGEL(IEND,IDD)).AND.RE
1MIND*(ROTPTL(IEND,IDD)).LE.DABS(RANGEU(IEND,IDD)))THEN
RN(IEND,IDD)=RN(IEND,IDD)+1.
BETASH(IEND,IDD)=-0.014*DSQRT(RYSHTL(IEND,NPC)/RYSHTL(IEND,IDD))
GAMMA(IEND,IDD)=-0.01*DSQRT(RN(IEND,IDD))
BMMPN(IEND,IDD)=BMYSH(IEND,NPC)*DEXP(BETASH(IEND,IDD)*RN(IEND,IDD)
1+GAMMA(IEND,IDD)*(RYSHTL(IEND,NPC)/RYSHTL(IEND,IDD)))
 IF(DABS(BMMPN(IEND,IDD)).LT.DABS(BMCR(IEND,IDD)))THEN
 BMMP(IEND,IDD)=1.01*BMCR(IEND,IDD)
 IF(DABS(BMMP(IEND,IDD)).GT.DABS(BMYSH(IEND,NPC))) THEN
 BMMP(IEND,IDD)=BMYSH(IEND,NPC)
 ELSE
 END IF
 ELSE
 BMMP(IEND,IDD)=BMMPN(IEND,IDD)
 END IF
 IF (DABS(BMMP(IEND,IDD)).LT.DABS(BMPP(IEND,IDD)))THEN
 BMMP(IEND,IDD)=BMPP(IEND,IDD)
```

```
       ELSE
       END IF
      RMAXPL(IEND,IDD)=RMAXTL(IEND,IDD)-BMMP(IEND,IDD)/GAL2
      ELSE
      END IF
      ELSE
      IF(REMIND*(ROTPTL(IEND,IDD)).GT.DABS(RANGEU(IEND,IDD)))THEN
      RN(IEND,IDD)=1.
      RMAXTL(IEND,IDD)=RYSHTL(IEND,IRR)
      RYSHTL(IEND,IPC)=RMAXTL(IEND,IDD)
      BMYSH(IEND,IPC)=BMYSH(IEND,IDD)+(RYSHTL(IEND,IPC)-RYSHTL(IEND,IDD)
     1)*1./(1./EKEPSH(IEND,IPC)+1./GAL2)
      RMAX(IEND,IDD)=RMAXTL(IEND,IDD)-BMYSH(IEND,IPC)/GAL2
      RYSH(IEND,IPC)=RMAX(IEND,IDD)
      BETASH(IEND,IDD)=-0.014*DSQRT(RYSHTL(IEND,IPC)/RYSHTL(IEND,IDD))
      GAMMA(IEND,IDD)=-0.01*DSQRT(RN(IEND,IDD))
      BMMPN(IEND,IDD)=BMYSH(IEND,IPC)*DEXP(BETASH(IEND,IDD)*RN(IEND,IDD)
     1+GAMMA(IEND,IDD)*(RYSHTL(IEND,IPC)/RYSHTL(IEND,IDD)))
      IF(DABS(BMMPN(IEND,IDD)).LT.DABS(BMCR(IEND,IDD))) THEN
      BMMP(IEND,IDD)=1.01*BMCR(IEND,IDD)
       IF(DABS(BMMP(IEND,IDD)).GT.DABS(BMYSH(IEND,IPC))) THEN
       BMMP(IEND,IDD)=BMYSH(IEND,IPC)
       ELSE
       END IF
      ELSE
      BMMP(IEND,IDD)=BMMPN(IEND,IDD)
      END IF
      IF (DABS(BMMP(IEND,IDD)).LT.DABS(BMPP(IEND,IDD)))THEN
      BMMP(IEND,IDD)=BMPP(IEND,IDD)
      ELSE
      END IF
      RMAXPL(IEND,IDD)=RMAXTL(IEND,IDD)-BMMP(IEND,IDD)/GAL2
      ELSE IF(REMIND*(ROTPTL(IEND,IDD)).GE.DABS(RANGEL(IEND,IDD)).AND.RE
     1MIND*(ROTPTL(IEND,IDD)).LE.DABS(RANGEU(IEND,IDD)))THEN
```

```
      RN(IEND,IDD)=RN(IEND,IDD)+1.
      BETASH(IEND,IDD)=-0.014*DSQRT(RYSHTL(IEND,IPC)/RYSHTL(IEND,IDD))
      GAMMA(IEND,IDD)=-0.01*DSQRT(RN(IEND,IDD))
      BMMPN(IEND,IDD)=BMYSH(IEND,IPC)*DEXP(BETASH(IEND,IDD)*RN(IEND,IDD)
     1+GAMMA(IEND,IDD)*(RYSHTL(IEND,IPC)/RYSHTL(IEND,IDD)))
       IF(DABS(BMMPN(IEND,IDD)).LT.DABS(BMCR(IEND,IDD)))THEN
       BMMP(IEND,IDD)=1.01*BMCR(IEND,IDD)
       IF(DABS(BMMP(IEND,IDD)).GT.DABS(BMYSH(IEND,IPC))) THEN
       BMMP(IEND,IDD)=BMYSH(IEND,IPC)
       ELSE
       END IF
       ELSE
       BMMP(IEND,IDD)=BMMPN(IEND,IDD)
       END IF
       IF (DABS(BMMP(IEND,IDD)).LT.DABS(BMPP(IEND,IDD)))THEN
       BMMP(IEND,IDD)=BMPP(IEND,IDD)
       ELSE
       END IF
      RMAXPL(IEND,IDD)=RMAXTL(IEND,IDD)-BMMP(IEND,IDD)/GAL2
      ELSE
      END IF
      END IF
      KFAC=0
      KSPRNG=2
      FACTOR=0.
      GO TO 300
C
C     RULE. 12 UNLOADING AFTER RULE 11
C
 240  IDD=INDSH(IEND)
      IF(REMIND*DBM(IEND).LT.0.0)GO TO 250
      IKK=IDD+10
 666  FORMAT(4(2X,E10.4),I3)
      FAC=(BMYSH(IEND,IKK)-BMTOT(IEND))/DBM(IEND)
```

```
      IF(FAC.GE.FACTOR)GO TO 300
      FACTOR=FAC
      KFAC=IEND
      KSPRNG=2
      BM=BMYSH(IEND,IKK)
      ROTSH=RYSH(IEND,IKK)
      KODESH=11
      EKSH=EKEPSH(IEND,14)
      IDK=IDD
      GO TO 300
 250  FAC=(BMCR(IEND,IDD)-BMTOT(IEND))/DBM(IEND)
      IDB=3-IDD
      IKK=IDD+9
      IF(FAC.GE.FACTOR)GO TO 300
      FACTOR=FAC
      BM=BMCR(IEND,IDD)
      ROTSH=REVPCR(IEND,IDD)
      KFAC=IEND
      KSPRNG=2
      KODESH=13
C
C     DETERMINE  MINIMUM UNLOADING SLOPE.
C
      IF(DABS(RMAX(IEND,IDB)).EQ.DABS(RCR(IEND,IDB)))THEN
      EKUMIN=(BMCR(IEND,IDB)-BMCR(IEND,IDD))/(RCR(IEND,IDB)-RCR(IEND,IDD
     1))
      ELSE
      EKUMIN=(BMPP(IEND,IDB)-BMCR(IEND,IDD))/(ROTP(IEND,IDB)-REVPCR(IEND
     1,IDD))
      END IF
      EKEPSH(IEND,15)=EKEPSH(IEND,IKK)
      IF(DABS(EKEPSH(IEND,15)).LT.DABS(EKUMIN)) THEN
      EKEPSH(IEND,15)=EKUMIN
      ELSE
```

```
      END IF
      IF(DABS(EKEPSH(IEND,15)).LT.DABS(EKEPSH(IEND,13))) EKEPSH(IEND,15)
     1=EKEPSH(IEND,13)
      EKSH=EKEPSH(IEND,15)
      REVPSH(IEND,IDD)=REVPCR(IEND,IDD)-BMCR(IEND,IDD)/EKEPSH(IEND,15)
      IDK=IDD
      GO TO 300
C
C     RULE 13. UNLOADING AFTER 12.
C
  260 IDD=INDSH(IEND)
      IF(REMIND*DBM(IEND).LT.0.0)GO TO 270
      IKK=IDD+12
      IRR=IDD+10
      KODYSH(IEND)=14
      EKRL=(BMYSH(IEND,IRR)-BMYSH(IEND,IKK))/(RYSH(IEND,IRR)-RYSH(IEND,I
     1KK))
      EKEPSH(IEND,12)=EKRL
      EKHSH(IEND)=EKEPSH(IEND,12)
      KFAC=0
      KSPRNG=2
      FACTOR=0.0
      GO TO 300
  270 MINDSH(IEND)=IDD+12
      KDPSSH(IEND)=KODSH
      FAC=-BMTOT(IEND)/DBM(IEND)
      IF(FAC.GE.FACTOR)GO TO 300
      FACTOR=FAC
      BM=0.
      ROTSH=REVPSH(IEND,IDD)
      KFAC=IEND
      KSPRNG=2
      KODESH=9
      IDK=3-IDD
```

```
      IDB=IDK
C
C     DETERMINE RELOADING SLOPE.
C
      IF(RMAX(IEND,IDB).EQ.RCR(IEND,IDB))THEN
      EKLSH=BMCR(IEND,IDB)/(RCR(IEND,IDB)-REVPSH(IEND,IDD))
      ELSE
      EKLSH=BMPP(IEND,IDB)/(ROTP(IEND,IDB)-REVPSH(IEND,IDD))
      END IF
      EKEPSH(IEND,13)=EKLSH
      EKSH=EKLSH
C
C     DETERMINE THE BREAKING POINTS AT CRACKING LOAD AND AT THE PRIMARY
C     CURVE.
C
      RREMIN=-1.*REMIND
      IRR=IDB+2
      IKK=IDB+4
      IPC=IDB+14
      IF(RMAX(IEND,IDB).EQ.RCR(IEND,IDB)) THEN
      ROTCRI(IEND,IDB)=RCR(IEND,IDB)
      KFLAG1(IEND)=3
      ELSE IF(DABS(RMAX(IEND,IDB)).LT.DABS(RYSH(IEND,IDB)))THEN
      ROTCRI(IEND,IDB)=REVPSH(IEND,IDD)+BMCR(IEND,IDB)/EKEPSH(IEND,13)
C     RREMIN=-1.*REMIND
      IF(RREMIN*ROTCRI(IEND,IDB).GE.DABS(RMAXPL(IEND,IDB)))THEN
      ROTCRI(IEND,IDB)=0.99*RMAXPL(IEND,IDB)
        IF(RREMIN*ROTCRI(IEND,IDB).LE.RREMIN*REVPSH(IEND,IDD))THEN
           IF(BMCR(IEND,IDB)*ROTCRI(IEND,IDB).LT.0.)THEN
           REVPSH(IEND,IDD)=1.01*ROTCRI(IEND,IDB)
           ELSE
           REVPSH(IEND,IDD)=0.99*ROTCRI(IEND,IDB)
           END IF
        ROTSH=REVPSH(IEND,IDD)
```

```
        ELSE
        END IF
      EKEPSH(IEND,13)=BMCR(IEND,IDB)/(ROTCRI(IEND,IDB)-REVPSH(IEND,IDD))
      EKSH=EKEPSH(IEND,13)
      ELSE
      END IF
      EKEPSH(IEND,14)=(BMMP(IEND,IDB)-BMCR(IEND,IDB))/(RMAXPL(IEND,IDB)-
     1ROTCRI(IEND,IDB))
      IF(RREMIN*ROTCRI(IEND,IDB).LE.DABS(RCR(IEND,IDB)).AND.DABS(EKEPSH(
     1IEND,14)).GE.DABS(EKEPSH(IEND,IRR))) THEN
      RYSH(IEND,IPC)=RYSH(IEND,IRR)
      BMYSH(IEND,IPC)=BMYSH(IEND,IRR)
      EKEPSH(IEND,14)=(BMYSH(IEND,IPC)-BMCR(IEND,IDB))/(RYSH(IEND,IPC)-R
     1OTCRI(IEND,IDB))
      KFLAG1(IEND)=11
      KFLAG2(IEND)=3
      ELSE
      IF(DABS(EKEPSH(IEND,14)).LE.DABS(EKEPSH(IEND,IRR))) GO TO 275
      RYSH(IEND,IPC)=(RCR(IEND,IDB)*EKEPSH(IEND,IRR)-ROTCRI(IEND,IDB)*EK
     1EPSH(IEND,14))/(EKEPSH(IEND,IRR)-EKEPSH(IEND,14))
      IF(DABS(RYSH(IEND,IPC)).GE.DABS(RYSH(IEND,IDB)))THEN
 275  IF(DABS(EKEPSH(IEND,14)).LE.DABS(EKEPSH(IEND,IKK))) THEN
      BMYSH(IEND,IPC)=BMYSH(IEND,IDB)
      RYSH(IEND,IPC)=RYSH(IEND,IDB)
       IF(RREMIN*ROTCRI(IEND,IDB).GE.DABS(RYSH(IEND,IDB))) THEN
       ROTCRI(IEND,IDB)=0.99*RYSH(IEND,IDB)
        IF(RREMIN*ROTCRI(IEND,IDB).LE.RREMIN*(REVPSH(IEND,IDD)))THEN
           IF(BMCR(IEND,IDB)*ROTCRI(IEND,IDB).LT.0.)THEN
           REVPSH(IEND,IDD)=1.01*ROTCRI(IEND,IDB)
           ELSE
           REVPSH(IEND,IDD)=0.99*ROTCRI(IEND,IDB)
           END IF
        ROTSH=REVPSH(IEND,IDD)
        ELSE
```

```
   END IF
  EKEPSH(IEND,13)=BMCR(IEND,IDB)/(ROTCRI(IEND,IDB)-REVPSH(IEND,IDD)
1 )
  EKSH=EKEPSH(IEND,13)
  ELSE
  END IF
 EKEPSH(IEND,14)=(BMYSH(IEND,IDB)-BMCR(IEND,IDB))/(RYSH(IEND,IDB)-
1ROTCRI(IEND,IDB))
 ELSE
 RYSH(IEND,IPC)=(BMYSH(IEND,IDB)-BMCR(IEND,IDB)+EKEPSH(IEND,14)*ROT
1CRI(IEND,IDB)-EKEPSH(IEND,IKK)*RYSH(IEND,IDB))/(EKEPSH(IEND,14)-EK
2EPSH(IEND,IKK))
 BMYSH(IEND,IPC)=BMYSH(IEND,IDB)+EKEPSH(IEND,IKK)*(RYSH(IEND,IPC)-R
1YSH(IEND,IDB))
 END IF
 KFLAG1(IEND)=11
 KFLAG2(IEND)=5
 ELSE
 BMYSH(IEND,IPC)=BMCR(IEND,IDB)+EKEPSH(IEND,IRR)*(RYSH(IEND,IPC)-RC
1R(IEND,IDB))
 KFLAG1(IEND)=11
 KFLAG2(IEND)=3
 END IF
 END IF
 ELSE
 ROTCRI(IEND,IDB)=REVPSH(IEND,IDD)+BMCR(IEND,IDB)/EKEPSH(IEND,13)
 IF(RREMIN*ROTCRI(IEND,IDB).GE.DABS(RMAXPL(IEND,IDB)))THEN
 ROTCRI(IEND,IDB)=0.99*RMAXPL(IEND,IDB)
   IF(RREMIN*ROTCRI(IEND,IDB).LE.RREMIN*REVPSH(IEND,IDD))THEN
      IF(BMCR(IEND,IDB)*ROTCRI(IEND,IDB).LT.0.)THEN
      REVPSH(IEND,IDD)=1.01*ROTCRI(IEND,IDB)
      ELSE
      REVPSH(IEND,IDD)=0.99*ROTCRI(IEND,IDB)
      END IF
```

```
      ROTSH=REVPSH(IEND,IDD)
      ELSE
      END IF
     EKEPSH(IEND,13)=BMCR(IEND,IDB)/(ROTCRI(IEND,IDB)-REVPSH(IEND,IDD))
     EKSH=EKEPSH(IEND,13)
     ELSE
     END IF
     EKEPSH(IEND,14)=(BMMP(IEND,IDB)-BMCR(IEND,IDB))/(RMAXPL(IEND,IDB)-
    1ROTCRI(IEND,IDB))
     IF(RREMIN*ROTCRI(IEND,IDB).LE.DABS(RCR(IEND,IDB)).AND.DABS(EKEPSH(
    1IEND,14)).GE.DABS(EKEPSH(IEND,IRR))) THEN
     RYSH(IEND,IPC)=RYSH(IEND,IKK)
     BMYSH(IEND,IPC)=BMYSH(IEND,IKK)
     EKEPSH(IEND,14)=(BMYSH(IEND,IPC)-BMCR(IEND,IDB))/(RYSH(IEND,IPC)-R
    1OTCRI(IEND,IDB))
     KFLAG1(IEND)=11
     KFLAG1(IEND)=5
     ELSE
C
C    BREAKING POINT ON THE PRIMARY CURVE.
C
     IF(DABS(EKEPSH(IEND,14)).LE.DABS(EKEPSH(IEND,IKK))) THEN
     BMYSH(IEND,IPC)=BMYSH(IEND,IKK)
     RYSH(IEND,IPC)=RYSH(IEND,IKK)
      IF(RREMIN*ROTCRI(IEND,IDB).GE.DABS(RYSH(IEND,IKK))) THEN
      ROTCRI(IEND,IDB)=0.99*RYSH(IEND,IKK)
       IF(RREMIN*ROTCRI(IEND,IDB).LE.RREMIN*REVPSH(IEND,IDD))THEN
          IF(BMCR(IEND,IDB)*ROTCRI(IEND,IDB).LT.0.)THEN
          REVPSH(IEND,IDD)=1.01*ROTCRI(IEND,IDB)
          ELSE
          REVPSH(IEND,IDD)=0.99*ROTCRI(IEND,IDB)
          END IF
       ROTSH=REVPSH(IEND,IDD)
       ELSE
```

```
          END IF
         EKEPSH(IEND,13)=BMCR(IEND,IDB)/(ROTCRI(IEND,IDB)-REVPSH(IEND,IDD)
     1 )
         EKSH=EKEPSH(IEND,13)
         ELSE
         END IF
        EKEPSH(IEND,14)=(BMYSH(IEND,IKK)-BMCR(IEND,IDB))/(RYSH(IEND,IKK)-
     1ROTCRI(IEND,IDB))
        ELSE
        RYSH(IEND,IPC)=(BMYSH(IEND,IDB)-BMCR(IEND,IDB)+EKEPSH(IEND,14)*ROT
     1CRI(IEND,IDB)-EKEPSH(IEND,IKK)*RYSH(IEND,IDB))/(EKEPSH(IEND,14)-EK
     2EPSH(IEND,IKK))
        BMYSH(IEND,IPC)=BMYSH(IEND,IDB)+EKEPSH(IEND,IKK)*(RYSH(IEND,IPC)-R
     1YSH(IEND,IDB))
        END IF
        KFLAG1(IEND)=11
        KFLAG2(IEND)=5
        END IF
        END IF
        GO TO 300
C
C       RULE 14. RELOADING AFTER RULE 13.
C
  280   IDD=INDSH(IEND)
        IF(REMIND*DBM(IEND).LT.0.0)GO TO 290
        IKK=IDD+10
        FAC=(BMYSH(IEND,IKK)-BMTOT(IEND))/DBM(IEND)
        IF(FAC.GE.FACTOR)GO TO 300
        FACTOR=FAC
        BM=BMYSH(IEND,IKK)
        ROTSH=RYSH(IEND,IKK)
        KFAC=IEND
        KSPRNG=2
        EKSH=EKEPSH(IEND,14)
```

```
      KODESH=11
      IDK=IDD
      GO TO 300
290   IKK=IDD+12
      FAC=(BMYSH(IEND,IKK)-BMTOT(IEND))/DBM(IEND)
      IF(FAC.GE.FACTOR)GO TO 300
      FACTOR=FAC
      BM=BMYSH(IEND,IKK)
      ROTSH=RYSH(IEND,IKK)
      KFAC=IEND
      KSPRNG=2
      EKSH=EKEPSH(IEND,15)
      KODESH=13
      IDK=IDD
300   RETURN
      END
```